

**THE ANALYSIS AND DISCRIMINATION OF
PYROLYSIS PRODUCTS FROM BIOLOGICAL AND
NON-BIOLOGICAL SOURCES**

By

GINA FRANCESCA GABRIEL

Centre for Forensic Science
Department of Pure and Applied Chemistry
University of Strathclyde

**A thesis presented in fulfilment of the requirements for the degree of
Doctor of Philosophy**

2015

Centre for Forensic Science
Department of Pure and Applied Chemistry
University of Strathclyde

**THE ANALYSIS AND DISCRIMINATION OF
PYROLYSIS PRODUCTS FROM BIOLOGICAL AND
NON-BIOLOGICAL SOURCES**

**PhD THESIS
GINA FRANCESCA GABRIEL
2015**

This thesis is the result of the author's original research. It has been composed by the author and has not been previously submitted for examination which has led to the award of a degree. The copyright of this thesis belongs to the author under the terms of the United Kingdom Copyright Acts as qualified by the University of Strathclyde Regulation 3.50. Due acknowledgement must always be made of the use of any material contained in, or derived from, this thesis.

Signed:

Date:

ABSTRACT

This work involves the limited use of human tissue samples. These samples were obtained through body donation and under full ethical approval from the University of Strathclyde ethics committee. Products generated through pyrolysis of common materials can act as background compounds, interfering with the analysis and identification of potential human remains. The development of a robust methodology for the generation and analysis of volatile products from biological (porcine and human tissues) and non-biological (textile materials) sources stands at the core of this study, combined with examining various factors that causes these profiles to deviate. This process began with the validation of porcine samples as a substitute of human samples through the identification of similar key indicators, characteristic to both tissues. Interestingly, different temperature ranges (pre- and post-ignition) and type of porcine tissues utilised were found to effect the type of key indicators detected; and as such, has convincingly resolved key indicators reported in previous research literature. In addition, key indicators of pure and blended textiles were also established and the effects of blended fibres towards the overall thermal properties of the textile, highlighted. Alterations to the key indicators of individual porcine and textile samples were examined, subjectively and objectively, when both samples were burnt together (combined samples). Subjective analysis involved the scrutiny of the chromatographic output, revealing the dominance of key indicators of porcine samples over textiles for majority of the combined samples. EIC and EIP proved to be a beneficial tool in extracting key indicators of porcine samples in the presence of contamination (textiles). At 70% presence, SOFM provided an objective and successful classification and discrimination of pyrolytic data according to the type of pyrolysis product detected across textiles, porcine bones and also in the combined textile-bone samples while underlining meaningful associations amongst similar groups. Overall, although this work suggests that pyrolytic data can be unpredictable, such as its dependence on various factors, with suitable analytical and statistical techniques, it has revealed pertinent information on the key indicators of porcine, human and textiles samples and the inter- and intra-molecular changes that occur to them during pyrolysis.

ACKNOWLEDGEMENTS

Firstly, I would like to thank my Lord Jesus for giving me the opportunity to fulfil my dreams of studying in Scotland and also in guiding me throughout the entire PhD.

I wish to express my sincere gratitude to my supervisor, Prof. Dr. Niamh Nic Daeid who has been a tremendous mentor, guide and encourager throughout these years and for allowing me to enjoy the learning curve and grow as a research scientist. Deepest appreciation is also due to Dr. Lorraine Gibson who stepped in to be my co-supervisor towards the end of this project. I am also forever grateful to the expert laboratory assistance provided by the incredible Jim Christie (Patman) throughout the duration of my study, failing which, I would not be able to independently operate and maintain the GC-MS as I would now. I would like to thank the Ministry of Education (MOE) and Universiti Kebangsaan Malaysia (UKM) for believing in me and supporting me financially in the course of studying the PhD.

Special thanks go to Dr.Nicola, Dr.Felicity, Dr.Linda, Dr.Ally, Laura, Tina (Owly), Dr.Sara, Dr.Yuva and Dr.Wan for making the entire PhD journey fun-filled and enduring. I cherish the friendship fostered here and cheers to many more years of success and happy memories.

My biggest thanks and gratitude goes to my family and closest friends. Words are not enough to express how grateful I am to my ever loving, supportive and handsome husband, Jaccob, for all your sacrifices, care and concern that you have extended to me. I am forever grateful for the surprise drop-ins to the office to check how I'm doing on my stressful days and all the little treats that made this journey all the more bearable. I would like to appreciate my parents, Mr. and Mrs. Gabriel, brothers (especially Mark 'Fish') and my extended family for their continual support, prayers, love and encouragement. Also to Gordon (Big Gee), Kala (Partner in Crime), Tass (Tassimo), Joshua (Moo) and Valerie (Diva) for always praying, encouraging and joining me in lots of crazy, adrenalin pumping activities and adventures. Friends for life!

PUBLICATIONS, POSTERS AND PRESENTATIONS

Niamh Nic Daeid and **Gina Gabriel**, Fire Investigation and Evidence Recovery, Encyclopaedia of Forensic and Legal Medicine 2nd Edition, November 2014 – Book Chapter.

Gina Gabriel and Niamh Nic Daeid, Identification of Key Indicators of Human and Porcine Tissues, Proceedings University of Strathclyde Research Day, July 2014, Glasgow, Scotland – Poster Presentation.

Gina Gabriel and Niamh Nic Daeid, The Analysis of Thermal Decomposition Products Generated from Undecomposed and Decomposed Porcine and Human Tissues under Laboratory Conditions, Proceedings Scottish Student Forensic Research Symposium, 1st Meeting, March 2014, Glasgow, Scotland – Oral Presentation (Best Oral Presenter).

Gina Gabriel and Niamh Nic Daeid, Effects of Temperature on the Detection of *n*-aldehydes Generated from Different Porcine Tissues under Laboratory Conditions, Proceedings Scottish Student Forensic Research Symposium, 1st Meeting, March 2014, Glasgow, Scotland – Poster Presentation.

Gina Gabriel and Niamh Nic Daeid, Systematic Study on the Analysis of Thermal Decomposition Products Generated from the Combustion of Porcine and Human Tissue under Laboratory Conditions, Proceedings American Academy of Forensic Science, 66th Meeting, February 2014, Seattle, USA – Oral Presentation.

Gina Gabriel and Niamh Nic Daeid, Effects of Different Heat Exposure Times and Temperatures on the Chromatographic Profile derived from Porcine Samples under Laboratory Conditions, Proceedings American Academy of Forensic Science, 66th Meeting, February 2014, Seattle, USA – Poster Presentation.

Gina Gabriel and Niamh Nic Daeid, Comparison of Different Extraction Techniques in the Analysis of Pyrolysis Products Derived from Porcine Bone, Proceedings European Academy of Forensic Science Conference 6th Meeting, August 2012, The Hague, Netherlands – Poster Presentation.

KEY ABBREVIATIONS

ACS	Activated Carbon Strip
ANN	Artificial Neural Network
ASTM	American Society for Testing Materials
EIC	Extracted Ion Chromatogram
EIP	Extracted Ion Profile
GC-MS	Gas Chromatography-Mass Spectrometry
ILR	Ignitable Liquid Residues
LOI	Limiting Oxygen Index
<i>m/z</i>	Mass-to-Charge ratio
NIST	National Institute of Standards and Technology
PAN	Polyacrylonitrile
PET	Polyethylene Terephthalate
PMI	Post-Mortem Interval
PU	Polyurethane
PVC	Polyvinylchloride
RSD	Relative Standard Deviation
SOFM	Self-Organising Feature Maps
SOM	Self-Organising Maps
STDEV	Standard Deviation
TIC	Total Ion Chromatogram
VOC	Volatile Organic Compounds

TABLE OF CONTENTS

Abstract	iii
Acknowledgement	iv
Publications, Posters and Presentations	v
Key Abbreviations	vi
Table of Contents	vii
Thesis Outline	xv
CHAPTER 1: INTRODUCTION	1
1.1 FIRES AND HUMAN REMAINS	1
1.2 BONE	2
1.2.1 Macroscopic and Microscopic Components of Bone	2
1.2.2 Macroscopic and Microscopic Structure of Bone	4
1.3 THE COMBUSTION PROCESS	6
1.4 PYROLYSIS / THERMAL DECOMPOSITION PROCESS	6
1.4.1 Mechanisms of Pyrolysis	11
1.4.1.1 Random Scission	11
1.4.1.2 Side Group Scission / Side Group Elimination / Chain Stripping	12
1.4.1.3 Monomer Reversion / Depolymerisation / Unzipping	13
1.4.2 Pyrolysis and Combustion of Polymers	14
1.4.3 Pyrolysis and Combustion of Hydrocarbons	17
1.4.4 Pyrolysis and Combustion of Carbohydrates and Fats	19
1.5 THERMAL ALTERATIONS TO BONE	21
1.5.1 Stages of Heat-Induced Modification in Bone	21
1.6 INTERFERING PYROLYSIS PRODUCTS AND THEIR IMPLICATION IN FORENSIC FIRE ANALYSIS	23
1.7 EXTRACTION OF PYROLYSIS PRODUCTS FROM FIRE DEBRIS SAMPLES	27
1.7.1 Passive Headspace Diffusion using Activated Carbon Strip (ACS)	28
1.8 INSTRUMENTAL ANALYSIS	30
1.8.1 Chromatography and Gas Chromatography (GC)	30
1.8.2 Instrumentation of Gas Chromatography	32

1.8.2.1	GC Injection Port / Inlet	33
1.8.2.2	Gas Supply and Flow Controllers	33
1.8.2.3	Analytical Column and Oven	34
1.8.2.4	Detector	35
1.8.2.5	Data Acquisition System	36
1.8.3	Gas Chromatography-Mass Spectrometry (GC-MS)	37
1.8.3.1	Ionisation Source	37
1.8.3.2	Mass Analyser	39
1.8.3.3	MS Detector	40
1.9	RESEARCH OBJECTIVES	43
1.10	REFERENCES	44

CHAPTER 2: GAS CHROMATOGRAPHY – MASS SPECTROMETRY (GC-MS) INSTRUMENTAL VALIDATION AND METHODOLOGY DEVELOPMENT

2.1	INTRODUCTION	61
2.2	VALIDATION OF GC-MS INSTRUMENTATION	61
2.2.1	Specificity / Selectivity	62
2.2.2	Precision	62
2.2.3	Limit of Detection (LOD) and Limit of Quantitation (LOQ)	64
2.2.4	Sensitivity	64
2.2.5	Accuracy	64
2.2.6	Linearity	64
2.2.7	Peak shape	65
2.2.8	Band Broadening	66
2.3	METHODOLOGY VALIDATION: GENERATION AND EXTRACTION OF PYROLYSIS PRODUCTS USING PASSIVE HEADSPACE ADSORPTION WITH ACTIVATED CARBON STRIP (ACS)	67
2.4	EXPERIMENTAL METHODS	68
2.4.1	Preparation of the Grob Test Mixture	68
2.4.2	GC-MS Experimental Set-Up	69

2.4.3	Validation of ACS Recovery Method using Porcine Bone as a Test Sample	70
2.4.3.1	Preparation of the Bone Samples	71
2.4.3.2	Pyrolysis of Bone Samples using the ACS Process	72
2.4.3.3	Extraction of Pyrolysis Products from Bone Samples using the ACS Process	72
2.5	RESULTS AND DISCUSSION	75
2.5.1	Assessment of GC-MS Instrumental Performance	75
2.5.2	Pyrolysis of the Porcine Samples	78
2.5.2.1	Temperature Profile of Bone Samples	78
2.5.2.2	Identification of Best Sample Weight, Post Deprivation Sampling Time and ACS Size	80
2.5.2.3	Identification of Peaks in the Total Ion Chromatogram (TIC)	84
2.6	CONCLUSIONS	92
2.7	REFERENCES	93

CHAPTER 3: THE EFFECTS OF TEMPERATURE AND TIME OF EXPOSURE ON THE PYROLYTIC PROFILE DERIVED FROM PORCINE AND HUMAN TISSUES **99**

3.1	INTRODUCTION	99
3.2	COMPOSITION OF THE HUMAN BODY	100
3.2.1	Structure and Composition of Muscle	104
3.2.2	Structure and Composition of Ribs	105
3.3	THERMAL DECOMPOSITION OF THE HUMAN BODY	106
3.4	EXPERIMENTAL METHODS	110
3.4.1	Sample Preparation: Porcine Tissue Samples	110
3.4.1.1	Porcine Bone	110
3.4.1.2	Porcine Muscle	110
3.4.1.3	Porcine Rib	110
3.4.2	Sample Preparation: Human Tissue Samples	110
3.4.2.1	Human Toe	110
3.4.3	Generation of Thermal Decomposition Products	111

3.4.4	Gas Chromatography – Mass Spectrometry	112
3.5	RESULTS AND DISCUSSION	113
3.5.1	Porcine Samples - Effects of Temperature	113
3.5.1.1	Porcine Bone Pre-Ignition Samples (200 °C – 250 °C)	113
3.4.1.2	Porcine Bone Post-Ignition Samples (> 250 °C)	115
3.5.1.3	Porcine Muscle Pre-Ignition Samples (200 °C – 250 °C)	118
3.5.1.4	Porcine Rib Pre-Ignition Samples (200 °C – 250 °C)	121
3.5.2	Porcine Samples - Effects of Time of Exposure	126
3.5.3	Human Samples - Effects of Temperature	132
3.5.3.1	Post-Ignition Human Samples (> 250 °C)	132
3.5.3.2	Comparison of Pyrolysis Products Generated from Post-Ignition Human and Porcine Samples	136
3.6	CONCLUSIONS	145
3.7	REFERENCES	146

CHAPTER 4: METHODOLOGY DEVELOPMENT FOR THE GENERATION, ANALYSIS AND CHARACTERISATION OF PYROLYSIS PRODUCTS FROM VARIOUS TEXTILE MATERIALS 152

4.1	INTRODUCTION	152
4.2	NATURAL FIBRES	152
4.2.1	Plant Fibres	153
4.2.1.1	Cotton	153
4.2.1.2	Denim	158
4.2.1.3	Linen	159
4.2.2	Animal Fibres	160
4.2.2.1	Wool	160
4.2.2.2	Silk	163
4.2.2.3	Leather	165
4.3	SYNTHETIC FIBRES	167
4.3.1	Polyester	168
4.3.2	Nylon	170
4.3.3	Acrylic	173

4.3.4	Spandex / Elastane	176
4.4	SEMI-SYNTHETIC FIBRES	177
4.4.1	Rayon	177
4.4.1.1	Viscose	178
4.4.1.2	Modal	178
4.5	FIBRE BLENDS	179
4.6	EXPERIMENTAL METHODS	180
4.6.1	Textile Samples	180
4.6.2	Generation of Thermal Decomposition Products	181
4.6.2.1	Preliminary Method Validation for Optimal Generation of Pyrolysis Products from Textile Samples	181
4.6.2.1.1	Control Samples / Unburnt Textiles	181
4.6.2.1.2	Burnt Textiles	181
4.6.3	Passive Headspace Adsorption with Activated Carbon Strip (ACS)	182
4.6.4	Gas Chromatography – Mass Spectrometry	182
4.7	RESULTS AND DISCUSSION	183
4.7.1	Control Samples / Unburnt Textiles	183
4.7.2	Temperature Profile and Burning Behaviour of Textiles	186
4.7.2.1	Pre-Optimised Burnt Textiles	186
4.7.2.2	Post-Optimised Burnt Textiles	194
4.7.3	Pyrolysis Products of Textiles	194
4.7.3.1	100% Cotton (A)	194
4.7.3.2	95% Cotton + 5% Elastin (B)	198
4.7.3.3	50% Cotton + 50% Modal (D)	201
4.7.3.4	100% Acrylic (E)	206
4.7.3.5	50% Acrylic + 50% Cotton (F)	212
4.7.3.6	80% Nylon + 20% Elastin (H)	217
4.7.3.7	100% Denim (J)	223
4.7.3.8	96% Wool + 4% LYCRA [®] (L)	226
4.7.3.9	64% Polyester + 33% Rayon + 3% Elastin (N)	230
4.7.3.10	50% Polyester + 50% Viscose (O)	235
4.7.3.11	100% Leather (Q)	240

4.8 CONCLUSIONS	246
4.9 REFERENCES	248

CHAPTER 5: GENERATION, ANALYSIS AND DISCRIMINATION OF PYROLYSIS PRODUCTS FROM PORCINE BONE IN THE PRESENCE OF TEXTILES USING PATTERN RECOGNITION TECHNIQUES **266**

5.1 INTRODUCTION	266
5.2 INTERFERING PYROLYSIS PRODUCTS	267
5.3 PATTERN RECOGNITION IN GC-MS DATA ANALYSIS AND INTERPRETATION	268
5.3.1 Extracted Ion Current / Chromatogram (EIC) and Extracted Ion Profile (EIP)	270
5.3.2 Self-Organising Feature Maps (SOFM)	275
5.4 EXPERIMENTAL METHODS	280
5.4.1 Pyrolysis Products from Textile Samples in the Presence of Porcine Bone	280
5.4.1.1 Textile Samples	280
5.4.1.2 Porcine Bone Samples	280
5.4.1.3 Generation and Extraction of Thermal Decomposition Products	281
5.4.1.4 Gas Chromatography – Mass Spectrometry	281
5.4.2 Pattern Recognition	281
5.4.2.1 Extracted Ion Chromatogram (EIC) and Extracted Ion Profile (EIP)	281
5.4.2.2 Self-Organising Feature Maps (SOFM)	282
5.4.2.2.1 SOFM of Individual Textile Samples	283
5.4.2.2.2 SOFM of Combined Samples	284
5.5 RESULTS AND DISCUSSION	285
5.5.1 Temperature Profile Associated with the Burning of Combined Samples	285
5.5.2 Pyrolysis Products	285
5.5.2.1 Porcine Bone + 100% Cotton (AA)	285
5.5.2.2 Porcine Bone + 95% Cotton + 5% Elastin (BB)	291
5.5.2.3 Porcine Bone + 50% Cotton + 50% Modal (DD)	298

5.5.2.4	Porcine Bone + 100% Acrylic (EE)	304
5.5.2.5	Porcine Bone + 50% Acrylic + 50% Cotton (FF)	311
5.5.2.6	Porcine Bone + 80% Nylon + 20% Elastin (HH)	317
5.5.2.7	Porcine Bone + 100% Denim (JJ)	324
5.5.2.8	Porcine Bone + 96% Wool + 4% LYCRA® (LL)	329
5.5.2.9	Porcine Bone + 64% Polyester + 33% Rayon + 3% Elastin (NN)	334
5.5.2.10	Porcine Bone + 50% Polyester + 50% Viscose (OO)	341
5.5.2.11	Porcine Bone + 100% Leather (QQ)	348
5.5.3	Application of Extracted Ion Chromatogram (EIC) and Extracted Ion Profile (EIP) for the Identification of Key Indicators of Porcine Bone	356
5.5.3.1	EIC and EIP of Porcine Bone (Post-Ignition)	356
5.4.3.2	EIC and EIP of Porcine Bone in the Presence of Textiles	360
5.5.4	Self-Organising Feature Maps (SOFM) Model Validation	360
5.5.4.1	SOFM Classification of Individual Textile Samples	361
5.5.4.1	SOFM Classification of Combined Samples	364
5.6	CONCLUSIONS	370
5.7	REFERENCES	372
CHAPTER 6: GENERAL CONCLUSIONS AND FUTURE WORK		382
6.1	SUMMARY OF CONCLUSIONS	382
6.2	RECOMMENDATION FOR FUTURE WORK	386
APPENDICES		388
APPENDIX 1.0		389
	PYROLYSIS PRODUCTS GENERATED ACROSS SIX SETS OF REPEATS FROM PORCINE BONE	
APPENDIX 2.0		392
	PYROLYSIS PRODUCTS FROM 50% COTTON + 33% VISCOSE + 17% POLYESTER (C)	
APPENDIX 3.0		393
	PYROLYSIS PRODUCTS FROM 100% NYLON (G)	
APPENDIX 4.0		395

PYROLYSIS PRODUCTS FROM 100% SILK (I)	
APPENDIX 5.0	396
PYROLYSIS PRODUCTS FROM 100% VISCOSE (K)	
APPENDIX 6.0	396
PYROLYSIS PRODUCTS FROM 100% POLYESTER (M)	
APPENDIX 7.0	397
PYROLYSIS PRODUCTS FROM 64% POLYESTER + 32% VISCOSE + 4% ELASTIN (P)	
APPENDIX 8.0	399
EIC and EIP of Porcine Bone in the Presence of Textiles (Combined Samples)	
EIC AND EIP OF PORCINE BONE IN THE PRESENCE OF COTTON AND COTTON BLENDS	399
EIC AND EIP OF PORCINE BONE IN THE PRESENCE OF ACRYLIC AND ACRYLIC BLENDS	403
EIC AND EIP OF PORCINE BONE IN THE PRESENCE OF NYLON-ELASTIN BLEND	406
EIC AND EIP OF PORCINE BONE IN THE PRESENCE OF DENIM	406
EIC AND EIP OF PORCINE BONE IN THE PRESENCE OF WOOL-LYCRA [®] BLEND	406
EIC AND EIP OF PORCINE BONE IN THE PRESENCE OF POLYESTER AND POLYESTER BLENDS	410
EIC AND EIP OF PORCINE BONE IN THE PRESENCE OF LEATHER	410
REFERENCES	414

THESIS OUTLINE

Chapter one of this thesis presents an introduction to the main topic, focusing on the process of combustion and pyrolysis, and the effects of interfering pyrolysis products in the extraction, analysis and interpretation of fire debris. The chapter also gives an overview on the structures of bone and its reaction towards heat.

Chapter two provides an in depth description of the techniques employed to validate instrumentation. It also outlines the first stage of this work which presented the methods used for optimising and validating the parameters in the methodology in which pyrolysis products are generated from porcine tissue utilising passive headspace extraction with activated carbon strip (ACS) coupled with GC-MS.

Chapter three involves validating the use of *n*-aldehydes as key indicators of biological remains by identifying the presence and absence of *n*-aldehydes across different temperatures, exposure durations, and across different types of porcine tissue. The work then examines the pyrolysis products generated from human and pig tissue, to identify their similarities and differences.

Chapter four presents the pyrolysis products for a variety of pure and blended textiles (natural, synthetic and semi-synthetic) and in particular, examines the thermal behaviour of each textile and the reproducibility of the production of these pyrolysis products.

Chapter five presents the pyrolysis products generated from textiles in the presence of porcine samples and the subsequent pattern recognition techniques using extracted ion chromatogram (EIC), extracted ion profile (EIP) and chemometric analysis using self-organising feature maps (SOFM) for separating and categorising the pyrolysis products generated from burning both porcine and textile samples together.

Chapter 6 provides the overall conclusions of the study and also recommendations for future work.

CHAPTER 1: INTRODUCTION

1.1 Fires and Human Remains

The purpose of this work was to develop a robust in-house laboratory methodology that emulates real life fire scenarios (as far as possible) for the generation, extraction, analysis and identification of key indicators of human tissue samples and, to test various factors that cause the profile to deviate. The literature in terms of the work conducted to identify pyrolysis products from human remains is poor. In criminal burning, fires are often used as a tool to destroy evidence, prevent recovery, detection and identification of human remains [1]. The extent of fragmentation and damage exerted by heat towards the body are known to cause thermal alterations that can render the body unrecognisable to the human eye, particularly if majority of the remains have been consumed with the remaining hard tissues rendered into pieces and left unrecognisable and obscured by the severely charred scene, a common situation that occurs during flashover conditions (simultaneous ignition of fuel load in compartmental fires to form a fully developed fire [2]) [3-5].

If knowledge of the pyrolysis products and the presence of key indicators of human remains are identified, as has been studied and developed in detail for a range of ignitable liquid residues (ILR) [6], the analyst can then be made aware of the chromatographic patterns that specifically indicate the presence of human remains in fire debris. This can indefinitely facilitate the proper examination, analysis and distinction of fire debris samples, particularly for cases where human remains are not suspected to be present or have been totally consumed by the fire. In the presence of contaminating pyrolysis products, that can come from a range of fuel load in the fire scene, the identification of these key indicators of human remains would not only prevent any misinterpretation and misidentification, but to also avoid any false positive or false negative conclusions from the examination of unknown patterns from fire debris samples containing human remains.

According to the National Fire Protection Association (NFPA) report in 2012, a staggering 1,375,000 fires were reported in the United States (U.S.), out of which 2,855 led to death [7]. In the United Kingdom (U.K.), the Department for Communities and Local Government mentioned in their annual Fire Statistics Great Britain 2011-2012 that 272, 000 fires were reported and from these, 11,300 caused injuries and 380 deaths [8]. Across both continents, arson remains to be the single most abundant cause of fires. The NFPA's annual survey (Fire Loss in the United States) reported that each year in the U.S., an estimated 267,000 fires are attributed to arson, which caused over 2,000 injuries and 475 deaths [9]. In the U.K., arson is a significant cause of fire cases in England and Wales with 27,208 cases recorded across the U.K. in 2011-2012 [10]. In Scotland, 15,061 deliberate fires were documented in the year 2012-2013 that resulted with 14 deaths [11]. Buyuk and Kocak [12] also mentioned that out of 70% of fire deaths, 10% are found to be deliberately caused to conceal crimes.

1.2 Bone

Across the tissues in the human body, teeth and bones are the most resilient and are most often encountered intact when a body is recovered from a fire scene. Bone is classified as hard tissue as it exhibits incredible durability and tensile strength, and is resistant to many kinds of decay [9]. Since bones are the last layer to be exposed to heat, they are often encountered in a scene after a fire.

1.2.1 Macroscopic and Microscopic Components of Bone

Bones are the basis of the skeletal structure in the human body and perform diverse physical and metabolic functions, such as provision of structural support and levers for movement and locomotion, protection of visceral organs, storage of marrow cells and mineral ion reservoirs, and homeostasis [13-15].

Being an organ that is only found in vertebras [16], bones can come in various forms: long, short, flat and irregular [17]. It is a tissue that allows growth and remodelling, and facilitates constant changes in its composition and microscopic structure to

accommodate external stresses and injuries [9, 18, 19]. A living bone is basically a vascularised connective tissue that contains water, blood, fat and a composite of nanometre-sized bioapatite mineral crystals (calcium phosphate) deposited in an organic matrix of collagen fibres [8, 20, 21].

To simplify this, bones are predominantly made up of three major parts: water, organic matrix and inorganic minerals [22], in proportion; 50% to 70% are minerals, 20% to 40% are organic matrix, 5% to 10% are water and less than 3% are lipids [15]. The amount of water present in bone, either existing freely or bonded to other molecules, varies, and is said to hold the power that dictates a bone's mechanical behaviour [16, 18].

Comprising 90% of the organic matrix is type I collagen, a structural fibrous protein that undergoes mineralisation and covalent cross-linking to provide bone with its flexibility / elasticity and tensile / mechanical strength [9, 13, 18, 20, 23]. Type I collagen molecules are highly organised, comprising three helical amino acids twisted into a triple helix, which are then grouped into bundles [24]. Elastin and other non-collagenous protein make up the rest of the 10% in the matrix [16, 25].

The inorganic salts, responsible for impregnating and enclosing the cross-linked collagen, are mainly calcium and phosphate although other impurities such as hydrogen phosphate, sodium, magnesium, potassium, citrate and carbonate also exist in minute amounts [26]. Having high binding affinity towards each other, calcium and phosphate combine and, in turn, form plate-shaped [27] microscopic hydroxyapatite crystals, $\text{Ca}_{10}(\text{PO}_4)_6(\text{OH})_2$ [9, 28], that arrange themselves transversely to the collagen fibres [29]. The term carbonated apatite (dahllite) has also been used sparingly to describe these crystals as it has been documented that minor amounts of phosphate in the crystals are displaced by carbonate [16, 30]. These crystals provide bones with their compressive, load-bearing strength and hardness [8, 18].

Figure 1.0 demonstrates the assembly of collagen fibres and hydroxyapatite crystals in bone.

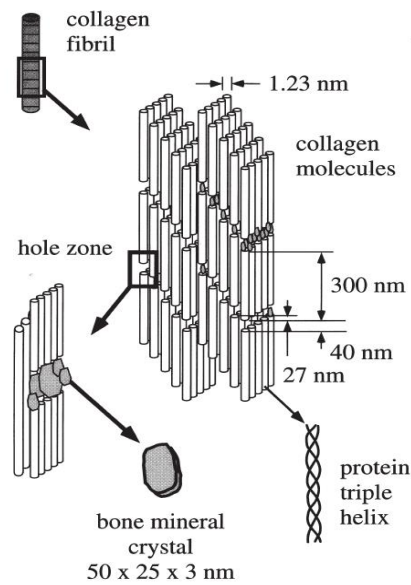


Figure 1.0: Assembly of collagen fibres and hydroxyapatite crystals in bone [13]

Both the organic and inorganic constituents are in close association with each other, forming a two-phase composite that affords bones their remarkable properties, without which bones would not be as strong, resistant and thermally stable as presumed [20, 31-33].

1.2.2 Macroscopic and Microscopic Structure of Bone

Macroscopically, a long bone can be sectioned into four parts: epiphysis (rounded ends of long bones), diaphysis (long hollow central shaft), metaphysis (cone-shaped area below the growth plate at both ends of the bone) and the epiphyseal plate (plates of cartilage).

A cross-section of the bone illustrates two very different types of bone tissue, namely cortical (compact) bone and trabecular (cancellous / spongy) bone. About 80% of the bones in the human body are compact bones and the remaining 20% are cancellous bones; both are primarily made up of osteons [15], arranged in a lamellar pattern [15, 34]. These bones are readily distinguishable based on their degree of porosity / density [35]. Bones that have a density of less than 70% are categorised as trabecular whereas bones with a density of more than 70% are categorised as cortical [36]. Figure 1.1 illustrates the different macroscopic sections of a bone.

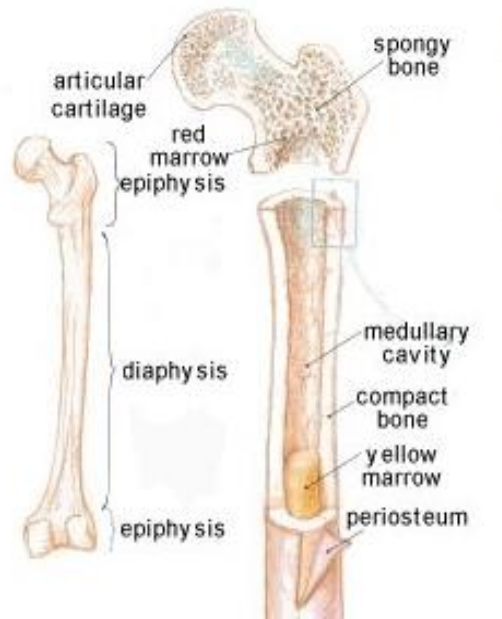


Figure 1.1: Macroscopic structure of long bone [37]

With its dense and compact structure, cortical bone forms a cortex around the circumference of cancellous bone, and is the primary component of the diaphysis [13, 15]. Thus, it is not surprising that this cortical structure is attributed to providing mechanical strength to bone. Having a porosity of 5% to 10%, cortical bone only allocates space for cells, blood channels (Haversian canal and Volkmann's canal) and erosion cavities [16, 18]. In contrast, trabecular bone is extremely porous (75% to 95%) in order to accommodate the bone marrow [18]. Trabecular bone is made up of a honeycomb network of rods, interspersed in the bone marrow compartment and is the main component of the epiphysis [15, 16, 18, 36].

The components and structure of bone vary from one individual to another and also within the same individual [38]. This can be attributed to diet, development, genetics and many other factors [39]. This is clearly seen in Forbes *et al.* [40] and Mitchell *et al.*'s [38] studies. They discovered that different types of bone (long bone: ulna, tibia; and flat bone: rib) varied in their chemical composition, especially in their fat and water content. Ribs possessed the highest water and protein content, whereas the ulna had the highest mineral content (calcium and phosphorous).

1.3 The Combustion Process

Fire is an exothermic oxidation reaction between a fuel and an oxidiser (most often oxygen in the surrounding air) that proceeds at such a rate as to be self-sustaining and yields detectable heat and light [41-43]. Robert Boyle was the first scientist to discover combustion and highlighted the need of an element in air required for combustion to occur [44]. Antoine-Laurent Lavoisier, went on to identify this element as oxygen and mentioned that fire was indeed a chemical reaction that converts matter while releasing energy in the form of heat and light [45]. It is made up of a number of chemical reactions that are occurring not only concurrently but together with a series of oxidative reactions [8] that are expressed physically in the form of flame and heat [10]. This process can also be referred to as combustion [17]. The production of heat and flames characterises an exothermic (heat releasing) reaction [8, 9].

1.4 Pyrolysis / Thermal Decomposition Process

Heat generated from a fire can induce the degradation and decomposition of a particular material, be it natural or synthetic. Thermal degradation and thermal decomposition are two different terms and should not be used interchangeably [46]. According to the American Society for Testing and Materials (ASTM) E176-13 [47], thermal degradation refers to the process of heat application that affects the material's physical and mechanical structure, whereas thermal decomposition refers to the various chemical changes the material experiences at elevated temperatures [46]. The latter is also referred to as pyrolysis, the process of vaporisation of a particular material by heat. The volatile products generated will burn and produce more volatile and combustion products [48]. In a fire scenario, pyrolysis is depicted to be the main force that drives the spread of fire as it dictates the rate of heat release generated by the fire [49]. Numerous views over the definition of pyrolysis can be observed across the literature [8, 43, 50].

The word ‘pyrolysis’ is taken from the Greek-derived word, where *pyro* refers to fire and *lysis* means separating [8]. Pyrolysis is defined as a thermochemical decomposition of organic material (solid or liquid) into smaller compounds at elevated temperatures (heat) above ambient temperature [51] in the absence of oxygen [52, 53] or any other oxidants, that is necessary for almost all solids (or liquids) to burn / combust [54]. Jones and De Neve [53] mentioned in their study that pyrolysis involves a great deal of physical and chemical modifications of the fuel, with the formation of numerous by-products. They went on to propose a figurative means of demonstrating pyrolysis as a whole and this is illustrated in Figure 1.2.

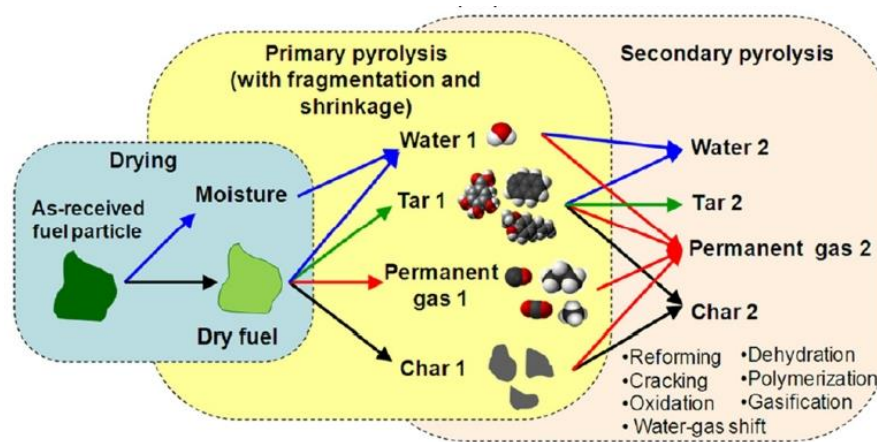


Figure 1.2: Pyrolysis model [53]

Although pyrolysis refers to a process that does not involve oxygen, the degradation process that precedes pyrolysis, and combustion, requires and is accelerated in the presence of oxygen [55]. The presence of oxygen induces oxidation, a reaction in which an element / fuel combines with oxygen; a vital chemical process that occurs in order for flames to exist [8]. In the presence of an ignition source, oxygen and fuel absorbs energy from heat and becomes activated. Once this occurs, a redox reaction takes place (oxidation and reduction) as the oxygen and fuel loses and gains electrons. Because electrons are neither created nor destroyed in a chemical reaction, oxidation and reduction are linked and it is not possible to have one without the other [56, 57]. In order for flames to form, enough volatiles have to be generated by the fuel (generated when an ignition source is applied to the fuel to cause pyrolysis) and, when mixed with adequate amounts of oxygen, combustion is facilitated and

sustained. With increasing oxygen levels, more free radicals are formed, that facilitates increasing attacks to the polymer's structure and integrity, and in turn generates more heat to fuel pyrolysis.

Generally, heat from the fire causes the macromolecule fuel structure to undergo devolatilisation as bonds that hold the molecules together are subjected to distress. As a result, depolymerisation, vaporisation and cross-linking of the fuel matrix occurs and causes the fuel to decompose into simpler compounds, namely liquid (tar), vapours and gases, and residual solid (char) [9, 10, 58]. The residual solid that is left behind is basically a charred residue and is primarily made up of carbon. It is the gaseous vapour formed during pyrolysis that is ultimately combusted in a flaming fire, not the solid / liquid fuel [54].

The energy needed to break two bonds in order to release a volatile compound would depend on the thermal stability and energy of the bonds within the polymer [59]. Bonds that are the weakest undergo breakdown first, before other sites in the polymer, that in turn dictates the polymer's subsequent decomposition pathways [55]. Polymers that are of high molecular weight and / or contain ring structures and cross-links are relatively harder to pyrolyse as these features make it possible for two bonds in the polymer to break apart closer in a chain without the release of a volatile, increasing their stability [55, 59]. Table 1.0 illustrates the various bonds and energy required to break these bonds (bond enthalpy).

Table 1.0: Bond and bond energy. Adapted from [60].

Bond	Bond enthalpy (kJ/mol)	Bond	Bond enthalpy (kJ/mol)
Single bonds		Multiple bonds	
H-H	436	C=C	619
H-N	393	C=N	615
H-O	460	C=O	724
H-S	368	C=S	477
C-H	414	N=N	418
C-C	347	P=P	490
C-N	276	S=S	351
C-O	351	O=O	499
C-S	255	O=S	469
N-N	393	C≡C	812
N-O	176	C≡N	891
O-O	142	N≡N	941

The rate of pyrolysis is predominantly a function of temperature and therefore heat – mainly heat flux. Heat flux refers to the rate at which heat is transferred per unit area upon or through a particular surface and is measured in W/m^2 [41]. With increasing heat, more pyrolysis products are generated as the rise in temperature facilitates the generation of smaller and more volatile molecules, as compared to heating at lower temperatures [54, 61]. Nonetheless, the rate of pyrolysis is also governed by other factors such as surface area of fuel, vapour pressure, and the presence of oxygen, hydrogen and water vapour [62, 63].

Besides temperature and heat flux, another important determinant of pyrolysis is thermal inertia (I). Thermal inertia refers to the measure of ignitability or responsiveness of a material to temperature variations [64]. It provides a quantitative value as to the amount of heat that must be added to a material to increase its temperature [10], and is influenced by three main factors; thermal conductivity (the quantity of heat transmitted through a unit thickness of a material), density (mass per unit volume of a material) and specific heat capacity (the amount of heat required to raise the temperature of a material by one degree) [9, 64, 65]. Equation 1.0 expresses the formula that determines thermal inertia in relation to the three factors mentioned above. If the value of (I) is high, it translates that the material in question is more resistant to ignition, thus higher amounts of heat and longer durations of exposure is required to heat up the material, and *vice versa*.

$$I = \sqrt{kpc} \quad \text{Equation 1.0}$$

where,

k is the thermal conductivity

p is the density

c is the specific heat capacity, and

I is the thermal inertia

Pyrolysis is said to occur at temperatures above 250 °C, commonly occurring within a temperature range of 500 °C to 800 °C [51]. As it is a function of heat and therefore temperature, thermal degradation and pyrolysis can be classified into three phases based on their temperature profiles [51, 54]:

- thermal degradation – 100 °C to 300 °C
- mild pyrolysis – 300 °C to 500 °C
- vigorous pyrolysis – above 500 °C

As temperatures and duration of exposure to heat flux in a fire typically fluctuate across these temperature ranges, this could in turn affect the chemical properties of the remaining fuel which is present after the fire. This is supported by DeHaan *et al.*'s [66] findings upon subjecting subcutaneous fat to various temperatures: samples exposed to 300 °C did not generate any pyrolysis products whereas temperatures reaching 500 °C were suggested to be the optimal temperatures to generate these products. Temperatures exceeding 700 °C were excessive and found to have caused the decomposition of volatile products. In the case of cadaveric remains in a fire, variation in temperatures and durations of exposure to heat to which the body is exposed could potentially alter the chemical composition, analytical profile and ultimately the presence of potential key volatile indicators of human remains [66].

Compounds subjected to pyrolysis undergo breakdown in three main ways, through: random scission, side-group scission and monomer reversion [54, 61, 67]. These three mechanisms are responsible for majority of the pyrolysis products generated in a fire, and, with the increase in temperature, they generate even smaller radicals and volatile molecules [54]. Other mechanisms such as cross-linking or char formation do not significantly affect the resulting pyrolysis products; thus, they don't play an important role in forensic fire analysis [61]. It is also important to note that a particular combustible material can go through more than one type of breakdown mechanism simultaneously, depending on polymer size and susceptibility of the polymer chain to a certain type of pyrolysis mechanism [54].

1.4.1 Mechanisms of Pyrolysis

1.4.1.1 Random Scission

Random scission occurs when a long chain hydrocarbon undergoes breakage at random locations on the carbon-to-carbon backbone that supports the molecular structure, producing smaller molecules of varying chain lengths [54, 61, 67]. The scission occurs at random as the carbon-to-carbon bonds are all of similar strengths at any location. The scission produces free radicals that will later form oligomers such as alkanes, alkenes and alkadienes of varying sizes as illustrated in Figure 1.3.

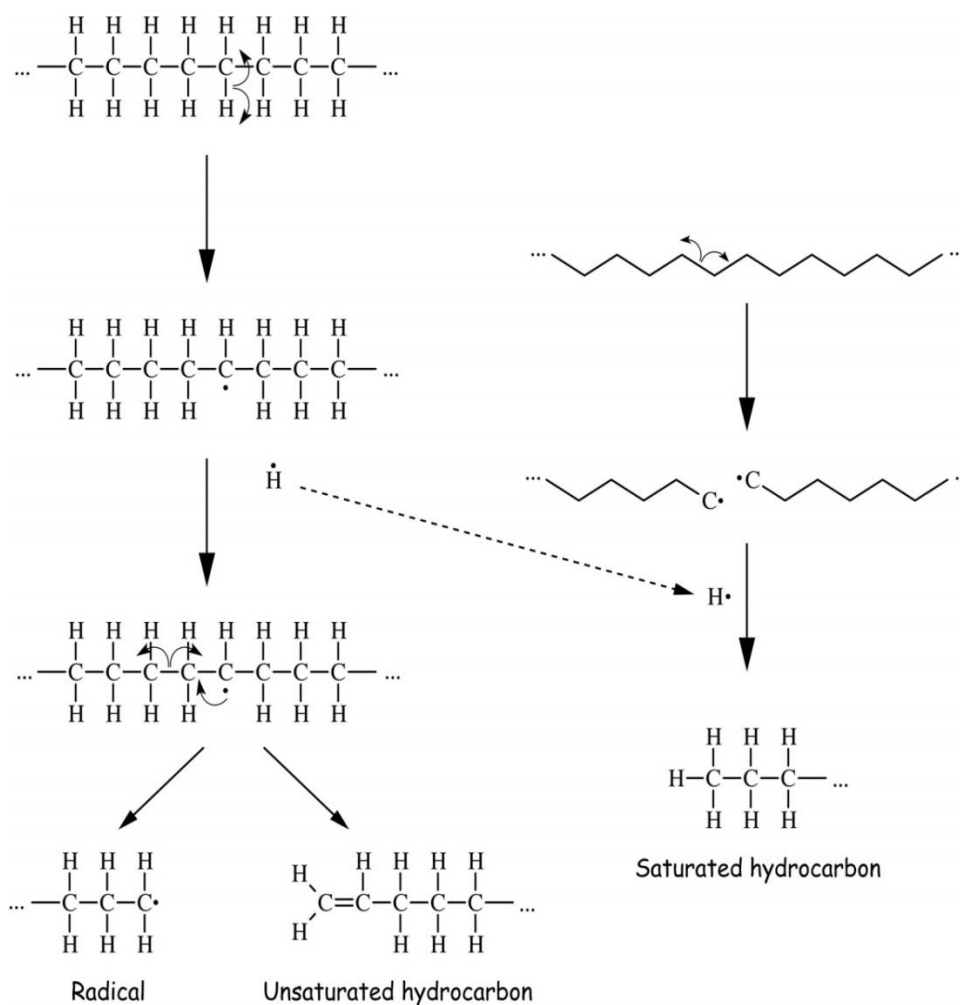


Figure 1.3: Polyethylene random scission mechanism [61, 68]

1.4.1.2 Side Group Scission / Side Group Elimination / Chain Stripping

The side group scission mechanism refers to when scission occurs to groups attached to the side of the backbone (carbon-to-side) rather than the backbone itself (carbon-to-carbon), causing the backbone to become polyunsaturated with double bonds [54]. Figure 1.4 illustrates the side group scission of polyvinylchloride where the lower energy carbon-to-chlorine bond is broken first to generate a chlorine radical, followed by the carbon-to-hydrogen bond that generates a hydrogen free radical. Both these by-products combine to form hydrogen chloride while the polyunsaturated backbone reforms itself to yield aromatic compounds such as benzene, toluene, ethylbenzene, styrene, naphthalene and other polycyclic aromatic hydrocarbons (PAHs) [50, 61].

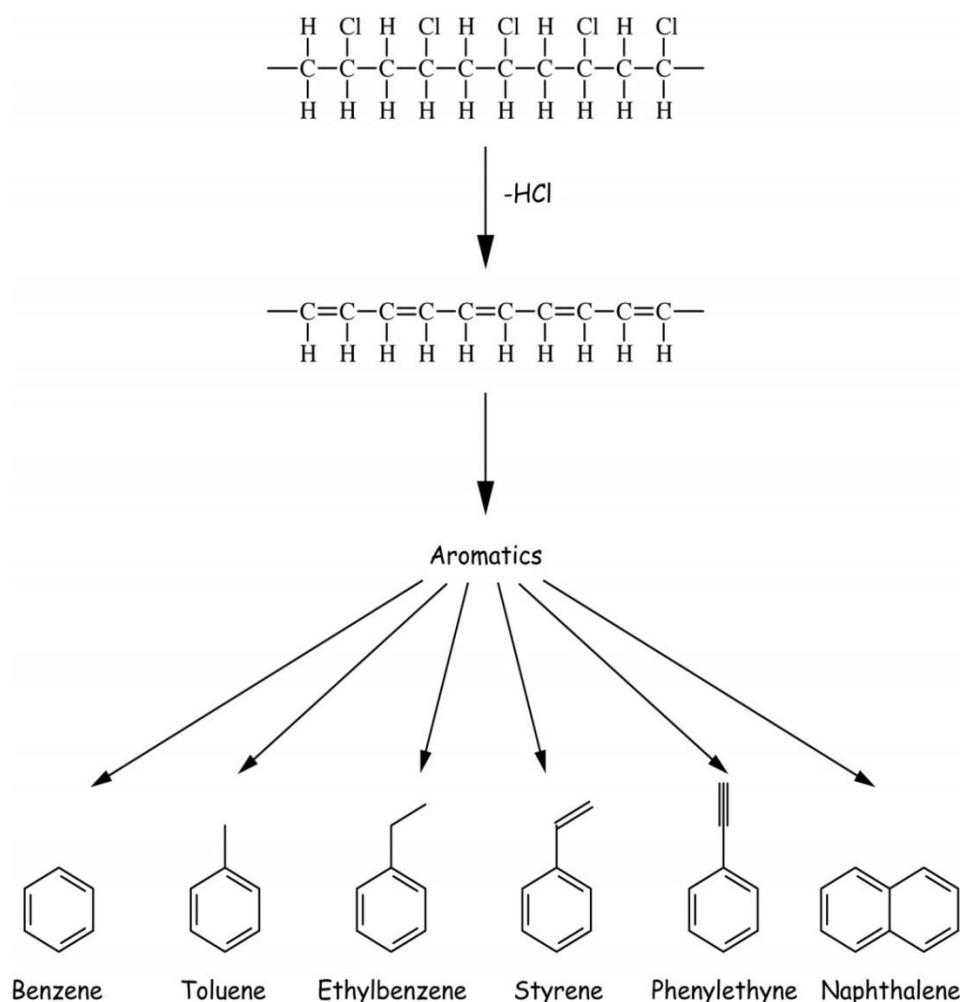


Figure 1.4: Polyvinylchloride side group scission mechanism [54, 68]

1.4.1.3 Monomer Reversion / Depolymerisation / Unzipping

Monomer reversion involves the depolymerisation (reversing the polymerisation process) and breaking of chains to return the polymer to its monomer form [50, 61]. Using polymethylmethacrylate (PMMA) as an example for monomer reversion (Figure 1.5), beta scission (thermal cracking of a hydrocarbon at the C-C bond to generate radicals) occurs at every other carbon-to-carbon bond to generate its monomer, methylmethacrylate [61]. This mechanism does not always occur independently in a typical fire scene as it is only capable of generating a singular end product, a highly unlikely event in a complex fire. Usually, monomer reversion occurs simultaneously with a number of other pyrolysis mechanisms [54].

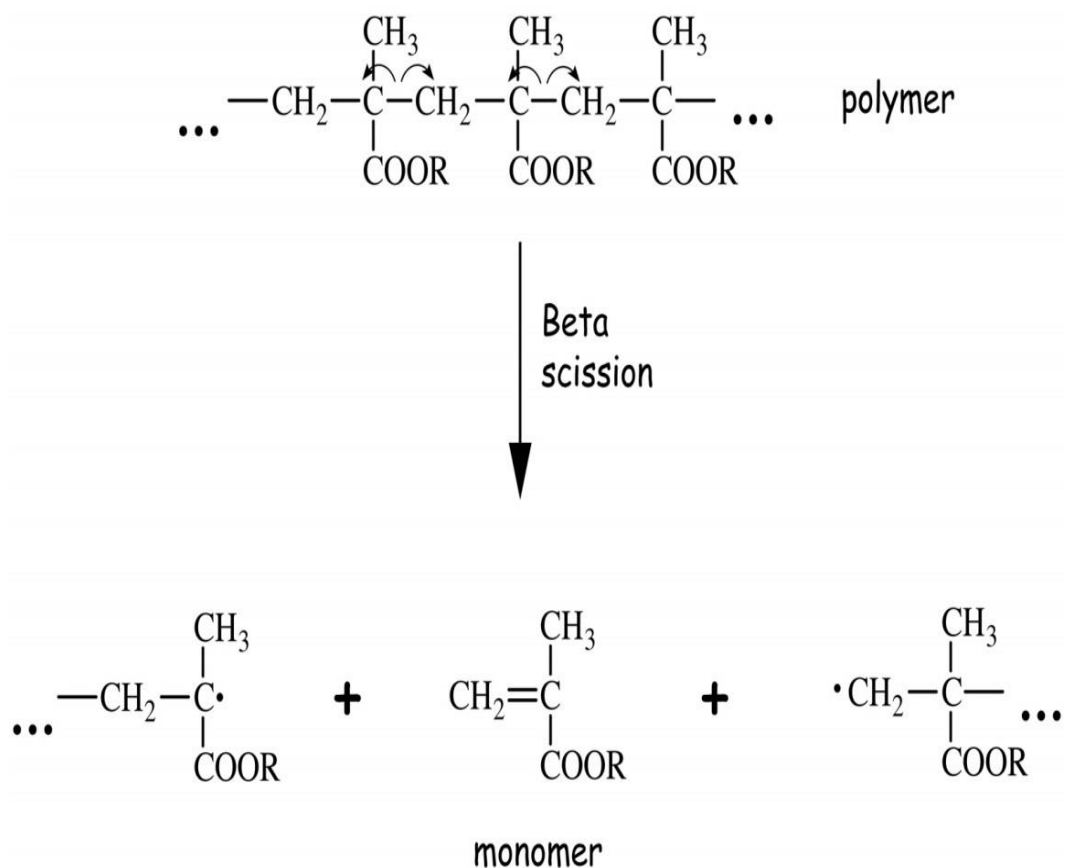


Figure 1.5: Polymethylmethacrylate monomer reversion mechanism [68]

1.4.2 Pyrolysis and Combustion of Polymers

Cellulose is one of the most common natural polymers encountered in fire scenes, as it is the building block for materials such as wood, carpets, upholstery and textiles.

Made up of repetitive glucose units, cellulose undergoes both physical and chemical changes through combustion and pyrolysis [69]. During combustion, heat is applied to the cellulose molecule that causes molecular decomposition into smaller compounds and, at the same time, producing enough heat to generate volatile products through pyrolysis [69, 70]. These volatile products include aldehydes, ketones, furans, levoglucosan, acid, acid esters and aromatics [69, 71, 72].

The pyrolysis of cellulose occurs by two different pathways (experiencing three different stages: initial, main and char decomposition), depending on the temperature applied to the material during the heating process [69]. At the initial stage, (temperatures below 300 °C but above 80 °C), marked physical changes are noticeable with damage occurring predominantly in the amorphous region of the material. Cellulose undergoes cross-linking and dehydration, generating H₂O and CO₂, and leaving behind a carbon backbone commonly known as char [73]; at temperatures above 300 °C where main pyrolysis occurs, pyrolysis and char decomposition are apparent at the crystalline region of the molecule.

The majority of the pyrolysis products are generated within the range of 300 °C to 380 °C, where the dehydrated chain undergoes random scission of the C-O bond, unzipping the chain to form levoglucosan and L-glucose, that will in turn generate volatiles, oxygenates and flammable gases that fuel combustion [46, 70, 73, 74]. At temperatures above 380 °C to 450 °C, char decomposition occurs, whereby the remaining char releases more H₂O and CO₂ and becomes even more dehydrated, releasing carboxyl and carbonyl products in the process [69, 75]. Figure 1.6 provides a schematic illustration of cellulose pyrolysis and the type of products generated across the temperatures.

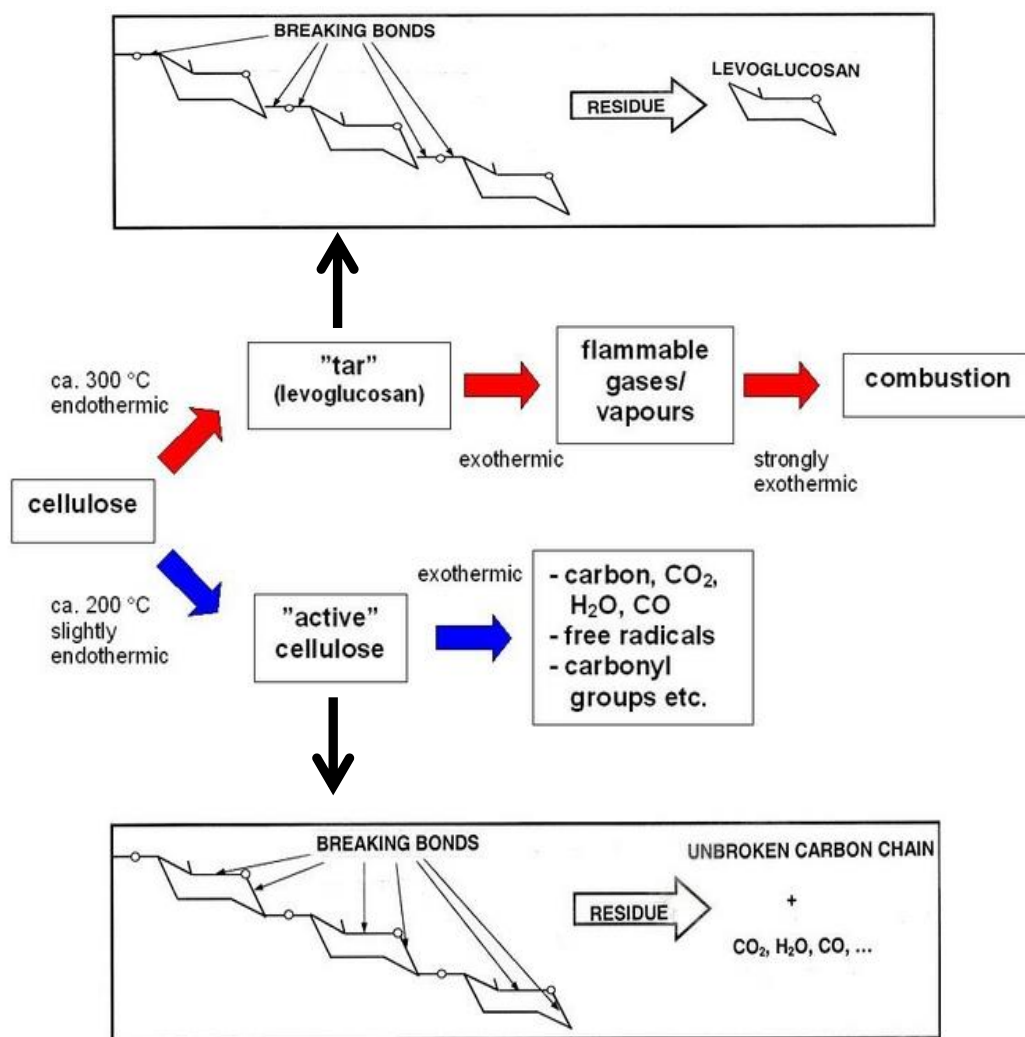


Figure 1.6: Pyrolysis pathways for cellulose [76]

Besides natural polymers like cellulose, other major synthetic polymers such as polyolefins, styrene, vinyl and acrylate are also commonly encountered in fire scenes [77]. According to Waste Watch 2003 [78], the building and construction sector in the UK utilised a staggering 800,000 tonnes of plastic in their industry, out of which 480,000 tonnes were of polyvinylchloride (PVC), a type of vinyl polymer. Other common polymers used included polyurethane, polystyrene, polyesters, polyethylene, polyamide, rubber, polycarbonates and polyacrylonitrile [77-79]. These synthetic polymers can be classified into three groups; thermoplastic (polyester, acrylic, nylon), thermosets (epoxy, vinyl ester, phenolic resin) and elastomers (isoprene) [55, 79]. Thermoplastics are a group of polymers that soften and melt when heated whereas thermosets do not melt, instead they release volatiles

and forms infusible and insoluble char as their end product while elastomers refer to a group of rubber-like polymers.

When heated, each of these polymers undergo various pyrolysis mechanisms depending on which group of polymers they belong to [55], generating a variety of pyrolysis products as explained in Table 1.1. Knowledge of the types of pyrolysis products generated from these commonly encountered materials is essential for the forensic scientist to prevent a false positive or false negative conclusion in a fire investigation, as these products can act as interfering products in the identification of ignitable liquid residues (ILR) and potentially human or animal remains.

Table 1.1: Common polymers encountered in fire scenes, including their decomposition mechanisms and pyrolysis products generated. Adapted from [77].

Polymers	Decomposition Mechanisms	Pyrolysis Products
Polyolefins		
Polyethylene	random scission	<i>n</i> -alkanes, <i>n</i> -alkenes, <i>n</i> -alkadienes
Polypropylene	random scission	branched alkanes, branched alkenes, branched alkadienes
Polyisobutylene	random scission monomer reversion	branched alkanes, branched alkenes, branched alkadienes
Syrene		
Polystyrene	monomer reversion side-group scission	styrene, aromatics
Poly(α -methylstyrene)	monomer reversion	α -methyl-styrene
Vinyl		
Polyvinylchloride	side-group scission	aromatics, chlorinated compounds
Polyvinylidenechloride	side-group scission	aromatics, chlorinated compounds
Polytetrafluoroethylene	monomer reversion	tetrafluoroethylene
Polyvinylacetate	side-group scission	aromatics, acetic acid
Polyvinylalcohol	side-group scission	aromatics
Acrylate		
Polymethylacrylate	random scission	methanol, oxygenated compounds
Polymethylmethacrylate	monomer reversion	methylmethacrylate
Polyamide		
Nylon 6	random scission cross-linking	oxygenated compounds
Nylon 6-6	random scission cross-linking	oxygenated compounds
Polyesters		
Polyethyleneterephthalate	random scission (CO bonds)	oxygenated compounds
Polyethylenaphthalate	random scission (CO bonds)	oxygenated compounds

Table 1.1 continued

Rubber		
Polybutadiene	monomer reversion (followed by dimerisation)	butadiene, alkene
Polyisoprene	monomer reversion (followed by dimerisation)	dipentene, alkene
Polyacrylonitrile and Copolymers		
Polyacrylonitrile	side-group scission	aromatics
Styrene-acrylonitrile (SAN)	side-group scission	aromatics

1.4.3 Pyrolysis and Combustion of Hydrocarbons

Hydrocarbon materials, the resultant products from the combination of hydrogen and carbon, make up most of the important fuel packages encountered in fires. The basic form of this is methane, CH₄, the key component in natural gas. Upon oxidation, methane undergoes over 100 intermediate reactions before producing carbon dioxide and water [9, 42].

The first step involves the loss of hydrogen atoms, generating ethane and acetylene together with free radicals (unstable molecular species) such as –OH, –CH₂O and –CHO. However, these free radicals require high temperatures to exist; thus, upon the expiration of fire they condensate to form pyrolysis products, noticeable on surfaces after the fire has been extinguished [8]. It is important to note that, when dealing with more complex hydrocarbons, a whole range of free radicals can be generated, proportional to the increase in intermediate reactions [8].

Hydrocarbons can be classified into a number of groups [8], namely:

- straight chain / normal / *n*-alkanes
- branched / iso / aliphatic/ paraffinic alkanes
- aromatics
- cycloparaffins

The final class of hydrocarbons that are frequently encountered are the cycloparaffins. They are made up of rings consisting of five, six or seven carbons but without the double bonds that characterise aromatics; cyclohexane, C₆H₁₂ (Figure 1.11), is an example.

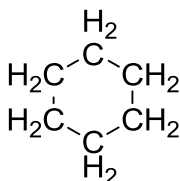


Figure 1.11: Molecular structure of cyclohexane

1.4.4 Pyrolysis and Combustion of Carbohydrates and Fats

In most countries, extensive use is made of wood, especially in building structures [80], making them one of the most common fuels encountered in structural fires. The main constituent of wood is cellulose, a carbohydrate. The monomer of any carbohydrate is glucose, with a molecular formula of C₆H₁₂O₆. Cellulose (C₆H₁₀O₅) is basically a network of glucose units which, when subjected to heat, exhibits the same burning profile of glucose, as illustrated below [8]:



The molecules in carbohydrates are large and complex, and they contain high levels of oxygen, indicating that they are partially oxidised to begin with [8]. Like other fuels, not all of the carbon undergoes complete oxidation to form carbon dioxide as oxygen is not always readily available in a typical fire scenario [9]. The residual carbon undergoes incomplete combustion and releases a variety of volatile products instead.

Besides cellulose, vegetable and animal fats also play a significant role in fuelling fires. Fats are basically composed of glycerol and fatty acids; a fatty acid is a long hydrocarbon chain with a terminal carboxyl group [8, 9]. Their monomers are known as triglycerides, a molecule composed of three fatty acids adhered to a glycerol molecule as illustrated in Figure 1.12.

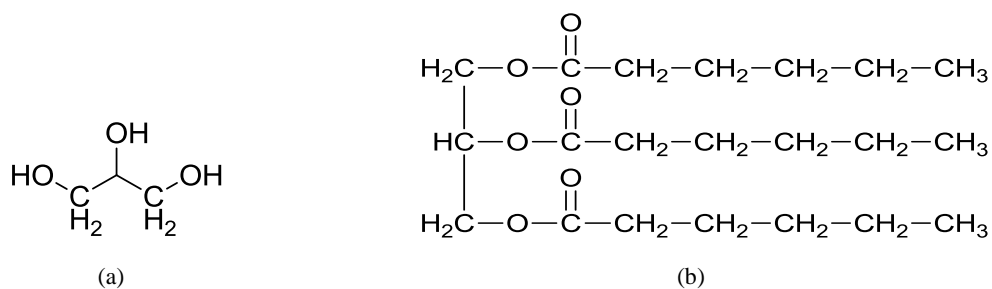


Figure 1.12: Chemical structure of (a) glycerol and (b) triglyceride

When fat is burnt, it melts at relatively low temperatures [81] and the vapours have been documented to ignite at temperatures around 250 °C [82]. The auto-ignition temperature (AIT) of fat has been documented to be within the range of 350 °C to 355 °C [17, 66]. When fat is heated at low temperatures for extended durations, charcoal is formed, and, when subjected to higher temperatures under moderate heating durations (300 °C to 500 °C for more than 30 minutes), a range of hydrocarbons, acids, aromatics, oxygenates and alkenes have been detected [83, 84]. However, when pyrolysed at high temperatures of 400 °C to 1000 °C for short durations (10 seconds), fats have been documented to decompose to generate *n*-aldehydes and a number of straight and branched hydrocarbons [83, 85].

Previous experiments have shown that animal fat (pig fat) and, by extension, human body fat have similar burning profiles and are impossible to tell apart; thus, pig fat is a good model for human fat [81, 86]. The National Fire Protection Association Handbook cited that animal fat outputs a high heat of combustion of 39.8 kJ/g [87]. In order for fats to actively contribute in a fire, the dermis layer of the body has to undergo splitting upon contact with an external flame to facilitate the rendering of the subcutaneous fat layer [88]. Once fat ignites, it will readily burn, generating flames of 700 °C to 800 °C [88], given that there is a steady supply of melted fat and significant amounts of heat are generated from the initial flames. The availability of a porous and carbonaceous wick (clothing, carpets, drapes, bedding) for the rendered fat to be absorbed onto, will facilitate the continuous combustion of fats once the initial heat source / flames is removed, failing which the flames will not self-sustain [81, 88]. According to Stryer [89], an average 70 kg male stores energy reserves of

100,000 kcal in tryglycerols (fats), 25,000 kcal in protein and only 640 kcal in carbohydrate. A case study conducted by DeHaan [88] and DeHaan *et al.* [86] also corroborated this as they found the best fuel in the human body to be subcutaneous fat, generating heat of 120-130 kW from 26 kg of fat. From this, it is evident that fats will play the leading role in the combustion of a human body and, for certain cases, contribute actively in a fire [90].

1.5 Thermal Alterations to Bone

Once heat penetrates soft tissues in the body and reaches the bones, it will substantially alter the bones' chemical and structural integrity. Bone starts to lose its collagen cross-link stability together with the minerals that hold its structure together [20]. Crystallisation of bone minerals [91], consumption of organic matrix and loss of water will all cause bones to calcinate, dehydrate, fracture and shrink [8, 9, 92].

1.5.1 Stages of Heat-Induced Modification in Bone

One of the first few researchers that identified the stages of heating to bone, in terms of the changes to its microscopic morphology was Shepard in the 1950s [93]. He classified six progressive stages of heating damage, further refined by Shipman *et al.* [94] into five stages and by Mayne Correia [95]. A holistic and robust approach to the categorisation of heat-induced modification to bone was proposed by Thompson [96], having adopted and modified the main work of Mayne Correia. He suggested that all heat-induced changes to bone fall into one of four main categories, based on the temperature exposure (Figure 1.13), and in a sequence following dehydration, decomposition, inversion and fusion (Table 1.2) [97].

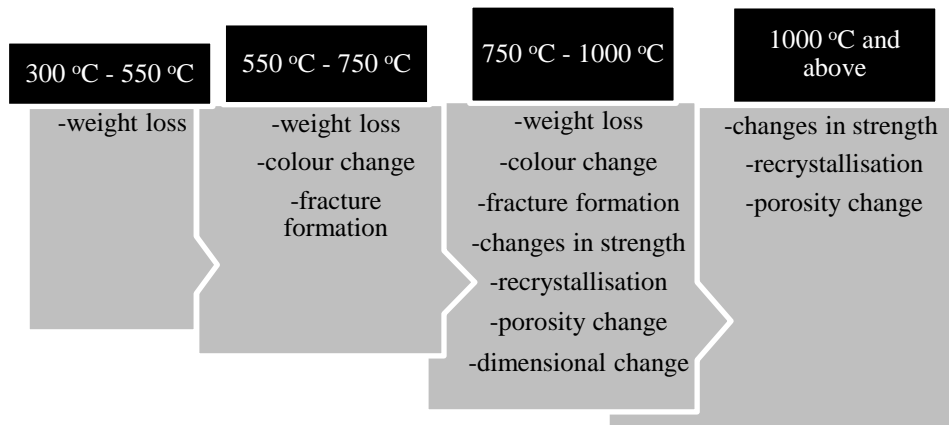


Figure 1.13: Relationship between temperature and heat-induced changes to bone. Adapted from Thompson [97].

Table 1.2: The four stages of heat-induced modification to bone. Adapted from [97].

Temperature Range (°C)	Stage of Transformation	Observation
100 - 600	Dehydration	Fracture patterns Weight loss
300 - 800	Decomposition	Colour change Weight loss Reduction in mechanical strength Changes in porosity
500 - 1000	Inversion	Increase in crystal size
Above 700	Fusion	Reduction in dimension Increase in crystal size Increase in mechanical strength Changes in porosity

Dehydration is the first thermal decomposition stage that bone undergoes, caused by the loss of physisorbed (adsorbed) or chemisorbed (bonded) water [95, 98], and also from the breakage of hydroxyl bonds in the apatite crystals [94]. Loss of water occurs as water molecules adhered to the crystal's surface and organic material disperses, causing widespread of cracks and warping of the bone [94, 99].

Upon dehydration, and with increasing temperatures typically between 350 °C to 525 °C, bone undergoes significant thermal decomposition, where the organic components of bone are pyrolysed and burned off, decreasing the organic content in bone that lead to the loss of mass [94, 95, 99].

Inversion is attained when changes in the crystal size occur as hydroxyapatite crystals begin to convert to β -tricalcium phosphate $\text{Ca}_3(\text{PO}_4)_2$ with the elimination of carbonates [96] to form carbon dioxide and calcium oxide [95]. Although the conversion process results in the formation of smaller crystals, recrystallisation also occurs concurrently, fusing the smaller crystals to form larger crystals, resulting in a range of crystal morphology [91, 94, 100].

At temperatures above 700 °C [94], the apatite crystals will begin to melt and cohere in the crystal matrix to fill up spaces left by the diminished water and organic compounds [7]. This is when bone enters the fusion phase. As a result, there is significant shrinkage and reduction in bone size. Although shrinkage occurs at all four stages, it is most evident and substantial at the fusion stage [96].

1.6 Interfering Pyrolysis Products and Their Implication in Forensic Fire Analysis

As discussed previously, a fire scene can be presented with a variety of fuels, natural or synthetic, which, when pyrolysed, generate volatiles and products that can cause interference in fire debris analysis [54]. More often than not, when fire investigators suspect that a fire scene is of a malicious nature, fire debris will be collected and submitted for analysis to the laboratory in an attempt to identify which, if any, contains ILR. The extraction process that follows is very simple, utilising readily available and established standard protocols as per ASTM [101-104]. However, it is the interpretation of these chromatographic results that poses a challenge to the forensic scientist and requires extensive skill, knowledge and experience. To complicate matters, the presence of these interfering and contaminating pyrolysis products renders this task even more complex as it then requires effective isolation of the target compounds from background interferences [105-109].

When a fire scene involves human remains, potential key indicators of human remains could also be masked by these interfering products, especially if the key indicators of human remains share similar chromatographic profiles with other

materials and are present in low concentrations. These key indicators of human remains have been reported to be a homologous series of *n*-aldehydes, documented to be present in pyrolysis products generated from both porcine and human samples [66, 110]. Other compounds such as *n*-alkanes, *n*-alkenes, aromatics, cycloalkanes, cycloalkenes, nitriles and light oxygenates have also been documented to have generated from cadaveric remains, but these compounds are also generated from household items and ILR, so they can be classified as interfering pyrolysis products.

Interfering products are defined as a ‘set of products found in a sample that interfere with the proper identification of target compounds’, typically ILR [68]. Pyrolysis products interfere with the analysis by generating volatiles that are either similar in range or emulate the mass-to-charge ratio (m/z) or chromatographic peaks of the target molecules [54, 111, 112]. In terms of ILR analysis, usually, the remaining ignitable liquid that is left behind after a fire has occurred will be low in abundance, as it will have been consumed massively in the fire. Thus, it is difficult to distinguish and separate ILR signals from other pyrolytic signals that are present in the background with similar low concentrations [108, 109]. This can, in turn, lead to a false positive conclusion of the presence of ignitable liquid in a fire scene and, at worst, a wrong conviction. From another perspective, a false negative can also be attained when one assumes that these peaks are only generated from interfering pyrolysis products and not from ILR. This can happen when there is a lack of knowledge about the type of volatiles that are generated from various fuels, including those from human remains [54].

Contaminating products can come from various sources [113] but are mainly classified into three groups, namely: substrate background products / actual petroleum products that are present in the substrate material; pyrolysis products released from the combustion of the substrate; and combustion products (Figure 1.14) [43, 77, 108, 109, 113-115]. Stauffer proposed a comprehensive chart to illustrate the breakdown of these sources according to phases, as exemplified in Figure 1.15; pre-fire, ignition, extended fire, extinguishment, and sampling.

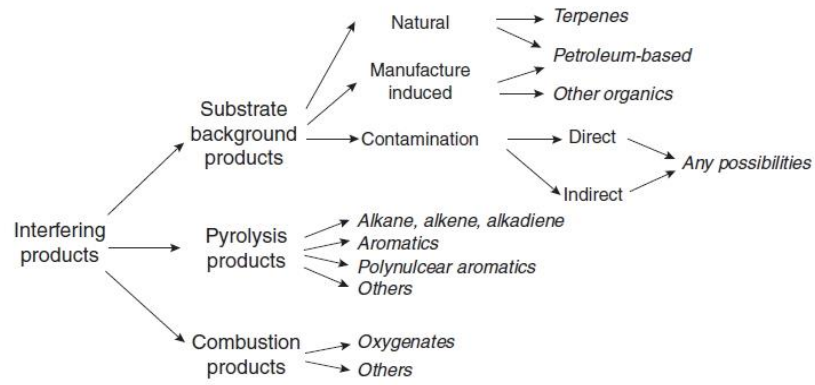


Figure 1.14: Breakdown of interfering products according to three main sources [77]

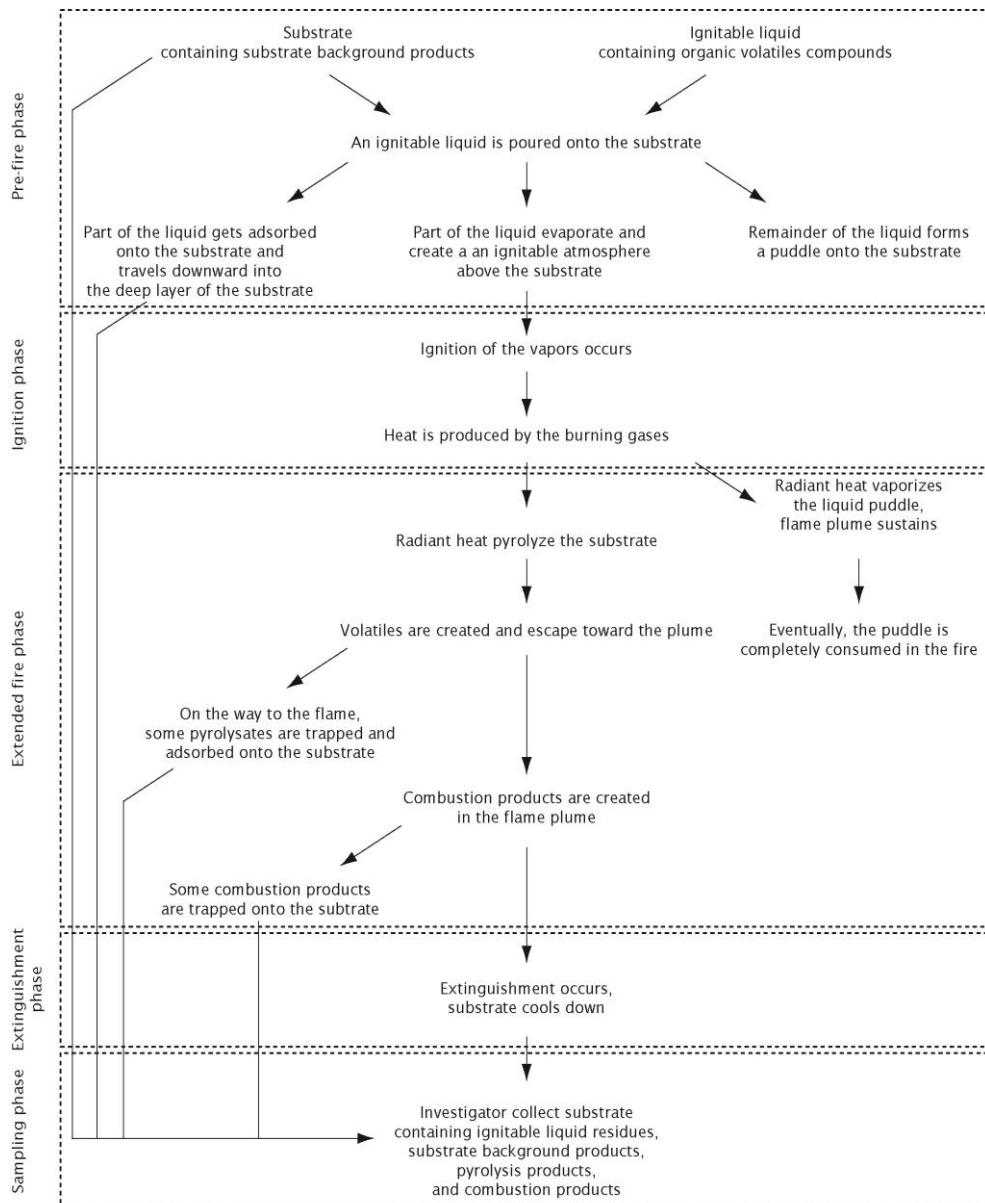


Figure 1.15: Formation of interfering products in a typical fire scene [68]

Although these interfering compounds can result from the pyrolysis of other compounds, they are almost always seen coming from natural or synthetic polymeric organic materials such as carpet, wood, padding and floor tiles [106, 108, 109, 116-119] – materials used ubiquitously in homes and buildings. Over the years, numerous researchers have conducted studies to demonstrate the generation of these interfering pyrolysis products over a wide range of materials. To name a few, Keto [109] discussed in detail the similarities between the pyrolysis products of polyethylene and heavy petroleum residues. Comparable results were also noted with the chromatographic similarities between asphalt pyrolates and heavy petroleum distillates [120]. Howard and McKague [118] recorded that the burning of carpet generated similar target compounds, namely toluene, xylenes and styrene – aromatics that are usually an indicator for the identification of gasoline. Bertsch [107] also documented similar results in which the presence of styrene, methyl-styrene, small amounts of aromatics and high levels of naphthalene and methyl-naphthalene were present naturally from burnt carpet and carpet padding. Lentini *et al.* [111] identified petroleum-based products naturally occurring in a variety of samples prior to burning.

In a case of false positive, Stone and Lomonte [117] looked into an arson case in which the suspect was wrongly convicted because turpentine was identified and led to the conclusion of ILR, but in fact it was actually a component normally occurring in wood padding [117]. If control samples were taken and information and knowledge on the pyrolytic profile of wood padding was readily available and known to the investigator, this situation could have been avoided. Similarly, in terms of the pyrolysis profile of cadaveric remains, very little research looking into the pyrolysis products generated from human or animal remains [66] have been conducted, and this should be examined further in order to prevent any future misinterpretation and misidentification in fire scene investigation. Proper analytical technique(s) and suitable diagnostic analysis also have to be undertaken to effectively isolate and identify these interfering background products from the target compounds.

1.7 Extraction of Pyrolysis Products from Fire Debris Samples

Once the fire debris evidence has been packed and sent to the laboratory, it is the job of the forensic scientist to examine the evidence thoroughly, to conduct proper extraction and to apply suitable analytical techniques, and finally to interpret the results of the analysis. A schematic representation of the process is depicted in Figure 1.16.

Extraction is conducted to separate the target components from a sample, to remove impurities and pre-concentrating them on an extracting material. It is performed to prevent sample loss and take full advantage of high detection limits [121]. Various extraction techniques exist to recover pyrolysis products from fire debris [122]. The headspace adsorption extraction technique combined with chromatographic separation of the target compounds is the most commonly used method recommended by the American Society for Testing and Materials (ASTM) E1412-00 [122, 123].

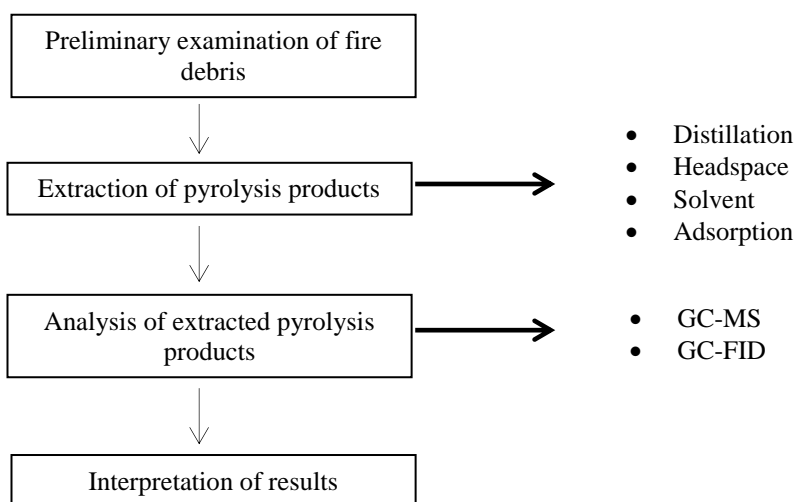


Figure 1.16: Laboratory analysis of fire debris. Adapted from [61].

1.7.1 Passive Headspace Diffusion using Activated Carbon Strip (ACS)

Passive or static headspace diffusion is one of the most common extraction methods used in forensic laboratories [61, 124].

Passive headspace diffusion is a process that involves the migration of volatile target compounds onto an adsorbent material (porous polymer or carbon) by diffusion, at ambient or heated temperatures at specific time intervals. The adsorbent material will then be desorbed by solvent extraction or thermal desorption for further analytical procedures [17, 125-127]. The entire process is relatively quick (minimal sample preparation), non-tedious (minimal or no monitoring), inexpensive, simple, relatively sensitive and, most importantly, non-destructive [121, 124, 125, 128]. Its non-destructive nature allows for sample archiving, as it does not cause the total depletion of the sample, contrary to active headspace sampling [129]. This is verified by Waters and colleagues [125] as they reported no substantial depletion in volatile concentration over multiple passive headspace sampling of the same sample across one, three and six months.

Passive headspace sampling of volatiles is commonly coupled with an adsorbent known as activated carbon [103, 124]. This adsorbent was initially introduced by Twibell and Holm [130] in the form of charcoal-coated ferromagnetic wires, whereby a thin layer of highly activated charcoal was used to coat the wires which were left in the headspace for one to two hours to undergo passive adsorption before being subjected to heat (thermal desorption) via the Curie point pyrolysis system to facilitate desorption [131]. In 1982, Juhala [132] modified this method with the introduction of Plexiglass beads and charcoal-coated copper wires that facilitated direct introduction into the sample headspace, and desorption was done using a solvent elution technique (with carbon disulfide) instead of thermal desorption. The use of this carbon wire adsorption / solvent extraction (CWSE) [121] technique facilitated headspace exposure and accommodated solvent extraction. However, since the coated wires and beads were fragile in nature, more often than not, the detachment of charcoal was observed [128]. Tranthim-Fryer [121] addressed this issue by utilising strips of aluminium or copper to provide support for the activated

charcoal and recommended the use of *n*-pentane as a solvent of choice to counter the damaging effects of carbon disulfide.

In recent years, the use of C-bags and diffuse flammable liquid extraction (DFLEX[®]) devices, commonly known as activated carbon strip (ACS) has gained popularity due to their *in situ* trapping that aids in preventing contamination and the loss of residual accelerants from the sample [128, 133-135]. They are also portable to crime scenes and can be used with ease, either with or without heating, and require very minimal monitoring. Both are usually suspended within the headspace of the sample with a magnet / string (Figure 1.17) and adsorption continues to take place until equilibrium between the headspace, the adsorbent and the sample is attained [61]. C-bags are basically made up of granular activated charcoal enclosed within a wrapping of porous paper, whereas ACS are adsorbent carbon impregnated on a polymer membrane [128, 136], originally taken from organic vapour detection badges and adapted for laboratory use by removing the plastic coverings [128]. The adsorbents are then desorbed using solvents or thermal desorption [127, 137].

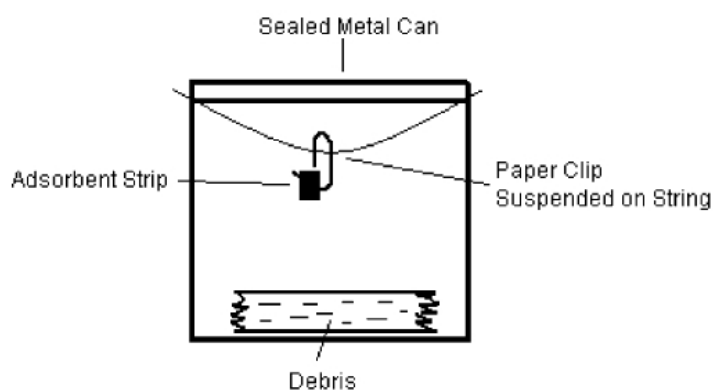


Figure 1.17: Experimental setup for ACS for passive headspace sampling [129]

ACSs are a highly porous material with a random structural arrangement of graphite; they are usually derived from cotton, coal and wood, compounds known to have high carbon contents, and also from some synthetic polymers [138]. Due to their highly porous structure and large surface areas, ACSs are deemed sensitive and can be applied to a wide range of ignitable liquids and hydrocarbons extraction, from

boiling points of 0 °C to 250 °C [139]. They are also able to retain as low as 0.2 µL of standard accelerant material (SAM) [128].

The use of ACS minimises sample preparation time significantly and eliminates any source of contamination; they are also inexpensive and very easy to work with [129]. In addition to this, they do not react with nitrogen or oxygen (do not undergo oxidation) [140] and do not suffer any interference in the presence of water as they are hydrophobic in nature [121, 128]. This makes them particularly useful in fire cases as most samples are often collected after fire extinguishment via water. Also, since they do not require monitoring, they significantly reduce analyst work time, especially because they can be sampled at ambient temperatures or left to be heated for hours at elevated temperatures [128]. This also offers flexibility to the analysis as samples that are not suitable for heating can be placed at ambient temperatures and *vice versa* [128]. In addition, ACS allows episodic sampling as more than one strip can be placed in a sample container per time. If the other is not needed for immediate analysis, archiving is made possible with no hassle [136].

1.8 Instrumental Analysis

1.8.1 Chromatography and Gas Chromatography (GC)

According to McNair and Miller [141], the term ‘chromatography’ initially came into use in the early nineteenth century when Tswett scientifically described it in one of his publications. Fifty years later, Martin and James [142] adopted the basis of this technique and brought forth gas chromatography (GC), a separation technique that utilises gas as the mobile phase, and it was then made commercially available in 1953 [143]. Its ability to separate a variety of volatile components in a fast, simple and accurate way has made it one of the most used universal separation technique in analytical laboratories [141, 144]. The use of GC was pioneered in the field of forensic science when Lucas [145] utilised this instrument in 1960 to separate and identify petroleum-based ignitable liquids in suspected arson cases. Since then, it has undergone modification and evolution of various kinds to create an automated, user-friendly, online, integrated system that is seen in laboratories nowadays. Its use has been an international phenomenon in various fields of forensic science, including fire

debris analysis [121, 125, 146-148], toxicology [149-152], biology [153-155], trace evidence [156], drugs [157-159], explosives [160] and environmental studies [130, 161, 162].

According to the International Union of Pure and Applied Chemistry (IUPAC), chromatography is defined as ‘a physical method of separation in which the components to be separated are distributed between two phases, one of which is stationary (stationary phase) while the other (the mobile phase) moves in a definite direction’ [163]. Principally, chromatography involves the relative separation and interaction of analytes in a two-phased partitioning system based on their affinity and equilibrium with the mobile and stationary phases [164]. The mobile phase (gas, liquid, supercritical liquid) serves as a transporter in which the analytes can be either be distributed on or dissolved within, prior to being carried through the stationary phase [141, 143]. The stationary phase is typically a solid or liquid bonded on a solid (bonded phase) or immobilised onto it (immobilised phase) with a large surface area that can be either packed in a tube (column) or on thin layers coated onto an inert support such as glass, plastic or aluminium [48, 163, 164].

Upon introduction into the analytical instrument, the vaporised analytes are carried by the mobile phase and partition from one another based on their differing affinities for the stationary and mobile phases. The relationship is inversely proportional, whereby when a target analyte distributes itself more strongly in the stationary phase, it moves slower through the system; whereas analytes that have high affinities for the mobile phase elute faster. Hence, the migration rate is mainly controlled by the distribution and equilibrium of the components between these two phases. Equilibrium between these two phases is attained according to the equilibrium constant (partition constant), K_C [141, 165], or distribution coefficient, K_D [143, 166], as represented in Equations 1.1 and 1.2, respectively.

$$K_C = \frac{[A_s]}{[A_m]} \quad \text{Equation 1.1}$$

where,

$[A]_s$ is the equilibrium concentration of analyte A in the stationary phase, and

$[A]_m$ is the equilibrium concentration of analyte A in the mobile phase

$$K_D = \frac{\text{Concentration of component in the stationary phase}}{\text{Concentration of component in the mobile phase}} \quad \text{Equation 1.2}$$

The components' affinities for either of the phases is governed by various factors, including the differences in molecular charge, vapour pressure, size or mass, polarity, redox potential, ionisation constant and structure [141, 165].

1.8.2 Instrumentation of Gas Chromatography

Typically, a gas chromatography instrument is made up of a combination of six main components, each playing a significant role in making the instrument effective and reliable. Every part has to function optimally on its own and, at the same time, interacting with one another, failing which the separation process would be hampered. Figure 1.18 presents a general gas chromatography system that comprises an injection port, gas supply and flow controllers, oven, analytical column, detector and recorder / data acquisition system [141, 143, 164].

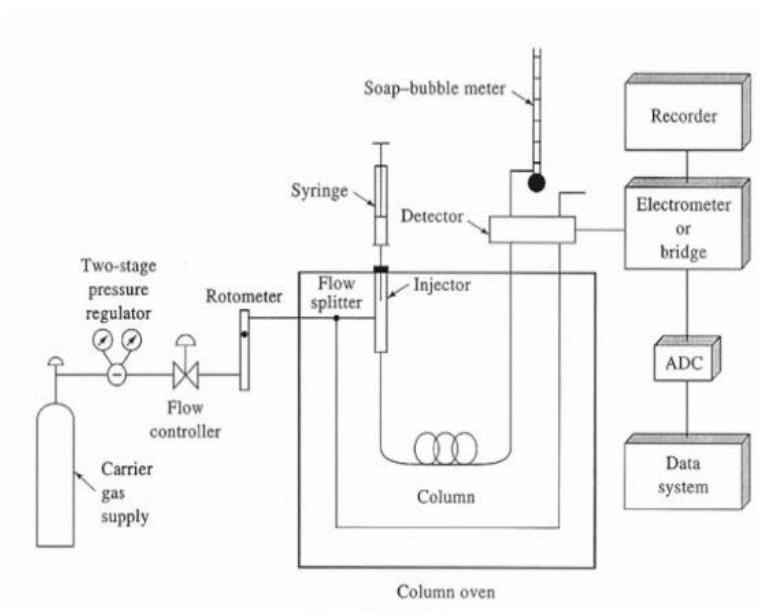


Figure 1.18: Instrumentation and set up of a typical gas chromatography [167]

1.8.2.1 GC Injection Port / Inlet

The injection port is the start off point of any analytical analysis in a GC instrument. Sealed with an inlet septum, this heated chamber serves to introduce samples into the column upon vaporisation. Samples are usually introduced into the injection port with a glass-coated stainless steel micro-syringe, typically 10 μL , which is sharp enough to penetrate the barricading septum. The injection port is usually made of a metal cylinder with a hollow space to accommodate a glass liner that is usually packed with variable amounts of glass wool. The purpose of the glass wool is to further clean up any impurities in the sample to safeguard the column from any impurities. As one end of the liner accepts the introduced sample, the other end is connected to the initial part of the column with a narrowed insert that serves to minimise band-broadening by controlling the amount of sample being transited into the column. The temperature of the injection port has to be high enough to ensure rapid vaporisation of the sample and, at the same, to be low enough to ensure thermal decomposition of the sample does not occur. It is typically kept between 100 °C and 300 °C for normal experimental conditions. Two modes of injection are normally observed, namely split and split-less injections. In the split mode, only small portions of the sample being injected are allowed into the column and the rest is purged out to prevent column overloading. Split-less mode allows the entire sample to enter into the column and is a mode that is usually applied when dealing with very trace amounts of samples. Once the sample has been converted into a gaseous state, it is then mixed with the carrier gas and migrated into the analytical column [141, 143, 164].

1.8.2.2 Gas Supply and Flow Controllers

The mobile phase of a GC is gaseous in nature and functions to transfer gaseous samples through the column, as well as to provide a conducive environment in which the detector has optimum sensitivity [141]. Among the common gases used are nitrogen (N_2), hydrogen (H_2) and helium (He), and the gas used is determined based on the type of detector employed [168]. When a mass spectrometer (MS) is used as the detector, helium is usually the preferable carrier gas as it does not interfere with the mass spectral patterns of the compounds [164, 169]. Hydrogen is also commonly

used, but because of its reactive nature, it is prone to fires and explosions and has to be handled with extreme caution. Nitrogen is usually used when the GC is coupled with a flame ionisation detector (FID), which is known for its high sensitivity but tends to extend the analysis time. An FID can also be used with helium as the carrier gas.

A carrier gas has to be inert to ensure no chemical interaction with the sample [167]. It also has to be up to 99.999% pure as the presence of any form of impurity, be it water or oxygen, can damage the analytical column as well as inducing high detector background and ghost peaks [141, 168]. The mobile phase is controlled by standard pressure regulators; a stainless steel diaphragm connected with a safety valve and an inlet filter. Besides preventing particulate matter (e.g. water, hydrocarbon, oxygen) from entering the column, they serve to prevent any air leaks in the system and to maintain a constant flow rate and pressure. Constant flow rate and pressure are essential to preserve column efficiency and the accuracy of quantitative analysis [141, 143]; the flow rate is usually within the range of 1 to 2 mL/min [167]. Once the mobile phase has engaged with the gaseous sample in the injection port, it moves through the length of the column and exit through the detector [141, 164, 167].

1.8.2.3 Analytical Column and Oven

The column, contained within an oven and connected to the injection port at one end and to the detector at the other end, is deemed to be the core of a GC. Basically, there are two types of columns, packed columns and capillary columns, and both are usually made of temperature-stable materials such as glass, stainless steel or Teflon[®] [141, 167]. Packed columns are stainless steel columns that are packed tightly with a liquid stationary phase coated on an inert solid support with a large surface area. They are less sensitive than capillary columns (open tubular columns) and have been replaced for most laboratory analyses. In contrast to packed columns, capillary columns are made up of a thin film of a liquid phase that coats the interior wall of the fused silica tubing and are not filled with any packing material [141, 143]. The open tubular structure facilitates the production of long lengths of columns that in turn gives them the ability to provide high efficiency of separation for complex matrices

[61, 170]. According to the ASTM E1618-11 for ignitable liquid residue analysis [168], a bonded phase methylsilicone or phenylmethylsilicone column is recommended for laboratory analyses using Gas Chromatography – Mass Spectrometry (GC-MS).

In order to optimise separation and analysis, the column (type, length, internal diameter, thickness) and temperature applied has to be carefully judged. All of these factors will directly affect the retention time and efficiency of the chromatographic process. Oven temperature also has to be monitored closely and, with modern automated temperature programming, gradual ramping of the oven temperature (ambient temperature to 360 °C) at specific intervals is made possible with no hassle, facilitating differing separation rates of molecules at reasonable speed [48, 141]. Temperatures above 360 °C are not recommended as this will not only denature samples but also subject the column to distress and, over time, lead to the degradation of its silica coating. Preferably, column temperatures have to be maintained above the ‘dew point’ but not above the boiling point of the sample [141]. Proper care during column installation, shortening and conditioning, as well as effective sample preparation technique, are also important to lengthen the life span of a column [143]. Once the samples are exposed to the stationary phase, separation of molecules begins based on their different affinities for either of the phases. This will in turn lead to differences in elution and detection time of each component in the sample mixture [17].

1.8.2.4 Detector

Once the component reaches the end of the column, it is lead into the detector by the mobile phase. The detector responds by producing electrical signals based on the physical and chemical properties of the compound [17, 141, 171]. The amplitude of these signals is directly proportional to the amount / concentration of the analyte present in the sample, facilitating quantification. The efficiency of a detector is a function of temperature and, as such, has to be maintained at temperatures that prevent condensation of the separated components. If condensation occurs, peak broadening is indefinite with increasing risk of peak loss. In the case of a thermal

conductivity detector, baseline stability and optimal detector output are preserved by strict regulation of temperature (± 0.1 °C) [141]. On the other hand, ionisation detectors require close monitoring of mass flow rates rather than temperatures. As long as the temperature is high enough to not cause condensation, these detectors work relatively fine at a range of temperatures.

Besides temperature, other factors like sample concentration, flow rate, selectivity, time constant, noise, sensitivity, minimum detectability and linear range all effect a detector's function and, in turn, the quality of data output [141]. Among the common detectors encountered in forensic analysis are the mass spectrometer (MS), flame ionisation detector (FID), electron capture detector (ECD), nitrogen / phosphorus detector (NPD), and a range of other detectors as represented in Table 1.3.

Table 1.3: Commonly available detectors. Adapted from [141].

Detector	Selectivity
Flame Ionisation Detector (FID)	No
Thermal Conductivity Detector (TCD)	No
Electron Capture Detector (ECD)	Halogen
Nitrogen / Phosphorus Detector (NPD)	Nitrogen, Phosphorus and Halogen
Photoionisation Detector (PID)	Aromatics
Helium Ionisation Detector (HID)	No

1.8.2.5 Data Acquisition System

The data acquisition system captures signals generated from the detector and is responsible for detecting the retention time of the component, that is, the time elapsed between the introduction of the sample into the injection port to the component's elution out of the column. The data is displayed in the form of a chromatogram. As capillary columns generate speedy elution and narrowed peaks, an integrated microprocessor or an online computer-based data system is probably the best means to capture the large load of data generated [141, 164]. Both the microprocessor and computer-based data system utilise an analogue-to-digital processor, but the computer system goes on to connect the data into a PC system, allowing multiple chromatographic analyses with software that facilitates data modification and manipulation. The latter has since replaced the microprocessor, as it

is very user-friendly with significantly greater flexibility and speed, and has modern storing, reporting and display features [141].

1.8.3 Gas Chromatography-Mass Spectrometry (GC-MS)

Although gas chromatography (GC) can achieve excellent separation, it is only capable of capturing the retention time of a compound based on the partition coefficient but lacks the ability for unique identification of compounds. The mass spectrometer (MS), can facilitate qualitative identification and quantification of organic compounds. By coupling both the GC and MS together, the two instruments complement each other and form a powerful analytical tool. Besides its high resolving and identification power, the GC-MS is very sensitive to trace amounts of samples (ppm / ppb) and is able to cover a mass-to-charge (m/z) range of 10-800 [172]. An experimental setup of the GC-MS is demonstrated in Figure 1.19 where the mass spectrometer is illustrated to have three main sections: ionisation source, mass analyser / filter and the detector [173].

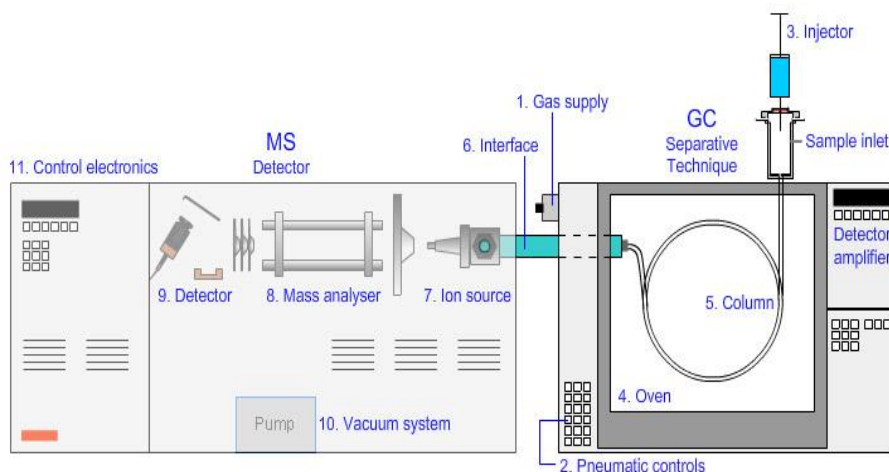


Figure 1.19: An experimental setup of the GC-MS [174]

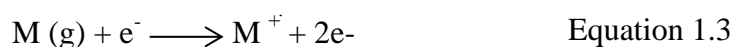
1.8.3.1 Ionisation Source

As the gaseous mixture exits the GC column, it is transmitted along a heated transfer line into the inlet of the MS and is introduced into the ionisation chamber. The entire MS system is maintained under a vacuum state using a turbo molecular pump (high speed) or a diffusion pump (low speed) at elevated temperatures between 200 °C and 300 °C. A vacuum state ensures zero charged particle collision that, in turn, aids in reducing background noise and unwanted peaks [175]. As the pressure in the MS is

lower compared to the GC, an interface that utilises a capillary direct is required to reduce this pressure to a functional range of 10^{-5} and 10^{-6} torr; it also serves to eliminate a huge part of the carrier gas volume, reducing flow rates to a manageable level for the MS [141, 164].

Once the gaseous compounds are in the ionisation chamber, they are converted into ions. This can happen in a number of ways, either via chemical ionisation (CI) or electrical ionisation (EI). In CI, ions are formed by subjecting the gaseous compounds to an oxidised reagent gas (methane) that induces sample ionisation via free radical formation. This method is relatively low energy and does not induce much fragmentation. It is usually present in GC-MS systems specialised for pesticide and explosive analysis. In EI, gaseous compounds are bombarded with high energy electrons generated from electron beams, causing them to undergo ionisation. EI is of much use in organic analysis and will be looked into further [141, 143, 173, 175].

In EI, high energy electrons generated from a heated tungsten or rhenium filament are guided through a narrow path by an appropriate potential behind the filament, towards the anode trap. A 70eV high energy electron beam is formed by focusing these excited electrons at one spot magnetically (Figure 1.20). When the neutral gaseous samples enter the chamber, these excited electrons bombard and collide with them continuously, inducing ionisation. The ionisation process causes loss of an electron from the molecule, rendering it in a form of a single positively charged molecular ion (parent ion), as represented in Equation 1.3.



As energy continues to build up on the bonds that hold the molecules together, continuous bombardment causes further fragmentation, especially for ions that are still unstable. This generates even more fragment ions, commonly known as daughter ions, each with its own unique relative abundance and m/z values that characterises a particular molecule [48, 61, 141, 143, 173, 175, 176].

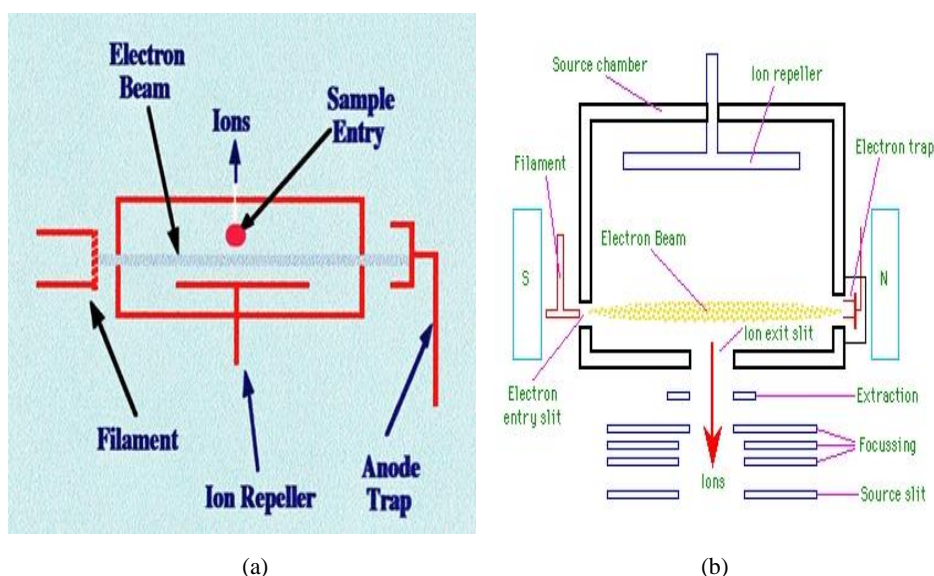


Figure 1.20: Electrical ionization chamber (a) [176] and (b) [177]

1.8.3.2 Mass Analyser

Positive ions that are formed in the ionisation chamber are then drawn into the mass analyser by charged lenses. They are then separated according to their m/z values via magnetic or electrical fields. Among the most commonly encountered analysers are ion traps, time of flight and, in the case, of forensic science, the quadrupole analyser. Introduced in 1968 by Finnigan Instruments [178], the quadrupole mass analyser benefits from its simplicity in operation, petite size, rapid scanning and capturing abilities – all features that are essential in forensic analysis. The term ‘quadrupole’ is derived from the four parallel hyperbolic rods that are strategically positioned in the pathway of ions in the ionisation chamber, as illustrated in Figure 1.21.

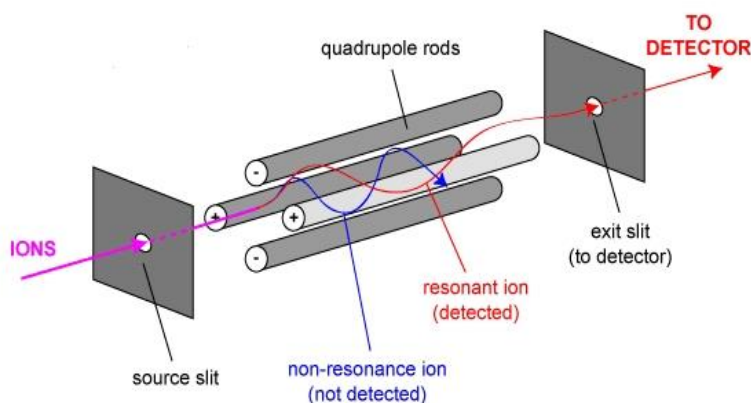


Figure 1.21: A quadrupole mass analyser [177]

Each of these rods is positioned in a way that each holds a charge that repels its adjacent partner. With the introduction of a fixed direct current (DC) into the system, the rods undergo alternate charge potentiating in a synchronised manner. Upon the entry of the positive ion through the narrowed slit, this rapid charge alternation across the rods causes the ions to experience a constant attraction-repulsion mechanism, moving them in a spiral formation down the pathway towards the negatively-charged detector. With the combination of a fixed direct current and a linear increase in alternating radio frequency (RF), the electromagnetic field acts as a mass filter and is modified by mass selective ejection to allow ions that possess a specific m/z value to orbit through the cavity without hitting the rods. As they reach the detector, the ions' m/z is captured and converted into a spectrum. Other fragmenting ratios that are too heavy or too light will either be neutralised upon hitting the rods and be expelled or removed by the vacuum [141, 143, 177, 179].

1.8.3.3 MS Detector

At the terminal end of the MS lies its detector, an uninterrupted 12 to 24 dynode version of an electron multiplier with large active surface areas that serve to collect and identify separated m/z values. Dynodes are metal plates that are usually made up of a combination of copper and beryllium and can come in the form of a discrete or continuous dynode; the latter is commonly encountered in laboratory GC-MS (Figure 1.22) [141, 172].

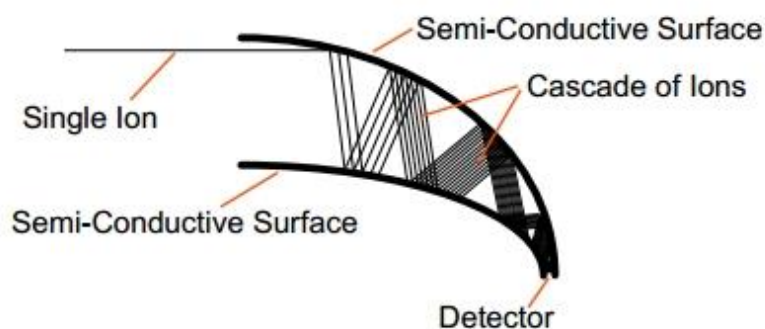


Figure 1.22: Continuous dynode electron multiplier [141]

As illustrated in Figure 1.22, the continuous dynode electron multiplier / channel electron multiplier is made up of a pair of semi-conductive surfaces that are situated at opposing sites along the entire length of the detector. Ions that are emitted from the mass analyser bombard the semi-conductive surface, generating a flow of electrons that is then amplified extensively by the potential difference that exists between the two semi-conductive surfaces. Secondary electron multiplication strengthens the initial weak signal up to 1 million fold or in the order of 10^4 - 10^8 [141, 172, 180]. These electrical signals are then transmitted to a computerised data acquisition system that converts them into a readable chromatogram containing mass spectra representing the m/z values versus the abundance of the sample [166]. Ion identification can then be conducted manually or by using softwares such as the National Institute of Standards and Technology (NIST) library. In the mass spectrum, the most abundant ion (given a percentage of 100%) is referred to as the base peak and the fragment peaks are plotted as a percentage of this base peak. Figure 1.23 illustrates the mass spectrum of hexane whereby the base peak is at m/z 57 with the remaining m/z 43 and 29 as fragment peaks of the hexane molecule.

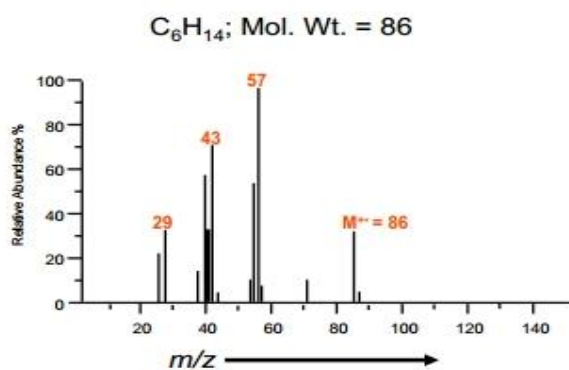


Figure 1.23: Mass spectrum of hexane [141]

Data obtained from the mass spectrum can be tabulated in a scan acquisition (SCAN) mode or in a selective ion monitoring (SIM) mode [141, 172]. In the SCAN, a universal range of data is scanned, typically between 40 to 400 atomic mass unit (AMU), and is displayed in the form of a total ion chromatogram (TIC). Commonly used for the identification of unknown compounds, SCAN is good for qualitative analysis although it experiences reduced sensitivity and slower acquisition rates as

compared to SIM. SIM is utilised when analysing specific target analytes with pre-determined m/z values. Because SIM is ion specific, its sensitivity is greatly enhanced and acquisition rates are rapid. However, because SIM does not scan all masses, it cannot be used for any qualitative analyses. Figure 1.24 demonstrates the differences in chromatograms produced by the SIM and SCAN modes.

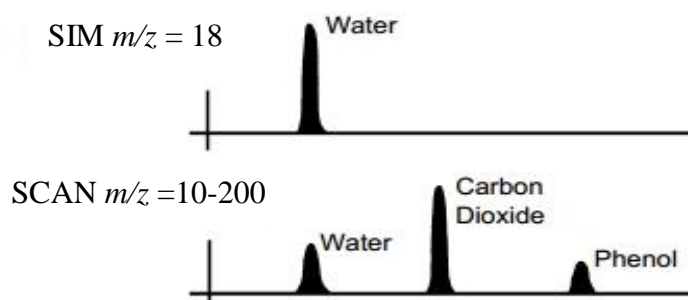


Figure 1.24: Comparison of chromatograms produced by SIM and SCAN modes [141]

1.9 Research Objectives

Interfering pyrolysis products can significantly complicate the identification of key indicators which may identify the presence of biological remains in fire debris analysis. These interfering products can come from various sources in a fire scene, and if the type of pyrolysis products generated from human or animal samples are known, the data interpretation process would be facilitated.

The first stage of this study was the development and validation of a robust methodology for generating pyrolysis products from animal tissue (porcine) under laboratory conditions, using passive headspace adsorption with ACS coupled with GC-MS. The various factors affecting the presence and abundance of pyrolysis products generated and extracted were optimised. The optimised methodology was then applied to human tissue and commonly encountered textile materials; to identify, compare and contrast the types of pyrolysis products generated across these samples and, to assess the factors that influence their pyrolytic profiles.

The next stage involved the generation of pyrolysis products from 'combined samples' (porcine and textile); to identify, compare and contrast the types of pyrolysis products generated when these samples are burnt together. The final stage investigated the ability of pattern recognition techniques to categorise and discriminate individual contributors in the combined samples.

1.10 References

1. Ubelaker, D.H., *The Forensic Evaluation of Burned Skeletal Remains: A Synthesis*. Forensic Science International, 2009. **183**(1-3): p. 1-5.
2. Dehaan, J.D., *Kirk's Fire Investigation*. 5th Edition. 2002, Upper Saddle River, NJ: Prentice Hall.
3. Fairgrieve, S.I., *Fire and Combustion, in Forensic Cremation: Recovery and Analysis*. 2008, Boca Raton: Florida: CRC Press.
4. Icove, D.J. and Dehaan, J.D., *Forensic Fire Scene Reconstruction*. 2009, Upper Saddle River, NJ: Pearson/Prentice Hall.
5. Fanton, L., Jdeed, K., Tilhet-Coartet, S., and Malicier, D., *Criminal Burning*. Forensic Science International, 2006. **158**(2): p. 87-93.
6. National Centre for Forensic Science. *Substrate Database*. 2006. University of Central Florida.
7. Karter, M.J.J., *Fire Loss in the United States During 2012*. 2013, National Fire Protection Association, Fire Analysis and Research Division: Quincy, MA.
8. Chowdhury, N., Rowe, I., and Sayer, G., *Fire Statistics Great Britain 2011 to 2012*, in Fire Statistics Great Britain. 2012, Department for Communities and Local Government London, UK.
9. United States Fire Administration, *National Fire Incident Reporting System: U.S. Fire Statistics*. [Online][January 1996, February 2014]. Available from: <http://www.usfa.fema.gov/statistics/estimates/index.shtm>.
10. Taylor, P. and Bond, S., *Crimes Detected in England and Wales 2011/12*, in Home Office Statistical Bulletin. 2012, Home Office Statistics under National Statistics Code of Practice: London, UK.
11. Bennison, L., *Statistical Bulletin Crime and Justice Series: Fires in Scotland 2012-2013*, in A National Statistic Publication for Scotland. 2013, The Scottish Government, Edinburgh: Scotland, UK.
12. Büyük, Y. and Koçak, U., *Fire-Related Fatalities in Istanbul, Turkey: Analysis of 320 Forensic Autopsy Cases*. Journal of Forensic and Legal Medicine, 2009. **16**(8): p. 449-454.

13. Rho, J.Y., Kuhn-Spearing, L., and Zioupos, P., *Mechanical Properties and the Hierarchical Structure of Bone*. Medical Engineering and Physics, 1998. **20**(2): p. 92-102.
14. Weiner, S., Traub, W., and Wagner, H.D., *Lamellar Bone: Structure-Function Relations*. Journal of Structural Biology, 1999. **126**(3): p. 241-255.
15. Clarke, B., *Normal Bone Anatomy and Physiology*. Clinical Journal of the American Society of Nephrology, 2008. **3**(3): p. 131-139.
16. Currey, J.D., *Bones: Structure and Mechanics*. 2002, Princeton: New Jersey: Princeton Univ Press.
17. Agu, K., *Investigation of the Thermal Degradation Products of Bone*, in Centre for Forensic Science, Department of Pure and Applied Chemistry. 2011, University of Strathclyde: Glasgow, Scotland.
18. Martin, R.B., Burr, D.B., and Sharkey, N.A., *Skeletal Tissue Mechanics*. 1998, New York, USA: Springer.
19. Symes, S.A., Rainwater, C.W., Chapman, E.N., Gipson, D.R., and Piper, A.L., *Patterned Thermal Destruction of Human Remains in a Forensic Setting*, in The Analysis of Burned Human Remains, ed. C.W. Schmidt and S.A. Symes. 2008, London, UK: Academic Press. p. 15-54.
20. Trebacz, H. and Wojtowicz, K., *Thermal Stabilization of Collagen Molecules in Bone Tissue*. International Journal of Biological Macromolecules, 2005. **37**(5): p. 257-262.
21. Collins, M.J., Nielsen-Marsh, C.M., Hiller, J., Smith, C.I., Roberts, J.P., Prigodich, R.V., Wess, T.J., Csapo, J., Millard, A.R., and Turner-Walker, G., *The Survival of Organic Matter in Bone: A Review*. Archaeometry, 2002. **44**(3): p. 383-394.
22. Kerr, J.B., *Atlas of Functional Histology*. 1999, St. Louis and London: Mosby International Limited.
23. Zioupos, P., Currey, J.D., and Hamer, A.J., *The Role of Collagen in the Declining Mechanical Properties of Aging Human Cortical Bone*. Journal of Biomedical Materials Research, 1999. **45**(2): p. 108-116.
24. Nielsen-Marsh, C.M., Gernaey, A., Turner-Walker, G., Hedges, R., Pike, A., and Collins, M., *The Chemical Degradation of Bone*, in Human Osteology,

- Archaeology and Forensic Science, ed. M. Cox and S. Mays. 2000, New York, USA: Cambridge Univ Press.
25. Kollias, N., Zonios, G., and Stamatias, G.N., *Fluorescence Spectroscopy of Skin*. *Vibrational Spectroscopy*, 2002. **28**(1): p. 17-23.
 26. Kuhn-Spearing, L., Rey, C., Kim, H.M., and Glimcher, M.J., *Carbonated Apatite Nanocrystals of Bone*, in *Synthesis and Processing of Nanocrystalline Powder*. ed. D.L. Bourell. 1996, Warrendale, PA: The Minerals, Metals and Materials Society.
 27. Weiner, S. and Traub, W., *Bone Structure: From Angstroms to Microns*. *The Journal of the Federation of American Societies for Experimental Biology*, 1992. **6**(3): p. 879-885.
 28. White, T.D. and Folkens, P.A., *The Human Bone Manual*. 2005, MA, USA: Elsevier: Academic Press.
 29. Landis, W.J., Song, M.J., Leith, A., Mcewen, L., and Mcewen, B.F., *Mineral and Organic Matrix Interaction in Normally Calcifying Tendon Visualized in Three Dimensions by High-Voltage Electron Microscopic Tomography and Graphic Image Reconstruction*. *Journal of Structural Biology*, 1993. **110**(1): p. 39-54.
 30. Weiner, S. and Wagner, H.D., *The Material Bone: Structure-Mechanical Function Relations*. *Annual Review of Materials Science*, 1998. **28**(1): p. 271-298.
 31. Sweeney, A.W., Byers, R.K., and Kroon, R.P. *Mechanical Characteristics of Bone and Its Constituents*, in *American Society of Mechanical Engineers Human Factor Conference*. 1965. New York, USA: American Society of Mechanical Engineers (ASME).
 32. Nalla, R.K., Kinney, J.H., and Ritchie, R.O., *Mechanistic Fracture Criteria for the Failure of Human Cortical Bone*. *Nature Materials*, 2003. **2**(3): p. 164-168.
 33. Yeni, Y.N. and Fyhrie, D.P., *Collagen-Bridged Microcrack Model for Cortical Bone Tensile Strength*, in *BioEngineering Conference*. 2001, American Society of Mechanical Engineers (ASME)-BED Publications. p. 293-294.

34. Kobayashi, S., Takahashi, H.E., Ito, A., Saito, N., Nawata, M., Horiuchi, H., Ohta, H., Iorio, R., Yamamoto, N., and Takaoka, K., *Trabecular Minimodeling in Human Iliac Bone*. *Bone*, 2003. **32**(2): p. 163-169.
35. Carter, D.R. and Hayes, W.C., *The Compressive Behavior of Bone as a Two-Phase Porous Structure*. *The Journal of Bone and Joint Surgery: American Volume*, 1977. **59**(7): p. 954.
36. Gibson, L.J., *The Mechanical Behaviour of Cancellous Bone*. *Journal of Biomechanics*, 1985. **18**(5): p. 317-328.
37. National Space Biomedical Research Institute, *Human Physical Development*. [Online] [January 2012, May 2012]. Available from: http://www.nsbri.org/humanphysspace/focus6/ep_development.html.
38. Mitchell, H.H., Hamilton, T.S., Steggerda, F.R., and Bean, H.W., *The Chemical Composition of the Adult Human Body and Its Bearing on the Biochemistry of Growth*. *Journal of Biological Chemistry*, 1945. **158**(3): p. 625-637.
39. Nürnberg, K., Wegner, J., and Ender, K., *Factors Influencing Fat Composition in Muscle and Adipose Tissue of Farm Animals*. *Livestock Production Science*, 1998. **56**(2): p. 145-156.
40. Forbes, R.M., Cooper, A.R., and Mitchell, H.H., *The Composition of the Adult Human Body as Determined by Chemical Analysis*. *Journal of Biological Chemistry*, 1953. **203**(1): p. 359-366.
41. Dehaan, J.D., *Kirk's Fire Investigation*. 6th Edition. 2007, New Jersey: Pearson: Prentice Hall.
42. Dehaan, J.D., *Fire and Bodies*, in *The Analysis of Burnt Human Remains*, ed. C.W. Schmidt and S.A. Symes. 2008, London, UK: Academic Press. p:1-13.
43. Drysdale, D., *An Introduction to Fire Dynamics*. 2002, Scotland, UK: John Wiley and Sons.
44. Reville, W., *Robert Boyle, the Father of Chemistry*, in *Public Awareness and Understanding of Science*. 2004, Irish Times 2001: University College, Cork.
45. Corry, R.A. and Kolko, D.J., *Fundamentals of Fire Investigation: Handbook of Firesetting in Children and Youth*. Academic Press: USA, imprint of Elsevier Science, 2002.

46. Beyler, C.L. and Hirschler, M.M., *Section 1, Chapter 7: Thermal Decomposition of Polymers*, in SFPE Handbook of Fire Protection Engineering, ed. P.J. Dinunno. 2002, National Fire Protection Association, (NFPA) Inc. : Quincy, MA.
47. ASTM International E176-13, *Standard Terminology of Fire Standards*. 2014. American Society for Testing and Materials (ASTM) International: West Conshohocken, PA.
48. Mat Desa, W.N.S., *The Discrimination of Ignitable Liquids and Ignitable Liquid Residues Using Chemometric Analysis*, in Centre for Forensic Science, Department of Pure and Applied Chemistry. 2012, Univeristy of Strathclyde: Glasgow, Scotland.
49. Yang, L., Chen, X., Zhou, X., and Fan, W., *The Pyrolysis and Ignition of Charring Materials under an External Heat Flux*. *Combustion and Flame*, 2003. **133**(4): p. 407-413.
50. Wampler, T.P., *Analytical Pyrolysis: An Overview*, in *Applied Pyrolysis Handbook*, ed. T.P. Wampler. 1995, New York, USA: Marcel Dekker.
51. Moldoveanu, E., *Analytical Pyrolysis of Natural Organic Polymers*, in *Techniques and Instrumentation in Analytical Chemistry*. Vol. **20**. 1998, Macon, GA: Brown and Williamson Tobacco Corp: Elsevier Science.
52. Purevsuren, B. and Davaajav, Y., *Investigation on Pyrolysis of Casein*. *Journal of Thermal Analysis and Calorimetry*, 2001. **66**(3): p. 743-748.
53. Jones, J. and De Neve, S., *Mechanisms of Pyrolysis*. New Zealand Biochar Reseach Centre, 2011.
54. Stauffer, E., *Concept of Pyrolysis for Fire Debris Analysis*. *Science and Justice*, 2003. **43**(1): p. 29-40.
55. Price, D. and Horrocks, A.R., *Combustion Processess of Textile Fibres*, in *Handbook of Fire Resistant Textiles*, ed. F.S. Kilinc. 2013, The Textile Institute: Woodhead Publishing: Cambridge, UK.
56. Boter, R., *Interactive Concepts in Biochemistry*. [Online] [January 2002, April 2014]. Available from: <http://www.wiley.com/college/boyer/0470003790/reviews/redox/redox.htm>.

57. Sisler, H.H. and Vanderwerf, C.A., *Oxidation-Reduction: An Example of Chemical Sophistry*. Journal of Chemical Education 1980. **57**(1): p. 42.
58. De Jong, W., Di Nola, G., Venneker, B.C.H., Spliethoff, H., and Wojtowicz, M.A., *TG-FTIR Pyrolysis of Coal and Secondary Biomass Fuels: Determination of Pyrolysis Kinetic Parameters for Main Species and NOx Precursors*. Fuel, 2007. **86**(15): p. 2367-2376.
59. Kilinc, F.S., *Handbook of Fire Resistant Textiles*. 2013, Cambridge, UK: The Textile Institute: Woodhead Publishing.
60. Chang, R., *Physical Chemistry for the Biosciences* 2005, USA: University Science Books.
61. Stauffer, E., Dolan, J.A., and Newman, R., *Fire Debris Analysis*. 2008, San Diego, USA: Academic Press.
62. Irwin, W.J., *Analytical Pyrolysis: A Comprehensive Guide*. 1982, New York, USA: Matthew Dekker.
63. Martinez-Escandell, M., Torregrosa, P., Marsh, H., Rodriguez-Reinoso, F., Santamaria-Ramirez, R., Gomez-De-Salazar, C., and Romero-Palazon, E., *Pyrolysis of Petroleum Residues: I. Yields and Product Analyses*. Carbon, 1999. **37**(10): p. 1567-1582.
64. Hopkins, D.J. and Quintiere, J.G., *Material Fire Properties and Predictions for Thermoplastics*. Fire Safety Journal, 1996. **26**(3): p. 241-268.
65. Vettori, R.L., *Estimates of Thermal Conductivity for Unconditioned and Conditioned Materials Used in Fire Fighters' Protective Clothing*. 2005: Department of Homeland Security, US Fire Administration.
66. Dehaan, J.D., Brien, D.J., and Large, R., *Volatile Organic Compounds from the Combustion of Human and Animal Tissue*. Science and Justice, 2004. **44**(4): p. 223-236.
67. CDS Analytical Inc., *Degradation Mechanisms: Random Scission*, in Applications Information using Advanced GC Sample Handling Technology. 2000, CDS Analytical Inc: Oxford, PA.
68. Stauffer, E., *Intefering Products of Common Polymers Found in Fire Scenes*, in Third Annual TWGFEX Symposium of Fire and Explosion Debris

- Analysis and Scene Investigation, ed. E. Stauffer. 2003: Orlando, Florida. p. 1-94.
69. Price, D., Horrocks, A.R., Akalin, M., and Farooq, A.A., *Influence of Flame Retardants on the Mechanism of Pyrolysis of Cotton (Cellulose) Fabrics in Air*. Journal of Analytical and Applied Pyrolysis, 1997. **40**: p. 511-524.
 70. Zhu, P., Sui, S., Wang, B., Sun, K., and Sun, G., *A Study of Pyrolysis and Pyrolysis Products of Flame-Retardant Cotton Fabrics by DSC, TGA, and PY-GC-MS*. Journal of Analytical and Applied Pyrolysis, 2004. **71**(2): p. 645-655.
 71. CDS Analytical Inc., *Pyrolysis-GS/MS of Clothing Fibres-Cotton and Poly(Ethylene Terephthalate)*, in Applications Information Using Advanced Sample Handling Technology. 2014, CDS Analytical Inc.: Oxford, PA.
 72. Nakanishi, S., Morikawa, J., and Hashimoto, T., *Flame Retardation of Cellulosic Fibers Characterized by Apparent Activation Energy of Thermal Degradation*. Textile Research Journal, 1999. **69**(3): p. 208-213.
 73. Nimlos, M.R. and Evans, R.J., *Levoglucosan Pyrolysis*. Fuel Chemistry, 2002. **47**(1): p. 393-394.
 74. Kawamoto, H., Murayama, M., and Saka, S., *Pyrolysis Behavior of Levoglucosan as an Intermediate in Cellulose Pyrolysis: Polymerization into Polysaccharide as a Key Reaction to Carbonized Product Formation*. Journal of Wood Science, 2003. **49**(5): p. 469-473.
 75. Chatterjee, P.K. and Conrad, C.M., *Kinetics of the Pyrolysis of Cotton Cellulose*. Textile Research Journal, 1966. **36**(6): p. 487-494.
 76. VTT, SP Tratek and KTH Biotechnology, Innofirewood, *Innovative Eco-Efficient High Fire Performance Wood Products for Demanding Applications: Burning of Wood*. [Online] [June 2013, June 2014]. Available from: <http://virtual.vtt.fi/virtual/innofirewood/stateoftheheart/database/burning/burning.html>.
 77. Stauffer, E., *Sources of Interference in Fire Debris Analysis*, in Fire Investigation, ed. N. Nic Daeid. 2004, Boca Raton, Florida: CRC Press. p. 191.

78. Waste Watch and Recoup, *Plastics in the UK Economy: A Guide to Polymer Use and the Opportunities for Recycling*. [Online] [April 2003, June 2014]. Available from: www.plasticsintheuk.org.uk.
79. Shalaby, S.M., *Chapter 3: Thermoplastic Polymers*, in *Thermal Characterization of Polymeric Materials*, ed. E.A. Turi. 1981, New York, USA: Academic Press: Elsevier.
80. Babrauskas, V., *Charring Rate of Wood as a Tool for Fire Investigations*. *Fire Safety Journal*, 2005. **40**(6): p. 528-554.
81. Dehaan, J.D., Campbell, S.J., and Nurbakhsh, S., *Combustion of Animal Fat and Its Implications for the Consumption of Human Bodies in Fires*. *Science and Justice*, 1999. **39**: p. 27-38.
82. Babrauskas, V., *Ignition Handbook*. 2003, Issaquah WA: Fire Science Publishers. p. 1116.
83. Maher, K.D. and Bressler, D.C., *Pyrolysis of Triglyceride Materials for the Production of Renewable Fuels and Chemicals*. *Bioresource Technology*, 2007. **98**(12): p. 2351-2368.
84. Purevsuren, B., Avid, B., Narangerel, J., Gerelmaa, T., and Davaajav, Y., *Investigation on the Pyrolysis Products from Animal Bone*. *Journal of Materials Science*, 2004. **39**(2): p. 737-740.
85. Fortes, I.C.P. and Baugh, P.J., *Study of Calcium Soap Pyrolysates Derived from Macauba Fruit (Acrocomia Sclerocarpa M.). Derivatization and Analysis by GC/MS and CI-MS*. *Journal of Analytical and Applied Pyrolysis*, 1994. **29**(2): p. 153-167.
86. Dehaan, J.D. and Nurbakhsh, S., *Sustained Combustion of an Animal Carcass and Its Implications for the Consumption of Human Bodies in Fires*. *Journal of Forensic Sciences*, 2001. **46**(5): p. 1076.
87. National Fire Protection Association (NFPA), *Fire Protection Handbook*. 1990. National Fire Protection Association (NFPA).
88. Dehaan, J.D., *Sustained Combustion of Bodies: Some Observations**. *Journal of Forensic Sciences*, 2012.
89. Stryer, L., *Biochemistry*. 3rd Edition. 1988, New York, USA: W.H Freeman and Company. p. 1089.

90. Richards, N.F., *Fire Investigation - Destruction of Corpses*. Medicine, Science and the Law, 1977. **17**(2): p. 79-82.
91. Holden, J.L., Phakey, P.P., and Clement, J.G., *Scanning Electron Microscope Observations of Heat-Treated Human Bone*. Forensic Science International, 1995b. **74**(1): p. 29-45.
92. Eckert, W.G., James, S., and Katchis, S., *Investigation of Cremations and Severely Burned Bodies*. The American Journal of Forensic Medicine and Pathology, 1988. **9**(3): p. 188.
93. Shepard, A.O., *Ceramics for the Archaeologist*. Vol. **609**. 1956, Washington DC, USA: Carnegie Institution of Washington.
94. Shipman, P., Foster, G., and Schoeninger, M., *Burnt Bones and Teeth: An Experimental Study of Color, Morphology, Crystal Structure and Shrinkage*. Journal of Archaeological Science, 1984. **11**(4): p. 307-325.
95. Mayne Correia, P.M., *Fire Modification of Bone: A Review of the Literature*, in Forensic Taphonomy: The Postmortem Fate of Human Remains, ed. W.D. Haglund and M.H. Sorg. 1997, Boca Raton, Florida: CRC Press.
96. Thompson, J.U., *Heat-Induced Dimensional Changes in Bone and Their Consequences for Forensic Anthropology*. Journal of Forensic Science, 2005. **50**(5): p. 1008-1015.
97. Thompson, J.U., *Recent Advances in the Study of Burned Bone and Their Implications for Forensic Anthropology*. Forensic Science International, 2004. **146**: p. S203-S205.
98. Rootare, H.M. and Craig, R.G., *Vapor Phase Adsorption of Water on Hydroxyapatite*. Journal of Dental Research, 1977. **56**(12): p. 1437-1448.
99. Ubelaker, D.H., *Human Skeletal Remains: Excavation, Analysis, Interpretation*. 3rd Edition. Vol. **2**. 1989, Washington, DC, USA: Adline Publishing Co. p. 172.
100. Herrmann, B., *On Histological Investigations of Cremated Human Remains*. Journal of Human Evolution, 1977. **6**(2): p. 101-103.
101. ASTM International E1386-10, *Standard Practice for Separation of Ignitable Liquid Residues from Fire Debris Samples by Solvent Extraction*. 2012.

- American Society for Testing and Materials (ASTM) International: West Conshohocken, PA.
102. ASTM International E1388-12, *Standard Practice for Sampling of Headspace Vapors from Fire Debris Samples*. 2012. American Society for Testing and Materials (ASTM) International: West Conshohocken, PA.
 103. ASTM International E1412-07, *Standard Practice for Separation of Ignitable Liquid Residues from Fire Debris Samples by Passive Headspace Concentration with Activated Charcoal*. 2012. American Society for Testing and Materials (ASTM) International: West Conshohocken, PA.
 104. ASTM International E2154-01, *Separation and Concentration of Ignitable Liquid Residues from Fire Debris Samples by Passive Headspace Concentration with Solid Phase Microextraction (SPME)*. 2012. American Society for Testing and Materials (ASTM) International: West Conshohocken, PA.
 105. Almirall, J.R. and Furton, K.G., *Characterization of Background and Pyrolysis Products That May Interfere with the Forensic Analysis of Fire Debris*. *Journal of Analytical and Applied Pyrolysis*, 2004. **71**(1): p. 51-67.
 106. Clodfelter, R.W. and Hueske, E.E., *A Comparison of Decomposition Products from Selected Burned Materials with Common Arson Accelerants*. *Journal of Forensic Science*, 1977. **22**: p. 116.
 107. Bertsch, W., *Volatiles from Carpet: A Source of Frequent Misinterpretation in Arson Analysis*. *Journal of Chromatography A*, 1994. **674**(1): p. 329-333.
 108. Dehaan, J.D. and Bonarius, K., *Pyrolysis Products of Structure Fires*. *Journal of the Forensic Science Society*, 1988. **28**(5): p. 299-309.
 109. Keto, R.O., *GC/MS Data Interpretation for Petroleum Distillate Identification in Contaminated Arson Debris*. *Journal of Forensic Sciences*, 1995. **40**: p. 412-412.
 110. McLellan, S.A., *An Investigation of the Volatiles Produced from Pyrolysis of the Body*, in Centre for Forensic Science, Department of Pure and Applied Chemistry. 1999, University of Strathclyde: Glasgow, Scotland.
 111. Lentini, J.J., Dolan, J.A., and Cherry, C., *The Petroleum-Laced Background*. *Journal of Forensic Sciences*, 2000. **45**(5): p. 968-989.

112. Lentini, J.J., *Incidental Accelerants*. National Fire and Arson Report, 1983. **2**(3): p. 3.
113. Stauffer, E., *Identification and Characterization of Interfering Products in Fire Debris Analysis*, in College of Arts and Science. 2001, Florida State University: Miami, USA.
114. Cavanagh, K., Pasquier, E.D., and Lennard, C., *Background Interference from Car Carpet-The Evidential Value of Petrol Residues in Cases of Suspected Vehicle Arson*. Forensic Science International, 2002. **125**(1): p. 22-36.
115. Nic Daeid, N., *An Introduction to Fires and Fire Investigation*, in Fire Investigation, ed. N. Nic Daeid. 2004, Boca Raton, Florida: CRC Press.
116. Nowicki, J., *An Accelerant Classification Scheme Based on Analysis by Gas Chromatography/Mass Spectrometry (GC-MS)*. 1990: National Emergency Training Center.
117. Stone, I. and Lomonte, J., *False Positions in Analysis of Fire Debris*. The Fire and Arson Investigator, 1984. **34**(3): p. 36-40.
118. Howard, J. and Mckague, A.B., *A Fire Investigation Involving Combustion of Carpet Material*. Journal of Forensic Sciences, 1984. **29**(3): p. 919-922.
119. Fernandes, M., Lau, C., and Wong, W., *The Effect of Volatile Residues in Burnt Household Items on the Detection of Fire Accelerants*. Science and Justice, 2002. **42**(1): p. 7-15.
120. Lentini, J. and Waters, L., *Isolation of Accelerant-Like Residues from Roof Shingles Using Headspace Concentration*. Arson Analysis Newsletter, 1982. **6**(3): p. 48.
121. Tranthim-Fryer, D.J., *The Application of a Simple and Inexpensive Modified Carbon Wire Adsorption/Solvent Extraction Technique to the Analysis of Accelerants and Volatile Organic Compounds in Arson Debris*. Journal of Forensic Science, 1990. **35**: p. 271-280.
122. Williams, M.R., *Advances in Fire Debris Analysis*, in Department of Chemistry, College of Sciences. 2007, University of Central Florida Orlando, Florida.

123. ASTM International E1412-00, *Standard Practice for Separation and Concentration of Ignitable Liquid Residues from Fire Debris Samples by Passive Headspace Concentration*. 2012. American Society for Testing and Materials (ASTM) International: West Conshohocken, PA.
124. Newman, R.T., Dietz, W.R., and Lothridge, K., *The Use of Activated Charcoal Strips for Fire Debris Extractions by Passive Diffusion. Part 1: The Effects of Time, Temperature, Strip Size, and Sample Concentration*. Journal of Forensic Science, 1996. **41**(3): p. 361-370.
125. Waters, L.V. and Palmer, L.A., *Multiple Analysis of Fire Debris Samples Using Passive Headspace Concentration*. Journal of Forensic Sciences, 1993. **38**: p. 165-165.
126. Caddy, B. and Smith, F.P., *Methods of Fire Debris Preparation for Detection of Accelerants*. Forensic Science Review, 1991(3): p. 57-69.
127. Borusiewicz, R., Zadora, G., and Zieba-Palus, J., *Application of Head-Space Analysis with Passive Adsorption for Forensic Purposes in the Automated Thermal Desorption-Gas Chromatography-Mass Spectrometry System*. Chromatographia, 2004. **60**: p. 133-142.
128. Dietz, W.R., *Improved Charcoal Packaging for Accelerant Recovery by Passive Diffusion*. Journal of Forensic Sciences, 1991. **36**(1).
129. Pert, A.D., Baron, M.G., and Birkett, J.W., *Review of Analytical Techniques for Arson Residues*. Journal of Forensic Sciences, 2006. **51**(5): p. 1033-1049.
130. Twibell, J.D. and Home, J.M., *Novel Method for Direct Analysis of Hydrocarbons in Crime Investigation and Air Pollution Studies*. Nature Materials, 1977. **268**(5622): p. 711-713.
131. Twibell, J.D., Home, J.M., and Smalldon, K.W., *A Splitless Curie Point Pyrolysis Capillary Inlet System for Use with the Adsorption Wire Technique of Vapour Analysis*. Chromatographia, 1981. **14**(6): p. 366-370.
132. Juhala, J.A., *The Method for Adsorption of Flammable Vapors by Direct Insertion of Activated Charcoal into Fire Debris Samples*. Arson Analysis Newsletter, 1982. **6**(2): p. 32-36.
133. Massey, D., Pasquier, E.D., and Lennard, C., *Solvent Desorption of Charcoal Strips (DFLEX[®]) in the Analysis of Fire Debris Samples: Replacement of*

- Carbon Disulfide*. Canadian Society of Forensic Science Journal, 2002. **35**(4): p. 195-208.
134. Massey, D., Du Pasquier, E., and Lennard, C. *Optimisation of Fire Debris Analysis with DFLEX[®]*, in Proceedings of the International Association of Forensic Science. 2002. Montpellier, France: International Association of Forensic Science.
 135. Frontela, L., Pozas, J.A., and Picabea, L., *A Comparison of Extraction and Adsorption Methods for the Recovery of Accelerants from Arson Debris*. Forensic Science International, 1995. **75**(1): p. 11-23.
 136. Bertsch, W. and Ren, Q., *The Chemical Analysis of Fire Debris for Potential Accelerants*, in Handbook of Analytical Separations 2. Elsevier Science: New York, 2000. **2**: p. 617-678.
 137. Borusiewicz, R., Zieba-Palus, J., and Zadora, G., *Application of Head-Space Analysis with Passive Adsorption to the Chromatographic Detection and Identification of Accelerants in the ATD–GC–MS System*. Problems of Forensic Sciences, 2002. **51**: p. 87-95.
 138. Marsh, H. and Rodriguez-Reinoso, F., *Activated Carbon*. 2006, Oxford, UK: Elsevier Science.
 139. Newman, R., *Modern Laboratory Techniques Involved in the Analysis of Fire Debris Samples*, in Fire Investigation, ed. N. Nic Daied. 2004, Boca Raton, Florida: CRC Press.
 140. Cafe, T. and Stern, W., *Is It an Accidental Fire or Arson*. Forensic and Scientific Services, 2004.
 141. Mcnair, H.M. and Miller, J.M., *Basic Gas Chromatography*. 2nd Edition. Vol. **2**. 2009, Hobokwn, New Jersey: John Wiley and Sons.
 142. James, A.T. and Martin, A.J.P., *Gas-Liquid Partition Chromatography: A Technique for the Analysis of Volatile Materials*. Analyst, 1952. **77**(921): p. 915-932.
 143. Stafford, D.T., *Forensic Gas Chromatography*, in Gas Chromatography in Forensic Science, ed. J. Robertson. 1992, Chicago, USA: Ellis Horwood Limited.
 144. Nic Daeid, N., *Fire Investigation*. 2004, Boca Raton, Florida: CRC Press.

145. Lucas, D.M., *The Identification of Petroleum Products in Forensic Science by Gas Chromatography*. Journal of Forensic Sciences, 1960. **5**(2): p. 236-247.
146. Yoshida, H., Kaneko, T., and Suzuki, S., *A Solid Phase Microextraction Method for the Detection of Ignitable Liquids in Fire Debris*. Journal of Forensic Sciences, 2008. **53**(3): p. 668-676.
147. Wu, C.H., Chen, C.L., Huang, C.T., Lee, M.R., and Huang, C.M., *Identification of Gasoline Soot in Suspect Arson Cases by Using Headspace Solid Phase Microextraction with GC/MS*. Analytical Letters, 2004. **37**(7): p. 1373-1384.
148. Wineman, P.L. and Keto, R.O., *Target-Compound Method for the Analysis of Accelerant Residues in Fire Debris*. Analytica Chimica Acta, 1994. **288**(1-2): p. 97-110.
149. Wardencki, W., Michulec, M., and J., C., *A Review of Theoretical and Practical Aspects of Solid Phase Microextraction in Food Analysis*. International Journal of Food Science and Technology, 2004. **39**(7): p. 703-717.
150. Vichi, S., Castellote, A.I., Pizzale, L., Conte, L.S., Buxaderas, S., and Lopez-Tamames, E., *Analysis of Virgin Olive Oil Volatile Compounds by Headspace Solid-Phase Microextraction Coupled to Gas Chromatography with Mass Spectrometric and Flame Ionization Detection*. Journal of Chromatography A, 2003. **983**(1): p. 19-33.
151. Ducki, S., Miralles-Garcia, J., Zumbe, A., Tornero, A., and Storey, D.M., *Evaluation of Solid-Phase Micro-Extraction Coupled to Gas Chromatography-Mass Spectrometry for the Headspace Analysis of Volatile Compounds in Cocoa Products*. Talanta, 2008. **74**(5): p. 1166-1174.
152. Isidorov, V.A., Bakier, S., and Grzech, I., *Gas Chromatographic-Mass Spectrometric Investigation of Volatile and Extractable Compounds of Crude Royal Jelly*. Journal of Chromatography B, 2012(885-886): p. 109-116.
153. Agius, R., Nadulski, T., Kahl, H.G., Schrader, J., Dufaux, B., Yegles, M., and Pragst, F., *Validation of a Headspace Solid-Phase Microextraction GC-*

- MS/MS for the Determination of Ethyl Glucuronide in Hair According to Forensic Guidelines*. Forensic Science International, 2010. **196**(1): p. 3.
154. Poon, K.F., Lam, P.K.S., and Lam, M.H.W., *Determination of Polychlorinated Biphenyls in Human Blood Serum by SPME*. Chemosphere, 1999. **39**(6): p. 905-912.
 155. Almirall, J.R., Wang, J., Lothridge, K., and Furton, K.G., *The Detection and Analysis of Ignitable Liquid Residues Extracted from Human Skin Using SPME/GC*. Journal of Forensic Sciences, 2000. **45**(2): p. 453-461.
 156. Wang, Y., *Sample Preparation / Concentration for Trace Analysis in GC-MS in Chemistry Department*. 1997, Virginia Polytechnic Institute and State University: Virginia, USA. p. 104.
 157. Bonadio, F., Margot, P., Delemont, O., and Esseiva, P., *Headspace Solid-Phase Microextraction (Hs-SPME) and Liquid-Liquid Extraction (LLE): Comparison of the Performance in Classification of Ecstasy Tablets (Part 2)*. Forensic Science International, 2008. **182**(1): p. 52-56.
 158. Lord, H. and Pawliszyn, J., *Microextraction of Drugs*. Journal of Chromatography A, 2000. **902**(1): p. 17-63.
 159. Brown, S.D., Rhodes, D.J., and Pritchard, B.J., *A Validated Spme-Gcms Method for Simultaneous Quantification of Club Drugs in Human Urine*. Forensic Science International, 2007. **171**(2): p. 142-150.
 160. Furton, K.G., Almirall, J.R., Bi, M., Wang, J., and Wu, L., *Application of Solid-Phase Microextraction to the Recovery of Explosives and Ignitable Liquid Residues from Forensic Specimens*. Journal of Chromatography A, 2000. **885**(1): p. 419-432.
 161. Vuckovic, D., Zhang, X., Cudjoe, E., and Pawliszyn, J., *Solid-Phase Microextraction in Bioanalysis: New Devices and Directions*. Journal of Chromatography A, 2010. **1217**(25).
 162. Trimble, T.A., You, J., and Lydy, M.J., *Bioavailability of PCBs from Field-Collected Sediments: Application of Tenax Extraction and Matrix-SPME Techniques*. Chemosphere, 2008. **71**(2): p. 337-344.
 163. Ettre, L.S., *The Beginnings of Headspace Analysis*. LCGC Asia Pacific, 2002. **20**(12): p. 1120-1129.

164. Braithwaite, A. and Smith, F.J., *Chromatographic Methods*. 5th Edition, ed. C.A. Hall. 1996, Dordrecht, The Netherlands: Kluwer Academic Publishers.
165. Robinson, K. and Robinson, J., *Contemporary Instrumental Analysis*. 3rd Edition. 2000, New Jersey, USA: Prentice Hall. p. 840.
166. Stafford, D.T., *Chapter 7: Chromatography*. 2nd Edition, in *Principles of Forensic Toxicology*, ed. B. Levine. 2003, USA: American Association of Clinical Chemistry Inc.
167. *Gas Chromatography and GC X GC*. [Online] [January 2012, February 2013]. Available from: <http://www.chemistry.mcmaster.ca/courses/4p03/Week%2012%20Notes.pdf>.
168. ASTM International E1618-11, *Standard Test Method for Ignitable Liquid Residues in Extracts from Fire Debris Samples by Gas Chromatography-Mass Spectrometry*. 2012. American Society for Testing and Materials (ASTM) International: West Conshohocken, PA.
169. Handley, A.J. and Adlard, E.R., *Gas Chromatography Techniques and Applications*, in *Pharmaceutical Analysis*, ed. J.M. Chalmers and A.J. Handley. 2001, Sheffield, UK: Sheffield Academic Press.
170. Lentini, J.J., *Analysis of Ignitable Liquid Residues*, in *Scientific Protocols for Fire Investigation*, ed. J.J. Lentini. 2006, Boca Raton, Florida: Taylor and Francis Gp: CRC Press.
171. Scott, R.P.W., Library for Science, *Principles and Practice of Chromatography: Detectors in Chromatography* [Online] [January 2010, October 2012]. Available from: <http://www.chromatography-online.org/topics/detector.html>.
172. McNair, H.M., Pierce Biotechnology Inc., *Introduction to GC/MS*. [Online] [July 2006, October 2012]. Available from: [http://www.cal-tox.org/Download/proceedings/1106/conklin_intro%20to%20gcms\(b\).pdf](http://www.cal-tox.org/Download/proceedings/1106/conklin_intro%20to%20gcms(b).pdf).
173. Jayaram, S.K., *A Comprehensive Chemical Examination of Methylamphetamine Produced from Pseudoephedrine Extracted from Cold Medication*, in Centre for Forensic Science, Department of Pure and Applied Chemistry. 2012, University of Strathclyde: Glasgow, Scotland.

174. Crawford Scientific, LC GC's CHROMacademy, *GC-MS Set-Up*. 2013, LC GC's CHROMacademy: Duluth, USA.
175. De Hoffmann, E., *Mass Spectrometry*, in Kirk-Othmer Encyclopedia of Chemical Technology. 2000, John Wiley and Sons, Inc.
176. Scott, R.P.W., Library for Science, *Analytical Spectroscopy: Electron Impact Ionization*. [Online] [January 2010, October 2012]. Available from: <http://www.analyticalspectroscopy.net/ap8-3.htm>.
177. Gates, P. *Gas Chromatography Mass Spectrometry*. NERC Life Sciences Mass Spectrometry, 2012. Life Sciences Mass Spectrometry Facility: University of Bristol.
178. Brock, D. C., *A Measure of Success*. Chemical Heritage Magazine: Chemical Heritage Foundation. [Online] [August 2010, July 2014] Available from: <http://www.chemheritage.org/discover/media/magazine/articles/29-1-a-measure-of-success.aspx?page=2>.
179. Davis, U.C., *Gas Chromatography*, in ChemWiki: The Dynamic Chemistry Textbook. 2010. The Regents of the University of California: California, USA.
180. ETP: SGE Group, *Electron Multipliers for Mass Spectrometry*. [Online] [September 2011, October 2012]. Available from: http://www.bgb-analytik.de/pdf/SGE_Multiplier.pdf.

CHAPTER 2: GAS CHROMATOGRAPHY – MASS SPECTROMETRY (GC-MS) INSTRUMENTAL VALIDATION AND METHODOLOGY DEVELOPMENT

2.1 Introduction

Prior to analysis of any test samples, the instrument of choice has to be calibrated and validated to ensure optimum and efficient performance. Validation is necessary for all laboratory based methodologies as this process guarantees the robustness, reliability, validity and consistency of the results / data obtained [1-3]. Validation can be conducted in a number of ways, that ultimately depends on the type of sample, nature of the analysis (qualitative / quantitative) and the instrument utilised. Validation is most commonly carried out using a series of standard experiments that employ either one or all of these techniques; calibration models, internal standards, external standards, reference standards, to generate data that will then be used to access the method's specificity / selectivity, precision (repeatability / reproducibility), sensitivity, limit of detection (LOD) / limit of quantitation (LOQ), accuracy and linearity [1-9].

2.2 Validation of GC-MS Instrumentation

When it comes to GC-MS validation, a commercial or in-house mixture of known standards / test mixture, commonly referred to as the Grob mixture [10], is often utilised. This test mixture is composed of compounds possessing a variety of functional groups often including hydrocarbons, fatty acid methyl esters, alcohols, aldehydes, organic acids and bases. Repetitive analysis of the Grob mixture facilitates an understanding of the ability of the analytical column, chromatographic and detector conditions to deliver accurate and reliable analytical results. In addition to the abovementioned factors, the analysed standard test mixture gives data points that can then be used to determine peak shape, peak resolution, peak asymmetry, band broadening and etc.

2.2.1 Specificity / Selectivity

In chromatographic analysis, selectivity, α refers to the relative interaction of two compounds with the stationary phase and can be expressed as a ratio of the time compound 'y' spends in the stationary phase, t'_y to the time compound 'x' spends in the stationary phase, t'_x [11], as illustrated in Equation 2.0.

$$\alpha = \frac{t'_y}{t'_x} \quad \text{Equation 2.0}$$

In method validation, according to the International Conference on Harmonisation (ICH) [12], specificity / selectivity refers to '*the ability to assess unequivocally the analyte in the presence of components which may be expected to be present*'. It refers to the extent to which the method and instrument are able to generate good separation, identification and quantification of the target component(s) in the presence of interferences, impurities, degradants and contaminants from endogenous and exogenous sources [1, 3, 6]. It is often tested by adding interfering compounds which are expected to be present in the test samples, into the blank samples.

2.2.2 Precision

Precision refers to the measure of closeness of the analytical results to each other, for a number of replicate measurements of the same homogenous sample, under the same analytical conditions [1, 2, 12]. It is commonly expressed in terms of the method's repeatability and reproducibility [1, 2].

Repeatability conditions expresses the precision of the method and instrument through multiple measurements under the same operating conditions (same analyst, same instrument, same day, same material, same laboratory) [1, 3]. Deviation from any of these settings is referred to as reproducible conditions, a measure of precision of multiple measurements between settings. While repeatability aims to verify the capability of an identical method to produce same results under the same conditions, reproducibility validates the ability of an identical method to produce same results under different settings. Both repeatability and reproducibility can be assessed

through a series of calculations of the mean and standard deviation (Equation 2.1 and Equation 2.1, respectively) of the peak area or peak height of the analyte(s).

$$Mean = \frac{\sum X_1 + X_2 + X_3 + \dots + X_n}{n} \quad \text{Equation 2.1}$$

where X_i represents the data value and n represents the total number of data measurements (sample size).

$$s = \sqrt{\frac{\sum_{i=1}^n (x_i - \bar{x})^2}{n-1}} \quad \text{Equation 2.2}$$

where x_i represents each value in the sample, \bar{x} represents the mean of x values and n refers to the total number of data measurements (sample size).

Peak area refers to the integration of the mass per unit volume / concentration of the analyte in relation to time, giving an accurate value of the analyte mass [13]. It is a data point that is widely used in chromatography due to its accuracy, as it is independent of peak tailing and asymmetry. Peak height is measured from the integrated section of the baseline to the peak's apex point and is seldom used as it is severely affected by peak tailing, asymmetry and band broadening, with the exception of Gaussian shaped peaks (bell shaped) [9, 14].

From the mean and standard deviation values, the relative standard deviation (RSD) of a given set of data can then be calculated. RSD, also commonly known as the coefficient of variation, measures the standard deviation relative to the mean (Equation 2.3), providing information pertaining to the precision of an instrument, within and between one analysis to the next [15, 16]. The RSD is expressed in the form of a percentage, and a value of 5% or lower has been accepted to indicate good instrument precision, although this value varies across a wide range of analysis [15]. Generally, the closer the value of the % RSD is to 0, the more precise the results [1].

$$\% RSD = \frac{s}{\bar{x}} \times 100 \quad \text{Equation 2.3}$$

where s refers to standard deviation and \bar{x} refers to the mean of x values.

2.2.3 Limit of Detection (LOD) and Limit of Quantitation (LOQ)

Limit of detection (LOD) refers to the point of lowest concentration of the analyte that can be detected and identified by the detector or the lowest concentration that can be distinguished from background noise with a certain degree of certainty (signal-to-noise ratio of 3 is widely accepted [1]), but not necessarily quantitated. Limit of quantitation (LOQ) refers to the lowest concentration of the analyte that can be quantitated with acceptable precision and accuracy, under certain conditions [1-3, 6]. Both LOD and LOQ can be determined through several techniques that all rely on the analysis of standards with known concentrations to establish the minimum level at which the analyte can be reliably detected / quantified [1, 3]. However, LOD is not a reliable indicator for validation as it largely dependent on the detector's sensitivity and is effected by small changes in the analytical system (temperature, purity) [1].

2.2.4 Sensitivity

Often confused with the LOD, sensitivity is a measure of the ability of the analytical method to detect small changes and differences in the mass / concentration of the analyte [1] and can be enhanced by employing a highly sensitive detector.

2.2.5 Accuracy

Accuracy of an analytical method is a measure of the closeness between the known concentration / mass of an analyte to the identified value upon experimentation [1, 2, 6]. It is commonly expressed as a percentage and accessed by calculating the ratio of the reference analyte of known concentrations to the concentration values identified from experimentation. The closer the known and experimental values are, the more accurate the analytical method.

2.2.6 Linearity

Linearity refers to a range of detectability that facilitates a directly proportional relationship between the response and the concentration of the analyte in the sample [1-3, 6]. It can be determined by injecting five or more known concentrations of standards at increasing levels to generate a calibration curve. From the calibration curve, the Goodness of Fit test is conducted to determine the regression / correlation

coefficient (r) that in turn governs the linearity of the results [1]. A value of 0.999 is often expected as a criteria of linearity and provides a conclusion that the results are highly linear [1, 2].

2.2.7 Peak shape

Peak shape can be assessed in terms of its resolution and asymmetry. Peak resolution (R_s) gives a quantitative measurement as to the degree of separation between two adjacent peaks, taking into consideration the mean peak width at the base (Equation 2.4) [2, 17, 18]. When the calculated R_s gives a value of one or above, a conclusion that the peaks are well separated from one another can be deduced.

$$R_s = \frac{(tr)_B - (tr)_A}{\frac{(wb)_A + (wb)_B}{2}} \quad \text{Equation 2.4}$$

where,

tr_A is the retention time of peak A,

tr_B is the retention time of peak B,

wb_A is the width at the base of peak A,

and wb_B is the width at the base of peak B

Peak asymmetry (A) measures peak tailing (T), a term used to express the deviation or skewness of a peak from its ideal symmetrical shape, which usually occurs when compounds have high affinity for the stationary phase of the column [18]. Peak tailing renders the process of quantification more difficult and less accurate as the skewed peak shape makes it problematic to access where the peak ends [2]. It is calculated by dividing the right (b) and left (a) halves of the peak width at 10% of the peak height (Equation 2.5).

$$A = \frac{b}{a} \quad \text{Equation 2.5}$$

An ideal peak shape is expected when the value of A is one [9]. When the value exceeds one, the peak is said to be tailing, whereas with values below one, the peak is said to be fronting. Generally, A values between 0.9-2 is recommended [2].

2.2.8 Band Broadening

Band broadening (HETP) is a condition that causes unwanted spreading of an analyte as it journeys through the column [19]. This phenomenon reduces the efficiency of the column and chromatographic separation, leading to poor resolution, reduced quality and accuracy of the results obtained [11, 19]. In 1956, J. J. Van Deemter introduced an equation (The Van Deemter Equation) to illustrate the major factors effecting band broadening [19] as detailed in Equation 2.6 and Equation 2.7, respectively [11].

$$HETP = A + \frac{B}{\bar{u}} + C\bar{u} + D\bar{u} \quad \text{Equation 2.6}$$

where,

$$\bar{u} = \frac{L}{t_m} \text{ cm/s} \quad \text{Equation 2.7}$$

where,

HETP is the height equivalent to a theoretical plate,

A is the Eddy diffusion,

B is the molecular diffusion in the mobile phase,

C is the resistance to mass transfer in the stationary phase,

D is the resistance to mass transfer in the mobile phase,

\bar{u} is the average linear carrier gas velocity,

L is the column length,

and t_m is the time spent in the mobile phase

Eddy diffusion (A) is facilitated through non-homogenous column packaging that allows analytes travelling within a band, to deviate from its original path into various directions, leading to band broadening [19]. It's effect can be reduced by ensuring the use of a tight and uniformly packed narrow column and small stationary phase particles (internal diameter of 2-4 mm) [20]. Molecular diffusion (B) occurs when a concentration gradient is established in the mobile phase [19, 20]. This causes the band of analytes to diffuse from highly concentrated areas to low concentrated areas, dispersing in every direction. To prevent the concentration gradient to develop in the

system, the use of a tightly packed column and a high mobile phase flow rate is recommended. (C) and (D) occur from mass transfer, where (C) refers to the diffusion of analytes in the stationary phase while (D) refers to the rate at which analytes travel through the mobile phase between contacts with the stationary phase [19, 20]. Both are formed due to the porousness of the stationary phase and the high flow rate of the mobile phase. Analytes can get stuck deep into the pore of the stationary phase, or at the surface of the pore or do not enter at all and this causes the analytes to be held up at different durations, causing band broadening and variation in elution time. It can be fixed by reducing the diameter of the particles in the stationary phase and applying lower carrier gas flow rates. Band broadening can be effectively reduced by minimising the values of (A), (B), (C) and (D) and optimising \bar{u} .

2.3 Methodology Validation: Generation and Extraction of Pyrolysis Products using Passive Headspace Adsorption with Activated Carbon Strip (ACS)

One of the most common extraction techniques utilised for fire debris analysis is passive headspace extraction with activated carbon strip (ACS) [17, 21]. This extraction system is simple, direct and useful for the detection of a wide range of volatile compounds, however various experimental parameters have to be optimised based on the chemistry of the sample of interest, in order for the extraction technique to work most efficiently.

Two of these parameters include temperature and extraction time. A number of studies have been conducted to identify the optimum temperature and adsorption time for ACS, and various propositions have been made based on the different type of samples used [22-26]. Dietz [23] proposed the application of 90 °C for one hour or at ambient temperature for 24 hours for the extraction of standard accelerant mixture (SAM) while Smith and Warnke [22] identified good diagnostic profiling of petroleum products; 60 °C for two hours for gasoline and 90 °C for four hours for diesel. Newman *et al.* [27] reported that temperatures below 60 °C were insufficient

to volatilise high molecular weight hydrocarbons of C₁₅ and above. At elevated temperatures but below 90 °C, high molecular weight compounds were easily volatilised, although displacements of lighter hydrocarbons were noted with the increase in heating profiles. They concluded that temperatures above 90 °C should not be attempted as it induced unwanted decomposition and pyrolysis of the sample. This finding is also supported by the ASTM E1412-07 [28]. In terms of extraction time, at elevated temperatures, carbon strips are able to adsorb C₇ to C₁₀ hydrocarbons when exposed for short periods of time; with extended exposures, higher molecular weight hydrocarbons ranging from C₁₄ to C₂₀ were seen to be adsorbed [17, 29]. In order to accommodate all factors, including practicality, an adsorption time between 16 to 24 hours at temperatures between 60 °C to 90 °C is recommended [24]. Stauffer [17] also proposed similar temperature ranges but with an exposure time of 12 to 16 hours. Newman [24] recommended the use of a minimal 8 mm × 8 mm ACS size for efficient extraction whereas Mat Desa [30] identified optimal extraction of ignitable liquids using ACS size of 5 mm × 25 mm.

Most research confirms the ASTM E1412-07 guideline for passive headspace sampling with activated carbon [28], which recommends the use of an ACS of at least 10 mm × 10 mm, incubated at temperatures between 60 °C to 80 °C for 16 to 18 hours. The desorption process suggests eluting the ACS with a suitable solvent such as carbon disulfide, *n*-pentane or diethyl ether before injection into the GC-MS [28]. However, even when using accepted standard methods such as the ASTM E1412-07, undertaking simple validation studies to ensure optimisation to the specific matrix under test is advisable [24, 25, 31-36].

2.4 Experimental Methods

2.4.1 Preparation of the Grob Test Mixture

A known standard mixture containing 14 high purity 99% analytical grade hydrocarbon compounds (BDH Chemicals and Sigma, UK) was prepared; the compounds were toluene (C₇H₈), octane (C₈), 1,4-dimethyl-benzene / *p*-xylene (C₈H₁₀), 3-ethyl-toluene / *m*-ethyl-toluene (C₉H₁₂), 2-ethyl-toluene / *o*-ethyl-toluene (C₉H₁₂), 1,2,4-trimethyl-benzene (C₉H₁₂), decane (C₁₀), undecane (C₁₁), dodecane

(C₁₂), tetradecane (C₁₄), pentadecane (C₁₅), hexadecane (C₁₆), octadecane (C₁₈) and eicosane (C₂₀). The range of compounds detailed above was chosen as they were present consistently in the pyrolytic work conducted by Agu [46] on porcine bone (of which this study was an extension).

Each compound was prepared as a separate 100 mg/mL standard stock solution in pentane (HPLC Grade, VWR International, Leicestershire, UK) using the appropriate weight (solid samples) or volume (liquid samples) of sample based on its density. A 1 mg/mL standard solution containing all 14 compounds was prepared by combining 1 mL from each of the stock solutions and diluting the mixture with pentane in a 100 mL volumetric flask.

2.4.2 GC-MS Experimental Set-Up

The Grob test mixture was analysed with a Hewlett Packard 6890 Series Gas Chromatography (GC) system coupled with a SCAN (scan acquisition mode) operating Hewlett Packard 5973 Mass Selective Detector (MSD) following the ASTM E1387-01 standard method [37]. The GC vial containing the Grob mixture was placed in an auto sampler. Three different GC-MS experimental settings were explored, as detailed in Table 2.0, and the setting that produced the best separation and chromatographic output of the Grob mixture was determined to be setting 2.

Table 2.0: Three different GC-MS experimental settings explored

Setting	Injector Temperature (°C)	Oven Ramping				
		Initial temperature (°C)	Duration (min)	Ramping Rate (°C/min)	Final temperature (°C)	Duration (min)
1	200	30	3	10	260	1
2	250	40	5	15	280	2
3	300	50	7	20	300	3

The instrument was then set-up according to the optimised parameters in setting 2. The injector was set at 250 °C with 1 µL of sample being injected into the GC. A split ratio of 20:1 was applied to the instrument with a split flow of 32.7 mL/min. Helium was used as a carrier gas, flowing at a constant rate of 1 mL/min. The column employed in this experiment was a 128-0122 DB-1MS column (25 m × 0.2 mm inner diameter and 0.33 µm film thickness). The initial oven temperature was set

at 40 °C and held for 5 minutes before ramping at 15 °C/min to 280 °C, and held for 2 minutes. The detector was maintained at 250 °C. The MS Quad was set at 150 °C and the Ion Source (70eV) at 230 °C. The chromatographic system was controlled with a Hewlett Packard Chemstation software to facilitate data acquisition, peak integration and data manipulation. To ensure optimal functions of the instrument, weekly tuning of the mass spectrometer (MS) with perfluorotributylamine (PFTBA) and an air and water check were conducted. MS tuning values with an isotopic ratio of 1:4:10 and the air and water check values of less than 5% were maintained throughout the experimental work.

The Grob test mixture was inserted into six GC vials (Agilent, UK) and each one injected once into the GC. The peak response, in terms of peak area, was assessed for each compound to determine peak resolution, asymmetrical values, mean, standard deviation and RSD values in order to assess the instrument's precision.

2.4.3 Validation of ACS Recovery Method using Porcine Bone as a Test Sample

Pig bones were chosen as a substitute for human sample as previous research suggested that there are substantial similarities between the two in terms of the bone anatomy, morphology, physiology and remodelling characteristics [38-43]. Pigs also share similar internal anatomy and fat distribution to humans [44, 45].

2.4.3.1 Preparation of the Bone Samples

Long pork bones were obtained from The Country Shop, Glasgow, Scotland, UK on a weekly basis to ensure the freshness of the bones. The bones were taken from animals aged less than six months, and were labelled according to the date obtained and stored in the laboratory freezer. The bones were left to defrost naturally at room temperature for 30 to 40 minutes before sample preparation. Once defrosted, each bone was held securely in a bench vice and a hacksaw was used to cut off the epiphysis on both ends of the bone. The epiphysis was removed to reduce variation in bone composition that might affect the repeatability and reproducibility of the extraction process. Any remaining soft tissue on the bone was removed with scissors

and tweezers. The diaphysis of the bone was cut into varying weights of approximately 15 g, 20 g and 25 g, ± 1.50 g in each case. Each bone fragment was then placed in a 125 mL tin can (WA Products, UK) with its lid removed. Empty tin cans and unused ACS strips were also sampled and analysed as control samples. Results showed that the tin cans and ACS did not generate any contaminants that could interfere with the pyrolysis study.

2.4.3.2 Pyrolysis of Bone Samples using the ACS Process

Pyrolysis of the bone sample

As a starting point, a tin can containing approximately 15 g of pork bone was attached to a retort stand and the can was heated over a Bunsen flame until the ignition of fat occurred (Figure 2.0).

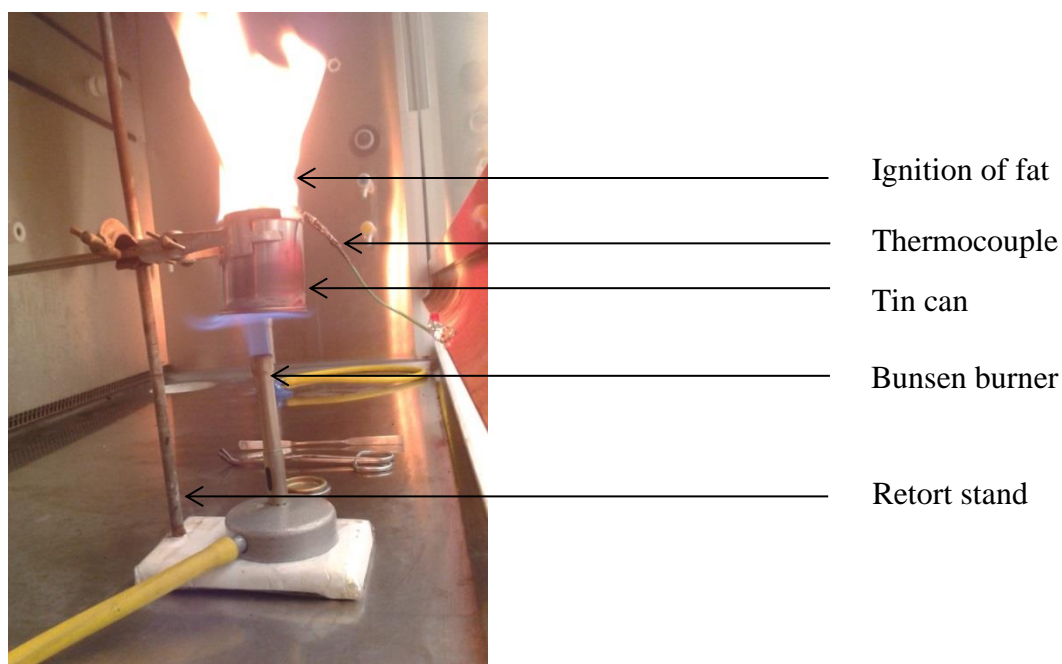


Figure 2.0: Experimental set-up for the generation of pyrolysis products

The temperature in the headspace of the tin (above sample) was monitored using a k thermocouple linked to a PicoLog TC-08 data logger (Pico Technology Limited, UK) connected to a laptop computer, (suspended at the headspace of the sample) to facilitate temperature recording per second. The sample was occasionally agitated with a spatula to help facilitate the ignition process. Once ignited, the sample was

allowed to burn for 5 minutes. The Bunsen flame and the thermocouple were removed ten seconds before the lid was placed on the tin causing the flame to extinguish.

2.4.3.3 Extraction of Pyrolysis Products from Bone Samples using the ACS Process

Optimisation of the pyrolysis and ACS extraction process

The passive headspace ACS extraction methodology utilised in this experiment was based on the experimental design developed by Agu [46], and adapted from the ASTM E1412-07 [28]. The lid was removed from the tin 1 minute after extinguishment and was immediately sealed with another lid to which four ACS of different sizes: 5 mm × 20 mm, 10 mm × 20 mm, 8 mm × 8 mm and 10 mm × 10 mm (ACS, 3M Corporation, USA) were attached. This entire process was repeated four times with different post-deprivation sampling times, defined as the time the sample was allowed to cool after extinguishment before a lid containing the ACS was used to seal the tin, which were 2 minutes, 3 minutes, 4 minutes and 5 minutes, respectively. The entire process was then repeated for the other two sample weights of bone samples (20 g and 25 g).

Once the tins were sealed with the lids bearing the ACS, they were left to incubate in an oven for 16 hours at 80 °C. During this period, pyrolysis products undergo volatilisation and are adsorbed onto the ACS. After 16 hours, the ACS were removed from the lid and placed in a GC vial (Agilent, UK) to be desorbed with 1 mg/mL of pentane (HPLC grade, WVR International, Leicestershire, UK) containing 0.5 mg/mL of tetrachloroethylene, C₂Cl₄ (Sigma, UK) as the internal standard. Tetrachloroethylene was chosen as the internal standard as it does not interfere with the analysis and elutes approximately in the middle of the chromatogram [47, 48]. The GC vials containing the desorbed strips were then analysed using the GC-MS methods detailed in section 2.4.2.

Figure 2.1 illustrates the extraction process post-pyrolysis and Table 2.1 gives a summary of the factors accessed in the optimisation of the pyrolysis and ACS extraction process.



ACS hooked to a paper clip held
by a magnet on the lid

Lid with ACS used to seal tin
containing pyrolysed sample

Incubate for 16 hours at 80
°C in an oven

Desorb with 1 mL of pentane
containing 0.5 mg/mL of C_2Cl_4

Analyse with GC-MS

Figure 2.1: Schematic representation of passive headspace diffusion extraction technique with ACS-GC-MS

Based on the number and consistency of chromatographic peaks obtained upon extraction and analysis, an optimised sample weight, and the most productive post-deprivation sampling time and ACS size was determined. Following this, six intra-variation (within tin) and inter-variation (between tins) repeat extractions and analysis were conducted on the optimised factors, to determine the repeatability and reproducibility of the pyrolysis and extraction system. Identification of the consistently appearing peaks across both inter- and intra-variation repeats was also conducted. Table 2.2 summarises the inter- and intra-variation repeat extractions and analysis conducted upon the optimisation of the pyrolysis and ACS extraction process.

Table 2.2: Summary of the inter- and intra-variation repeat experiments for the optimisation of the pyrolysis and ACS extraction process

Sample weight (g)	Optimised weight
ACS size (mm)	X
Post-deprivation sampling time (min)	Y
Inter-variation repeats	6X × 6
Intra-variation repeats	1X × 6

2.5 Results and Discussion

2.5.1 Assessment of GC-MS Instrumental Performance

To determine instrumental performance and precision, responses from six injections of the same Grob test mixture injected into six individual vials were assessed. Mean, standard deviation and RSD values across six injections were calculated from the peak area of the GC-MS output for each of the 14 compounds within the test mixture. Table 2.3 tabulates the compounds represented in the chromatogram according to their retention time, peak asymmetric factor, standard deviation and RSD values and Figure 2.2 illustrates a chromatographic display of all 14 components as a function of their retention time and abundance.

Table 2.3: Average retention time and peak area, peak asymmetric factor, standard deviation and relative standard deviation values from the retention time and peak area of 14 compounds present in the standard test mixture ($n=6$)

No	Compound	Peak Asymmetric Factor	Average Retention Time (min)	Retention Time (min)		Average Peak Area	Peak Area	
				STDEV	% RSD		STDEV	% RSD
1	toluene	0.83	4.11	0.006	0.16	5890265	40883.6	0.69
2	C ₈	1.08	5.60	0.005	0.10	3618659	40459.7	1.12
3	<i>p</i> -xylene	1.00	7.04	0.004	0.10	4048835	66823.9	1.65
4	<i>m</i> -ethyl toluene	1.07	8.73	0.003	0.04	3978513	77610.9	1.95
5	<i>o</i> -ethyl toluene	1.02	8.99	0.001	0.01	3117945	55310.3	1.71
6	1,2,4-trimethylbenzene	1.10	9.22	0.001	0.01	2172208	40984.8	1.89
7	C ₁₀	1.02	9.50	0.004	0.00	4192505	76184.0	1.82
8	C ₁₁	1.23	10.75	0.001	0.00	3367776	58329.9	1.73
9	C ₁₂	1.35	11.83	0.001	0.00	2251762	47899.0	2.13
10	C ₁₄	0.67	13.71	0.000	0.00	1914764	59397.4	3.10
11	C ₁₅	1.36	14.56	0.001	0.00	3747416	79076.5	2.11
12	C ₁₆	0.92	15.35	0.003	0.02	3538918	129434.2	3.66
13	C ₁₈	1.06	16.82	0.001	0.01	28906305	1006188.0	3.48
14	C ₂₀	1.05	18.00	0.002	0.01	29397841	878360.0	2.99

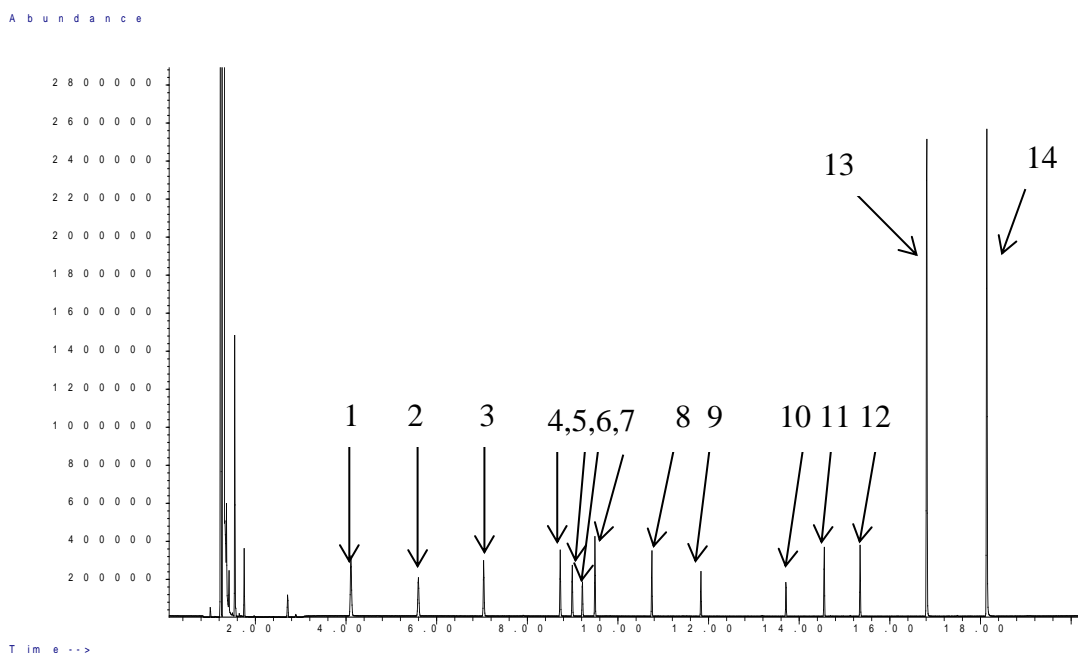


Figure 2.2: Chromatogram of 1 mg/mL of standard Grob mixture

From Table 2.3, the peak asymmetric factor values reveal that most of the peaks experienced very slight tailing or fronting, with values fluctuating between 0.67 and 1.36. These slight variations from the ideal peak shape were within an acceptable range with indications of good chromatographic response [49].

Excellent repeatability and reproducibility in terms of the retention time and response / peak areas across six injections of the Grob mixture was observed with retention time % RSD values in the range of 0.00-0.16% and peak area % RSD values within the range of 0.69%-3.66%. All 14 compounds were fully resolved from one another and appear consistently at specific time intervals, demonstrating excellent separation (Figures 2.2 and 2.3).

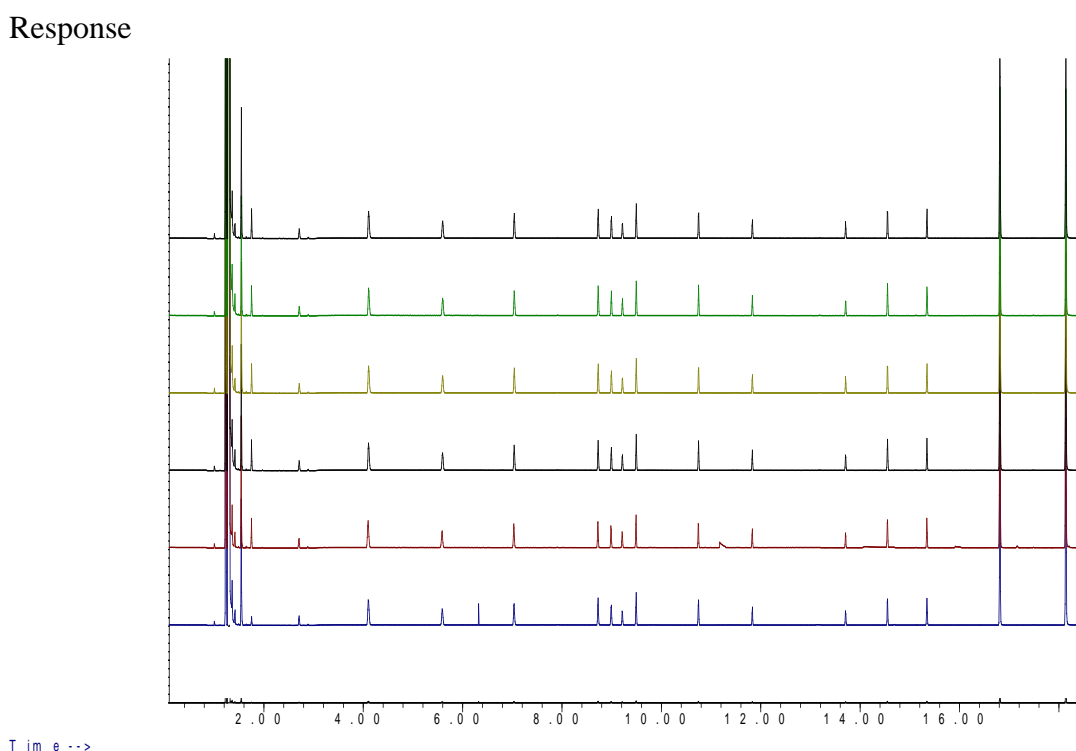


Figure 2.3: Overlay of six chromatograms with each representing individual injections of the standard Grob mixture

2.5.2 Pyrolysis of the Porcine Samples

Three different weights of porcine bone were selected and systematically analysed. This occurred in two phases;

Initially, the porcine samples were prepared and analysed using the method adapted from ASTM E1412-07 [28] in order to elucidate the nature of the pyrolysis products obtained and the temperature profile of the process.

Secondly, once the pyrolysis profile of the bone samples was established, the pyrolysis process and ACS extraction method were further refined and finally optimised using different sample sizes, post-deprivation sampling times and ACS sizes. The influence of each variable was identified and discussed. The results obtained in this section were used as a basis for further experimental work explored in this study.

2.5.2.1 Temperature Profile of Bone Samples

An illustration of the temperature profiles of porcine bone samples of different weights (15 g, 20 g and 25 g) is presented in Figure 2.4.

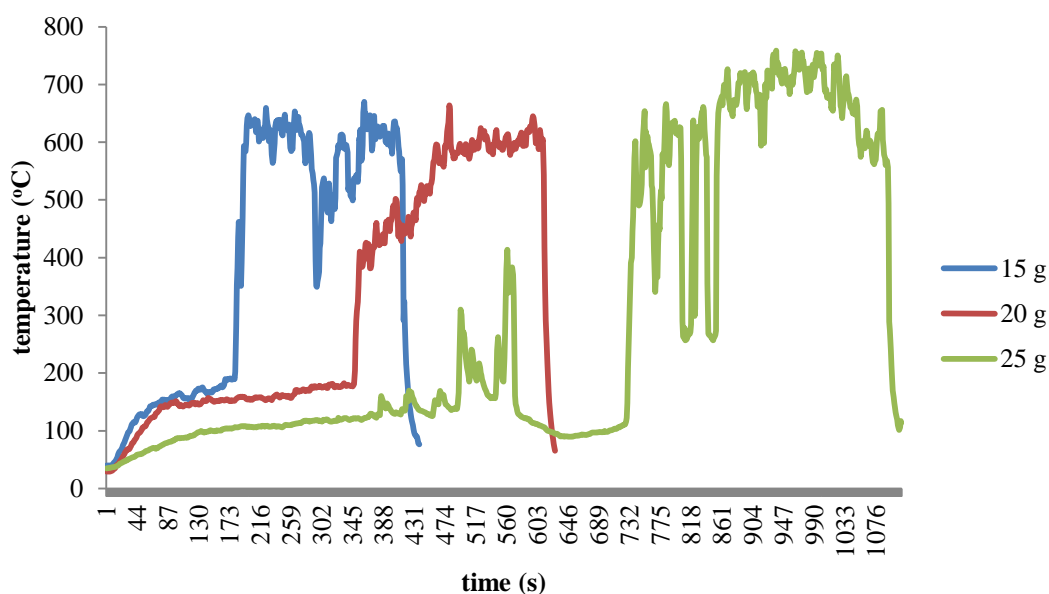


Figure 2.4: Temperature profiles from initial heat application up to five 5 minutes post-ignition across 15 g, 20 g and 25 g bone samples

Each temperature profile exhibits an initial rise in temperature to approximately 100 °C as the flame of the Bunsen burner impinges on the base of the tin. Once the temperature reaches approximately 200 °C, volatile components derived from the fatty components associated with the bone sample were noted to auto-ignite and flames were observed rising from the bone sample within the tin. As fats melt at relatively low temperatures [40], auto-ignition of fat at these temperature ranges (200 °C to 250 °C) is expected and has been documented in previous studies [50], although in some cases higher auto-ignition temperatures were suggested (300 °C to 355 °C [39, 46]).

Auto-ignition was evidenced by the rapid rise in temperature of the sample. Across the 15 g, 20 g and 25 g samples, the lightest sample auto-ignited within the shortest timeframe (at 169 seconds) followed by the 20 g sample (at 337 seconds) and finally the heaviest sample (at 715 seconds). This indicates that variation in sample weight directly affects the time taken for the sample to auto-ignite and corroborates the outcome observed by Agu [46]. Sample sizes of less than 15 g were found to produce little or no pyrolysis products under the experimental condition outlined. Similar findings were also reported by Agu [46] under the same experimental conditions.

Once auto-ignition occurred, the temperatures in each case rose rapidly to between 650 °C to 750 °C. If left undisturbed, the flames would burn continuously for a period of time as long as there was a steady supply of melted fat (fuel) from the sample. In this study, the flames burnt for between 5 and 10 minutes post-ignition depending on the sample weight before self-extinguishing. As expected flames from the 15 g sample self-extinguished quickest, followed by the 20 g sample and finally the 25 g sample. This is because larger bone samples contain larger amounts of fats in comparison to smaller samples and, hence, are able to generate more melted fat to fuel the flames for longer.

Within this work, the flames were extinguished within 5 minutes after ignition as Agu [46] suggested that no pyrolysis products were recovered if the samples were allowed to continuously burn and self-extinguish. Agu further suggested that the

length of time for which a sample was allowed to burn affected the pyrolysis products being generated and suggested an optimum burning time of 5 minutes to be the best time for the generation of detectable pyrolysis products [46].

2.5.2.2 Identification of Best Sample Weight, Post-Deprivation Sampling Time and ACS Size

For each sample weight, the total ion chromatogram (TIC)s were used to identify peaks that consistently appeared across six repetitive experiments. Peaks that did not appear consistently across the repetitive experiments were discarded. An example of the TICs for 15 g, 20 g and 25 g sample extracted using ACS 5 mm × 20 mm at 4 minutes post-deprivation time is illustrated in Figure 2.5. The total peak area and total number of consistently appearing peaks within each chromatogram as a function of the sample weight was calculated and plotted against both the ACS sizes and the post-deprivation sampling times and are presented in Figures 2.6 and 2.7, respectively.

Figure 2.6 clearly demonstrates that 25 g of pork bone (Figure 2.6(c)) was the best weight to generate pyrolysis products of considerably large total peak areas as compared to the 15 g (Figure 2.6(a)) and 20 g (Figure 2.6(b)) samples. Similarly, Figure 2.7 also establishes that sample weights of 25 g (Figure 2.7(c)) produced more pyrolysis products, with detection possible of up to 80 peaks as compared to 15 g (Figure 2.7(a)) and 20 g (Figure 2.7(b)) samples that produced an average of 65 to 68 peaks, respectively. Further experimentation with larger sample weights (> 25 g) was not conducted as the 125 mL tin cans could not accommodate larger sample sizes.

With the optimised sample weight identified, a closer look at both 25 g sample weight graphs (Figure 2.6(c) and Figure 2.7(c)) illustrated that the best achievable way to generate reproducible results were by allowing the 25 g sample to cool for 4 minutes post-deprivation and extracting with an ACS of 10 mm × 20 mm. A representative chromatogram of these optimised parameters is illustrated in Figure 2.8.

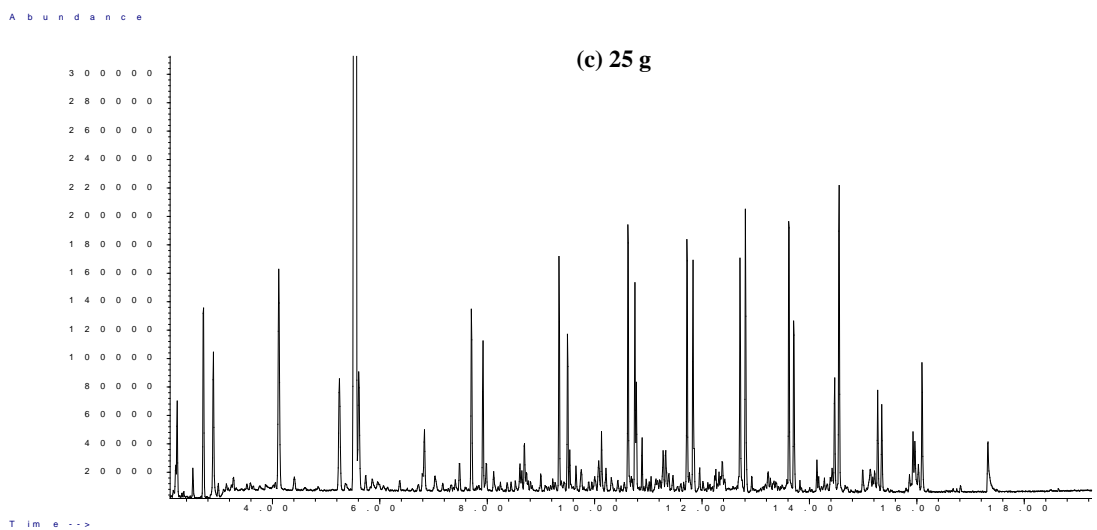
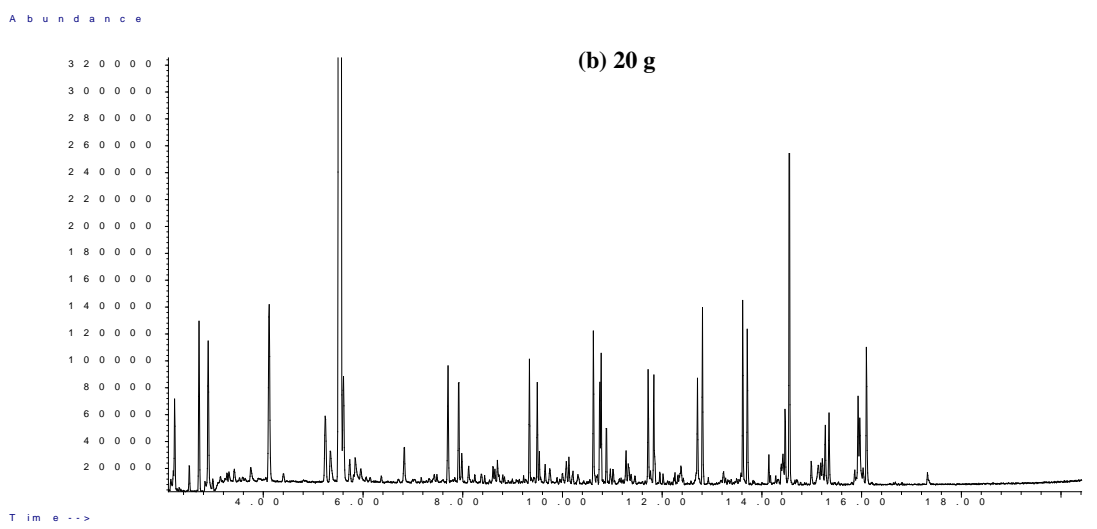
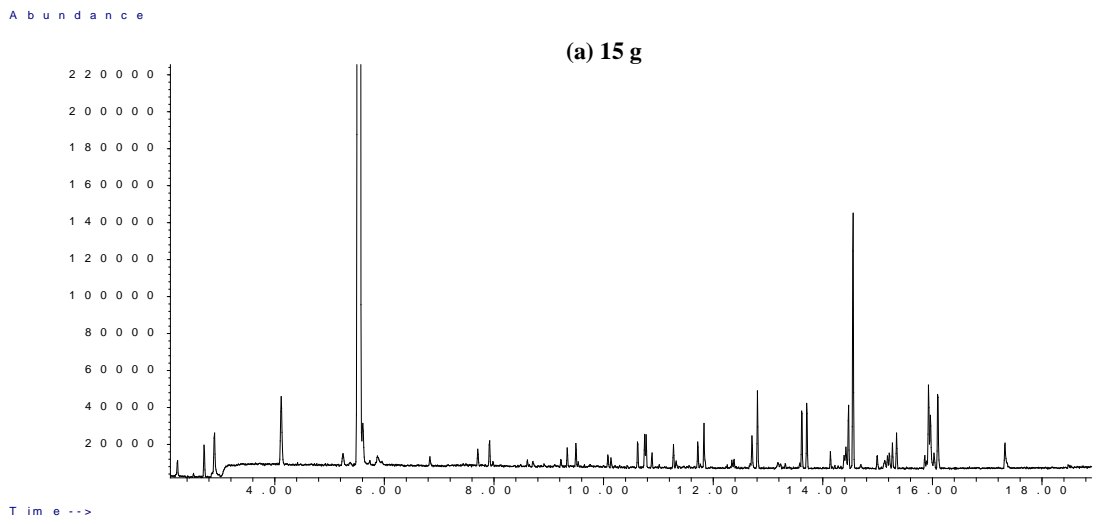
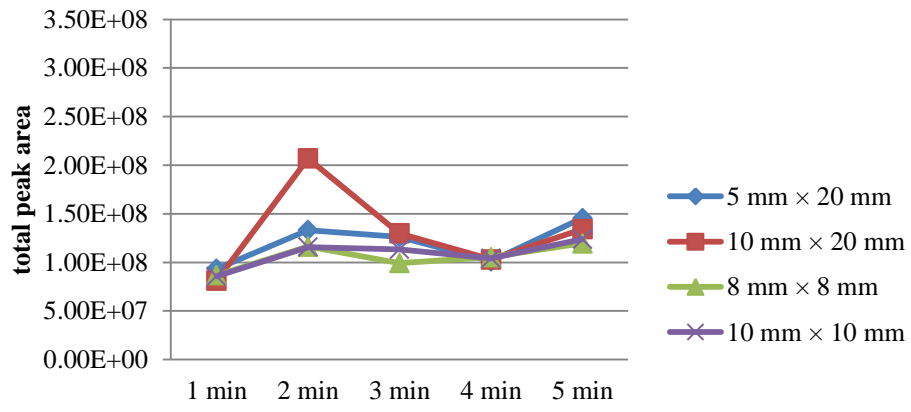
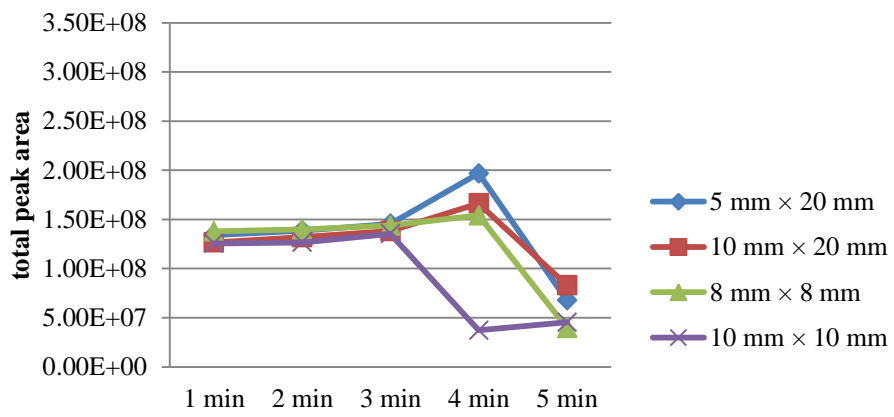


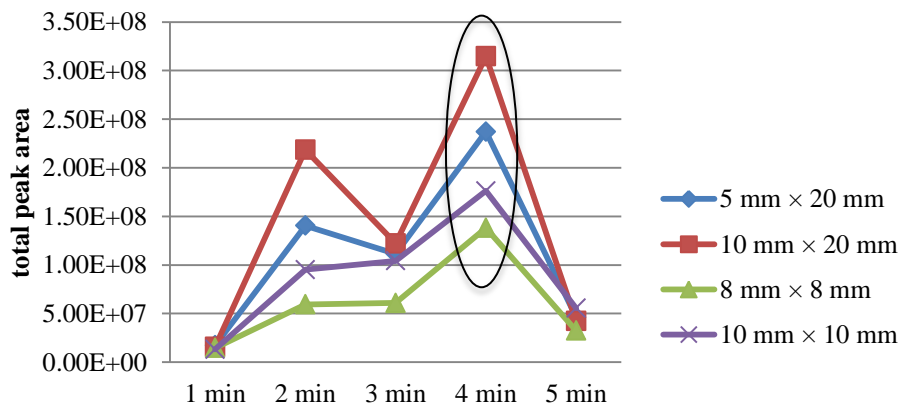
Figure 2.5: Individual TICs for (a) 15 g, (b) 20 g and (c) 25 g sample extracted using ACS of 5 mm × 20 mm at 4 minutes post-deprivation sampling time



post-deprivation sampling time
15 g
(a)



post-deprivation sampling time
20 g
(b)



post-deprivation sampling time
25 g
(c)

Figure 2.6: Post-deprivation sampling times (1 to 5 minutes) plotted against total peak area for (a) 15 g, (b) 20 g and (c) 25 g of pork bone samples across four ACS sizes (5 mm × 20 mm, 10 mm × 20 mm, 8 mm × 8 mm and 10 mm × 10 mm)

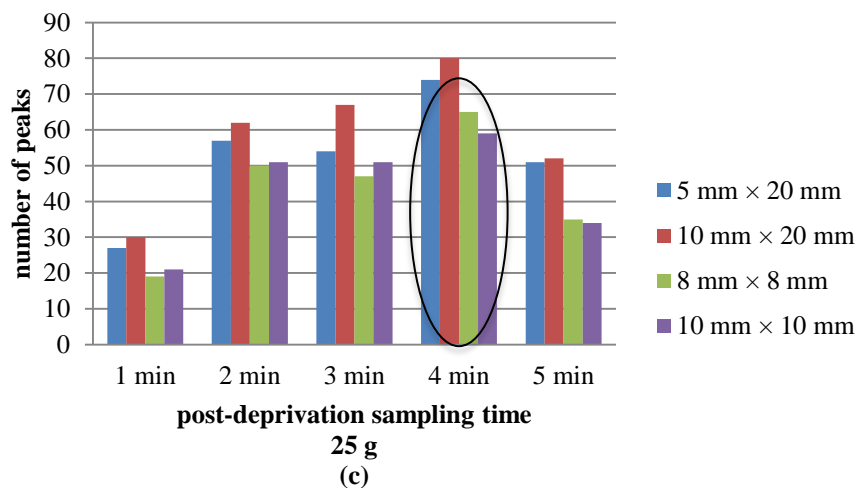
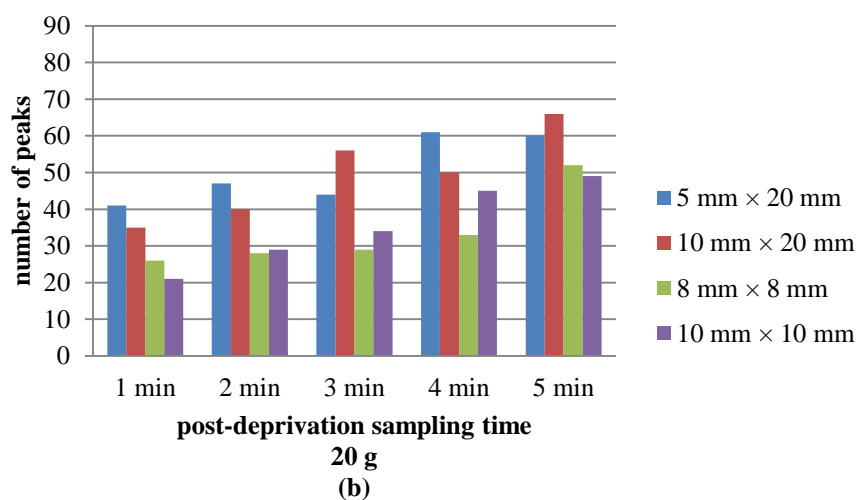
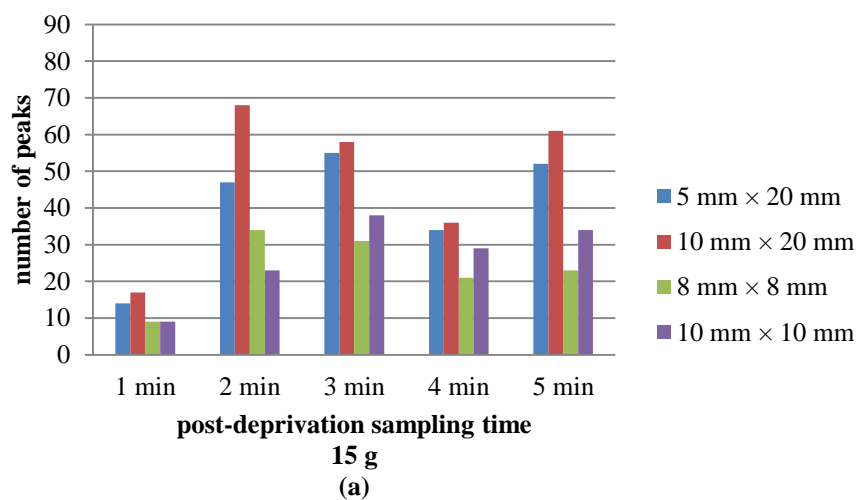


Figure 2.7: Post-deprivation sampling times (1 to 5 minutes) plotted against the number of peaks for (a) 15 g, (b) 20 g and (c) 25 g of pork bone samples across four ACS sizes (5 mm × 20 mm, 10 mm × 20 mm, 8 mm × 8 mm and 10 mm × 10 mm)

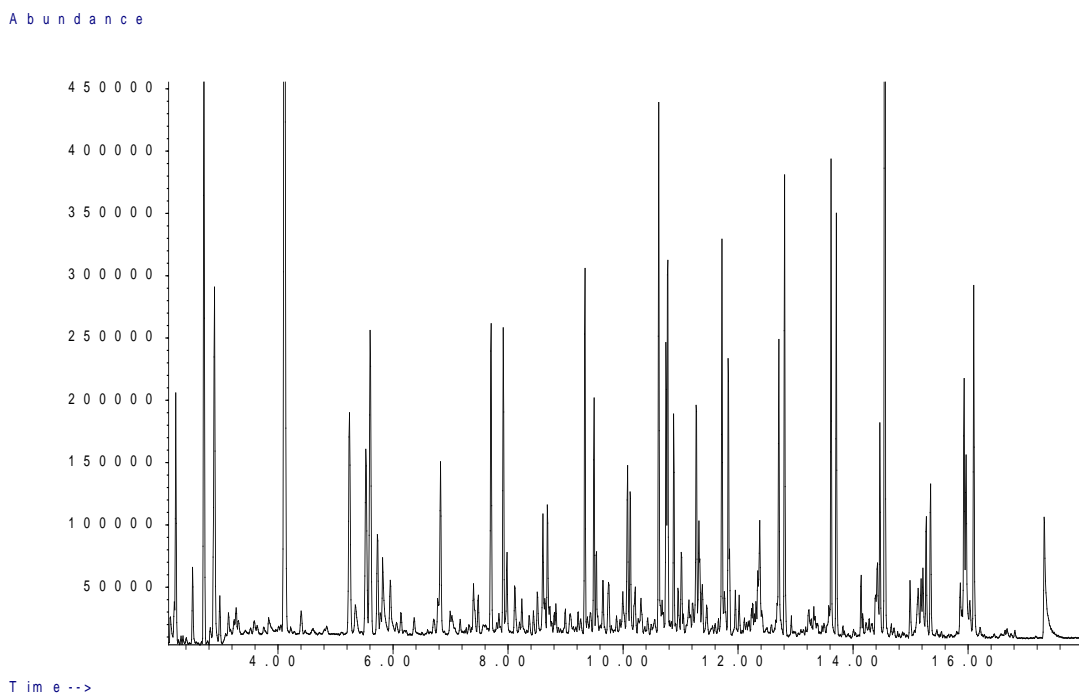


Figure 2.8: A representative chromatogram of the optimised parameters - 25 g pyrolysed bone sampled at 4 minutes post-deprivation sampling time using an ACS of 10 mm × 20 mm

2.5.2.3 Identification of Peaks in the Total Ion Chromatogram (TIC)

Using the optimised conditions detailed previously, the total ion chromatograms (TIC)s generated as a result of GC analysis were scrutinised for the identification of peaks that appeared consistently across the six repeat pyrolysis and extractions. Peaks that did not appear consistently across the six repeats are detailed in Appendix 1.0. In total, 26 peaks appeared in all six repetitive extractions, both in the inter- and intra-variation repeats. The National Institute of Standards and Technology (NIST) library and standard mixtures were utilised to identify the peaks based on their retention times and m/z values. Based on the peak areas of these repetitive peaks, peak area % RSD values were calculated for both inter- and intra-variation repeats as detailed in Tables 2.4 and 2.5, respectively. These % RSD values were then used to assess the analytical method's precision: repeatability and reproducibility. An overlay of the TICs of the inter- and intra-variation repeats are presented in Figures 2.9 and 2.10, respectively and the 26 peaks labelled in Figure 2.11.

Table 2.4: Peak area % RSD calculations for 26 peaks and an internal standard across the six intra-variation repeats. * I.S. refers to the internal standard

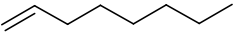
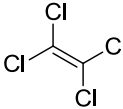
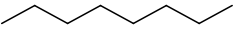
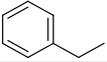
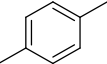
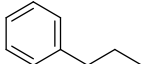
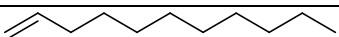
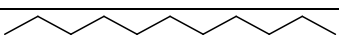
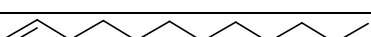
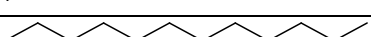
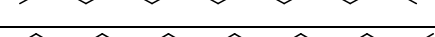
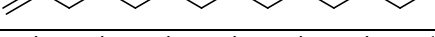
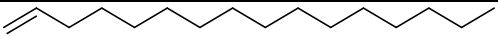
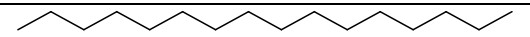
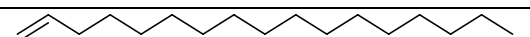
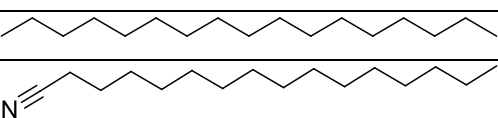
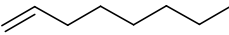
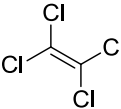
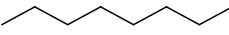
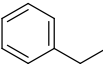
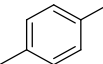
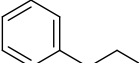
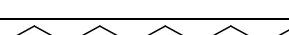
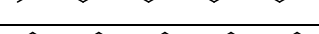
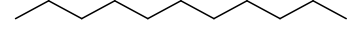
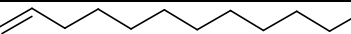
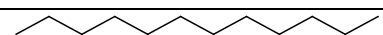
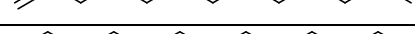
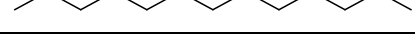
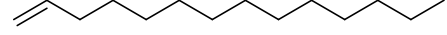
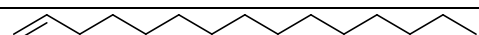
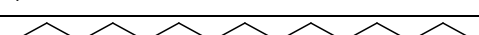
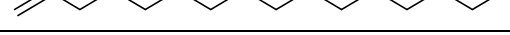
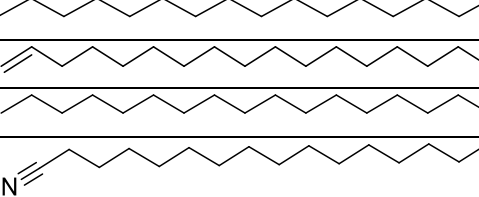
No	Retention Time (min)	Compound	Molecular Structure	% RSD
1	2.22	benzene		60.1
2	4.11	toluene		44.3
3	5.24	1-octene		36.7
4	5.52	tetrachloroethylene (I.S.*)		3.1
5	5.60	octane		24.4
6	6.82	ethyl-benzene		65.5
7	6.94	<i>p</i> -xylene		68.8
8	7.70	1-nonene		25.8
9	7.91	nonane		44.6
10	8.61	propyl-benzene		39.4
11	9.33	1-decene		28.4
12	9.49	decane		53.2
13	10.62	1-undecene		24.5
14	10.75	undecane		65.1
15	11.72	1-dodecene		72.1
16	11.83	dodecane		40.5
17	12.70	1-tridecene		33.7
18	12.81	tridecane		38.5
19	13.61	1-tetradecene		45.5
20	13.70	tetradecane		33.3
21	14.47	1-pentadecene		58.9
22	14.55	pentadecane		56.6
23	15.21	1-hexadecene		63.6
24	15.34	hexadecane		41.6
25	15.92	1-heptadecene		49.9
26	16.10	heptadecane		63.9
27	17.32	hexadecanitrile		78.9

Table 2.5: Peak area % RSD calculations for 26 peaks and an internal standard across the six inter-variation repeats. * I.S. refers to the internal standard

No	Retention Time (min)	Compound	Molecular Structure	% RSD
1	2.22	benzene		63.8
2	4.11	toluene		57.2
3	5.24	1-octene		37.5
4	5.52	tetrachloroethylene (I.S.*)		3.3
5	5.60	octane		27.2
6	6.82	ethyl-benzene		78.1
7	6.94	<i>p</i> -xylene		81.7
8	7.70	1-nonene		23.1
9	7.91	nonane		52.2
10	8.61	propyl-benzene		42.5
11	9.33	1-decene		26.6
12	9.49	decane		57.1
13	10.62	1-undecene		21.9
14	10.75	undecane		63.4
15	11.72	1-dodecene		46.3
16	11.83	dodecane		46.0
17	12.70	1-tridecene		32.7
18	12.81	tridecane		37.0
19	13.61	1-tetradecene		46.3
20	13.70	tetradecane		41.7
21	14.47	1-pentadecene		60.7
22	14.55	pentadecane		57.9
23	15.21	1-hexadecene		58.2
24	15.34	hexadecane		46.1
25	15.92	1-heptadecene		83.5
26	16.10	heptadecane		68.3
27	17.32	hexadecanitrile		81.2

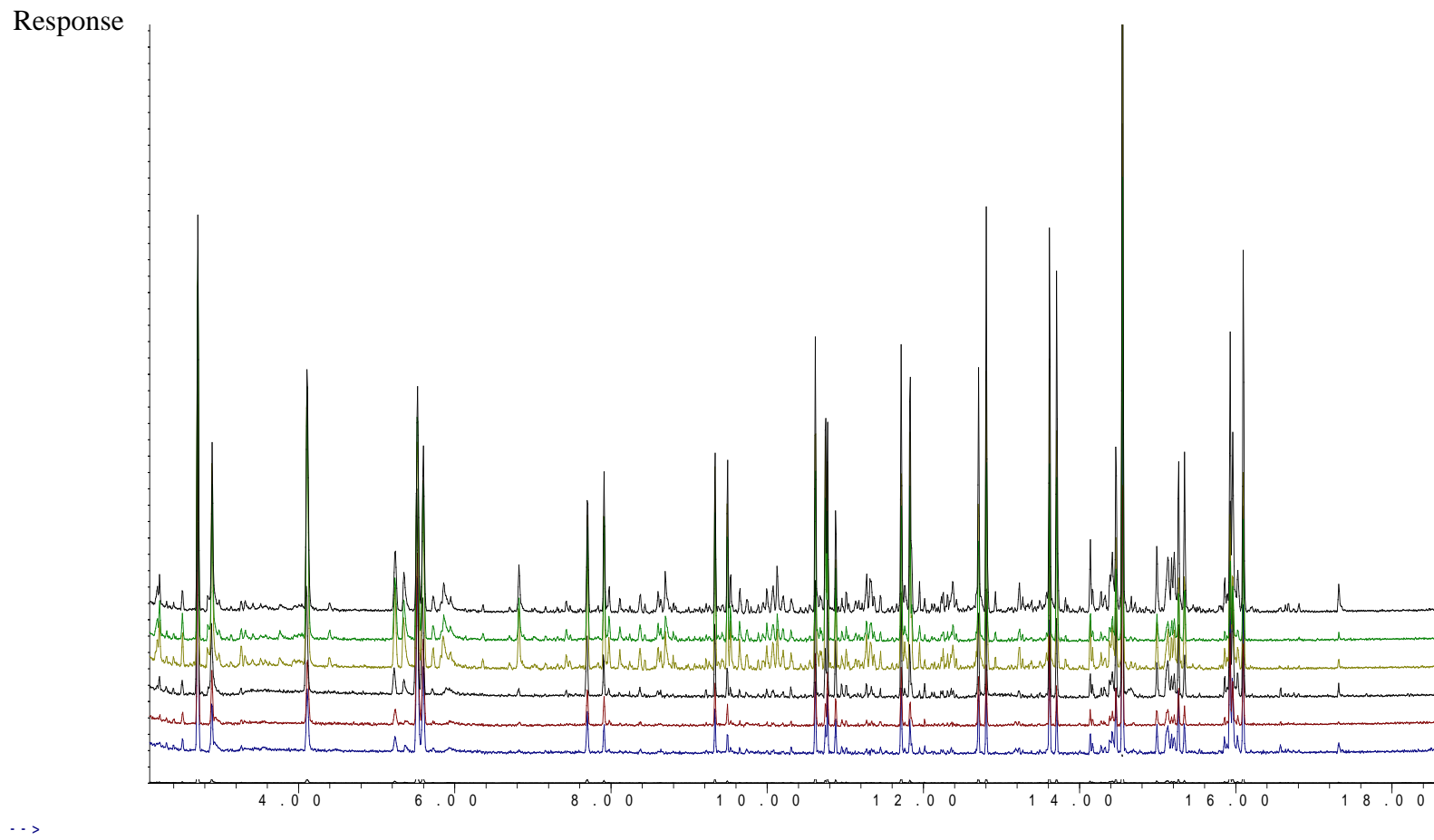


Figure 2.9: Intra sample variation - overlay of six TICs generated from the same 25 g pyrolysed bone sampled at 4 minutes post-deprivation sampling time using a 10 mm × 20 mm ACS

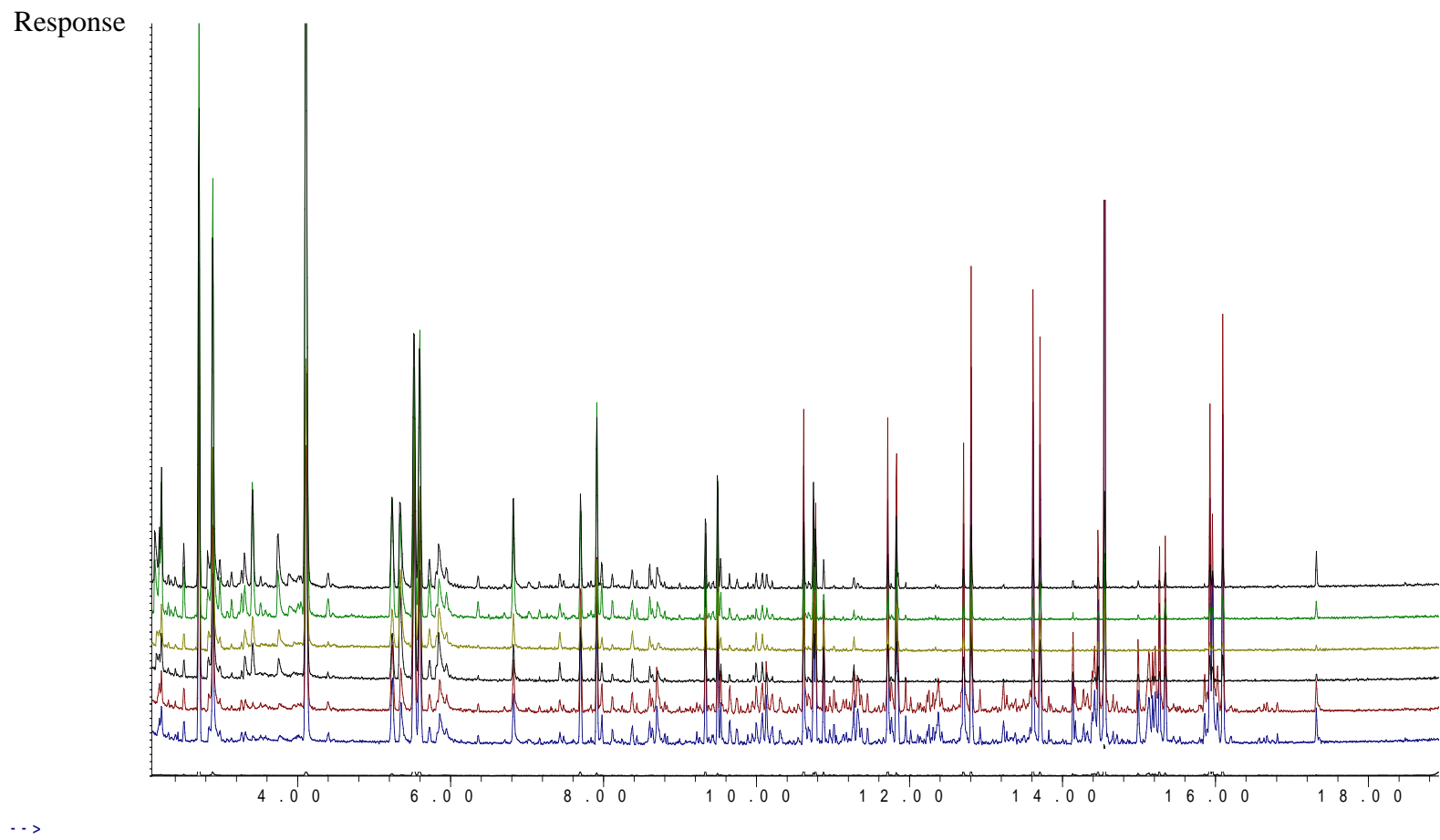


Figure 2.10: Inter sample variation - overlay of six TICs generated from different 25 g pyrolysed bone sampled at 4 minutes post-deprivation sampling time using a 10 mm × 20 mm ACS

Abundance

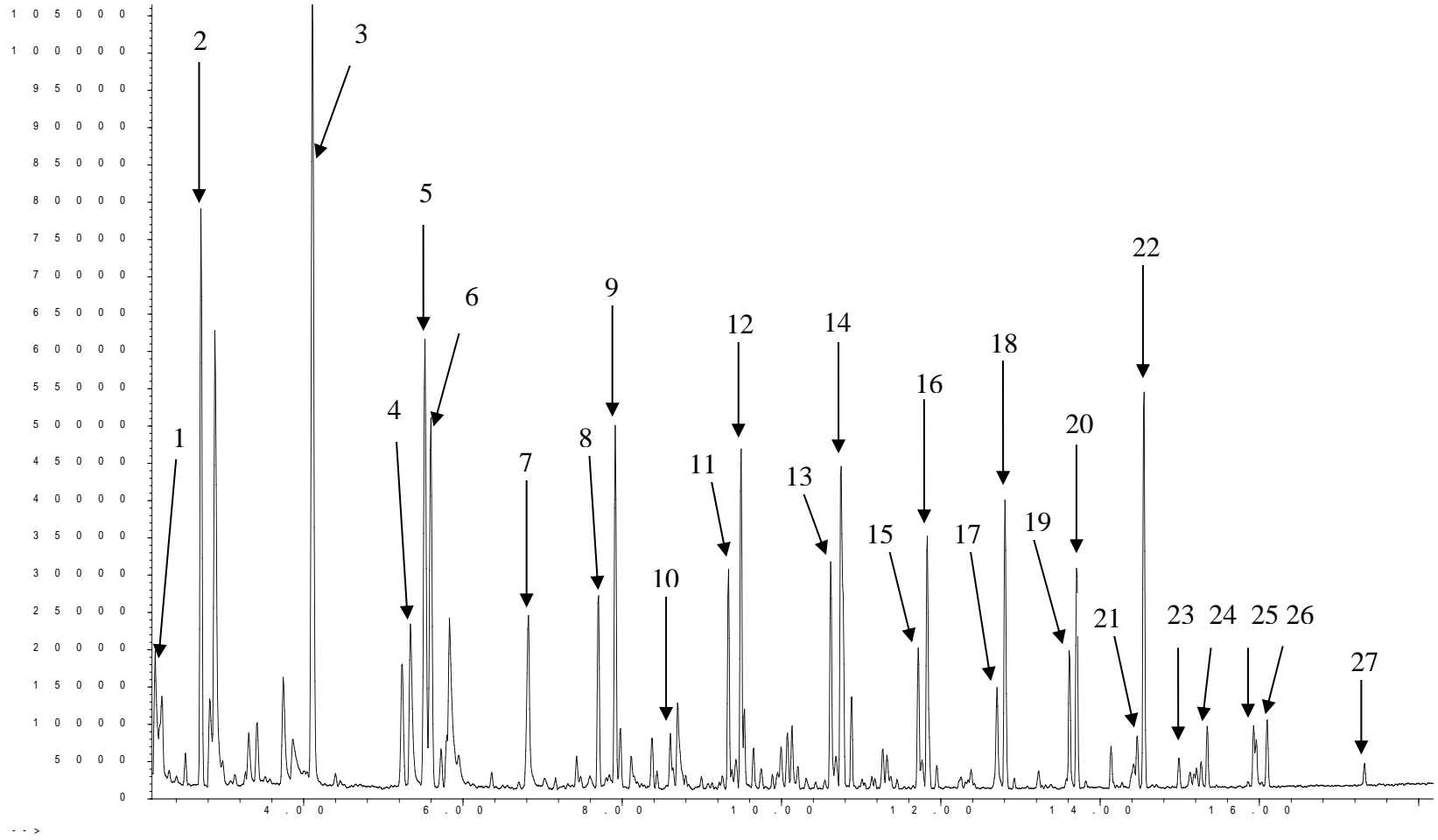


Figure 2.11: A representative TIC of pyrolysed porcine bone consisting 26 repeatable pyrolysis products and an internal standard (4) represented in the form of retention time labelled peaks

From Tables 2.4 and 2.5, the main peaks that consistently appear across the porcine bone samples are the C₈ to C₁₇ *n*-alkanes and *n*-alkenes together with some aromatics, *n*-alkyl-benzenes and a nitrile. However, no *n*-aldehydes were revealed. Similar results were noted by Purevsuren *et al.* [51] in his study on the pyrolysis of cattle bone whereby the presence of *n*-alkanes, *n*-alkenes, aromatics and nitriles were noted with the absence of *n*-aldehydes. Pyrolysed triglyceride oil (fats) studies have also documented the presence of predominant species of *n*-alkanes and *n*-alkenes with no *n*-aldehydes [52]. Agu [46] also reported similar results to this study. This is contrary to DeHaan *et al.* [39] and McLellan [53] who detected *n*-aldehydes including *n*-pentanal, *n*-hexanal and 3-methyl-butanal in burnt pork tissues. DeHaan *et al.* [39] also identified the presence of C₅ to C₁₅ aldehydes together with some straight and branched-chain *n*-alkenes and *n*-alkanes, aromatic, unsaturated and cyclic hydrocarbons from pyrolysed porcine fat. While isomers of *n*-alkenes, methyl-alkane nitriles and alkane nitriles, *n*-cycloalkanes and *n*-cycloalkanes, dienes, alkyl-pyrroles, *n*-alkyl-benzenes and substituted alkyl-benzenes, aromatics, substituted benzenes, cyano-alkene, disulfide, an alkyne and a ketone were detected, although inconsistently from porcine bone pyrolysis (Appendix 1.0), the absence of *n*-aldehydes in this study can be due to a variety of factors, including variation in experimental methodology, temperatures attained and exposure durations during the burning process; all of these factors were further explored.

Similar pyrolysis products to those of porcine fat have been documented from the combustion of polyethylene [39, 54]. This can cause interferences in the positive identification of animal or human remains at a fire scene. DeHaan *et al.* [39] suggested the use of a limited range of pyrolysis compounds and variation in peak ratios to distinguish polyethylene and porcine samples. The pyrolysis of polyethylene produced higher ranges of *n*-aldehydes of up to C₂₃, whereas the combustion of porcine fat produced *n*-aldehydes within the range of C₁₅ to C₁₈. In terms of peak ratio for polyethylene, *n*-alkenes are said to produce the highest peak ratio followed by *n*-alkanes, dienes and *n*-aldehydes in descending order. Similar *n*-alkene peak ratios were also produced by porcine fat; however, the distinguishing factor lies in the ratio of *n*-alkanes and *n*-aldehydes that were relatively proportional to each other with little or no presence of diene. Although the pyrolysis of polyethylene produced

similar *n*-alkanes, *n*-alkenes and light *n*-alkyl-benzenes as pyrolysed bone fat, it can be identified by the presence of high amounts of pyridines, pyrroles, amides and alkyl-nitriles – compounds that were not present (consistently) from bone fat pyrolysis [54].

The % RSD values for peak area documented in Tables 2.4 and 2.5, respectively are relatively high for almost all peaks except for the internal standard with 3.1% and 3.3% for the intra- and inter-variation repeats, respectively. The fact that the RSD values of the internal standard were relatively low indicates the column was functioning with good precision across the six inter- and intra-variation repeats. The other pyrolytic peaks with high RSD values indicate that the quantity / abundance of the 26 pyrolysis products varied across the repeats. Similar results were also noted in the pyrolysis studies conducted by Agu [46] and DeHaan *et al.* [39]. The variations in the abundance of pyrolysis products generated can be due to various factors such as oxygen availability, diaphysis variation and temperatures attained during the auto-ignition period. Agitation of the sample was also used to speed up the auto-ignition process and this would vary from sample to sample. Variation in the fat content from one bone diaphysis to another or within the same diaphysis can also influence the abundance of products detected. Besides this, temperatures attained during the auto-ignition process also varied for samples of similar weights, 25 g, ranging from 650 °C to 750 °C (Figure 2.12).

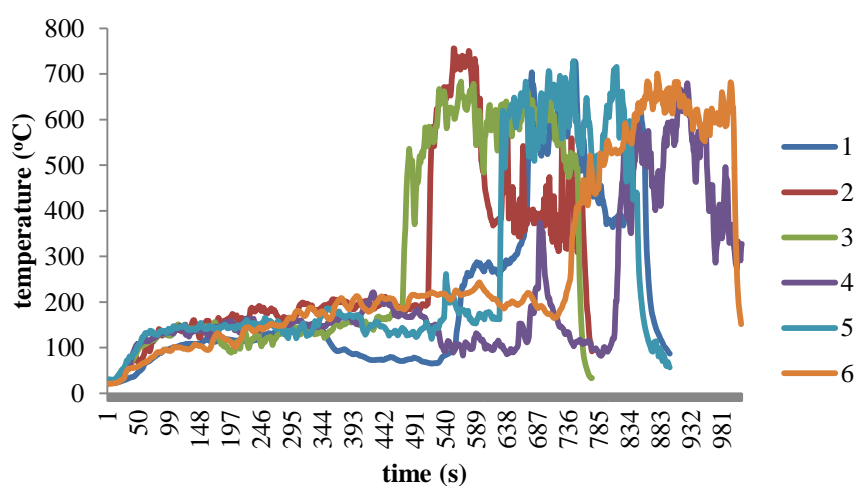


Figure 2.12: Temperature profiles of six 25 g bone samples combusted at similar environmental conditions

These factors are believed to differ from one burning to the other even though samples were combusted in the same fume hood with similar air flow and placed at consistent distance from the Bunsen flame. With regards to the dynamic nature of fire, these phenomena are very much expected as fires are rarely reproducible and almost always vary significantly in their combustion profiles. Thus, quantitative reproducibility in terms of the abundance of pyrolysis products is rarely observed [39].

2.6 Conclusions

A series of experiments conducted to determine the column's performance and instrument precision has demonstrated that the chosen GC-MS instrument and method were suitable to carry out the experimental analysis required for this study. The experimental procedure for the generation of pyrolysis products from porcine bone has been validated and proven to generate reproducible and optimal pyrolysis products of C₈ to C₁₇ *n*-alkanes and *n*-alkenes, *n*-alkyl-benzenes, aromatics and a nitrile from sample weight of 25 g sampled at 4 minutes post-deprivation with a 10 mm × 20 mm ACS strip size.

2.7 References

1. Laboratory and Scientific Section (LSS), United Nations Office on Drugs and Crime, *Guidance for the Validation of Analytical Methodology and Calibration of Equipment Used for Testing of Illicit Drugs in Seized Materials and Biological Specimens*. 2009. United Nations Office on Drugs and Crime, Vienna: Austria.
2. Ng, L.L., *Reviewer Guideline: Validation of Chromatographic Methods*. 1994, Center for Drug Evaluation and Research, Food and Drug Administration (FDA). p. 669-671.
3. Huber, L., *Validation of Analytical Methods*. 1998, LC-GC International: Agilent Technologist.
4. Yilmaz, B. and Arslan, S., *Development and Validation of GC-MS Method for Determination of Metoprolol in Human Urine*. *Journal of Chromatographic Science*, 2010. **48**(8): p. 613-617.
5. Boumrah, Y., Rosset, M., Lecompte, Y., Bouanani, S., Khimeche, K., and Dahmani, A., *Development of a Targeted GC/MS Screening Method and Validation of an HPLC/DAD Quantification Method for Piperazines–Amphetamines Mixtures in Seized Material*. *Egyptian Journal of Forensic Sciences*, 2014. **4**(3): p. 90-99.
6. Gambaro, V., Benvenuti, C., Ferrari, L.D., Dell'acqua, L., and Farè, F., *Validation of a GC/MS Method for the Determination of Tramadol in Human Plasma after Intravenous Bolus*. *II Farmaco*, 2003. **58**(9): p. 947-950.
7. Meyer, M.R., Welter, J., Weber, A.A., and Maurer, H.H., *Development, Validation, and Application of a Fast and Simple GC–MS Method for Determination of Some Therapeutic Drugs Relevant in Emergency Toxicology*. *Therapeutic Drug Monitoring*, 2011. **33**(5): p. 649-653.
8. Wang, G., Vincent, M., Rodrigues, W., Agrawal, A., Moore, C., Barhate, R., Abolencia, E., Coulter, C., Soares, J., and Zheng, Y-F., *Development and GC-MS Validation of a Highly Sensitive Recombinant G6PDH-Based Homogeneous Immunoassay for the Detection of Buprenorphine and*

- Norbuprenorphine in Urine*. Journal of Analytical Toxicology, 2007. **31**(7): p. 377-382.
9. LC-GC Chromacademy, *Quantitative & Qualitative HPLC*. 2014, LC-GC CHROMacademy: Duluth, USA.
 10. Grob Jr, K., Grob, G., and Grob, K., *Comprehensive, Standardized Quality Test for Glass Capillary Columns*. Journal of Chromatography A, 1978. **156**(1): p. 1-20.
 11. Stafford, D.T., *Forensic Gas Chromatography*, in Gas Chromatography in Forensic Science, ed. I. Tebbett. 1992, England, UK: Ellis Horwood.
 12. Ewg, I.M. *ICH Harmonised Tripartite Guideline: Validation of Analytical Procedures Text and Methodology Q2(R1)*, in International Conference on Harmonisation of Technical Requirements for the Registration of Pharmaceuticals for Human Use. 2002.
 13. Scott, K., Chromatography Online: *Quantitative Chromatographic Analysis - Peak Area Measurements from Quantitative Chromatographic Analysis*. [Online] [January 2014, January 2015]. Available from: <http://www.chromatography-online.org/quant/Chromatographic%20Data/Data%20Processing/Peak%20Area%20Measurements.php>.
 14. Agilent Technologies Inc., *Fundamentals of Liquid Chromatography (HPLC)*, in HPLC Basis. 2014, Agilent Technologies Inc., p. 2-37.
 15. Miller, J.N. and Miller, J.C., *Statistics and Chemometrics for Analytical Chemistry*. 6th Edition. 2005: Prentice Hall. 268.
 16. Cojocariu, C., Silcock, P., and Kotz, A., *Validation of GC-MS/MS for Detection and Confirmation of Low-Level Dioxins*. 2014, Thermo Fisher Scientific: California, USA.
 17. Stauffer, E., Dolan, J.A., and Newman, R., *Fire Debris Analysis*. 2008, San Diego, USA: Academic Press.
 18. McNair, H.M. and Miller, J.M., *Basic Gas Chromatography*. 2nd Edition. Vol. 2. 2009, Hobokwn, New Jersey: John Wiley and Sons.
 19. LCGC's CHROMacademy: Crawford Scientific, *Band Broadening*, in The Theory of HPLC. 2014.

20. Stafford, D.T., *Forensic Gas Chromatography in Gas Chromatography in Forensic Science*, in *Gas Chromatography in Forensic Science*, ed. J. Robertson. 1992, Chicago, USA: Ellis Horwood Limited.
21. Pert, A.D., Baron, M.G., and Birkett, J.W., *Review of Analytical Techniques for Arson Residues*. *Journal of Forensic Sciences*, 2006. **51**(5): p. 1033-1049.
22. Smith, E.T. and Warnke, M.M., *Arson Analysis by Static Headspace Enrichment and Gas Chromatography Using Simplex Optimization*, in *Pittsburgh Conference on Analytical Chemistry and Applied Spectroscopy (Pittcon)*. 2003. Orlando, Florida.
23. Dietz, W.R., *Improved Charcoal Packaging for Accelerant Recovery by Passive Diffusion*. *Journal of Forensic Sciences*, 1991. **36**(1).
24. Newman, R.T., Dietz, W.R., and Lothridge, K., *The Use of Activated Charcoal Strips for Fire Debris Extractions by Passive Diffusion. Part 1: The Effects of Time, Temperature, Strip Size, and Sample Concentration*. *Journal of Forensic Science*, 1996. **41**(3): p. 361-370.
25. Massey, D., Du Pasquier, E., and Lennard, C. *Optimisation of Fire Debris Analysis with DFLEX[®]*, in *Proceedings of the International Association of Forensic Science*. 2002. Montpellier, France.
26. Bertsch, W. and Ren, Q., *The Chemical Analysis of Fire Debris for Potential Accelerants*, in *Handbook of Analytical Separations*. Elsevier Science: New York, 2000. **2**: p. 617-678.
27. Newman, R., *Modern Laboratory Techniques Involved in the Analysis of Fire Debris Samples*, in *Fire Investigation*, ed. N. Nic Daied. 2004, Boca Raton, Florida: CRC Press.
28. ASTM International E1412-07, *Standard Practice for Separation of Ignitable Liquid Residues from Fire Debris Samples by Passive Headspace Concentration with Activated Charcoal*. 2012. American Society for Testing and Materials (ASTM) International: West Conshohocken, PA.
29. Nic Daeid, N., *An Introduction to Fires and Fire Investigation*, in *Fire Investigation*, ed. N. Nic Daeid. 2004, Boca Raton, Florida: CRC Press.
30. Mat Desa, W.N.S., *The Discrimination of Ignitable Liquids and Ignitable Liquid Residues Using Chemometric Analysis*, in *Centre for Forensic Science*,

Department of Pure and Applied Chemistry. 2012, Univeristy of Strathclyde: Glasgow, Scotland.

31. Lentini, J.J. and Armstrong, A.T., *Comparison of the Eluting Efficiency of Carbon Disulfide with Diethyl Ether: The Case for Laboratory Safety*. Journal of Forensic Sciences, 1997. **42**: p. 307-311.
32. Frontela, L., Pozas, J.A., and Picabea, L., *A Comparison of Extraction and Adsorption Methods for the Recovery of Accelerants from Arson Debris*. Forensic Science International, 1995. **75**(1): p. 11-23.
33. Demers-Kohls, J.F., Ouderkirk, S.L., Buckle, J.L., and Norman, W.E., *Evaluation of the DFLEX[®] Device for Fire Debris Analysis*. Journal Canadian Society of Forensic Science, 1994. **27**: p. 99-99.
34. Dolan, J., *Recent Advances in the Applications of Forensic Science to Fire Debris Analysis*. Analytical and Bioanalytical Chemistry, 2003. **376**(8): p. 1168-1171.
35. Waters, L.V., and Palmer, L.A., *Multiple Analysis of Fire Debris Samples Using Passive Headspace Concentration*. Journal of Forensic Sciences, 1993. **38**: p. 165-165.
36. Massey, D., Pasquier, E.D., and Lennard, C., *Solvent Desorption of Charcoal Strips (DFLEX[®]) in the Analysis of Fire Debris Samples: Replacement of Carbon Disulfide*. Canadian Society of Forensic Science Journal, 2002. **35**(4): p. 195-208.
37. ASTM International E1387-01, *Standard Test Method for Ignitable Liquid Residues in Extracts from Fire Debris Samples by Gas Chromatography*. 2002. American Society for Testing and Materials (ASTM) International: West Conshohocken, PA.
38. Pearce, A.I., Richards, R.G., Milz, S., Schneider, E., and Pearce, S.G., *Animal Models for Implant Biomaterial Research in Bone: A Review*. European Cells and Materials, 2007. **13**: p. 1-10.
39. Dehaan, J.D., Brien, D.J., and Large, R., *Volatile Organic Compounds from the Combustion of Human and Animal Tissue*. Science and Justice, 2004. **44**(4): p. 223-236.

40. Dehaan, J.D., Campbell, S.J., and Nurbakhsh, S., *Combustion of Animal Fat and Its Implications for the Consumption of Human Bodies in Fires*. Science and Justice, 1999. **39**: p. 27-38.
41. Hillier, M.L. and Bell, L.S., *Differentiating Human Bone from Animal Bone: A Review of Histological Methods*. Journal of Forensic Sciences, 2007. **52**(2): p. 249-263.
42. Thorwarth, M., Schultze-Mosgau, S., Kessler, P., Wiltfang, J., and Schlegel, K.A., *Bone Regeneration in Osseous Defects Using a Resorbable Nanoparticulate Hydroxyapatite*. Journal of Oral and Maxillofacial Surgery, 2005. **63**(11): p. 1626-1633.
43. Raab, D.M., Crenshaw, T.D., Kimmel, D.B., and Smith, E.L., *A Histomorphometric Study of Cortical Bone Activity During Increased Weight Bearing Exercise*. Journal of Bone and Mineral Research, 1991. **6**(7): p. 741-749.
44. Catts, E.P. and Goff, M.L., *Forensic Entomology in Criminal Investigations*. Annual Review of Entomology, 1992. **37**(1): p. 253-272.
45. Anderson, G.S. and Vanlaerhoven, S.L., *Initial Studies on Insect Succession on Carrion in Southwestern British Columbia*. Journal of Forensic Sciences, 1996. **41**: p. 617-625.
46. Agu, K., *Investigation of the Thermal Degradation Products of Bone*, in Centre for Forensic Science, Department of Pure and Applied Chemistry. 2011, University of Strathclyde: Glasgow, Scotland.
47. Hubschamann, H-J., *Handbook of GC/MS: Fundamentals and Applications*. Vol. 2. 2009, Weinheim: Wiley-VCH Verlag GmbH and Co.
48. Walbridge, J. and Keifer, K., *GC-MS Tuning Solutions, Internal and Surrogate Standard*, Sigma Aldrich Co. 2014, USA.
49. Dolan, J.W., *Peak Tailing and Resolution*. LCGC Asia Pacific, 2005. **5**(3): p. 430-437.
50. Babrauskas, V., *Ignition Handbook*. 2003, Issaquah WA: Fire Science Publishers. p. 1116.

51. Purevsuren, B., Avid, B., Gerelmaa, T., Davaajav, Y., Morgan, T.J., Herod, A.A., and Kandiyoti, R., *The Characterisation of Tar from the Pyrolysis of Animal Bones*. *Fuel*, 2004. **83**(7–8): p. 799-805.
52. Lima, D.G., Soares, V.C., Ribeiro, E.B., Carvalho, D.A., Cardoso, Ã.R.C., Rassi, F.V.C., Mundim, K.C., Rubim, J.C., and Suarez, P.A., *Diesel-Like Fuel Obtained by Pyrolysis of Vegetable Oils*. *Journal of Analytical and Applied Pyrolysis*, 2004. **71**(2): p. 987-996.
53. Mcllellan, S.A., *An Investigation of the Volatiles Produced from Pyrolysis of the Body*, in Centre for Forensic Science, Department of Pure and Applied Chemistry. 1999, University of Strathclyde: Glasgow, Scotland.
54. Purevsuren, B., Avid, B., Narangerel, J., Gerelmaa, T., and Davaajav, Y., *Investigation on the Pyrolysis Products from Animal Bone*. *Journal of Materials Science*, 2004. **39**(2): p. 737-740.

CHAPTER 3: THE EFFECTS OF TEMPERATURE AND TIME OF EXPOSURE ON THE PYROLYTIC PROFILE DERIVED FROM PORCINE AND HUMAN TISSUES

3.1 Introduction

As pyrolysis is a function of temperature, variation in temperatures applied to a sample would certainly impact the pyrolysis process and the type of pyrolysis products generated. In relation to temperature, pyrolysis is also governed by heat flux, the rate at which heat is transferred per unit area, where shorter burning times would transfer less heat over a unit of sample. This could in turn alter the pyrolytic profile generated from the burning material. Besides temperature, the type of tissue that undergoes pyrolysis could also experience different thermal decomposition processes that could alter the pyrolysis profile generated. In the analysis of pyrolysis products from porcine samples in Chapter 2 (2.5.2.3), no *n*-aldehydes were detected from burnt porcine bones, although they were detected consistently in other studies [1, 2]. This variation in the pyrolytic profile could be due to one or all of the above-mentioned parameters.

In this chapter, the sample generation process is systematically altered to explore the full range of chemical products derived from the sample matrix. This included testing different variables: temperature, tissue type and exposure duration. These variables were altered systematically to ascertain if any of them influenced the generated of *n*-aldehydes in particular and, if so, which influenced the product generation to the greatest degree.

When subjected to heat, *n*-aldehydes undergo thermal decomposition to form various products depending on the type of aldehyde. For example, at 450 °C to 600 °C, acetaldehyde breaks down to form carbon monoxide and methane, whereas propionaldehyde generates similar products along with ethane [3]. Table 3.0 also shows that common aldehydes evaporate at relatively moderate temperatures of 209 °C and below. In a typical fire scene, temperatures would certainly supersede 209 °C

and have been documented to typically reach 900 °C and above [4]. At these temperature ranges, the detection of *n*-aldehydes from human or animal samples would certainly be very challenging and problematic as the *n*-aldehydes would likely decompose and break down at temperatures above their boiling points. Table 3.0 also illustrates some of the commonly encountered aldehydes and their properties.

Table 3.0: Structure, boiling point and polarity of commonly encountered *n*-aldehydes. Adapted from [5],[6] and [7].

Aldehyde	Structure	Boiling Point (°C)	Solubility in Water
Formaldehyde / Methanal		- 21	Very soluble
Acetaldehyde / Ethanal		21	Very soluble
Propionaldehyde / Propanal		49	Soluble
Butyraldehyde / Butanal		75	Soluble
Pentanal		103	Slightly soluble
Hexanal		129	Insoluble
Heptanal		153	Insoluble
Octanal		171	Insoluble
Nonanal		195	Insoluble
Decanal		209	Insoluble

3.2 Composition of the Human Body

The human body is made up of various organic and inorganic elements that cohere to form cells, tissues, organs and systems. Eleven interactive systems exist in the human body: respiratory, digestive, nervous, cardiovascular, skeletal, endocrine, integument, immune, reproductive, urinary and lymphatic, and they work together to perform various processes and tasks that support normal bodily functions [8].

Water is the major constituent as it makes up 65% to 95% of the human body [9]. The remainder is made up of 10–30% protein, 10% lipids, 5% minerals and 1–2% carbohydrate [10, 11]. Mitchell *et al.* [12] and Forbes *et al.* [13] conducted compositional studies on human bodies and obtained similar results in terms of water and protein proportion in the human body. As a water molecule comprises one oxygen and two hydrogen atoms, oxygen accounts for 65% of all the elements in the

human body by mass, followed by carbon and hydrogen [14]. The other elements include hydrogen, nitrogen, calcium, and phosphorus. Table 3.1 gives an overview of the major and minor elements in the human body and their percentages by mass.

Table 3.1: Major and minor elements in the human body. Adapted from [9].

Element	Percentage by Mass (%)
Oxygen	65
Carbon	18
Hydrogen	10
Nitrogen	3
Calcium	1.5
Phosphorus	1.2
Potassium	0.2
Sulfur	0.2
Chloride	0.2
Sodium	0.1
Magnesium	0.05
Iron, Cobalt, Copper, Zinc, Iodine, Selenium, Fluoride	Trace

The subunits of proteins are carbon, hydrogen, oxygen, nitrogen and phosphorus while some proteins can also contain sulfur. Proteins are the key structural material in the human body and are often described in terms of their molecular structure – fibrous or globular (Table 3.2) [11]. They also make up the majority of the constituents in muscular tissues [10].

Table 3.2: Types of proteins and their functions in the human body. Adapted from [11].

Overall Structure	Function	Examples
Fibrous	Structural framework	Collagen: tensile strength of bones, tendons and ligaments Elastin: durability and flexibility in ligaments Keratin: structural protein for hair and nails
	Movement	Actin and Myosin: contraction in muscle cells
Globular	Catalysis	Protein enzymes: biochemical reaction
	Transport	Haemoglobin: transport of oxygen in blood

Consisting of carbon, oxygen and hydrogen, lipids are the third largest building block of the human body. Lipids can be broken down into triglycerides, phospholipids, steroids and other minor lipid substances (Table 3.3) [11]. Their major function is to provide thermal insulation and mechanical protection from injury, as well as to serve as an energy reservoir for the body. The melting point of a

lipid largely depends on the length of the carbon chain and the level of saturation [15]. Generally, longer, more saturated fats have higher melting points and *vice versa*. Table 3.4 outlines the melting points of some animal fats. Oleic acid, stearic acid and palmitic acid are the common saturated and unsaturated fatty acids found in humans and animals [15]. Oleic acid, an unsaturated fatty acid, is the most prevalent acid found in animal fat. Across all the tissues, adipose contains the highest level of lipids, with up to 60–85% accumulated in adipocytes (fat cells) [16], out of which 90–95% are triglycerides [10, 17].

Table 3.3: Types of lipids and their functions in the human body. Adapted from [11].

Lipid Type	Location and Function
Triglyceride	In fat deposits for insulation, protection and energy source
Phospholipids	In cell membrane for integrity of the membrane
Steroids	
Cholesterol	To manufacture steroids
Sex Hormones	Male and female hormone for reproduction
Other lipids	
Lipoprotein	To transport fatty acid and cholesterol in bloodstream
Eicosanoids	In cell membrane to control uterine contraction, gastrointestinal tract motility, and inflammation responses

Table 3.4: Melting points of fats from pig, cow and lamb. Adapted from [15].

Animal	Melting Point (°C)
Pig	
Back fat	30–40
Leaf fat	43–48
Cow	
External fat	32–43
Kidney fat	40–50
Lamb	
External fat	32–46
Kidney fat	43–51

The monomers of carbohydrates are sugars / glucose that contain carbon, hydrogen and oxygen. The levels of oxygen in these compounds are much higher as compared to lipids and usually follow the 1:2 oxygen:hydrogen ratio. Three types of carbohydrates can be found in the human body and they are monosaccharides, disaccharides and polysaccharides. Their structural representation is displayed in Figure 3.1, Figure 3.2 and Figure 3.3, respectively. Monosaccharides are single units of sugar (glucose) whereas disaccharides are built from a combination of two monosaccharides (maltose). Polysaccharides are polymers of simple sugars linked

together to form long chains (cellulose). The main function of carbohydrates is to provide a readily available energy source to support bodily functions. In excess, they are converted to glycogen and stored in different tissues for future energy supply.

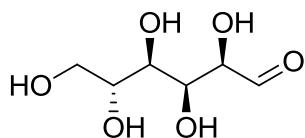


Figure 3.1: Monosaccharide (glucose)

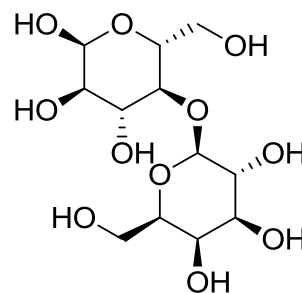


Figure 3.2: Disaccharide (maltose)

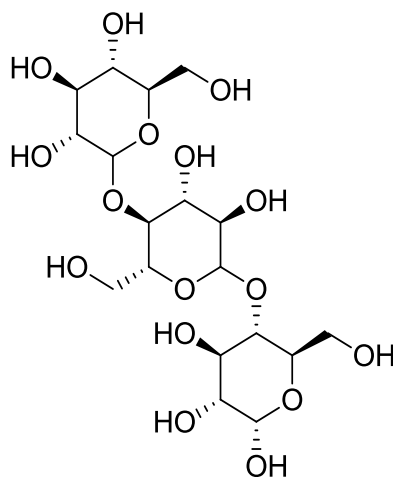


Figure 3.3: Polysaccharide (cellulose)

As different tissues and organs contain various proportions of organic and inorganic elements, it is expected that some parts of the human body are more vulnerable than others to the effects of heat exposure [18, 19]. Certain parts of the body that have greater concentrations of subcutaneous fat, the human body's main fuel in a fire, will readily burn and when subjected to heat, these fats will melt to form a viscous liquid which then auto-ignites, generating flames that burn at very high temperatures [1, 20]. Other parts of the body with high water and protein content and low fat content, take longer to burn or do not burn at all, unless under specific circumstances. However, this also depends on the length of time the body is exposed to the fire [21,

22]. For example, a moderate fuelled fire under normal circumstances would cause severe damage to the torso areas but not to the upper limbs and head, whereas a fire fuelled by ignitable liquid could last longer and attain higher temperatures that could in turn consume more parts of the human body [18, 23]. For the purpose of this work, three types of tissues were examined, bone (described in detail in Chapter 1), rib and muscle.

3.2.1 Structure and Composition of Muscle

In humans, the skeletal muscle accounts for 32%–40% [24] of normal human body weight, whereas in animals, it constitutes a larger percentage range of 35%–65% [15]. Muscles are made up of a collection of muscle fibres (75% to 92%), nerve endings, connective tissues and blood vessels that are bounded together (Figure 3.4). Muscle tissue is composed of 65% to 80% water, 16% to 22% protein, 3% to 13% lipid, 1% to 2% inorganic minerals and 0.5% to 1.5% carbohydrate [15, 16].

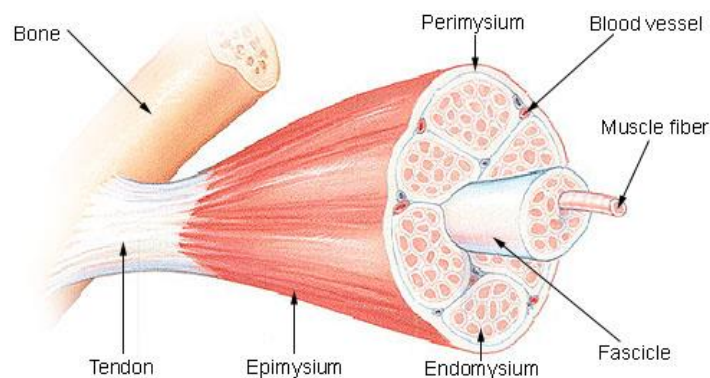


Figure 3.4: Structure of muscle tissues [25]

Proteins that are found in muscle tissues are predominantly myofibrils and sarcoplasmic proteins [15, 16]. Myofibril proteins are characterised as long, thin and cylindrical rods that primarily exist in the form of actin (thin filaments) and myosin (thick filaments). These myofibrils are responsible for the movement and contraction of muscles [26]. Sarcoplasmic protein, such as myoglobin and haemoglobin, exists in the form of pigments and enzymes. They are primarily involved in the transportation and storage of oxygen in the human body [15]. Other proteins such as collagen, elastin and reticulin are also present in muscle tissues but in low amounts.

Lipids are present at low concentrations in muscle tissues, typically below 3%. However, muscles are one of the three major organs (the other two being adipose and liver) that store and hydrolyse fat in a controlled way for internal use or transportation to energy deprived organs (Figure 3.5) [27].

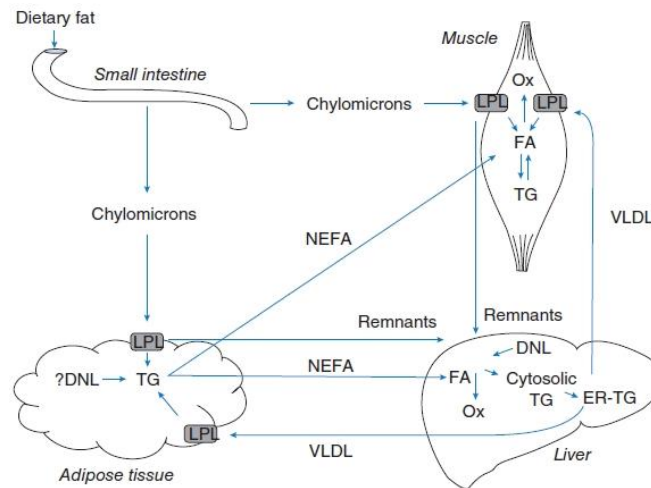


Figure 3.5: Lipid storage and metabolism between adipose tissue, muscle and liver [27]

Carbohydrates found in muscle tissues are primarily glycogen, a polymer of sugar that is formed when there is excess glucose in the body. Glycogen in muscle tissues functions as a secondary source of energy supply for the muscle tissues themselves and the entire human body when needed. Inorganic minerals found in muscles can vary but they are normally ferum, zinc, sodium, potassium, calcium, magnesium and chloride. [28].

3.2.2 Structure and Composition of Ribs

Ribs are flat bones [29] with irregular structures that join together to form lateral walls which give form to the thorax [30]. They also provide a cage of protection for the lungs and heart and play a crucial role in respiration [31]. A typical rib consists of a vertebral extremity, shaft / body and sternal extremity (Figure 3.6) [30, 32]. The spherical head articulates with the transverse process of the thoracic vertebrae through a tubercle and is connected to the rib by the neck. The sternal extremity refers to the other end of the rib that articulates with the sternum via the costal hyaline cartilage [30, 31]. There are 12 pairs of ribs in the human body that

correspond to the number of vertebrae (from cervical to lumbar) in the backbone [30, 31]. From the 12 pairs of ribs, seven pairs are called true ribs while the remaining five pairs are false ribs. The last two pairs of the false ribs are known as floating ribs. True ribs are ribs that are implanted directly to the sternum by their cartilages, whereas false ribs are ribs that have cartilages joining together but not directly to the sternum. Floating ribs are the bottom two ribs that are not attached to any cartilages or the sternum, but they are hanging and loosely connected to the abdominal muscles.

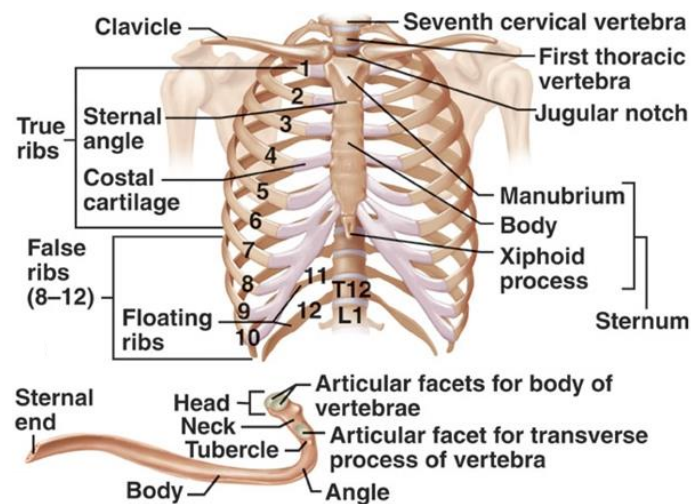


Figure 3.6: Structure of the human rib cage [32]

Ribs are characterised by their flattened, irregular structure that appears to have undergone a certain degree of twisting to facilitate breathing. The flat side of the rib takes a smoother; more rounded form at the upper edges as it approaches the lungs, whereas the lower edges remain sharp and grooved to provide extra support for arteries and nerves. As ribs are generally bones, their organic and inorganic components are similar to other bones although they may vary in proportions. Ribs have been documented to have the lowest fat percentage as compared to the other bones (i.e. femur and vertebrae) [33]. Henrique *et al.* [34] conducted a compositional study on the ninth, tenth and eleventh ribs and identified that these ribs contain 60% muscle, 59% water, 21% fat, 20% protein and 5% minerals. However, these values vary and can differ from one rib to another. For instance, Woodard [35] mentioned

that calcium and phosphate levels in the tenth rib were much higher as compared to the values recorded from the second to sixth ribs.

3.3 Thermal Decomposition of the Human Body

When subjected to heat, the human body undergoes various physical and chemical changes, internally and externally. Fat from the human body can be pyrolysed and its volatile products can act as a suitable source to fuel a fire. The next step in this study focuses on systematically generating pyrolysis products from human samples under the laboratory conditions previously outlined and optimised in Chapter 2. The purpose was two-fold, firstly to identify and categorise pyrolysis products from human samples and secondly, to compare these products with those generated from porcine tissue in order to assess the efficacy of the porcine model in representing human tissue, particularly for pyrolytic data.

It is uncommon for a fire to completely destroy all features of a human body and, even more so, reducing it completely to ash [36, 37]. In most fire scenarios, the fire will be short-lived or will not generate sufficient temperatures to cause the total destruction of a human body, especially when dealing with hard, robust structures like bones and teeth [23, 38]. According to Eckert *et al.* [39], Spitz [36] and Bohnert *et al.* [40], at constant temperatures exceeding 850 °C to 1000 °C for a period of 1 to 2 hours, an adult human body can undergo complete destruction, typically in a crematorium; even so, portions of the human body, such as the skull, pelvic bone and dentition, may still remain. The temperature and duration of an uncontrolled fire is often far less than that achieved within a crematorium and can fluctuate as the fire develops, however under certain circumstances such as flashover conditions, majority of the human remains can be consumed and rendered to ashes [4, 8-9].

However, the human body is a complex fuel package, rendering a variety of fuels that have different burning properties (Table 3.5) and, given the right circumstances, can dynamically contribute to fuelling a fire [41]. These include the availability of a porous structure or wick for the melted body fat to be absorbed into and also

adequate heating by the primary heat source [19, 41, 42]. With external ignition, the human body can sustain combustion for up to 7 hours [18] and can undergo dramatic microscopic, macroscopic, physical and chemical changes (Table 3.6), burning in a relatively predictable fashion [43].

This occurs in a predictable sequence of damage beginning from the epidermis, dermis, subcutaneous fat, muscle, internal organs and finally bone [44]. The degree of burning is classified according to the damage sustained by these tissues [43]. First degree burns involve damage to the superficial epidermis layer, whereas second degree burns are characterised by the destruction of this epidermis layer. Damage to and destruction of the dermis and hypodermis indicate the onset of third degree burns and are commonly expressed as a loss of sensation to the nerve endings. Once the destruction of the entire skin layer is complete, fourth degree burns follow with damage to muscles, tendons, internal organs and ultimately the bone [36].

Table 3.5: Fuels represented in the human body and their major building blocks. Adapted from [41].

Organ	Composition
Skin: Proteinaceous	
Epidermis	cellular structure and does not have mechanical strength [45] made primarily from keratinocytes [46] thin, easily separated at 4–5 kW/m ² , or 54 °C
Dermis	thick and strong [45] made primarily from collagen (70% of its dry weight) and elastin [45] higher water content, minimal contribution to fuel package
Subcutaneous fat	made up of adipocytes highest heat content: 32–34 kJ/g [42] low melting point: burns as a viscous liquid main fuel from body in a fire [41]
Muscle tendons	proteinaceous, microfilaments made up of actin and myosin moderate water content poor fuel: 4–5 kJ/g [47]
Internal organs	proteinaceous high water content: no contribution to heat release rate
Bone	made up of minerals (hydroxyapatite crystals), organic content (fibrous protein collagen) and water [48] fat-rich (contribution to fire only when large bones split due to external fire, usually occurring at 670 °C to 810 °C for 1 hour [40])

Table 3.6: Effects of fire on the human body. Adapted from [40].

Time	Effects of fire on the human body
10 min	Pugilistic attitude Face tissues charred Skull, metacarpals and fingers free of soft tissues
20 min	Visible calvaria (skull cap), ribs and sternum Sparse soft tissues on face; heat fracture on calvaria Thoracic muscles charred Hands largely destroyed; partially visible ulna and radius Carbonisation of leg muscles
30 min	Tabula externa of calvaria crumbling Thoracic and abdominal cavity exposed; organs blackened and shrunken Hands and distal forearms burnt away with severely charred muscles Tibia and distal femur free of soft tissue; exposed long bones calcined with longitudinal fractures
40 min	Calvaria comes off and brain showing Bones of face begin to disintegrate Shrunken and charred organs with bumpy surface Ribs free from soft tissue Forearms completely consumed; upper arms largely free of soft tissue
50 min	Bones on face largely destroyed; base of skull showing; Vertebral bodies calcined Organs largely consumed by fire Arms burnt away Calcined stumps of the thighs
60 min	Destruction of the skull leaving on central part of the facial bones Intervertebral discs destroyed Internal organs reduced to ashes

In recent years, research on the pyrolysis products generated from fresh human and pig tissues has begun and is gaining more interest. Pioneer studies in this field utilised fresh porcine tissues and identified the presence of *n*-aldehydes (*n*-pentanal, *n*-hexanal and 3-methyl-butanal), toluene and ethyl-benzene as by-products of pyrolysis [2]. In a preliminary study by DeHaan and Brien [1], limited amounts of human and porcine fat was subjected to open-burning flames and they identified the presence of C₅ to C₁₀ *n*-aldehydes together with some aromatics and cyclic hydrocarbons in both samples. Although they mentioned that there were slight differences in the human and porcine fat profiles, DeHaan, Brien and Large [1] when on to refute this idea through their pyrolysis probe experiment using chicken, porcine and human fat. They identified a variety of *n*-alkanes, *n*-alkenes, *n*-aldehydes and light aromatics from all three samples with no differences in their pyrolysis profiles, suggesting that they are good representations of human fat.

3.4 Experimental Methods

3.4.1 Sample Preparation: Porcine Tissue Samples

3.4.1.1 Porcine Bone

Porcine bone samples were prepared as per 2.4.3.1. Six bone samples of $25 \text{ g} \pm 1.50 \text{ g}$ were cut and each one placed into a 125 mL tin can (WA Products, UK) without a lid.

3.4.1.2 Porcine Muscle

Fresh pork loin chops were obtained from Aldi Stores, High Street, Glasgow, Scotland, UK on a daily basis to ensure the freshness of the sample. Six muscle samples of $25 \text{ g} \pm 1.50 \text{ g}$ were cut and each one placed into a 125 mL tin can (WA Products, UK) without a lid.

3.4.1.3 Porcine Rib

Fresh pork ribs were obtained from Tesco Stores, St. Enoch Square, Glasgow, Scotland, UK on a daily basis to ensure the freshness of the sample. Each rib was held securely on a bench vice and a hacksaw was used to remove a $25 \text{ g} \pm 1.50 \text{ g}$ rib sample. Six separate rib samples were prepared in this way and placed individually into a 125 mL tin can (WA Products, UK) without a lid.

3.4.2 Sample Preparation: Human Tissue Samples

3.4.2.1 Human Toe

Five unembalmed human toe samples, originating from one individual, were obtained from the University of Strathclyde's Department of Biomedical Engineering under full ethical approval. The toe samples were kept at $-18.3 \text{ }^{\circ}\text{C}$. The individual's medical record was obtained and cross-referenced to ensure the circumstances leading to death would not interfere with the outcome of this study. All of the samples were thawed for several hours at room temperature. Once thawed, the toe samples were transferred into five individual 125 mL tin cans (WA Products, UK) without a lid.

3.4.3 Generation of Thermal Decomposition Products

Thermal decomposition products were generated according to the optimised methodology established in 2.4.3, with modification according to the factor(s) assessed.

For all three porcine tissues, these factors include temperature and burning time. The tin can containing the porcine sample was heated over a Bunsen flame so that it reached (i) temperatures between 200 °C and 250 °C (pre-ignition) and (ii) temperatures in excess of 250 °C (post-ignition). Pre-ignition samples refer to samples that were exposed to temperatures below 250 °C but not necessarily indicate that the samples are capable of experiencing post-ignition temperatures (above 250 °C). Post-ignition samples refer to samples that are exposed to, and were capable of burning at temperatures above 250 °C. Six repeat samples of each porcine tissue type at each temperature range were prepared.

In order to determine the effects of the length of time that the samples were exposed to heat to the generation of thermal decomposition products, six porcine muscle samples were each placed in a 125 mL tin can (WA Products, UK) without a lid and heated over a Bunsen flame for 450 seconds, 500 seconds, 550 seconds, 600 seconds, 650 seconds and 700 seconds. The optimal exposure duration was identified based on the number of peaks detected and a further six repeats of the optimised exposure duration were conducted.

For human toe samples, modification in burning time was required as each sample was less than 5 g in weight, thus the amount of fat present within the samples would not sustain burning for 5 minutes upon auto-ignition. As a consequence, the burning time upon auto-ignition was shortened to 1 minute.

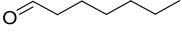
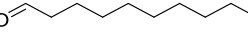
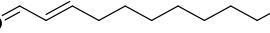
Once the designated temperature and / or duration of exposure was attained, the Bunsen flame and thermocouple were removed and an empty lid was placed onto the tin for the samples to cool down for 4 minutes. Samples were then extracted with a

10 mm × 20 mm ACS, using the optimised passive headspace extraction method previously detailed in section 2.4.3.3.

3.4.4 Gas Chromatography – Mass Spectrometry

The GC-MS analysis for all porcine and human samples was conducted following the method in 2.4.2. In addition to the Grob mixture, a known standard mixture was also analysed which contained analytical grade *n*-aldehydes: pentanal (98% Sigma Aldrich), hexanal (98% Sigma Aldrich), heptanal (95% Sigma Aldrich), octanal (99% Sigma Aldrich), nonanal (95% Sigma Aldrich), decanal (98% Sigma Aldrich), undecenal (96% Sigma Aldrich) and dodecanal (92% Sigma Aldrich). These *n*-aldehydes, detailed in Table 3.7, were chosen as they were documented to be present from the pyrolysis of animal and human tissues [1, 49].

Table 3.7: Retention time and molecular structure of eight *n*-aldehydes present in the standard mixture

Retention Time (min)	Compound	Molecular Structure
4.80	Pentanal	
7.45	Hexanal	
9.44	Heptanal	
10.98	Octanal	
12.26	Nonanal	
13.38	Decanal	
14.73	Undecenal	
15.38	Dodecanal	

The total ion chromatogram (TIC) produced for each sample was analysed based on the retention times and *m/z* values. Each significant peak was then identified by comparing data against the National Institute of Standards and Technology (NIST) library and the standard mixture.

The compounds appearing in the pre-ignition (200 °C – 250 °C) porcine samples were compared to those produced in the post-ignition (> 250 °C) porcine samples.

The compounds appearing in the post-ignition porcine bone samples were compared and contrasted to the ones appearing consistently across the five repeats of human toe samples.

3.5 Results and Discussion

3.5.1 Porcine Samples - Effects of Temperature

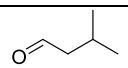
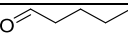
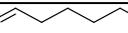
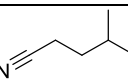
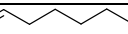
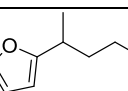
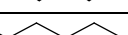
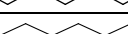
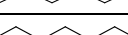
3.5.1.1 Porcine Bone Pre-Ignition Samples (200 °C – 250 °C)

The derived products are presented in Table 3.8 and a representative total ion chromatogram (TIC) of a heated porcine bone prior to ignition is labelled and displayed in Figure 3.7 (set 5).

The samples produced predominantly *n*-aldehydes with some less consistent, heavier *n*-alkanes (except for pentadecane) and *n*-alkenes. Also present in two of the six samples were 4-methyl-pentanenitrile and 2-pentyl-furan. Across the repeats, the qualitative reproducibility of the detected products was poor. The TIC also revealed low abundance of pyrolysis products which was not unexpected given the temperature of the exposure. It is also noted that no aromatics were detected from porcine bone pre-ignition samples.

The maximum temperature attained during the heating process in the headspace above the samples were recorded to be in the range of 224 °C to 237 °C with exposure to heat ranging from 9.1–9.8 minutes as illustrated in Figure 3.8.

Table 3.8: 11 compounds identified based on the *m/z* values and retention times for six porcine bone samples heated at temperatures below 250 °C

No	Retention Time (min)	Compound	Molecular Structure	Set					
				1	2	3	4	5	6
1	3.81	3-methyl-butanal				√	√	√	
2	4.79	pentanal					√	√	√
3	7.45	hexanal					√	√	√
4	8.09	4-methyl-pentanenitrile			√	√			
5	9.45	heptanal							√
6	10.96	2-pentyl-furan						√	√
7	10.98	octanal						√	√
8	12.44	undecene			√	√	√		
9	14.50	tridecene				√	√	√	
10	15.32	1-tetradecene					√	√	
11	16.27	pentadecane		√	√	√	√	√	√

Abundance

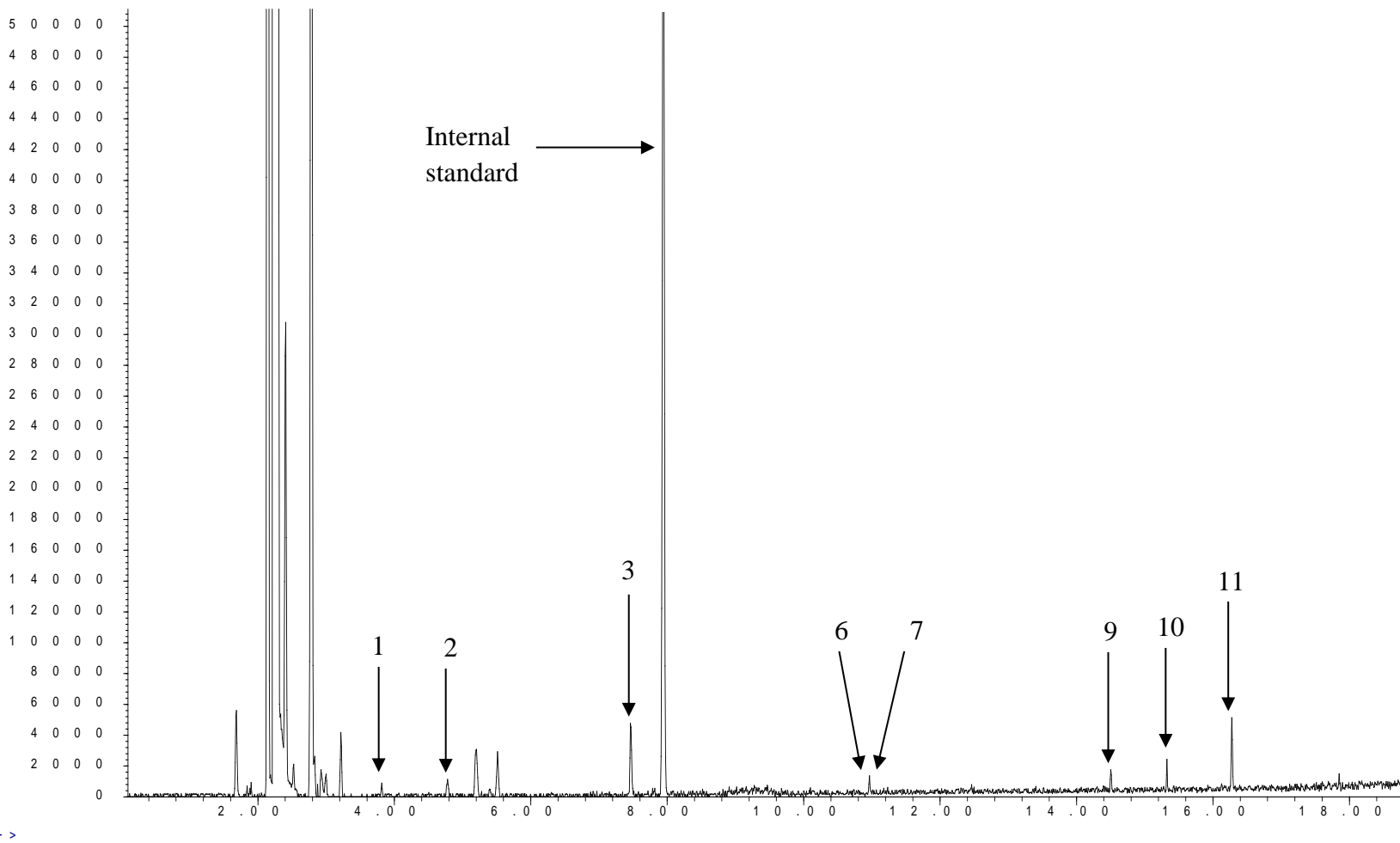


Figure 3.7: A representative TIC of heated porcine bone prior to the onset of auto-ignition (< 250 °C) (set 5)

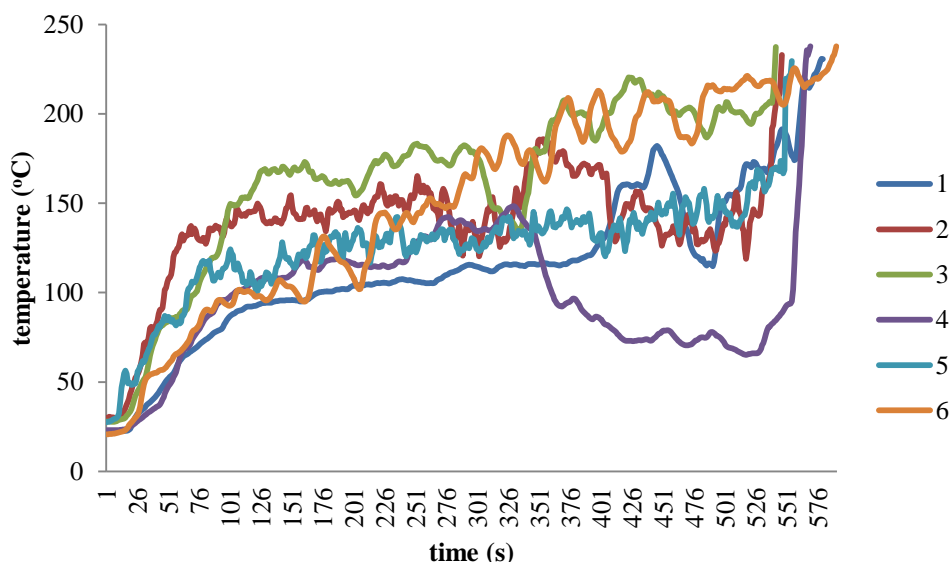


Figure 3.8: Overlay of six time temperature profiles of heated porcine bones prior to the onset of auto-ignition (< 250 °C)

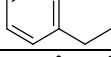
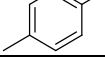
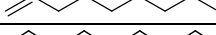
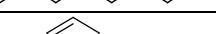
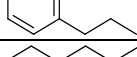
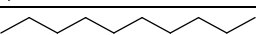
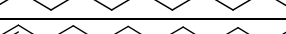
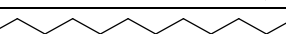
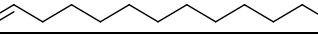
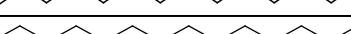
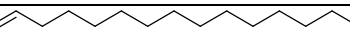
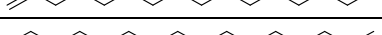
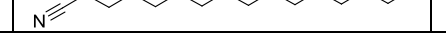
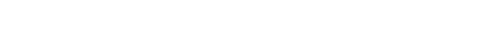
3.4.1.2 Porcine Bone Post-Ignition Samples (> 250 °C)

The derived products are presented in Table 3.9 and a representative total ion chromatogram (TIC) of a burnt porcine bone post-ignition is labelled and displayed in Figure 3.9 (set 6).

The samples produced the consistent presence of the C₈ to C₁₇ *n*-alkanes and *n*-alkenes together with some aromatics, *n*-alkyl-benzenes and a nitrile. However, no *n*-aldehydes were revealed. Across the repeats, the qualitative reproducibility of the detected products was good with high abundance of the pyrolysis products detected.

All of the samples ignited and burned continuously for 5 minutes prior to the intended oxygen deprivation, where maximum temperature ranges between 650 °C to 750 °C were recorded in the headspace above the samples, as illustrated in Figure 3.10.

Table 3.9: 26 compounds identified based on the m/z values and retention times for six porcine bone samples burnt at temperatures upon auto-ignition ($> 250\text{ }^{\circ}\text{C}$)

No	Retention Time (min)	Compound	Molecular Structure	Set					
				1	2	3	4	5	6
1	2.22	benzene		√	√	√	√	√	√
2	4.11	toluene		√	√	√	√	√	√
3	5.24	1-octene		√	√	√	√	√	√
4	5.60	octane		√	√	√	√	√	√
5	6.82	ethyl-benzene		√	√	√	√	√	√
6	6.94	<i>p</i> -xylene		√	√	√	√	√	√
7	7.70	1-nonene		√	√	√	√	√	√
8	7.91	nonane		√	√	√	√	√	√
9	8.61	propyl-benzene		√	√	√	√	√	√
10	9.33	1-decene		√	√	√	√	√	√
11	9.49	decane		√	√	√	√	√	√
12	10.62	1-undecene		√	√	√	√	√	√
13	10.75	undecane		√	√	√	√	√	√
14	11.72	1-dodecene		√	√	√	√	√	√
15	11.83	dodecane		√	√	√	√	√	√
16	12.70	1-tridecene		√	√	√	√	√	√
17	12.81	tridecane		√	√	√	√	√	√
18	13.61	1-tetradecene		√	√	√	√	√	√
19	13.70	tetradecane		√	√	√	√	√	√
20	14.47	1-pentadecene		√	√	√	√	√	√
21	14.55	pentadecane		√	√	√	√	√	√
22	15.21	1-hexadecene		√	√	√	√	√	√
23	15.34	hexadecane		√	√	√	√	√	√
24	15.92	1-heptadecene		√	√	√	√	√	√
25	16.10	heptadecane		√	√	√	√	√	√
26	17.32	hexadecanitrile		√	√	√	√	√	√

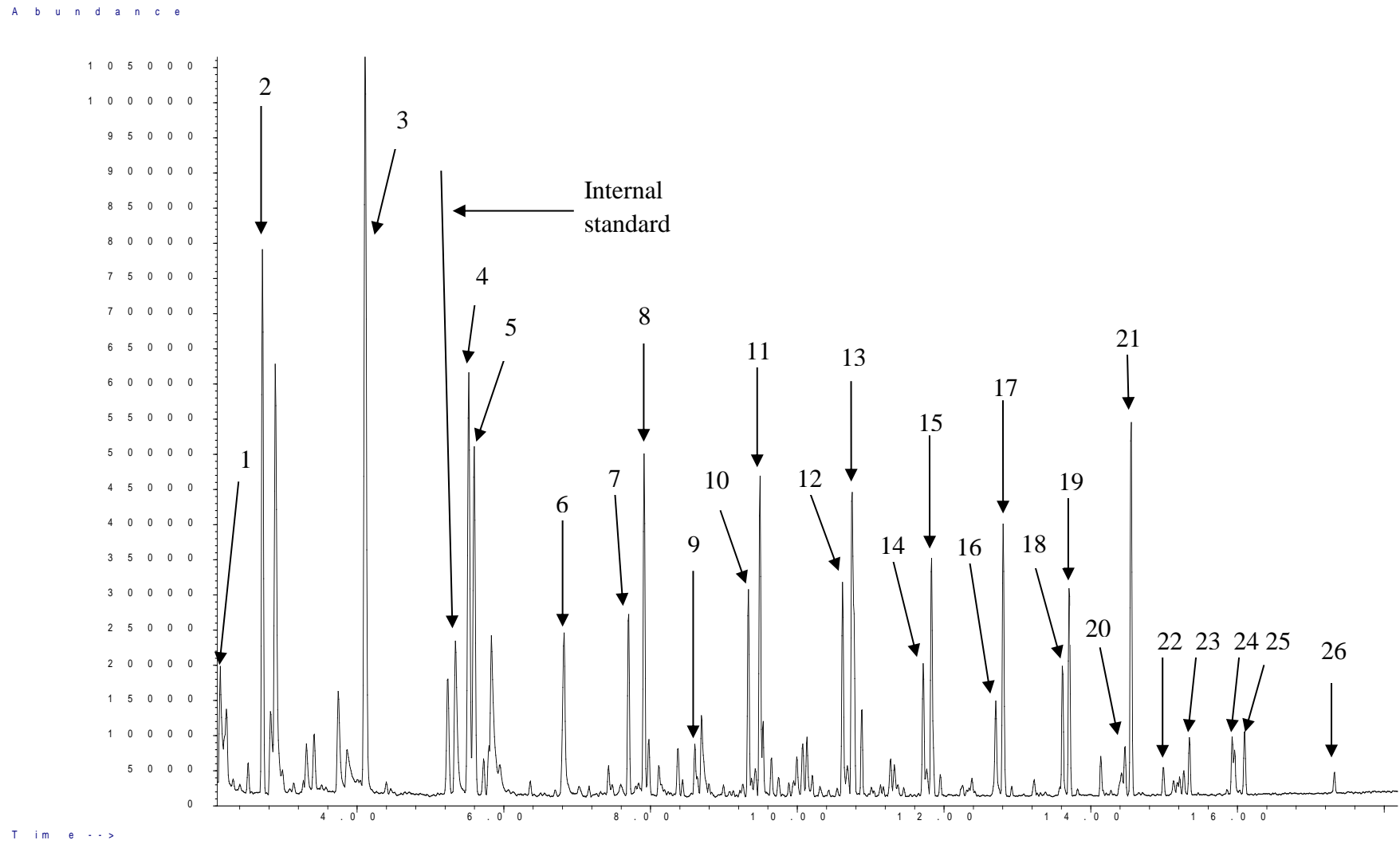


Figure 3.9: A representative TIC of a burnt porcine bone upon to the onset of auto-ignition (> 250 °C) (set 6)

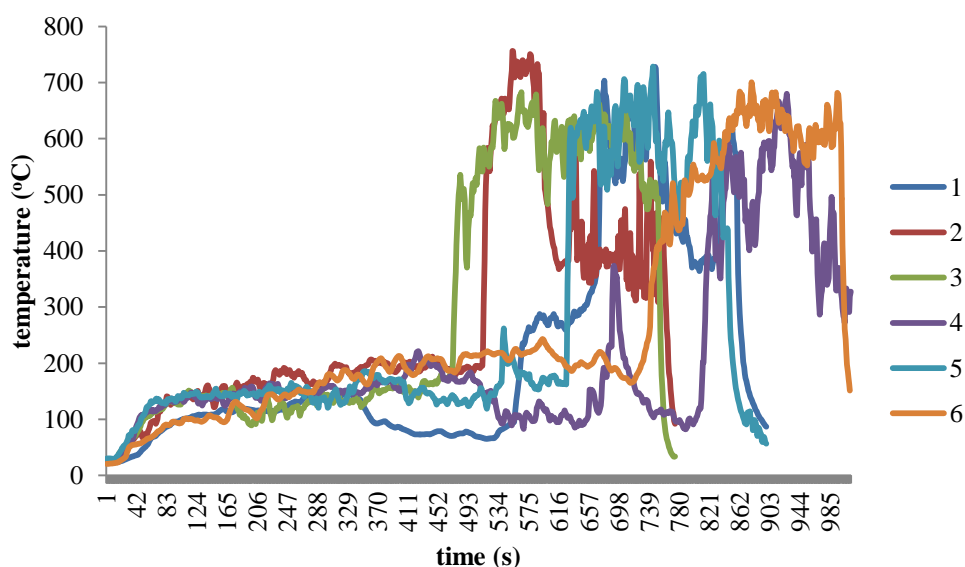


Figure 3.10: Overlay of six time temperature profiles of burnt porcine bones upon the onset of auto-ignition (> 250 °C)

3.5.1.3 Porcine Muscle Pre-Ignition Samples (200 °C – 250 °C)

When porcine muscle was heated, auto-ignition did not occur. Samples heated for extended durations experienced significant charring and did not generate any residual pyrolysis products upon analysis.

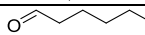
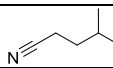
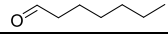
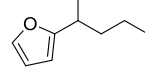
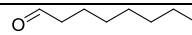
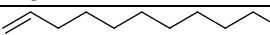
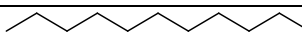
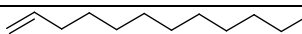
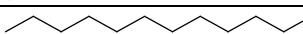
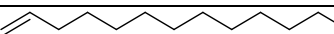
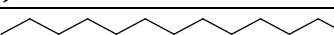
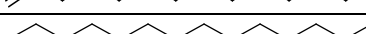
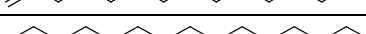
The results of the repetitive analysis of pre-ignition porcine muscle samples are tabulated in Table 3.10 and a representative total ion chromatogram (TIC) of a heated porcine muscle is labelled and illustrated in Figure 3.11 (set 1).

The heated porcine muscle samples generated a variety of *n*-aldehydes, *n*-alkanes and *n*-alkenes. Toluene, 4-methyl-pentanenitrile, 2-pentyl-furan and ethanedial were also present among the hydrocarbons. However, while the rest of the products appeared with relatively good qualitative reproducibility across the samples, 4-methyl-pentanenitrile was only detected in two out of the six samples. In terms of consistently appearing products, the *n*-aldehydes of 3-methyl-butanal, pentanal, hexanal, heptanal, octanal, nonanal and heptadecenal were relatively consistent across the six repeats, appearing in more than four of the six repeats. *n*-Alkanes and *n*-alkenes were detected in more than half of the samples, as well as some unknown

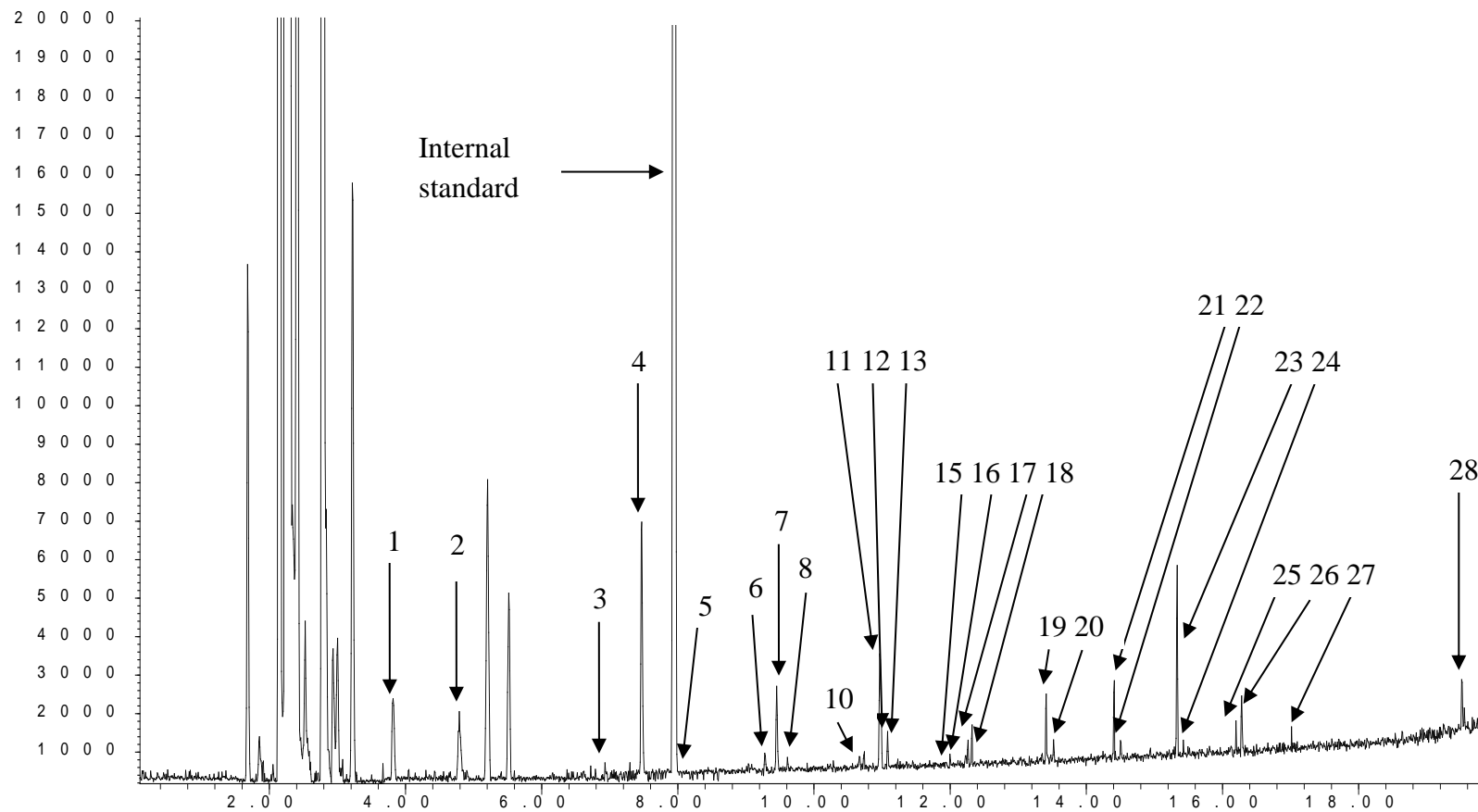
compounds appearing in two or three repeats. The TIC also displays that the abundance of pyrolysis products detected was higher than porcine bone pre-ignition.

The maximum temperature attained during the heating process in the headspace above the samples were recorded to be in the range of 200 °C to 211 °C with exposure to heat ranging from 5–9.3 minutes as illustrated in Figure 3.12.

Table 3.10: The 24 compounds identified based on the m/z values and retention times for six porcine muscle samples heated at temperatures below 250 °C and four unknown compounds

No	Retention Time (min)	Compound	Molecular Structure	Set					
				1	2	3	4	5	6
1	3.81	3-methylbutanal		√	√	√	√	√	√
2	4.79	pentanal		√	√	√	√	√	√
3	6.91	toluene		√	√	√		√	
4	7.45	hexanal		√	√	√	√	√	√
5	8.09	4-methylpentanenitrile		√	√				
6	9.27	ethanedial		√	√		√	√	√
7	9.45	heptanal		√	√	√	√		√
8	9.61	1-nonene		√	√	√	√		
9	9.73	unknown	-				√		√
10	10.67	unknown	-	√	√	√			
11	10.96	2-pentyl-furan		√	√	√	√	√	√
12	10.98	octanal		√	√	√	√		√
13	11.08	1-decene		√	√	√	√		
14	11.23	decane			√	√	√		
15	11.99	unknown	-	√	√	√			√
16	12.26	nonanal		√		√	√		√
17	12.31	1-undecene		√	√	√	√		
18	12.45	undecane		√	√	√			
19	13.41	1-dodecene		√	√	√	√		
20	13.53	dodecane		√	√	√	√		
21	14.40	1-tridecene		√	√	√	√		
22	14.50	tridecane		√	√	√	√		
23	15.32	1-tetradecene		√	√	√	√		√
24	15.42	tetradecane		√	√		√		
25	16.19	1-pentadecene		√	√	√	√		
26	16.27	pentadecane		√	√	√	√		
27	17.01	heptadecenal		√	√	√	√		
28	19.52	unknown	-	√			√		√

Abundance



Time -->

Figure 3.11: A representative TIC of heated porcine muscle prior to the onset of auto-ignition (< 250 °C) (set 1)

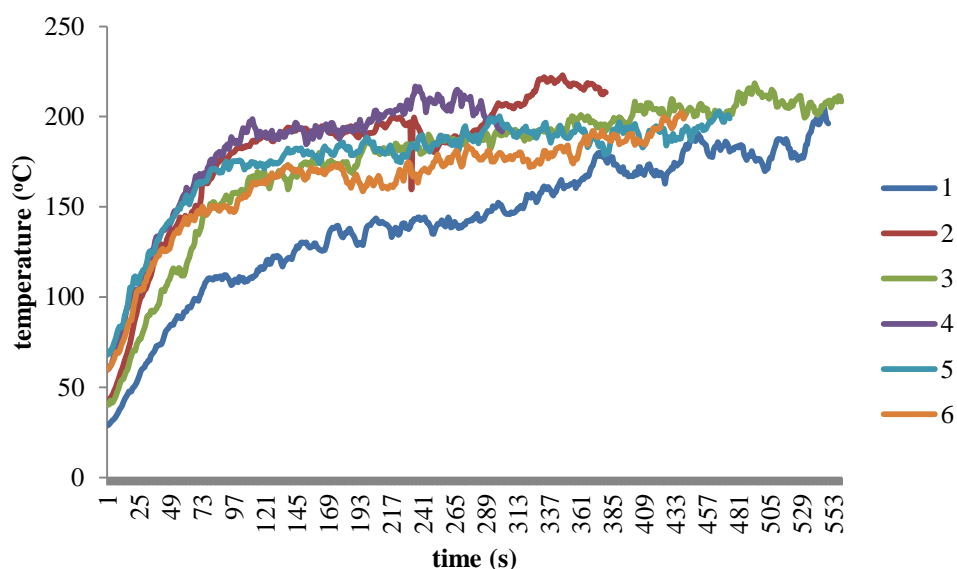


Figure 3.12: Overlay of six time temperature profiles of heated porcine muscles prior to the onset of auto-ignition (< 250 °C)

3.5.1.4 Porcine Rib Pre-Ignition Samples (200 °C – 250 °C)

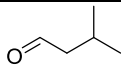
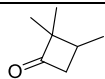
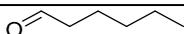
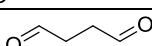
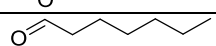
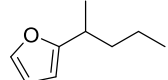
Similar to porcine muscles, porcine ribs did not display any signs of auto-ignition (> 250 °C). Samples heated for extended durations experienced significant charring and did not generate any residual pyrolysis products upon analysis.

The results of the repetitive analysis of pre-ignition porcine rib samples are tabulated in Table 3.11 and a representative total ion chromatogram (TIC) of a heated porcine rib is labelled and illustrated in Figure 3.13 (set 4).

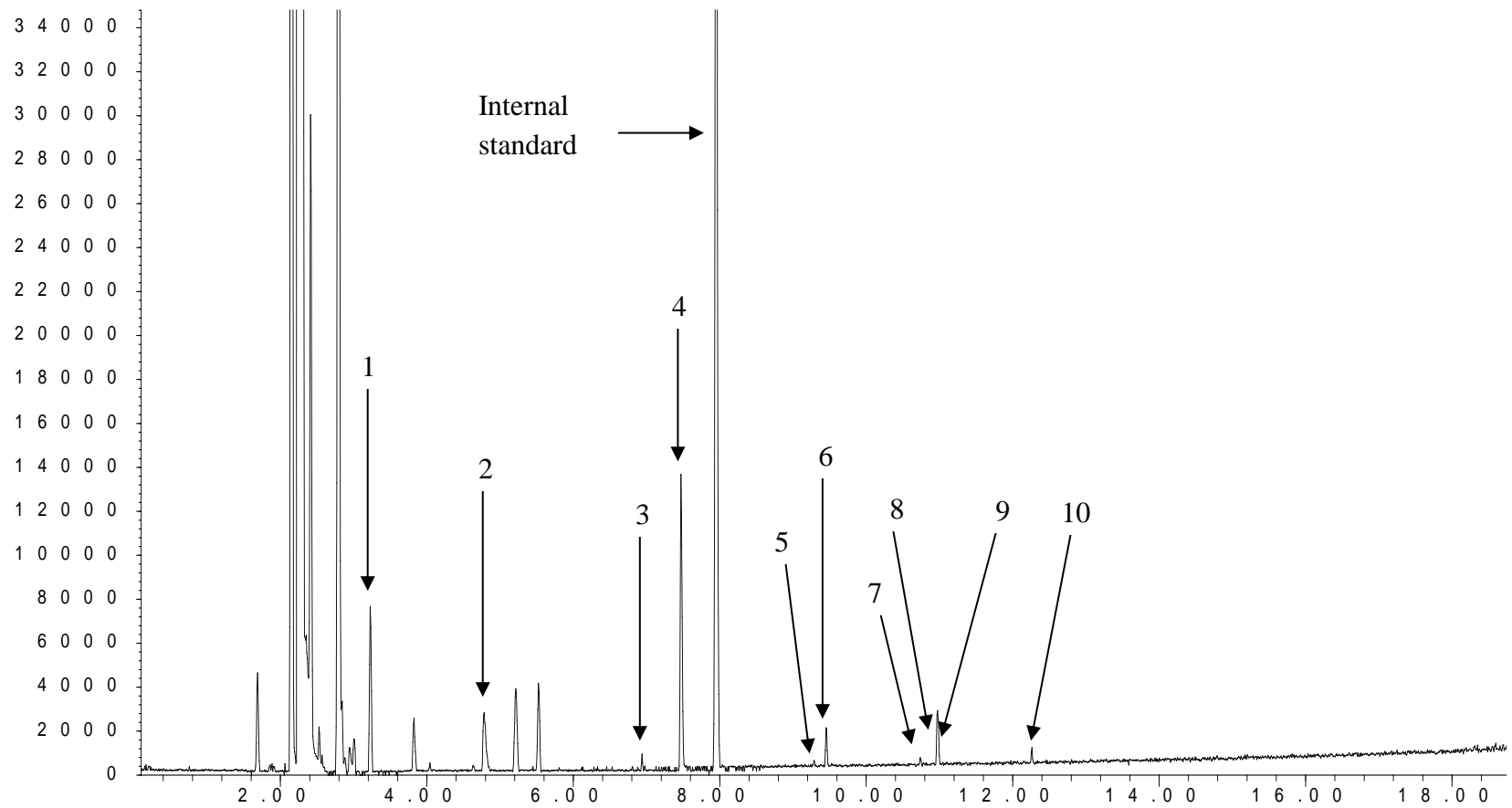
Porcine ribs heated at temperatures prior to ignition generated a homologous series of *n*-aldehydes, 2-pentyl-furan, butanedial and 2,2,3-trimethyl-cyclobutanone. 3-Methyl-butanal, pentanal, hexanal, heptanal and octanal were present in all of the repeats, whereas nonanal was only present in four of the six repeats. One unidentified compound at 10.73 minutes was noted to be consistently present at low concentrations across the repeats. No *n*-alkanes, *n*-alkenes or aromatics were detected in any of the six repeats. Good qualitative reproducibility was attained as the consistencies of repeatable products across a wide range of intensities were displayed across the six sets of sampling. The TIC also displays that the abundance of pyrolysis products detected was higher than porcine bone pre-ignition.

The maximum temperature attained during this experiment across the headspace above the six samples were in the range of 177 °C to 209 °C with exposure to heat ranging from 9.6–12.4 minutes as illustrated in Figure 3.14.

Table 3.11: Nine compounds identified based on the m/z values and retention times for six porcine rib samples heated at temperatures below 250 °C and one unknown

No	Retention Time (min)	Compound	Molecular Structure	Set					
				1	2	3	4	5	6
1	3.81	3-methyl-butanal		√	√	√	√	√	√
2	4.79	pentanal		√	√	√	√	√	√
3	6.93	2,2,3-trimethyl-cyclobutanone		√	√	√	√	√	√
4	7.45	hexanal		√	√	√	√	√	√
5	9.38	butanedial		√	√	√	√	√	√
6	9.45	heptanal		√	√	√	√	√	√
7	10.73	unknown	-	√	√	√	√	√	√
8	10.96	2-pentyl-furan		√	√	√	√	√	√
9	10.98	octanal		√	√	√	√	√	√
10	16.27	nonanal				√	√	√	√

Abundance



Time -->

Figure 3.13: A representative TIC of heated porcine rib prior to the onset of auto-ignition (< 250 °C) (set 4)

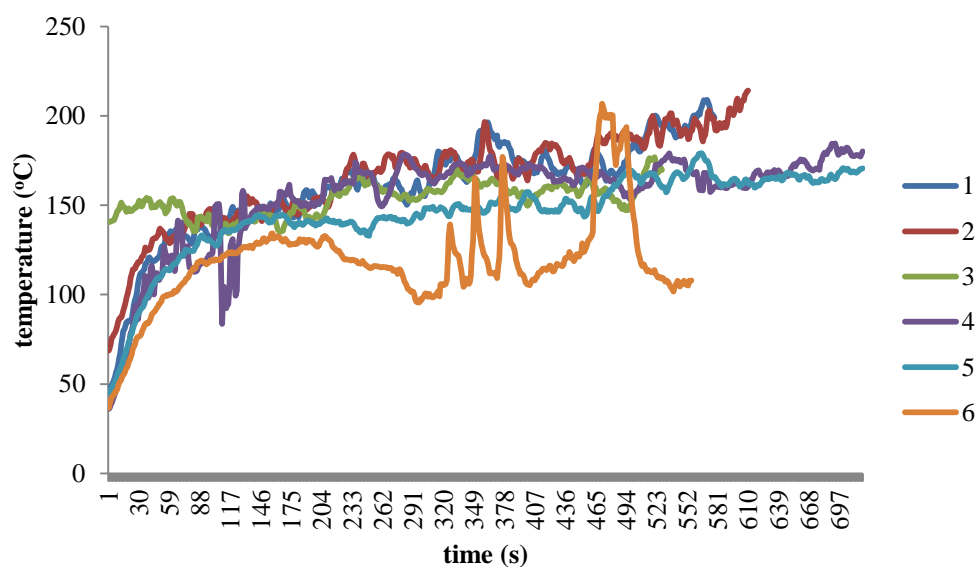


Figure 3.14: Overlay of six time temperature profiles of heated porcine ribs prior to the onset of auto-ignition (< 250 °C)

Variations in retention times for pyrolysis products generated from porcine bone samples subjected to temperatures above 250 °C, as compared to the rest of the samples discussed in this chapter, is due to the change in the DB-1MS column used during the analysis. The column was replaced as it displayed signs of degradation.

The types of pyrolysis products generated across porcine samples are clearly matrix and temperature dependent. All three; porcine bone, muscle and rib samples exposed to temperatures prior to auto-ignition generated predominantly *n*-aldehydes with porcine bone and muscle samples also producing some less consistent *n*-alkanes and *n*-alkenes. Apart from this, no detectable differences were noted in terms of the type of products generated during pyrolysis for pre-ignition samples across the three types of porcine tissues.

A noticeable difference is, however, documented in the ability of porcine bones to undergo auto-ignition, which was not experienced by porcine muscles or ribs. This could be due to the low levels of fat and / or high water and protein content in porcine muscle or rib tissues or the inability of these tissues to absorb enough heat to form volatile products (high thermal inertia) required for auto-ignition. This finding is clearly supported by DeHaan's [18] study in which he mentioned that certain parts

of the human anatomy with lower fat content such as the hand, feet and lower leg, do not readily burn and most of the time only respond to a direct external fire rather than heat. Other parts such as the torso, upper legs and pelvis that have high fat content burn readily in the presence of flames and heat [18, 19].

Porcine bone samples exposed to temperatures upon ignition generated predominantly *n*-alkanes, *n*-alkenes, aromatics, *n*-alkyl-benzenes and a nitrile. The abundance and number of pyrolysis products generated from auto-ignited samples were significantly higher and consistent across all the repeats (Figure 3.9 and Table 3.9) as compared to all the pre-ignition samples (bones: Figure 3.7 and Table 3.8, muscles: Figure 3.11 and Table 3.10, ribs: Figure 3.13 and Table 3.11).

The obvious difference noted across pre- and post-ignition samples is the presence of *n*-aldehydes in pre-ignition samples but their absence in post-ignition samples. In the literature, a homologous series of *n*-aldehydes has been consistently documented from the pyrolysis of both porcine and human tissues [1, 2]. These *n*-aldehydes are said to have generated from the pyrolysis of fat (triglycerides) [50]. However, other pyrolysis studies have documented the presence of predominant species of *n*-alkane and *n*-alkenes with no detection of *n*-aldehydes from fats [51].

The differences in the presence and absence of *n*-aldehydes generated from pyrolysed samples has been shown to be directly related to the temperature ranges to which the samples were exposed. When looking at the temperature profiles for pre-ignited bone, muscle and rib samples and post-ignition bone samples (Figures 3.8, 3.12 and 3.14 and Figure 3.10, respectively), temperatures attained in the pre-ignition samples were all below 250 °C whereas the latter was in the range of 650 °C to 750 °C. Higher temperatures facilitate the formation of more free radicals which in turn, attack and break double bonds and the carbon backbone of the generated molecules, resulting in smaller, more stable compounds [52]. These higher temperature ranges could have caused the decomposition and oxidation of *n*-aldehydes, breaking them into smaller, undetectable compounds [1, 49]. The flames produced during auto-ignition may have also consumed these volatile *n*-aldehydes [53]. These findings are

corroborated by Agu's [49] study where she commented that *n*-aldehydes were only detected significantly prior to or in the first minute upon ignition and were not detected at all after that [49].

In addition to this, variations in the methodologies employed could also potentially alter and affect the generation and detection of *n*-aldehydes [54]. Although DeHaan *et al.* [1] mentioned in his study that temperatures above 700 °C proved to generate less straight-chain *n*-aldehydes due to fragmentation and oxidation, they however reported detecting varying amounts of *n*-aldehydes, low molecular weight *n*-alkanes and *n*-alkenes from samples exposed at 500 °C and 700 °C utilising a microfurnace (contained environment and provides more control on the combustion and pyrolysis process) CDS pyrolysis probe exposed for 10 seconds [1]. Contrary to DeHaan *et al.*'s findings, Purevsuren *et al.* [55] detected high molecular weight *n*-alkanes and *n*-alkenes but no *n*-aldehydes when he used a retort pyrolyser at 500 °C to 700 °C for about 4 to 5 hours. Similar to Purevsuren's work, the long burning duration and different burning methodology utilised in this work could have caused the decomposition and / or consumed of any *n*-aldehydes that could have been generated.

3.5.2 Porcine Samples - Effects of Time of Exposure

Porcine muscle samples were chosen to be exposed to heat for a range of time frames because they created the widest range of pyrolysis products across the three types of porcine tissue samples.

From the six exposure durations applied, samples exposed to heat for 450 seconds generated the best result and produced the greatest number of pyrolysis products as seen in the overall results tabulated in Table 3.12. These were predominantly a homologous series of *n*-aldehydes, *n*-alkanes, *n*-alkenes, *n*-alkyl-benzenes, aromatics and nitriles. Across the six durations of heat exposure to which porcine muscle was subjected, *n*-aldehydes of 3-methyl-butanal, pentanal, hexanal, heptanal, octanal and nonanal, plus toluene and 2-pentyl-furan appeared consistently in all samples.

Table 3.12: 33 compounds identified based on the m/z values and retention times generated from six porcine muscle samples heated across six different exposure durations

No	Retention Time (min)	Compound	Time (s)					
			450	500	550	600	650	700
1	3.81	3-methyl-butanal	√	√	√	√	√	√
2	4.15	benzene	√	√		√	√	√
3	4.79	pentanal	√	√	√	√	√	√
4	5.26	2-methyl-butanenitrile	√				√	
5	6.91	toluene	√	√	√	√	√	√
6	7.45	hexanal	√	√	√	√	√	√
7	8.09	4-methyl-pentanenitrile	√				√	
8	8.58	2-furanmethanol	√	√	√		√	√
9	8.91	ethyl-benzene	√				√	
10	9.27	ethanedial	√	√	√		√	√
11	9.45	heptanal	√	√	√	√	√	√
12	9.61	1-nonene	√	√				
13	10.25	2-heptenal	√		√	√	√	√
14	10.58	1-heptanol			√			
15	10.96	2-pentyl-furan	√	√	√	√	√	√
16	10.98	octanal	√	√	√	√	√	√
17	11.08	1-decene	√					
18	11.35	nonyne			√			
19	11.47	2,3-heptanedione		√				
20	11.65	2-octenal			√			√
21	11.89	1-octanol			√			√
22	12.26	nonanal	√	√	√	√	√	√
23	12.31	1-undecene	√					
24	12.85	2-nonenal			√	√		
25	12.99	pentyl-benzene	√				√	√
26	13.41	1-dodecene	√			√		√
27	13.48	benzenepropanenitrile	√				√	√
28	13.93	2-decenal			√	√		√
29	14.40	1-tridecene	√					√
30	15.32	1-tetradecene	√			√	√	√
31	16.19	tetradecane	√					
32	16.27	pentadecane	√		√	√	√	√
33	17.01	heptadecenal	√			√		√
Total			26	13	18	16	20	22

Figure 3.15 illustrates the temperatures attained across the six heat exposure durations to which muscle samples were subjected. The headspace above the samples exposed to heat for 450, 500, 550, 600, 650 and 700 seconds, respectively attained a maximum temperature of 70 °C, 80 °C, 92 °C, 64 °C, 207 °C and 124 °C, respectively.

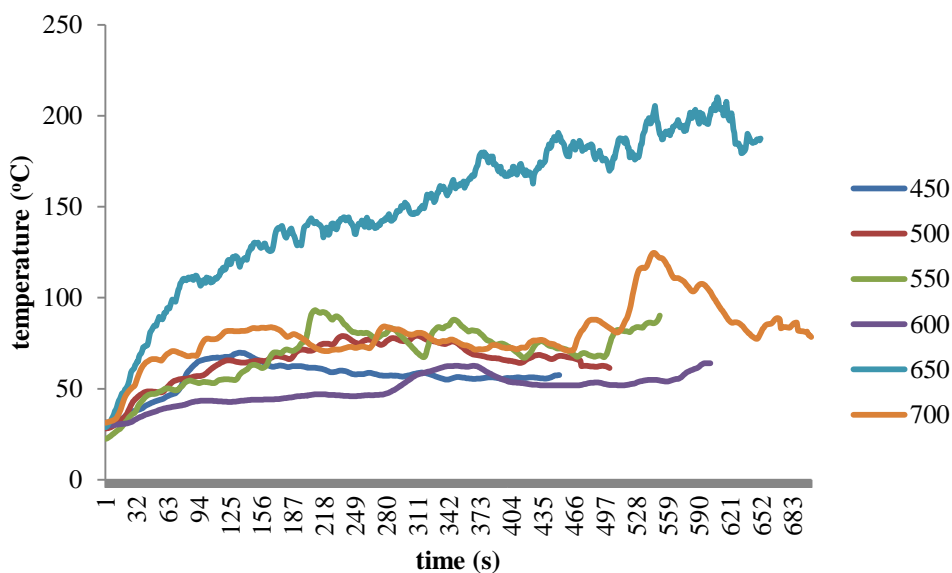
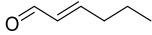
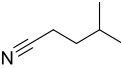
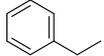
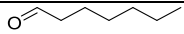
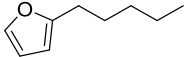
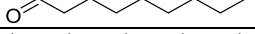
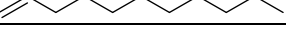
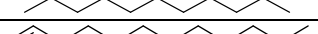
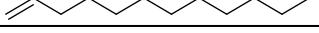
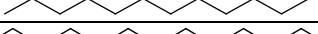
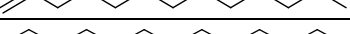
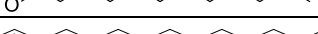
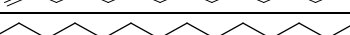
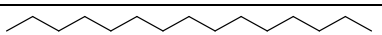
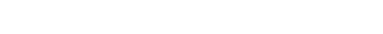


Figure 3.15: Overlay of six heat exposure duration time temperature profiles of heated porcine muscles

Porcine muscle samples were then subjected to six repetitive heating for 450 seconds. The results of the repetitive analysis are tabulated in Table 3.13. A representative total ion chromatogram (TIC) of a heated porcine muscle (set 4) and an overlay of the six repetitive samples at 450 seconds are illustrated in Figure 3.16 and Figure 3.17, respectively.

The temperature profiles obtained for the six repetitive samples at 450 seconds (Figure 3.18) and the consistency of pyrolysis products detected, detailed in Table 3.13 demonstrate that qualitative reproducibility was difficult to obtain and the only consistent products appearing in all six repeat samples were *n*-aldehydes of 3-methyl-butanal, pentanal and hexanal. Maximum temperatures attained across the headspace above the six repeats varied and were between 70 °C to 135 °C.

Table 3.13: The 27 compounds identified based on the m/z values and retention times for porcine muscle samples across six repeats exposed to heat for 450 seconds

No	Retention Time (min)	Compound	Molecular Structure	Set					
				1	2	3	4	5	6
1	3.81	3-methylbutanal		√	√	√	√	√	√
2	4.15	benzene					√	√	√
3	4.79	pentanal		√	√	√	√	√	√
4	6.91	toluene					√		√
5	7.45	hexanal		√	√	√	√	√	√
6	7.73	hexenal					√	√	
7	8.09	4-methylpentanenitrile				√	√		
8	8.91	ethylbenzene				√	√		√
9	9.27	ethanedial					√	√	
10	9.45	heptanal					√	√	
11	9.60	1-nonene					√	√	
12	10.96	2-pentyl-furan					√	√	√
13	10.98	octanal						√	√
14	11.08	1-decene					√	√	
15	12.26	nonanal					√	√	√
16	12.31	1-undecene					√	√	
17	12.44	undecane					√	√	
18	13.40	1-dodecene					√	√	√
19	13.52	dodecane					√	√	
20	14.40	1-tridecene					√	√	
21	14.50	tridecane					√	√	
22	14.83	2-dodecenal							√
23	15.32	1-tetradecene					√	√	√
24	15.41	tetradecane					√	√	
25	16.00	hexadecenal					√	√	
26	16.27	pentadecane					√	√	√
27	17.01	heptadecenal					√	√	

Abundance

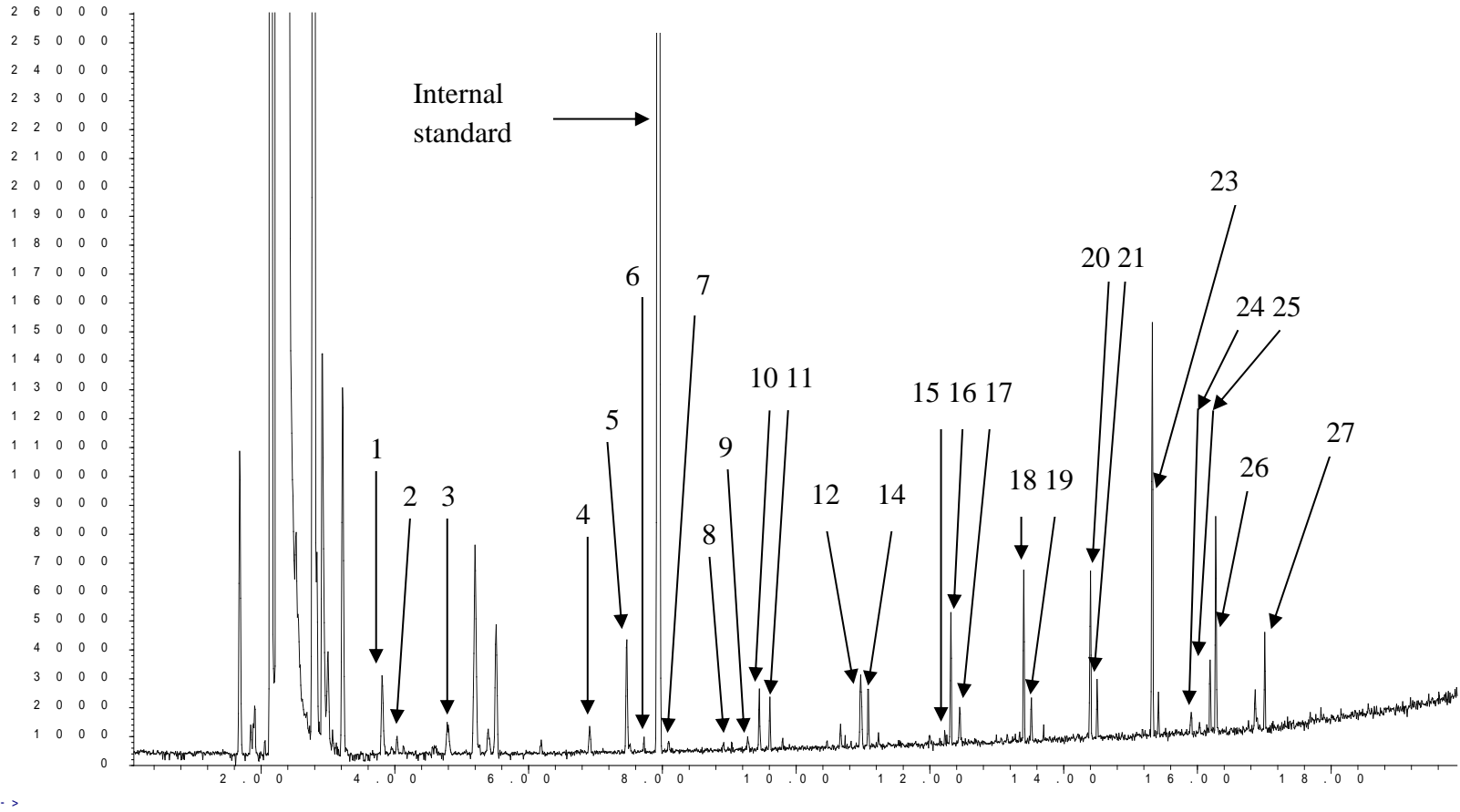


Figure 3.16: A representative TIC of heated porcine muscle exposed to heat for 450 seconds (set 4)

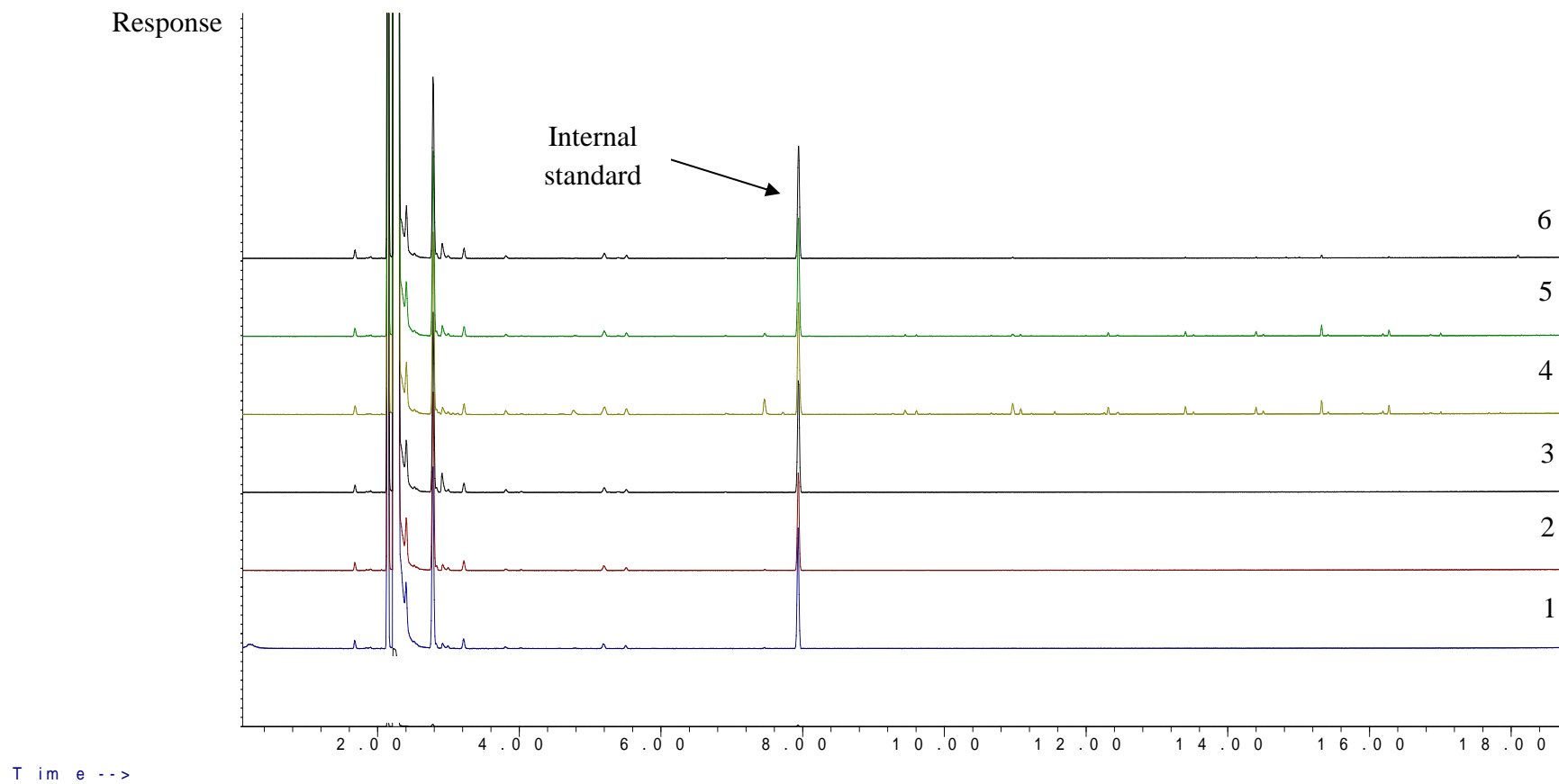


Figure 3.17: Overlay of six TICs of porcine muscle samples exposed to heat for 450 seconds

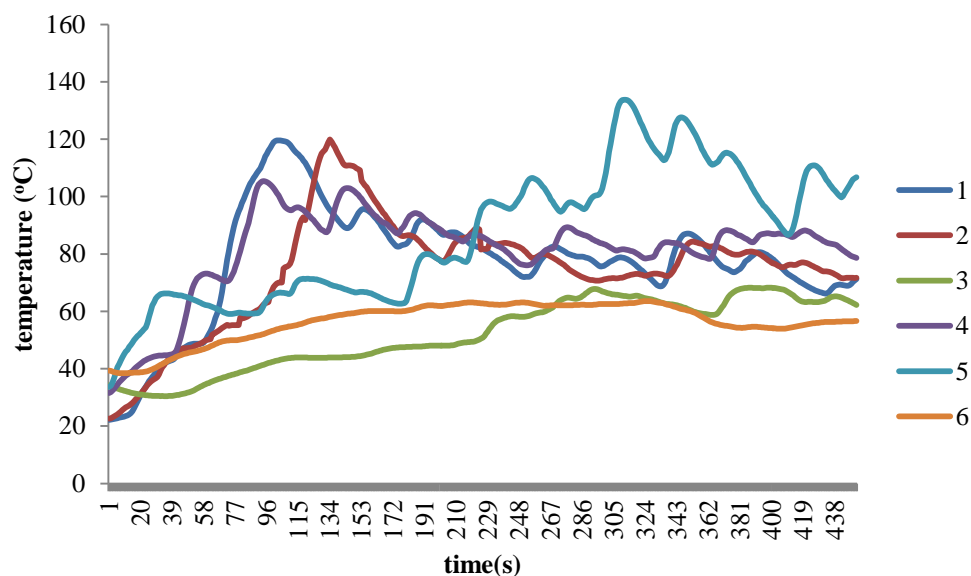


Figure 3.18: Six time temperature profiles of porcine muscle samples exposed to heat for 450 seconds

Although the duration of heat exposure did affect the generation of pyrolysis products, the temperatures attained by the samples during this exposure period played a more significant role in determining the absence and presence of pyrolysis products. This is supported by the clear inconsistencies observed across the type and number of pyrolysis products generated and the temperature profiles across six samples exposed to heat for the same duration of 450 seconds. Higher temperatures held at longer durations not unsurprisingly, generates more pyrolysis products [55]. This clearly demonstrates that the effects of fires can be very unpredictable and vary considerably from one sample to another.

3.5.3 Human Samples - Effects of Temperature

3.5.3.1 Post-Ignition Human Samples (> 250 °C)

The derived products are presented in Table 3.14. The pyrolysis of five human toe samples produced a range of products, namely *n*-alkanes, *n*-alkenes, light aromatics, *n*-alkyl-benzenes, nitriles, disulfide, furan and an alkyl-cycloalkane.

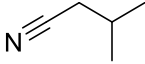
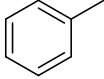
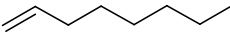
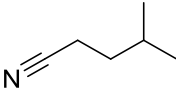
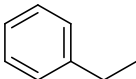
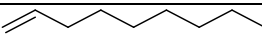
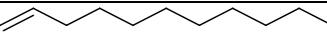
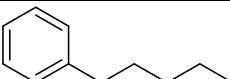
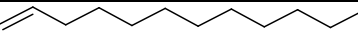
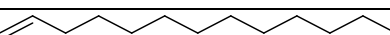
From the 32 products detected, only 22 were consistently present across the five repeats; these products include *n*-alkanes, *n*-alkenes, light aromatics, *n*-alkyl-benzenes and methyl-nitriles as detailed in Table 3.15. A representative total ion

chromatogram (TIC) of a burnt human toe sample is labelled and displayed in Figure 3.19 (set 4). *n*-Alkyl-benzenes (*p*-xylene, *o*-xylene, butyl-benzene and hexyl-benzene), an alkane (tetradecane), an alkene (heptadecene), a nitrile (hexanenitrile), a disulfide (dimethyl disulfide), an alkyl-cycloalkane (methyl-cyclohexane) and an alkyl-furan (2-pentyl-furan) were among those that were inconsistently present.

Table 3.14: 32 compounds identified based on the *m/z* values and retention times for burnt human toe samples

No	Retention Time (min)	Compound	Set				
			1	2	3	4	5
1	3.01	benzene	√	√	√	√	√
2	3.94	3-methyl-butanenitrile	√	√	√	√	√
3	4.76	dimethyl disulfide			√	√	
4	5.67	toluene	√	√	√	√	√
5	5.99	1-methyl-cyclohexane				√	
6	6.65	1-octene	√	√	√	√	√
7	6.93	octane	√	√	√	√	√
8	7.04	4-methyl-pentanenitrile	√	√	√	√	√
9	7.87	hexanenitrile	√			√	
10	7.92	ethyl-benzene	√	√	√	√	√
11	8.11	<i>p</i> -xylene	√			√	
12	8.51	<i>o</i> -xylene				√	
13	8.70	1-nonene	√	√	√	√	√
14	8.90	nonane	√	√	√	√	√
15	8.96	2-nonene	√		√	√	
16	10.12	2-pentyl-furan					√
17	10.24	1-decene	√	√	√	√	√
18	10.40	decane	√	√	√	√	√
19	10.96	butyl-benzene	√	√	√		
20	11.48	1-undecene	√	√	√	√	√
21	11.60	undecane	√	√	√	√	√
22	11.79	2-undecene	√	√	√	√	√
23	12.15	pentyl-benzene	√	√	√	√	√
24	12.59	1-dodecene	√	√	√	√	√
25	12.71	dodecane	√	√	√	√	√
26	13.23	hexyl-benzene				√	
27	13.59	1-tridecene	√	√	√	√	√
28	13.69	tridecane	√	√	√	√	√
29	14.51	1-tetradecene	√	√	√	√	√
30	14.61	tetradecane					√
31	15.45	pentadecane	√	√	√	√	√
32	16.86	1-heptadecene					√

Table 3.15: 22 consistently present compounds identified based on the m/z values and retention times for burnt human toe samples ($n=5$)

No	Retention Time (min)	Compound	Molecular Structure
1	3.01	benzene	
2	3.94	3-methyl-butanenitrile	
3	5.67	toluene	
4	6.65	1-octene	
5	6.93	octane	
6	7.04	4-methyl-pentanenitrile	
7	7.92	ethyl-benzene	
8	8.70	1-nonene	
9	8.90	nonane	
10	8.96	2-nonene	
11	10.24	1-decene	
12	10.40	decane	
13	11.48	1-undecene	
14	11.60	undecane	
15	11.79	2-undecene	
16	12.15	pentyl-benzene	
17	12.59	1-dodecene	
18	12.71	dodecane	
19	13.59	1-tridecene	
20	13.69	tridecane	
21	14.51	1-tetradecene	
22	15.45	pentadecane	

A b u n d a n c e

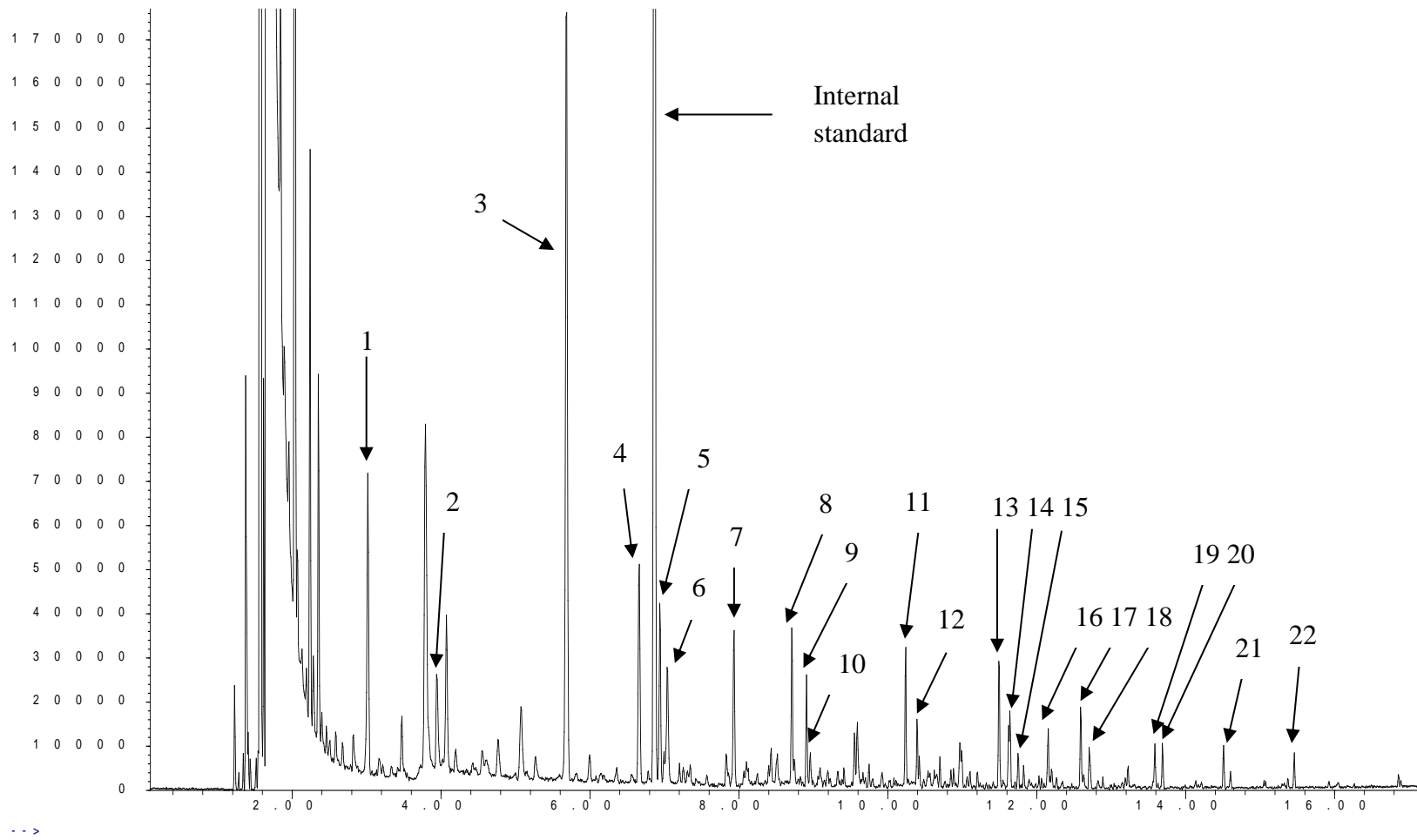


Figure 3.19: A representative TIC of a burnt human toe sample (set 4)

Figure 3.20 demonstrates a typical time temperature profile of the headspace above the burnt human toes. A patterned rise and fall in temperature was observed across the human toe samples. Temperatures began to rise once the Bunsen flame was applied to the base of the tin and, from then on, the sample experienced a gradual rise in its temperature profile until auto-ignition occurred approximately around 200 °C. From this point forward, temperatures rose steeply, typically reaching temperatures in excess of 700 °C before plateauing. The flames were extinguished after 1 minute and the tin covered for 4 minutes and then the pyrolysis products extracted.

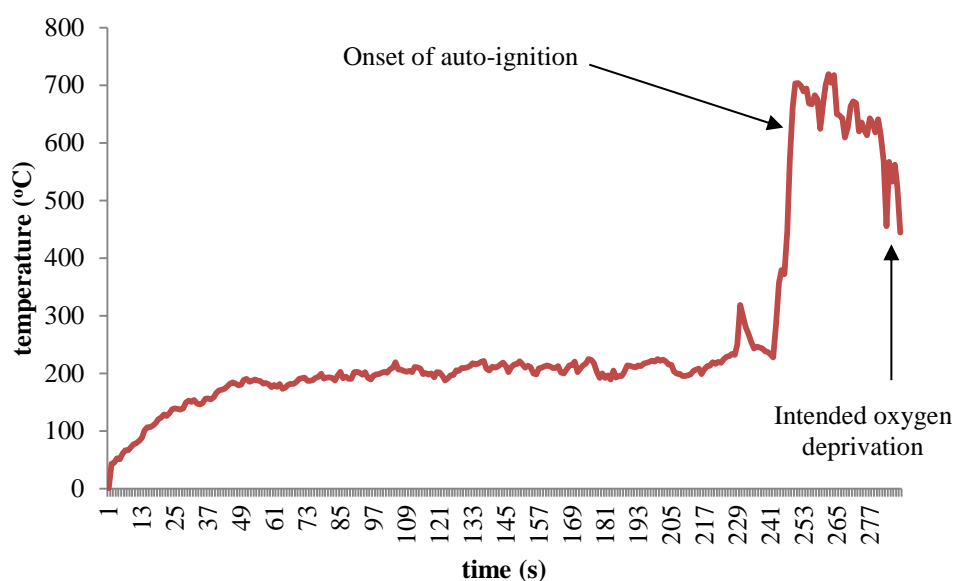


Figure 3.20: Typical time temperature profile of burnt human toes

3.5.3.2 Comparison of Pyrolysis Products Generated from Post-Ignition Human and Porcine Samples

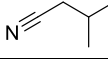
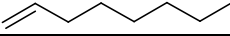
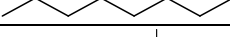
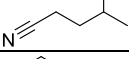
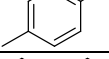
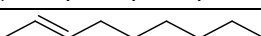
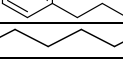
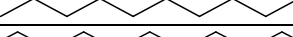
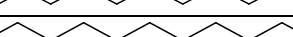
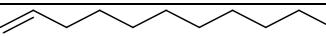
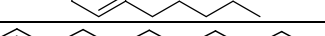
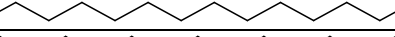
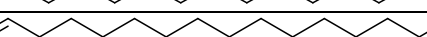
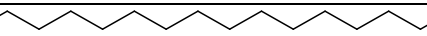
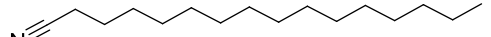
Comparison of the consistently present products generated from the pyrolysis of porcine bones (3.4.1.2) and human toes was conducted to identify similarities and differences across both types of samples as detailed in Table 3.16.

While both samples contained similar pyrolytic profiles of *n*-alkanes, *n*-alkenes and light aromatics, some compounds were detected consistently in the pyrolysis of porcine bone but not in human toes; these compounds were higher molecular weight *n*-alkanes and *n*-alkenes (with the exception of pentadecane in human toes), *p*-

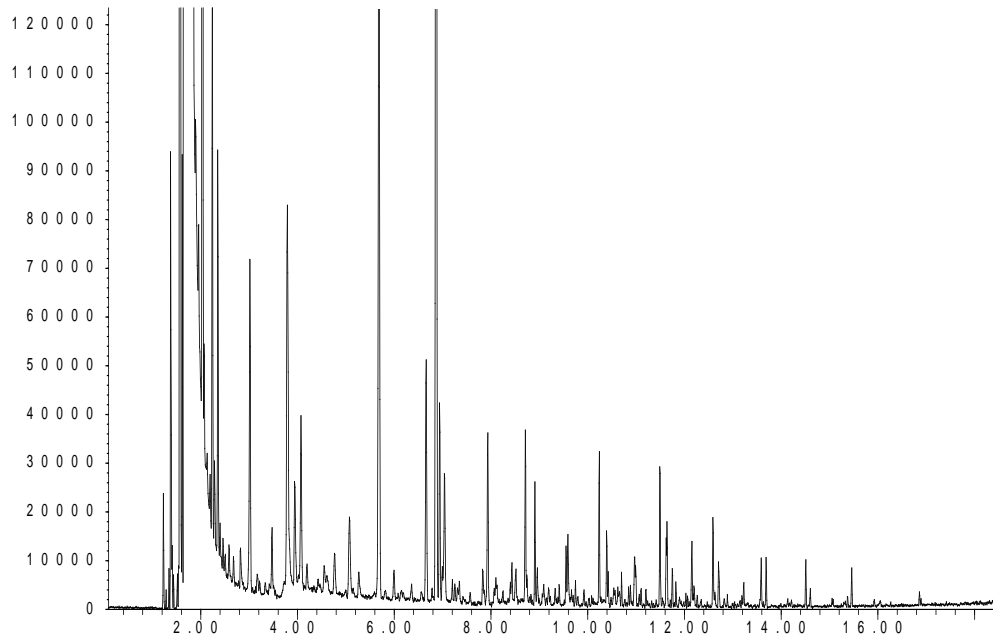
xylene, propyl-benzene and hexadecanitrile. Although not detected consistently across the five sets of repeats, these products (tetradecane, heptadecene and *p*-xylene) were detected in one or more of the sets of human toe samples (Table 3.14). The presence of dimethyl disulfide, *n*-alkyl-benzenes, 2-pentyl-furan and *o*-xylene detected inconsistently from human toe samples is also highlighted. With the exception of 2-pentyl-furan and *o*-xylene, the remaining inconsistently detected pyrolysis products from human toe samples were also present inconsistently across porcine bone samples (Appendix 1.0). In terms of consistently appearing compounds, slightly more pyrolysis products were generated from porcine samples (26) as compared to those generated by human toe samples (22). Variation in the number of products detected could be due to the differences in sample size. Human toe samples were of 5 g or lesser in weight in comparison to the 25 g porcine bone samples. With lesser fat supply, human toe samples could only burn for short durations and this would not have facilitated the generation of more, and high molecular weight pyrolysis products. This could also be due to the differences in the composition of human toes in comparison to porcine bones. The human toe consist of a network of nail, skin, muscle and soft tissues (abductor hallucis in the big toe and abductor digiti minimi for the other toes), nerves, blood vessels and bone [63, 64] whereas porcine bone samples only contained bone with no other tissues. As both samples possess different chemistry and composition, with varying proportions of water, protein, lipids, minerals and carbohydrates, it is not surprising that their profiles would display some differences as the comparison was not like-to-like, as observed by Dehaan *et al.* [1].

Pyrolysis products of 3-methyl-butanenitrile, 4-methyl-butanenitrile and pentyl-benzene, which were present in the burnt human samples, were not detected consistently in porcine bone samples. However, these products, with the exception of pentyl-benzene, were detected inconsistently in a number of sets of repeats porcine bone samples, detailed in Appendix 1.0. The differences in the pyrolysis compounds detected across both samples were minimal and, when comparing their TICs in Figures 3.21 (a) and (b), both appear to have similar chromatographic profiles. Similar outcomes were also documented in the literature [1, 19].

Table 3.16: Comparison of the consistently detected pyrolysis products generated from burnt porcine bone and human toe samples

No	Compounds	Molecular Structure	Burnt Human Toe	Burnt Porcine Bone
1	benzene		√	√
2	3-methyl-butanenitrile		√	
3	toluene		√	√
4	1-octene		√	√
5	octane		√	√
6	4-methyl-pentanenitrile		√	
7	ethyl-benzene		√	√
8	<i>p</i> -xylene			√
9	1-nonene		√	√
10	nonane		√	√
11	2-nonene		√	
12	propyl-benzene			√
13	1-decene		√	√
14	decane		√	√
15	1-undecene		√	√
16	undecane		√	√
17	2-undecene		√	
18	pentyl-benzene		√	
19	1-dodecene		√	√
20	dodecane		√	√
21	1-tridecene		√	√
22	tridecane		√	√
23	1-tetradecene		√	√
24	tetradecane			√
25	1-pentadecene			√
26	pentadecane		√	√
27	1-hexadecene			√
28	hexadecane			√
29	1-heptadecene			√
30	heptadecane			√
31	hexadecanitrile			√
Total compounds			22	26

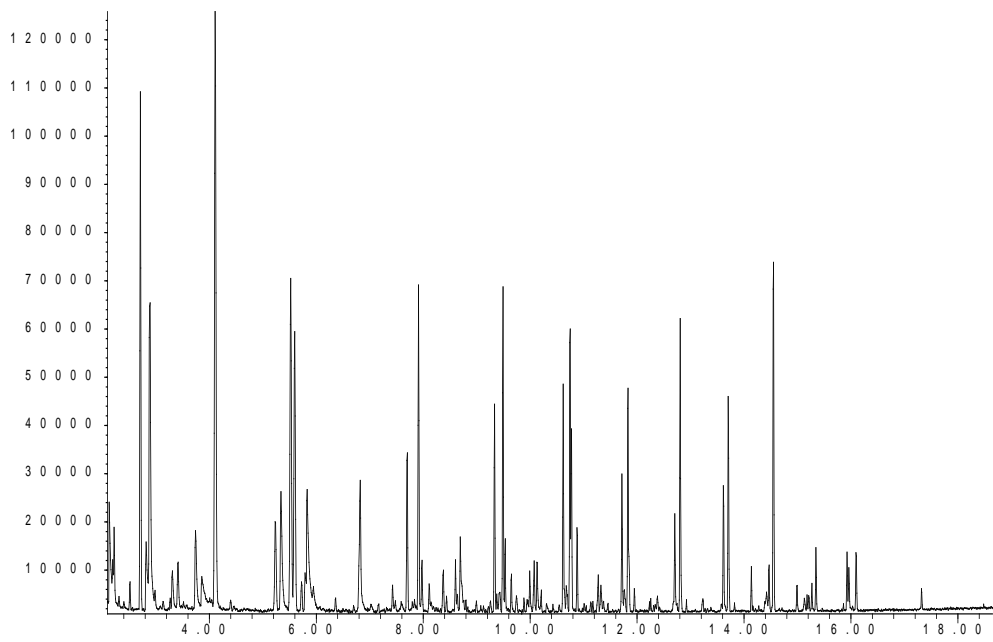
Abundance



Time -->

(a)

Abundance



Time -->

(b)

Figure 3.21: Representative TICs of burnt (a) human toe and (b) porcine bone

Both human and porcine samples generated low and medium molecular weight C₈ to C₁₅ *n*-alkanes and *n*-alkenes, together with some aromatics, *n*-alkyl-benzenes and nitrile(s) (Table 3.16). Porcine samples generated higher molecular weight C₁₆ to C₁₇ *n*-alkanes and *n*-alkenes as well. Low molecular weight and medium molecular weight *n*-alkanes and *n*-alkenes and aromatics were seen to be present in prior studies on human and porcine fat / tissue [1, 2, 55]. However, high molecular weight *n*-alkanes and *n*-alkenes together with nitriles have only been mentioned once as present in animal bone pyrolysis analysis [55]. (This excludes the findings in Agu's research [49] of which this study was an extension).

The low vapour pressures of higher molecular weight *n*-alkanes and *n*-alkenes require analysis using higher temperatures and longer lengths of time in order to be resolved [52]. If experimental procedures and analytical techniques do not facilitate these temperatures and durations, then these compounds will not volatilise and, hence, will not be detected [54]. This is seen in DeHaan *et al.*'s [1] study, whereby a microfurnace CDS pyrolysis probe was utilised to generate pyrolysis products at various low and high temperatures for 10 seconds. Although some of the temperatures were high enough, the short exposure duration could have limited the volatilisation of these high molecular weight compounds and could be the reason why they were not detected. Utilising condensation techniques to capture pyrolysed water and tar at 500 °C to 700 °C for about 4 to 5 hours, Purevsuren *et al.* [55] managed to detect these high molecular weight *n*-alkanes and *n*-alkenes. Similarly in this study, heavy hydrocarbons were detected as; (1) the burning duration of the samples were between 13-16 minutes at temperatures exceeding 700 °C, and (2) the adsorption temperature was set at 80 °C for 16 hours (optimised for the extraction of pyrolysis products in prior experiments), recommended by the ASTM [56, 57] and several authors [58-60] as they are high enough to volatilise high molecular weight compounds without displacing low molecular weight compounds. Temperatures lower than this did not have the capacity to volatilise high molecular weight compounds, whereas temperatures higher than this caused a high rate of displacement of low molecular weight compounds and unwanted decomposition of volatiles.

Table 3.17 provides a summary of the type of tissues and type of pyrolysis products generated in this study in comparison to those reported in the literature.

n-Aldehydes were not detected from the pyrolysis of either porcine or human samples in this work. Such products have been previously documented in the literature, particularly in pyrolysed human and animal fat [1, 2], Discussed in detail in the previous section, the absence of *n*-aldehydes has been shown to be directly related to the temperature and length of exposure time of the sample to heat. When looking at the temperature profiles for porcine and human samples (Figures 3.10 and 3.20, respectively), temperatures attained during the experiment were in the range of 650 °C to 750 °C and held for either 5 minutes (porcine) or 1 minute (human). These high temperature ranges have most likely caused the degradation and oxidation of *n*-aldehydes, breaking them into smaller, undetectable compounds [1, 49]. Similar situations would be expected to occur in a typical fire. In the context of human identification using unburnt VOC, Vass *et al.* [61] developed an approach using a ratio of aldehydes, ketones, alcohols and amides, generated from the odour of each species, in order to differentiate bones from pig, human, deer and dog. However, for burnt samples, odour analysis would be redundant given the effects of heat on these remains.

Table 3.17 continued

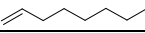
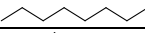
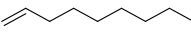
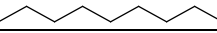
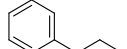
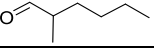
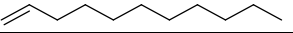
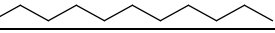
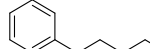
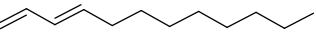
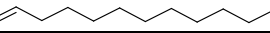
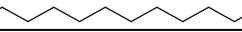
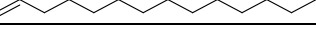
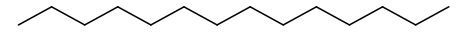
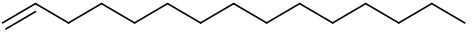
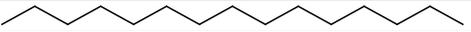
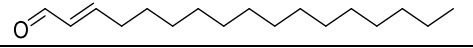
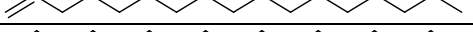
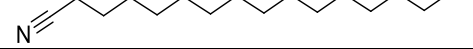
toluene		√	√		√		√		√
1-octene		√	√					√	√
octane		√	√					√	√
ethyl-benzene		√	√				√		√
<i>p</i> -xylene			√						√
1-nonene		√	√		√			√	
nonane		√	√					√	√
2-nonene		√							
propyl-benzene			√						
1-decene		√	√		√			√	√
decane		√	√		√			√	√
nonanal					√	√		√	
methyl-hexanal								√	
1-undecene		√	√		√				√
undecane		√	√	√	√				√
2-undecene		√							
pentyl-benzene		√							
dodecadiene								√	
1-dodecene		√	√		√			√	√
dodecane		√	√		√		√	√	√
decanal								√	
cyclodecene								√	√
1-tridecene		√	√		√			√	√
tridecane		√	√	√	√			√	√
1-tetradecene		√	√	√	√				√

Table 3.17 continued

tetradecane			√		√				√
1-pentadecene			√		√				√
pentadecane		√	√	√	√				√
heptadecenal					√				
1-hexadecene			√						√
hexadecane			√						√
1-heptadecene			√						√
heptadecane			√						
hexadecanitrile			√						

3.6 Conclusions

Pyrolysis products generated from three different types of porcine tissues displayed similar chromatographic profiles for pre-ignition samples, generating mainly *n*-aldehydes. The main differences noted amongst these tissues were the inability of porcine muscle and rib samples to attain auto-ignition, whereas porcine bone readily auto-ignited; this illustrated that differences in tissue sampling from a fire scene can certainly influence the type of pyrolysis products detected. This information could also be useful to researchers when selecting certain parts of porcine tissue to simulate human tissue for laboratory generation of pyrolysis data.

The effects of temperature on the chromatographic output of pyrolysed tissues are clearly seen for pre-ignition and post-ignition samples. Pre-ignition samples generated a homologous series of *n*-aldehydes, whereas no *n*-aldehydes were detected in the latter samples. Post-ignition porcine bone generated a consistent presence of *n*-alkanes, *n*-alkenes, aromatics, *n*-alkyl-benzenes and a nitrile. As *n*-aldehydes have been documented to be potential key indicators of human remains, failure to detect them in this study at elevated temperatures clearly demonstrates that their presence and absence is temperature dependent. This renders unreliable the use of *n*-aldehydes to be key indicators of human remains in a fire and has convincingly resolved the previous research literature. The duration of exposure to heat did not generate repeatable results across a series of six samples as the temperatures attained and held by the samples during the course of exposure to heat fluctuated and appeared to have more of an influence on the type and number of products generated. This study has clearly demonstrated that, even in a laboratory-controlled environment, pyrolysis profiles generated from samples exposed to an open flame can vary in an unpredictable way.

Pyrolysis products generated from porcine and human tissues exposed to an open flame under laboratory conditions displayed similar chromatographic profiles across the species, demonstrating the ability of porcine samples to act as a reasonable substitute for human samples in the analysis of pyrolysis products.

3.7 References

1. Dehaan, J.D., Brien, D.J., and Large, R., *Volatile Organic Compounds from the Combustion of Human and Animal Tissue*. Science and Justice, 2004. **44**(4): p. 223-236.
2. McLellan, S.A., *An Investigation of the Volatiles Produced from Pyrolysis of the Body*, in Centre for Forensic Science, Department of Pure and Applied Chemistry. 1999, University of Strathclyde: Glasgow, Scotland.
3. Berces, T., *Thermal Decomposition of Aldehydes and Ketones*, in Decomposition and Isomerization of Organic Compounds, ed. R.G. Compton, C.H. Bamford, and C.F.H. Tipper. Vol. **5**. 1971, Amsterdam, The Netherlands: Elsevier Publishing Company.
4. Babrauskas, V., *Temperatures in Flames and Fires*. 2014, Fire Science and Technology Inc., (2008-2014): Issaquah, WA.
5. Timberlake, K., *Chemistry: An Introduction to General, Organic, and Biological Chemistry*. 10th Edition. 2009, Los Angeles, California: Pearson: Prentice Hall.
6. Brown, W. H., *Aldehydes*. Encyclopaedia Britannica. [Online] [January 2014, November 2014]. Available from: <http://www.britannica.com/EBchecked/topic/13527/aldehyde>.
7. Royal Society of Chemistry (RSC), *Names and Identifies: Aldehydes*. [Online] [January 2014, August 2014]. Available from: <http://www.chemspider.com/Chemical-Structure.7883.html>.
8. Sherwood, L., *Human Physiology: From Cells to Systems*. 7th Edition. 2008, Belmont, California: Brooks/Cole: Cengage Learning.
9. Chang, R., *Chemistry*. Vol. **9**. 2007, Boston, USA: McGraw Hill.
10. Janaway, R.C., Percival, S.L., and Wilson, A.S., *Chapter 14: Decomposition of Human Remains*, in Microbiology and Aging: Clinical Manifestations, ed. S.L. Percival. 2009, New York, USA: Springer Science and Business Media.
11. Marieb, E.N. and Hoehn, K., *Human Anatomy & Physiology*. 7th Edition. 2007, USA: Pearson Education.

12. Mitchell, H.H., Hamilton, T.S., Steggerda, F.R., and Bean, H.W., *The Chemical Composition of the Adult Human Body and Its Bearing on the Biochemistry of Growth*. Journal of Biological Chemistry, 1945. **158**(3): p. 625-637.
13. Forbes, R.M., Cooper, A.R., and Mitchell, H.H., *The Composition of the Adult Human Body as Determined by Chemical Analysis*. Journal of Biological Chemistry, 1953. **203**(1): p. 359-366.
14. Helmenstine, A. M., *Chemistry Chemical Composition of the Human Body*. [Online] [April 2014, July 2014]. Available from: <http://chemistry.about.com/chemicalcomposition/a/Chemical-Composition-Of-The-Human-Body.htm>.
15. *Composition of Muscle Tissue*. [Online] [February 2013, July 2014]. Available from: www.depts.ttu.edu/meatscience/docs/8_Composition_of_Muscle.pptx.
16. *Structure of Muscle Tissue and Associated Tissues*. [Online] [January 2013, July 2014]. Available from: <http://www.as.nchu.edu.tw/lab/409%E8%AC%9B%E7%BE%A9/Structure%20of%20Muscle%20Tissue%20II.pdf>.
17. Brook, C.G.D., *Composition of Human Adipose Tissue from Deep and Subcutaneous Sites*. British Journal of Nutrition, 1971. **25**(03): p. 377-380.
18. Dehaan, J.D., *Sustained Combustion of Bodies: Some Observations**. Journal of Forensic Sciences, 2012.
19. Dehaan, J.D., Campbell, S.J., and Nurbakhsh, S., *Combustion of Animal Fat and Its Implications for the Consumption of Human Bodies in Fires*. Science and Justice, 1999. **39**: p. 27-38.
20. Drysdale, D., *An Introduction to Fire Dynamics*. 2002, Scotland, UK: John Wiley and Sons.
21. Dehaan, J.D., *Fire and Bodies*, in *The Analysis of Burnt Human Remains*, ed. C.W. Schmidt and S.A. Symes. 2008, London, UK: Academic Press. p:1-13.
22. Dehaan, J.D., *Kirk's Fire Investigation*. 6th Edition. 2007, New Jersey: Pearson: Prentice Hall.
23. Dehaan, J.D., *Kirk's Fire Investigation*. 5th Edition. 2002, Upper Saddle River, NJ: Prentice Hall.

24. *Principle of Animal Physiology: Muscle Physiology*. [Online] [January 2014, July 2014]. Available from: <https://www.uta.edu/biology/bernard/classnotes/3442/08%20Animal%20Physiology%20-%20Muscle%20Physiology.pdf>.
25. National Cancer Institute, National Institutes of Health, *Structure of Skeletal Muscle*. [Online] [April 2014, June 2014] Available from: <http://training.seer.cancer.gov/anatomy/muscular/structure.html>.
26. Cooper, G.M., *The Cell: A Molecular Approach* 2000, Sinauer Associates: Sunderland, MA.
27. Frayn, K., Arner, P., and Yki-Jarvinen, H., *Fatty Acid Metabolism in Adipose Tissue, Muscle and Liver in Health and Disease*. *Essays Biochem*, 2006. **42**: p. 89-103.
28. Robertson, J.D., *Studies on the Chemical Composition of Muscle Tissue II. The Abdominal Flexor Muscles of the Lobster Nephrops Norvegicus (L.)*. *Journal of Experimental Biology*, 1961. **38**(4): p. 707-728.
29. Clarke, B., *Normal Bone Anatomy and Physiology*. *Clinical Journal of the American Society of Nephrology*, 2008. **3**(3): p. 131-139.
30. Frandson, R.D., Wilke, W.L., and Fails, A.D., *Anatomy and Physiology of Farm Animals*. 7th Edition. 2009, Blackwell, UK: John Wiley and Sons.
31. Bell, J., Bell, C., and Godman, J.D., *The Anatomy and Physiology of the Human Body*. Vol. **1**. 1827, New York, USA: Collins and Co.
32. Saladin, K.S. and Mcfarland, R.K., *Human Anatomy*. 2007, Phillipines: McGraw-Hill International Edition.
33. Field, R.A., Riley, M.L., Mello, F.C., Corbridge, J.H., and Kotula, A.W., *Bone Composition in Cattle, Pigs, Sheep and Poultry*. *Journal of Animal Science*, 1974. **39**(3): p. 493-499.
34. Henrique, W., Sampaio, A.A.M., Leme, P.R., Alleoni, G.F., and Lanna, D.P.D., *Estimativa Da Composição Química Corporal De Tourinhos Santa Gertrudes a Partir Da Composição Química E Física Das 9-10-11^a Costelas*. *Revista Brasileira de Zootecnia*, 2003. **32**(3): p. 709-726.
35. Woodard, H.Q., *The Elementary Composition of Human Cortical Bone*. *Health Physics*, 1962. **8**(5): p. 513-517.

36. Spitz, W.U., *Thermal Injuries*, in *Medicolegal Investigation of Death: Guidelines for the Application of Pathology to Crime Investigation*, ed. C.C. Thomas. 1993, 3rd Edition. Springfield, IL: Charles C. Thomas. p. 413-443.
37. Murray, K.A. and Rose, J.C., *The Analysis of Cremains: A Case Study Involving the Inappropriate Disposal of Mortuary Remains*. *Journal of Forensic Sciences*, 1993. **38**(1): p. 98-103.
38. Symes, S.A., Dirkmaat, D.C., Ousley, S., Chapman, E., and Cabo, L., *Recovery and Interpretation of Burned Human Remains*. 2012, Final Technical Report: U.S Department of Justice: USA. p. 229.
39. Eckert, W.G., James, S., and Katchis, S., *Investigation of Cremations and Severely Burned Bodies*. *The American Journal of Forensic Medicine and Pathology*, 1988. **9**(3): p. 188.
40. Bohnert, M., Rost, T., and Pollak, S., *The Degree of Destruction of Human Bodies in Relation to the Duration of the Fire*. *Forensic Science International*, 1998. **95**(1): p. 11-21.
41. Dehaan, J.D., *Sustained Combustion of Bodies: Some Observations**. *Journal of Forensic Sciences*, 2012.
42. Dehaan, J.D. and Nurbakhsh, S., *Sustained Combustion of an Animal Carcass and Its Implications for the Consumption of Human Bodies in Fires*. *Journal of Forensic Sciences*, 2001. **46**(5): p. 1076.
43. Fairgrieve, S.I., *Fire and Combustion Forensic Cremation: Recovery and Analysis*. 2008, Boca Raton: Florida: CRC Press.
44. Pope, E.J., *The Effects of Fire on Human Remains: Characteristics of Taphonomy and Trauma*, in *Department of Anthropology*. 2008, University of Arkansas: Fayetteville, AR. p. 525.
45. Kollias, N., Zonios, G., and Stamatias, G.N., *Fluorescence Spectroscopy of Skin*. *Vibrational Spectroscopy*, 2002. **28**(1): p. 17-23.
46. Brakebusch, C. and Fässler, R., *$\beta 1$ Integrin Function in Vivo: Adhesion, Migration and More*. *Cancer and Metastasis Reviews*, 2005. **24**(3): p. 403-411.

47. Chizzolini, R., Zanardi, E., Dorigoni, V., and Ghidini, S., *Calorific Value and Cholesterol Content of Normal and Low-Fat Meat and Meat Products*. Trends in Food Science and Technology, 1999. **10**(4-5): p. 119-128.
48. Currey, J.D., *Bones: Structure and Mechanics*. 2002, Princeton: New Jersey: Princeton Univ Press.
49. Agu, K., *Investigation of the Thermal Degradation Products of Bone*, in Centre for Forensic Science, Department of Pure and Applied Chemistry. 2011, University of Strathclyde: Glasgow, Scotland.
50. Maher, K. and Bressler, D., *Pyrolysis of Triglyceride Materials for the Production of Renewable Fuels and Chemicals*. Bioresource Technology, 2007. **98**(12): p. 2351-2368.
51. Lima, D.G., Soares, V.C., Ribeiro, E.B., Carvalho, D.A., Cardoso, Ã.R.C., Rassi, F.V.C., Mundim, K.C., Rubim, J.C., and Suarez, P.A., *Diesel-Like Fuel Obtained by Pyrolysis of Vegetable Oils*. Journal of Analytical and Applied Pyrolysis, 2004. **71**(2): p. 987-996.
52. Stauffer, E., *Concept of Pyrolysis for Fire Debris Analysis*. Science and Justice, 2003. **43**(1): p. 29-40.
53. Almirall, J.R. and Furton, K.G., *Characterization of Background and Pyrolysis Products That May Interfere with the Forensic Analysis of Fire Debris*. Journal of Analytical and Applied Pyrolysis, 2004. **71**(1): p. 51-67.
54. Paczkowski, S. and Schütz, S., *Post-Mortem Volatiles of Vertebrate Tissue*. Applied Microbiology and Biotechnology, 2011. **91**(4): p. 917-935.
55. Purevsuren, B., Avid, B., Gerelmaa, T., Davaajav, Y., Morgan, T., Herod, A., and Kandiyoti, R., *The Characterisation of Tar from the Pyrolysis of Animal Bones*. Fuel, 2004. **83**(7): p. 799-805.
56. ASTM International E1412-07, *Standard Practice for Separation of Ignitable Liquid Residues from Fire Debris Samples by Passive Headspace Concentration with Activated Charcoal*. 2012. American Society for Testing and Materials (ASTM) International: West Conshohocken, PA.
57. ASTM International E1388-12, *Standard Practice for Sampling of Headspace Vapors from Fire Debris Samples*. 2012. American Society for Testing and Materials (ASTM) International: West Conshohocken, PA.

58. Newman, R.T., Dietz, W.R., and Lothridge, K., *The Use of Activated Charcoal Strips for Fire Debris Extractions by Passive Diffusion. Part 1: The Effects of Time, Temperature, Strip Size, and Sample Concentration*. Journal of Forensic Science, 1996. **41**(3): p. 361-370.
59. Nic Daeid, N., *Fire Investigation*. 2004, Boca Raton, Florida: CRC Press.
60. Stauffer, E., Dolan, J.A., and Newman, R., *Fire Debris Analysis*. 2008, San Diego, USA: Academic Press.
61. Vass, A.A., Smith, R.R., Thompson, C.V., Burnett, M.N., Dulgerian, N., and Eckenrode, B.A., *Odor Analysis of Decomposing Buried Human Remains**. Journal of Forensic Sciences, 2008. **53**(2): p. 384-391.
62. Purevsuren, B., Avid, B., Gerelmaa, T., Davaajav, Y., Morgan, T.J., Herod, A.A., and Kandiyoti, R., *The Characterisation of Tar from the Pyrolysis of Animal Bones*. Fuel, 2004. **83**(7-8): p. 799-805.
63. *Sole of the Foot: Muscles* [Online] [2014, May 2015]. Available from: <http://www.gla.ac.uk/t4/~fbis/files/fab/tutorial/anatomy/sole3.html>.
64. Encyclopaedia Britannica. *Hands and Feet*. Human Skeletal System [Online] [January 2015, May 2015]. Available from: <http://www.britannica.com/EBchecked/topic/547358/human-skeletal-system/41870/Hands-and-feet>.

CHAPTER 4: METHODOLOGY DEVELOPMENT FOR THE GENERATION, ANALYSIS AND CHARACTERISATION OF PYROLYSIS PRODUCTS FROM VARIOUS TEXTILE MATERIALS

4.1 Introduction

Textile materials have been found to cause significant fire risk both in Europe [1] and in the UK [2]. More often than not, a fire scene is commonly surrounded by various textile based materials that are used in the manufacture of carpets, upholstery, sofas, curtains, bedding and clothing. Knowledge and understanding of the volatile products generated from these textile materials in a fire is crucial in order to determine their potential in generating any interfering volatile products that may rise within the analytical results generated from fire debris samples.

Numerous studies have looked into the pyrolysis products generated from specific types of natural or synthetic fibre under various environmental conditions. This study intends to take the existing work a step further, by looking into the systematically generated pyrolysis products from common fibres encountered in fire scenes and utilised as clothing, such as cotton, polyester, nylon, wool, leather, silk and acrylic, but also to include a combination of these common textiles with other fibres such as modal, elastin, viscose, rayon, linen and spandex (LYCRA[®]) in various proportions to see the effects of these blends on the resultant mechanism, interaction and type of pyrolysis products generated.

4.2 Natural Fibres

Natural fibres, such as cotton, wool and silk, are elongated fibres that can be found naturally in the ecosystem. Obvious variations in their physical structure and chemical properties distinguish whether these fibres are produced by animals or plants. In terms of their physical structure, animal fibres such as wool and silk tend to be rougher and bulkier in comparison to plant fibres (e.g. cotton, hemp, flax) that possess a softer, more pliable texture [3]. The building block of plant fibres is

predominantly cellulose, thus making these fibres susceptible to odourless burning and acidic reactions, whereas animal fibres are made up of proteins (i.e. a polypeptide chain of amino acids) that burn reluctantly with a pungent odour and suffer immediate deterioration in the presence of an alkali. Both of these categories of fibres are extremely useful and have been manipulated to generate desirable materials that are used around the world today [4, 5].

4.2.1 Plant Fibres

4.2.1.1 Cotton

Produced by the plant genus *Gossypium*, cotton is one of the most widely produced and used natural agricultural fibre worldwide [4, 6]. Originally commercialised in India, these fibres are now used internationally because of their versatility and favourable physical characteristics (e.g. tensile strength, absorbency, softness, ease of cleaning and handling) and performance [7, 8]. Most (60%) commercialised cotton is used in the clothing industry (e.g. shirts, socks, dresses, jackets, pants, denim) and the remaining 40% used in home furnishings (curtains, sofas, bedspreads, comforters, napkins) and other applications (fire-proof apparel, cotton wool, gauze bandages, compresses) [4, 8, 9].

Cotton consists of a number of layers of material. The outer layer (cuticle) of cotton is primarily made up of wax, serving as a protective barrier against water and microbial degradation [6, 8]. The underlying layer is filled with pectin substances either in the form of pectic acid or pectic salts, and finally hemicellulose and cellulose makes up the innermost layer of the primary and secondary wall. The primary wall comprises crystalline cellulose fibres, whereas the secondary wall is made up of compacted, winding parallel fibres that contains the most cellulose [6]. Figure 4.0 provides a schematic representation of the various layers in a cotton fibre.

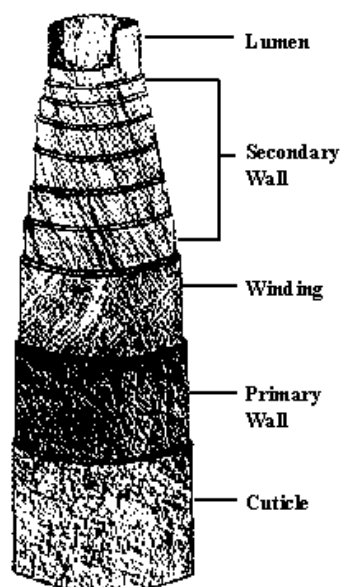


Figure 4.0: A schematic representation of the various layers in a cotton fibre [10]

Each cotton fibre is predominantly made up of polysaccharide chains of cellulose (Figure 4.1), namely repeatable units of linear D -glucopyranose linked together by the β -1,4-glycosidic bonds (Figure 4.2), making up to 80-95% of its composition [7, 8, 11-13]. These glucan units normally arrange themselves in two forms, either regularly in the crystalline region or irregularly in the amorphous region [11, 13]. These arrangements across both regions largely dictate the physical, chemical and reactivity of the fibre in general.

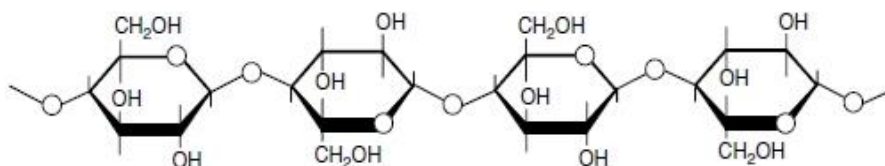


Figure 4.1: Cellulose polymer [6]

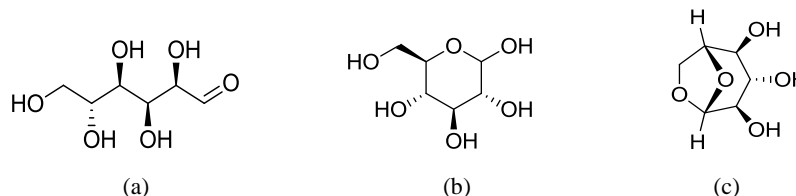


Figure 4.2: Chemical structure of (a) D -glucose, (b) glucopyranose and (c) levoglucosan

Other non-cellulosic compounds such as wax and pectin are found on the cuticle and in the underlying layers of cotton, whereas protein, water and other substances are either found inside the lumen or in-between the pores in the amorphous region of the fibre [6-8, 11]. Inorganic ions such as potassium, magnesium, calcium, sodium and iron are also present in varying amounts throughout the cotton layers [14]. Table 4.0 reveals the composition and proportion of various constituents in a typical cotton fibre.

Table 4.0: Composition and proportion of cotton's major constituents and inorganic ions. Adapted from [6], [8] and [14].

Major Constituent	Range (%)
Cellulose	80-95
Water	6-8
Hemicellulose and Pectin	4-6
Protein	1.0-1.9
Other (acid and pigments)	0.5-2.5
Wax and Fats	0.5-1.0
Ash	0.1-1.8
Inorganic Ion	Range (ppm)
Potassium	2000-6500
Magnesium	400-1200
Calcium	400-1200
Sodium	100-300

As cotton is predominantly cellulose, it possesses similar thermal behaviour to cellulose [15] and can either undergo smouldering combustion or flaming combustion; the latter is much more common [15]. Smouldering combustion occurs when oxygen levels are too low to facilitate flames but high enough to oxidise solid cellulose. It occurs at a much slower rate as compared to flaming combustion. Flaming combustion involves both solid and gas phases, where heat causes endothermic decomposition of cellulose, forming volatile gases which when mixed with oxygen will, in the presence of an ignition source, result in flaming ignition of the volatile gases [6].

With a low limiting oxygen index (LOI) (minimum concentration of oxygen that is required to support the combustion of a material) of 18.4%, (Table 4.1) similar to that of regenerated cotton fibres (e.g. rayon, viscose, modal) [16, 17], cotton ignites and burns rapidly [18]. Fibres with LOI values of < 21% are considered highly

flammable, 21-25% are moderately flammable and > 25% possess low flammability [19]. According to Matthews [7] and Wakelyn *et al.* [6], although cotton can withstand relatively high temperatures before experiencing any alterations, at 120-160 °C, cellulose experiences dehydration and weight loss that eventually leads to structural collapse. Abidi *et al.* [20] reported that non-cellulosic compounds present in the cuticle and primary wall of cotton tend to breakdown first as they possess lower decomposition temperatures as compared to cellulose. Cellulose heated above 140 °C experiences further loss in tensile strength and is discoloured to a scorched yellow [6]. Temperatures above 200 °C induces further weight loss of up to 62% [21], causing complete loss of tensile strength and turns the cotton brown.

Table 4.1: Limiting oxygen index (LOI) values for commonly encountered fibres. Adapted from [22], [23] and [24].

Fibre	LOI (vol%)
Cotton	18.4
Rayon	18.9
Viscose	18.9
Acrylic	18.2
Nylon 6	20-21.5
Nylon 6,6	20-21.5
Polyester	20-21
Silk	22.8
Wool	25

When pyrolysed, cellulose in cotton decomposes into smaller fragments. These fragments can be used to characterise the parent molecule, making them useful as diagnostic fragments [5, 25]. Pyrolysis of cellulose occurs at two stages: primary and secondary pyrolysis [6]. Primary pyrolysis occurs at 200 °C to 290 °C where H₂O, CO₂ and CO are generated. The first stage of secondary pyrolysis occurs between 290 °C and 310 °C. This stage generates anhydroglucoses (levoglucosan), whereas the second stage (310-350 °C) is characterised by the presence of furans, ketones and *n*-aldehydes. Generally, cotton possesses similar auto-ignition and pyrolysis temperatures of 350 °C [22].

Typically, the pyrolysis of cotton generates carbonaceous residue (solid), liquids and volatile gases [26, 27]. The proportions of solid, liquid and gas generated from cotton largely depends on the pyrolysis environment to which the cotton is subjected. It has

been reported that pyrolysis of pure cotton under vacuum conditions generates 15% solids, 65% liquids and 20% gases [6].

The residual carbonaceous solid can exist in three different forms depending on the temperature to which the cotton was subjected (Figure 4.3) [15]. At temperatures between 300 °C to 400 °C, aliphatic char is formed. At higher temperatures ranging from 400 °C to 600 °C, carbonaceous solid is formed and can either exist as an oxidised char or an aromatic char depending on the type of pyrolysis mechanisms it undergoes.

Levoglucosan (1,6-anhydro- β -D-glucopyranose) (Figure 4.2c), an intermediate by-product formed mainly through rapid depolymerisation [28] and random scission of the 1,4-glycosidic bond [27], followed by intramolecular rearrangement of the monomer units [28] at 300 °C, has been reported to be a major pyrolysis constituent of cotton [21, 25-27]. At temperatures above 350 °C, levoglucosan breaks down into smaller, more volatile fragments [25] through dehydration, decomposition and fragmentation. Compounds such as furans (e.g. methyl-furan, dimethyl-furan) and *n*-aldehydes (e.g. furfural, 5-methyl-furfural, acetaldehyde, glyceraldehyde) have been detected at high levels from the decomposition and dehydration of levoglucosan [5, 15, 25, 27, 29-31]. Other volatile compounds such as hydrocarbons, ketones (methyl iso-propyl ketone, acetone, 2,3-butanedione, 3-methyl-3-buten-2-one), aromatics (toluene and benzene), ether, methyl esters, pyrans, alcohol, carbonyl compounds and acrolein have also been documented to be volatile products generated from the pyrolysis of cotton across a range of temperatures [25, 27, 29, 30, 32-34].

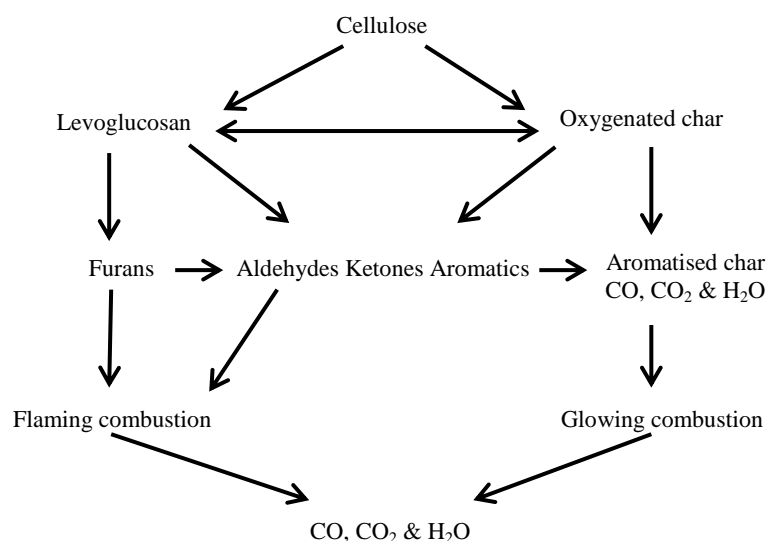


Figure 4.3: Pyrolysis model for cotton (cellulose) decomposition in air. Adapted from [35].

4.2.1.2 Denim

Denim, popularly known for its strength and durability [36] initially originated in Nîmes, France where it was largely used for sails [37]. Its original name, *serge de Nîmes* (fabric of Nîmes), was shortened to form ‘denim’ [37]. The fabric was then modified to make trousers and ultimately dyed (indigo dye) to give denim its characteristic blue colour, seen in modern jeans nowadays.

Denim is essentially made from cotton fibres that have been twill weaved into a diagonal dipping to create a sturdy fabric [38]. The amount and type of weaving ultimately dictates the pattern and style of denim as the end product. Although most denim is made from 100% cotton, it can also contain small fractions of elastane / spandex to give it some form of elasticity and polyester to reduce shrinkage and wrinkles [38]. The elemental composition of denim is presented in Table 4.2. With cotton (cellulose) being its only or major component, the thermal decomposition of denim follows the pathways of cotton pyrolysis.

Table 4.2: Elemental composition of denim. Adapted from [36].

Elements	Percentage (wt%)
C	43.2
O	50.2
H	6.2
N	0.3

4.2.1.3 Linen

Bast fibres are fibres that are produced from the bast surrounding stems in plants [39], located between the cuticle-epidermis layer and the inner woody tissues [40]. Bast are specialised long, cellulose-rich fibres that are very strong and resistant [41-43]. A form of bast fibre include the light amber flax (*Linum usitatissimum* L.) fibres [42] that are used to manufacture linen [40]. Linen is a widely used textile in the apparel and interior designing industry and is valued for its comfort, high tenacity, high moisture regain, excellent tensile strength, easy handling and distinctive appearance [43, 44].

The organisation of tissues in flax fibres can be distinguished into identifiable sections: outer cuticle layer, epidermis, thin-wall parenchyma cells, flax fibre bundles, cambium and inner woody cells [40, 42, 45]. The outer cuticle comprises lipids, including waxes, cutin, and aromatics [46, 47] that serve as a first line of defence against biological and mechanical attack and water loss. This is followed by the adjacent epidermis layer, made up of epidermal cells that border one side of a wall of parenchyma cells. Fibre bundles border the other side of the parenchyma wall and contain high levels of pectin and sugars. Pectin is essentially a heteropolysaccharide that consists of D -galacturonic acid linked together by α -bonds, and serves as a natural binder [42]. The next section is referred to as the cambium. The cambium produces tissues that are specialised for secondary growth and also contain high levels of pectin. The cortex of inner woody cells primarily contains xylem and other structural cells that are highly lignified, providing strength, rigidity, water conduction and microbial protection for the plant [42, 43].

Flax fibres are essentially cellulose, although their cellulose content is not as high as in cotton; cellulose accounts for 65-80% of the composition of linen [31, 48]. The remaining non-cellulosic compounds that make up to 17% of flax include pectin, lignin (higher than in cotton) [49], hemicellulose, waxes, protein and aromatics [46]. Similar to denim, cellulose accounts for the majority of the components in linen and, thus, when subjected to heat, linen undergoes similar thermal decomposition mechanisms [31, 45, 50] to cotton.

4.2.2 Animal Fibres

Wool and silk are the most common animal fibres encountered in the textile industry. They possess individual characteristics that make them unique desirable. Although both wool and silk are produced by animals and are essentially protein, the distinctive amino acids that serve as building blocks for the polypeptide chain are different across both fibres and can be distinguished from one another easily [51].

4.2.2.1 Wool

Wool is an epidermal growth of keratin fibrous protein, typically in the form of fleeces on the outer surface of (primarily) sheep [3, 52]. This yellowish white fibre is characterised by its rough, curly appearance and consists of multiple fibres twined together in staples. Wool's durability, high tensile strength, softness, crimps, serration and felting characteristics has made it a highly desirable material particularly in the textile and furnishing industry where it is used to make woollen clothing, blankets, upholstery, carpets and rugs [53-55].

Wool fibres are formed within hair follicles and undergo keratinisation before they are then driven out onto the surface of the animal [56]. A typical wool fibre has two parts, the follicle and the shaft, and are categorised into three distinguishable sections: the cortex, core and outer layer [3, 56, 57]. The cortex is referred to as the medullary canal where soft, globular / cortex cells are embedded. The core is enclosed by a middle section that comprises long, spindle-shaped cells that make up the majority of the fibre. The outer layer, made up of spiked, flattened / cuticle cells, bounds the medullary canal and middle section, running along the length of the fibre from the tip to the root.

The building block of wool is essentially protein (Figure 4.4), typically long chains of helical polypeptide, of at least 18-25 units of α -amino acids [52, 55, 58], distinguished from silk by the presence of sulfur-containing α substituents, mainly L-cysteine (Figure 4.5) [59]. The α -carbon in the polypeptide can be attached to either two hydrogen atoms or one hydrogen atom and one R side group. The chemistry of the R group determines if the fibre is hydrophilic, acidic or basic.

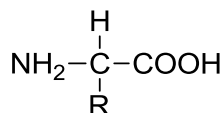


Figure 4.4: Chemical building block of protein

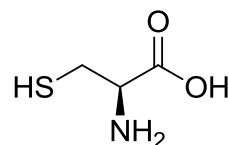


Figure 4.5: Chemical arrangement of L-cysteine

Three types of major proteins are found in wool fibres, intermediate filament (IF) protein, high tyrosine-glycine (HTG) proteins and intermediate filament associated proteins (IFAPs) [60]. (IF) proteins are fibrillary proteins, whereas (HTG) proteins are rich in tyrosine and glycine. (IFAPs) refer to a group of matrix proteins with high sulfur content like cysteine (Figure 4.5) which makes up at least 10% to 12% of wool's composition and contains reactive disulfide bonds that can be easily oxidised to carbon disulfide. It is also the first molecule to decompose when heat is applied to wool [55, 58]. When reduced, disulfide bonds produce thioglycollic acid [58]. The general elemental composition of wool is presented in Table 4.3.

Table 4.3: Elemental composition of wool. Adapted from [58].

Elements	Composition (%)
C	40-50
O	23-25
N	15-16
H	6-7
S	3-4

Besides proteins, wool also contains contaminants such as wool grease, suint and dirt which cumulatively can account for to 20-30% of raw wool [56, 58, 60]. Wool grease includes esters of long chain fatty acids, alcohols and sterols that form wax. Suint are water soluble salts such as potassium, carbonate and bicarbonate, and dirt can be a number of contaminants including sand, soil, skin and dead cuticles. While most of these contaminants disappear during the scouring process in wool preparation, some, typically wax, can linger at low concentrations in the final product [58].

Upon application of heat, wool does not melt or soften [22]. With its high ignition temperature of 570-600 °C, high LOI of 25-28% and low heat of combustion (energy released in the form of heat during combustion) (20.5 kJ/g), wool is the most flame resistant of all natural fibres [55, 58]. This is attributed to its high nitrogen content

(15-16%), high moisture content (10-16%) and high sulfur content (3-4%) (Table 4.3) [22, 55, 58], allowing its fibres to be resistant to ignition and flame propagation [18].

Due to its complex protein structure, wool breaks down and produces char and dissipating ash as its end products [18, 22]. Thermal decomposition of wool follows the loss of moisture at 100 °C. Initial decomposition is seen at 200 °C to 240 °C with the rupture of its helical structure [61], followed by an endothermic reaction at temperatures above 230 °C to 295 °C, typically marked with the emission of H₂S and sulfur compounds from the breakdown of disulfide bonds [22, 58, 62] in cysteine [63]. Wool undergoes rapid weight loss and the onset of pyrolysis at temperatures above 245 °C [22], releasing flammable volatiles and producing char [63]. While volatiles are released continuously throughout pyrolysis, some compounds evolve at specific temperature ranges: sulfur dioxide at 270-320 °C, thiols at 250-320 °C, nitriles at 340-480 °C, and phenol and 4-methyl-phenol at 370-400 °C [18].

At its ignition temperature (570-600 °C), the pyrolysis process continues to generate more volatile pyrolysis products with increasing levels of char [22, 62]. Ingham *et al.* [62] documented a lower ignition temperature of 385 °C for wool and mentioned that, at temperatures above 500 °C, most of the volatile products are consumed and can no longer be detected. In general, the pyrolysis of wool produces a variety of products, namely methane, carbon monoxide, ammonia, hydrogen sulfide, hydrogen cyanide, acetaldehyde, acrylonitrile, isobutyronitrile, toluene, isovaleronitrile, 2-methyl-butyronitrile, indole, skatole, phenols and amino acids [62, 64, 65]. Acetaldehyde is a break down product of alanine and proline, and isovaleronitrile is produced by leucine. Isobutyronitrile and 2-methyl-butyronitrile are both produced from the decomposition of valine and isoleucine [64]. Phenolic compounds and *para*-cresol (methyl-phenol) are generated from the pyrolysis of tyrosine, whereas indole and skatole are breakdown products of tryptophan [34, 65, 66]. Phenylalanine has been reported to be the parent compound that breaks down to generate toluene and phenyl-acetonitrile in wool and silk [65, 67].

4.2.2.2 Silk

Silk is an animal fibre produced by the insect order Lepidoptera [56]. Continuous filaments are produced by the larvae of caterpillars (silk worms) during the pupae stage and used to build their cocoons [57]. The outstanding strength, elasticity, high regain, softness, resistance to creasing and its luxurious appearance has made silk very prominent in the clothing and drapery industry [55, 68, 69].

As silk is an animal fibre, its monomers are primarily made up of proteins of 16 α -amino acids [55]. Silk is basically composed of 70-80% fibroin, 17-30% globular protein (sericin) and 0.4-0.8% waxes [56, 57] (Table 4.4).

Table 4.4: Composition of raw silk [70]

Compounds	Percentage
Fibroin	70-80
Sericin	17-30
Moisture	10-11
Carbohydrates and Starch	1.2-1.6
Inorganic Matter	0.7
Waxy Matter	0.4-0.8
Pigment	0.2

Fibroin forms the inner layer of silk fibres and is principally made up of glycine (R=H), alanine (R=CH₃) and serine (R=CH₂OH) and constitute 80% of the total amino acids found in silk, where serine contributes 10% [55, 57]. These amino acid repeat unit (glycine-alanine-serine) position themselves compactly in the crystalline region of the fibre, contributing to the formation of the β -sheet structure in silk [56, 57] (Figure 4.6).

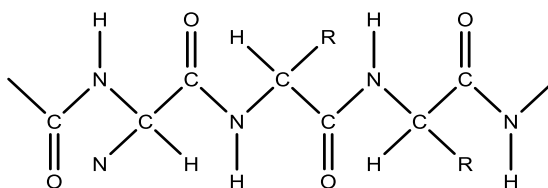


Figure 4.6: Regular arrangement of polypeptide chain [57]

Other amino acids such as tyrosine and valine can also be found in varying proportions in silk fibres (Table 4.5). These groups of amino acids are bulky,

hindering compact orientation, forming an amorphous region in the silk fibre [57]. Sericin (glue-like protein) forms the outer layer of silk fibres, encapsulating the fibroin. Sericin binds the silk fibres together and serves as a protective barrier against any mechanical or chemical damage [56, 57].

Silk possesses good thermal stability up to 140 °C and has a high LOI of 23% [55, 57]. When subjected to temperatures in the region of 100 °C, water molecules are vaporised within the amorphous region of the fibre and dehydration occurs [70]. As the temperature rises to 150 °C, the onset of thermal decomposition follows [57, 70]. Primary decomposition causes further dehydration, weight loss and the release of volatile products from the fibre (> 250 °C) [55, 70]. It has been reported that the pyrolysis temperature of silk occurs between 320 °C and 400 °C [55, 70, 71]. During this period of secondary decomposition, proteins that form the crystalline structure break down and release by-products in the form of volatile gases [70]. Similar to wool, the end product of silk is a char, which is formed through the dehydration and cross-linking characteristics of the hydroxyl group, particularly in serine [55, 59]. Also, as silk and wool are predominantly protein, they share similar thermal decomposition pathways and pyrolytic profiles.

Table 4.5: Side-group proteins in silk and wool fibres. Adapted from [56].

Side Group Protein	g amino acid per 100 g protein	
	Silk Fibroin	Wool Keratin
INERT		
Alanine	26.4	4.1
Glycine	43.8	6.5
Isoleucine	1.4	0.0
Leucine	0.8	9.7
Phenylalanine	1.5	1.6
Valine	3.2	5.5
ACIDIC		
Aspartic acid	3.0	7.3
Glutamic acid	2.0	16.0
BASIC		
Arginine	1.1	8.6
Histidine	0.5	0.7
Lysine	0.9	2.5
HYDROXYL		
Serine	12.6	9.5
Tyrosine	10.6	6.1
OTHERS		
Cysteine	0.0	11.8

4.2.2.3 Leather

Leather is a group of natural, fibrous protein based textile [72]. The raw material for leather making is obtained from the skin of animals, such as reptiles, birds or fish, and subjected to chemical and mechanical tanning processes to preserve the skin from decay, heat and moisture damage in addition to enhancing its properties [73-75]. Leather is regarded for its high tensile strength; good resistance to tear, flexing or puncture; poor heat conduction; good thermal insulation; permeability to air; favourable thermostatic properties and resistance to heat and flame [73, 76]. As such, leather is widely used in the manufacture of footwear (up to 60%) [77], upholstery and clothing.

In the making of leather [73, 78], the epidermis (including hair follicles, fur, sweat glands; < 1% thickness) and sub-cutaneous (including connective tissues and fat; 14-15% thickness) layers are removed. What is left is the thick dermis layer (85% thickness), containing bundles of three-dimensional connective fibre networks interspaced with proteins (globulin-collagen), that is then processed to produce tanned leather. The surface of the dermis that borders the epidermis is referred to as the 'grain', whereas the area that borders the dermis and sub-cutaneous layer is referred to as the 'split'. The grain can undergo a variety of chemical treatments but the most common are chromium and vegetable tanning and their final composition is illustrated in Table 4.6 [72, 78]. Once tanned, the material is then dyed, dried and staked (softened). Finishing is the final process of leather treatment and is conducted to protect the leather from abrasion, wear and tear and to also cover any defects (scars, veins, growth marks, shade and grain variation) in the final product.

Table 4.6: Properties of tanned leather. Adapted from [72, 79, 80].

Analysis (wt%)	Finished leather trimming	Unfinished leather trimming	Chromium-tanned shavings	Vegetable-tanned shavings
Moisture	12	12	7.1	5.9
Ash	4.5	7.2	67.0	59.0
Volatiles	66.7	65.7	9.6	3.9
Carbon	51.9	29.2	44.3	52.4
Hydrogen	6.3	6.7	3.1	0.9
Nitrogen	12.7	12.4	14.2	6.6
Sulfur	1.1	2.2	1.8	1.1

There are four types of leather: pure aniline, semi-aniline, corrected grain and suede split [78]. Pure aniline is the softest of all leathers; however, due to minimal chemical processing, it is susceptible to weathering and external damage. Semi-aniline is much more resistant as it has a layer that is slightly covered with organic pigments. Corrected grain is the most heavily pigmented, thus making it the most resistant of leathers. Suede split is a type of leather that is widely used in upholstery, shoes, garments and handbags. It refers to the under layer of leather that has been split, dyed and buffed to generate a velvet appearance.

When leather is subjected to temperatures below 200 °C for short durations, it maintains its structural integrity and resists damage; temperatures higher than this result in pyrolysis [76]. The pyrolysis of leather forms volatile gases, oils and carbonaceous residues [79]. When ignited, leather smoulders for extended durations while experiencing shrinkage [76]. According to Caballero *et al.* [80] and Font *et al.* [81], the pyrolysis of leather occurs in two distinctive temperature dependent stages, generating as its major products ammonia, hydrogen cyanide, and sulfur dioxide through the degradation of polypeptides, as well as carbon dioxide through the decarboxylation of carboxylates [79]. Toluene, naphthalene and methyl-naphthalene have also been detected from the pyrolysis of watch strap leather at 400-535 °C [82]. Carbonaceous residues are formed throughout the pyrolysis process via decomposition, polymerisation and polycondensation, yielding about 40-48% in proportion, and can be reduced to ashes (containing chromium trioxide and ammonium carbonate) with increasing temperatures up to 1200 °C [72, 80]. Oils formed have been identified to be asphaltene, aliphatic, aromatic and polar in nature [79].

Besides natural leather, artificial / synthetic leather (such as faux, vinyl or leatherette) is also popular, as it is much cheaper, provides better flexibility and is more versatile in comparison to real leather [83]. Artificial leather refers to a group of natural fibre or synthetic leathers that are commonly plasticised / coated with polyvinylchloride (PVC) or polyurethane (PU) and treated to resemble real leather [83, 84]. In comparison to PVC leather (plasticised and dyed), which is only used to

manufacture low stress tolerance materials, PU leather (cotton coated with PU) is much more commonly utilised for the production of upholstery, bags, shoes and belts, as it is much more flexible, resistant, durable and possesses high tensile strength – all favourable properties required for the production of good quality, strong material.

In general, when artificial leather is subjected to heat, it has been reported to undergo immediate ignition accompanied by slow smouldering and burning, forming ash as its end product [76]. Artificial leather has higher heat release rates and generates more smoke (carbon monoxide) in comparison to its natural counterpart, making it highly susceptible to fires [76].

PVC leather, however, is relatively resistant to fire and can barely sustain a flame, it can undergo combustion and pyrolysis to generate a variety of aromatics and chlorinated compounds through side group scission [85]. Across a range of temperatures (500-1000 °C), PVC decomposes to generate benzene, hydrogen cyanide, chlorinated aliphatic hydrocarbons, monoaromatic and polyaromatic hydrocarbons, naphthalene, chloro-benzenes, *n*-alkenes and a range of volatile and semi-volatile products [86-91]. As PU is made from amines and isocyanates, the pyrolysis of PU causes the polymer to undergo decomposition across the 350-850 °C via the breakdown of urethane and ester linkages, generating amines, aromatic amines, amino-isocyanates, diisocyanates, dienes, cyclic compounds, diols, hydrogen cyanide, styrene, benzene and naphthalene [81, 92, 93].

4.3 Synthetic Fibres

Accounting for 68% of all fibres produced worldwide [94], synthetic fibres are man-made fibres that were developed to enhance and improve the physical and chemical properties of natural fibres [56]. These fibres are divided into three main groups: synthetic fibres, made from the polymerisation of petroleum oils and petrochemicals to form long, linear chains (e.g. polyester, nylon, acrylic, elastane); semi-synthetic regenerated fibres, made from the regeneration of the polymer structure of naturally

occurring fibres (e.g. viscose, rayon, modal); and inorganic fibres, fibres that are made from glass, carbon, metal and ceramic (e.g. acetate) [56, 94, 95]. The four main groups under synthetic fibres are polyester, nylon, acrylic and polyolefins. Other synthetic fibres also include spandex / elastane (LYCRA®).

4.3.1 Polyester

Polyesters are one of the most common and widely used synthetic polymer [95]. Polyester's characteristic traits of resistance to abrasion and water, good elasticity and rigidity, strength and versatility as well as being cheap to produce and manufacture, has made its application very favourable in the manufacture of clothing, home furnishings, reinforced fibres, insulation, and as packaging and film material for food and drinks [85, 95-98].

Polyester is essentially a white thermoplastic composed of linear chain macromolecules consisting of at least 85% diol (ethane-1,2-diol / ethylene glycol) by mass and 15% dicarboxylic acid (benzene-1,4-dicarboxylic acid / terephthalic acid) (Figure 4.7), which are linked together by ester bonds [94, 99]. Polyesters can be referred to in two ways, depending on what they are used for [100]: 65% of polyesters are manufactured for the clothing and textile industry and are simply referred to as 'polyester fibres', whereas in the plastic and bottle industry (35%), they are referred to as 'polyethylene terephthalate' (PET) [96, 100].

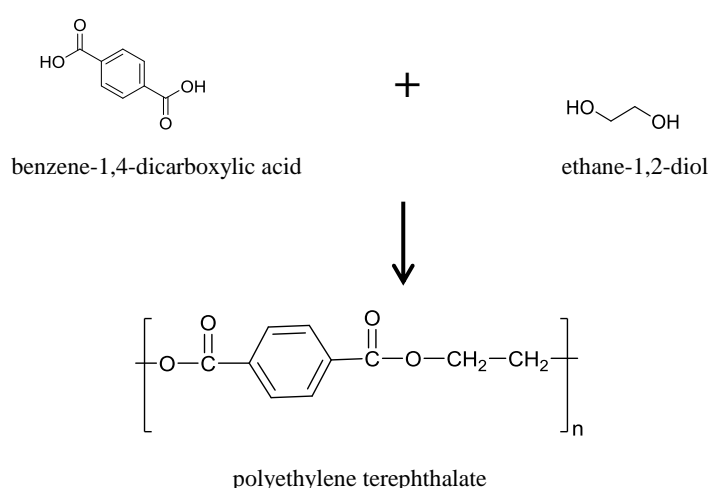


Figure 4.7: Monomers of polyester and chemical structure of polyester

The majority of polyester fibres are synthesised through condensation polymerisation reactions and in particular by a process called continuous polymerisation, where the fibre is subjected to elevated temperatures and forced through fine holes to form long strands of fibres, in the presence of a catalyst [96, 98, 101]. The physical and chemical properties of polyester can vary as they depend on the end product and level of polymerisation during manufacture. Generally, upon heating, polyester softens at 80-90 °C [22], and at its melting point of 200-260 °C, the fibres melt and fuse together to form hard beads [98, 102]. With the increase in temperature, these melted fibres ignite with difficulty and have been documented to auto-ignite at 450-530 °C [22, 103, 104]. The thermal decomposition temperature of polyester can range from 230-450 °C up to 570-900 °C depending on the size and type of molecules in the polymer and the duration of burning [5, 105-109]. Table 4.7 gives an overview of some of the thermochemical properties of polyester.

Table 4.7: Thermochemical properties of polyester. Adapted from [108] and [22].

Thermochemical property	Measured value
Melting point	250-300 °C
Heat of combustion	25-32 MJ/kg
Flash ignition	400 °C
Auto-ignition	450-500 °C
Flame temperature	750 °C

As polyester is essentially carbon, oxygen and hydrogen, its thermal decomposition pathway generates volatile hydrocarbons and oxygenates, together with carbon dioxide, carbon monoxide and water [103, 108, 110]. When heated to its thermal decomposition temperature above 300 °C, random scission of the C-O ester bond occurs, generating highly flammable, intermediate compounds (i.e. ethylene oxide, vinyl-alcohol, methane, diethyl ether, 2-methyl-1,3-dioxolane, acetaldehyde) that are then subjected to further decomposition at the C-C bonds to generate smaller, more stable compounds [107, 108, 111, 112]. The pyrolysis of polyesters have been documented to generate a series of *n*-aldehydes (acetaldehyde, benzaldehyde, butanaldehyde, formaldehyde), aromatics and aromatic esters (benzene, toluene, *p*-xylene, phenol, biphenyl), furan (tetrahydro-furan), vinyl-terephthstyrenes, naphthalene, ketones, *n*-alkanes (methane, butane), *n*-alkene (butane), *n*-cycloalkanes

and *n*-cycloalkenes together with acid and acid esters (benzoic acid, terephthalic acid esters, benzoic acid, ethenyl ester;) [34, 56, 85, 103, 106-110, 113, 114].

Although a range of volatile products can be formed through the pyrolysis of polyesters, the type of products detected largely depends on the temperatures attained during pyrolysis [115]. Lower temperature episodes, particularly at the initial stage of decomposition, have been noted to generate acetaldehyde, formaldehyde, and carbon dioxide as their main pyrolysis products, whereas at higher temperatures, aromatic and aliphatic hydrocarbons, methyl acetate, alcohols and acids were detected at high levels [107, 115]. Edge *et al.* [111] and Dzieciol and Trzeszczynski [115] documented a maximum presence of acetaldehyde at 300 °C and 400 °C, respectively. At 500 °C, maximum levels of benzoic acid, formaldehyde, methyl-alcohol and dioxane were recorded [103, 115], whereas temperatures above 700 °C generated high levels of aromatics, branched alkenes, naphthalene, benzaldehyde and acetophenone [5, 106].

4.3.2 Nylon

Nylons are long chains of aliphatic polyamides that are widely used as a synthetic polymer in the fabric and plastic industry [109, 116, 117]. The monomers of nylon are repetitive units of either amino acid or equal portions of diamine and dicarboxylic acid, which are linked together through peptide bonds and possess amide repeating units (–CO–NH–) (Figure 4.8) [109, 118, 119] of which, less than 85% are attached to two aromatic rings in the polymer chain [98].

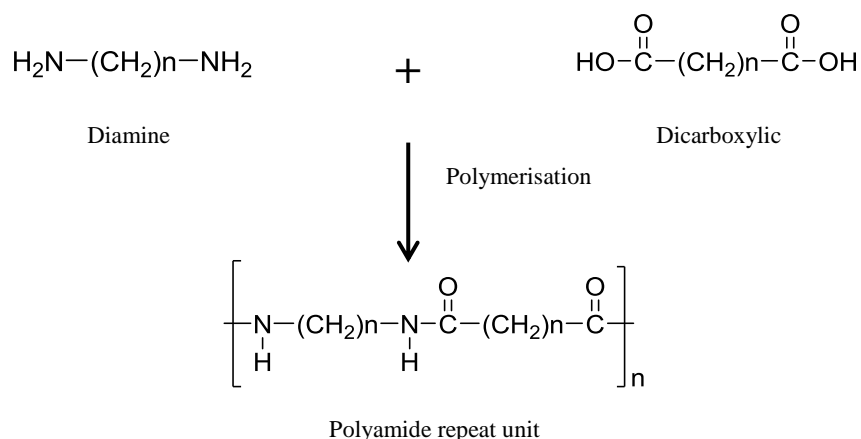


Figure 4.8: Monomers of nylon

Nylons can be either aliphatic (nylon 6, nylon 6,6), aliphatic / aromatic or aromatic polyamides [109]. While aliphatic and a mixture of aliphatic / aromatic nylons are common, aromatic nylons such as Nomex[®] are specifically designed for the production of protective clothing as they possess extremely high thermal stability [117, 118]. Nylons are categorised and named based on the composition of their monomers [116, 117]. When nylons are made from the hydrolytic polymerisation of ω -amino carboxylic acids, single numbered nylons are formed (nylon 6, nylon 12). If the monomers are made up of diamine-dicarboxylic acids that undergo polycondensation, double numbered nylons are formed (nylon 6,6, nylon 6,12). Nylon 6, with a chemical formula of $[-NH-(CH_2)_6-C(O)-]_n$ is generated through the polymerisation of caprolactam in the presence of water [109], whereas nylon 6,6 $[-NH-(CH_2)_6-NH-C(O)-(CH_2)_4-C(O)-]_n$, being one of the most widely used groups of nylon, is made from the hexamethylenediamine salt of adipic acid [109, 117]. Nylon 12 $[-NH-(CH_2)_{11}-CO-]_n$ is formed through the polymerisation of α -lauryl lactam, while nylon 6,12 $[-NH-(CH_2)_6-NH-C(O)-(CH_2)_{10}-CO-]_n$ contains the monomer hexamethylenediamine and 1,12-dodecanedioic acid [119].

As nylons can exist in a number of different forms and polymer sizes, their thermal properties and flammability vary and have been documented to generate a range of volatile products that differ based on their composition, length of molecule / hydrocarbon chain and pyrolysis temperature (Table 4.8) [108, 109, 117, 118, 120].

Table 4.8: Thermal properties of nylon. Adapted from [117, 118, 121, 122].

Nylon	Melting Point (°C)	Ignition Temperature (°C)	Minimum Thermal Decomposition Temperature (°C)
	172-260	421-590	310-380
Nylon 6	215-220		583
Nylon 12	179-210		310-380
Nylon 6,6	250-260		310-340
Nylon 6,12	218		310-380

As a class, nylons are moderately resistant to thermal decomposition (LOI of 21%) [59] and have been documented to resist decomposition up to 340 °C [118]. Aliphatic nylons tend to decompose at lower temperatures (300-400 °C) as compared to aromatic nylons (> 451 °C), as the latter contain relatively stable aromatic rings that

are difficult to decompose [109, 118]. As temperatures rise above 310 °C (up to 900 °C), nylon undergoes pyrolysis and typically generates carbon dioxide and water as its major products, together with mononitriles, amides, amines, ketones, dienes, acids, hydrocarbons and char (depending on the circumstances) [109, 116-119, 123, 124]. The presence of branched *n*-alkenes, benzaldehyde, indene, acetophenone and naphthalene were also documented from nylon carpets burnt in tin cans in Almirall *et al.*'s study [125]. The main pyrolysis pathway responsible for the generation of a range of pyrolysis products from nylons is mainly due to the scission of the peptide bonds (C(O)-NH), along with the C-C(O) and C-C bonds [109, 118, 123]. These scissions give rise to NH₃, CO₂, CO and low molecular weight fragments that subsequently undergo further decomposition to generate flammable volatiles [59]. Random scission of the weak C-N bonds generates amides and alkenes, and with dehydration, nitriles are formed. Further hydrolysis of the peptide bonds leads to the formation of amines and acids. When the C-C bonds break, various hydrocarbons, dienes, nitriles and cyclic compounds are formed.

Looking into specific nylon groups, nylon 6, when heated, softens and melts at 50 °C and 215 °C, respectively [22]. It undergoes decomposition at 400 °C and pyrolysis at 600 °C to generate a range of pyrolysis products as described above, whereby its main route of thermal decomposition is through depolymerisation, to form its monomer, caprolactam [59, 109, 110, 116]. Volatile at 140 °C [59], caprolactam is a specific nylon 6 by-product, produced in high yield during pyrolysis and formed when the polyamide undergoes C-N bond cleavage (cyclisation of amino hexanoic acid) at the polymer backbone [56]. It has also been detected in minor amounts coming from the pyrolysis of nylon 6,6 and nylon 6,12 [109, 119]. Nylon 6 has also been reported to generate benzonitrile and toluene at higher temperature ranges, typically between 800-950°C [119]. Through the cleavage of the C-N, C-O and C-C bonds, the pyrolysis of nylon 12 produces more fragment molecules as compared to nylon 6, generating lauryl lactam as its major product together with toluene, mononitriles, hydrocarbons, acids, amides and a range of C₂-C₁₂ nitriles at 800-950 °C [109, 116, 119].

Nylon 6,6 has been documented to soften at 50 °C, melt at 265 °C and experience the onset of pyrolysis between 310-403 °C [22], where the carbonyl-methylene (CO=CH₂) bond in apidic acid undergoes free radical attack and subsequently suffers carbon monoxide loss to form cyclopentanone as its major by-product [126], together with nitriles, ketones, aromatics, olefins, dimers and trimers [109, 118, 119, 123, 127, 128]. Nylon 6,6 also has a high ignition temperature of 530 °C and LOI of 20-21.0% [22]. Nylon 6,12 undergoes cyclisation (structural rearrangement leading to the formation of cyclic products) to generate lauryl lactam, caprolactam, toluene and undecane-nitrile as its major product that, undergoes further decomposition to produce nitriles (mononitriles and dinitriles) and cyclic oligomers [116, 119, 127].

With increasing temperature and burning duration, nylon loses most of its mass due to the thermal breakdown and generation of volatile pyrolysis products. The residual char that is formed during this process can undergo further decomposition to ultimately generate carbon dioxide, water, ammonia and hydrogen cyanide [119].

4.3.3 Acrylic

In the textile industry, acrylics refers to linear macromolecules consisting of not less than 85% acrylonitrile repeating units [-CH₂-CH(CN)-] and not more than 15% additives and copolymers [94, 129]. In general, acrylics are made up of 68% carbon, 26.4% nitrogen and 5.6% hydrogen [130, 131]. Acrylics possess high elasticity, excellent heat retention and a soft and flexible texture, making them useful as blankets, sweaters, socks and home furnishings [94, 98, 129, 131].

Because pure polyacrylonitrile (PAN) fibres don't dye well, acrylics that are manufactured for the synthetic fibre industry contain acrylonitrile (90-94%) as the main constituent (Figure 4.9), with the additional presence of one or two polymerised copolymers [98, 129, 132]. Copolymers can be either neutral (vinyl acetate, methyl acrylate, methyl methacrylate, ethyl acrylate) or ionic (styrene sulfonate, allyl sulfonate) in nature [129]. The common copolymers that are utilised in the manufacture of acrylics are vinyl acetate and methyl acrylate (Figure 4.10) [132].

Other monomers such as styrene sulfonate and ethyl acrylate can also be used to synthesise acrylic (Figure 4.11) [132].

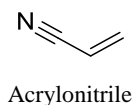


Figure 4.9: Chemical structure of acrylonitrile



Figure 4.10: Chemical structure of common monomers of acrylic

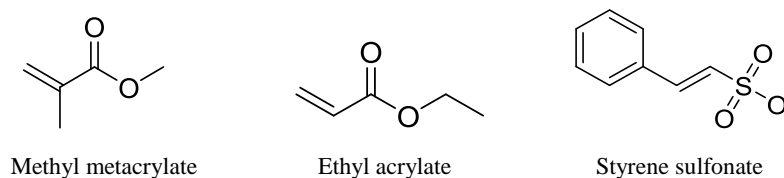


Figure 4.11: Chemical structure of other monomers of acrylic

When heat is applied, acrylic softens and melts at 100 °C and > 220 °C, respectively [22], and it has been reported to undergo three distinctive temperature-dependent pyrolysis stages: 250-350 °C, 350-550 °C and > 550 °C [133]. Across these stages, the processes of volatilisation (homolytic cleavage (the bond electron pair is split evenly between two products) and chain scission forming free radicals) and cyclisation compete with the production of char, and they are largely governed by the heating rate and oxygen availability [130, 133-135]. These free radicals attack the polymer chain to cause fragmentation into smaller, more stable products. The residual solid that is left after volatilisation and decomposition constitutes char.

At 280-590 °C, the pyrolysis of acrylic generates, as its major products, cyanogen, hydrogen cyanide, nitriles (acrylonitrile, acetonitrile, vinyl acetonitrile), cyano-alkanes and cyano-alkenes [130, 136], while at 700 °C, in addition to these products,

acids, nitriles (isobutyronitrile, propionitrile, methacrylonitrile), substituted aromatics, dimers, trimers, tetramers and acrylates (ethyl acrylate, methyl methacrylate, butyl acrylate) have been reported to be present [34, 132, 137]. Substituted aromatic compounds such as dicyano-benzene are formed through an additional pyrolysis mechanism: dehydrogenation and / or dehydrocyanide reactions followed by cyclisation of the polymer [134], whereas substituted alkanes and alkenes (dicyano-propene and dicyano-butene) are formed through the elimination of the HCN and methyl radical, respectively [130].

As pyrolysis is a function of temperature, higher temperatures cause more rapid fragmentation, inducing larger yields of volatile species (dicyano- / tricyano- / tetracyano- alkane and alkene) [130] and low molecular weight products (hydrocyanic acid, acetonitrile, acrylonitrile, methacrylonitrile, low molecular weight hydrocarbon) [130, 137]. However, once the maximum temperature is attained for the yield of specific compounds, their production starts to decrease, as observed by Minagawa *et al.* [137] who reported that the yield of acetonitrile and acrylonitrile dwindled after 700 °C and 800 °C, respectively (Figure 4.12).

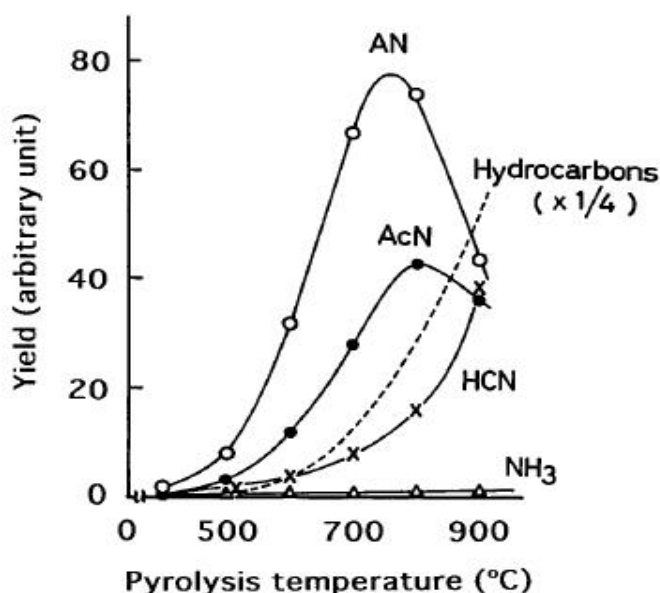


Figure 4.12: Temperature-dependent yield of acrylonitrile (AN), acetonitrile (AcN), hydrocarbons, hydrogen cyanide (HCN) and ammonia (NH₃) [137]

4.3.4 Spandex / Elastane

Known for its outstanding elasticity [138] and its wide application in sportswear and swimwear [139], spandex (or elastane) is made from synthetic fibres containing long chains of at least 85% segmented polyurethane linkage units (synthesised from polyester and diisocyanate) (Figure 4.13) and the remaining 15% polyurea [139-142]. As the resultant polymer contains both long fibres in the amorphous region and short, rigid fibres in the crystalline structure, these network arrangements are responsible for the formation of an elastomeric fibre [140, 142], facilitating stretching and recoiling [143] and giving the fibre its superior stretchability, strength, versatility, lightweight nature and resistance to abrasion [140, 144].

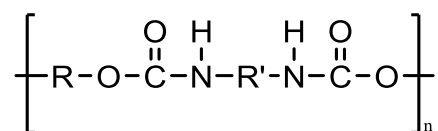


Figure 4.13: Polyurethane repeat unit

The synthesis of spandex requires pre-polymers that form the backbone of the polymer, stabilisers to secure integrity and colorant for selling purposes. The common pre-polymers used in the manufacture of spandex is macroglycol (polyester / polycarbonate), a long chain of polymer containing –OH groups at both ends which is responsible for flexibility and diisocyanate, the short chain polymer containing –NCO groups at both ends which provides rigidity and strength. These pre-polymers are then reacted together and commonly undergo a solution dry spinning (dissolved in solvent which is then evaporated) technique to generate the desired fibres [141, 144]. Other techniques like the melt extrusion (heat and pressure is applied to polymer fibres and is forced through fine holes continuously), reaction spinning (chemicals are added to increase the viscosity of the fibres during spinning) and solution wet spinning (fibres submerged in a chemical bath) can also be utilised to generate spandex fibres (Figure 4.14) [142]. LYCRA® and Dorlastan® are some of the common trade names of spandex / elastane [144].

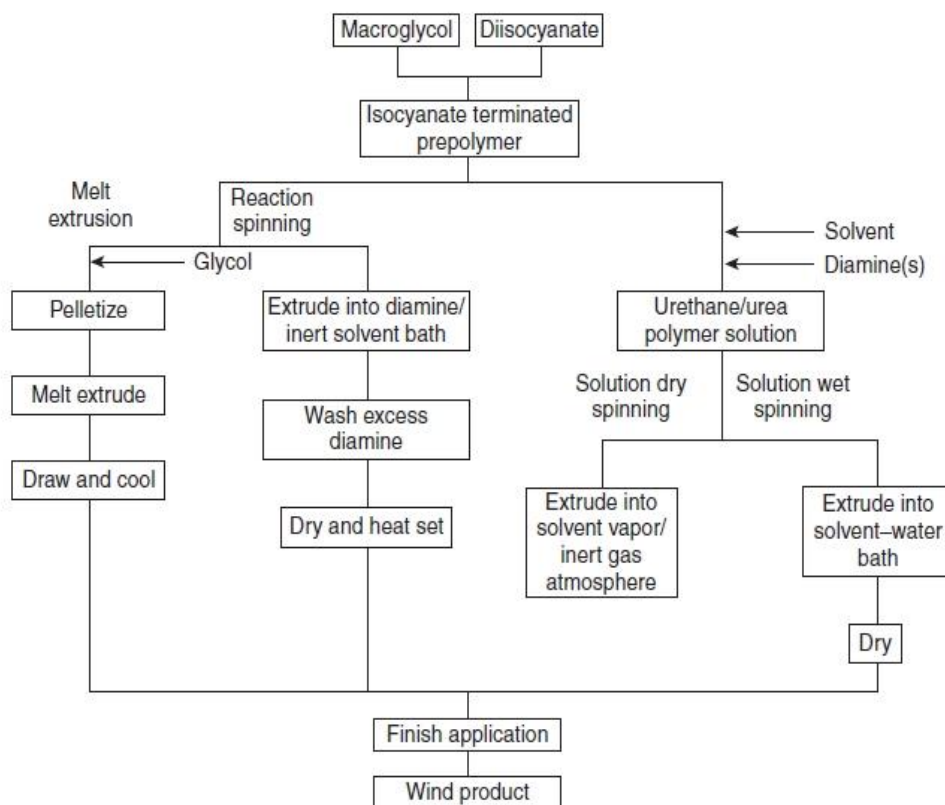


Figure 4.14: Spandex manufacturing methods [142]

The physical and chemical properties of spandex / elastane depend on the processing conditions and pre-polymers used during the manufacturing process [139, 142]. In general, spandex fibres have shown good thermal stability up to 200 °C [139]. Across 190-205 °C, spandex fibres undergo complete stretching comparable to that of melting, where the physical cross-linking between the segments are broken down.

4.4 Semi-Synthetic Fibres

4.4.1 Rayon

Rayon is a semi-synthetic fibre, made of purified cellulose fibres obtained from wood pulp that has been chemically modified and solidified [145, 146]. According to the Federal Trade Commission [147], rayon refers to regenerated cellulose fibres in which substituents have not replaced more than 15% of the hydrogens in the hydroxyl group [68]. The fibres undergo a process called spinneret to form soft filaments that then become the regenerated cellulose fibres. Besides having a soft and comfortable feel, rayon fibres are highly absorbent and drape well; they are also

versatile and don't insulate heat [148]. They are used widely in clothing, home furnishings and the manufacture of industrial products. In general, rayon has a melting point of 150 °C and burns rapidly, emitting yellow flames [146]. The most common forms of rayon are viscose and modal [97]. Both of these textiles are essentially 100% cellulose, although they have undergone different processes and have their own individual characteristics [149].

4.4.1.1 Viscose

Viscose is a group of rayon that is made up of regenerated cellulose (cellulose xanthate), often blended with varying proportions of other fibres, and is commonly used in the manufacture of textiles [145, 150]. Its starting material is wood pulp containing short cotton fibres that have been steeped in an alkaline solution and treated with carbon disulfide; it is then dissolved in a sodium hydroxide solution and spun to become viscose [94, 145, 146, 151]. Viscose is easily dyed at low temperatures, possesses good abrasion and sunlight resistance and can be used for woven or non-woven fabrics, (e.g. rubber and cellophane) [148]. As viscose is essentially cellulose, its thermal properties are similar to cellulose, where it has been documented to pyrolyse at 350 °C and auto-ignite at 420 °C [22].

4.4.1.2 Modal

Modal is an improved version of viscose, containing regenerated cellulose fibres that originate from beech wood rather than wood pulp [94]. These fibres undergo a higher degree of polymerisation and modified precipitating baths (additives added during the spinning process) [149], thus enhancing their physical and chemical properties so that they are more resistant and have better dry and wet tensile strength, good dimensional stability, moisture regain, air permeability, a pleasant texture (soft and silky) and resistance to shrinkage and fading [94, 148]. These properties have made modal very popular in the manufacture of sleepwear, towels, bath robes, exercise clothing and underwear, either on its own or blended with cotton, wool or other synthetic fibres [148].

4.5 Fibre Blends

While natural and synthetic fibres are relatively versatile and desirable in their pure state, more often than not they are sold in the form of blends with other fibres to enhance favourable features and / or to improve the textile's characteristics [44, 49, 98, 112]. For example, linen combined with 15% polyester is shown to improve the fabric's abrasion properties, while linen-rayon blends possess increased elasticity and crease resistance [152]. Cotton blended with high molecular weight modal fibres possesses better tensile strength, flexibility and endurance [149] whereas a cotton-wool blend produces textiles with lower shrinkage properties while maintaining the favourable characteristics of wool [98].

Although fibre blends can improve a textile's properties, an opposite outcome can also occur, especially in the fibre's thermal properties as observed by Ordoyno and Rowan [153]. They identified that the presence of wool in polyester reduced the synthetic fibre's thermal stability as a result of the chemical interactions between the by-products of both fibres. The physical and thermal properties of blended fibres can be quite different from each fibre's individual properties, and this should be taken into consideration when dealing with cases of blended polymers [109].

Since all fibre polymers are chemically different, the process of pyrolysis generates specific volatile fingerprints characteristic of each fibre that can be used as an indicator and positive identifier of the fibre [154]. When it comes to blended fibres, although they are subjected to various thermal decomposition pathways (either individually, concurrently or co-pyrolysed with the mixture of fibres present), the thermal decomposition is an intramolecular one, independent of the other type(s) of fibre(s) in the blend [5]. As such, the pyrolysis profile generated from a fibre blend is more of a superimposition of two fibres rather than a merged one [65, 154, 155]. However, the intermolecular reactions between the molecules during pyrolysis [109] can potentially alter the characteristic by-products relied on for individual fibre identification [109], especially if the proportions of the fibre blends are not equal or if these by-products are produced at low levels or not present at all [22].

Knowledge of these interactions in fibre blends is essential in identifying potential interferences and understanding the pyrolysis mechanism involved during these interactions, as well as the type of volatile products generated as an outcome of this process [156]. Perlstein [51] studied the use of pyrolysis products as a diagnostic tool for identifying the individual fibres that made the textile blends of polyester with cotton and polyester with wool. He proposed the use of identified diagnostics peaks from the pyrolysis of individual fibres rather than the pattern recognition method to identify individual fibres in blended fabrics. Yang and Hardin [157] also reported this, particularly for polyester and cotton blends, and proposed an additional use of a calibration chart and regression curve to determine ratio calculation for fabric blends.

4.6 Experimental Methods

4.6.1 Textile Samples

20 different used (not new) textiles were sampled as per Table 4.9. These materials were chosen as they represent common fabrics used in the textile and home furnishing industry. Each textile was cut using scissors into 12 swatches, (8.5 cm × 3 cm) and placed in a 125 mL tin can (WA Products, UK). The first six swatches were used as control samples, and the second set of six swatches were subjected to burning / pyrolysis.

Table 4.9: The composition of a range of 20 used textiles

Label	Composition
A	100% cotton
B	95% cotton + 5% elastin
C	50% cotton + 33% viscose + 17% polyester
D	50% cotton + 50% modal
E	100% acrylic
F	50% acrylic + 50% cotton
G	100% polyester
H	100% viscose
I	65% polyester + 35% cotton
J	64% polyester + 32% viscose + 4% elastin
K	64% polyester + 33% rayon + 3% elastin
L	50% polyester + 50% viscose
M	47% viscose + 28% linen + 22% polyester + 3% elastin
N	100% nylon
O	80% nylon + 20% elastin
P	96% wool + 4% LYCRA [®]
Q	100% silk
R	100% denim
S	100% leather
T	95% cotton + 5% spandex

4.6.2 Generation of Thermal Decomposition Products

4.6.2.1 Preliminary Method Validation for Optimal Generation of Pyrolysis Products from Textile Samples

4.6.2.1.1 Control Samples / Unburnt Textiles

Six samples from each textile type were placed into individual ($n=6$) 125 mL tin cans (WA Products, UK) and sealed with a lid containing one ACS 10 mm \times 20 mm (ACS, 3M Corporation, USA) that was hooked onto a medium-sized paper clip and held firmly on the inner part of the lid by individual magnets placed on the outer part of the lid. The tin containing the textile sample and the ACS was left to incubate in an oven for 16 hours at 80 °C. This was to allow any volatile products present in the unburnt textile to undergo volatilisation and to be adsorbed onto the ACS.

4.6.2.1.2 Burnt Textiles

A preliminary experiment was conducted to identify the burning behaviour of all textiles in Table 4.9 and to aid in narrowing down the number of textiles which would be subjected to further experimentation.

A tin can containing the textile sample was attached to a retort stand at a position measuring 20 cm from the base of the stand. The tin can was then heated over a Bunsen flame and held in place until ignition occurred. The temperature in the tin was monitored using a k thermocouple linked to a PicoLog TC-08 data logger (Pico Technology Limited, UK) connected to a laptop computer to facilitate temperature recording per second. Using an aluminium sticky tape, the end of the thermocouple was attached to the tin so that it hung above the headspace of the textile sample. If the sample ignited, it was allowed to burn for a specific textile-dependent duration (until the flames reduced in size and a drop in temperature was noted) before the flame was extinguished through oxygen deprivation by a lid being placed onto the tin. To facilitate this, the Bunsen flame and the thermocouple were removed 10 seconds before the lid was placed on the tin. The lid was removed 4 minutes after extinguishment and the tin immediately sealed with another lid bearing one 10 mm \times 20 mm ACS (ACS, 3M Corporation, USA).

If the sample did not ignite, it was heated until two thirds of the sample was consumed and a drop in temperature was noted. A lid was then placed onto the tin and it was allowed to cool for 4 minutes before immediately being sealed with another lid bearing one 10 mm × 20 mm ACS (ACS, 3M Corporation, USA).

The entire process was repeated six times for each textile type.

4.6.3 Passive Headspace Adsorption with Activated Carbon Strip (ACS)

The headspace extraction was undertaken according to the optimised method in 2.2.4.3.

4.6.4 Gas Chromatography – Mass Spectrometry

The GC-MS analysis was conducted following the optimised method from 2.4.2.

The total ion chromatogram (TIC) produced for each control (unburnt) and burnt textile sample was analysed based on the retention times and m/z values. Each significant peak from both the unburnt and burnt samples, was then identified by comparing the data against the National Institute of Standards and Technology (NIST) library and standard mixtures. The burning behaviour of each textile was recorded, together with its time-temperature profile.

The full range of textiles was then narrowed down to a smaller set of textiles which would be utilised for further experimentation. This was done in a two-step elimination process: (1) through scrutiny of the TIC of each textile, eliminating those that were producing little or no pyrolysis products, and (2) for those textiles that produced considerable amounts of pyrolysis products, they were narrowed down based on the consistency and number of pyrolysis products generated across six sets of repeat samples. These reduced groups of textiles from (1) were then subjected to another round of pyrolysis, six times for each textile type, adhering to the methods in 4.6.2.1.2, 4.6.3 and 4.6.4. Pyrolysis products that appeared in at least four of the six repeat samples were considered as major identifying peaks for that particular textile.

4.7 Results and Discussion

4.7.1 Control Samples / Unburnt Textiles

A preliminary experiment was conducted to determine the use of new and used clothing for this study. Results indicated that there were no significant differences across the range of pyrolysis products generated from both types of samples, with the exception of limonene which was present in used clothing. This compound could have potentially transferred onto used clothing from citrus-based detergents / cleaners used to wash clothing or from the use of perfumes / fragrances containing citrus oil extracts [158-160]. Given that the clothing and textiles involved in a fire scene are more likely to have been used rather than brand new, and because no noticeable differences were detected in the type of pyrolysis products generated from new and used clothing, the next stage of this work subjected used clothing for further experimentation.

Control samples refer to textile samples in Table 4.9 that were not subjected to pyrolysis and burning but to volatilisation at 80 °C for 16 hours in the oven. This was undertaken in order to ascertain if any volatile products were naturally present in the substrate prior to pyrolysis or combustion. If present, these volatile products, which are referred to as substrate background products [85], can cause potential interference in the interpretation of pyrolytic data obtained from fire scenes, particularly for the positive identification of ignitable liquid residues (ILR) and potentially human remains.

From the 20 different textile types and blends, only three textiles generated detectable volatiles in the control samples: 100% cotton (A), 65% polyester + 35% cotton (I) and 80% nylon + 20% elastin (O); the volatiles are detailed in Table 4.10. Textile (A) produced *n*-butyl ether, textile (I) generated an alkane group that could not be specified given the less discriminative *m/z* abundances while textile (O) produced ethyl-benzene and *p*-xylene. The peak height (h) and area (a) of the four volatile products were as follows: *n*-butyl ether (h 1075, a: 27218), alkene (h:1512, a:15723), ethyl-benzene (h:758, a:1214) and *p*-xylene (h:1218, a:18800). These products were detected at relatively low levels in comparison to those which would

be expected post-pyrolysis and post-combustion. The remaining 17 textiles did not generate any detectable substrate background products.

Table 4.10: Presence and absence of substrate volatile products generated from 20 different textile types and blends

Label	Composition	Volatiles	Retention Time (min)	Compound	<i>m/z</i>
A	100% cotton	√	9.52	<i>n</i> -butyl ether	44, 57, 87
B	95% cotton + 5% elastin	×	-	-	-
C	50% cotton + 33% viscose + 17% polyester	×	-	-	-
D	50% cotton + 50% modal	×	-	-	-
E	100% acrylic	×	-	-	-
F	50% acrylic + 50% cotton	×	-	-	-
G	100% polyester	×	-	-	-
H	100% viscose	×	-	-	-
I	65% polyester + 35% cotton	√	15.53	alkane	57, 71, 85
J	64% polyester + 32% viscose + 4% elastin	×	-	-	-
K	64% polyester + 33% rayon + 3% elastin	×	-	-	-
L	50% polyester + 50% viscose	×	-	-	-
M	47% viscose + 28% linen + 22% polyester + 3% elastin	×	-	-	-
N	100% nylon	×	-	-	-
O	80% nylon + 20% elastin	√	9.04 9.21	ethyl-benzene <i>p</i> -xylene	91, 106 91, 105, 106
P	96% wool + 4% LYCRA [®]	×	-	-	-
Q	100% silk	×	-	-	-
R	100% denim	×	-	-	-
S	100% leather	×	-	-	-
T	95% cotton + 5% spandex	×	-	-	-

Substrate background products have been discussed in Chapter 1 (1.5). These products can complicate the analysis and interpretation of target molecules, particularly in the identification of ignitable liquid residue (ILR) and potential human remains [161, 162]. Target molecules are compounds used to identify the presence of specific ILR based on the type, abundance and clustering pattern of the peaks detected [91]. If these target molecules are present in a sample, it can be indicative of the presence of ILR, thus helping investigators to determine the cause of and circumstances leading to the fire.

Substrate background products can come from a range of unburnt items found at fire scenes, either natural or synthetic, these include shoes, furniture, upholstery, clothing, kitchen appliances, flooring and many more [125, 161-165]. They have been reported to produce compounds that have the same boiling point ranges to the target compounds of ILR [91, 164, 166]. For example, the natural occurrence of turpentine in unburnt pine wood padding misled investigators to conclude that ILR was present at a fire scene, as this is a target molecule for ILR identification [167]. Unburnt polyethylene bags produce a range of *n*-alkanes [162], while vinyl floorings have been reported to generate TXIB (2,2,4-trimethyl-1,3-pentanediol diisobutyrate) and Isopar H, both of which are isoparaffinic products from petroleum distillates in ILR [165]. Other compounds such as toluene, branched cycloalkanes, C₉-aldehydes, octanol and C₃-alkyl-benzene have also detected from unburnt synthetic floorings [91]. Unburnt boots and walking shoes are also known to produce toluene and a range of other ignitable liquid volatiles resulting from the manufacturing process (adhesive) [161] or picked up from the environment [161, 168].

In the case of clothing, unburnt synthetic leather has been reported to produce hexanal, decanal, octanal, ethyl-hexanol and furan-methanol [91]. Particularly for cotton-based materials, low levels of toluene and *p*-xylene have been detected as well; however, at low levels these compounds are expected to have been generated from the environment or occur as a consequence of the manufacturing process [91, 168]. Similar findings were also noted in this study from 100% unburnt cotton with the presence of low levels of *n*-butyl ether.

The presence and abundance of the substrate background products generated from textiles (A), (I) and (O) in this study were scrutinised in the next stage of the work where the textiles were subjected to burning. This was to identify if the presence and proportion of these volatile products differ in any way after burning [91].

4.7.2 Temperature Profile and Burning Behaviour of Textiles

4.7.2.1 Pre-Optimised Burnt Textiles

In the first step elimination process, all of the textiles in Table 4.9 generated considerable amounts of pyrolysis products with the exception of 65% polyester + 35% cotton (I), 47% viscose + 28% linen + 22% polyester + 3% elastin (M) and 95% cotton + 5% spandex (T). These three textiles were, as a consequence, omitted from further scrutiny and the sample set relabelled in Table 4.11 to avoid confusion. This reduced set of 17 textile samples that were subjected to further six burnings exhibited variations in their thermal and burning properties, detailed in Table 4.11.

Across the six repeats, the following textiles auto-ignited: 100% cotton (A), 95% cotton + 5% elastin (B), 50% cotton + 33% viscose + 17% polyester (C), 50% cotton + 50% modal (D), 80% nylon + 20% elastin (H), 100% viscose (K) and 100% leather (Q). For textiles (H) and (K), four and five out of the six samples respectively, auto-ignited while the rest did not experience auto-ignition. Maximum temperatures attained during the auto-ignition of textiles (A), (B), (C), (D), (H), (K) and (Q) were in the range of 490-780 °C (Figures 4.15, 4.16, 4.17, 4.18, 4.22, 4.25 and 4.31, respectively).

100% acrylic (E), 100% silk (I), 96% wool + 4% LYCRA[®] (L) and 100% polyester (M) did not auto-ignite. The maximum temperatures attained across these textiles were below 300°C (Figures 4.19, 4.23, 4.26 and 4.27, respectively).

In terms of auto-ignition, the remaining textiles exhibited a mixture of results as, across the six repetitive samples within the same textile type, some auto-ignited while others did not. For 50% acrylic + 50% cotton (F), 100% nylon (G), 100% denim (J) and 50% polyester + 50% viscose (O), more than half of the repeats did not auto-ignite (Figures 4.20, 4.21, 4.24 and 4.29, respectively). In 64% polyester + 33% rayon + 3% elastin (N) and 64% polyester + 32% viscose + 4% elastin (P), exactly half of the repeats ignited (Figures 4.28 and 4.30, respectively).

Table 4.11: Thermal behaviours of textiles and their blends

Label	Composition	Ignition	Max Temperature Attained (°C)	Other observation
A	100% cotton	Yes	720 (Figure 4.15)	-
B	95% cotton + 5% elastin	Yes	710 (Figure 4.16)	-
C	50% cotton + 33% viscose + 17% polyester	Yes	780 (Figure 4.17)	-
D	50% cotton + 50% modal	Yes	490 (Figure 4.18)	Yellow smoke
E	100% acrylic	No	290 (Figure 4.19)	Yellow smoke, pungent odour Appears melted
F	50% acrylic + 50% cotton	No-5 out of 6 did not ignite, 1 ignited	500 (Figure 4.20)	Yellow smoke
G	100% nylon	No-4 out of 6 did not ignite, 2 ignited	580 (Figure 4.21)	-
H	80% nylon + 20% elastin	Yes-4 out of 6 ignited, 2 did not ignite	620 (Figure 4.22)	-
I	100% silk	No	270 (Figure 4.23)	Yellow smoke
J	100% denim	No-4 out of 6 did not ignite, 2 ignited	580 (Figure 4.24)	-
K	100% viscose	Yes-5 out of 6 ignited, 1 did not ignite	720 (Figure 4.25)	-
L	96% wool + 4% LYCRA®	No	275 (Figure 4.26)	Yellow smoke, pungent odour
M	100% polyester	No	245 (Figure 4.27)	Appears melted
N	64% polyester + 33% rayon + 3% elastin	Yes- half ignited, half did not ignite	620 (Figure 4.28)	-
O	50% polyester + 50% viscose	No-4 out of 6 did not ignite, 2 ignited	550 (Figure 4.29)	-
P	64% polyester + 32% viscose + 4% elastin	Yes-half ignited, half did not ignite	615 (Figure 4.30)	-
Q	100% leather	Yes	705 (Figure 4.31)	-

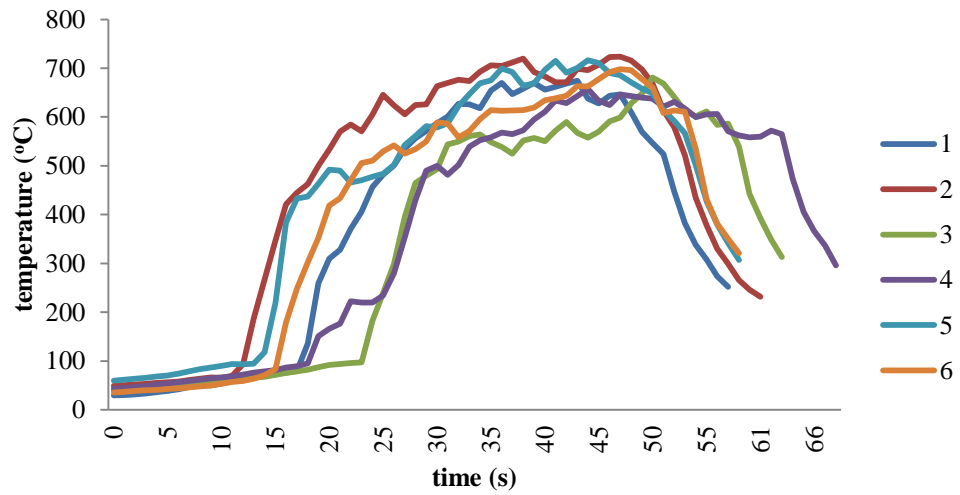


Figure 4.15: Time-temperature profile of 100% cotton (A)

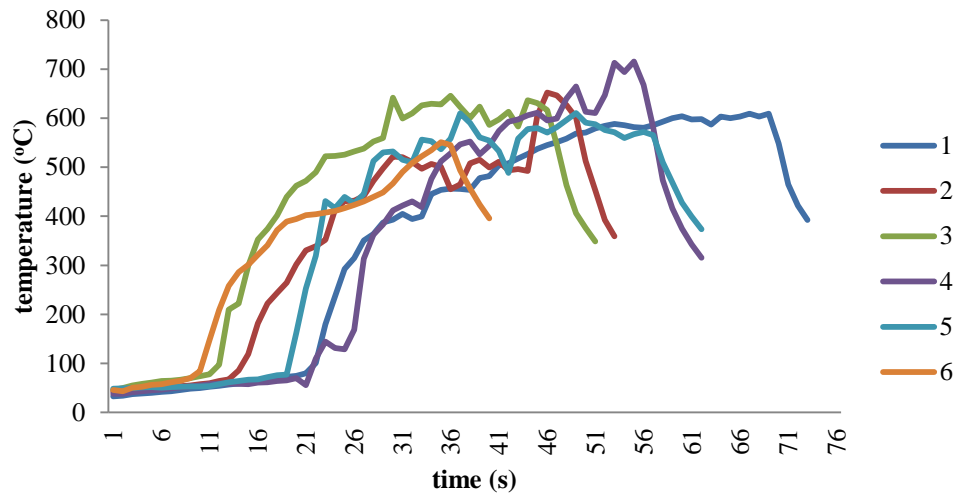


Figure 4.16: Time-temperature profile of 95% cotton + 5% elastin (B)

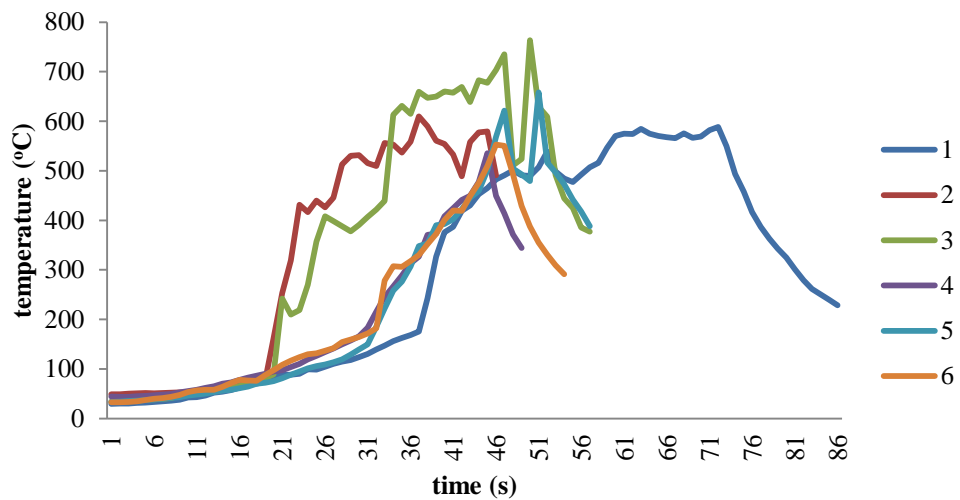


Figure 4.17: Time-temperature profile of 50% cotton + 33% viscose + 16% polyester (C)

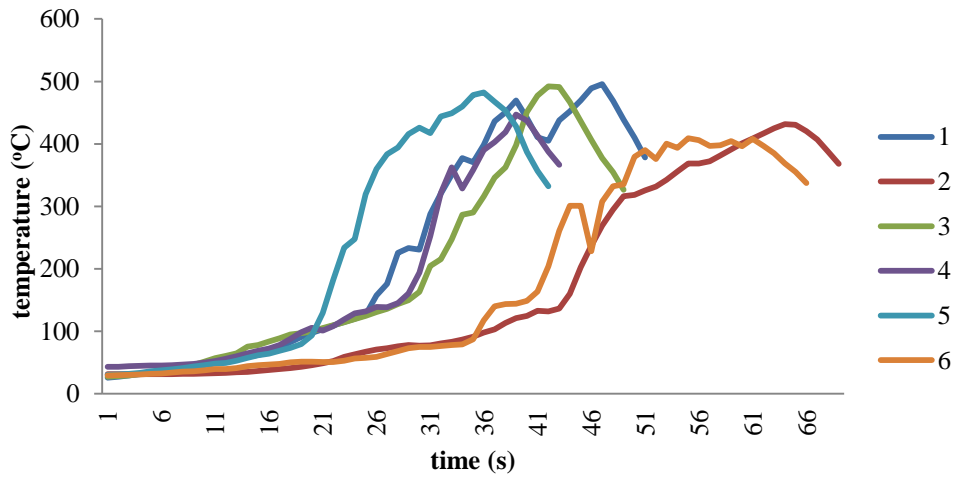


Figure 4.18: Time-temperature profile of 50% cotton + 50% modal (D)

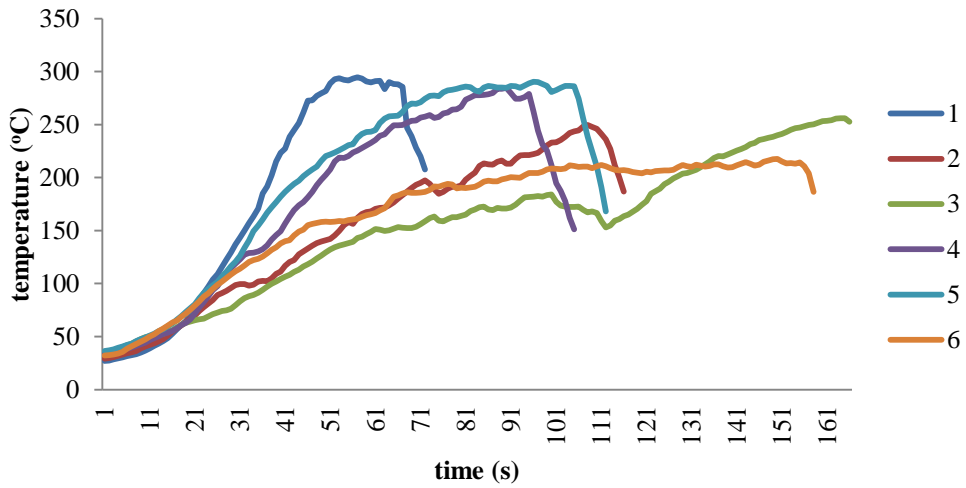


Figure 4.19: Time-temperature profile of 100% acrylic (E)

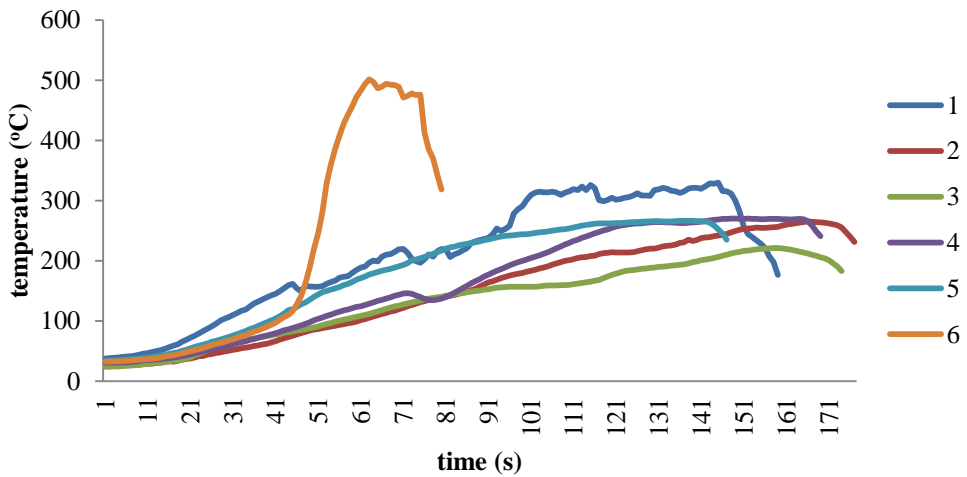


Figure 4.20: Time-temperature profile of 50% acrylic + 50% cotton (F)

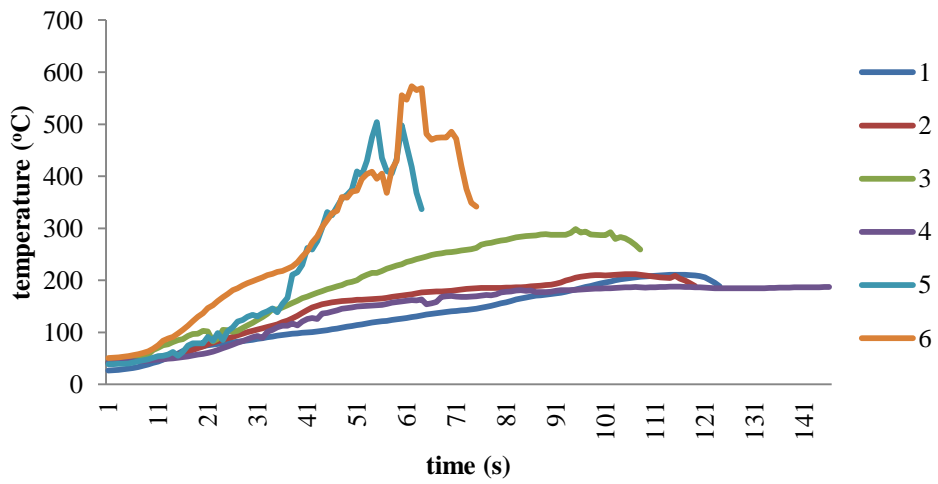


Figure 4.21: Time-temperature profile of 100% nylon (G)

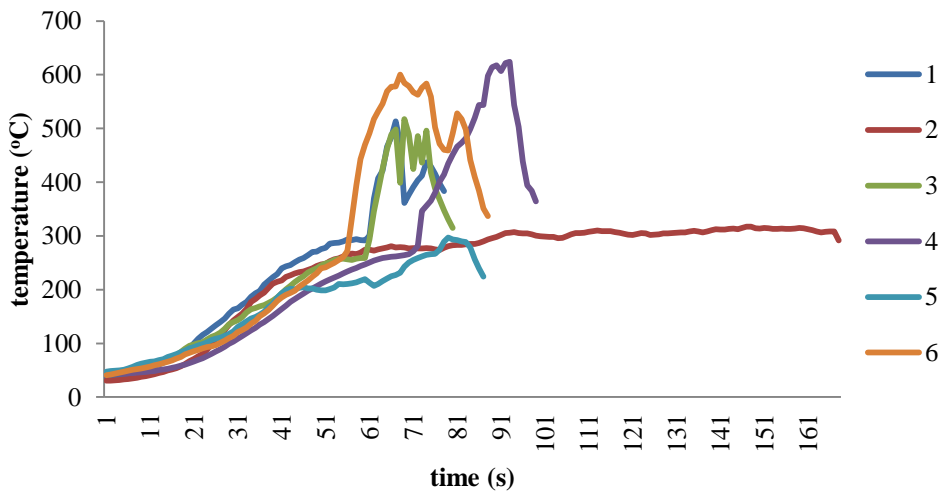


Figure 4.22: Time-temperature profile of 80% nylon + 20% elastin (H)

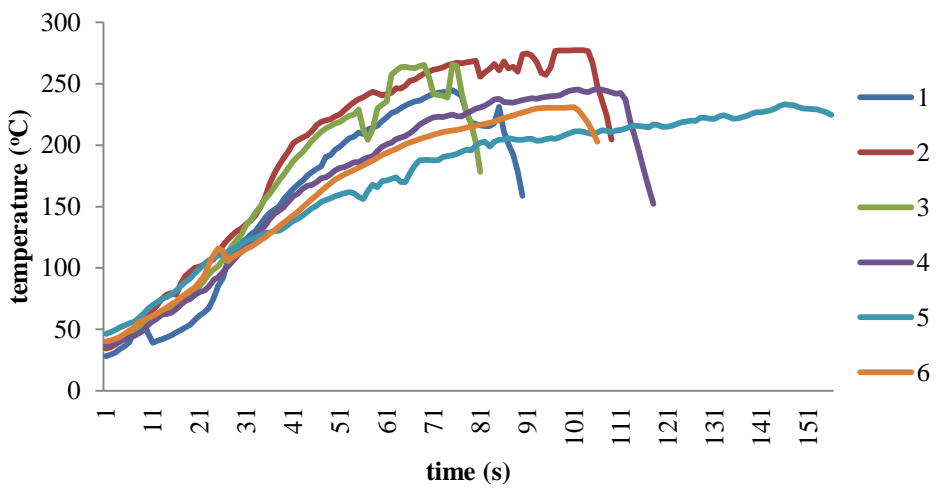


Figure 4.23: Time-temperature profile of 100% silk (I)

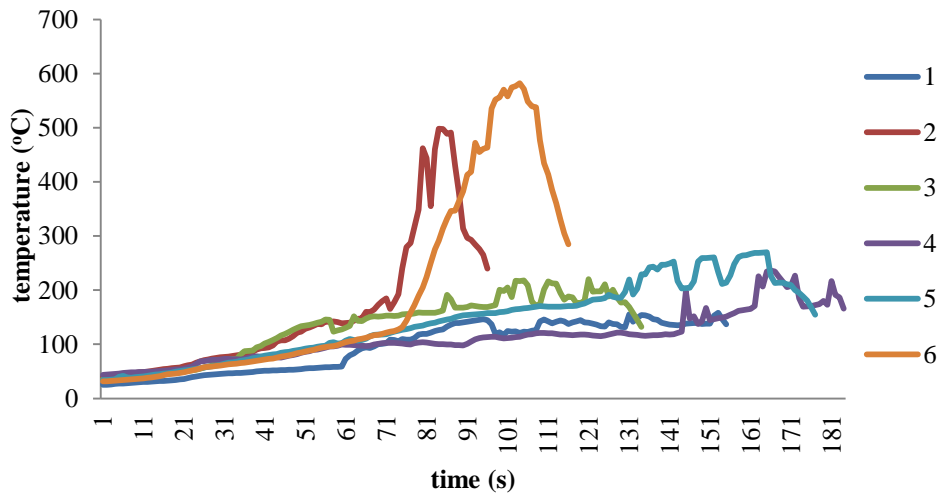


Figure 4.24: Time-temperature profile of 100% denim (J)

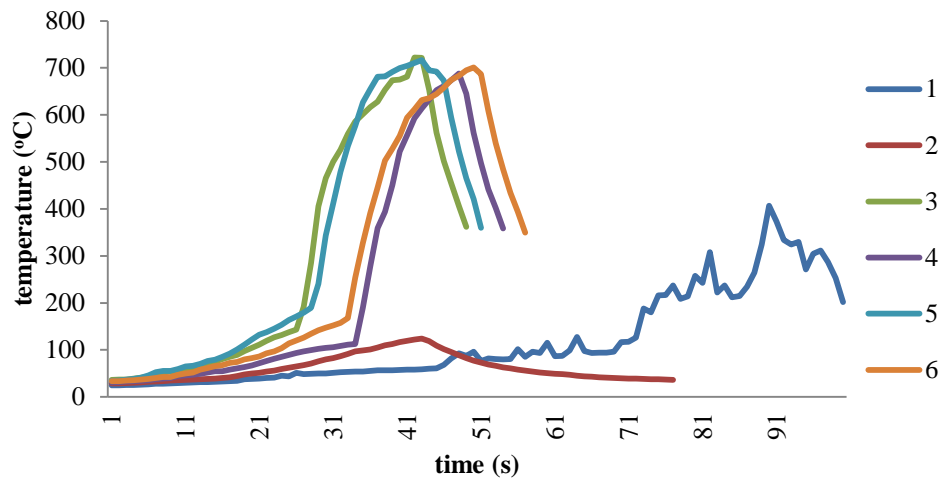


Figure 4.25: Time-temperature profile of 100% viscose (K)

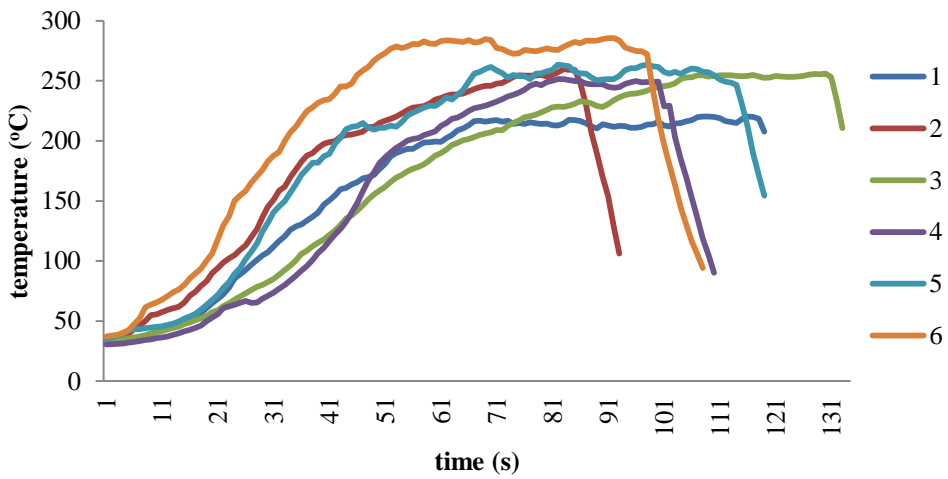


Figure 4.26: Time-temperature profile of 96% wool + 4% LYCRA® (L)

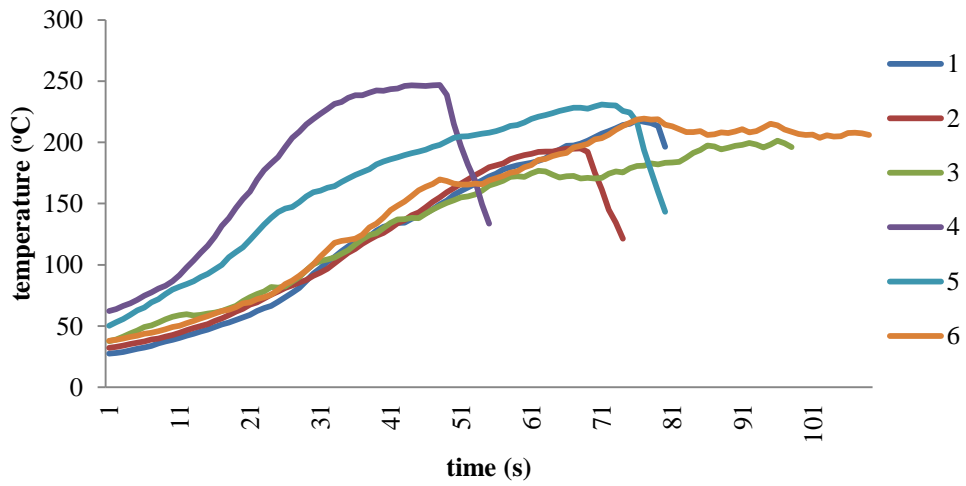


Figure 4.27: Time-temperature profile of 100% polyester (M)

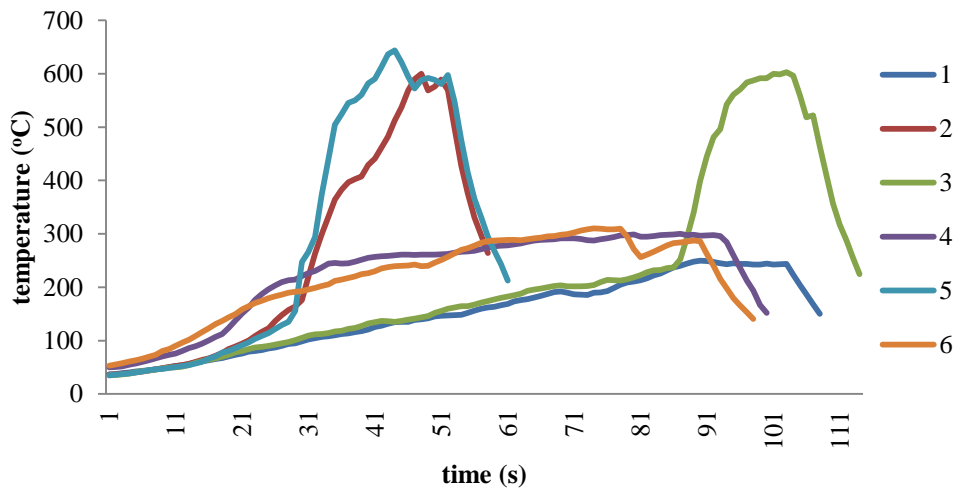


Figure 4.28: Time-temperature profile of 64% polyester + 33% rayon + 3% elastin (N)

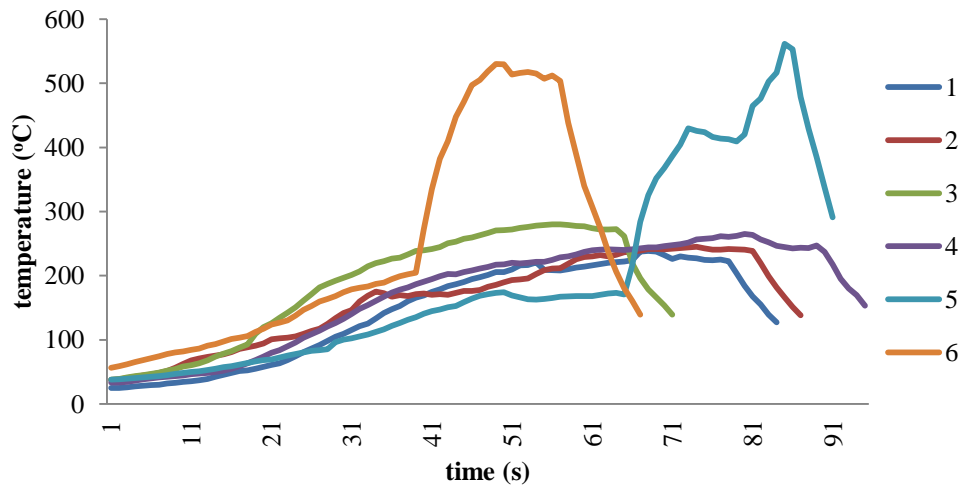


Figure 4.29: Time-temperature profile of 50% polyester + 50% viscose (O)

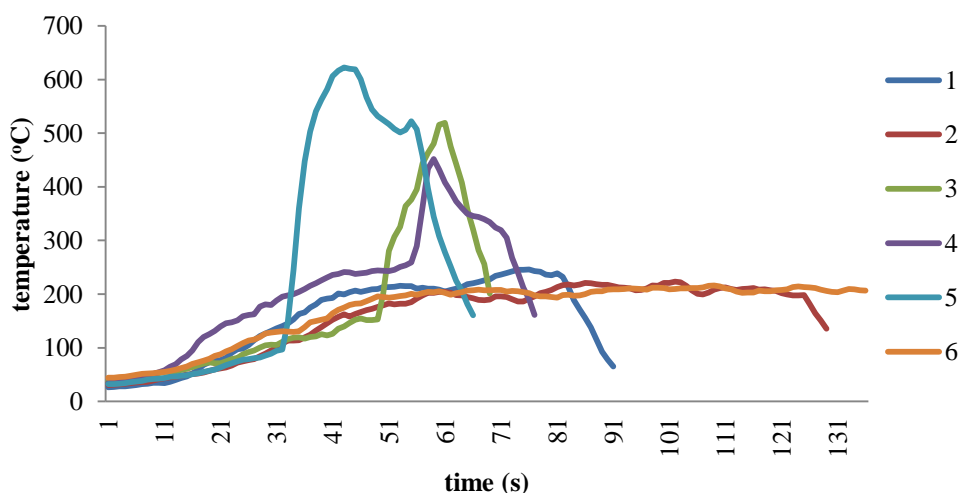


Figure 4.30: Time-temperature profile of 64% polyester + 32% viscose + 4% elastin (P)

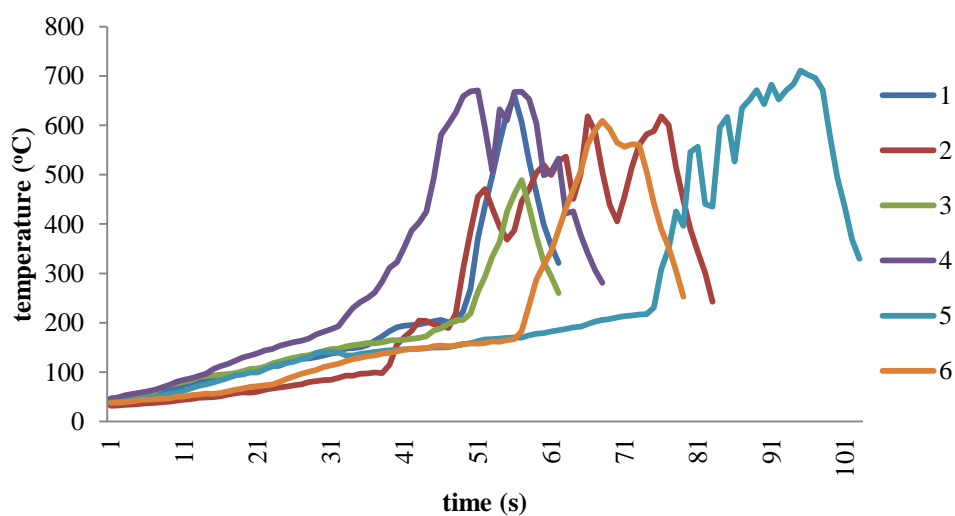


Figure 4.31: Time-temperature profile of 100% leather (Q)

Across all the textile types, acrylic (E) and the acrylic-cotton blend (F), the cotton-modal blend (D), pure silk (I) and wool (L) generated visible yellow smoke during the burning process. Yellow smoke can be generated from the breakdown of disulfide bonds in the monomer molecule to form sulfur-based compounds (e.g. sulfur dioxide, hydrogen disulfide, carbon disulfide) at elevated temperatures [22, 58]. Both acrylic (E) and polyester (M) were observed to have melted rather than undergone burning / charring. Similar findings were also observed by Wright and Adams [169] and the Fashion Laboratory [170], as illustrated in Table 4.12 as part of the compilation of the burning properties of some common natural, semi-synthetic and synthetic fibres.

Table 4.12: Burning properties of natural, semi-synthetic and synthetic fibres. Adapted from [170].

Fibres	Behaviour to flame	Behaviour in flame	Type of smoke	Odour
NATURAL				
Cellulosic Cotton Linen	Does not melt or shrink, moves away from flame	Burns quickly without melting	Grey	Burnt paper
Protein Wool Silk	Melts down, curls up and moves away from flame	Burns slowly, yellow flame	Grey	Burnt hair
SEMI-SYNTHETIC				
Rayon Viscose	Does not melt or shrink	Burns quickly without melting, yellow flame	Grey	Burnt paper
ARTIFICIAL				
Polyamide	Melts down and shrinks away from flame	Burns slowly and melts, yellow flame	Grey	Boiled celery
Polyester	Melts down and shrinks away from flame	Burns slowly and melts, yellow flame	Black	Aromatic, sweet
Acrylic	Melts down and shrinks away from flame	Burns and melts, bright flame	Black	Acrid, pungent

4.7.2.2 Post-Optimised Burnt Textiles

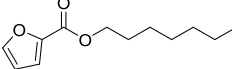
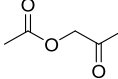
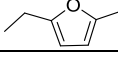
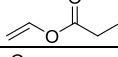
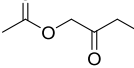
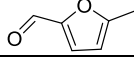
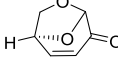
The remaining textiles were subjected to further six burnings and the alphabetical numbering for the optimised textiles follows those detailed in Table 4.11. In the second step elimination process, textiles that did not generate consistent pyrolysis products in at least three of the six repeats were eliminated. From the list of textiles in Table 4.11, 50% cotton + 33% viscose + 17% polyester (C), 100% nylon (G), 100% silk (I) 100% viscose (K), 100% polyester (M) and 64% polyester + 32% viscose + 4% elastin (P), were omitted from scrutiny in the next stage of study and the results for the remaining textiles tabulated.

4.7.3 Pyrolysis Products of Textiles

4.7.3.1 100% Cotton (A)

The pyrolysis of pure cotton produced a range of products, particularly aromatics, furans, ketones, acid and acid esters, *n*-aldehydes, *n*-alkyl-benzenes and levoglucosenone (Table 4.13). *n*-Butyl ether was not detected from the burnt cotton samples even though it was present in the control samples (Table 4.10).

Table 4.13: Pyrolysis products generated from 100% cotton (A)

No	Retention Time (min)	Compound	Molecular Structure	Set					
				1	2	3	4	5	6
1	2.72	methacrylaldehyde		√	√	√	√	√	√
2	2.99	pyruvaldehyde					√	√	√
3	3.20	2-methyl-furan		√	√	√	√	√	√
4	4.27	benzene		√	√	√	√	√	√
5	4.38	3-methyl-3-buten-2-one		√	√	√	√	√	√
6	5.12	propanoic acid					√		√
7	5.56	2,5-dimethyl-furan		√	√	√	√	√	√
8	7.06	toluene		√	√	√	√	√	√
9	7.85	2-furancarboxylic acid, heptyl ester		√	√	√	√	√	√
10	8.15	furfural		√	√		√	√	√
11	8.69	1-(acetyloxy)-2-propanone					√		√
12	9.03	ethyl-benzene		√	√	√	√	√	√
13	9.20	<i>p</i> -xylene		√	√	√	√	√	√
14	9.60	2-ethyl-5-methyl-furan					√		√
15	10.27	propanoic acid, ethenyl ester		√	√		√	√	√
16	10.31	1-(acetyloxy)-2-butanone		√	√		√	√	√
17	10.37	5-methyl-2-furancarboxaldehyde					√		√
18	12.15	levoglucosenone					√		√

In terms of qualitative reproducibility, *n*-aldehydes of methacrylaldehyde, furfural / 2-furancarboxaldehyde, aromatics and *n*-alkyl-benzenes (benzene, toluene, ethyl-benzene, *p*-xylene), furans (2-methyl-furan, 2,5-dimethyl-furan), ketones (3-methyl-3-buten-2-one, 1-(acetyloxy)-2-butanone) and acid esters (2-furancarboxylic acid, heptyl ester; propanoic acid, ethenyl ester) appeared in at least five of the six sets, while the remaining compounds were less consistent. A representative TIC (set 6) of textile (A) is represented in Figure 4.32.

Levoglucosenone, detected in two of the six sets is reported to be the major intermediate pyrolysis product of cellulose at temperatures of 300 °C [6, 21, 25-27]. At temperatures above 300 °C, this intermediate product undergoes decomposition to generate a range of furans, *n*-aldehydes and ketones [5, 6, 15, 27, 29, 30, 32, 33]. All six samples auto-ignited and attained maximum temperatures of 650-719 °C during pyrolysis (Figure 4.15). At these high temperatures, the generated levoglucosenone would have undergone decomposition into smaller, more stable compounds, which would explain why it was not detected in the majority of the samples.

Pyrolysis products such as methacrylaldehyde, pyruvaldehyde, furfural, 2-methyl-furan, benzene, toluene, 5-methyl-2-furancarboxaldehyde, 3-methyl-3-buten-2-one and the ketones that were detected in this study have been reported in the literature to be the major identifying peaks from the pyrolysis of cotton [25, 27, 29, 30, 32, 33, 82].

No *n*-alkanes, *n*-alkenes, *n*-cycloalkanes and *n*-cycloalkenes were revealed which is contrary to what that has been mentioned in some of the literature (C_1 - C_6 *n*-alkanes and *n*-alkenes) [27, 32, 33]. While acetic acid, 1,3-butadiene-1-carboxylic acid and 2,2-diethoxypropionate, ethyl ester [27, 29, 32] have been reported to be by products of cotton pyrolysis (none of which were detected in this study), this work identified the consistent presence of an additional two acid esters (i.e. 2-furancarboxylic acid, heptyl ester; propanoic acid, ethenyl ester).

Abundance

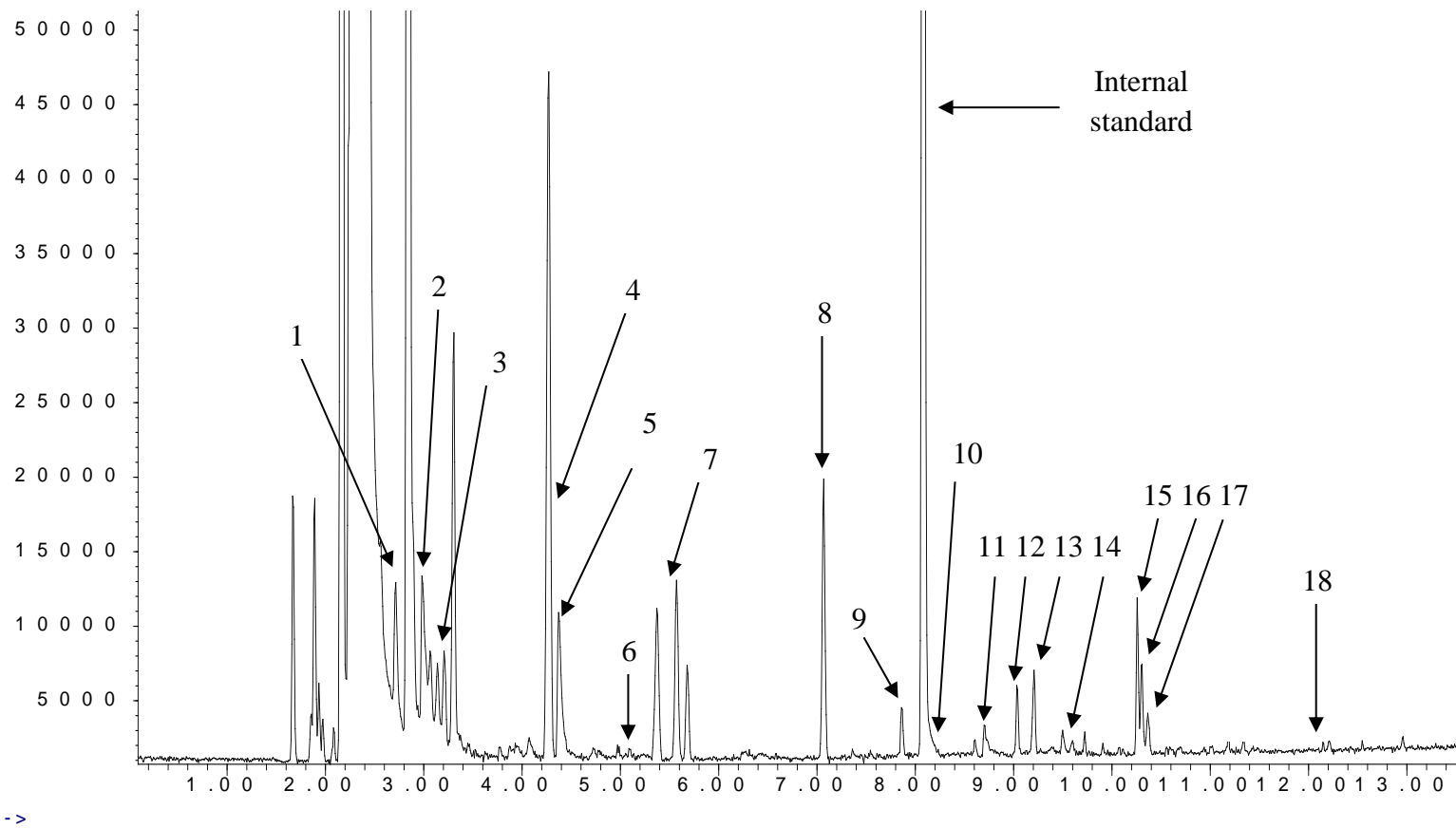


Figure 4.32: A representative TIC of 100% cotton (A) (set 6)

4.7.3.2 95% Cotton + 5% Elastin (B)

The pyrolysis of 95% cotton + 5% elastin produced a greater number of products, similar to 100% cotton (Table 4.13), but with the addition of ether, oxy-alkane, oxy-alkene, *n*-alkene, alcohol, *n*-cycloalkene, furans, limonene, acid esters and aromatic functional groups (Table 4.14), none of which were detected in pure cotton.

Table 4.14: Pyrolysis products from 95% cotton + 5% elastin (B)

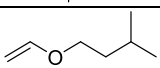
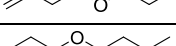
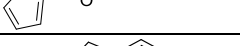
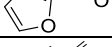
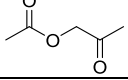
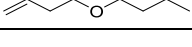
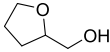
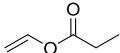
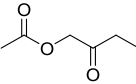
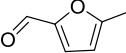
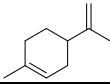
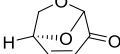
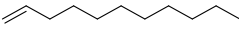
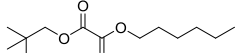
No	Retention Time (min)	Compound	Molecular Structure	Set					
				1	2	3	4	5	6
1	2.71	methacrylaldehyde		√		√		√	√
2	2.99	pyruvaldehyde		√		√		√	√
3	3.20	2-methyl-furan		√		√		√	√
4	3.57	tetrahydro-furan		√		√	√	√	√
5	3.92	2,3-dihydro-furan		√		√		√	√
6	4.27	benzene		√		√	√	√	√
7	4.38	3-methyl-3-buten-2-one		√		√		√	√
8	4.98	1-(ethenyloxy)-3-methyl-butane		√	√	√	√	√	√
9	5.12	propanoic acid		√				√	
10	5.56	2,5-dimethyl-furan		√		√		√	√
11	7.06	toluene		√		√	√	√	√
12	7.44	3-butenyl propyl ether		√		√		√	√
13	7.65	1-propoxy-butane		√		√		√	√
14	7.86	2-furancarboxylic acid, heptyl ester		√		√		√	√
15	8.15	furfural		√		√			
16	8.22	3-methylene-cycloheptene				√		√	√
17	8.70	1-(acetyloxy)-2-propanone		√				√	√
18	9.04	ethyl-benzene		√		√		√	√
19	9.15	2-propenoic acid, methyl ester		√				√	√
20	9.20	<i>p</i> -xylene		√		√		√	√
21	9.34	4-butoxy-1-butene		√		√		√	√

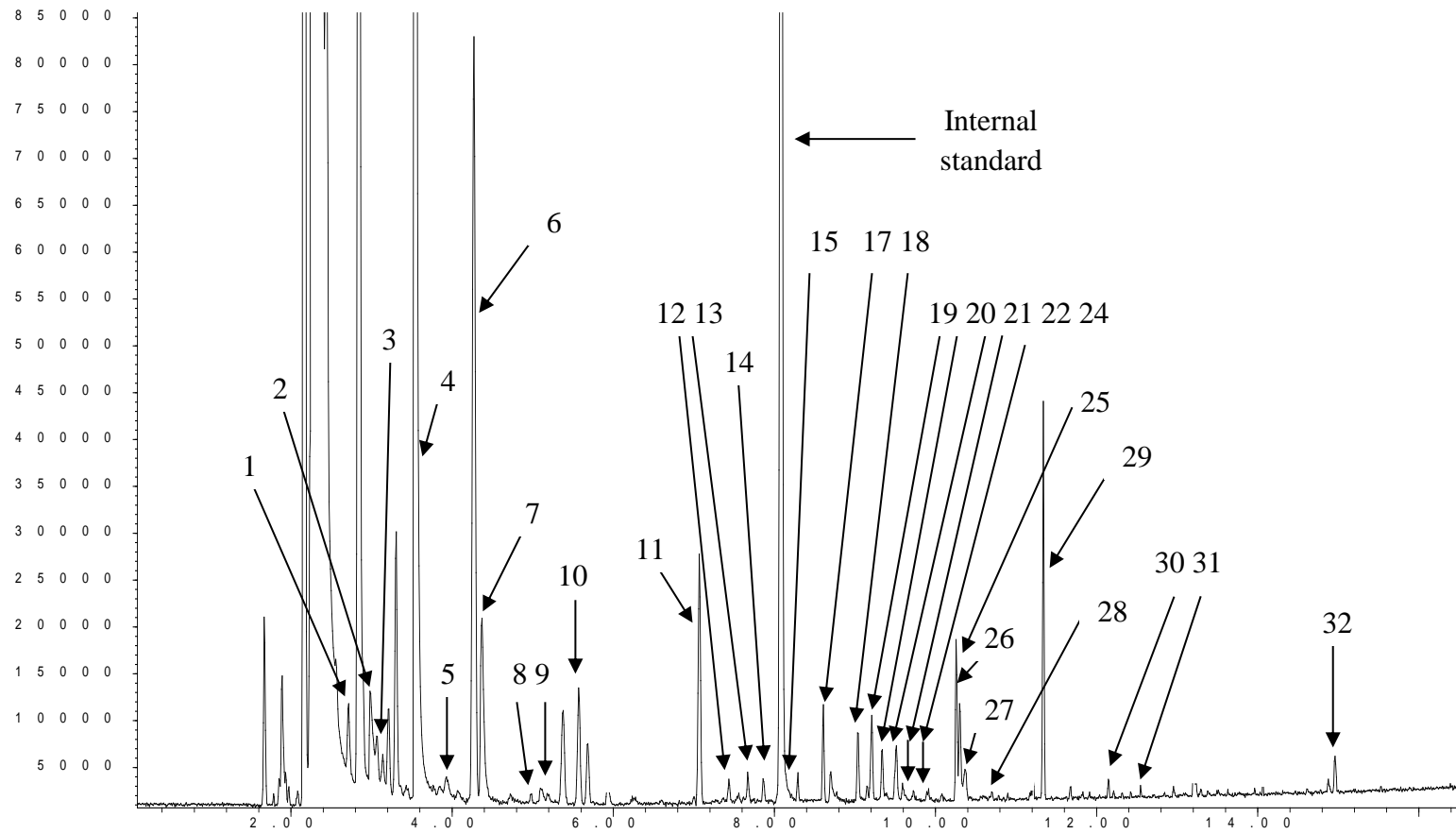
Table 4.14 continued

22	9.60	<i>o</i> -xylene		√		√		√	
23	9.73	1-nonene						√	√
24	9.90	2-furanmethanol, tetrahydro-		√		√		√	√
25	10.27	propanoic acid, ethenyl ester		√		√		√	√
26	10.30	1-(acetyloxy)-2-butanone		√		√		√	√
27	10.37	5-methyl-2-furancarboxaldehyde		√		√		√	
28	10.70	1,3,5-trimethyl-benzene		√		√		√	√
29	11.68	limonene		√				√	
30	12.15	levoglucosenone		√					
31	12.42	1-undecene		√				√	
32	14.97	oxalic acid, hexyl neopentyl ester		√					√

In terms of qualitative reproducibility, the following appeared in at least four of the six sets: *n*-aldehydes (methacrylaldehyde, pyruvaldehyde), aromatics and *n*-alkyl-benzenes (benzene, toluene, ethyl-benzene, *p*-xylene, 1,3,5-trimethyl-benzene), furans (2-methyl-furan, tetrahydro-furan, 2,3-dihydro-furan, 2,5-dimethyl-furan), ketones (3-methyl-3-buten-2-one, 1-(acetyloxy)-2-butanone), oxy-alkanes and oxy-alkenes (1-(ethenyloxy)-3-methyl-butane, 1-propoxy-butane, 4-butoxy-1-butene), acid esters (2-furancarboxylic acid, heptyl ester; propanoic acid, ethenyl ester), ether (3-butenyl propyl ether) and an alcohol (2-furanmethanol, tetrahydro-). Other compounds were inconsistent across the repeats. A representative TIC (set 1) of textile (B) is represented in Figure 4.33.

Looking at the temperatures attained across the repeats (Figure 4.16), sets 2 and 4, with the lowest number of pyrolysis products detected, experienced the highest temperatures (652-715 °C). These temperatures could have resulted in secondary decomposition of the volatiles generated during the pyrolysis process. Other samples experienced maximum temperatures between 551-641 °C, and produced a greater variety of pyrolysis products.

Abundance



Time -->

Figure 4.33: A representative TIC of 95% cotton + 5% elastin (B) (set 1)

Limonene, detected in two of the six sets of repeats, are a group of flammable, cyclic terpenes (consisting of two isoprene units) [171] found in essential oils, particularly from citrus oil extracts [159, 160]. It is known for its citrus-like scent and is often used in the cosmetic, fragrance and detergent industry [172]. Its presence could have been due to the use of detergents, cleaning agents or perfumes applied to the clothing prior to burning that volatilised when heat was applied. This is corroborated by Agu [173] and Lentini *et al.* [161] who both detected the presence of limonene from the pyrolysis of used wool clothing, cotton shirts and cardboard. Limonene has also been reported to be produced naturally and released during the pyrolysis of wood [161, 174], particularly white and yellow pinewood [82]. Under reduced pressure conditions, high concentrations of limonene have also been reported to have been generated from the pyrolysis of rubber in vehicle tyres [175]. The presence of 2-furanmethanol, tetrahydro-; from textile (B) has also been detected previously from cellulosic materials [162].

4.7.3.3 50% Cotton + 50% Modal (D)

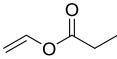
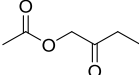
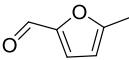
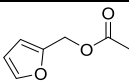
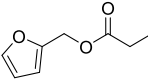
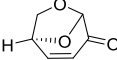
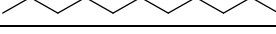
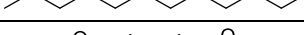
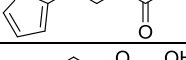
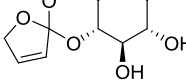
The pyrolysis of 50% cotton + 50% modal generated similar groups of compounds to textiles (A) and (B), but with additional dioxolane, ketones, sugar, *n*-alkanes, *n*-alkenes, acid and acid esters (Table 4.15).

However, when looking at the qualitative reproducibility, most of the compounds did not appear consistently across the six repetitive test sets. Pyrolysis products that appeared in at least four of the six repeats were *n*-aldehydes (furfural), furans (2-methyl-furan, 2,5-dimethyl-furan) and aromatics and *n*-alkyl-benzenes (benzene, toluene, ethyl-benzene, *p*-xylene). The list of compounds is presented in Table 4.15 and a representative TIC (set 6) of textile (D) is represented in Figure 4.34.

Table 4.15: Pyrolysis products generated from 50% cotton + 50% modal (D)

No	Retention Time (min)	Compound	Molecular Structure	Set					
				1	2	3	4	5	6
1	2.71	methacrylaldehyde			√			√	√
2	2.99	pyruvaldehyde			√			√	√
3	3.09	acetic acid							√
4	3.20	2-methyl-furan		√	√		√		√
5	3.92	2-methyl-1,3-dioxolane			√			√	√
6	4.27	benzene		√	√	√	√	√	√
7	4.38	3-methyl-3-buten-2-one			√			√	√
8	5.12	propanoic acid						√	√
9	5.56	2,5-dimethyl-furan		√	√			√	√
10	6.15	3-penten-2-one							√
11	6.82	propanoic acid, 2-methyl						√	√
12	7.00	propanoic acid, 2-oxo-, methyl ester						√	√
13	7.06	toluene		√	√		√	√	√
14	7.45	pentanoic acid						√	√
15	7.85	1-octene		√					
16	7.86	1-(2-furanyl)-ethanone			√			√	√
17	8.15	furfural		√	√			√	√
18	8.69	1-(acetyloxy)-2-propanone						√	√
19	9.04	ethyl-benzene		√	√		√	√	√
20	9.20	p-xylene		√	√			√	√
21	9.48	2-methyl-2-cyclopenten-1-one						√	√
22	9.54	2-furanmethanol, 2-formate						√	√
23	9.60	2-ethyl-5-methyl-furan						√	√
24	9.68	2-methyl-3-octanone						√	√
25	9.73	1-nonene		√	√				√

Table 4.15 continued

26	10.27	propanoic acid, ethenyl ester			√				√	√
27	10.31	1-(acetyloxy)-2-butanone							√	√
28	10.37	5-methyl-2-furancarboxaldehyde							√	√
29	10.70	1,3,5-trimethylbenzene			√					√
30	10.76	2,5-dihydro-3,5-dimethyl-2-furanone							√	√
31	10.84	2-furanmethanol, acetate							√	√
32	11.18	1-decene		√	√					√
33	11.83	acetophenone		√					√	√
34	12.03	2-furanmethanol, propanoate							√	√
35	12.15	levoglucosenone							√	√
36	12.42	1-undecene		√						√
37	12.55	undecane		√						
38	13.51	dodecane							√	√
39	13.63	butanoic acid, 2-furan-, methyl ester							√	√
40	13.83	4,6-O-furylidene-D-glucopyranose								√

Abundance

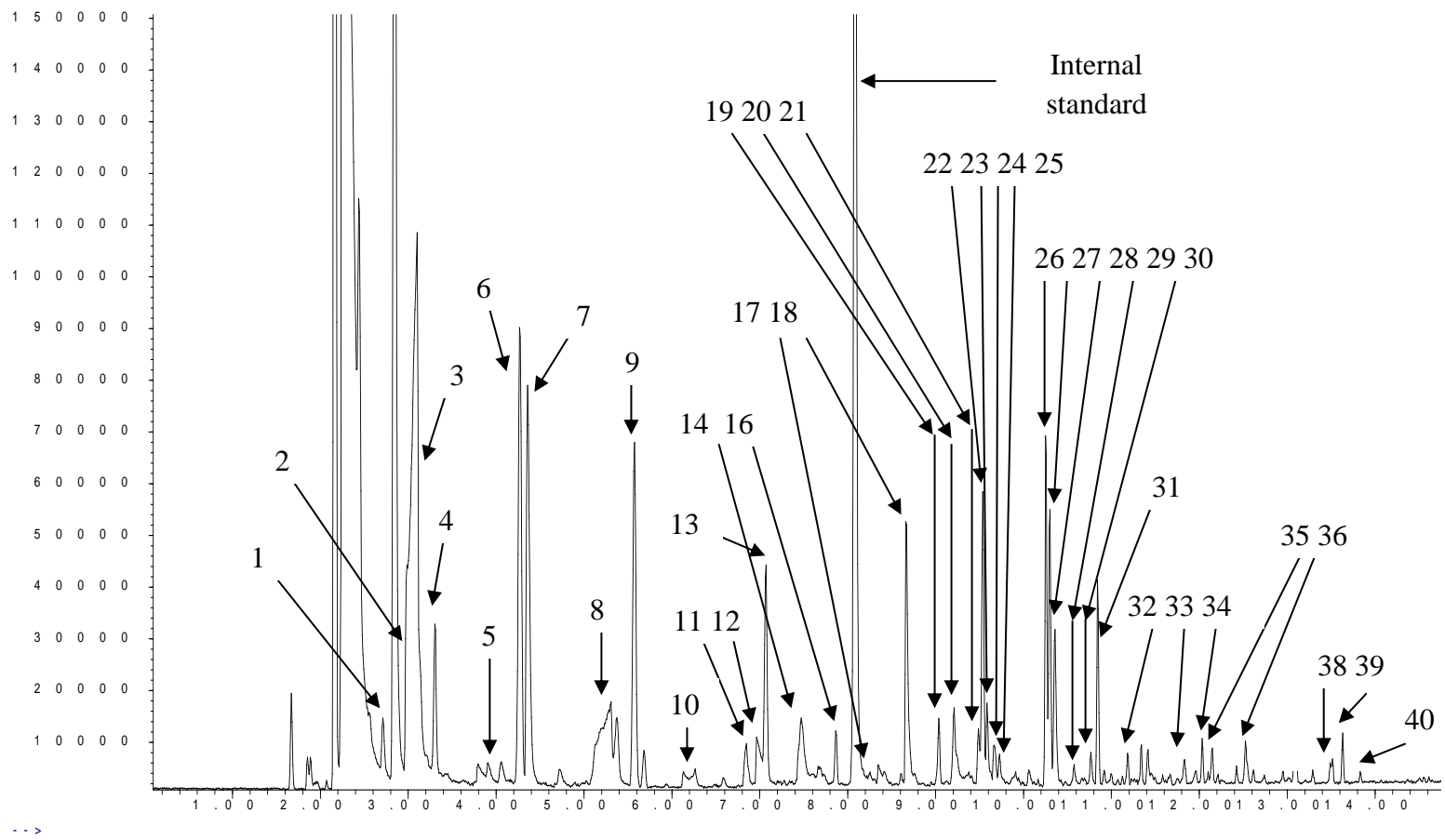


Figure 4.34: A representative TIC of 50% cotton + 50% modal (D) (set 6)

In terms of temperatures attained across the six sets of repeats (Figure 4.18), the highest temperature (492 °C) was recorded in set 3, which was also the set that generated the least pyrolysis products. The remaining sets attained maximum temperature of between 409 °C and 478 °C. Temperatures attained in textile (D) were much lower in comparison to those attained in textiles (A) and (B).

Although modal is essentially cotton, its fibres have undergone treatment of various kinds which alter its chemical structure, thermal properties, thermal decomposition mechanism and as a consequence, the resulting pyrolysis products. Similar outcomes are expected of other cellulose based textiles such as viscose, rayon and denim, depending on the percentage of these fibres in the textile. Dioxolane detected in textiles (D) refers to a group of organic acetal compound containing the dioxolane ring. It has good water solubility and is often used as a solvent and a monomer or comonomer in the synthesis of polymers [176]. It possesses an auto-ignition temperature of 273 °C [177] and is most likely to have been generated from the pyrolysis of modal rather than cotton, as it was not seen in textiles (A) or (B). The same is true for the additional acids, acid esters, ketones and alcohols that were seen only in textile (D). The presence of acetic acid and furanmethanol compounds detected in textile (D) was also reported by Stauffer *et al.* [162], having generated from the pyrolysis of different forms of cellulosic materials. The presence of a sugar; 4,6-O-furylidene-D-glucopyranose in textile (D) is expected as both cellulosic components (cotton and modal) are essentially made up of sugar monomers, namely D-glucopyranose [7, 8]. A glucopyranose derivative was also detected from the pyrolysis of 50% cotton + 33% viscose + 17% polyester (C) (Appendix 2.0), with majority of its pyrolysis products (although inconsistently) detected in textile (D).

As the percentage of cotton reduces from textiles (A) to (B) to (D), a shift is seen in the pyrolysis profile generated: *n*-alkanes, *n*-alkenes, dioxolanes, aromatic groups and alcohols start to appear, and an increase in the number of ketones and acid esters is observed. The increase in the percentage of the additional fibre seems to have increased the complexity of the pyrolysis profile as compared to cotton on its own.

Another observation was that, although all three fibres auto-ignited, the maximum temperatures they attained decreased proportionally with the percentage of cotton: from 719 °C (A) (100% cotton) to 715 °C (B) (95% cotton) and dropping markedly to 492 °C for textile (D) (50% cotton). Cotton, with an LOI of 18.4% [16], burns readily at its pure state however, in the presence of an additional fibre such as elastin or modal, the thermal behaviour of cotton obviously changes. For textile (B), maximum temperatures attained were relatively high and similar to textile (A) as the percentage of elastin was minor (5%) in (B), and in textile (D), where the proportions of fibres were equal (50% cotton, 50% modal), a marked change in temperature was noted with a difference of over 200 °C from textiles (A) and (B) to textile (D).

This observation is expected; as the percentage of the blended fibre increases, its thermal properties are dominantly displayed. This observation is supported by Cardamone [18] who reported that textiles containing two or more fibre blends exhibited distinctive burning behaviour, not characteristics of their individual fibres, and this burning profile has been reported to be largely influenced by the proportions of the individual fibres in the blends. If the proportion of one fibre is significantly higher than the other, the majority of the burning behaviour of that textile blend is expected to be similar to that of the highly proportioned fibre [19, 156].

4.7.3.4 100% Acrylic (E)

The pyrolysis of pure acrylic generated a variety of nitriles and derivatives, aromatics and derivatives, *n*-alkyl-benzenes, cyanide and cyanic compounds, pyridine, pyrazine, piperidine, *n*-alkanes, *n*-alkenes, acid esters and acid salt, *n*-aldehyde, ketone, naphthalene and amines (Table 4.16) with good qualitative reproducibility across all six samples. While the majority of the pyrolysis products appeared consistently across all or at least in five of the six sets, benzene and *N,N*-dimethyl-1-tetradecanamine were only detected in four and three of the six repeats, respectively. A representative TIC (set 3) of textile (E) is represented in Figure 4.35.

The majority of the products were seen to be nitriles of various kinds: *n*-alkane / *n*-alkene nitrile, methyl-nitrile, *n*-alkane / *n*-alkene dinitrile, methyl- *n*-alkane / -*n*-

alkene nitrile, benzonitrile, and cyanic compounds; iso- / cyano-alkane- / *n*-alkene-benzene, corresponding to those presented in pervious literature [130, 132, 136, 137]. These nitrile and cyanic based compounds are expected as the monomers of acrylic are acrylonitrile repeating units [-CH₂-CH(CN)-] [127]. When heat is applied, the monomers break down to form unstable radicals that in turn cleave the polymer backbone, accompanied by elimination of hydrogen, cyclisation (structural rearrangement to form cyclic products) of C≡N and conjugation, to yield a variety of cyanic and nitrile constituents, depending on the temperature to which it is subjected [130, 133, 134].

Table 4.16: Pyrolysis products from 100% acrylic (E)

No	Retention Time (min)	Compound	Molecular Structure	Set					
				1	2	3	4	5	6
1	2.60	propanenitrile		√	√	√	√	√	√
2	2.95	2-methyl-2-propenenitrile		√	√	√	√	√	√
3	3.21	isobutyronitrile		√	√	√	√	√	√
4	3.65	3-butenenitrile		√	√	√	√	√	√
5	4.00	butanenitrile		√	√	√	√	√	√
6	4.27	benzene		√		√	√	√	
7	4.77	2-pentenenitrile		√	√	√	√	√	√
8	5.43	2-methyl-butanenitrile		√	√	√	√	√	√
9	5.54	2-methyl-3-butenenitrile		√	√	√	√	√	√
10	6.33	methallyl cyanide		√	√	√	√	√	√
11	6.77	pentenenitrile		√	√	√	√	√	√
12	6.79	2-methyl-2-butenenitrile		√	√	√	√	√	√
13	6.98	pentanenitrile		√	√	√	√	√	√
14	7.06	toluene		√	√	√	√	√	√
15	7.26	2,2'-iminobis-acetonitrile		√	√	√	√	√	√
16	7.81	1-isocyano-butane		√	√	√	√	√	√
17	7.91	3-methyl-2-methylene-butanenitrile		√	√	√	√	√	√
18	8.22	4-methyl-pentanenitrile		√	√	√	√	√	√
19	8.55	5-cyano-1-pentene		√	√	√	√	√	√
20	8.82	3-hexenedinitrile		√	√	√	√	√	√

Table 4.16 continued

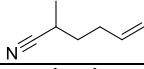
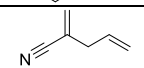
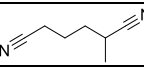
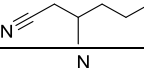
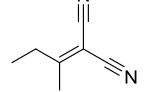
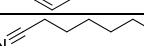
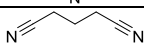
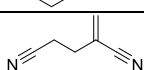
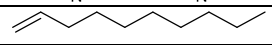
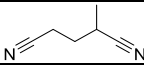
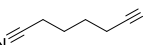
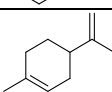
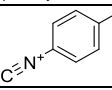
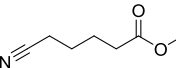
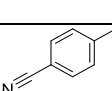
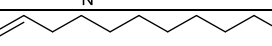
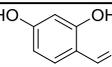
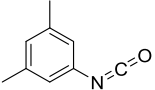
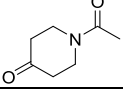
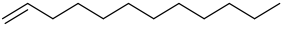
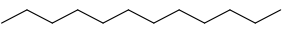
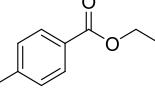
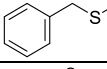
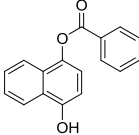
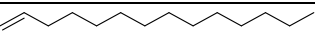
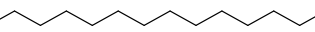
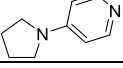
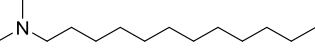
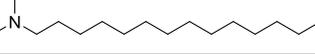
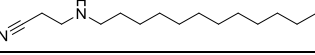
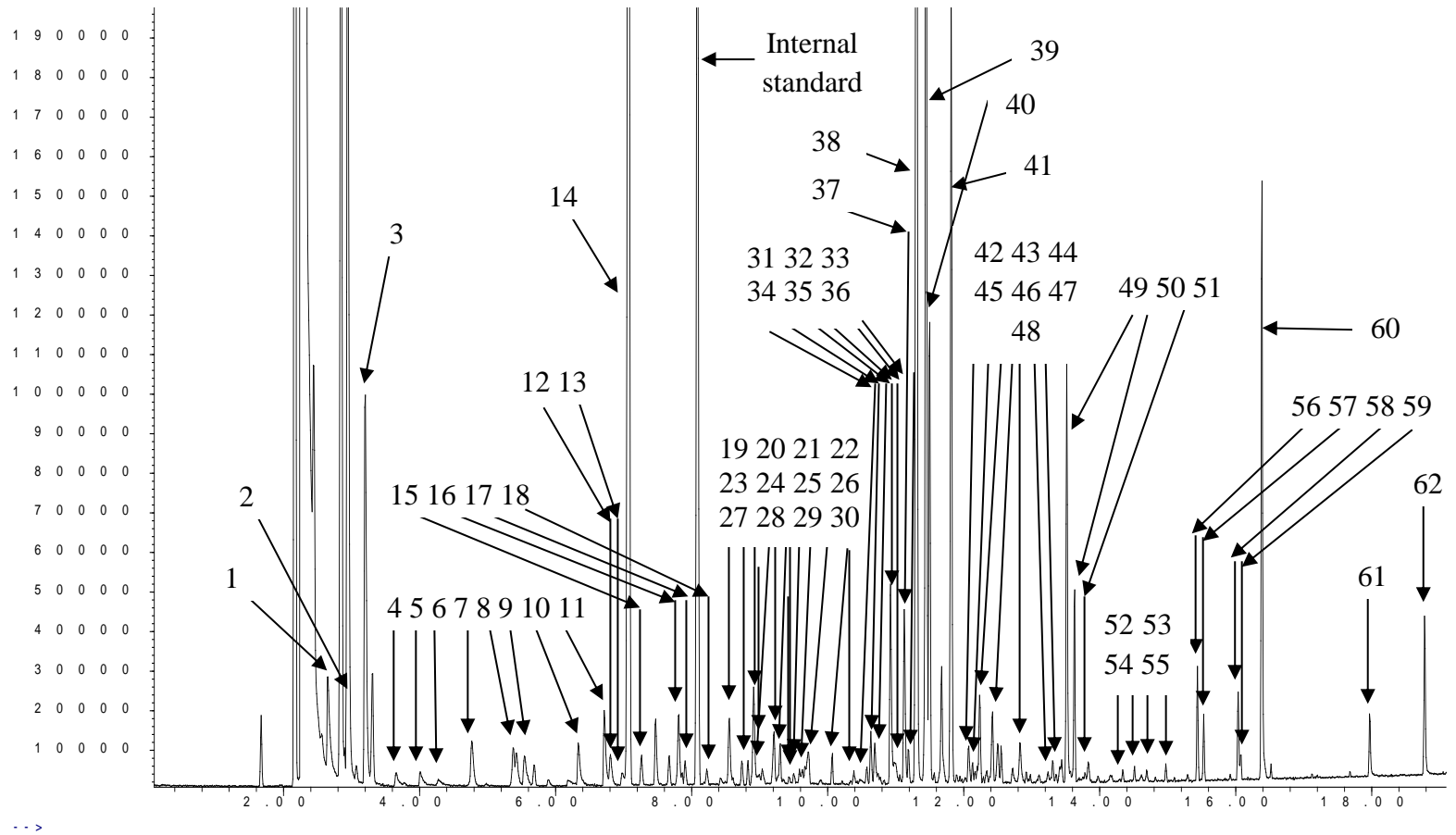
21	8.92	hexanenitrile		√	√	√	√	√	√
22	9.04	ethyl-benzene		√	√	√	√	√	√
23	9.20	<i>p</i> -xylene		√	√	√	√	√	√
24	9.31	2-methyl-5-hexenenitrile		√	√	√	√	√	√
25	9.51	styrene		√	√	√	√	√	√
26	9.62	2-methylene-4-pentenitrile		√	√	√	√	√	√
27	9.66	2-methyl-hexanedinitrile		√	√	√	√	√	√
28	9.71	3-methyl-hexanenitrile		√	√	√	√	√	√
29	10.06	(1-methylpropylidene)-propanedinitrile		√	√	√	√	√	√
30	10.40	benzaldehyde		√	√	√	√	√	√
31	10.57	heptanonitrile		√	√	√	√	√	√
32	10.64	benzonitrile		√	√	√	√	√	√
33	10.68	3,5-dimethyl-pyridine		√	√	√	√	√	√
34	10.94	pentanedinitrile		√	√	√	√	√	√
35	10.99	cyclohexanecarbonitrile		√	√	√	√	√	√
36	11.13	2-methylene-pentanenitrile		√	√	√	√	√	√
37	11.18	1-decene		√	√	√	√	√	√
38	11.30	2-methyl-pentanedinitrile		√	√	√	√	√	√
39	11.44	hexanedinitrile		√	√	√	√	√	√
40	11.50	1-(methylethenyl)-pyrazine		√	√	√	√	√	√
41	11.68	limonene		√	√	√	√	√	√
42	12.07	1-isocyano-4-methyl-benzene		√	√	√	√	√	√
43	12.13	pentanoic acid, 5-cyano-, methyl ester		√	√	√	√	√	√
44	12.24	4-methyl-benzonitrile		√	√	√	√	√	√
45	12.42	1-undecene		√	√	√	√	√	√
46	12.90	2,4-dihydroxy-benzaldehyde		√	√	√	√	√	√

Table 4.16 continued

47	13.33	3,5-xylylisocyanate		√	√	√	√	√	√
48	13.44	1-acetyl-4-piperidone		√	√	√	√	√	√
49	13.52	1-dodecene		√	√	√	√	√	√
50	13.63	dodecane		√	√	√	√	√	√
51	13.84	3,3-dimethyl-piperidine		√	√	√	√	√	√
52	14.34	ethyl 4-methylbenzoate			√	√	√	√	√
53	14.51	1-tridecene		√	√	√	√	√	√
54	14.69	[(methylsulfenyl)-methyl]-benzene		√	√	√	√	√	√
55	14.97	naphthalene-1,4-diol, 4-O-benzoyl(ether)		√	√	√	√	√	√
56	15.43	1-tetradecene		√	√	√	√	√	√
57	15.53	tetradecane		√	√	√	√	√	√
58	16.04	1-pentadecene		√	√	√	√	√	√
59	16.07	4-pyrrolidinopyridine		√	√	√	√	√	√
60	16.38	N, N-dimethyl-1-dodecanamine			√	√	√	√	√
61	17.98	N, N-dimethyl-1-tetradecanamine			√	√	√		
62	18.77	3-(dodecylamino)-propanenitrile			√	√	√	√	√

Abundance



Time -->

Figure 4.35: A representative TIC of 100% acrylic (E) (set 3)

The 100% acrylic (E) was part of the group of textiles that did not undergo auto-ignition. Throughout the burning process, the highest temperatures attained across the sets were below 300 °C, ranging from 210 °C to 294 °C (Figure 4.19). Although acrylic has a low LOI of 18% [129], no ignition occurred in any of the tests. This can be explained by Bajaj's [129] findings in which he documented the melting point of dry polyacrylonitrile to be 320 °C, where the molecule undergoes cyclisation before reaching its melting point. Contrary to this, other researchers have documented that acrylic melts at temperatures above 220 °C [22] and undergoes significant pyrolytic decomposition at temperatures between 290-590 °C [22, 130]. Temperatures attained in this study might not have been high enough to induce significant decomposition to produce enough flammable volatiles to cause ignition. This is supported by Horrocks *et al.* [133] who reported that, at temperatures of 250-350 °C, the dominant process that occurs is cyclisation, while at higher temperatures, volatilisation takes over and this causes the fibre to produce more volatile flammables that readily ignites.

Major products that have been reported from the pyrolysis of acrylic at various temperature ranges are as follows: cyanogen, hydrogen cyanide, acrylonitrile, acetonitrile and vinyl-acetonitrile at 280-450 °C [136]; hydrogen cyanide, acetonitrile, acrylonitrile, methacrylonitrile, 1,3-dicyano-propene, 1,3-dicyano-butene, 2,4-dicyano-butene, 1,3-dicyano-butane, 2,4,6-tricyano-hexene, 1,3,5-tricyano-hexane, 1,3,5-tricyano-hexane and 2,4,6,8-tetracyano-octene at 590 °C [130]; hydrogen cyanide, acetonitrile, acrylonitrile, acetic acid, methacrylonitrile, 1,3-dicyano-propene, 1,3-dicyano-butene and 1,3,5-tricyano-hexane at 700°C [132]; and hydrogen cyanide, acrylonitrile, acetonitrile, propionitrile, isobutyronitrile and methacrylonitrile at 500-900 °C [137]. The pyrolysis of acrylic has been reported occur at temperatures between 500-700 °C, in which random fragmentation and secondary decomposition yield abundant volatiles and particularly high levels of hydrogen cyanide, acetonitrile and acrylonitrile [137]. These products were however, not detected in this study. Similar findings were also documented by Surianarayanan *et al.* [130] and it appears to be temperature related; at temperatures below 425 °C, as in this study, these products were not detected. Notwithstanding this, a significant number of thermal decomposition products were observed.

In addition to this, ammonia, reported in the literature from the pyrolysis of polyacrylonitrile [137] was also not detected in this work, similar to findings by Causin *et al.* [132] and Minagawa *et al.* [137]. Ammonia requires extended periods and elevated temperatures to form. Although the pyrolysis process was relatively long in this study, the temperatures attained by the samples were too low to facilitate the release of ammonia [137]. Although hydrogen cyanide, acetonitrile, acrylonitrile and ammonia were not detected in this work, cyanic compounds, amine groups, benzaldehydes, styrene, pyrazine, pyridine, piperidine, naphthalene and high molecular weight *n*-alkanes and *n*-alkenes were all present in the samples upon analysis. These compounds could have resulted as a consequence of the various cleavage and scission pathways the fibre was subjected to during the early stages of thermal decomposition.

4.7.3.5 50% Acrylic + 50% Cotton (F)

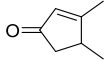
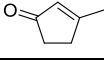
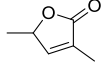
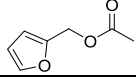
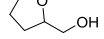
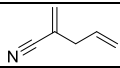
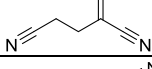
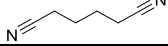
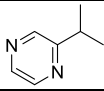
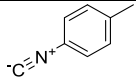
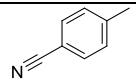
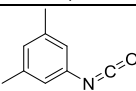
The pyrolysis of 50% acrylic + 50% cotton generated a variety of compounds (Table 4.17) similar to those from 100% acrylic (E) but with the absence of the long chain *n*-alkanes and *n*-alkenes, pyridine, piperidine, acid ester, *n*-aldehyde, naphthalene and amines (Table 4.16).

In terms of qualitative reproducibility, the pyrolysis products generated by the acrylic-cotton blend were less consistent across the sets as compared to those from 100% acrylic (E). However, most of the products were detected in at least four of the six repeat samples. A representative TIC (set 4) of textiles (F) is represented in Figure 4.36.

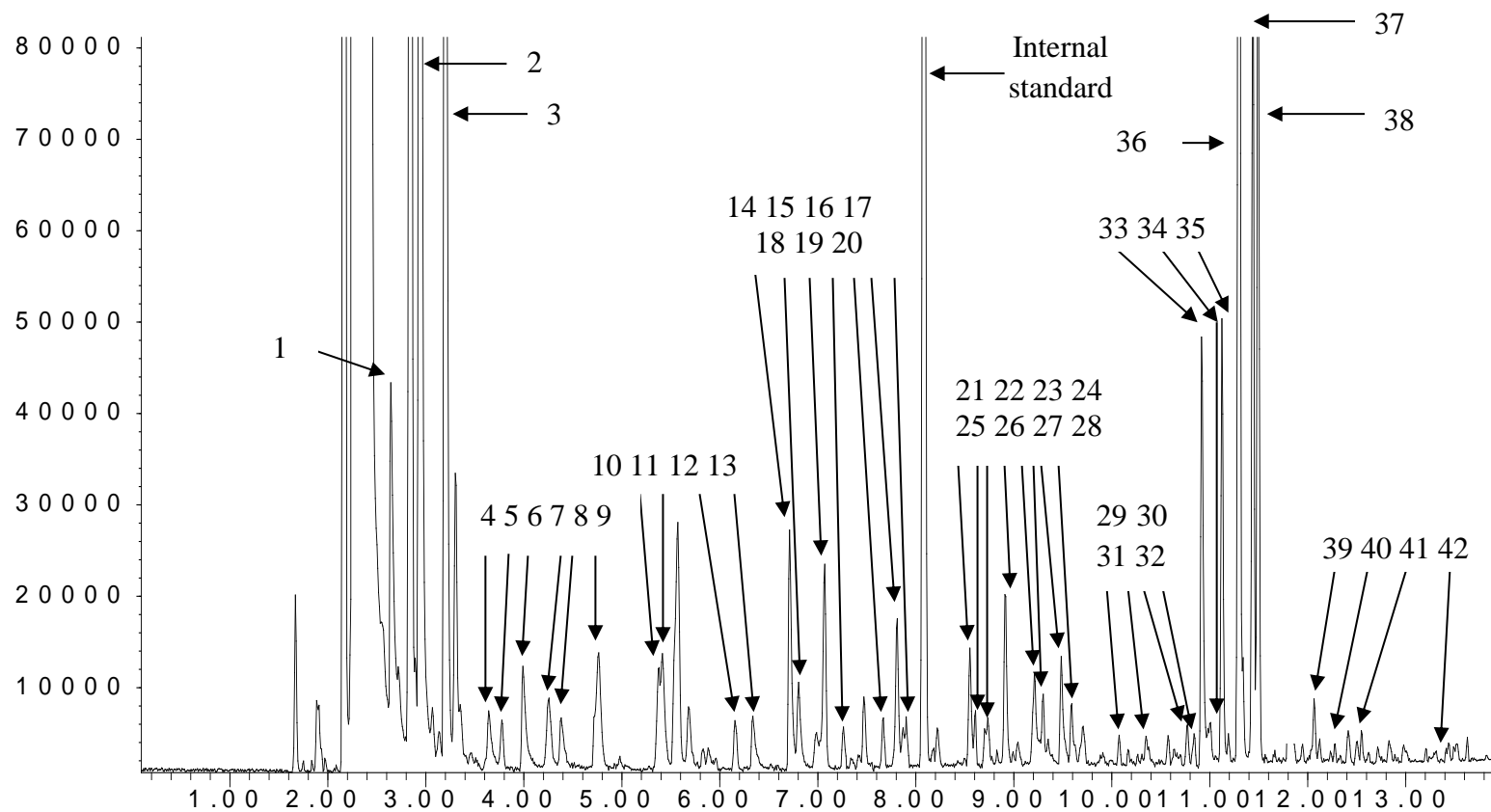
Table 4.17: Pyrolysis products from 50% acrylic + 50% cotton (F)

No	Retention Time (min)	Compound	Molecular Structure	Set					
				1	2	3	4	5	6
1	2.60	propanenitrile		√	√	√	√	√	√
2	2.95	2-methyl-2-propenenitrile		√	√	√	√	√	√
3	3.21	isobutyronitrile		√	√	√	√	√	√
4	3.65	3-butenenitrile				√	√	√	
5	3.77	propyl-cyclopropane		√	√	√	√	√	
6	4.00	butanenitrile		√	√	√	√		
7	4.27	benzene		√	√	√	√		√
8	4.38	3-methyl-3-buten-2-one		√	√	√	√		√
9	4.78	2-pentenenitrile		√	√	√	√		
10	5.45	2-methyl-butanenitrile		√	√	√	√		
11	5.56	2,5-dimethyl-furan		√	√	√	√		√
12	6.15	1-methyl-1H-pyrrole				√	√		
13	6.34	methallyl cyanide				√	√		
14	6.75	pentenenitrile		√	√	√	√		
15	6.80	2-methyl-2-butenenitrile				√	√		√
16	7.06	toluene		√	√	√	√		
17	7.25	2,2'-iminobis-acetonitrile				√	√		√
18	7.67	3-methyl-2-methylene-butanenitrile				√	√		
19	7.81	4-methyl-pentanenitrile		√	√	√	√		√
20	7.87	2-ethyl-5-methyl-furan				√	√		
21	8.55	5-cyano-1-pentene		√	√	√	√		√
22	8.69	1,6:2,3-dianhydro-4-O-acetyl-β-D-allopyranose				√	√		√
23	8.92	hexanenitrile		√	√	√	√		√
24	9.04	ethyl-benzene		√	√	√	√		√
25	9.20	p-xylene		√	√	√	√		√
26	9.30	2-methyl-5-hexenenitrile		√		√	√		√
27	9.50	2-dimethyl-2-cyclopenten-1-one				√	√		√
28	9.58	1-(1H-pyrazol-4-yl)-ethanone		√		√	√		√

Table 4.17 continued

29	10.08	3,4-dimethyl-2-cyclopenten-1-one		√		√	√		√
30	10.35	3-methyl-2-cyclopenten-1-one				√	√		√
31	10.77	2,5-dihydro-3,5-dimethyl-2-furanone				√	√		√
32	10.84	2-furanmethanol, acetate				√	√		√
33	10.94	pentanedinitrile		√	√	√	√	√	√
34	11.00	2-furanmethanol, tetrahydro-				√	√		√
35	11.13	2-methylene-pentanedinitrile		√	√	√	√	√	√
36	11.30	2-methyl-pentanedinitrile		√	√	√	√	√	√
37	11.44	hexanedinitrile		√	√	√	√	√	√
38	11.50	(1-methylethenyl)-pyrazine		√	√	√	√	√	√
39	12.07	1-isocyano-4-methyl-benzene		√		√	√		√
40	12.24	4-methyl-benzonitrile		√		√	√		√
41	12.50	pyrazine		√		√	√		√
42	13.30	3,5-xylylisocyanate					√		√

Abundance



Time -->

Figure 4.36: A representative TIC of 50% acrylic + 50% cotton (F) (set 4)

The acrylic-cotton blend (F) also generated additional groups of compounds not seen in 100% acrylic (E): sugar, ketones, furan, alcohol, pyrrole and alkyl-cycloalkane. These additional compounds, particularly 3-methyl-3-buten-2-one, 2,5-dimethyl-furan, 2-ethyl-5-methyl-furan, 2-dimethyl-2-cyclopenten-1-one, 2,5-dihydro-3,5-dimethyl-2-furanone; 2-furanmethanol, acetate; and 2-furanmethanol, tetrahydro-; are attributed to be by-products from the pyrolysis of the cotton counterpart in the textile mixture, as they were seen to be present in the pyrolysis profile of cotton blends in textiles (A), (B) and (D). Although not detected in the pyrolysis of cotton blend in textiles (A) and (B), the presence of a pyranose compound; 1,6:2,3-dianhydro-4-O-acetyl- β -D-allopyranose detected in textile (F) is most likely a result of the decomposition of the sugar monomer present in cellulose [178] and has been previously mentioned in the literature to be an isomeric form of levoglucosan [27]. This claim is further corroborated with the detection of different forms of pyranose from the pyrolysis of 50% cotton + 50% modal (D) and 50% cotton + 33% viscose + 17% polyester (C) (Appendix 2.0). Additional ketone groups, pyrrole, and alkyl cycloalkane detected in textiles (F) could potentially be by-products of the pyrolytic interaction between cotton and acrylic or from the thermal decomposition of cotton at temperatures below 500 °C.

An overlap in the aromatic profiles produced by both pure cotton (A) and pure acrylic (E) was noted, whereby benzene, toluene, ethyl-benzene and *p*-xylene were all produced by both the natural and synthetic fibres. Thus, these volatiles should not be used as characteristic identifying products for either fibre in blends although they are present consistently and at high concentration across the two different groups of fibres.

Although the proportions of acrylic and cotton in the textile are equal, and their pyrolytic profiles are expected to be a superimposition of the two fibres rather than a merged one, the volatile profile generated in this study clearly demonstrates the dominant features of acrylic, which produced more than half of the volatile products in the pyrolytic profile as compared to cotton. From the 42 volatile products generated, only eight were produced from the pyrolysis of cotton. Similarly, the

burning behaviour of the cotton-acrylic blend (F) was also largely influenced by the presence of acrylic rather than cotton. This is particularly noted when five of the six textiles did not auto-ignite and reached maximum temperatures in the range of 221-321 °C only (Figure 4.20). It was only the sixth repeat that ignited and reached a maximum temperature of 482°C. This failure to auto-ignite was also documented in pure acrylic fibres (E). As cotton has proven to auto-ignite easily and experience secondary decomposition [6] at temperatures between 280-310 °C [18], the presence of acrylic must have prevented the auto-ignition of the cotton fibres in the blended textiles. The possible intermolecular reaction between the acrylic and cotton fibres clearly altered the thermal properties of each individual fibre, particularly for cotton.

4.7.3.6 80% Nylon + 20% Elastin (H)

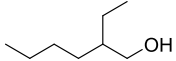
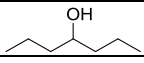
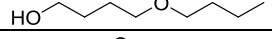
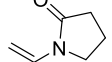
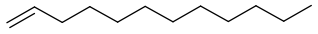
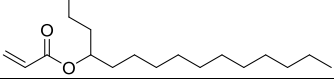
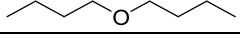
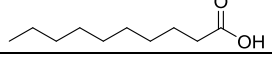
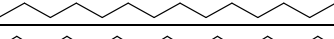
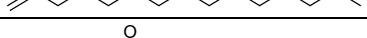
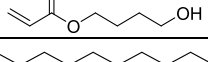
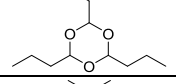
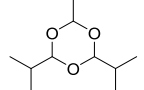
The pyrolysis of 80% nylon + 20% elastin generated a range of products: dienes, furan, nitriles, aromatics, *n*-alkyl-benzenes, alkyl-cycloalkane / cycloalkene, cyanic compounds, acids, *n*-alkanes, *n*-alkenes, *n*-cycloalkanes, cyclic / dialkyl-ether, alkyl- / oxy-alcohols, capro- / aromatic ketones, *n*-aldehyde oligomer, lactam compounds, caprolactam and acrylic ester (Table 4.18).

In terms of qualitative reproducibility, compounds that appeared in at least four of the six sets were of furan (tetrahydro-furan), aromatics (benzene, toluene), nitrile (hexanenitrile), alcohol (4-butoxy-1-butanol), ethers (dibutyl ether, *n*-butyl ether), acid (*n*-decanoic acid) and caprolactam. The remaining pyrolysis products generated were present in only half or less of the repeats. A representative TIC (set 3) of textile (H) is represented in Figure 4.37.

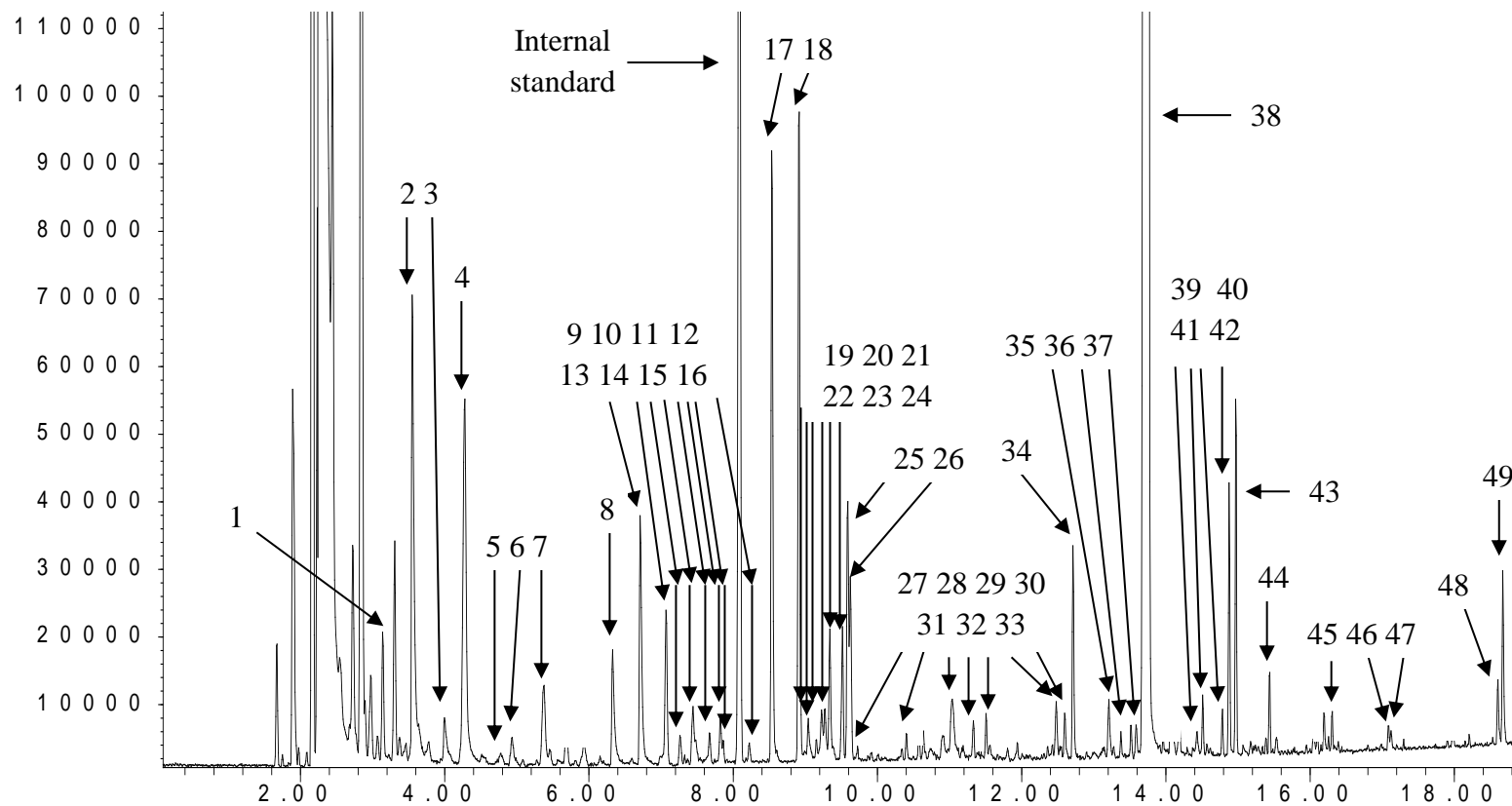
Table 4.18: Pyrolysis products from 80% nylon + 20% elastin (H)

No	Retention Time (min)	Compound	Molecular Structure	Set					
				1	2	3	4	5	6
1	2.97	1,2-hexadiene				√	√		
2	3.57	tetrahydro-furan			√	√	√	√	√
3	4.00	butanenitrile				√	√		√
4	4.27	benzene		√		√	√	√	√
5	4.87	3-pentenenitrile				√	√		
6	4.99	ethenyl-cyclobutane		√		√	√		
7	5.46	1,5-heptadiene				√	√		
8	6.34	methallyl cyanide				√	√		√
9	6.71	pentanenitrile				√	√		√
10	7.06	toluene		√		√	√		√
11	7.26	2,2'-iminobis-acetonitrile				√	√		√
12	7.44	pentanoic acid				√	√		√
13	7.67	1-propoxy-butane				√	√		√
14	7.82	3-methylene-heptane				√	√		√
15	7.85	1-octene				√	√		√
16	8.23	1,5-cyclooctadiene				√	√		√
17	8.54	5-cyano-1-pentene				√	√		√
18	8.92	hexanenitrile		√	√	√	√	√	√
19	9.04	ethyl-benzene				√	√		√
20	9.20	p-xylene				√	√		√
21	9.31	2-methyl-5-hexenenitrile				√	√		
22	9.35	4-butoxy-1-butene				√	√		√
23	9.52	n-butyl ether		√	√	√	√		√
24	9.60	1,2-diethenyl-cyclobutane			√	√		√	
25	9.62	2-methylene-4-pentenenitrile			√	√		√	
26	10.40	6-cyano-1-hexene			√	√		√	
27	10.63	benzonitrile			√	√		√	
28	10.90	5-hexenoic acid			√	√		√	
29	11.04	propanedioic acid, propyl-			√	√		√	
30	11.30	3-hydroxypropyl-oxirane			√	√		√	

Table 4.18 continued

31	11.51	2-ethyl-1-hexanol			√	√		√	
32	12.47	caprolactone			√	√		√	
33	12.60	4-heptanol			√	√		√	
34	12.72	4-butoxy-1-butanol			√	√	√	√	
35	13.23	<i>N</i> -vinylbutyrolactam			√	√		√	
36	13.51	1-dodecene			√	√		√	
37	13.56	<i>N</i> -methylcaprolactam			√	√		√	
38	13.73	caprolactam			√	√	√	√	
39	14.43	<i>N</i> -acetylcaprolactam			√	√		√	
40	14.51	1-tridecene			√	√		√	
41	14.78	4-(prop-2-enoyloxy)-pentadecane			√	√		√	
42	14.88	dibutyl ether			√	√	√	√	
43	14.97	<i>n</i> -decanoic acid			√	√	√	√	
44	15.43	1-tetradecene			√	√		√	
45	16.34	pentadecane			√	√		√	
46	17.08	4-hydroxybutyl acrylate			√	√		√	
47	17.12	1-hexadecene			√	√		√	
48	18.60	2,4,6-tripropyl-1,3,5-trioxane			√	√		√	
49	18.67	2,4,6-tris(1-methylethyl)-1,3,5-trioxane			√	√		√	

Abundance



Time -->

Figure 4.37: A representative TIC of 80% nylon + 20% elastin (H) (set 3)

Although a range of products was generated, only three sets (sets 3, 4 and 6) generated considerable amounts of pyrolysis products, whereas the other three generated very low numbers of products (sets 1, 2 and 5). This directly corresponds to the temperature and burning duration attained by the fibres during pyrolysis. The nylon-elastin blend (H) was among the group of textiles that exhibited a mixture of results in terms of auto-ignition, as four of the textile samples ignited whereas the other two did not (Figure 4.22). Sets 1, 3, 4 and 6 ignited and attained maximum temperatures of 498-616 °C, and sets 3, 4 and 6 produced considerably more pyrolysis products in comparison to sets 2 and 5 which did not ignite (< 314 °C). In contrast to this, little pyrolysis products were detected in set 1 even though ignition was achieved however in this case, ignition was only sustained for a very short period of time. From this behaviour, it is evident that temperatures attained by the polyamide fibre during the burning process largely affects the presence and type of pyrolysis products detected [126]. Although only accounting for 20% of the fibre blend, the elastin could have interfered with nylon's ability to auto-ignite. This is expected as when the proportion of the blended fibre increases, its thermal properties are exerted to the blend or could even alter the overall burning properties to produce new characteristics, not identifiable to any of the individual fibres [18].

The following pyrolysis products detected are corroborated in the literature as thermal decomposition products from the pyrolysis of nylon across a range of temperatures; furans [179], aromatics [119, 125, 179], nitriles [109, 119], acids [56] and caprolactam [59, 109, 123]. Ether and alcohols have not been previously reported. Although low levels of ethyl-benzene and *p*-xylene were detected in the control samples of (H) (Table 4.10), they were only present in three of the six sets.

The thermal decomposition of nylon, particularly nylon 6, begins at temperatures above 310 °C [117, 118] and follows an intramolecular process accompanied by a hydrogen transfer that leads to the cleavage of the weak C-N bond [124]. This process, documented at 400-600 °C, is responsible for the generation of caprolactam, the main and specific by-product of nylon 6 [59, 109, 110, 116]. In this study, caprolactam was detected in high abundance in four of the six repeat samples (sets 3,

4, 5 and 6). Sets 3, 4 and 6 achieved temperatures above 518 °C and set 5 achieved a temperature of approximately 318 °C. Although temperatures were much lower than 400 °C in set 5, the generation of caprolactam was not inhibited. This is not surprising, as the minimum decomposition temperature for a range of nylon groups has been documented to be around 300-380 °C [117, 118, 121]. The absence of caprolactam in set 2 is most likely due to lower temperatures (302 °C) while although set 1 auto-ignited and reached temperatures of 498 °C, the duration of burning was very short. Caprolactam was also detected in five of the six sets of 100% silk (I) pyrolysis (Appendix 4.0). Being a natural polyamide [180], silk possesses similar molecules, namely *L*-lysine [56, 118] to synthetic nylon, (*L*-lysine is used to synthesise caprolactam, a monomer of nylon [181]) and thus during thermal decomposition, it undergoes pyrolytic breakdown to generate caprolactam. By contrast, the pyrolysis of 100% nylon (G) (Appendix 3.0) did not yield any caprolactam across the six sets of repeats. This could be due to the variation in the type of nylon used to synthesise textile (G), as caprolactam is a specific by-product indicative of nylon 6 only [109, 110], having detected inconsistently at low levels across nylon 6,6 and nylon 6,12 [119]. Besides caprolactam, *N*-acetylcaprolactam, *N*-methylcaprolactam, *N*-vinylbutyrolactam and caprolactone, all derivatives of caprolactam, were also detected in sets 3, 4 and 6. While *N*-acetylcaprolactam has been reported in the literature as a by-product of nylon 6 [109], the other three have not been previously reported from the pyrolysis of nylon 6.

The thermal decomposition process is then followed by the cleavage of the CO-CH₂ bond and subsequently the C-C bonds [109, 116, 118, 123]. The hydrocarbons, dienes, styrene, furan, nitriles, ketone, aromatics, acids and cyclic compounds detected in this study, and supported in the literature [109, 119, 123, 125, 179] are formed through the scission of the C-O and C-C bonds in the nylon molecule [109]. Nitriles are formed from the scission of the C-C bonds in molecules containing the C-N end group, while acids (hexanoic acid, hexenoic acid, decanoic acid) are formed through thermal hydrolysis that generates an acid end chain. Although low molecular weight *n*-alkanes and *n*-alkenes have been reported consistently in the literature [109, 118, 119, 179], only Almirall *et al.* [125] reported the presence of C₉ and C₁₄-C₁₅

branched alkenes from the pyrolysis of nylon carpets at 800 °C. This work established the presence of an additional high molecular weight *n*-alkane and *n*-alkene, pentadecane and hexadecane, respectively, detected at temperatures below 616 °C, in addition to the presence of *n*-aldehyde oligomers of 2,4,6-tripropyl-1,3,5-trioxane; 2,4,6-tris(1-methylethyl)-1,3,5-trioxane; and an acrylic ester (4-hydroxybutyl acrylate); although, they were only detected from three of the ignited set of fibres. The presence of these products could also be due to additional side chain reactions, as observed by Senoo *et al.* [126].

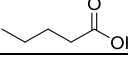
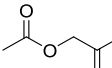
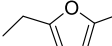
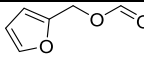
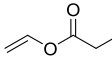
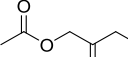
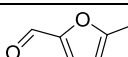
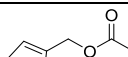
4.7.3.7 100% Denim (J)

The pyrolysis of 100% denim generated furans, dioxolanes, aromatics, *n*-alkyl-benzenes, ketones, acid and acid esters, *n*-aldehyde and caprolactam (Table 4.19). From the list of pyrolysis products generated across the repetitive samples, only furans (2-methyl-furan, 2,5-dimethyl-furan), dioxolane (2-methyl-1,3-dioxolane), aromatics (benzene, toluene), acid ester (propanoic acid, ethenyl ester; 2-furanmethanol, 2-formate; / formic acid, furfuryl ester;), ketones (3-methyl-3-buten-2-one and 1-(acetyloxy)-2-butanone) and *n*-aldehyde (5-methyl-2-furancarboxaldehyde) were present in at least four of the six sets of repeats. The remaining products were seen in less than half of the samples. A representative TIC (set 2) of textile (J) is represented in Figure 4.38.

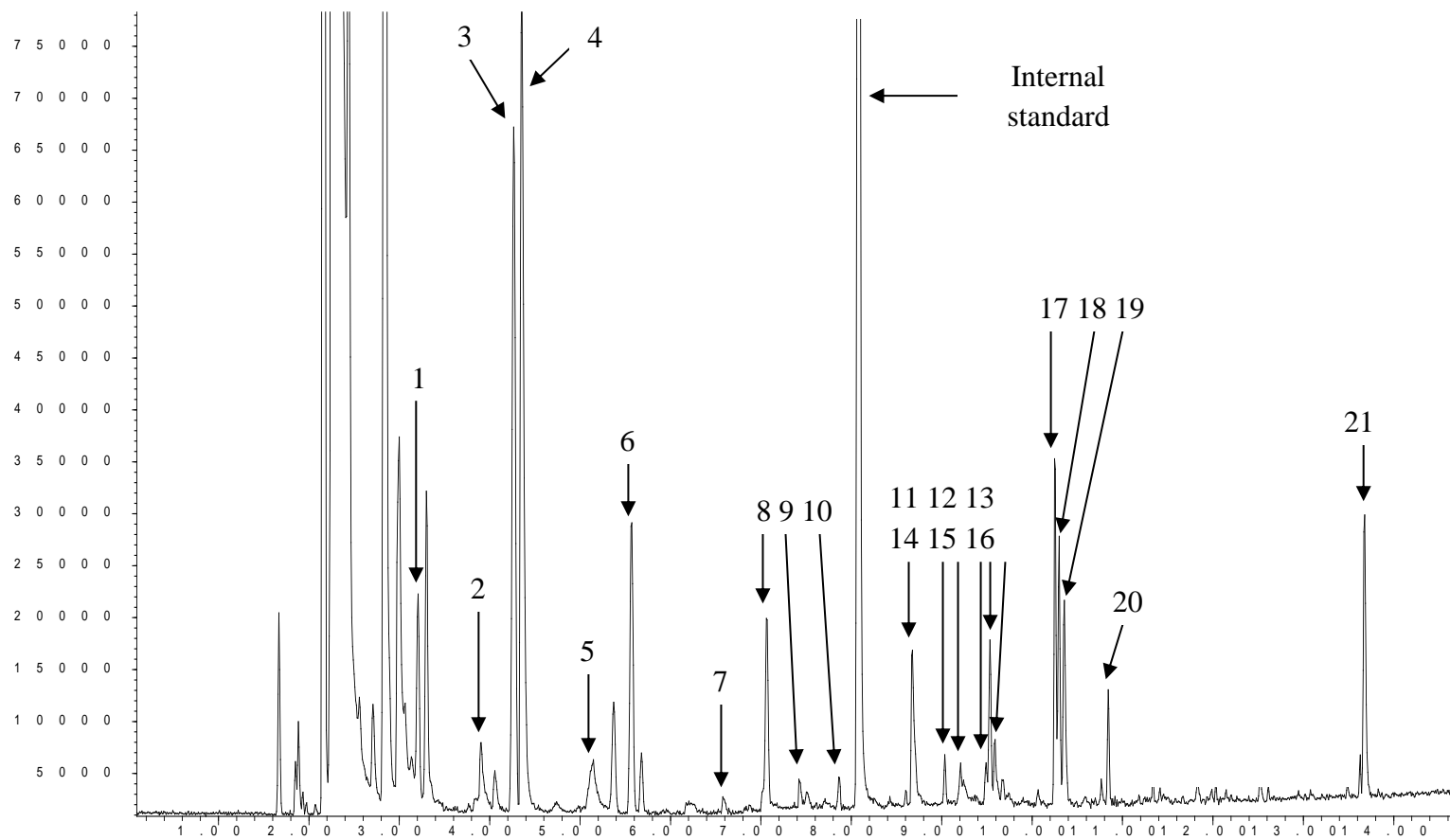
Since denim is cellulosic in nature, its burning properties are expected to be similar to those of cotton. However, its burning characteristics exhibited in Figure 4.24 displayed a mixture of results, as only two out of the six samples (sets 2 and 6) auto-ignited reaching maximum temperatures of 498-574 °C, similar to cotton, and generating more pyrolysis products in comparison to the remaining sets (sets 1, 3, 4 and 5). The remaining sets attained maximum temperatures of 121-268 °C while generating few or no pyrolysis products. Again, the presence of additives and the manufacturing process to which the fibre was subjected could have altered its burning characteristics. Neither levoglucosan nor any of its isomers were detected in the pyrolysis of denim, but the additional (although inconsistent) presence of an acid

ester (2-furanmethanol, 2-formate / formic acid, furfuryl ester) was noted. This acid ester was also present in 50% cotton + 50% modal (D) samples.

Table 4.19: Pyrolysis profile of 100% denim (J)

No	Retention Time (min)	Compound	Molecular Structure	Set					
				1	2	3	4	5	6
1	3.20	2-methyl-furan		√	√	√	√		√
2	3.90	2-methyl-1,3-dioxolane		√	√	√			√
3	4.27	benzene		√	√	√	√		√
4	4.38	3-methyl-3-buten-2-one		√	√	√	√		√
5	5.14	propanoic acid			√				√
6	5.56	2,5-dimethyl-furan		√	√	√	√		√
7	6.60	1,3-dioxolane			√				√
8	7.06	toluene		√	√	√	√		√
9	7.43	pentanoic acid			√				√
10	7.86	1-(2-furanyl)-ethanone			√	√			
11	8.67	1-(acetyloxy)-2-propanone			√	√			√
12	9.03	ethyl-benzene			√				
13	9.23	<i>p</i> -xylene			√				
14	9.48	2-ethyl-5-methyl-furan			√				√
15	9.54	2-furanmethanol, 2-formate		√	√	√			√
16	9.60	1-(1H-pyrazol-4-yl)-ethanone			√	√			√
17	10.25	propanoic acid, ethenyl ester		√	√	√			√
18	10.30	1-(acetyloxy)-2-butanone		√	√	√			√
19	10.37	5-methyl-2-furancarboxaldehyde		√	√	√			√
20	10.84	2-furanmethanol, acetate			√	√			√
21	13.73	caprolactam			√				√

Abundance



Time -->

Figure 4.38: A representative TIC of 100% denim (J) (set 2)

Most of the pyrolysis products detected in textile (J) are products of from pyrolysis of cotton identified across textiles (A), (B) and particularly in textile (D). As denim is essentially cotton, it is not surprising to see similar chromatographic output among these textiles. Having said that, the presence of caprolactam detected here, although at low concentrations is somewhat surprising. As mentioned in 4.7.3.6, caprolactam is an important intermediate pyrolysis product of nylon 6 and is used as a positive indicator of nylon 6 when present at high abundance [116]. Although denim is made from 100% cotton, additives such as spandex / elastane are usually added in small amounts to increase its performance and appearance [38]. Besides that, denim is also dyed with a mixture of phenylglycine reacted in potassium hydroxide-sodium hydroxide (KOH-NaOH) and sodium amide (NaNH₂) to create its characteristic indigo colour [182]. It has also been mentioned in the literature that the polyamine dye component commonly used in dyeing cellulosic textile materials contains an epoxidised polyamide group in its mixture [183]. Either one or all of these factors or the interactions between these factors, could have been responsible for the presence of caprolactam in denim as they could potentially contribute the N group needed to form the lactam molecule [36].

4.7.3.8 96% Wool + 4% LYCRA[®] (L)

The pyrolysis of 96% wool + 4% lycra[®] produced a range of nitriles, furans, aromatics, *n*-aldehyde, *n*-alkyl-benzenes, alkyl-aromatics, diazine, α -amino acid, alcohol, isocyanate and phenolic compounds (Table 4.20). The qualitative reproducibility of textile (L) was rather poor with only sets 1 and 4 producing more than one pyrolysis product. A representative TIC (set 1) of textile (L) is represented in Figure 4.39.

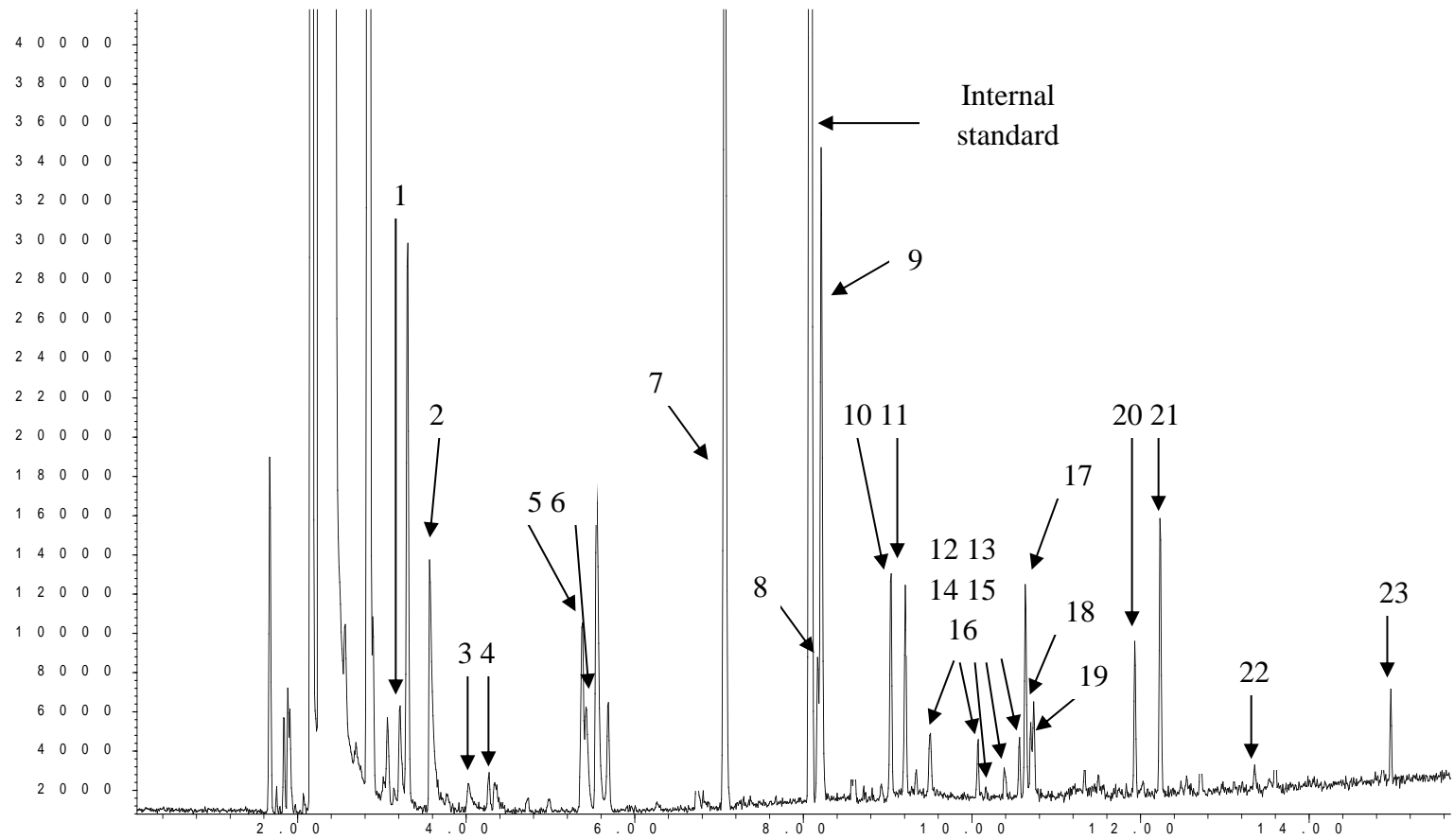
Textile (L) was part of the group of textiles that did not undergo auto-ignition. Maximum temperatures attained across the repeats were 217-282 °C (Figure 4.26). With its high LOI value of 25-28% and nitrogen, sulfur and moisture content [18, 22, 58], wool is known to be the natural fibre that is most resistant to flames and fires [55] and has been reported to auto-ignite only at higher temperatures of 570-600 °C [59]. However, some researchers have identified the ability of wool to auto-ignite at

temperatures as low as 385 °C [62]. None of these temperatures were attained in this study, even with prolonged burning.

Table 4.20: Pyrolysis products from 96% wool + 4% LYCRA® (L)

No	Retention Time (min)	Compound	Molecular Structure	Set					
				1	2	3	4	5	6
1	3.19	isobutyronitrile		√					
2	3.56	tetrahydro-furan		√			√		
3	4.00	butanenitrile		√			√		
4	4.27	benzene		√					
5	5.40	2-methyl-butanenitrile		√					
6	5.54	3-methyl-butanenitrile		√			√		
7	7.06	toluene		√			√		
8	8.16	bis(1,1-dimethylethyl)-diazene		√			√	√	
9	8.20	4-methyl-pentanenitrile		√			√		
10	9.03	ethyl-benzene		√			√		
11	9.20	p-xylene		√					
12	9.50	styrene		√					
13	10.06	5-methyl-hexanenitrile		√					
14	10.39	benzaldehyde		√					
15	10.55	propyl-benzene		√					
16	10.63	benzonitrile		√					
17	10.70	1-methylethyl-benzene		√					
18	10.72	phenol		√					
19	10.92	4-methyl-phenol		√					
20	11.94	L-arginine, N2-[(phenylmethoxy)carbonyl]-		√					
21	12.24	1-isocyano-3-methyl-benzene		√					
22	13.59	benzenepropanenitrile		√					
23	14.96	1-butoxy-4-butanol		√					

Abundance



Time -->

Figure 4.39: A representative TIC of 96% wool + 4% LYCRA® (L) (set 1)

Wool is essentially a helical chain of α -amino acid polypeptides containing chemically reactive disulfide bonds [55, 58]. The thermal degradation of wool begins as an endothermic reaction involving the dehydration of wool fibres at 120-160 °C [52], followed by cleavage of the weak disulfide bonds to produce small amounts of volatiles and inorganic compounds [22, 58, 62]; this progresses into an exothermic reaction involving a series of temperature-dependent pyrolysis stages that generate the major bulk of volatile products (> 245 °C) [18, 52]. The pyrolysis of wool is proven to be largely dependent on the temperature and duration of burning [32] and at certain temperatures, different types of pyrolysis products have been reported [18]. These products include furans, *n*-aldehydes, ketones, methyl-ketones, nitriles, alcohols, aromatics and phenolic compounds, reported from the pyrolysis of wool at various temperatures [18, 32, 64, 65, 67].

Across the literature, a number of products have been reported to be wool's major or distinctive pyrolysis products. Among them are phenol and 4-methyl-phenol at 370 °C and 480 °C, respectively [18]; toluene and nitriles at 590 °C [64], aromatic and phenolic compounds at 700 °C [65]; and alcohol, furan, *n*-aldehyde, aromatic and ketone at 800 °C [32]. These products were also present in this study, particularly in set 1. The majority of these products were also detected from the pyrolysis of 100% silk (I) (Appendix 4.0). This is not surprising as both silk and wool are made up of animal proteins and amino acids [52, 55]. These volatiles are by-products generated from the breakdown of various α -amino acids. While nitriles are formed through the pyrolysis of valine, alanine, leucine and isoleucine [64], phenolic compounds are generated from the pyrolysis of tyrosine [67], and phenylalanine breaks down to form aromatics [64]. Thiols and sulfur compounds, detected in previous work [18, 59] are formed through the decomposition of cysteine [18, 55] but were absent from the samples in this study. *L*-Arginine, an α -amino acid detected in this study, can be attributed to its presence at 7-10% in the polypeptide chain of wool [184]. The additional presence of styrene and diazene in this work is also highlighted.

4.7.3.9 64% Polyester + 33% Rayon + 3% Elastin (N)

The pyrolysis of 64% polyester + 33% rayon + 3% elastin generated a large number of products, namely *n*-aldehydes, furans, dioxolanes, *n*-alkyl-benzenes, ketones, acid and acid esters, methyl- alkenes and alkanes, aromatics and its derivatives, biphenyls, naphthalene, *n*-alkanes, *n*-alkenes and vinyl-benzenes as detailed in Table 4.21.

Across the six sample sets, qualitative reproducibility was poor as, out of the 59 pyrolysis products generated, only 14 were present in at least four of the six sets of repeats. These reproducible products were furans (2-methyl-furan, tetrahydro-furan, 2,5-dimethyl-furan), dioxolane (2-methyl-1,3-dioxolane), aromatics and *n*-alkyl-benzenes (benzene, toluene, ethyl-benzene, *p*-xylene), ketones (3-methyl-3-buten-2-one, 1-(acetyloxy)-2-butanone, acetophenone), *n*-aldehyde (1-furfural) and acid esters (2-propenoic acid, methyl ester; propanoic acid, ethenyl ester;). A representative TIC (set 4) of textile (N) is represented in Figure 4.40.

Table 4.21: Pyrolysis products from 64% polyester + 33% rayon + 3% elastin (N)

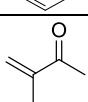
No	Retention Time (min)	Compound	Molecular Structure	Set					
				1	2	3	4	5	6
1	2.71	methacrylaldehyde		√			√	√	
2	2.99	pyruvaldehyde		√			√	√	
3	3.21	2-methyl-furan		√		√	√		√
4	3.56	tetrahydro-furan		√		√	√	√	√
5	3.80	2,3-dihydro-furan					√	√	
6	3.89	2-methyl-1,3-dioxolane		√		√	√	√	√
7	4.27	benzene		√	√	√	√	√	√
8	4.38	3-methyl-3-buten-2-one		√		√	√	√	√
9	5.12	propanoic acid					√	√	
10	5.56	2,5-dimethyl-furan		√		√	√	√	√
11	6.15	2,3-dimethyl-1-butene					√	√	
12	6.58	2-ethyl-1,3-dioxolane					√	√	

Table 4.21 continued

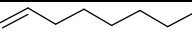
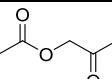
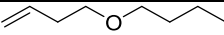
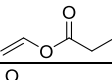
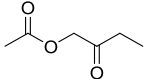
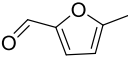
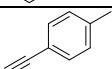
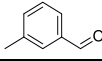
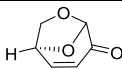
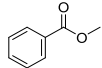
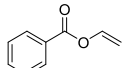
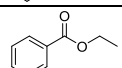
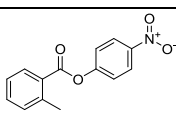
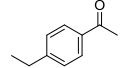
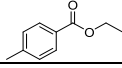
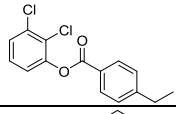
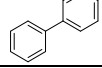
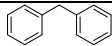
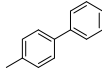
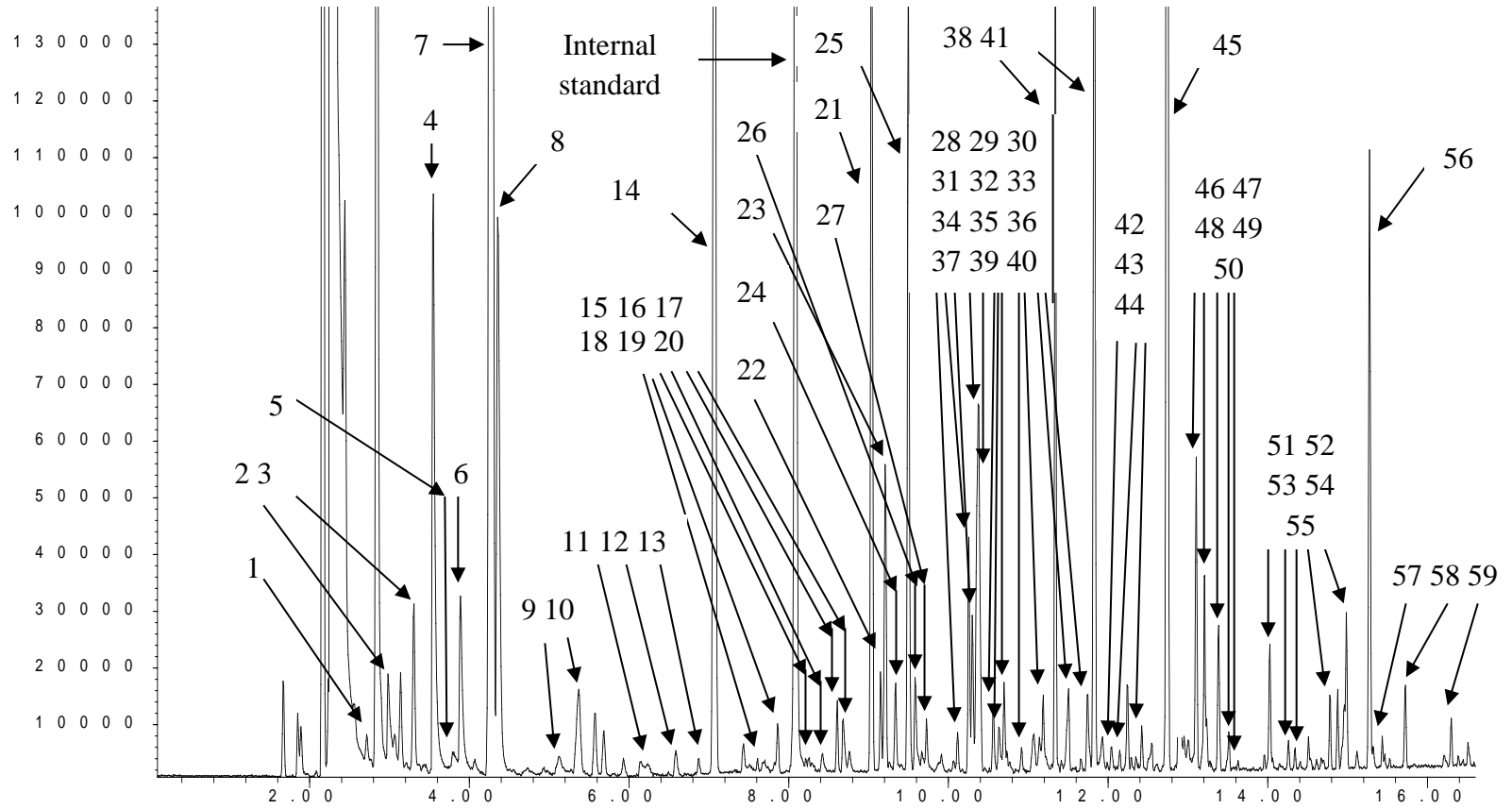
13	6.87	1-cyclobutyl-ethanone		√			√	√	
14	7.06	toluene		√		√	√	√	√
15	7.70	3-furfural					√	√	
16	7.85	1-octene					√	√	
17	8.16	1-furfural		√			√	√	√
18	8.42	3-methyl-3-penten-2-one					√	√	
19	8.69	1-(acetyloxy)-2-propanone		√			√	√	
20	8.77	1,3-dioxolane					√	√	
21	9.04	ethyl-benzene		√		√	√	√	√
22	9.16	2-propenoic acid, methyl ester		√		√	√	√	
23	9.20	<i>p</i> -xylene		√		√	√	√	√
24	9.35	4-butoxy-1-butene		√			√	√	
25	9.50	styrene		√			√	√	
26	9.60	1-(2-furanyl)-ethanone		√			√	√	
27	9.73	1-nonene					√		
28	10.12	1-methylethyl-benzene					√	√	
29	10.25	propanoic acid, ethenyl ester		√			√	√	√
30	10.30	1-(acetyloxy)-2-butanone		√			√	√	√
31	10.36	5-methyl-2-furancarboxaldehyde		√			√	√	
32	10.37	benzaldehyde					√	√	√
33	10.56	propyl-benzene					√	√	
34	10.64	benzonitrile					√	√	
35	10.71	1-ethyl-2-methyl-benzene					√	√	
36	10.91	α -methyl-styrene					√	√	
37	11.07	benzofuran					√	√	
38	10.20	1-decene					√	√	
39	11.50	1-propenyl-benzene					√	√	
40	11.75	1-ethynyl-4 methyl benzene					√	√	

Table 4.21 continued

41	11.83	acetophenone		√		√	√	√	√
42	12.03	3-methyl-benzaldehyde					√	√	
43	12.15	levoglucosenone		√			√	√	
44	12.24	benzoic acid, methyl ester		√			√	√	
45	12.73	benzoic acid, ethenyl ester					√	√	
46	13.10	benzoic acid, ethyl ester					√	√	√
47	13.23	1-(4-methylphenyl)-ethanone					√	√	
48	13.40	naphthalene					√	√	
49	13.51	1-tridecene					√		
50	13.64	tridecane					√		
51	14.02	<i>o</i> -toluic acid, 4-nitrophenyl ester					√	√	
52	14.26	1-(4-ethylphenyl)-ethanone					√	√	
53	14.34	<i>p</i> -toluic acid, ethyl ester					√	√	
54	14.51	1-tetradecene					√	√	
55	15.00	4-ethylbenzoic acid, 2,3-dichlorophenyl ester					√	√	
56	15.27	biphenyl					√	√	
57	15.43	1-pentadecene		√			√	√	
58	15.72	diphenylmethane					√	√	
59	16.21	4-methyl-1,1'-biphenyl					√	√	

Abundance



Time -->

Figure 4.40: A representative TIC of 64% polyester + 33% rayon + 3% elastin (N) (set 4)

The samples exhibited a mixture of burning properties as half of the samples ignited whereas the other half did not (Figure 4.28). Sets 2, 3 and 5 auto-ignited, reaching maximum temperatures between 598-636 °C, while maximum temperatures between 243-308 °C were attained for sets 1, 4 and 6. Polyesters are known to be quite resistant to heat, melting around 200-260 °C to form beads [98, 102] and igniting with difficulty at temperature ranges of 450-530 °C [103, 104]. The initial auto-ignition of textiles (N) in sets 2, 3 and 5 could have potentially been due to the rayon (purified cellulose) content of the textile rather than the polyester (cf. Table 4.11 in which 100% polyester (M) did not ignite across the six sets), as rayon is essentially cellulose and readily burns at lower temperatures [22]. Once ignited, the heat generated from the flames could have raised the temperature of the fibre high enough to induce the ignition of polyester.

Although low molecular weight aliphatic hydrocarbons (C₁-C₄) have been reported previously from the pyrolysis of polyester [115], this work identified the presence of high molecular weight *n*-alkanes and *n*-alkenes. These are attributed to be by-products of rayon pyrolysis. With a melting point of 150 °C [146], rayon undergoes thermal decomposition that follows the breakdown of cellulose to generate a variety of *n*-alkanes and *n*-alkenes, as seen in the pyrolysis of cellulosic fibres in textiles (B) and (D). These high molecular weight *n*-alkanes and *n*-alkenes together with 23 other pyrolysis products detected in textile (N) were also present from the pyrolysis of 100% nylon (G) (Appendix 3.0). These similarities are believed to be due to the chemical nature of these textiles; both are synthetic fibres commonly made from petroleum based products and share a range of similar pyrolysis products upon heat decomposition [118]. However, 100% nylon (G) can be distinguished from 64% polyester + 33% rayon + 3% elastin (N) through the range of additional nitriles and its derivatives in its pyrolytic profile. With similar composition and proportions, it is not surprising that a similar range of pyrolysis products to textiles (N) (with the exception of *n*-alkanes and *n*-alkenes) were also observed from the pyrolysis of 64% polyester + 32% viscose + 4% elastin (P) (Appendix 7.0), with the additional presence of terephthalic acid, 2-chlorophenyl ethyl ester; reported in textiles (P).

4.7.3.10 50% Polyester + 50% Viscose (O)

The pyrolysis of textile O (50% polyester + 50% viscose) generated less than half of the pyrolysis products detected in textile (N). Textile (O) generated furans, ketones, aromatics, acid esters, *n*-alkyl-benzenes, *n*-aldehydes, biphenyl, nitrile and dioxolane as detailed in Table 4.22.

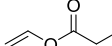
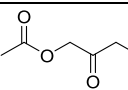
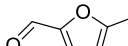
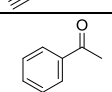
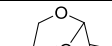
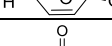
All of these pyrolysis products were present in textile (N), with textile (O) generating the additional presence of 1-(2-furanyl)-ethanone and *o*-xylene; however, no *n*-alkanes, *n*-alkenes or α -methyl-styrene were present in textile (O). The qualitative reproducibility across textile (O) also poor, with only four products present in at least four of the six sets of repeats. A representative TIC (set 6) of textile (O) is represented in Figure 4.41.

Similar to textile (N), textile (O) also exhibited a mixture of results in terms of auto-ignition characteristics: sets 5 and 6 auto-ignited with a maximum temperature of 561 °C and 529 °C, respectively, but the remaining sets did not auto-ignite reaching maximum temperatures of between 244-280 °C (Figure 4.29).

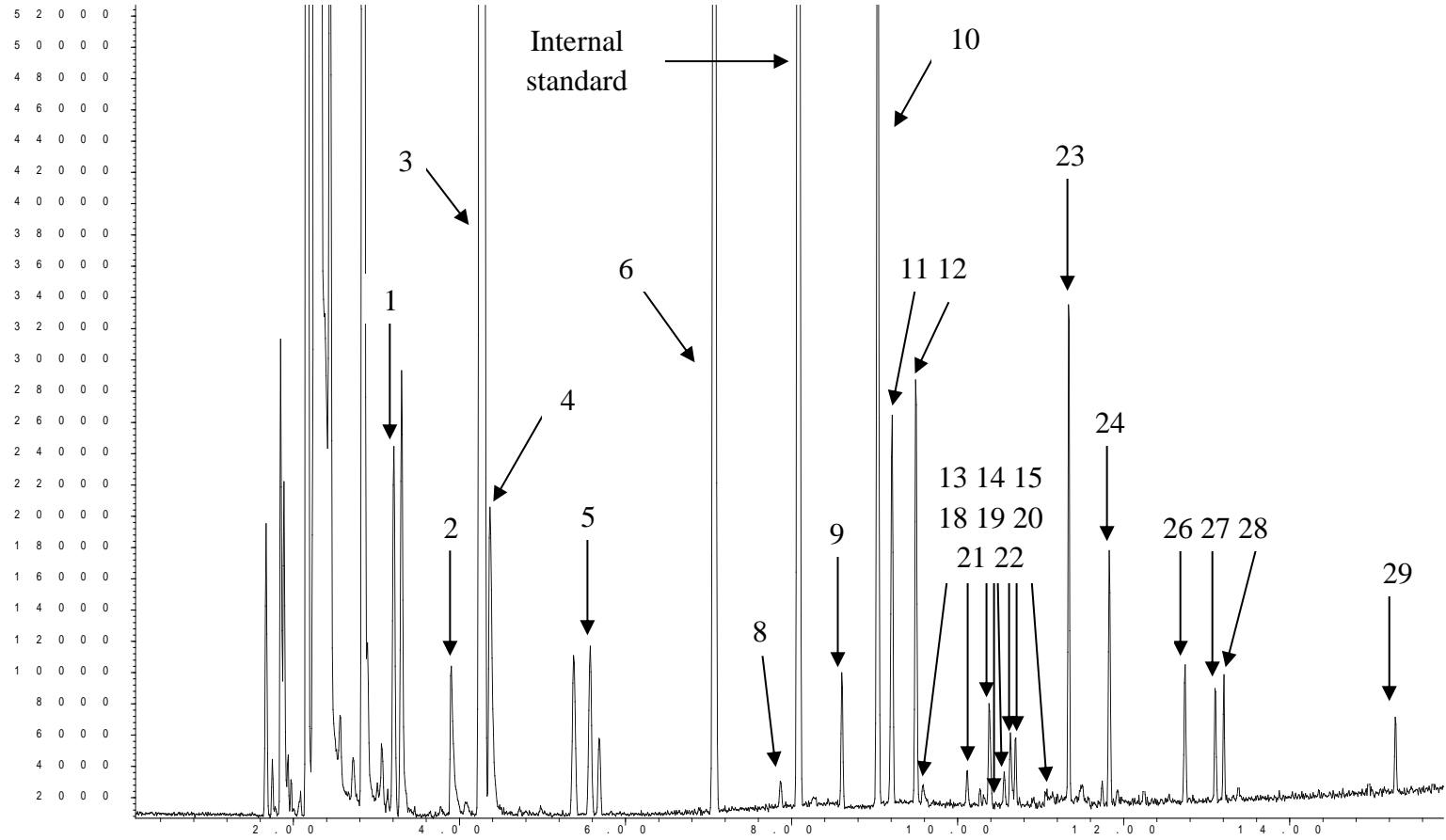
Table 4.22: Pyrolysis products from 50% polyester + 50% viscose (O)

No	Retention Time (min)	Compound	Molecular Structure	Set					
				1	2	3	4	5	6
1	3.21	2-methyl-furan		√		√			√
2	3.89	2-methyl-1,3-dioxolane		√		√			√
3	4.27	benzene		√		√		√	√
4	4.38	3-methyl-3-buten-2-one		√		√			√
5	5.56	2,5-dimethyl-furan		√		√			√
6	7.06	toluene		√		√		√	√
7	7.70	3-furfural		√		√			
8	7.86	1-(2-furanyl)-ethanone							√
9	8.69	1-(acetyloxy)-2-propanone							√

Table 4.22 continued

10	9.04	ethyl-benzene		√		√		√	√
11	9.20	<i>p</i> -xylene				√		√	√
12	9.50	styrene				√		√	√
13	9.60	<i>o</i> -xylene				√			√
14	10.12	1-methylethyl-benzene							√
15	10.25	propanoic acid, ethenyl ester		√		√			√
16	10.30	1-(acetyloxy)-2-butanone		√		√			
17	10.36	5-methyl-2-furancarboxaldehyde		√		√			
18	10.37	benzaldelyde		√		√		√	√
19	10.56	propyl-benzene							√
20	10.64	benzonitrile						√	√
21	10.71	1-ethyl-2-methyl-benzene							√
22	11.07	benzofuran							√
23	11.75	1-ethynyl-4 methyl benzene							√
24	11.83	acetophenone				√		√	√
25	12.15	levoglucosenone				√			
26	12.73	benzoic acid, ethenyl ester						√	√
27	13.10	benzoic acid, ethyl ester						√	√
28	13.40	naphthalene							√
29	15.27	biphenyl						√	√

A b u n d a n c e



T i m e -->

Figure 4.41: A representative TIC of 50% polyester + 50% viscose (O) (set 6)

The pyrolysis of polyester begins with the random scission of the weak C-O ester bonds to generate intermediate products, such as ethylene oxide, which in turn undergoes trans-esterification (substitution of a R ester group to a R' of an alcohol) at higher temperatures to generate acetaldehyde, formaldehyde, 2-methyl-1,3-dioxolane, vinyl and other intermediate products [34, 107, 108, 111]. While acetaldehyde and formaldehyde were not detected in this study, 2-methyl-1,3-dioxolane and vinyl products were detected in both textiles (N) and (O) and was also present from the pyrolysis of 64% polyester + 32% viscose + 4% elastin (P) (Appendix 7.0). However, as 2-methyl-1,3-dioxolane was also present in textiles (D) (50% cotton + 50% modal), (G) (100% nylon) (Appendix 3.0), (J) (100% denim) and (K) (100% viscose) (Appendix 5.0), it is not suitable to be utilised as a characteristic indicator of polyester.

With higher temperatures, typically 300-700 °C [5, 103, 106, 107, 111, 115], random scission of the polymer and breakdown of the strong C-C bonds takes place to form *n*-aldehydes, aromatics, low molecular weight *n*-alkanes and *n*-alkenes, aromatic esters, carboxylic acid and acid esters, furans, ketones, alkyl-benzenes and dioxolanes [34, 85, 103, 109, 110, 113], all of which were detected in this work. These high temperatures could also break other bonds in the molecule and cause inter- and intramolecular transformation to take place, generating complex products such as benzoic acid, ethenyl ester, naphthalene, styrene, toluene, biphenyl, ethylbenzene and phenol [82, 107, 115], all of which were present across both textiles (N) and (O).

Similar to other textiles, the pyrolysis of polyester is a function of temperature and, as such, the production, type and abundance of pyrolysis products generated are directly proportional to the temperature until a maximum production temperature is attained for a particular by-product [108, 115]. For example, Joseph and Tretsiakova-McNall [112], Edge *et al.* [111] and Dzieciol [115] all reported the maximum presence of acetaldehyde at 300 °C, 300 °C and 400 °C, respectively, whereas formaldehyde, methyl-alcohol and dioxane were reported to have a maximum production temperature of 500 °C [115]. Sugimura and Tsuge [185] reported that

biphenyl and benzene, as reported in textiles (N) and (O), were only detected at temperatures above 500 °C, having generated from terephthalic acid, while Kinoshita *et al.* [103] identified the increasing presence of benzoic acid and its derivatives, as seen in textiles (N) and (O), at temperatures of between 450-500 °C. Generally, lower temperatures generate *n*-aldehydes, ether and oxides, whereas higher temperatures facilitate the production of aromatics, aliphatic hydrocarbons, methyl acetates, branched alkenes, ketones, alcohols, acids and acid esters [103, 112, 115]. Besides temperature, the size and type of monomer molecules used to synthesise the resultant polymer also significantly influence the physical and thermal properties of polyester, as these characteristics dictate the fibre's melting point, thermal decomposition temperature, ignition temperature and the type of pyrolysis products generated [105-108].

While the majority of the products generated in textiles (N) and (O) are attributable to the thermal decomposition of the polyester content, the presence of a group of compounds indicates the pyrolysis of cotton / rayon / modal / viscose; these characteristic by-products are furans (2-methyl-furan, 2,5-dimethyl-furan), ketones (3-methyl-3-buten-2-one, 1-(acetyloxy)-2-butanone, 1-(acetyloxy)-2-propanone), acid ester (propanoic acid, ethenyl ester), *n*-aldehydes (5-methyl-2-furancarboxaldehyde, 1-furfural, 3-furfural, methacrylaldehyde, pyruvaldehyde) and levoglucosenone [5, 15, 29, 30, 32]. These volatile products were not only recorded in the pyrolysis of textiles (N) and (O), but also in the pyrolysis of textiles (A) (100% cotton, Table 4.13), (B) (95% cotton, Table 4.14) and (D) (50% cotton + 50% modal, Table 4.15). These products were also detected from the pyrolysis of 100% viscose (K) (Appendix 5.0) and 64% polyester + 32% viscose + 4% elastin (P) (Appendix 7.0), further supporting the contribution of the cellulose based fibre to the pyrolytic profile of textiles (N) and (O). The presence of benzoic acid, ethyl ester; in 100% viscose (K), 64% polyester + 33% rayon + 3% elastin (N) and 50% polyester + 50% viscose (O) indicates that this acid is formed through the decomposition of viscose / rayon rather than polyester.

As the percentage of polyester reduces from 64% in textile (N) to 50% in textile (O), the number of detected pyrolysis products reduced considerably from 59 to 29, generating fewer high molecular weight acid and acid esters, methyl-aromatics and aromatic substituents, together with the absence of *n*-alkanes, *n*-alkenes and α -methyl-styrene in textile (O) as compared to (N). With the reduction in the proportion of polyester and an increase in the presence of cellulosic fibres (rayon / viscose), the pyrolysis profile generated seemed to have been affected, with fewer polyester-based pyrolates in textile (O) as compared to textile (N). Similar to cotton blends in textiles (B) and (D), the blended fibres in textiles (N) and (O) seem to have altered the thermal characteristics of the each contributing fibre; as the proportion of polyester in the blended fibre increases, the dominance of the fibre in influencing the overall thermal properties of the textile and type of pyrolysis products generated also increased greatly and vice versa [18, 19, 109].

4.7.3.11 100% Leather (Q)

The pyrolysis of 100% leather generated a range of products, particularly *n*-alkanes, *n*-alkenes, alkyl- / cyclo- / vinyl- / chloro- / chloroethoxy- / dichloro- *n*-alkanes and *n*-alkenes, aromatics, *n*-alkyl-benzenes, furans, nitriles, ketones, sulfides, alkyl-aldehyde and pyrroles as detailed in Table 4.23.

Out of the 48 pyrolysis products generated, 21 were present in at least four of the six sets of repeats. They were aromatics and *n*-alkyl-benzenes (benzene, toluene, ethylbenzene), chloro-alkanes (1,2-dichloro-propane, 1-(2-chloroethoxy)-butane), nitriles (2-methyl-butanenitrile, 3-methyl-butanenitrile, 4-methyl-pentanenitrile), pyrrole (1-ethyl-1H-pyrrole), sulfides (dimethyl disulfide, dimethyl trisulfide), vinyl-cycloalkane (ethenyl-cyclobutane), *n*-alkane (tetradecane) and *n*-alkenes (1-octene, decene, undecene, dodecene, tridecene, tetradecene, pentadecene, 8-hexadecene). The majority of the pyrolysis products detected from 100% leather (Q) were also present from the pyrolysis of porcine bones (Table 2.3 and Appendix 1.0) and the human toe samples (Table 3.14).

All of the six sets of repeats of leather auto-ignited, attaining high maximum temperatures between 490-684 °C (Figure 4.31). From the six sets, set 4 was the only set that did not produce any detectable pyrolysis products. A representative TIC (set 6) of textile (Q) is represented in Figure 4.42.

Table 4.23: Pyrolysis products from 100% leather (Q)

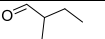
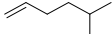
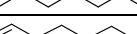
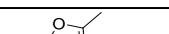
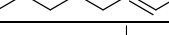
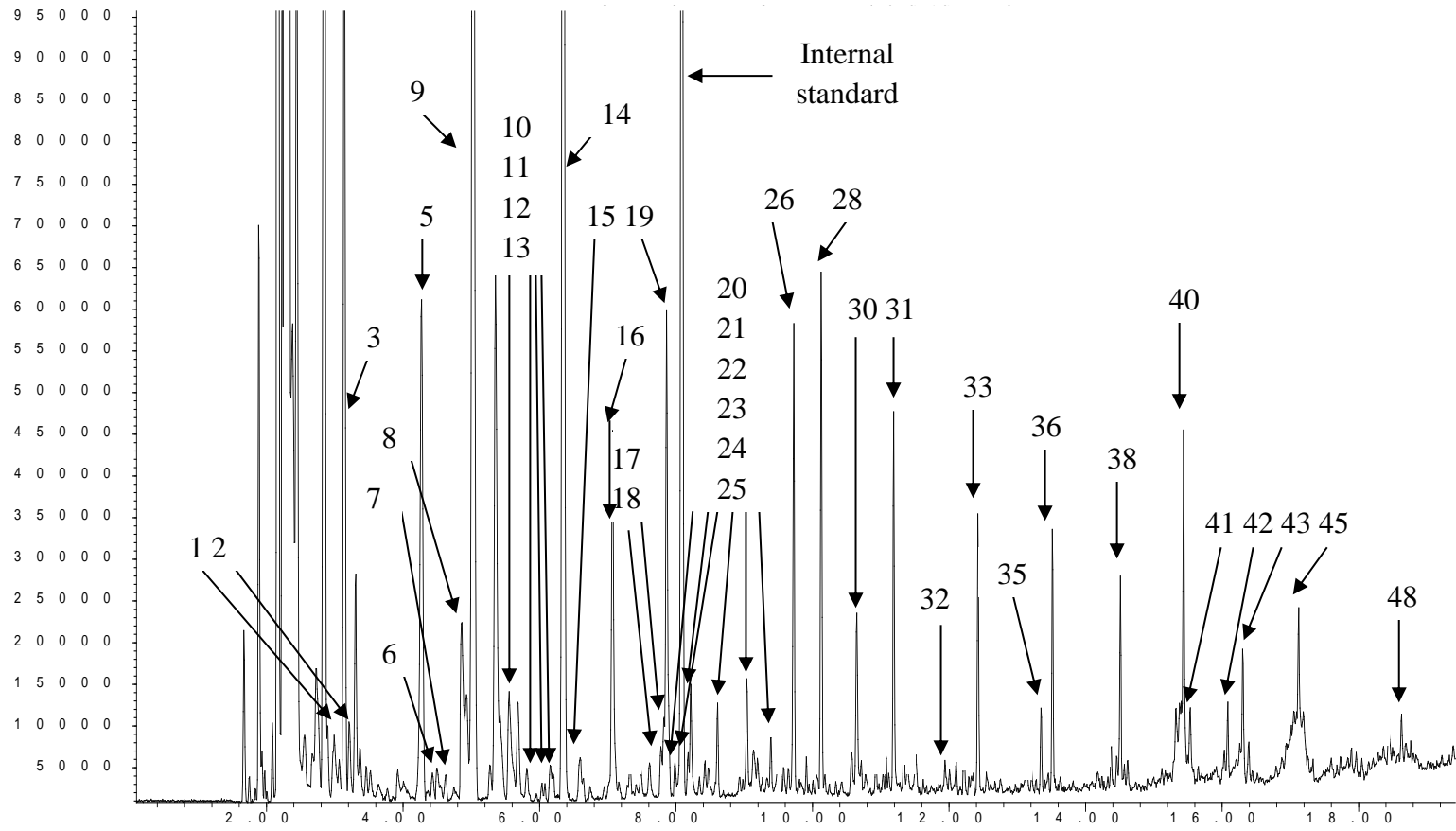
No	Retention Time (min)	Compound	Molecular Structure	Set						
				1	2	3	4	5	6	
1	3.00	2-ethyl-butanal								√
2	3.14	1-hexene			√	√				√
3	3.21	2-methyl-furan								√
4	3.48	3-methyl-cyclopentene			√					
5	4.27	benzene		√	√	√			√	√
6	4.43	5-methyl-1-hexene		√						√
7	4.50	tetrahydro-2-methyl-furan		√						√
8	4.90	ethenyl-cyclobutane		√	√	√				√
9	5.03	1,2-dichloro-propane		√	√	√				√
10	5.59	2-methyl-butanenitrile		√	√				√	√
11	5.74	3-methyl-butanenitrile		√	√				√	√
12	6.08	1-methyl-cyclohexane								√
13	6.16	3-ethenyl-cyclohexanone								√
14	6.36	dimethyl disulfide		√	√	√				√
15	6.60	methylene-cyclohexane								√
16	7.06	toluene		√	√	√			√	√
17	7.82	2-methylene-heptane			√	√				√
18	7.86	1-octene		√	√	√				√
19	7.98	2-ethyl-5-methyl-tetrahydro-furan								√
20	8.00	1-ethyl-1H-pyrrole		√	√	√				√
21	8.17	2-octene								√
22	8.22	4-methyl-pentanenitrile		√	√				√	√
23	8.48	(1-methylethyl)-cyclopentane								√
24	9.04	ethyl-benzene		√	√	√			√	√
25	9.20	<i>p</i> -xylene			√					√
26	9.72	1-nonene			√	√				√

Table 4.23 continued

27	9.90	nonane			√				
28	10.13	1-(2-chloroethoxy)-butane		√	√	√		√	√
29	10.34	3-methyl-1H-pyrrole			√				
30	10.64	dimethyl trisulfide		√	√	√			√
31	11.18	1-decene			√	√		√	√
32	11.95	butyl-benzene							√
33	12.42	1-undecene		√	√	√			√
34	12.55	undecane			√	√			
35	13.35	2-decanone							√
36	13.52	1-dodecene		√	√	√		√	√
37	13.63	dodecane			√				
38	14.51	1-tridecene		√	√	√		√	√
39	14.61	tridecane		√	√			√	
40	15.43	1-tetradecene		√	√	√		√	√
41	15.53	tetradecane		√	√			√	√
42	16.08	1-chloro-undecane		√					√
43	16.30	1-pentadecene		√	√	√		√	√
44	16.40	pentadecane		√	√			√	
45	17.12	8-hexadecene		√	√	√		√	√
46	17.24	1-hexadecene						√	
47	17.32	hexadecane						√	
48	18.62	1-heptadecene			√			√	√

Abundance



Time -->

Figure 4.42: A representative TIC of 100% leather (Q) (set 6)

Leather is essentially a polymerised chain of polypeptides that has undergone chemical and mechanical processes to provide its distinguishable properties [18, 74, 75]. When subjected to heat, leather decomposes to form carbonaceous residues, oils and gases [79, 81] and has been documented to auto-ignite and burn easily [77] at low temperatures of 200-250 °C [76, 186]. This is corroborated in the current study, as the onset of pyrolysis was reported to be at similar temperature ranges between 170-217 °C (Figure 4.31). Its high flammability is a result of the high volatile matter content in leather, facilitating rapid combustion [77].

The pyrolysis of leather can be categorised into two distinctive temperature dependent stages (primary and secondary), which generate a range of gases and volatiles [80, 81] such as ammonia, carbon dioxide, hydrogen cyanide, sulfur dioxide, aromatics, aliphatic and branched hydrocarbons, carboxylic acids, *n*-aldehydes, amines, nitrogenous compound (naphthalene, pyrrole), alcohols, nitriles and cyanic compounds [72, 79-82, 186-188]. While most of the organic compounds were detected, no cyanic compounds, alcohols, carboxylic acids or amines were detected in this work, although they are expected as the polypeptide chain is essentially a network of amino acids. When heated, the process of decarboxylation causes the protein to form a range of acids, amines, phenols and dioxan [187].

Out of the 48 products generated in this study, 20 of which were *n*-alkanes and *n*-alkenes with some of the remaining being hydrocarbon substitutes. Their presence has been reported previously in the literature, contributing up to 2% of the volatiles detected [188], depending on the temperature to which leather was subjected [79, 186, 188]. Heavy molecular weight hydrocarbons, as detected in this work, are formed through extended burning durations at elevated temperatures, as these factors facilitate volatilisation of the heavy hydrocarbons [166].

Since leather is formed from the skin of animals, it fundamentally contains high levels of water and protein with some lipids and minerals [77]. The protein make-up comprises of various amino acids that have been polymerised through condensation to form peptide bonds (-CO-NH-). As these bonds are present at every pair of amino

acids, the level of nitrogen in the polypeptide chain is very high, and when temperatures are high enough to break down the C-N bonds and any ring structure containing nitrogen in the polypeptide chain, nitrogenous compounds, such as nitriles and pyrroles, are formed, as detected in this work [72, 77, 79, 187]. Both of these products (nitriles and pyrroles) were also reported in the work of Font *et al.* [81]. Similar to hydrocarbons and nitriles, dimethyl disulfide and dimethyl trisulfide, that were detected in textiles (Q), are to be expected as leather contains sulfur and, when heated, the weak disulfide bonds within the polypeptide chain cleave to generate various forms of sulfur-based gases [77, 79], as seen in wool (4.7.3.8) [55, 58]. Besides generating from sulfur molecules within the polypeptide chain, sulfur gases such as sulfur dioxide have been reported to generate from decomposition of chromium sulfate, a chemical used in the chromium tanning process of leather [81]. The presence of chloro-based compounds (1-chloro-undecane, 1-(2-chloroethoxy)-butane, 1,2-dichloro-propane) in this work is also highlighted.

Besides temperature and heating duration, the raw material and the type of tanning process that it is subjected to can also significantly affect the burning properties, yield and type of pyrolysis product generated from leather [79, 186, 189, 190]. This is because different types of raw material and processes applied to leather generate a range of end products containing different levels of moisture, carbon, hydrogen, oxygen, nitrogen, sulfur and inorganic content, together with chemicals used in the tanning process [72, 79, 81, 186]. An example of this is illustrated in the works of Yilmaz *et al.* [79] and Font *et al.* [81] who identified that chromium tanned leather yielded more gaseous products, particularly sulfur dioxide, with increasing temperatures, whereas vegetable tanned leather did not.

In addition to pure leather, another group of important leather is artificial leather; leather plasticised with PVC or coated with PU [83, 84]. This type of leather is more susceptible to flames and can generate a variety of products, similar to pure leather but with the addition of chlorinated compounds, chlorinated aliphatic hydrocarbons, amines, aromatic amines, isocyanates, amino isocyanates and dienes, again

depending on the temperature and burning duration to which it is subjected [85-87, 92, 93, 173].

4.8 Conclusions

This work highlights the variation in the burning properties and type of pyrolysis products generated over a range of textiles: natural, semi synthetic and synthetic. These variations were not only demonstrated with textiles from different sources (i.e. animal, plant and manufactured) but also within the same group and within the same type of textile. Some of the textiles did not experience any auto-ignition while others did and, more interestingly, some textiles exhibited different burning behaviour within the same textile type. These factors should be taken into consideration when dealing with the identification of textile samples in fire scenes, as it has been shown that major identifying peaks of certain textiles are not always present as pyrolysis products.

This work has also established that each textile type can generate a specific group of compound(s) or product(s) which, when present together, are indicative of a particular type of textile. It should be noted, however, that the presence or absence of these characteristic products is largely dependent on temperature and burning duration. For cotton-based textiles, including rayon, modal, viscose and denim, these pyrolysis products include levoglucosenone, 2-methyl-furan, 2,5-dimethyl-furan, 2-ethyl-5-methyl-furan, 3-methyl-3-buten-2-one, 1-(acetyloxy)-2-propanone, 1-(acetyloxy)-2-butanone, 2-furancarboxylic acid, heptyl ester; 1-furfural, 5-methyl-2-furancarboxaldehyde, 2-furanmethanol, acetate; / acetic acid, furfuryl ester; 2-furanmethanol, 2-formate; / formic acid, furfuryl ester; 2-furanmethanol, tetrahydro-; propanoic acid, ethenyl ester; and pyranose sugars when present together. For acrylic fibres, the indicative pyrolysis products include a range of nitriles, dinitriles, methyl- / alkyl- nitriles, pyridines, pyrazine, piperidine, acrylate, cyanic and isocyanic compounds present together, whereas for nylon 6 they are caprolactam, lactam and caprolactone-based compounds, together with *n*-butyl ether and dibutyl ether. When present together, phenol, 4-methyl-phenol and α -amino acids are indicators of wool,

whereas α -methyl-styrene, phenyl and biphenyl products together with naphthalene and benzoic acid derivatives such as benzoic acid, ethenyl ester;, 4-ethylbenzoic acid, 2,3-dichlorophenyl ester; are positive identifiers of polyesters when present together. For leather utilised in this work, 1,2-dichloro-propane, 1-(2-chloroethoxy)-butane, dimethyl disulfide, dimethyl trisulfide, and high molecular weight *n*-alkenes are its major identifying peaks, and can be used to distinguish leather utilised in this work from human pyrolytic data. However as the source of the leather is not known, it is impossible to distinguish if the key indicators of leather identified in this work can be used for a range of different types of leather particularly if it's of different origins (raw material).

The influence of one or more blended fibres in a textile is also highlighted in this work. The presence of the blended fibre does not only influence the major fibre's physical characteristics, but also its chemical, thermal and pyrolytic properties. As the proportion of the blended fibre increases, its dominance over the other major fibre(s) becomes more apparent and has been shown to alter the widely known pyrolytic profile of the major fibre. However, the pyrolytic profiles of the individual fibres in the blend are still present, with the additional presence of products generated from the inter-molecular reactions between the pyrolysis mechanisms of the blended fibres.

4.9 References

1. Laitala, K., *Fire Hazards of Clothing Related to Accidents and Consumer Habits* 2004, Statens Institutt For Forbruksforskning (SIFO): Oslo, Norway.
2. Network, D.H.S., *Clothing Flammability Accidents Study*, in ODPM Final Research Report : BD2546 Sprinkler Effectiveness in Care Homes, ed. M. Shipp and P. Clark. 2006, Building Research Establishment Ltd (BRE): London, UK. p. 25.
3. International Textbook Company. *Classification of Textile Fibres: Wool*. [Online] [January 2014, December 2014]. Available from: <https://www.cs.arizona.edu/patterns/weaving/monographs/ics469.pdf>.
4. International Year of Natural Fibres, *Cotton Fibres*. [Online] [May 2009, August 2014]. Available from: <http://www.naturalfibres2009.org/en/fibres/cotton.html>.
5. CDS Analytical Inc., *Pyrolysis-GC/MS of Clothing Fibres-Cotton and Poly(Ethylene Terephthalate)*, in Applications Information Using Advanced Sample Handling Technology. 2014, CDS Analytical Inc: Oxford, PA.
6. Wakelyn, P.J., Bertoniere, N.R., French, A.D., Thibodeaux, D.P., Triplett, B.A., Rousselle, M-A., Goynes Jr, W.R., Edwards, J.V., Hunter, L., and Mcalister, D.D., *Chemical Properties of Cotton*, in Cotton Fiber Chemistry and Technology. 2010, New York, USA: CRC Press.
7. Matthews, M.J., *Chemical Properties of Cotton Fiber*. 5th Edition. Matthews' Textile Fibers, ed. H.P. Mauersberger. 1931, New York, USA: Wiley Interscience. p. 266-304.
8. Hedge, R.R., Atul Dahiya, M., and Kamath, M.G., *Materials Science and Engineering 554: Cotton Fibres*, in Nonwoven Science and Technology II, ed. L.C. Wadsworth, 2004.
9. Natural Fibres: *Cotton*. [Online] [April 2013, August 2014]. Available from: <http://www.globalnaturalfibres.org/cotton>.
10. Cotton Incorporated, *Cotton Morphology and Chemistry*. [Online] [January 2014, December 2014]. Available from: <http://www.cottoninc.com/product/NonWovens/Nonwoven-Technical-Guide/CottonMorphology-AndChemistry>.

11. Newling, B. and Batchelor, S.N., *Pulsed Field Gradient NMR Study of the Diffusion of H₂O and Polyethylene Glycol Polymers in the Supramolecular Structure of Wet Cotton*. The Journal of Physical Chemistry B, 2003. **107**(45): p. 12391-12397.
12. Han, J.S. and Rowell, J.S., *Chapter 5: Chemical Composition of Fibers*, in Paper and Composites from Agro Based Resources, ed. R.M. Rowell and R.A. Young. 1997, CRC Press: Madison, WI. p. 83-134.
13. Ciolacu, D., Ciolacu, F., and Popa, V.I., *Amorphous Cellulose—Structure and Characterization*. Cellulose Chemistry and Technology, 2011. **45**(1): p. 13.
14. Brushwood, D.E. and Perkins Jr, H.H. *Characterization of Sugars from Honeydew Contaminated and Normal Cottons*, in Beltwide Cotton Conferences 1994. Memphis, TN: National Conference Council.
15. Price, D., Horrocks, A.R., Akalin, M., and Farooq, A.A., *Influence of Flame Retardants on the Mechanism of Pyrolysis of Cotton (Cellulose) Fabrics in Air*. Journal of Analytical and Applied Pyrolysis, 1997. **40**: p. 511-524.
16. Tsafack, M.J. and Levalois-Grützmacher, J., *Flame Retardancy of Cotton Textiles by Plasma-Induced Graft-Polymerization (PIGP)*. Surface and Coatings Technology, 2006. **201**(6): p. 2599-2610.
17. Yang, C.Q., *Flame Resistant Cotton*, in Handbook of Fire Resistant Textiles, ed. F.S. Kilinc,. 2013, The Textile Institute: Woodhead Publishing: Cambridge, UK. p. 177-215.
18. Cardamone, J., *Fire Resistant Wool and Wool Blends*, in Handbook of Fire Resistant Textiles, ed. F.S. Kilinc,. 2013, The Textile Institute: Woodhead Publishing: Cambridge, UK.
19. Horrocks, A.R., Tunc, M., and Price, D., *Burning Behaviour of Textiles and Its Assessment by Oxygen-Index Methods*. 1st-3rd Edition. Vol. **18**. 1989: Textile Institute.
20. Abidi, N., Hequet, E., Cabrales, L., Gannaway, J., Wilkins, T., and Wells, L.W., *Evaluating Cell Wall Structure and Composition of Developing Cotton Fibers Using Fourier Transform Infrared Spectroscopy and Thermogravimetric Analysis*. Journal of Applied Polymer Science, 2008. **107**(1): p. 476-486.

21. Chatterjee, P.K. and Conrad, C.M., *Kinetics of the Pyrolysis of Cotton Cellulose*. Textile Research Journal, 1966. **36**(6): p. 487-494.
22. Horrocks, A.R., *Flame-Retardant Finishing of Textiles*. Coloration Technology, 1986. **16**(1): p. 62-101.
23. Horrocks, A.R., *Flame Retardant Finishes and Finishing*, in Textile Finishing, ed. D. Heywood,. Vol. **2**. 2003, West Yorkshire, UK: Soceity of Dyers and Colourist: Colourist Technology. 62-101.
24. Guan, J., Yang, C.Q., and Chen, G., *Formaldehyde-Free Flame Retardant Finishing of Silk Using a Hydroxyl-Functional Organophosphorus Oligomer*. Polymer Degradation and Stability, 2009. **94**(3): p. 450-455.
25. Kawamoto, H., Murayama, M., and Saka, S., *Pyrolysis Behavior of Levoglucosan as an Intermediate in Cellulose Pyrolysis: Polymerization into Polysaccharide as a Key Reaction to Carbonized Product Formation*. Journal of Wood Science, 2003. **49**(5): p. 469-473.
26. Madorsky, S.L., Hart, V.E., and Straus, S., *Thermal Degradation of Cellulosic Materials*. Journal of Research of the National Bureau of Standards, 1958. **60**(4): p. 343-349.
27. Shen, D.K. and Gu, S., *The Mechanism for Thermal Decomposition of Cellulose and Its Main Products*. Bioresource Technology, 2009. **100**(24): p. 6496-6504.
28. Li, S., Lyons-Hart, J., Banyasz, J., and Shafer, K., *Real-Time Evolved Gas Analysis by FTIR Method: An Experimental Study of Cellulose Pyrolysis*. Fuel, 2001. **80**(12): p. 1809-1817.
29. Nakanishi, S., Masuko, F., Hori, K., and Hashimoto, T., *Pyrolytic Gas Generation of Cotton Cellulose With and Without Flame Retardants at Different Stages of Thermal Degradation: Effects of Nitrogen, Phosphorus, and Halogens*. Textile Research Journal, 2000. **70**(7): p. 574-583.
30. Zhu, P., Sui, S., Wang, B., Sun, K., and Sun, G., *A Study of Pyrolysis and Pyrolysis Products of Flame-Retardant Cotton Fabrics by DSC, TGA, and PY-GC-MS*. Journal of Analytical and Applied Pyrolysis, 2004. **71**(2): p. 645-655.

31. Keheyan, Y., *PY/GC/MS Analyses of Historical Papers*. BioResources, 2008. **3**(3): p. 829-837.
32. Hiramatsu, K., *The Study of Pyrolytic Products of Polymer Materials by Mass-Spectroscopy the Mass-Spectroscopy of Pyrolytic Products of Wood Components*. Journal of the Mass Spectrometry Society of Japan, 1966. **14**(4): p. 215-224.
33. Hardin, I.R. and Wang, X.Q., *The Use of Pyrolysis-Gas Chromatography in Textiles as an Identification Method*, in *Modern Textile: Investigation of Textiles by Analytical Pyrolysis*, ed. M. Raheel. 1989, New York, USA: Marcel Dekker. p. 175-263.
34. Raheel, M., *Modern Textile Characterization Methods*. Vol. **13**. 1996, New York, USA: CRC Press.
35. Faroq, A.A., Price, D., Milnes, G.J., and Horrocks, A.R., *Use of Gas Chromatographic Analysis of Volatile Products to Investigate the Mechanisms Underlying the Influence of Flame Retardants on the Pyrolysis of Cellulose in Air*. *Polymer Degradation and Stability*, 1991. **33**(2): p. 155-170.
36. Ramos, M.E., González, J.D., Bonelli, P.R., and Cukierman, A.L., *Effect of Process Conditions on Physicochemical and Electrical Characteristics of Denim-Based Activated Carbon Cloths*. *Industrial and Engineering Chemistry Research*, 2007. **46**(4): p. 1167-1173.
37. Perkin, W.H., *Chemistry of Blue Jeans: Indigo Synthesis and Dyeing*. 2014.
38. Textile School, *Denim Fabrics*. [Online] [January 2014, August 2014]. Available from: <http://www.textileschool.com/articles/355/denim-fabrics>.
39. Tahir, P.M., Ahmed, A.B., Syeed, O.A., Azry, S., and Ahmed, Z., *Retting Process of Some Bass Plant Fibres*. *Bioresources*, 2011. **6**(4): p. 5260-5281.
40. Akin, D.E., *Flax Fiber*. *Kirk-Othmer Encyclopedia of Chemical Technology*. Vol. **11**. 2003, Athens, USA: John Wiley and Sons.
41. Akin, D.E., *Standards for Flax Fiber*. Trade Journal Publication in American Society for Testing and Materials (ASTM) International, 2005: p. 22-25.

42. Akin, D.E., *Chemistry of Plant Fibre*, in *Industrial Applications of Natural Fibres: Structure, Properties and Technical Applications*, ed. C. Stevens and J. Müssig. Vol. **10**. 2010, Athens, USA: John Wiley and Sons.
43. Akin, D.E., *Linen Most Useful: Perspectives on Structure, Chemistry, and Enzymes for Retting Flax*. Hindawi Publishing Corporation: ISRN Biotechnology, 2012. **2013**: p. 23.
44. Anandjiwala, R.D., Hunter, L., Kozlowski, R., and Zaikov, G., *Textiles for Sustainable Development*. 2007, New York, USA: Nova Science Publishers.
45. Kymäläinen, H-R. and Sjöberg, A.M., *Flax and Hemp Fibres as Raw Materials for Thermal Insulations*. *Building and Environment*, 2008. **43**(7): p. 1261-1269.
46. Buchert, J., Pere, J., Johansson, L-S., and Campbell, J.M., *Analysis of the Surface Chemistry of Linen and Cotton Fabrics*. *Textile Research Journal*, 2001. **71**(7): p. 626-629.
47. Akin, D.E., Morrison, W.H., Gamble, G.R., Rigsby, L.L., Henriksson, G., and Eriksson, K-E.L., *Effect of Retting Enzymes on the Structure and Composition of Flax Cell Walls*. *Textile Research Journal*, 1997. **67**(4): p. 279-287.
48. Focher, B., Marzetti, A., and Sharma, H.S.S., *Changes in the Structure and Properties of Flax Fibre During Processing*. *The Biology and Processing of Flax*, 1992: p. 329-342.
49. Bhat, G., Kamath, M.G., and Parikh, D.V., *Biodegradable/Compostable Composites from Lignocellulostic Fibres*, in *Textiles for Sustainable Development*, ed. R.D. Anandjiwala, L. Hunter, R. Kozlowski, and G. Zaikov. 2007, New York, USA: Nova Publishers.
50. CDS Analytical Inc., *Pyrolysis GC/MS of Plant Derived (Cellulostic) Textiles*. 2014, CDS Analytical Inc: Oxford, PA.
51. Perlstein, P., *Identification of Fibres and Fibre Blends by Pyrolysis Gas Chromatography*. *Analytica Chimica Acta*, 1983. **155**: p. 173-181.
52. Tian, C.M., Li, Z., Guo, H.Z., and Xu, J.Z., *Study on the Thermal Degradation of Flame Retardant Wools*. *Journal of Fire Sciences*, 2003. **21**(2): p. 155-162.

53. International Wool Textile Organisation (IWTO), *Wool, the Natural Fibre*. [Online] [January 2014, August 2014]. Available from: <http://www.iwto.org/wool/the-natural-fibre/>.
54. Livestock Production Management, *Physical and Chemical Properties of Wool*. [Online] [January 2014, August 2014]. Available from: <https://sites.google.com/site/viveklpm/wool/physical-and-chemical-properties-of-wool>.
55. Wilkie, C.A. and Morgan, A.B., *Fire Retardancy of Polymeric Materials*. 2nd Edition. 2012, Boca Raton, Florida: CRC Press: Taylor and Francis Grp.
56. Palenik, S.J., *Microscopical Examination of Fibres*, in *Forensic Examination of Fibres*, ed. J.R. Robertson, C. Roux, and K. Wiggins. 2002, CRC Press: London, UK.
57. Kozlowski, R., *Handbook of Natural Fibres: Types, Properties and Factors Affecting Breeding and Cultivation*, ed. R. Kozlowski. Vol. 1. 2012, USA: Elsevier.
58. Benisek, L., *Flame Retardance of Protein Fibers*, in *Flame-Retardant Polymeric Materials*, ed. M. Lewin, S.M. Atlas, and E.M. Pearce. 1975, Springer: Waldshut-Tiengen, Germany. p. 137-191.
59. Price, D. and Horrocks, A.R., *Combustion Processes of Textile Fibres*, in *Handbook of Fire Resistant Textiles*, ed. F.S. Kilinc. 2013, The Textile Institute: Woodhead Publishing: Cambridge, UK.
60. Mckinnon, J., *Some Chemistry of the Wool Industry Scouring and Yarn Production* 2014, Wool Research Organization of New Zealand: New Zealand.
61. Horrocks, A.R. and Davies, P.J., *Char Formation in Flame-Retarded Wool Fibres. Part 1. Effect of Intumescent on Thermogravimetric Behaviour*. *Fire and Materials*, 2000. **24**(3): p. 151-157.
62. Ingham, P.E., *The Pyrolysis of Wool and the Action of Flame Retardants*. *Journal of Applied Polymer Science*, 1971. **15**(12): p. 3025-3041.
63. Forouharshad, M., Montazer, M., Moghadam, M.B., and Saligheh, O., *Flame Retardancy of Wool Fabric with Zirconium Oxychloride Optimized by Central Composite Design*. *Journal of Fire Sciences*, 2010.

64. Takekoshi, Y., Sato, K., Kanno, S., Kawase, S., Kiho, T., and Ukai, S., *Analysis of Wool Fiber by Alkali-Catalyzed Pyrolysis Gas Chromatography*. Forensic Science International, 1997. **87**(2): p. 85-97.
65. CDS Analytical Inc., *Pyrolysis GC of Natural Fibres*, in Applications Information Using Advanced Sample Handling Technology. 2014, CDS Analytical Inc: Oxford, PA.
66. Danielson, N.D. and Rogers, L.B., *Determination of Tryptophan in Proteins by Pyrolysis Gas Chromatography*. Journal of Analytical Chemistry, 1978. **50**(12): p. 1680-1683.
67. Marmer, W.N. and Magidman, P., *Pyrolysis Gas Chromatography of Wool Part III: Detection and Quantitation of Tyrosine*. Textile Research Journal, 1990. **60**(7): p. 417-420.
68. Lewin, M., *Handbook of Fiber Chemistry*, ed. M. Lewin. 2010: CRC Press.
69. Reddy, R.M., *Innovative and Multidirectional Applications of Natural Fibre, Silk-A Review*. Academic Journal of Entomology, 2009. **2**(2): p. 71-75.
70. Babu, K.M., *Silk: Processing, Properties and Applications*. 2013, Cambridge, UK: The Textile Institute: Woodhead Publishing Limited.
71. Muralidhara, K.S. and Sreenivasan, S., *Thermal Degradation and Burning Behavior of Cellulose Based and Cellulose-Silk Blended Upholstery Fabric*. Journal of Scientific and Industrial Research, 2010. **69**: p. 879.
72. Muralidhara, H.S., Maggin, B., and Phipps Jr, H., *Conversion of Tannery Waste to Useful Products*. Resources and Conservation, 1982. **8**(1): p. 43-59.
73. Scottish Leather Group Company, *Understanding Leather*. 2014, Scottish Leather Group Company: Andrew Muirhead and Son Limited: Scotland, UK.
74. Erdem, M., *Chromium Recovery from Chrome Shaving Generated in Tanning Process*. Journal of Hazardous Materials, 2006. **129**(1): p. 143-146.
75. Cassano, A., Drioli, E., and Molinari, R., *Recovery and Reuse of Chemicals in Unhairing, Degreasing and Chromium Tanning Processes by Membranes*. Desalination, 1997. **113**(2): p. 251-261.
76. Kozłowski, R., Mieleniak, B., Muzyczek, M., and Fiedorow, R., *Flammability and Flame Retardancy of Leather*. Leather International, 2006.

77. Bahillo, A., Armesto, L., Cabanillas, A., and Otero, J., *Thermal Valorization of Footwear Leather Wastes in Bubbling Fluidized Bed Combustion*. Waste Management, 2004. **24**(9): p. 935-944.
78. Leather Resource LLC, *Leather*. [Online] [February 2008, September 2014]. Available from: <http://www.leatherresource.com/naturalcharacteristics.html>.
79. Yılmaz, O., Cem Kantarli, I., Yuksel, M., Saglam, M., and Yanik, J., *Conversion of Leather Wastes to Useful Products*. Resources, Conservation and Recycling, 2007. **49**(4): p. 436-448.
80. Caballero, J.A., Font, R., and Esperanza, M.M., *Kinetics of the Thermal Decomposition of Tannery Waste*. Journal of Analytical and Applied Pyrolysis, 1998. **47**(2): p. 165-181.
81. Font, R., Caballero, J.A., Esperanza, M.M., and Fullana, A., *Pyrolytic Products from Tannery Wastes*. Journal of Analytical and Applied Pyrolysis, 1999. **49**(1-2): p. 243-256.
82. Castelbuono, J., *The Identification of Ignitable Liquids in the Presence of Pyrolysis Products: Generation of a Pyrolysis Product Database*, in Department of Chemistry: College of Sciences. 2008, University of Central Florida Orlando, Florida. p. 122.
83. Taiwan External Trade Development Council (TAITRA), *PU/PVC Synthetic Leather Making Plant*. 2014. Bureau of Foreign Trade (BOFT).
84. Zhejiang Meitekang Synthetic Leather Co., Ltd, *Artificial Leather*. [Online] [June 2010, May 2014]. Available from: http://en.mtkleather.com/news_view.asp?id=13.
85. Stauffer, E., *Sources of Interference in Fire Debris Analysis*, in Fire Investigation, ed. N. Nic Daeid. 2004, Boca Raton, Florida: CRC Press. p. 191.
86. Aracil, I., Font, R., and Conesa, J.A., *Semivolatile and Volatile Compounds from the Pyrolysis and Combustion of Polyvinyl Chloride*. Journal of Analytical and Applied Pyrolysis, 2005. **74**(1): p. 465-478.
87. Mcneill, I.C., Memetea, L., and Cole, W.J., *A Study of the Products of PVC Thermal Degradation*. Polymer Degradation and Stability, 1995. **49**(1): p. 181-191.

88. Iida, T., Nakanishi, M., and Gotō, K., *Stabilization of Poly (Vinyl Chloride). I. Change in Color of Poly (Vinyl Chloride) Compounded with Some Metal Soaps*. Journal of Applied Polymer Science, 1975. **19**(1): p. 235-241.
89. Panagiotou, T., Levendis, Y.A., Carlson, J., and Vouros, P. *The Effect of the Bulk Equivalence Ratio on the PAH Emissions from the Combustion of PVC, Poly (Styrene), and Poly (Ethylene)*, in Symposium (International) on Combustion. 1996. Boston, USA: Elsevier.
90. Wang, Z., Wang, J., Richter, H., Howard, J.B., Carlson, J., and Levendis, Y.A., *Comparative Study on Polycyclic Aromatic Hydrocarbons, Light Hydrocarbons, Carbon Monoxide, and Particulate Emissions from the Combustion of Polyethylene, Polystyrene, and Poly (Vinyl Chloride)*. Energy and Fuels, 2003. **17**(4): p. 999-1013.
91. Jhaumeer-Laulloo, S., Maclean, J., Ramtoola, L.L., Duyman, K., and Toofany, A., *Characterisation of Background and Pyrolysis Products That May Interfere with Forensic Analysis of Fire Debris in Mauritius*. Pure and Applied Chemical Sciences, 2013. **1**(2): p. 51-61.
92. Zaikov, G.G., Steptalin, R.A., and Lomakin, S.M., *Chapter 1: Pyrolysis and Flammability of Polyurethane: Organophilic Clay Nanocomposites*, in Chemical Physics of Pyrolysis, Combustion, and Oxidation, ed. A.A. Berlin, I.A. Novakov, N.A. Khalturinskiy, and G.E. Zaikov. 2005, New York, USA: Nova Publishers.
93. Ohtani, H., Kimura, T., Okamoto, K., Tsuge, S., Nagataki, Y., and Miyata, K., *Characterization of Polyurethanes by High-Resolution Pyrolysis-Capillary Gas Chromatography*. Journal of Analytical and Applied Pyrolysis, 1987. **12**(2): p. 115-133.
94. European Man-Made Fibre Association, *Man Made Fibres*. 2014, European Man-Made Fibre Association: Brussels, Belgium.
95. IHS Global Spec, *Synthetic Fibres and Fabrics Information*. [Online] [January 2014, August 2014]. Available from: http://www.global-spec.com/learnmore/materials_chemicals_adhesives/composites_textiles_reinforcements/synthetic_fibers_fabrics_polymer_textiles.

96. CIEC the University of York, *Polymers: Polyesters*, in *The Essential Chemical Industry Online*. 2013, The University of York: UK.
97. Nawaz, S.M., Jamil, N.A., Farooq, A., and Mahmood, T., *Comparative Study of Shrinkage and Moisture Regain of Silk, Viscose Rayon and Polyester Filament Yarn*. *International Journal of Agriculture and Biology*, 2002. **4**: p. 493-495.
98. Cook, J.G., *Handbook of Textile Fibres: Man-Made Fibres*. 1984, Woodhead Publishing Ltd: India.
99. Plunkett, J.W., *Plunkett's Chemicals, Coatings & Plastics Industry Almanac*, ed. Plunkett Research Limited,. 2009.
100. Clark, J., *Polyesters*. *Understanding Chemistry*. [Online] [January 2004, August 2014], . Available from: <http://www.chemguide.co.uk/organicprops/esters/polyesters.html>.
101. *Polyester Fibre Manufacturing Process*. [Online] [January 2014, September 2014]. Available from: <http://www.cottonyarnmarket.net/OASMTP/POLYESTER%20FIBRE%20manufacturing%20process.pdf>.
102. Moncrieff, F.W., *Man-Made Fibres, Formerly Artificial Fibres*. 1963, New York, USA: John Wiley and Sons.
103. Kinoshita, R., Teramoto, Y., and Yoshida, H., *Kinetic Analysis of the Thermal Decomposition of Polyesters by Simultaneous TG-DTA/FT-IR*. *Thermochimica Acta*, 1993. **222**(1): p. 45-52.
104. Kasem, M.A. and Rouette, H.K., *Flammability and Flame Retardancy of Fabrics: A Review*. *Fire and Flammability Series*, 1974. **9**.
105. Garozzo, D., Giuffrida, M., and Montaudo, G., *Primary Thermal Decomposition Processes in Aliphatic Polyesters Investigated by Chemical Ionization Mass Spectrometry*. *Macromolecules*, 1986. **19**(6): p. 1643-1649.
106. Stauffer, E., *Identification and Characterization of Interfering Products in Fire Debris Analysis*, in *College of Arts and Science*. 2001, Florida State University: Miami, USA.
107. Zvanskii, B.V. and Krasev, S.Y., *Mechanism of Thermal Degradation of Polyester Fibre in a Furnace Pyrolyzer*. *Fibre Chemistry*, 1997. **29**(6): p. 363-366.

108. Braun, E. and Levin, B.C., *Polyesters: A Review of the Literature on Products of Combustion and Toxicity*. Fire and Materials, 1986. **10**(3-4): p. 107-123.
109. Moldoveanu, E., *Analytical Pyrolysis of Natural Organic Polymers*, in Techniques and Instrumentation in Analytical Chemistry. Vol. **20**. 1998, Macon, GA: Brown and Williamson Tobacco Corp: Elsevier Science.
110. Levchik, S.V. and Weil, E.D., *A Review on Thermal Decomposition and Combustion of Thermoplastic Polyesters*. Polymers for Advanced Technologies, 2004. **15**(12): p. 691-700.
111. Edge, M., Wiles, R., Allen, N.S., McDonald, W.A., and Mortlock, S.V., *Characterisation of the Species Responsible for Yellowing in Melt Degraded Aromatic Polyesters—I: Yellowing of Poly (Ethylene Terephthalate)*. Polymer Degradation and Stability, 1996. **53**(2): p. 141-151.
112. Joseph, P. and Tretsiakova-Mcnally, S., *Chapter 3: Chemical Modification of Natural and Synthetic Textile Fibres to Improve Flame Retardancy*, in Handbook of Fire Resistant Textiles, ed. F.S. Kilinc. 2013, Cambridge, UK: The Textile Institute: Woodhead Publishing.
113. Pohl, H.A., *The Thermal Degradation of Polyesters*. Journal of the American Chemical Society, 1951. **73**(12): p. 5660-5661.
114. Challinor, J.M., *Examination of Forensic Evidence*. Applied Pyrolysis Handbook, ed. T.P. Wampler. Vol. **2**. 2006, London, UK: CRC Press. p. 175.
115. Dzięcioł, M. and Trzeszczyński, J., *Volatile Products of Poly (Ethylene Terephthalate) Thermal Degradation in Nitrogen Atmosphere*. Journal of Applied Polymer Science, 2000. **77**(9): p. 1894-1901.
116. CDS Analytical Inc., *A Comparison of Nylon by Pyrolysis GC*, in Applications Information Using Advanced Sample Handling Technology. 2013, CDS Analytical Inc.: Oxford, PA.
117. Braun, E. and Levin, B.C., *Nylons: A Review of the Literature on Products of Combustion and Toxicity*. Fire and Materials, 1987. **11**(2): p. 71-88.
118. Beyler, C.L. and Hirschler, M.M., *Section 1, Chapter 7: Thermal Decomposition of Polymers*, in SFPE Handbook of Fire Protection

- Engineering (NFPA), ed. P.J. Dinunno. 2002, National Fire Protection Association (NFPA), Inc. : Quincy, MA.
119. Herrera, M., Matuschek, G., and Kettrup, A., *Main Products and Kinetics of the Thermal Degradation of Polyamides*. Chemosphere, 2001. **42**(5): p. 601-607.
 120. Crompton, T.R., *Characterisation of Polymers*. 2009, Smithers Rapra: Shawbury, UK.
 121. PAR Group Manchester, *Nylon 12*. [Online] [January 2014, November 2014]. Available from: <http://www.par-group.co.uk/UserDocs/Plastics%20-%20Technical/Nylon12.pdf>.
 122. Chemical Book, *24936-74-1(Nylon 6/12)*. [Online] [April 2007, February 2014]. Available from: http://www.chemicalbook.com/ChemicalProductProperty_US_CB7300743.aspx.
 123. Straus, S. and Wall, L.A., *Pyrolysis of Polyamides*. Journal of Research of the National Bureau of Standards, 1958. **60**(1): p. 39.
 124. Holland, B.J. and Hay, J.N., *Thermal Degradation of Nylon Polymers*. Polymer International, 2000. **49**(9): p. 943-948.
 125. Almirall, J.R. and Furton, K.G., *Characterization of Background and Pyrolysis Products That May Interfere with the Forensic Analysis of Fire Debris*. Journal of Analytical and Applied Pyrolysis, 2004. **71**(1): p. 51-67.
 126. Senoo, H., Tsuge, S., and Takeuchi, T., *Pyrolysis-Gas Chromatographic Analysis of 6-66-Nylon Copolymers*. Journal of Chromatographic Science, 1971. **9**(5): p. 315-318.
 127. Ballistreri, A., Garozzo, D., Giuffrida, M., and Montaudo, G., *Mechanism of Thermal Decomposition of Nylon 6,6*. Macromolecules, 1987. **20**(12): p. 2991-2997.
 128. Peebles, L.H. and Huffman, M.W., *Thermal Degradation of Nylon 66*. Journal of Polymer Science Part A-1: Polymer Chemistry, 1971. **9**(7): p. 1807-1822.
 129. Bajaj, P., *Acrylic Fibres*. Manufactured Fibre Technology, ed. V.B. Gupta and V.K. Kothari. 1997, London, UK: Chapman and Hall.

130. Surianarayanan, M., Vijayaraghavan, R., and Raghavan, K.V., *Spectroscopic Investigations of Polyacrylonitrile Thermal Degradation*. Journal of Polymer Science Part A: Polymer Chemistry, 1998. **36**(14): p. 2503-2512.
131. Bajaj, P. and Paliwal, D.K., *Some Recent Advances in the Production of Acrylic Fibres for Specific End Uses*. Indian Journal of Fibre and Textile Research, 1991. **16**: p. 89-99.
132. Causin, V., Marega, C., Schiavone, S., Guardia, V.D., and Marigo, A., *Forensic Analysis of Acrylic Fibers by Pyrolysis–Gas Chromatography/Mass Spectrometry*. Journal of Analytical and Applied Pyrolysis, 2006. **75**(1): p. 43-48.
133. Horrocks, A.R., Zhang, J., and Hall, M.E., *Flammability of Polyacrylonitrile and Its Copolymers II. Thermal Behaviour and Mechanism of Degradation*. Polymer International, 1994. **33**(3): p. 303-314.
134. Usami, T., Itoh, T., Ohtani, H., and Tsuge, S., *Structural Study of Polyacrylonitrile Fibers During Oxidative Thermal Degradation by Pyrolysis-Gas Chromatography, Solid-State Carbon-13 NMR, and Fourier-Transform Infrared Spectroscopy*. Macromolecules, 1990. **23**(9): p. 2460-2465.
135. Grassie, N. and Mcguchan, R., *Pyrolysis of Polyacrylonitrile and Related Polymers—III. Thermal Analysis of Preheated Polymers*. European Polymer Journal, 1971. **7**(10): p. 1357-1371.
136. Monahan, A.R., *Thermal Degradation of Polyacrylonitrile in the Temperature Range 280–450° C*. Journal of Polymer Science Part A-1: Polymer Chemistry, 1966. **4**(10): p. 2391-2399.
137. Minagawa, M., Onuma, H., Ogita, T., and Uchida, H., *Pyrolysis Gas Chromatographic Analysis of Polyacrylonitrile*. Journal of Applied Polymer Science, 2001. **79**(3): p. 473-478.
138. Marmarali, A.B., *Dimensional and Physical Properties of Cotton/Spandex Single Jersey Fabrics*. Textile Research Journal, 2003. **73**(1): p. 11-14.
139. Bhat, G., Chand, S., and Yakopson, S., *Thermal Properties of Elastic Fibers*. Thermochemica Acta, 2001. **367**: p. 161-164.

140. Advameg Inc., *Spandex*. [Online] [January 2014, September 2014]. Available from: <http://www.madehow.com/Volume-4/Spandex.html>.
141. Dreibelbis, R.L. and Houser, N.E., *Spandex Fiber with Copolymer Soft Segment*. 1991, Google Patents.
142. Boliek, J.E. and Denney, S.A., *Fibers, Elastomeric*, in Encyclopedia Of Polymer Science and Technology. 2009, Kirk-Othmer Encyclopedia of Chemical Technology: John Wiley and Sons. p. 1-18.
143. Lin, J-H., Chang, C-W., Lou, C-W., and Hsing, W-H., *Mechanical Properties of Highly Elastic Complex Yarns with Spandex Made by a Novel Rotor Twister*. Textile Research Journal, 2004. **74**(6): p. 480-484.
144. Industrievereinigung Chemiefaser E.V., *Elastane Fibres (Spandex Fibres)*. [Online] [January 2014, September 2014]. Available from: https://www.ivc-ev.de/live/index.php?page_id=73.
145. American Fiber Manufacturers Association: Fiber Economics Bureau, *Rayon Fibre(Viscose)*. [Online] [1997-2008, August 2014]. Available from: <http://web.archive.org/web/20080406101953/http://www.afma.org/ftutor/rayon.htm>.
146. AMEO: Conservation and Art Materials Encyclopedia Online, *Materials Database: Rayon Fibre*. [Online] [February 2013, August 2014] Available from: http://cameo.mfa.org/wiki/Rayon_fiber.
147. Federal Trade Commission, *Consumer Information*. [Online] [January 2013, September 2014]. Available from: <http://www.consumer.ftc.gov/>.
148. MJ Knit Import and Domestic, *Rayon Blends*. [Online] [January 2014, September 2014]. Available from: <http://www.aaatextiles.com/knit.Modal.html>.
149. Burrows, T. and Lenzing, A.G., *Flame Resistant Manmade Cellulostic D fibres*, in Handbook of Fire Resistant Textiles, ed. F.S. Kilinc. 2013, Cambridge, UK: The Textile Institute: Woodhead Publishing.
150. Wyss, G., *The Ripening of Viscose*. Industrial and Engineering Chemistry, 1925. **17**(10): p. 1043-1045.
151. *Unripened: Yarn Properties, Spinning of Viscose*. 1950, Google Patents.
152. Kernaghan, K., Stuart, T., Mccall, R.D., and Sharma, H.S.S., *Chapter 8: A Review on the Development of Rapid Analytical Techniques for Assessing*

- Physical Properties of Modified Linen*, in *Textiles for Sustainable Development*, ed. R.D. Anandjiwala, R. Kozlowski, G. Zaikov, and L. Hunter. 2007, New York, USA: Nova Science Publishers.
153. Ordoyno, N.F. and Rowan, S.M., *Interactions Observed During the Pyrolysis of Binary Mixtures of Textile Polymers*. *Thermochimica Acta*, 1978. **23**(2): p. 371-385.
 154. Wampler, T.P., *Analytical Pyrolysis: An Overview*, in *Applied Pyrolysis Handbook*, ed. T.P. Wampler. 1995, New York, USA: Marcel Dekker.
 155. Sharypov, V.I., Marin, N., Beregovtsova, N.G., Baryshnikov, S.V., Kuznetsov, B.N., Cebolla, V.L., and Weber, J.V., *Co-Pyrolysis of Wood Biomass and Synthetic Polymer Mixtures. Part I: Influence of Experimental Conditions on the Evolution of Solids, Liquids and Gases*. *Journal of Analytical and Applied Pyrolysis*, 2002. **64**(1): p. 15-28.
 156. Horrocks, A.R. and Anand, S.C., *Handbook of Technical Textiles*. 2000, Cambridge, UK: Woodhead Publishing Ltd.
 157. Yang, X-N. and Hardin, I.R., *Analytical Pyrolysis as a Method to Determine Blend Levels in Cotton/Polyester Yarns*. *Textile Chemist and Colorist*, 1991. **23**(4): p. 15-18.
 158. Jones, C.L., *Process for Producing Blended D-Limonene and Uses of the Blended Product*. 1985, Google Patents.
 159. Stauffer, E., *Intefering Products of Common Polymers Found in Fire Scenes*, in *Third Annual TWGFEX Symposium of Fire and Explosion Debris Analysis and Scene Investigation*, ed. E. Stauffer. 2003: Orlando, Florida. p. 1-94.
 160. Newman, R., *Interpretation of Laboratory Data*, in *Fire Investigation*, ed. N. Nic Daeid. 2004, Boca Raton, Florida: CRC Press. p. 155.
 161. Lentini, J.J., Dolan, J.A., and Cherry, C., *The Petroleum-Laced Background*. *Journal of Forensic Sciences*, 2000. **45**(5): p. 968-989.
 162. Stauffer, E., Dolan, J.A., and Newman, R., *Fire Debris Analysis*. 2008, San Diego, USA: Academic Press.
 163. Baerncopf, J. and Hutches, K., *A Review of Modern Challenges in Fire Debris Analysis*. *Forensic Science International*, 2014(224): p. 12-20.

164. Dehaan, J.D. and Bonarius, K., *Pyrolysis Products of Structure Fires*. Journal of the Forensic Science Society, 1988. **28**(5): p. 299-309.
165. Wells, S.B., *The Identification of Isopar H in Vinyl Flooring*. Journal of Forensic Sciences, 2005. **50**(4): p. 865-872.
166. Stauffer, E., *Concept of Pyrolysis for Fire Debris Analysis*. Science and Justice, 2003. **43**(1): p. 29-40.
167. Stone, I. and Lomonte, J., *False Positions in Analysis of Fire Debris*. The Fire and Arson Investigator, 1984. **34**(3): p. 36-40.
168. Coulson, S., Morgan-Smith, R., Mitchell, S., and McBriar, T., *An Investigation into the Presence of Petrol on the Clothing and Shoes of Members of the Public*. Forensic Science International, 2008. **175**(1): p. 44-54.
169. Wright, P.L. and Adams, C.H., *Toxicity of Combustion Products from Burning Polymers: Development and Evaluation of Methods*. Environmental Health Perspectives, 1976. **17**: p. 75.
170. Fashion Laboratory, *Identification of Textile Fibres by Means of Pyrognostic Analysis*. 2013.
171. Fernandes, M.S., Lau, C.M., and Wong, W.C., *The Effect of Volatile Residues in Burnt Household Items on the Detection of Fire Accelerants*. Science and Justice, 2002. **42**(1): p. 7-15.
172. The British Pharmacopoeia, the Official Source of British Pharmaceutical Standards. *Limonene*. [Online] [2014-2015, October 2014]. Available from: <http://www.pharmacopoeia.org.uk/>.
173. Agu, K., *Investigation of the Thermal Degradation Products of Bone*, in Centre for Forensic Science, Department of Pure and Applied Chemistry. 2011, University of Strathclyde: Glasgow, Scotland.
174. Faix, O., Meier, D., and Fortmann, I., *Thermal Degradation Products of Wood*. Holz als Roh-und Werkstoff, 1990. **48**(7-8): p. 281-285.
175. Pakdel, H., Pantea, D.M., and Roy, C., *Production of D-Limonene by Vacuum Pyrolysis of Used Tires*. Journal of Analytical and Applied Pyrolysis, 2001. **57**(1): p. 91-107.

176. BASF-The Chemical Company, *1,3-Dioxolane*. [Online] [June 2013, October 2014]. Available from: <http://www.basf.com/group/corporate/en/literaturedocument:/Sales+Products+Dioxolane-Brochure--1+3+Dioxolane-English.pdf>.
177. Lambiotte and Cie, *Dioxolane*. [Online] [January 2014, October 2014]. Available from: http://www.lambiotte.com/Dioxolane-product_view.htm?id=62.
178. National Center for Biotechnology Information, U.S. National Library of Medicine, *β -D-Allopyranose*. [Online] [April 2013, November 2014]. Available from: <http://pubchem.ncbi.nlm.nih.gov/compound/448388>.
179. Michal, J., Mitera, J., and Kubát, J., *Major Pyrolysis and Thermoxidative Products from Certain Polyamides*. *Fire and Materials*, 1981. **5**(1): p. 1-5.
180. Lawrence, S.A., *Heterocyclic Amines*, in *Amines: Synthesis, Properties and Applications*, ed. S.A. Lawrence. 2004, Cambridge, UK: Cambridge University Press.
181. Frost, J.W., *Synthesis of Caprolactam from Lysine*. 2013, Google Patents.
182. Cox, B.M., *Towards Renewable Commodity Chemicals: Biosynthesis of Phloroglucinol and Chemoenzymatic Synthesis of Caprolactam*, in Department of Chemistry. 2008, ProQuest: USA.
183. Christie, N.J., Cox, R.A., James, R.E., and Stevenson, J.C., *Finishing to Improve Crockfastness by Applying and Curing a Blocked Urethane Prepolymer and an Epoxidized Polyamine*. 1986, Google Patents.
184. Vickery, H.B. and Block, R.J., *The Basic Amino Acids of Wool*. *Journal of Biological Chemistry*, 1930. **86**(1): p. 107-111.
185. Sugimura, Y. and Tsuge, S., *Studies on Thermal Degradation of Aromatic Polyesters by Pyrolysis-Gas Chromatography*. *Journal of Chromatographic Science*, 1979. **17**(5): p. 269-272.
186. Bowden, W., *The Development of Downdraft Gasification for Leather Industry Wastes*. 2003, BLC Leather Technology Centre: Penn State, New York. p. 46.
187. Yanik, J., Ebale, S., Kruse, A., Saglam, M., and Yüksel, M., *Biomass Gasification in Supercritical Water: II. Effect of Catalyst*. *International Journal of Hydrogen Energy*, 2008. **33**(17): p. 4520-4526.

188. Midilli, A., Dogru, M., Akay, G., and Howarth, C.R., *Gasification of Leather Residues—Part II. Conversion into Combustible Gases and the Effects of Some Operational Parameters*. *Energy Sources*, 2004. **26**(1): p. 45-53.
189. Bilbao, R., Arauzo, J., and Millera, A., *Kinetics of Thermal Decomposition of Cellulose: Part I. Influence of Experimental Conditions*. *Thermochemica Acta*, 1987. **120**: p. 121-131.
190. Corté, P., Hérault, V., Castillo, S., and Traverse, J.P., *High-Temperature Gasification of Carbonaceous Materials by Flash Pyrolysis: Thermal Aspects*. *Fuel*, 1987. **66**(8): p. 1107-1114.

CHAPTER 5: GENERATION, ANALYSIS AND DISCRIMINATION OF PYROLYSIS PRODUCTS FROM PORCINE BONE IN THE PRESENCE OF TEXTILES USING PATTERN RECOGNITION TECHNIQUES

5.1 Introduction

Interfering products refers to a wide range of natural or synthetic [1] compounds that are commonly encountered in a fire scene that interfere with the analysis and identification of target compounds by generating characteristic volatiles that either are within the boiling point range or emulate the m/z values of the compound(s) of interest [2-5]. Interfering products can present in three major forms: substrate background products or actual petroleum products that are present in the substrate material, pyrolysis products released from the combustion of the substrate, and combustion products [1, 6-11]. When a scene involves human or animal remains, potential key indicators of these remains could also be masked by interfering products, especially if the key indicators share similar chromatographic profiles with the interfering compounds and are present at low concentrations. Thus, it is crucial that the analyst is aware of the possible presence of these products.

As the type of pyrolysis products from porcine bone (Chapter 2), human samples (Chapter 3) and from individual textiles (Chapter 4) have been established in previous chapters, this chapter concentrates on developing a robust methodology for the generation of pyrolysis products from porcine bone samples in the presence of contaminants – in this case, the textiles which produced the most repeatable products from Chapter 4 – under the laboratory conditions previously outlined. Data generated from the repeat experiments were used to ascertain the type and consistency of the pyrolysis products detected and how the combined chromatographic profiles varied from those of individual porcine and textile samples. The next stage of the work outlines the use of extracted ion current / chromatogram (EIC), extracted ion profile (EIP) and self-organising feature maps (SOFM) as a means to scrutinise and discriminate pyrolytic data obtained from porcine bone samples, individual textile samples, and the combination of porcine bone and textile samples.

5.2 Interfering Pyrolysis Products

Interfering compounds are almost always observed from natural or synthetic polymeric organic materials such as carpet, wood, padding and floor tiles [7, 8, 12-16], and textiles such as cotton, wool, polyester, acrylic and leather [5, 10]. The pyrolysis of natural, semi-synthetic and synthetic fibres has been studied, as detailed in Chapter 4. These interfering compounds can be present naturally in the original material or due to environmental transfers, and they may be generated during pyrolysis and / or combustion. They interfere with the analysis by generating fragments of the same m/z values as the target molecule or eluting in the same region as the target molecules [2, 5, 6, 16-19].

Characteristic databases are available for ignitable liquid residues (ILR), with established standards developed and published for the analysis of ILR by the American Standard for Testing and Materials (ASTM) [20-24], as these profiles are those commonly contaminated with the presence of interfering products [25, 26]. Sub-divided into light (C_4 - C_9), medium (C_8 - C_{13}) and heavy (C_9 - C_{20+}) petroleum distillates by the ASTM E1618-11 [22], these ILR have been studied and scrutinised over the years to identify their unique chromatographic patterns and chemical fingerprints. For example, petrol / gasoline has been identified through the presence of benzene, toluene, xylene, *n*-alkanes, *n*-alkyl-benzenes, indanes and naphthalenes at certain ratios [5, 7, 16, 19, 27-29]. The presence of kerosene and diesel are confirmed with high molecular weight *n*-alkanes, aromatics [29] and methyl-naphthalenes [22]. Xylene and toluene are major constituents of paint thinner [7, 16], whereas C_9 - C_{11} paraffins, *n*-alkyl-benzenes, *n*-alkyl-cycloalkanes and terpenes [29] indicate the presence of turpentine [16, 22].

Across the literature, cotton-based materials have been shown to generate toluene, a common aromatic used in the positive identification of ILR [5] and a series of *n*-alkanes, particularly present in the kerosene identification range [2]. Synthetic leather, commonly incorporated in the making of upholstery, produces *n*-alkenes and chloroalkanes, interfering with the elution of target compounds found in petrol [5].

Natural (wool) and synthetic (nylon) carpets are known to decompose to form benzene, toluene, xylene, styrene, indanes, naphthalene and C₃- and C₄-alkylbenzene [7, 16, 19], compounds used in the positive identification of petrol. Polyester-based materials generally produce light and midrange volatiles [7], together with naphthalene, styrene and ethylbenzene, complicating petrol identification [10]. The presence of kerosene, a common ILR, has also been detected from the decomposition of spandex [2]. In recent years, researchers have reported that blankets, carpets and clothing can act as wicks that, together with adequate fat, facilitate significant combustion of human remains / tissues in a fire [30-32]. In these situations, volatiles generated from the textile materials could have the potential either to emulate or to obscure any key volatile indicators of human or animal remains.

While widespread work has been conducted on the interfering products associated with ILR, a knowledge gap in terms of the possible interfering compounds for human / animal identification is still large. Currently, only a few researchers have started looking into generating and identifying potential volatile indicators of human / animal remains [33-35] in the absence of matrix contaminants. The work detailed here intends to fill this gap by looking into the effects of burning textile in the presence of porcine bone, to the pyrolytic profiles generated, using GC-MS data analysis processes and by adopting pattern recognition approaches.

5.3 Pattern Recognition in GC-MS Data Analysis and Interpretation

The classification and identification of ILR are largely dependent on pattern recognition techniques applied to the chromatographic outputs [36, 37]. Pattern recognition refers to the process of visually observing and analysing variables in order to recognise any emerging patterns and regularities in a dataset [38, 39]. It refers to a set of techniques whereby samples are classified according to a characteristic property using measurements that are indirectly related to the property, generating an empirical relationship or classification rule [40]. The rule / relationship is then applied to various samples to predict the characteristic property that is in question.

The property in question may be the class of ILR suspected in a fire scene and the measurements are the area / height / ratio / order of elution / retention time / mass-to-charge ratio of the chromatographic peak(s). These patterns are then used to answer the hypothesis or questions related to the process and experiment.

Pattern recognition can either be subjective or objective [41]. Subjective pattern recognition refers to visual patterns commonly identified using extracted ion current / chromatogram (EIC), extracted ion profile (EIP) and target compound chromatogram (TCC), whereby the unknown chromatographic patterns are subjectively compared to those derived from a series of established reference standards and classified by their mass-to-charge ratio and / or retention times, if there are sufficient similarities [21, 22, 26, 29, 36, 37, 42, 43]. Objective pattern recognition refers to the application of multivariate chemometric techniques (statistical techniques involving calculations of measurements on chemical data [38] when analysing and observing a number of target variables within and between groups [44]) utilised to perform comparison, classification and discrimination, objectively. These include principle component analysis (PCA), hierarchical cluster analysis (HCA), neural network, artificial neural network (ANN); self-organising feature maps (SOFM), and covariance mapping [38, 41, 45-54].

Most multivariate pattern recognition process involves two of the following sets of data [38, 55]:

- i. **labelled or supervised scheme**, where the technique requires the input of training algorithms of assigned groups to learn the structure of the data (i.e. it visualises the relationship between samples and variables that have been assigned to groups);
- ii. **exploratory data / unsupervised scheme**, where the technique does not require the input of training algorithms of assigned groups (i.e. it visualises the relationship between samples and variables but does not need them to be assigned to groups).

Multivariate analysis converts high dimensionality data into a two-dimensional format, facilitating a simpler and more valid interpretation by providing links between and within the samples and variables while revealing relationships, possible classification estimation and linkage of common vectors that otherwise, would not be visible under normal analytical conditions [41]. It is a powerful tool that facilitates the interpretation of complex data and has been widely used in the field of fire debris analysis, predominantly for ILR detection and classification, particularly in the presence of background interferences [39, 45, 47, 48, 51, 56].

5.3.1 Extracted Ion Current / Chromatogram (EIC) and Extracted Ion Profile (EIP)

GC-MS is well-known and favoured for its ability to provide a wealth of information, facilitate data manipulation and allow intricate levels of pattern recognition [26, 47, 49, 57]. One of these features includes the use of extracted ions [51, 57-59]. Each class of compound possesses one or more characteristic m/z ion(s) depending on its structure [58], and if these are known, the process of extracting pertinent structural indicators (fragment ions) from the entire data set can be conducted [58]. When characteristic m/z values are inputted into the GC-MS Data Analysis Software, the algorithm recovers any chromatographic peaks from the mass spectrum containing the identical m/z value(s), generating either an extracted ion current / chromatogram (EIC) or an extracted ion profile (EIP) [36, 49, 60].

In single ion EIC, individual ions are extracted independently, generating n number of chromatograms, corresponding to the number (n) of m/z values requested, resulting in a more discrete dataset that allows for better distinction between some classes. In summed EIP, a group of ions that represent a class of chemical compounds is extracted simultaneously, summarising data from multiple individual EICs to generate a more detailed chromatogram, containing patterns of relative ratios of similar class compounds across a range of boiling points [49, 57]. An example of alkyl-substituted aromatics, namely C_2 , C_3 and C_4 alkyl-benzenes (m/z 91, 105, 119), is utilised here to illustrate the difference across both types of extraction; they were extracted from the total ion chromatogram (TIC) of gasoline displayed in Figure 5.0

(a). Figures 5.0 (b), (c) and (d) illustrate the three individual EIC chromatograms of m/z 91, 105 and 119, respectively, whereas in Figure 5.0 (e), a summed EIP is generated with the use of all three m/z values in one chromatogram. The latter is much preferred as it requires the generation of only one chromatogram that contains a larger information pool at higher abundances required for analysis and interpretation [54]. EIP also facilitates a higher signal-to-noise ratio, aiding in reducing interferences from background compounds [22] while enabling ratios of compounds to be visually compared on one scale [36]. However, the use of EIP risks the loss of minor components that are not easily seen at the common baseline scale, and in these instances, EIC is a better option [36].

Similarly, the process can be applied to a whole range of compounds including *n*-alkenes, *n*-cycloalkanes and *n*-cycloalkenes, aromatics, ketones, alcohols, indanes and naphthalenes. For hydrocarbons, the characteristic ions are based on their successive alkyl / methylene (CH_2) group, generating a range of ion fragments in the order of 14 mass-to-charge units apart [47, 49, 57]. For example, in a complex TIC of gasoline (Figure 5.1(a)), the presence of saturated *n*-alkanes can be detected by inputting its major fragment ions (m/z 43, 57, 71, 85, 99; succession of 14) (Figure 5.1 (b)). This generates an EIP that highlights the presence of *n*-alkanes in a less complex chromatogram. Similarly with unsaturated *n*-alkenes, its corresponding fragment ions (m/z 41, 55, 69, 83, 97) reduce by two for each double bond in comparison to *n*-alkanes [47, 49].

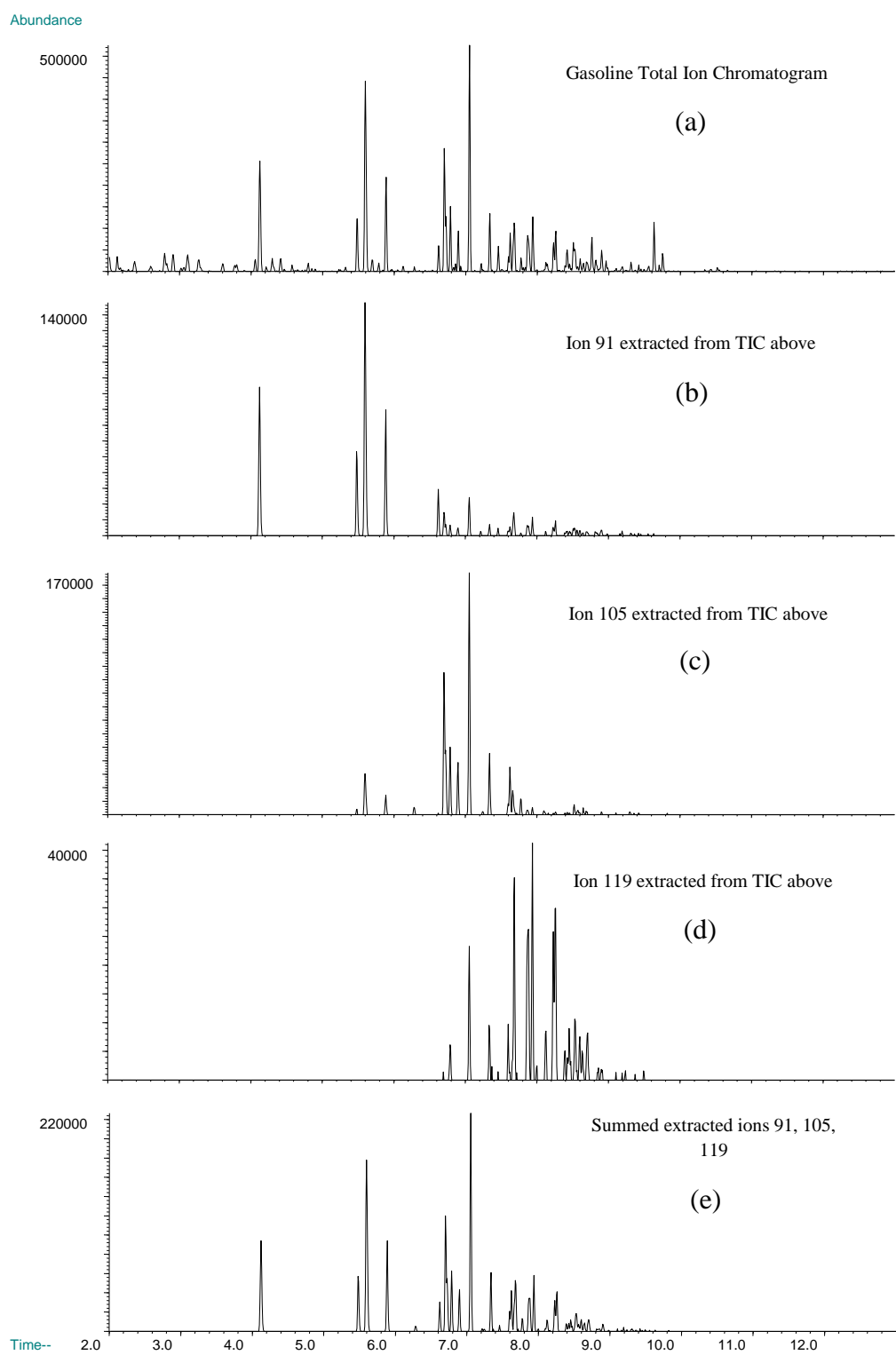


Figure 5.0: (a) TIC of gasoline, (b) EIC of ion 91, (c) EIC of ion 105, (d) EIC of ion 119, (e) EIP of ions 91, 105, 119 for *n*-alkyl-benzenes [57]

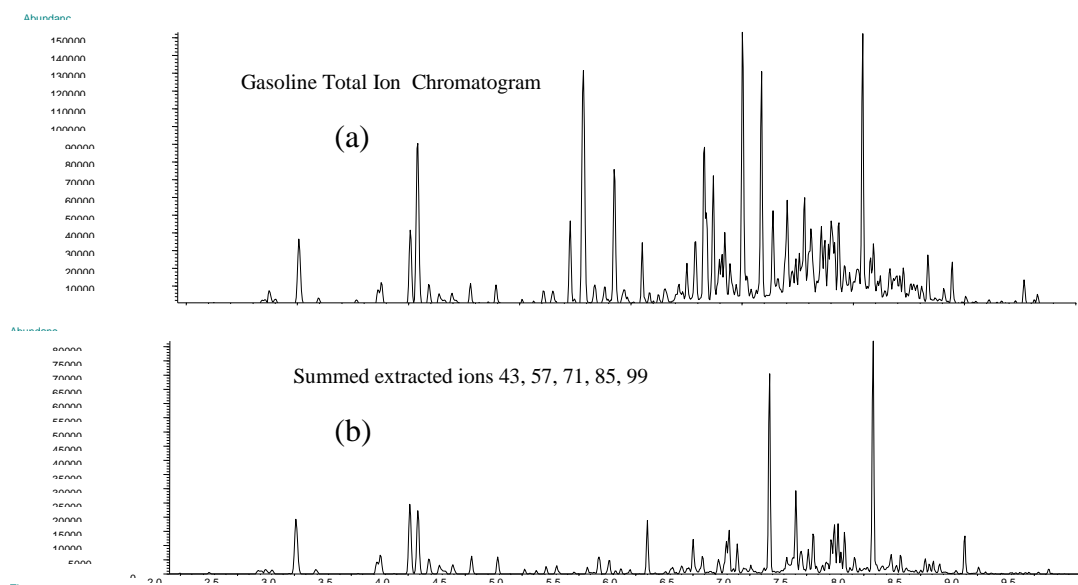


Figure 5.1: (a) TIC of gasoline and (b) EIP of ions 43, 57, 71, 85, 99 for *n*-alkanes [57]

However, the abundance of these fragment ions has to be considered for accurate identification, as the fragment ion m/z values are class-specific rather than class-exclusive [49, 57, 61]. Using the previous example, although *n*-alkanes are identified by their major fragment ions of 43, 57, 71, and 85, the possibility of this class of hydrocarbons possessing low abundances of minor fragment ions m/z 55, 69, and 73 (indicators of *n*-alkenes) is evident [57]. Thus, caution has to be applied when looking into the major and minor ion peak relative abundances in order to attain a more accurate and reliable interpretation. Similar caution is needed in cases where two or more different classes of compounds share one or more comparable fragment ions. This is the case with *n*-alkenes and *n*-cycloalkanes, as they both possess the same empirical formula of C_nH_{2n} [49]. When they fragment in the mass spectrometer, smaller *n*-cycloalkanes and the fragmentation of larger *n*-cycloalkanes generate fragment ions of m/z 41, 55 and 69, similar to those produced by *n*-alkenes [47]. However, *n*-cycloalkanes can be easily identified by the presence of the prominent ion 83, whereas *n*-alkenes are distinguishable by the presence of the prominent ion 55 [49, 58]. A compilation of the major fragment ions used in the identification of a range of fire-debris-related compounds is detailed in Table 5.0.

Table 5.0: Major class / compound indicative fragment ions for commonly encountered compounds in fire debris analysis. Adapted from [2, 22, 29, 36, 47, 49, 57, 58, 62].

Class / Compound	Major Fragment Ions						
<i>n</i> -alkanes (normal and iso)	29	43	57	71	85	99	+14
<i>n</i> -alkenes	41	55	69	83			
<i>n</i> -cycloalkanes	41	55	69	83	97		
<i>n</i> -aldehydes	44 [33]						
<i>n</i> -alkyl-cyclohexanes	82	83					
simple aromatics	91	105	119	133			
polynuclear aromatics	128	142	156	170			
<i>n</i> -alkyl-benzenes	91	92	105	106	119	120	
<i>n</i> -alkyl-styrenes	104	117	118	132	146		
indanes	117	118	131	132			
naphthalenes	128	142	156	170			
ketones	44	58	72	86			
alcohols	31	45	59				
phenol	95	109	123				
benzene	77	78					
monoterpenes	93	136					

***Bold numbers refer to the most prominent ion(s) for identification of the class**

** **+14 refers to the increase in m/z in the order of 14 for the fragment ions**

For the detection of petroleum-based ignitable liquids, the compounds of interest are saturated hydrocarbons (i.e. *n*-alkanes, both normal and iso), *n*-alkenes, cycloalkanes, and aromatics which are further classified into simple aromatics (mononuclear), polynuclear aromatics (naphthalenes) and indanes, and oxygenates. These compounds are not only found naturally in ignitable liquids but they are also present in fire debris analysis as interfering compounds [2, 22, 47, 49, 58]. The use of EIP and EIC in these cases has been well documented in the literature [2, 10, 12, 39, 47, 53, 58, 63, 64].

The extensive use of EIC and EIP in fibre debris analysis [58] is due to their ability to facilitate the collection of the entire dataset while allowing the analysis of the compound(s) of interest and, at the same time, solving the issues of co-elution of contaminants and allowing data to be filtered accordingly to reduce data load, interferences and complexity [26, 36, 47, 57]. Both EIC and EIP are also useful to reveal compounds at low concentrations that are not usually detected from routine analysis as they are likely to be obscured by the presence of stronger, more concentrated contributors [58]. EIC and EIP also simplifies the analysis procedure,

particularly in reducing the complexity of the datasets involved into a more manageable format for efficient comparison, identification and interpretation [54]. EIC and EIP are also particularly useful in distinguishing different classes of petroleum-based products (distillate, isoparaffinic, naphthalenic) and is useful in ILR detection [63, 65].

While subjective pattern recognition is proven to be useful, even in the presence of certain background contaminants [29, 36, 66], it has its own set of challenges and its limitations should be highlighted, particularly in the field of fire debris analysis and ILR identification. Certain guidelines must be followed in order to prevent incorrect analysis and interpretation [36]. This includes the need to select suitable fragment ion(s) from the set of standards for comparison, to compare an unknown sample to a set of known standards under identical chromatographic conditions and to perform visual comparisons not only on the EIC or EIP but also on the general patterns and peak ratios, and the overall relative abundances within the TIC. These guidelines render the process time consuming, tedious, and complex, relying heavily on the skillset, expertise and experience of the analyst who must know what to look for and how to go about distinguishing the peak(s) of interest from contaminants [26, 29, 36, 37, 43, 45, 66].

5.3.2 Self-Organising Feature Maps (SOFM)

In recent years, the use of self-organising feature maps (SOFM) / Kohonen neural network has gained more interest as an alternative approach for data visualisation involving forensic datasets. SOFM has been regarded to be an advanced artificial neural network (ANN) technique [41] that has demonstrated its effectiveness in analysing complex and non-linear data [67], predominantly in the field of drug design [67, 68], food science [69-71], environmental science and engineering [72-74] and lately in the field of forensic science [75-82].

The artificial neural network in SOFM was developed by Teuvo Kohonen in 1982 [83]. This network was developed using the human brain function as its model, loosely emulating its architecture in terms of how the brain neurons (basic unit)

process information and acquire knowledge [45, 84, 85]. Artificial neurons / nodes were then developed to collect signals and project points from a multi-dimensional space into a single or two-dimensional lattice, transforming these points into a visual and discrete topological feature map output [68, 84, 85]. The projection points are directly extracted from the multi-dimensional space onto the two-dimensional space, conserving their topology [67, 68, 85]. The closer the nodes are to each other, the more similar the compounds are as compared to those that are far apart. These neural networks self-organise themselves in an unsupervised scheme [68, 84] and facilitate the use of SOFM for [67, 68]:

- i. association
- ii. classification / clustering
- iii. modelling / perception
- iv. transformation / representation

The SOFM network is essentially made up of two distinct [86] yet fully connected layers; input layer and output layer [74, 76, 84]. The input layer is comprised of neurons that represent the variables within the dataset, where each neuron receives an individual input signal [76], whereas the output layer creates a two-dimensional lattice onto which the input patterns are mapped [41, 77, 78] and consists of map units / neurons that represent nodes in the final structure [76]. The connection between the two layers is characterised by weight, where the values represent the strength of the connection [76]. A typical layout of the SOFM is illustrated in Figure 5.2.

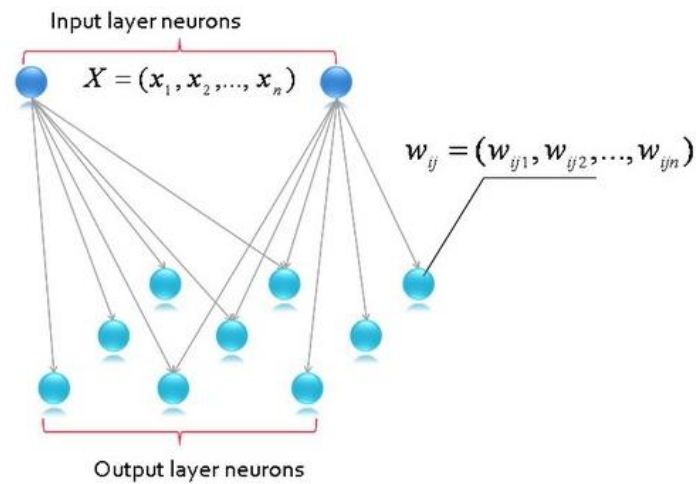


Figure 5.2: Two layer structure of the neural network in SOFM. X represents the number of input neurons. W_{ij} represents the random weight values assigned to each neuron [87]

The neural mapping process begins within the unsupervised, competitive learning scheme in SOFM when neurons in the output layers are assigned with random weight values upon the introduction of the input nodes to the input layer. Once this occurs, a two-step process follows [41, 74, 76, 78]:

- i. identification of the winning / best matching unit (BMU) neuron [88], which is the output neuron that is the closest in terms of its weight to the input vector and is identified when neurons in the output layer compete with each other.
- ii. updating optimised weight, whereby the weight of the winning neuron and the neighbouring neurons are tuned and updated so that they become closer to the input vectors.

As this process continues, the neural network self-organises to configure the mapping of similar input vectors onto similar output neurons, generating clusters of similar patterns, visualised in the form of a topological map. If the different clusters are to be visualised, an additional step of performing cluster boundaries is conducted [76].

The visualisation of the output data in SOFM can be conducted in a number of meaningful ways, depending on the nature of the information acquired and what type of output is desired. Some of the common visualisation techniques utilised is distance matrix (U-matrix, P-matrix), hit histogram, similarity colouring, and component planes [38, 88-90]. To illustrate the visualisation of similarity colouring with SOFM, 15 colours classified using the red, green, blue (RGB) values of 0 and 1 is taken as an example. White is given values of [1, 1, 1] while black is valued at [0, 0, 0]. The output map is presented in Figure 5.3. Obvious groupings can be identified from the map. The bottom right of the map consist of groups containing various shades of blue while shades of grey are grouped at the middle and middle top of the map. A closer look within the grey cluster, for example, reveals further clustering into light, medium and dark. Similarly, in the blue cluster shades of sky blue, dark blue, grey blue and cyan can be identified.

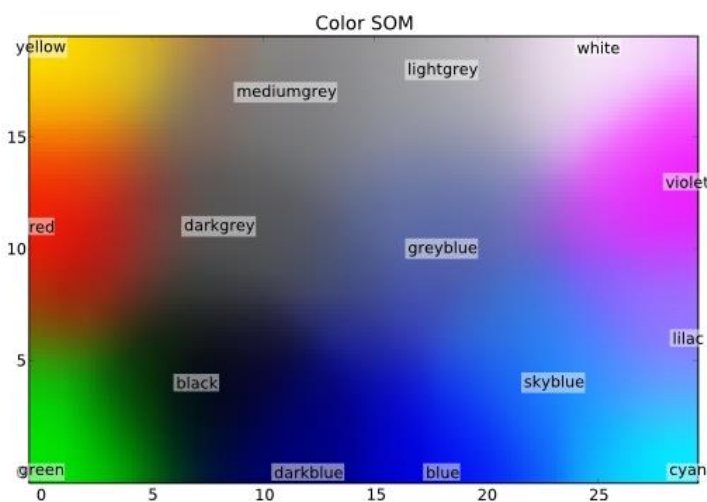


Figure 5.3: Similarity colouring SOFM map output shows similarities and differences across a range of colours [91]

In terms of the application of SOFM in the field of forensic science, a U-matrix visualisation for the classification of lighter fuels from the work of Mat Desa *et al.* [77] is used as an example. In their study, five types of lighter fluids were used and evaporated at six different concentrations. The output map is presented in Figure 5.4. Again, clear groupings can be identified from the map. The lighter fuel labelled ‘P’ can be seen clustering with borders in the middle of the map, whereas the ‘D’ labelled lighter fuel is grouped at the top left and middle of the map. Within each

cluster, a further grouping of the six different concentrations can be identified. For example, separation is observed for lighter fuels with concentrations labelled P10, P25, P50, P75, P90, P95 and P neat. This demonstrates that SOFM can perform very well for forensic data, particularly in the analysis and discrimination of ILR.

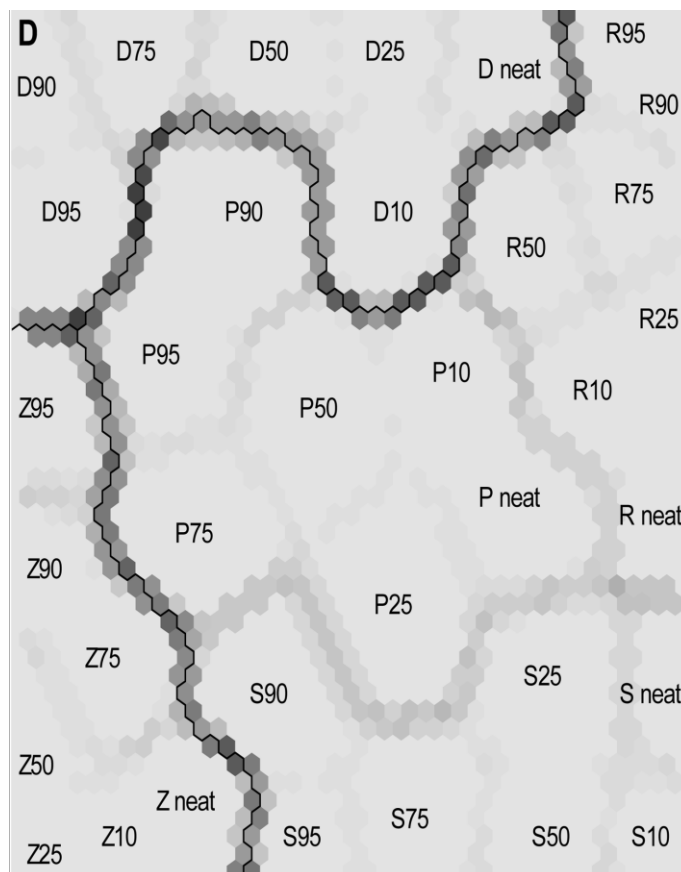


Figure 5.4: U-matrix SOFM topographic map output of five pure and evaporated lighter fuel samples. (D-Dunhill, P-Perma, R-Ronsonol, S-Swan, and Z-Zippo) [77]

Although SOFM has been proven to be a powerful tool in facilitating the grouping of data with similar characteristics from a multi-dimensional lattice to a two-dimensional space without affecting the topology of the input, its limitation is in its requirement for large quantities of pre-treated, good quality data in order to perform optimally [87], plus extra computational time for the neural network to learn patterns and algorithms [41].

5.4 Experimental Methods

5.4.1 Pyrolysis Products from Textile Samples in the Presence of Porcine Bone

5.4.1.1 Textile Samples

The optimised textiles from 4.7.2.2 were utilised in this study as detailed in Table 5.1. Each textile was cut using scissors into six swatches (8.5 cm × 3 cm), and each piece was placed in a 125 mL tin can (WA Products, UK) with its lid removed.

Table 5.1: A range of 11 optimised textiles based on their composition

Label	Composition
A	100% cotton
B	95% cotton + 5% elastin
D	50% cotton + 50% modal
E	100% acrylic
F	50% acrylic + 50% cotton
H	80% nylon + 20% elastin
J	100% denim
L	96% wool + 4% LYCRA [®]
N	64% polyester + 33% rayon + 3% elastin
O	50% polyester + 50% viscose
Q	100% leather

5.4.1.2 Porcine Bone Samples

Long pork bones were obtained from The Country Shop, Glasgow, Scotland, UK on a weekly basis to ensure the freshness of the samples. Each bone, was labelled according to the date obtained and stored in the laboratory freezer. The bones were left to defrost naturally at room temperature for 30 to 40 minutes before sample preparation. Once defrosted, each bone was held securely in a bench vice and a hacksaw was used to cut off the epiphysis on both ends of the bone. The epiphysis was removed to reduce variation in bone composition that might affect the reproducibility of the extraction process. Any remaining soft tissue on the bone was removed with scissors and tweezers. The diaphysis of the bone was then cut into 25 g ± 1.50 g samples ($n=6$). Each bone fragment was then placed beside the textile sample in the same 125 mL tin can (WA Products, UK), with its lid removed. The process was repeated six times for each textile type.

5.4.1.3 Generation and Extraction of Thermal Decomposition Products

The generation and extraction of thermal decomposition products followed the optimised methodology established in sections 2.4.3.2 and 2.4.3.3, respectively, with modification in the length of time for which the textile-porcine bone combinations were allowed to burn. For the purpose of this study, the term ‘combined samples’ is used to illustrate the combination of porcine bone and textile samples during the burning process. If auto-ignition occurred, the combined samples were allowed to burn to reach temperatures above 500 °C or until a reduction in the size of the flames occurred and when temperatures within the tin did not show any signs of increasing. These variables were determined through preliminary experiments with each of the combined samples. If auto-ignition did not occur, the combined samples were heated until two thirds of the samples were burnt. The experiment was repeated six times for each textile type in the presence of porcine bone.

5.4.1.4 Gas Chromatography – Mass Spectrometry

The GC-MS analysis utilised here followed the optimised method from section 2.4.2. The TIC produced for each combined sample was analysed based on the retention times and m/z values. Each significant peak was then identified by comparing mass spectrometric data against the National Institute of Standards and Technology (NIST) library and standard mixtures.

The compounds appearing in the individual porcine bone samples (Chapter 2) and individual, optimised textile samples (Chapter 4) were then compared to those generated from the combined samples.

5.4.2 Pattern Recognition

5.4.2.1 Extracted Ion Chromatogram (EIC) and Extracted Ion Profile (EIP)

Data acquisition was performed using the GC-MS Data Analysis MS Chemstation Software (version B.00.01 Hewlett Packard, Agilent Technologies) connected to the NIST/EPA/NIH Mass Spectral Library (NIST 08) (version 2.0*f*, Gaithersburg, MD) distributed by the National Institute of Standards and Technology (NIST)[®] 1987-2008, United States of America [92]. Extracted ion chromatograms (EIC)s and

extracted ion profiles (EIP)s were obtained from six of the total ion chromatograms (TIC)s of porcine bone post-ignition (identified in section 2.5.2.2) based on the m/z values of the consistently appearing characteristic products. These products were a series of C_8 to C_{17} n -alkanes and n -alkenes and a hexadecanitrile. EIC and EIP were applied from 5.50 minutes to 22.30 minutes for porcine bone samples. The pattern recognition process did not include any peaks prior to 5.50 minutes (except benzene and toluene) as it was masked by the solvent front. Although a number of aromatics and n -alkyl-benzenes were also consistently present in porcine samples, their m/z values were not inserted into the EIC and EIP as these products were not characteristic to porcine samples only, as they have been consistently reported across a range of ILR and other types of fuel load, as discussed previously.

Once the EIC and EIP was conducted and validated on porcine bone samples post-ignition, the characteristic m/z values were then applied to the TIC of the optimised set (i.e. the set with the highest number of pyrolysis products detected) within the combined samples (AA), (BB), (DD), (EE), (FF), (HH), (JJ), (LL), (NN), (OO) and (QQ), to determine the use and effectiveness of EIC and EIP in extracting the profile of porcine tissue in the presence of contaminants (i.e. textiles).

5.4.2.2 Self-Organising Feature Maps (SOFM)

Multivariate pattern recognition was conducted using the Self-Organizing Maps Viscovery Self Organising Map SOMine 5.0 Ink software powered by Viscovery® GmbH 2009. To estimate the general performance of the SOFM model in clustering and predicting classification for a given set of data, validation of the model was conducted using the original textile dataset, having selected the optimised set for each individual textile ($n=11$) (4.7.3) and the individual porcine bone data (2.5.2.3) ($n=1$). The entire dataset was partitioned into 12 SOM-ward clusters, corresponding to 11 textile types and one porcine bone, and reported in the form of flat clusters for visualisation.

Once the SOFM model was validated, the percentage of correct classification was determined. Performance values above 85% [41] demonstrate that the SOFM model

is capable of providing an objective analysis in the classification of complex data patterns from textile and porcine bone samples.

5.4.2.2.1 SOFM of Individual Textile Samples

Firstly, the type of compounds generated from the 11 individual textile types ($n=6$ for each textile, so 11×6), were combined into an Excel spreadsheet and labelled as 1 for present and 0 for absent. The data was then inputted into the SOFM software and the topological map was tuned to categorise the output into 11 SOM-ward clusters, labelled accordingly and reported in the form of clusters for visualisation.

The number of pyrolysis products generated for each set ($n=6$) within the same textile type was then identified and the percentage of the compounds present within each set was determined by dividing the sum of products generated by set x by the total number of pyrolysis product generated for that particular type of textile and multiplying by 100. This process was then applied to the other textile types across their sets of repeats.

The next stage involved the elimination of sets, according to the percentages of total compounds present. Percentages for the sets were rounded to the nearest whole number. An initial percentage of 100% was applied: sets that did not generate 100% of the total compounds detected within the same textile type were eliminated and the data was uploaded into the SOFM software. As mentioned previously, the topological map was tuned to categorise the output into 11 SOM-ward clusters (depending on how many textiles are represented), labelled accordingly and reported in the form of flat clusters for visualisation. The process was repeated for 90%, 80%, 70%, 60%, 50%, 40%, 30%, 20%, 10% and < 5%. SOFM map outputs were then compared to determine the percentage, and hence the group of pyrolysis products, for which the software is capable of producing distinctive separation between the textile types.

Once the percentage was determined, the datasets were then tuned to categorise the 11 clusters into a U-matrix visualisation map and also into six SOM-ward clusters,

corresponding to the six groups of textile types – cellulose base (A, B, D, J), acrylic base (E, F), nylon (H), wool (L), polyester base (N, O), and leather (Q) – and visualised in the form of flat clusters and U-matrix maps. U-matrix maps are used to outline boundary lines within the maps, emphasising any groupings and classifications within and between samples.

5.4.2.2.2 SOFM of Combined Samples

Similar to section 5.4.2.2.1, the type of compounds generated from the 11 combined samples ($n=6$ for each, so 11×6), were combined into an Excel spreadsheet and labelled as 1 for present and 0 for absent. The data was then entered into the SOFM software and the topological map was tuned to categorise the output into 11 SOM-ward clusters, labelled accordingly and reported in the form of flat clusters for visualisation.

Following this a single, optimised porcine bone data (2.5.2.3) was added into the spreadsheet of the combined samples and inserted into the SOFM software. The topological map was then tuned to categorise the output into 12 SOM-ward clusters, one for porcine bone and 11 for combined samples, labelled accordingly and reported in the form of flat clusters for visualisation.

After this, the most optimised (i.e. the most pyrolysis products generated (4.7.3)) textile data was added into the spreadsheet containing the combined samples and porcine bone data and uploaded into the SOFM software. This time, the topological map was then tuned to categorise the output into 23 SOM-ward clusters, one for porcine bone, 11 for individual textiles and 11 for combined samples, labelled accordingly and reported in the form of flat clusters for visualisation.

The procedure detailed in 5.4.2.2.1 was conducted in the next stage of the analysis for the percentage of total compounds present, but this time with the combined samples.

Once the percentage was determined, the datasets were then tuned to categorise the 11 clusters into a U-matrix visualisation map and also into six SOM-ward clusters, corresponding to the six groups of textile types – cellulose base (A, B, D, J), acrylic base (E, F), nylon (H), wool (L), polyester base (N, O), and leather (Q) and visualised in the form of flat clusters and U-matrix maps. As in 5.4.2.2.1, the U-matrix maps were used to outline boundary lines within the maps, emphasising any groupings and classifications within and between samples.

The final stage involved the addition of the optimised porcine bone and individual textile data to the spreadsheet of the optimised percentage data. The dataset was then tuned to categorise the output into 23 SOM- flat clusters and U-matrix clusters for visualisation; one for porcine bone, 11 for individual textiles and 11 for combined samples.

5.5 Results and Discussion

5.5.1 Temperature Profile Associated with the Burning of Combined Samples

The six sets of repeats for each combined sample all underwent auto-ignition at varying times and durations and exhibited varying thermal behaviour. This will be discussed in detail in the following sections.

5.5.2 Pyrolysis Products

5.5.2.1 Porcine Bone + 100% Cotton (AA)

The pyrolysis of pure cotton in the presence of porcine bone generated a wide range of products; which included *n*-alkanes, *n*-alkenes, *n*-cycloalkanes, *n*-cycloalkenes, alcohols, *n*-aldehydes, aromatics, *n*-alkyl-benzenes, furans, methyl-alkane / *n*-alkane nitriles, dienes, pyrroles, ketone, sulfide, alkyne, acid esters and a sugar (Table 5.2). A representative total ion chromatogram of the combined sample (AA) is illustrated in Figure 5.5.

Table 5.2: Pyrolysis products generated from 100% cotton in the presence of porcine bone (AA) across six repeats

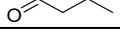
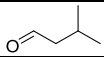
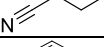
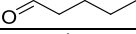
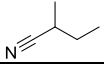
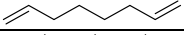
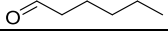
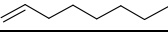
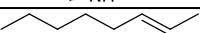
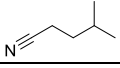
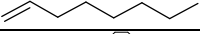
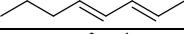
No	Retention Time (min)	Compound	Molecular Structure	Set					
				1	2	3	4	5	6
1	2.21	ethanol			√		√		
2	3.09	butanal			√		√		
3	3.16	2-butanone		√					
4	3.38	2-methyl-furan		√	√	√	√	√	√
5	3.46	ethyl acetate			√		√		
6	3.63	3-methyl-cyclopentene		√		√			
7	4.17	3-methyl-butanal			√		√		
8	4.20	butanenitrile				√			
9	4.27	benzene		√	√	√	√	√	√
10	4.95	pentanal			√		√		
11	5.11	cyclohexene		√		√		√	√
12	5.61	2-methyl-butanenitrile				√		√	√
13	5.72	2,5-dimethyl-furan		√		√	√	√	√
14	6.32	1-methyl-1H-pyrrole				√		√	√
15	6.49	dimethyl disulfide				√		√	√
16	6.70	vinyl-cyclopentane				√		√	√
17	6.90	pentanenitrile		√		√		√	
18	7.20	toluene		√	√	√	√	√	√
19	7.44	1-methyl-cyclohexene		√		√	√	√	
20	7.60	1,7-octadiene		√		√		√	
21	7.70	hexanal			√		√		
22	7.97	1-octene		√		√	√	√	√
23	8.00	1-ethyl-1H-pyrrole		√		√		√	√
24	8.29	2-octene		√		√	√	√	√
25	8.33	4-methyl-pentanenitrile		√		√	√	√	√
26	8.45	octene isomer		√	√	√	√	√	
27	8.53	bicyclooctane		√		√	√	√	
28	8.58	cyclooctene		√		√	√	√	
29	8.83	1-ethyl-cyclohexane		√		√		√	
30	9.04	1,6-undecadiene		√		√	√	√	
31	9.15	ethyl-benzene		√	√	√	√	√	√
32	9.23	2,4-octadiene		√		√	√	√	
33	9.31	<i>p</i> -xylene		√	√	√	√	√	

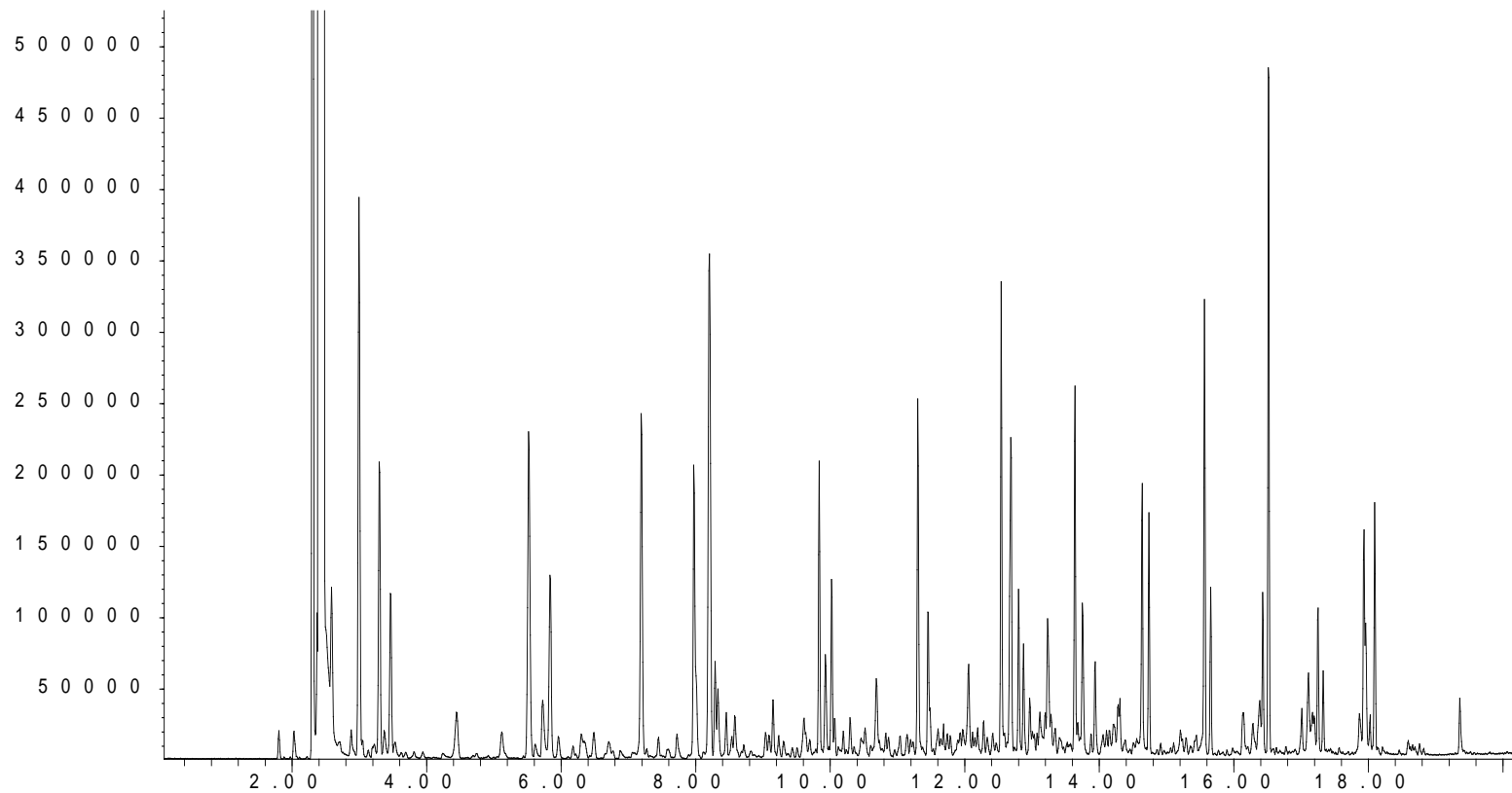
Table 5.2 continued

34	9.38	DL-xylose		√					
35	9.44	3-ethyl-cyclohexene		√		√	√	√	
36	9.51	2-heptanone			√	√	√	√	
37	9.60	styrene				√		√	
38	9.64	1,8-nonadiene		√			√	√	
39	9.67	heptanal			√		√		
40	9.70	<i>o</i> -xylene		√		√		√	
41	9.80	1-nonene		√		√	√	√	√
42	9.93	cyclooctane		√		√	√	√	
43	10.01	nonane		√	√	√	√	√	√
44	10.06	2-nonene		√		√	√	√	
45	10.19	nonene isomer					√	√	
46	10.30	1,3-nonadiene				√	√	√	
47	10.36	propyl-cyclohexane		√			√		
48	10.37	propanoic acid, ethenyl ester			√				
49	10.44	1-butyl-1H-pyrrole		√		√		√	√
50	10.48	2-heptenal			√		√		
51	10.53	butyl-cyclopentane		√		√	√		√
52	10.68	propyl-benzene				√	√	√	
53	10.83	2,4-nonadiene					√	√	
54	10.95	1-octen-3-ol			√			√	
55	11.04	1-ethyl-4-methyl-benzene		√		√		√	
56	11.19	2-pentyl-furan			√	√	√	√	
57	11.30	1-decene		√	√	√	√	√	√
58	11.46	decane		√	√	√	√	√	√
59	11.60	5-decene			√	√	√	√	
60	11.68	<i>cis</i> -3-decene		√		√		√	
61	11.97	1-pentyl-1H-pyrrole		√		√	√	√	
62	11.98	cyclodecene						√	√
63	12.06	butyl-benzene		√		√	√	√	√
64	12.11	3-decen-1-ol			√	√		√	
65	12.28	propylidencyclohexane		√			√	√	√
66	12.48	nonanal			√		√		
67	12.58	1-undecene		√	√	√	√	√	√
68	12.68	undecane		√	√	√	√	√	√
69	12.80	2-undecene		√		√	√	√	√
70	12.87	cycloundecene		√		√	√	√	

Table 5.2 continued

71	12.96	3-hexyl-cyclopentene		√		√	√	√	√
72	13.11	pentyl-benzene		√		√	√	√	
73	13.33	(1-methylbutyl)-benzene				√	√	√	
74	13.52	1-dodecene		√	√	√	√	√	√
75	13.63	dodecane		√	√	√	√	√	√
76	13.87	3-dodecene				√	√	√	
77	13.93	cyclododecene		√		√	√	√	
78	14.28	2,4-dodecadiene				√	√	√	
79	14.30	hexyl-benzene		√		√	√	√	
80	14.60	1-tridecene		√	√	√	√	√	√
81	14.73	tridecane		√		√	√	√	√
82	15.20	heptyl-cyclohexane		√		√	√	√	
83	15.29	heptyl-benzene		√		√	√	√	
84	15.44	1-cyclohexylheptane		√			√	√	
85	15.56	1-tetradecene		√	√	√	√	√	√
86	15.65	tetradecane		√	√	√	√	√	√
87	15.98	3-undecyl-cyclopentene		√		√	√	√	
88	16.58	1-hexadecyne				√	√	√	
89	16.4	1-pentadecene		√		√	√	√	√
90	16.56	pentadecane		√	√	√	√	√	√
91	17.01	nonyl-cyclohexane		√		√	√	√	
92	17.17	cyclohexadecene		√		√	√	√	
93	17.24	1-hexadecene		√		√	√	√	
94	17.32	hexadecane		√		√	√	√	
95	17.87	5-hexadecene				√	√	√	
96	17.96	1-heptadecene		√		√	√	√	
97	17.98	2-heptadecene		√		√	√	√	
98	18.01	heptadecane		√	√	√	√	√	
99	19.36	hexadecanitrile		√		√	√	√	

Abundance



Time -->

Figure 5.5: A representative TIC of porcine bone + 100% cotton (AA) (set 5)

Out of the 99 compounds generated, furans (2-methyl-furan, 2-pentyl-furan, 2-5-dimethyl-furan), aromatics, *n*-alkyl-benzenes, *n*-cycloalkanes and *n*-cycloalkenes, *n*-alkanes and *n*-alkenes, pyrroles, nitriles, dienes and a ketone appeared in at least four of the six repeats, exhibiting good reproducibility, while the remaining compounds were less consistent. With only 36 and 33 products detected respectively, sets 2 and 6 produced the lowest number of pyrolysis products while the remaining sets generated 68-83 products, with set 5 producing the highest amount. The presence of ethanol in sets 2 and 4 is also highlighted in this work.

All of the pyrolysis products generated by porcine bone (Table 2.3) were present in the combined samples (AA) with the exception of octane. However, only seven products from the pyrolysis of 100% cotton (A) (Table 4.13) were seen to be present in the combined samples (AA). They were 2-methyl-furan; 2,5-dimethyl-furan; propanoic acid, ethenyl ester; benzene; toluene; ethyl-benzene and *p*-xylene; the latter four were also present in porcine bone. Key indicators of cotton such as acids, acid esters, levoglucosenone, ketones or furancarboxyaldehyde were not detected in the combined samples, with the exception of the following: 2-methyl-furan (all sets); 2,5-dimethyl-furan (sets 1 and 3-6); propanoic acid, ethenyl ester (set 1); and DL-xylene, a sugar found in the cellulose structure of glucose [93] (set 2). The pyrolytic profile of porcine bone seemed to have dominated the type of compounds generated, in the combined sample (AA). The combined samples also generated the additional presence of *n*-aldehydes, methyl-alkane / alkane nitriles, dienes, cyclic compounds, *n*-alkyl-benzenes, alcohols, pyrroles, alkyne, acid ester and sulfide that were not documented to be present in either of the individual samples. However, the majority of these products with the exception of a few (*n*-aldehydes, alcohols, dienes, acid ester) were noted to have been present inconsistently, within the pyrolysis of porcine bone samples alone (Appendix 1.0).

n-Aldehydes of butanal, 3-methyl-butanal, pentanal, hexanal, heptanal, 2-heptenal and nonanal were detected in two sets (sets 2 and 4) of the combined samples (AA). These *n*-aldehydes were not documented to be present in porcine bone or 100% cotton samples. However, the presence of *n*-aldehydes, dienes and alcohols from the

pyrolysis of cotton over a range of temperatures has been documented in the literature [94-97]. Some or all of these *n*-aldehydes were also present in the work of McLellan [35] and DeHaan *et al.* [33], from the pyrolysis of human and porcine fat.

All of the combined samples (AA) auto-ignited, as evidenced by the temperature profiles across the six sets of repeats (Figure 5.6); similar results were also reported in the 100% cotton samples (A) (Table 4.11 and Figure 4.15). Both sets 2 and 4 experienced auto-ignition in the first two minutes of heat exposure, although the flames only lasted for less than 20 seconds before extinguishing. The other four sets auto-ignited much later and generated flames that were self-sustaining for a period of 1-2.5 minutes. Little to no fluctuations in temperature were noted in the combined samples (AA). The short burning durations in sets 2 and 4 could have prevented the generated *n*-aldehydes from undergoing decomposition. Similar observations were also observed in Agu's [34] work in the first minute upon auto-ignition and in the work of DeHaan *et al.* [33] when the samples were exposed to high temperatures for only 10 seconds. Maximum temperatures attained across the six sets of repeats were in the range of 335-630 °C.

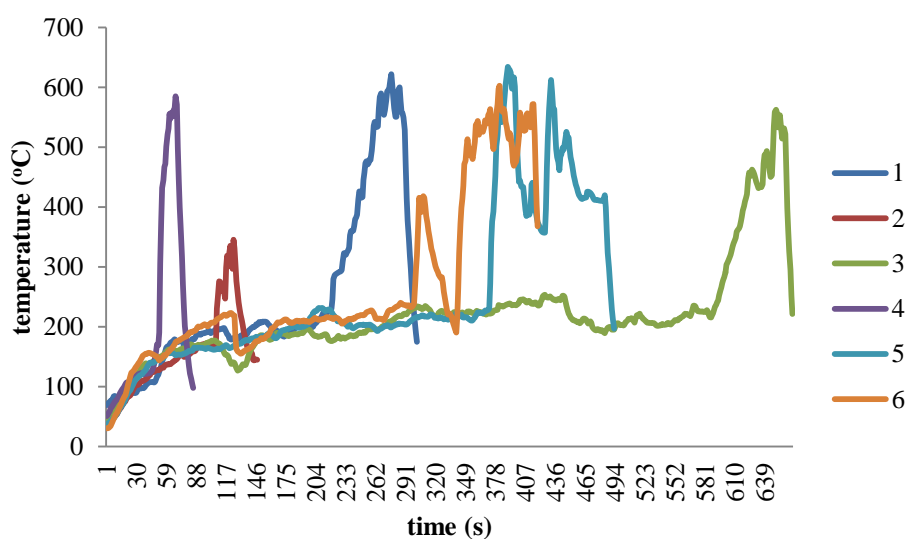


Figure 5.6: Time-temperature profiles of six 100% cotton + porcine bone samples (AA)

5.5.2.2 Porcine Bone + 95% Cotton + 5% Elastin (BB)

The pyrolysis of 95% cotton + 5% elastin in the presence of porcine bone also generated a wide range of products, similar to combined samples (AA) but with the

additional presence of *n*-cycloalkanes and *n*-cycloalkenes, methyl-alkane / *n*-alkane nitriles, furans, benzene derivatives and limonene, as detailed in Table 5.3. A representative total ion chromatogram of the combined sample (BB) is illustrated in Figure 5.7.

Compounds that appeared in at least four of the six repeats were *n*-alkanes, *n*-alkenes, aromatics, furans (2-methyl-furan, 2-pentyl-furan, 2,5-dimethyl-furan), pyrroles, *n*-cycloalkanes and *n*-cycloalkenes, methyl-alkane / *n*-alkane nitriles, *n*-alkyl-benzenes and an alkyne. The remaining compounds were present in half or less of the repeats. Set 6 produced the lowest number of pyrolysis products (26), whereas the remaining sets generated larger numbers of pyrolysis products (70-90), with set 4 generating the highest number of pyrolysis products. The presence of limonene is attributed to having generated from the used textile as it was also present in the (B) samples.

Similar outcomes with combined samples (AA) were noted in combined samples (BB), whereby all of the pyrolysis products generated from porcine bone (Table 2.3) were detected in combined samples (BB) with the exception of octane. Fifteen compounds which generated from 95% cotton + 5% elastin (B) (Table 4.14) were detected in the combined samples (BB); they were: 2-methyl-furan; tetrahydro-furan; 2,5-dimethyl-furan; limonene; *o*-xylene; 1,3,5-trimethyl-benzene; propanoic acid, ethenyl ester; 3-methyl-3-buten-2-one; 1-(acetyloxy)-2-butanone; nonene; undecene; benzene; toluene; ethyl-benzene and *p*-xylene; the latter six products were also seen in porcine bone samples. Only five key indicators of cotton were present in the combined samples (BB): 2-methyl-furan and 2,5-dimethyl-furan were in all sets, and 3-methyl-3-buten-2-one; 1-(acetyloxy)-2-butanone and propanoic acid, ethenyl ester; were only present in set 3. The presence of tetrahydro-furan, is attributed to have generated from the cotton counterpart in the combined samples, as cellulose in cotton decomposes to generate a range of furans as documented in the literature [94, 95, 97-100].

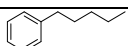
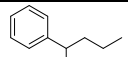
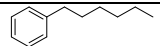
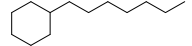
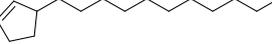
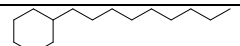
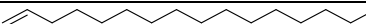
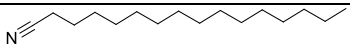
Table 5.3: Pyrolysis products generated from 95% cotton + 5% elastin in the presence of porcine bone (BB) across six repeats

No	Retention Time (min)	Compound	Molecular Structure	Set					
				1	2	3	4	5	6
1	3.09	butanal				√			
2	3.14	1,5-hexadiene			√		√		
3	3.16	2-butanone		√		√		√	
4	3.38	2-methyl-furan		√	√	√	√	√	√
5	3.63	3-methyl-cyclopentene		√	√		√	√	√
6	3.77	tetrahydro-furan				√		√	√
7	3.94	methyl-cyclopentane			√		√	√	
8	4.12	3-methyl-butanal				√			
9	4.22	butanenitrile		√	√			√	
10	4.27	benzene		√	√	√	√	√	√
11	4.61	3-methyl-3-buten-2-one				√			
12	4.75	2-methyl-1,3-pentadiene		√	√		√		
13	5.11	cyclohexene		√	√		√	√	
14	5.14	pentanal				√			
15	5.61	2-methyl-butanenitrile		√	√	√	√	√	
16	5.71	3-methyl-butanenitrile		√	√	√	√	√	√
17	5.72	2,5-dimethyl-furan		√	√	√	√	√	√
18	6.32	1-methyl-1H-pyrrole		√				√	
19	6.49	dimethyl disulfide		√	√	√	√	√	
20	6.65	ethyl-cyclopentane					√	√	
21	6.70	vinyl-cyclopentane		√			√		
22	6.72	methylene-cyclohexane		√			√	√	
23	6.90	pentanenitrile		√	√		√	√	
24	7.20	toluene		√	√	√	√	√	√
25	7.44	1-methyl-cyclohexene		√	√		√	√	
26	7.60	1,7-octadiene			√		√		
27	7.61	2-propyl-furan		√		√			
28	7.62	3,4-nonadiene			√		√		
29	7.70	hexanal				√			
30	7.97	1-octene		√	√	√	√	√	√
31	8.00	1-ethyl-1H-pyrrole		√	√	√	√	√	√
32	8.29	2-octene		√	√		√	√	
33	8.33	4-methyl-pentanenitrile		√	√	√	√	√	√
34	8.45	octene isomer				√	√	√	
35	8.53	bicyclooctane			√		√	√	
36	8.58	cyclooctene		√	√		√	√	
37	8.68	2,6-octadiene		√	√		√		

Table 5.3 continued

38	8.83	1-ethyl-cyclohexane			√		√	√	
39	9.08	hexanenitrile			√	√	√	√	
40	9.09	2-ethyl-cyclohexane		√	√		√	√	
41	9.15	ethyl-benzene		√	√	√	√	√	√
42	9.23	2,4-octadiene		√	√		√	√	
43	9.31	<i>p</i> -xylene		√	√	√	√	√	
44	9.44	3-ethyl-cyclohexene			√		√	√	
45	9.51	2-heptanone		√		√			
46	9.60	styrene			√		√	√	
47	9.67	heptanal				√			
48	9.70	<i>o</i> -xylene			√		√	√	
49	9.80	1-nonene		√	√	√	√	√	√
50	9.93	cyclooctane		√		√	√	√	
51	10.01	nonane		√	√	√	√	√	√
52	10.06	2-nonene			√	√	√	√	
53	10.19	nonene isomer		√	√		√	√	
54	10.30	1-propenyl-cyclohexane		√	√		√	√	
55	10.39	propanoic acid, ethenyl ester				√			
56	10.46	1-butyl-1H-pyrrole			√		√	√	
57	10.48	propyl-cyclohexane		√	√	√	√	√	
58	10.53	butyl-cyclopentane			√		√	√	
59	10.68	propyl-benzene		√	√	√	√	√	
60	10.73	1-(acetyloxy)-2-butanone				√			
61	10.78	1-ethyl-3-methyl-2-benzene			√	√	√	√	
62	10.82	1,3,5-trimethyl-benzene			√	√	√	√	
63	10.84	1-octen-3-ol		√	√	√			
64	11.04	1-ethyl-4-methyl-benzene		√	√		√	√	
65	11.19	2-pentyl-furan		√	√	√	√	√	
67	11.30	1-decene		√	√	√	√	√	√
68	11.46	decane		√	√	√	√	√	√
69	11.68	<i>cis</i> -3-decene			√		√	√	
70	11.79	limonene			√		√		
71	11.88	2-octenal				√			
72	11.97	1-pentyl-1H-pyrrole		√	√		√	√	
73	12.06	butyl-benzene		√	√	√	√	√	√
74	12.20	1-butyl-cyclohexene			√		√	√	
75	12.28	propylidencyclohexane		√	√		√	√	

Table 5.3 continued

76	12.48	nonanal				√			
77	12.58	1-undecene		√	√	√	√	√	√
78	12.59	5-undecene					√	√	
79	12.68	undecane		√	√	√	√	√	√
80	12.80	2-undecene		√	√	√	√	√	√
81	12.87	cycloundecene		√	√		√	√	
82	12.96	3-hexyl-cyclopentene		√		√	√	√	
83	13.11	pentyl-benzene		√		√	√	√	√
84	13.33	(1-methylbutyl)-benzene				√	√	√	
85	13.52	1-dodecene		√	√	√	√	√	√
86	13.67	5-dodecene				√	√	√	
87	13.63	dodecane		√	√	√	√	√	√
88	13.87	3-dodecene			√		√	√	
89	13.93	cyclododecene		√	√		√	√	
90	14.28	2,4-dodecadiene			√		√	√	
91	14.30	hexyl-benzene		√	√		√	√	
92	14.60	1-tridecene		√	√	√	√	√	√
93	14.73	tridecane		√	√	√	√	√	√
94	15.20	heptyl-cyclohexane			√		√	√	
95	15.56	1-tetradecene		√	√	√	√	√	√
96	15.65	tetradecane		√	√	√	√	√	√
97	16.14	nonyl-cyclopentane		√	√		√	√	
98	16.58	1-hexadecyne		√	√	√	√	√	
99	16.4	1-pentadecene		√	√	√	√	√	√
100	16.56	pentadecane		√	√	√	√	√	√
101	17.01	nonyl-cyclohexane		√	√	√	√	√	
102	17.24	1-hexadecene		√	√	√	√	√	
103	17.32	hexadecane		√	√	√	√	√	
103	17.87	5-hexadecene		√	√	√	√	√	
104	17.96	1-heptadecene		√	√	√	√	√	
105	17.98	2-heptadecene		√	√	√	√	√	
106	18.01	heptadecane		√	√	√	√	√	
107	19.36	hexadecanitrile		√	√	√	√	√	√

A b u n d a n c e

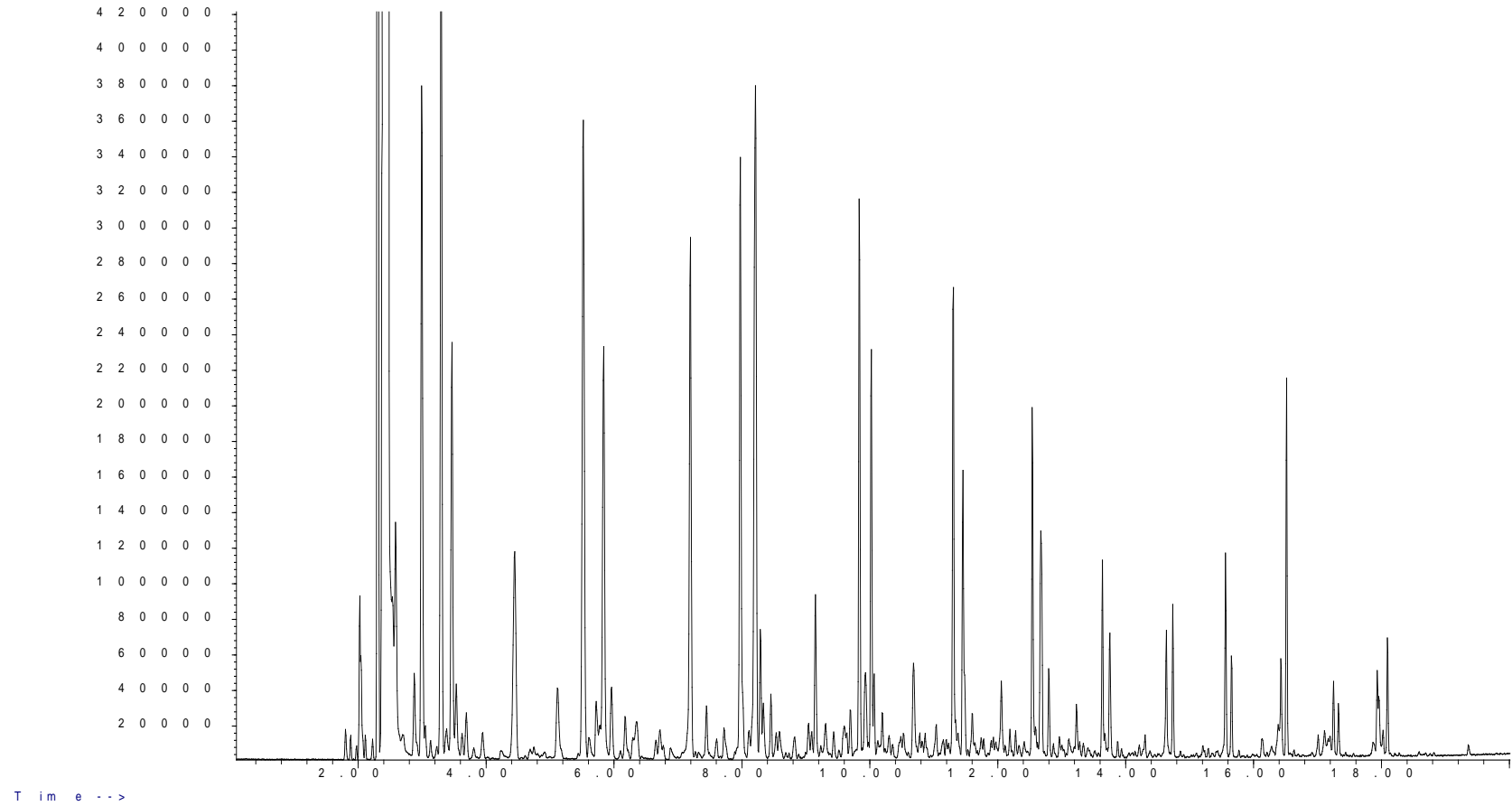


Figure 5.7: A representative TIC of porcine bone + 95% cotton + 5% elastin (BB) (set 4)

Similar to combined samples (AA), the pyrolytic profile of porcine bone seemed to have dominated the type of compounds generated in the combined samples in comparison to those generated by 95% cotton + 5% elastin (B). In addition, *n*-aldehydes, dienes, cyclic compounds, *n*-alkyl-benzenes, pyrroles, methyl-alkane /, alkane nitriles, sulfide, ketone, alkyne and alcohol that were detected in the combined sample were not present in either of the individual samples. However, majority of these products with the exception of a few (*n*-aldehydes, dienes, ketone, alcohol) were noted to have generated, although inconsistently, from porcine bone samples (Appendix 1.0). *n*-Aldehydes of butanal, hexanal, heptanal, 2-octenal and nonanal were only detected in set 3 of the combined samples (BB).

Examination of the temperature profiles across the six sets of repeats (Figure 5.8) reveal that set 3 experienced the shortest burning duration (35 seconds) upon auto-ignition. The remaining sets sustained auto-ignition for longer periods of time. Although set 1 auto-ignited rapidly in the early stages of heat exposure, it experienced a second burst of flames at 319 seconds that lasted for a longer duration. The double auto-ignition is thought to be due to the separate auto-ignition of: (1) porcine bone, (2) the cotton-elastin blend as 95% cotton + 5% elastin was part of the group of textiles that auto-ignited (Table 4.11 and Figure 4.16), and / or (3) the interaction of the bone and textile. Maximum temperatures attained across the six sets ranged from 504-706 °C, which were higher than those reported in (AA).

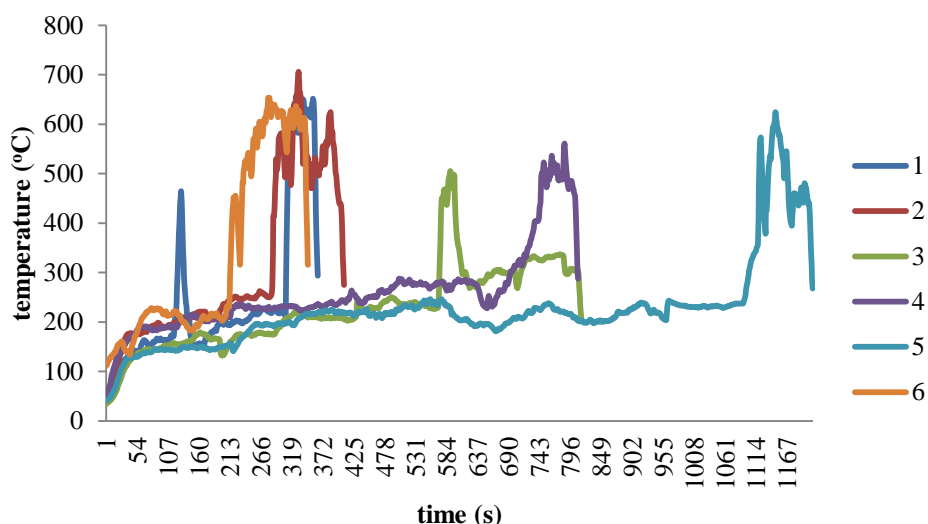


Figure 5.8: Time-temperature profiles of six 95% cotton + 5% elastin + porcine bone samples (BB)

5.5.2.3 Porcine Bone + 50% Cotton + 50% Modal (DD)

The pyrolysis of 50% cotton + 50% modal in the presence of porcine bone produced similar pyrolysis products to those from combined samples (AA) and (BB), but with better reproducibility (Table 5.4). Combined samples (DD) also produced additional acid, methyl acid, *n*-alkynes and levoglucosenone that were not detected in combined samples (AA) or (BB). A representative total ion chromatogram of the combined sample (DD) is illustrated in Figure 5.9.

While most of the pyrolysis products (79) generated across the six sets were reproducible (i.e. present in at least four of the six repeats), propanedioic acid, propyl; propanoic acid, ethenyl ester; levoglucosenone; dimethyl disulfide; *o*-xylene; *n*-aldehydes, *n*-cycloalkanes, *n*-cycloalkenes and dienes were present inconsistently across the six sets of repeats. The majority of the sets generated large numbers of pyrolysis products with set 4 producing the highest (89); set 6 produced the lowest (57). The presence of limonene here is attributed to having generated from the used textile utilised in this study.

Similar to (AA) and (BB), all of the pyrolysis products generated by porcine bone (Table 2.3) were present in the combined samples (DD) with the exception of octane. In combined samples (DD), however, more products from the pyrolysis from 50% cotton + 50% modal (D) (Table 4.15) were seen to be present as compared to (AA) and (BB). They were 2-methyl-furan; 2,5-dimethyl-furan; propanoic acid, ethenyl ester; levoglucosenone; 1,3,5-trimethyl-benzene; octane; decene; undecene; undecane; dodecene; benzene; toluene; ethyl-benzene and *p*-xylene. The latter nine were also present in porcine bone samples.

Table 5.4: Pyrolysis products generated from 50% cotton + 50% modal in the presence of porcine bone (DD) across six repeats

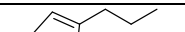
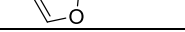
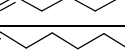
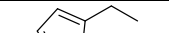
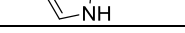
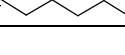
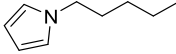
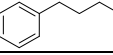
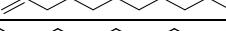
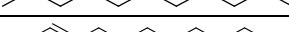
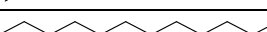
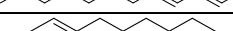
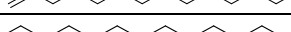
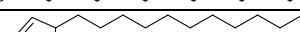
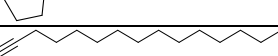
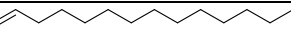
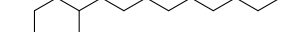
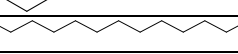
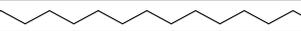
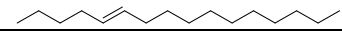
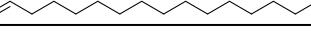
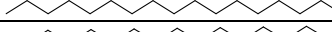
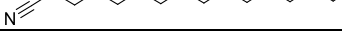
No	Retention Time (min)	Compound	Molecular Structure	Set					
				1	2	3	4	5	6
1	3.09	butanal		√			√	√	√
2	3.16	2-butanone		√	√	√	√	√	√
3	3.38	2-methyl-furan		√	√	√	√	√	√
4	3.63	3-methyl-cyclopentene			√		√		
5	3.80	3-methyl-1,2-pentadiene			√		√		
6	3.94	methyl-cyclopentane			√		√		
7	4.12	3-methyl-butanal		√				√	√
8	4.35	2-methyl-butanal		√					
9	4.27	benzene		√	√	√	√	√	√
10	4.75	2-methyl-1,3-pentadiene			√	√	√		
11	5.11	cyclohexene			√	√	√		
12	5.14	pentanal		√			√	√	√
13	5.61	2-methyl-butanenitrile		√	√	√	√	√	
14	5.71	3-methyl-butanenitrile		√	√	√	√	√	√
15	5.72	2,5-dimethyl-furan		√	√	√	√	√	√
16	6.22	3-methyl-cyclohexene			√		√		
17	6.32	1-methyl-1H-pyrrole			√	√	√	√	
18	6.49	dimethyl disulfide		√	√		√		
19	6.70	vinyl-cyclopentane			√	√	√	√	
20	6.77	4-methyl-cyclohexene			√	√	√		
21	7.20	toluene		√	√	√	√	√	√
22	7.44	1-methyl-cyclohexene			√	√	√	√	
23	7.60	1,7-octadiene			√	√	√		
24	7.62	3,4-nonadiene			√	√	√		
25	7.61	2-propyl-furan		√	√	√	√	√	√
26	7.70	hexanal		√			√	√	√
27	7.97	1-octene		√	√	√	√	√	√
28	8.00	1-ethyl-1H-pyrrole		√	√	√	√	√	√
29	8.29	2-octene		√	√	√	√	√	
30	8.33	4-methyl-pentanenitrile		√	√	√	√	√	
31	8.45	octene isomer		√	√	√	√	√	

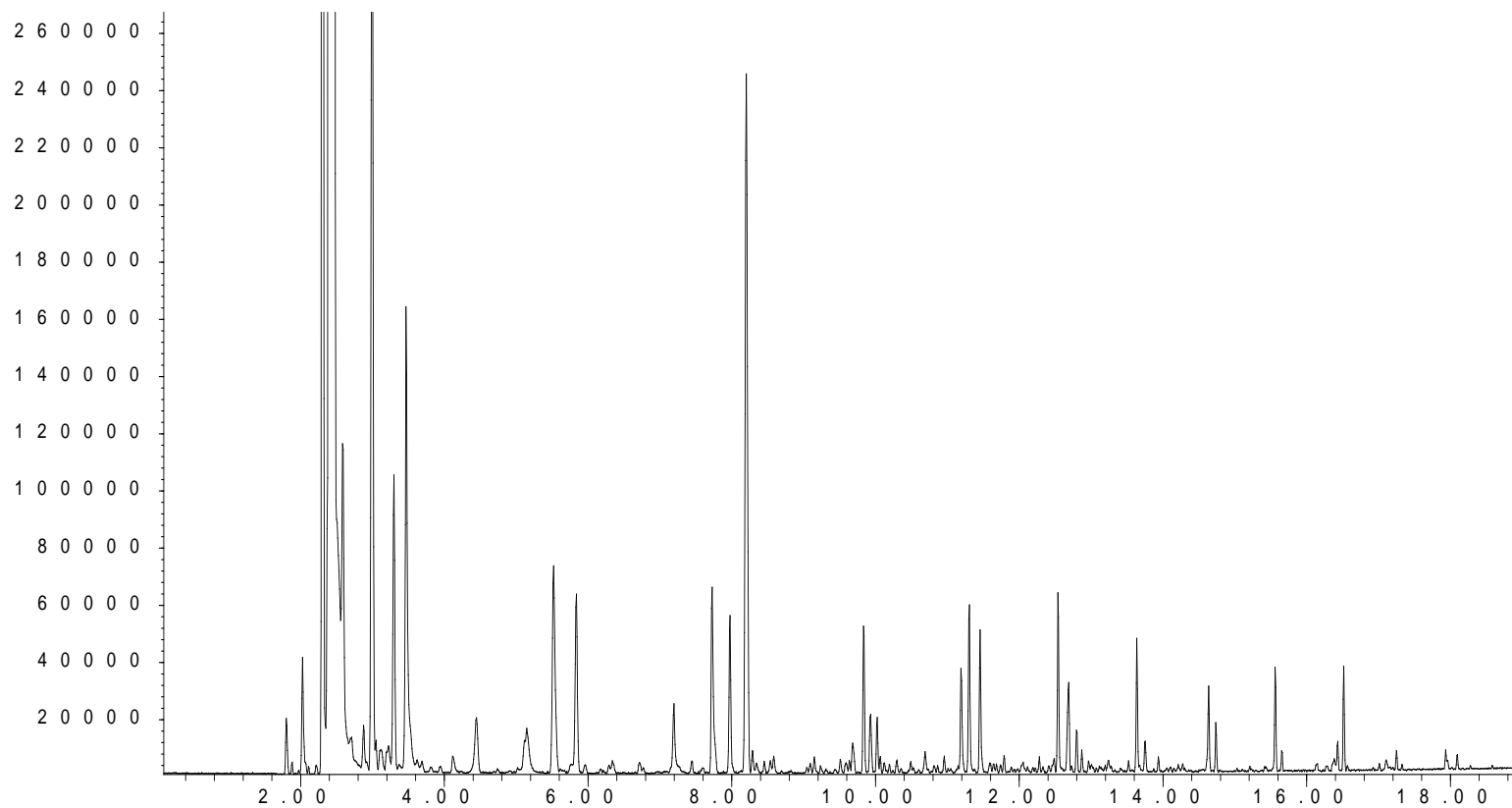
Table 5.4 continued

32	8.53	bicyclooctane		√	√	√	√	√	
33	8.58	cyclooctene			√	√	√	√	
34	8.87	levoglucosenone		√					
35	9.09	2-ethyl-cyclohexane			√	√	√	√	
36	9.15	ethyl-benzene		√	√	√	√	√	√
37	9.23	2,4-octadiene		√	√	√	√	√	√
38	9.31	<i>p</i> -xylene		√	√	√	√	√	√
39	9.38	propanedioic acid, propyl							√
40	9.44	3-ethyl-cyclohexene			√	√	√		
41	9.51	2-heptanone		√	√	√	√	√	√
42	9.60	cyclopropyl-cyclohexane			√	√	√		
43	9.64	1,8-nonadiene			√	√	√	√	
44	9.67	heptanal		√			√	√	√
45	9.70	<i>o</i> -xylene			√	√			
46	9.80	1-nonene		√	√	√	√	√	√
47	9.93	cyclooctane		√	√	√	√	√	
48	10.01	nonane		√	√	√	√	√	√
49	10.06	2-nonene		√	√	√	√	√	
50	10.11	pentanoic acid, 3-methyl, methyl ester		√	√		√	√	√
51	10.19	nonene isomer		√	√	√	√	√	
52	10.46	1-butyl-1H-pyrrole		√	√	√	√	√	
53	10.53	butyl-cyclopentane			√	√	√	√	
54	10.68	propyl-benzene		√	√	√	√	√	
55	10.75	propanoic acid, ethenyl ester						√	√
56	10.82	1,3,5-trimethyl-benzene		√	√	√	√	√	
57	10.84	1-octen-3-ol		√	√	√	√	√	√
58	11.04	1-ethyl-4-methyl-benzene		√	√	√	√	√	
59	11.19	2-pentyl-furan		√	√	√	√	√	√
60	11.30	1-decene		√	√	√	√	√	√
61	11.46	decane		√	√	√	√	√	√
62	11.60	5-decene		√	√	√	√		
63	11.68	<i>cis</i> -3-decene		√	√	√	√	√	√
64	11.79	limonene		√	√	√	√		√

Table 5.4 continued

65	11.97	1-pentyl-1H-pyrrole		√	√	√	√		
67	12.06	butyl-benzene		√	√	√	√	√	√
68	12.48	nonanal		√			√	√	√
69	12.58	1-undecene		√	√	√	√	√	√
70	12.68	undecane		√	√	√	√	√	√
71	12.80	2-undecene		√	√	√	√	√	√
72	12.87	cycloundecene		√	√	√	√	√	√
73	13.11	pentyl-benzene		√	√	√	√	√	√
74	13.52	1-dodecene		√	√	√	√	√	√
75	13.63	dodecane		√	√	√	√	√	√
76	13.93	cyclododecene		√	√	√	√	√	√
77	14.28	2,4-dodecadiene		√	√	√	√	√	√
78	14.30	hexyl-benzene		√	√	√	√	√	
79	14.60	1-tridecene		√	√	√	√	√	√
80	14.73	tridecane		√	√	√	√	√	√
81	15.20	heptyl-cyclohexane		√	√	√	√	√	
82	15.43	1-tetradecyne		√	√	√	√	√	√
83	15.56	1-tetradecene		√	√	√	√	√	√
84	15.65	tetradecane		√	√	√	√	√	√
85	16.14	nonyl-cyclopentane		√	√	√	√	√	√
86	16.58	1-hexadecyne		√	√	√	√	√	√
87	16.40	1-pentadecene		√	√	√	√	√	√
88	16.56	pentadecane		√	√	√	√	√	√
89	17.01	nonyl-cyclohexane		√	√	√	√	√	√
90	17.10	1-octadecyne		√	√	√	√	√	√
91	17.17	cyclohexadecane		√	√	√	√	√	√
92	17.24	1-hexadecene		√	√	√	√	√	√
93	17.32	hexadecane		√	√	√	√	√	√
94	17.87	5-hexadecene		√	√	√	√	√	√
95	17.96	1-heptadecene		√	√	√	√	√	√
96	18.01	heptadecane		√	√	√	√	√	√
97	19.36	hexadecanitrile		√	√	√			

Abundance



Time -->

Figure 5.9: A representative TIC of porcine bone + 50% cotton + 50% modal (DD) (set 4)

Key indicators of cotton and modal that were present in the combined samples (DD) included 2-methyl-furan; 2,5-dimethyl-furan in all samples; propanoic acid, ethenyl ester; in sets 5 and set 6 and levoglucosenone in set 1. The presence of additional acid esters, propanedioic acid, propyl; in sets 5 and 6, and pentanoic acid, 3-methyl, methyl ester; in sets 1, 2, 4-6 in combined samples (DD) is attributed to have generated from the decomposition of cellulose in cotton and modal as the pyrolysis of these fibres are expected to generate acid and acid esters of various carbon chain lengths [95, 96]. Although the key indicators of cotton and modal were present at higher numbers in (DD), the pyrolysis profile of porcine bone clearly dominated that of 50% cotton + 50% modal (D) in the combined samples (DD). The combined samples also generated additional methyl-alkane nitriles, dienes, cyclic compounds, *n*-alkyl-benzenes, *n*-alkynes, pyrroles, alcohol and sulfide that were not documented to be present in either of the individual samples. Similar to the combined samples (AA) and (BB), the majority of these products with the exception of a few (*n*-aldehydes, *n*-alkynes, dienes, alcohol) were noted to have occurred inconsistently with the porcine bone samples (Appendix 1.0). *n*-Aldehydes of butanal, 2-methyl-butanal (only in set 1), 3-methyl-butanal (only in set 1, 5-6), pentanal, hexanal, heptanal, and nonanal were also detected in the combined samples (DD), as observed in (AA) and (BB), across sets 1, 4, 5 and 6.

As evidenced by the temperature profiles across the six sets of repeats (Figure 5.10), all of the sets experienced large temperature fluctuations with a series of flame emissions during the burning process, in contrast to the combined (AA) samples and the majority of the combined (BB) samples. Sets 2-6 experienced auto-ignition at the early stages of heat application. In sets 2 and 6, the initial flames extinguished and subsequent flaming occurred thereafter with noted fluctuations in temperature. For set 5, the initial flames extinguished and two separate incidents of flaming developed subsequently. Set 1 auto-ignited much later, at 250 seconds; however, the flames extinguished with a marked drop in temperature before the second flaming occurred, increasing the temperature within the tin with noted fluctuations. The initial flames were sustained in sets 3 and 4. As in the combined (BB) samples, the multiple auto-ignition is thought to be due to the separate auto-ignition of: (1) porcine bone; (2) the

cotton-modal blend, as 50% cotton + 50% modal was part of the group of textiles that auto-ignited (Table 4.11 and Figure 4.18), and / or (3) the interaction of the bone and textile. Maximum temperatures attained across the six sets ranged from 596-728 °C, higher than those reported in (AA) and (BB).

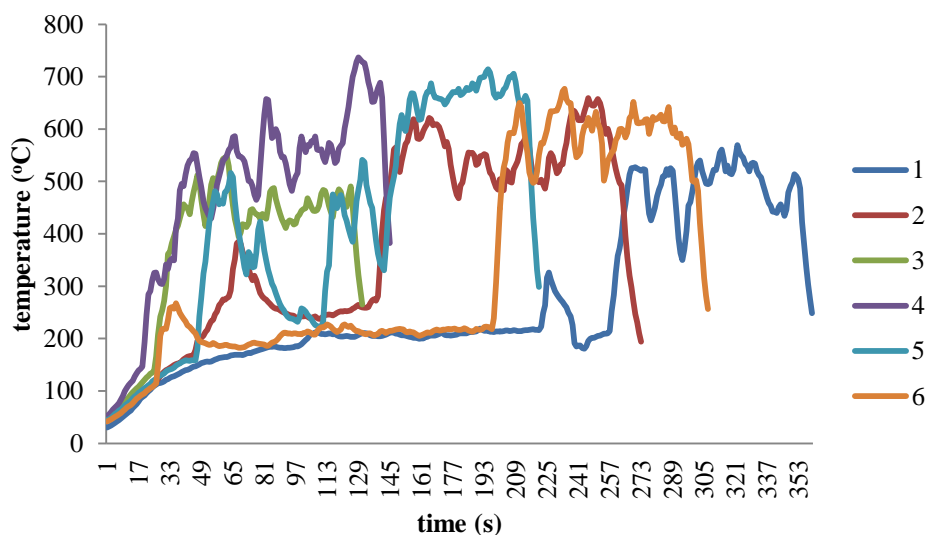


Figure 5.10: Time-temperature profiles of six 50% cotton + 50% modal + porcine bone samples (DD)

The additional pyrolysis products detected across (AA), (BB) and (DD) could have been generated by the pyrolysis of: (1) porcine bone, (2) the textile, and / or (3) through the pyrolytic interactions between the two samples.

5.5.2.4 Porcine Bone + 100% Acrylic (EE)

The pyrolysis of 100% acrylic in the presence of porcine bone generated a wide range of nitrile-based products (*n*-alkane / *n*-alkene / methyl- / methyl-alkane / methylene- nitrile / dinitrile), together with *n*-alkanes, *n*-alkenes, *n*-cycloalkanes and *n*-cycloalkenes, *n*-aldehydes, pyrroles, aromatics, *n*-alkyl-benzenes, dienes, furans, alkyne, acetate, sulfide, ketone, cyano-alkene and pyrazine (Table 5.5). A representative total ion chromatogram of combined sample (EE) is illustrated in Figure 5.11.

From the 105 products generated, less than half were present in at least four of the six repeats. These products were mostly nitriles and their derivatives, aromatics, *n*-alkanes, *n*-alkenes, *n*-alkyl-benzenes, cyano-alkene, ketone, pyrrole, furan and

pyrazine. Set 1 produced the highest number of pyrolysis products (82), whereas sets 5 and 6 had the lowest in number (33).

All of the pyrolysis products generated by porcine bone (Table 2.3) were present in the combined samples (EE) with the exception of octane and decane. While octane was also absent in the previous combined samples (AA), (BB) and (DD), the absence of decane in the combined sample (EE) was a new observation. Twenty-eight products from the pyrolysis of 100% acrylic (E) (Table 4.16) were detected in the combined samples (EE). These products included a range of nitriles and their derivatives, cyano-alkene (5-cyano-1-pentene), a pyrazine ((1-methylethenyl)-pyrazine), aromatics and *n*-alkyl-benzenes (benzene, toluene, ethyl-benzene, *p*-xylene, styrene), *n*-alkanes and *n*-alkenes (decene, undecene, dodecene, dodecane, tridecene, tetradecene, tetradecane, pentadecene). The aromatics (benzene, toluene, ethyl-benzene, *p*-xylene), *n*-alkanes and *n*-alkenes detected in the combined sample (EE) and the 100% acrylic (E) were also present in porcine bone. The range of nitriles and their derivatives, together with cyano-alkene and pyrazine, detected in the combined sample (EE) here served as reliable key indicators of acrylic. The remaining key indicators (pyridine, piperidine, cyanic and isocyanic compounds), detected in (E) were not present in combined samples (EE).

Both the acrylic and porcine bone in the combined samples (EE) had equal dominance in the total ion chromatogram, generating almost equal amounts of pyrolytic products and significant amounts of key indicators of both materials. Combined samples (EE) also generated the additional presence of *n*-aldehydes, dienes, cyclic compounds, *n*-alkyl-benzenes, furans, pyrroles, alkyne, alcohol, sulfide and acetate that were not detected in either of the separate samples. However, the majority of these products with the exception of a few (*n*-aldehydes, dienes, alkyne, acetate, ketone, alcohol) were noted to have been generated, although inconsistently, from porcine bone samples (Appendix 1.0). *n*-Aldehydes of pentanal, hexanal and heptanal were detected in sets 2-4 while nonanal was only present in sets 2 and 4 in the combined samples (EE).

Table 5.5: Pyrolysis products generated from 100% acrylic in the presence of porcine bone (EE) across six repeats

No	Retention Time (min)	Compound	Molecular Structure	Set					
				1	2	3	4	5	6
1	2.82	propanenitrile		√	√		√	√	√
2	3.13	2-methyl-2-propenenitrile		√	√			√	√
3	3.38	isobutyronitrile		√	√	√		√	√
4	3.47	ethyl acetate			√	√	√		
5	4.22	butanenitrile		√	√				
6	4.27	benzene		√	√	√	√		
7	5.11	cyclohexene		√					
8	5.14	pentanal			√	√	√		
9	5.61	2-methyl-butanenitrile		√	√	√	√	√	√
10	5.71	3-methyl-butanenitrile		√	√	√	√	√	√
11	6.32	1-methyl-1H-pyrrole		√					
12	6.49	dimethyl disulfide		√					
13	6.70	pyrrole		√					
14	6.90	pentanenitrile		√	√				
15	7.20	toluene		√	√	√	√	√	√
16	7.39	2,2'-iminobis-acetonitrile		√					
17	7.44	1-methyl-cyclohexene		√					
18	7.60	1,7-octadiene		√	√				
19	7.61	2-propyl-furan			√	√	√		
20	7.70	hexanal			√	√	√		
21	7.79	3-methyl-2-methylene-butanenitrile		√					
22	7.97	1-octene		√	√	√	√	√	√
23	8.00	1-ethyl-1H-pyrrole		√	√	√	√		
24	8.29	2-octene		√	√	√	√		
25	8.33	4-methyl-pentanenitrile		√	√	√	√	√	√
26	8.68	5-cyano-1-pentene		√	√				
27	9.02	3,5-octadiene		√					
28	9.08	hexanenitrile		√	√		√		
29	9.15	ethyl-benzene		√	√	√	√	√	√
30	9.23	2,4-octadiene		√					

Table 5.5 continued

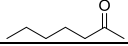
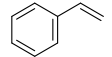
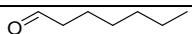
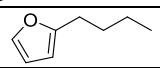
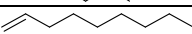
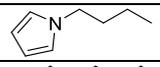
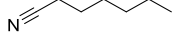
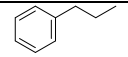
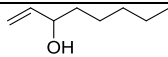
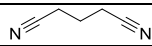
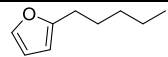
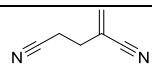
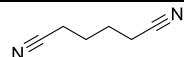
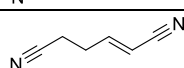
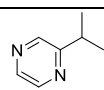
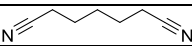
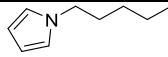
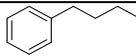
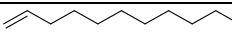
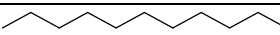
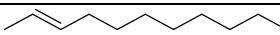
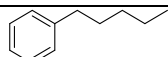
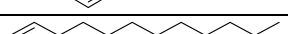
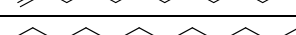
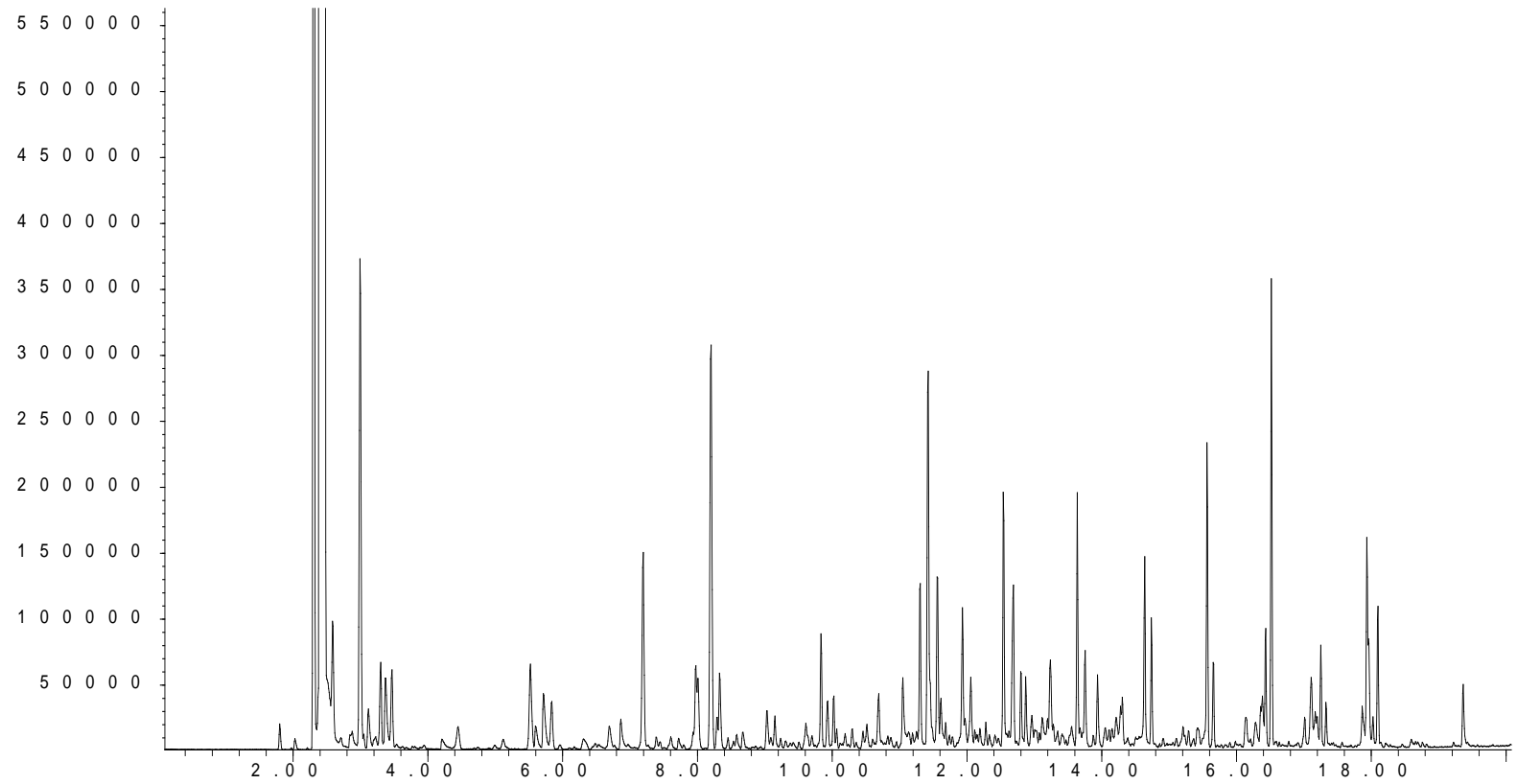
31	9.31	<i>p</i> -xylene		√						
32	9.51	2-heptanone		√	√	√	√			
33	9.60	styrene		√						
34	9.67	heptanal			√	√	√			
35	9.69	2-butyl-furan				√	√			
36	9.70	<i>o</i> -xylene		√		√				
37	9.80	1-nonene		√	√	√	√			
38	9.93	cyclooctane		√		√	√			
39	10.01	nonane		√	√	√	√	√	√	√
40	10.06	2-nonene		√	√	√	√			
41	10.30	1,3-nonadiene		√	√					
42	10.46	1-butyl-1H-pyrrole		√						
43	10.51	heptanonitrile		√						
44	10.68	propyl-benzene		√	√	√	√			
45	10.84	1-octen-3-ol		√	√					
46	11.05	pentanedinitrile		√	√	√	√	√	√	√
47	11.19	2-pentyl-furan		√	√	√	√	√	√	√
48	11.25	2-methylene-pentanedinitrile		√	√	√	√	√	√	√
49	11.30	1-decene		√	√	√	√	√	√	√
50	11.41	hexanedinitrile		√	√	√	√	√	√	√
51	11.56	hexenedinitrile		√	√	√	√	√	√	√
52	11.61	(1-methylethenyl)-pyrazine		√	√	√	√	√	√	√
53	11.94	heptanedinitrile		√	√	√	√	√	√	√
54	11.97	1-pentyl-1H-pyrrole		√	√					
55	12.06	butyl-benzene		√	√	√	√			
56	12.48	nonanal			√		√			
57	12.58	1-undecene		√	√	√	√	√	√	√
58	12.68	undecane		√	√	√	√	√	√	√
59	12.80	2-undecene		√	√	√	√			
60	12.87	cycloundecene		√		√	√			
61	13.11	pentyl-benzene		√	√	√	√			
62	13.52	1-dodecene		√	√	√	√	√	√	√
63	13.63	dodecane		√	√	√	√	√	√	√
82	13.93	cyclododecene		√	√		√	√	√	√

Table 5.5 continued

83	14.05	5,7-dodecadiene		√		√	√		
84	14.28	2,4-dodecadiene		√		√	√		
85	14.30	hexyl-benzene		√			√		
86	14.60	1-tridecene		√	√	√	√	√	√
87	14.73	tridecane		√	√	√	√	√	√
88	15.20	heptyl-cyclohexane		√					
89	15.29	heptyl-benzene		√					
90	15.42	cyclododecene		√		√	√		
91	15.56	1-tetradecene		√	√	√	√	√	√
92	15.65	tetradecane		√	√	√	√	√	√
93	16.14	nonyl-cyclopentane		√		√	√		
94	16.40	1-pentadecene		√	√	√	√	√	√
95	16.43	2-pentadecene		√	√	√			
96	16.56	pentadecane		√	√	√	√	√	√
97	17.01	nonyl-cyclohexane		√		√	√		
98	17.10	1-octadecyne		√		√	√		
99	17.17	cyclohexadecane		√		√	√		
100	17.24	1-hexadecene		√		√	√	√	√
101	17.32	hexadecane		√		√	√	√	√
102	17.87	5-hexadecene		√		√	√		
103	17.96	1-heptadecene		√	√	√	√	√	√
103	17.98	2-heptadecene		√		√	√		
104	18.01	heptadecane		√	√	√	√	√	√
105	19.36	hexadecanitrile		√		√	√		

Abundance



Time -->

Figure 5.11: A representative TIC of porcine bone +100% acrylic (EE) (set 1)

Examination of the temperature profiles across the six sets of repeats (Figure 5.12) reveals that sets 2, 3 and 4 experienced a steep rise in temperature within the first 55 seconds of heat application. Auto-ignition occurred thereafter but the flames only lasted for a short period (18-26 seconds). The short duration of burning across these sample sets could have prevented the generated *n*-aldehydes from undergoing decomposition. Sets 1, 5 and 6 auto-ignited much later and the flames were able to self-sustain for longer periods of time (around 108-126 seconds). However, these three sets experienced fluctuations in temperature and underwent a series of flaming events before stabilising. Temperatures recorded in set 1 were the highest at 661 °C and could be the reason set 1 generated the largest number of products. The series of flaming events is thought to be due the separate auto-ignition of: (1) porcine bone, which could have raised the temperatures in the tin, thus facilitating (2) the auto-ignition of acrylic (100% acrylic was part of the group of textiles that did not auto-ignite (Table 4.11 and Figure 4.19)); or (3) the interaction of the bone and textile. Maximum temperatures attained across the six sets of repeats were in the range of 388-640 °C.

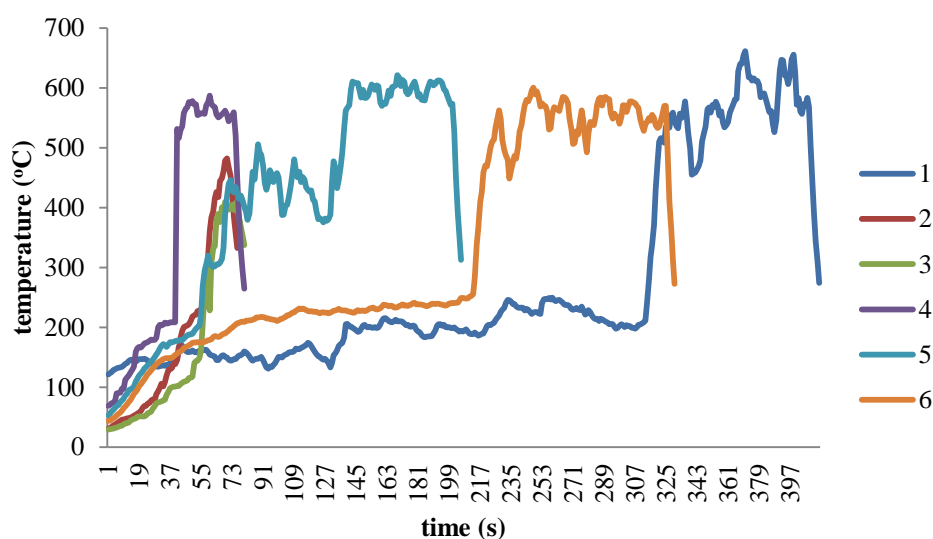


Figure 5.12: Time-temperature profiles of six 100% acrylic + porcine bone samples (EE)

5.5.2.5 Porcine Bone + 50% Acrylic + 50% Cotton (FF)

The pyrolysis of 50% acrylic + 50% cotton in the presence of porcine bone generated fewer but similar types of pyrolysis products as compared to (EE), as detailed in Table 5.6. A representative total ion chromatogram of combined sample (FF) is illustrated in Figure 5.13.

Poor reproducibility was noted in the combined samples (FF) as the majority of the pyrolysis products generated were detected in half or less of the repeats. From the 77 compounds detected, only 20 were present in at least four of the six sets, and these products were mostly *n*-alkanes and *n*-alkenes, together with a furan, limonene, toluene and cyclo-alkane. Half of the sets (sets 1, 2, 6) produced a considerable number of pyrolysis products (58, 68 and 65, respectively) whereas the other half (sets 3, 4, 5) generated fewer products (29, 28 and 16, respectively). Limonene detected here is attributed to the used textile utilised in this study.

All of the pyrolysis products generated by porcine bone (Table 2.3) were present in the combined samples (FF) with the exception of octane, propyl-benzene and hexadecanitrile. While octane was absent in the previous combined samples (AA), (BB), (DD) and (EE), the absence of propyl-benzene and hexadecanitrile in the combined samples (FF) was a new observation. Sixteen products from the pyrolysis of 50% acrylic + 50% cotton (F) (Table 4.17) were detected in the combined samples (FF): these included a range of nitriles and their derivatives, aromatics, pyrazine, pyrrole and a furan. From the sixteen products detected, only 2,5-dimethyl-furan is attributed from the cotton counterpart in the combined samples, as cellulose in cotton generates a range of furans during pyrolysis [94, 95, 97-100] and it was also present in the pyrolysis of 100% cotton (A). None of the acid esters, ketones and sugar, indicative of cotton, detected in (F) was present in the combined samples (FF).

Table 5.6: Pyrolysis products generated from 50% acrylic + 50% cotton in the presence of porcine bone (FF) across six repeats

No	Retention Time (min)	Compound	Molecular Structure	Set					
				1	2	3	4	5	6
1	2.82	propanenitrile			√				
2	3.13	2-methyl-2-propenenitrile			√				
3	3.13	1,5-hexadiene		√					√
4	3.38	isobutyronitrile			√				√
5	3.62	3-methyl-cyclopentene		√	√				√
6	3.94	methyl-cyclopentane			√				√
7	4.27	benzene		√	√		√		√
8	5.11	cyclohexene		√	√				
9	5.14	pentanal			√	√			
10	5.61	2-methyl-butanenitrile			√				√
11	5.71	3-methyl-butanenitrile							√
12	5.72	2,5-dimethyl-furan			√				
13	6.32	1-methyl-1H-pyrrole		√	√				√
14	6.49	dimethyl disulfide							√
15	6.70	vinyl-cyclopentane		√	√				
16	6.90	pentanenitrile			√				
17	7.20	toluene		√	√		√	√	√
18	7.44	1-methyl-cyclohexene		√	√				√
19	7.60	1,7-octadiene		√					√
20	7.61	2-propyl-furan			√	√			√
21	7.70	hexanal			√	√			
22	7.97	1-octene		√	√		√	√	√
23	8.00	1-ethyl-1H-pyrrole		√	√				√
24	8.29	2-octene		√	√				√
25	8.33	4-methyl-pentanenitrile		√	√				√
26	8.45	octene isomer		√	√				√
27	8.53	bicyclooctane		√	√				√
28	8.58	cyclooctene		√	√				√
29	9.04	1-methylethyl-cyclopentane		√	√				√

Table 5.6 continued

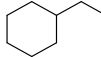
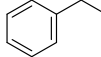
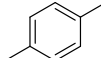
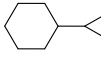
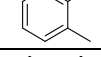
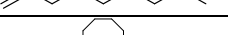
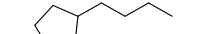
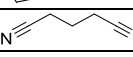
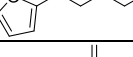
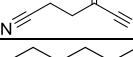
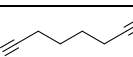
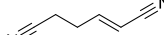
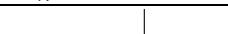
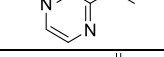
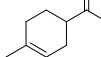
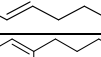
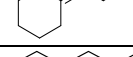
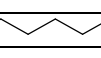
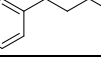
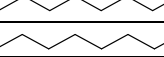
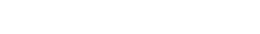
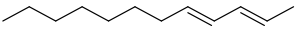
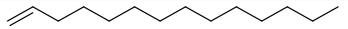
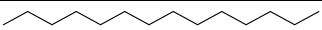
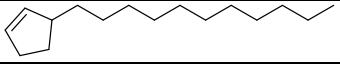
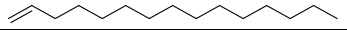
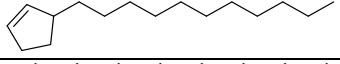
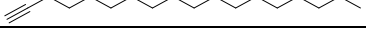
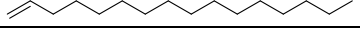
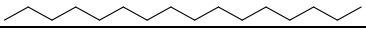
30	9.09	2-ethyl-cyclohexane		√	√				√
31	9.15	ethyl-benzene		√	√				√
32	9.31	<i>p</i> -xylene		√	√				√
33	9.58	cyclopropyl-cyclohexane		√	√				√
34	9.67	heptanal			√	√			
35	9.70	<i>o</i> -xylene		√					√
36	9.80	1-nonene		√	√	√	√	√	√
37	9.93	cyclooctane		√	√				√
38	10.01	nonane		√	√			√	√
39	10.06	2-nonene		√	√				√
40	10.53	butyl-cyclopentane		√	√				√
41	11.05	pentanedinitrile			√	√			
42	11.19	2-pentyl-furan		√	√	√	√		√
43	11.25	2-methylene-pentanedinitrile				√			
44	11.30	1-decene		√	√	√	√	√	√
45	11.41	hexanedinitrile			√	√	√		
46	11.46	decane		√	√	√		√	√
47	11.56	hexenedinitrile			√	√			√
48	11.61	(1-methylethenyl)-pyrazine			√	√			√
49	11.74	limonene		√	√		√		√
50	11.88	2-octenal				√			√
51	12.06	butyl-benzene		√	√				√
52	12.28	propylidencyclohexane		√	√		√		√
53	12.48	nonanal				√			√
54	12.58	1-undecene		√	√	√	√	√	√
55	12.68	undecane		√	√		√		√
56	12.80	2-undecene		√	√				√
57	12.87	cycloundecene		√	√				√
58	12.96	3-hexyl-cyclopentene		√	√				√
59	13.11	pentyl-benzene		√	√				√
60	13.52	1-dodecene		√	√	√	√	√	√
61	13.63	dodecane		√	√	√	√	√	√

Table 5.6 continued

62	13.93	cyclododecene		√	√				√
63	14.28	2,4-dodecadiene		√	√				√
64	14.60	1-tridecene		√	√	√	√	√	√
65	14.73	tridecane		√	√	√	√	√	√
66	15.56	1-tetradecene		√	√	√	√	√	√
67	15.65	tetradecane		√	√	√	√	√	√
68	16.14	nonyl-cyclopentane		√	√				√
69	16.40	1-pentadecene		√	√	√	√	√	√
70	16.56	pentadecane		√	√	√	√	√	√
71	17.01	nonyl-cyclohexane		√	√				√
72	17.10	1-octadecyne		√	√				√
73	17.24	1-hexadecene		√	√	√	√		√
74	17.32	hexadecane		√	√	√	√		√
75	17.96	1-heptadecene		√	√	√	√		√
76	17.98	2-heptadecene		√	√	√			√
77	18.01	heptadecane		√	√	√	√		√

A b u n d a n c e

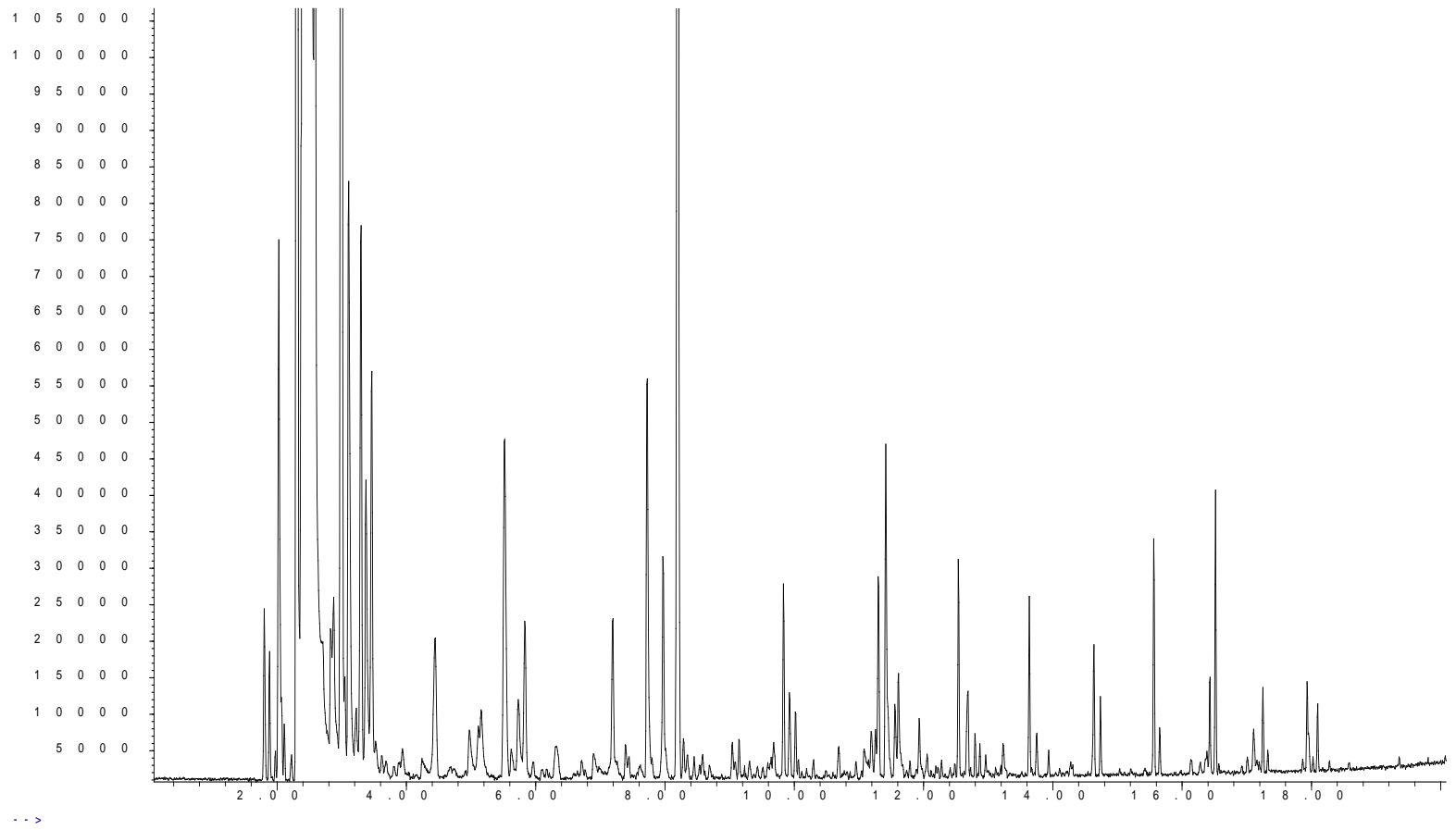


Figure 5.13: A representative TIC of porcine bone + 50% acrylic + 50% cotton (FF) (set 2)

A distinctive difference was noted in 50% acrylic + 50% cotton (F) as compared to 50% cotton + 50% modal (D) and 100% acrylic (E): *n*-alkanes or *n*-alkenes were present in (D) and (E) but not in (F). In the combined samples (FF), the range of *n*-alkanes and *n*-alkenes were present. A range of nitriles and their derivatives and pyrazine that served as key indicators of 50% acrylic + 50% cotton (F) were present in the combined samples (FF). The remaining key indicators (pyridine, piperidine, cyanic and isocyanic compounds), detected in (F) were not present in combined samples (FF). Similar to (EE), the pyrolytic profile of combined samples (FF) had equal dominance from 50% acrylic + 50% cotton (F) and porcine bone, with 16 and 23 key indicators detected, respectively.

The combined samples (FF) also generated the additional presence of *n*-aldehydes, dienes, cyclic compounds, *n*-alkyl-benzenes, pyrroles, alkyne and sulfide that were not documented to be present in either of the individual samples. As in the combined samples (EE), majority of these products were noted to have been previously generated, although inconsistently, from the porcine bone samples (Appendix 1.0). Of the *n*-aldehydes present in the combined samples (FF), pentanal, hexanal and heptanal were detected in sets 2 and 3 while 2-octenal and nonanal were present in sets 3 and 6.

As evidenced by the temperature profiles across the six sets of repeats (Figure 5.14), all of the sets experienced large temperature fluctuations with most demonstrating a series of flame emissions during the burning process. Sets 1 and 5 experienced two flaming episodes; (1) the first upon heat application but was not self-sustaining and (2) the second flare that occurred much later. The initial flames were sustained in sets 2, 3, 4 and 6, experiencing fluctuations throughout except in set 4. The series of flames experienced across the sets is believed to be due the separate auto-ignition of: (1) porcine bone, which could have increased the temperatures in the tin to cause (2) the auto-ignition of the acrylic-cotton blend, as 50% acrylic + 50% cotton was part of the group of textiles that did not auto-ignite with the exception of one sample (Table 4.11 and Figure 4.20), and / or (3) as the interaction between bone and the textile, as seen in combined samples (AA), (BB), (DD) and (EE). Maximum temperatures

attained across the six sets of repeats of (FF) were 616-692 °C, higher than those attained in the combined samples (EE).

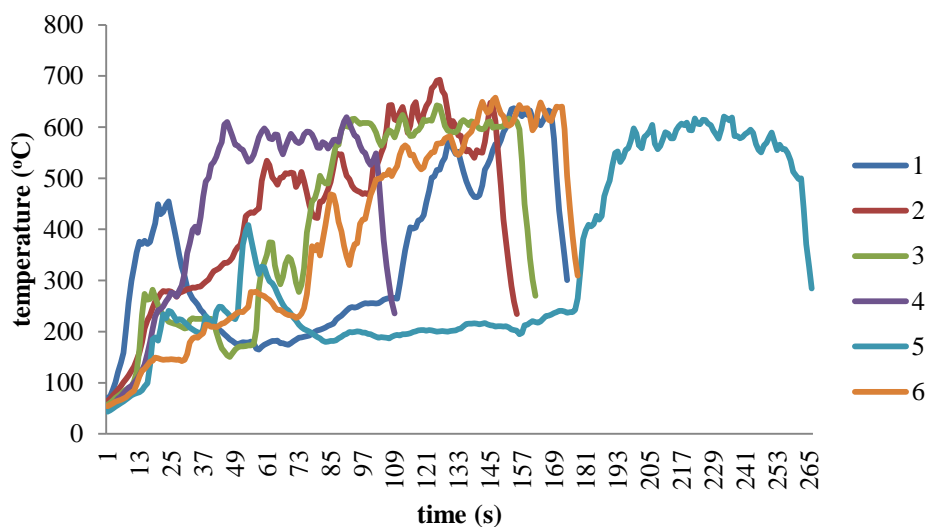


Figure 5.14: Time-temperature profiles of six 50% acrylic + 50% cotton + porcine bone samples (FF)

Similar to the cotton blends (AA, BB and DD), the presence of additional pyrolysis products detected in (EE) and (FF) could have been generated by the pyrolysis of: (1) porcine bone, (2) the textile, and / or (3) through the pyrolytic interactions between the two samples.

5.5.2.6 Porcine Bone + 80% Nylon + 20% Elastin (HH)

The pyrolysis of 80% nylon + 20% elastin in the presence of porcine bone generated a variety of products, particularly *n*-alkane / methyl-alkane / methylene nitrile, together with *n*-alkanes, *n*-alkenes, *n*-cycloalkanes and *n*-cycloalkenes, *n*-aldehydes, pyrrole, aromatics, *n*-alkyl-benzenes, dienes, furans, *n*-alkynes, cyano-alkenes, sulfide, ketone, acid, methyl acid and caprolactam (Table 5.7). A representative total ion chromatogram of the combined sample (HH) is illustrated in Figure 5.15.

In combined samples (HH), 47 out of the 86 compounds detected were present in at least four of the six repeats. These products were mainly aromatics, *n*-alkanes, *n*-alkenes, *n*-cycloalkenes, *n*-alkyl-benzenes, methyl-alkane / alkane nitriles, limonene, caprolactam, alkyne, ketone, pyrrole and a furan. Set 6 generated the highest number of pyrolysis products (76), followed closely by sets 1 and 5 (62 and 72, respectively);

set 2 had the lowest number of pyrolysis products (26). Similar to the other combined samples, limonene detected here is attributed to having generated from the used textile utilised in this work.

All of the pyrolysis products generated by porcine bone (Table 2.3) were present in the combined samples (HH) with the exception of octane. Twenty-one products from the pyrolysis of 80% nylon + 20% elastin (H) (Table 4.18) were present in the combined samples (HH). These products included a range of nitriles and their derivatives, cyano-alkenes, diene, acid, caprolactam, aromatics, *n*-alkanes and *n*-alkenes. The aromatics, *n*-alkanes and *n*-alkenes detected in the combined samples (HH) were also present in the porcine bone samples. In the combined samples (HH), the only key indicator of nylon that was present was caprolactam. Lactam and caprolactone-based compounds, together with *n*-butyl ether and dibutyl ether, were not present. Hexenoic acid and 6-cyano-1-hexene detected across both (H) and (HH) samples could potentially be useful indicators of nylon 6; however both compounds were only present in three or less of the repeats in both the individual textile (H) and the combined (HH) samples. 6-cyano-1-hexene was also present in one of the six sets of repeats of porcine bone pyrolysis (Appendix 1.0). Similar to (AA), (BB) and (DD), the presence of key indicators of porcine bone dominated the pyrolytic profile of the combined samples (HH) in comparison to the presence of key indicators of textile (80% nylon + 20% elastin).

The combined samples also generated additional *n*-aldehydes, dienes, cyclic compounds, *n*-alkyl-benzenes, *n*-alkynes, methyl-alkane / methylene- nitrile, sulfide, methyl acid and pyrrole that were not present consistently in either of the textile or porcine bone samples. *n*-Aldehydes of 3-methyl-butanal, pentanal, hexanal and octanal were present across sets 1 and 2 while butanal and heptanal were only present in set 2.

Table 5.7: Pyrolysis products generated from 80% nylon + 20% elastin in the presence of porcine bone (HH) across six repeats

No	Retention Time (min)	Compound	Molecular Structure	Set					
				1	2	3	4	5	6
1	2.82	propanenitrile							√
2	3.10	butanal			√				
3	3.13	1,5-hexadiene						√	√
4	3.37	2-methyl-furan		√					
5	3.38	isobutyronitrile							√
6	4.12	3-methyl-butanal		√	√				
7	4.25	butanenitrile						√	√
8	4.27	benzene		√	√	√	√	√	√
9	4.74	2-methyl-1,3-pentadiene						√	√
10	5.11	cyclohexene					√	√	√
11	5.14	pentanal		√	√				
12	5.61	2-methyl-butanenitrile				√	√	√	√
13	5.71	3-methyl-butanenitrile				√	√	√	√
14	6.49	dimethyl disulfide				√			√
15	6.90	pentanenitrile						√	√
16	7.20	toluene		√		√	√	√	√
17	7.44	1-methyl-cyclohexene						√	√
18	7.60	1,7-octadiene						√	√
19	7.70	hexanal		√	√				
20	7.97	1-octene		√		√	√	√	√
21	8.00	1-ethyl-1H-pyrrole		√		√	√	√	√
22	8.29	2-octene		√			√	√	√
23	8.33	4-methyl-pentanenitrile		√		√	√	√	√
24	8.45	octene isomer		√			√	√	√
25	8.53	bicyclooctane						√	√
26	8.67	5-cyano-1-pentene		√				√	√
27	9.08	hexanenitrile		√		√	√	√	√
28	9.15	ethyl-benzene		√		√	√	√	√
29	9.23	2,4-octadiene						√	√
30	9.31	p-xylene		√				√	√
31	9.44	4-butoxy-1-butene						√	√

Table 5.7 continued

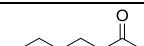
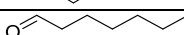
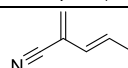
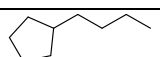
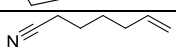
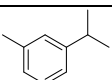
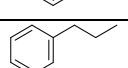
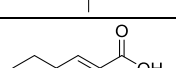
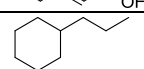
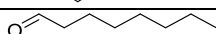
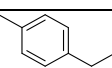
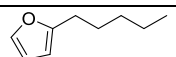
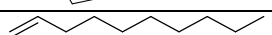
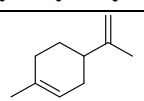
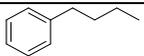
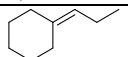
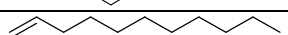
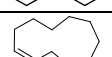
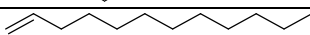
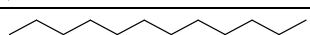
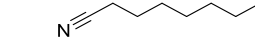
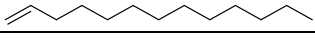
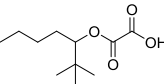
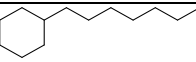
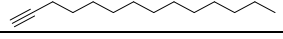
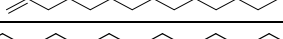
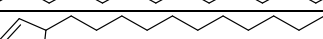
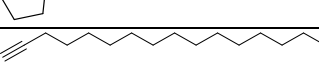
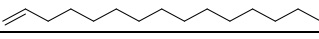
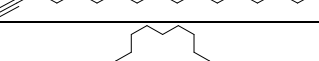
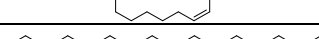
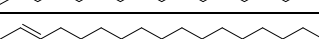
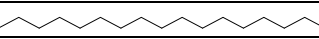
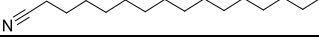
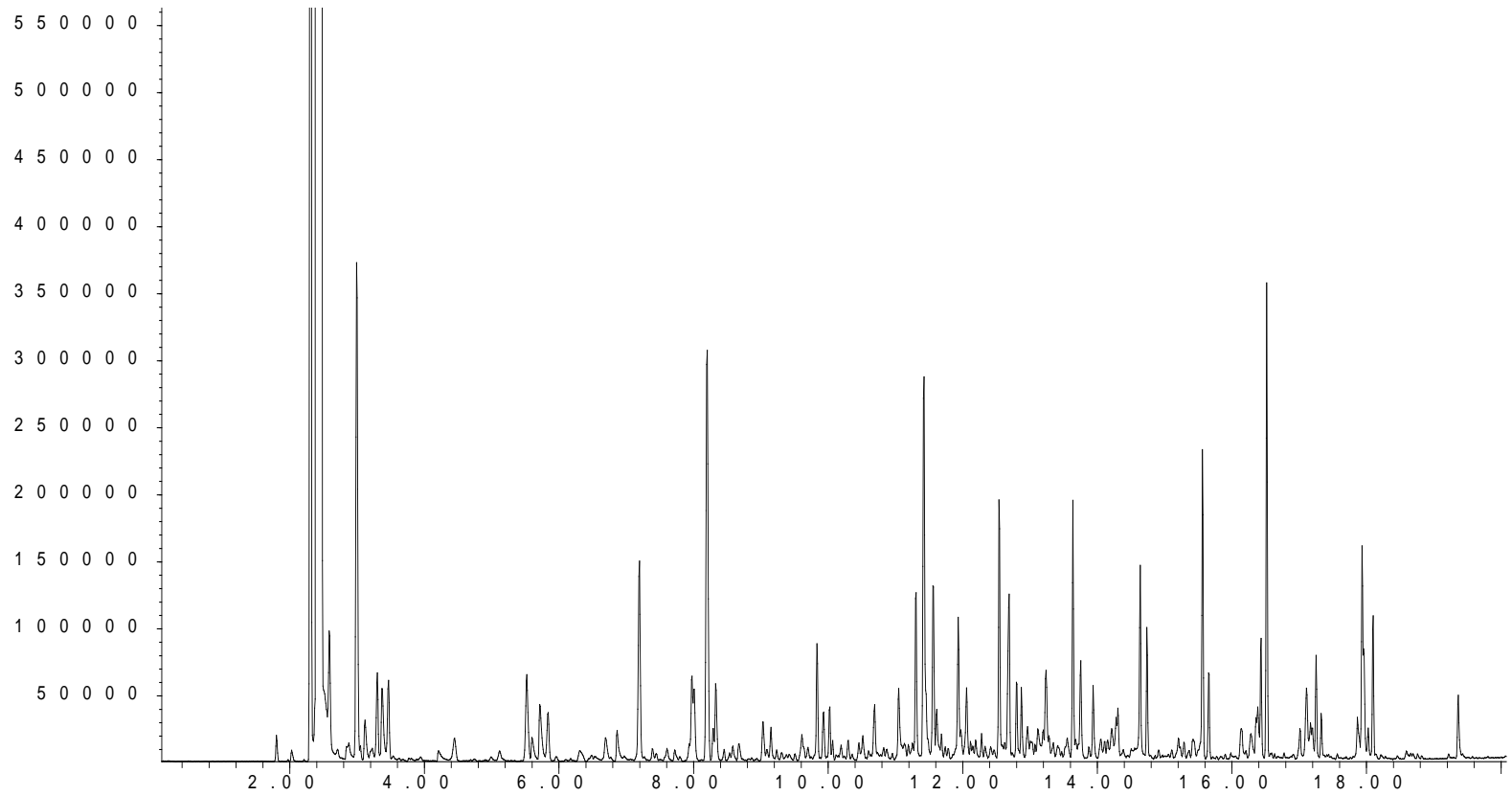
32	9.50	2-heptanone		√	√			√	
33	9.62	styrene					√	√	√
34	9.67	heptanal			√				
35	9.70	<i>o</i> -xylene						√	√
36	9.74	2-methylene- petanenitrile		√				√	√
37	9.80	1-nonene		√	√	√	√	√	√
38	9.93	cyclooctane		√			√	√	√
39	10.01	nonane		√		√	√	√	√
40	10.06	2-nonene		√			√	√	√
41	10.21	nonene isomer						√	√
42	10.51	butyl-cyclopentane						√	√
43	10.52	6-cyano-1-hexene		√				√	√
44	10.65	1-methyl-3-(1- methylethyl)- benzene			√	√		√	√
45	10.69	propyl-benzene		√		√	√	√	√
46	10.82	1,3,5-trimethyl- benzene		√				√	√
47	10.83	hexenoic acid		√					
48	10.85	propyl- cyclohexane		√				√	√
49	10.96	octanal		√	√				
50	11.03	1-ethyl-4-methyl- benzene		√				√	√
51	11.19	2-pentyl-furan		√	√	√	√		√
52	11.30	1-decene		√	√	√	√	√	√
53	11.46	decane		√		√	√	√	√
54	11.74	limonene		√	√		√	√	√
55	12.06	butyl-benzene		√	√		√	√	√
56	12.28	propylidencyclo hexane		√				√	√
57	12.58	1-undecene		√	√	√	√	√	√
58	12.68	undecane		√		√	√	√	√
59	12.80	2-undecene		√		√	√	√	√
60	12.87	cycloundecene		√		√		√	√
61	13.11	pentyl-benzene		√		√	√	√	√
62	13.52	1-dodecene		√	√	√	√	√	√
63	13.63	dodecane		√	√	√	√	√	√

Table 5.7 continued

64	13.82	caprolactam		√	√	√	√	√	√
65	13.93	cyclododecene		√					√
66	14.30	octanenitrile		√		√		√	√
67	14.60	1-tridecene		√	√	√	√	√	√
68	14.73	tridecane		√	√	√	√	√	√
69	15.09	oxalic acid, butyl-neopentyl-ester		√					
70	15.21	heptyl-cyclohexane				√	√	√	√
71	15.40	1-tetradecyne		√				√	
72	15.56	1-tetradecene		√	√	√	√	√	√
73	15.65	tetradecane		√	√	√	√	√	√
74	16.14	nonyl-cyclopentane		√		√	√	√	√
75	16.28	1-hexadecyne		√		√		√	√
76	16.40	1-pentadecene		√	√	√	√	√	√
77	16.56	pentadecane		√	√	√	√	√	√
78	17.01	nonyl-cyclohexane		√		√	√	√	√
79	17.10	1-octadecyne		√		√	√	√	√
80	17.17	cyclohexadecene		√		√	√	√	√
81	17.24	1-hexadecene		√	√	√	√	√	√
82	17.32	hexadecane		√		√	√	√	√
83	17.96	1-heptadecene		√		√	√	√	√
84	17.98	2-heptadecene		√		√	√	√	√
85	18.01	heptadecane		√		√	√	√	√
86	19.36	hexadecanenitrile				√	√	√	√

Abundance



Time -->

Figure 5.15: A representative TIC of porcine bone + 80% nylon + 20% elastin (HH) (set 6)

The temperature profiles of the six sets of repeats (Figure 5.16) illustrate fluctuations in the temperatures attained, as observed in a number of previous combined samples. While the initial flames were sustained in set 1 with fluctuations throughout, sets 2 and 3 experienced similar fluctuations but with two distinctive flaming episodes instead. Set 5 experienced similar patterns to sets 2 and 3 but with shorter burning durations between the first and second flaming events. Set 4 took the longest to auto-ignite, exhibiting the first signs of auto-ignition at 346 seconds; and the second flame at 437 seconds while set 6 experienced three flaming episodes, at 138 seconds, 160 seconds and 253 seconds, respectively.

The flaming events and the presence of additional pyrolysis products detected in the combined samples (HH) could have been generated by the pyrolysis of: (1) porcine bone, (2) the nylon-elastin blend, as 80% nylon + 20% elastin was part of the group of textiles that auto-ignited with the exception of two (Table 4.11 and Figure 4.22), and / or (3) the pyrolytic interactions between the two samples. Maximum temperatures attained across the six sets of repeats were 535-667 °C.

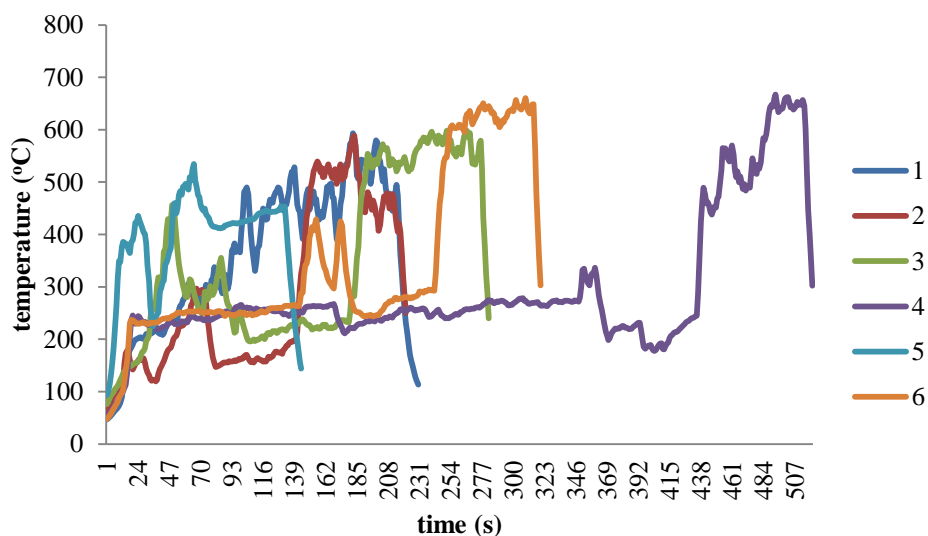


Figure 5.16: Time-temperature profiles of six 80% nylon + 20% elastin + porcine bone samples (HH)

5.5.2.7 Porcine Bone + 100% Denim (JJ)

The pyrolysis of 100% denim in the presence of porcine bone generated 60 products in total, and these products were *n*-alkanes, *n*-alkenes, *n*-cycloalkanes and *n*-cycloalkenes, *n*-aldehydes, aromatics, *n*-alkyl-benzenes, dienes, methyl-alkane nitriles, furans, limonene, alkyne and sulfide as detailed in Table 5.8. A representative total ion chromatogram of the combined sample (JJ) is illustrated in Figure 5.17.

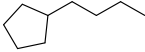
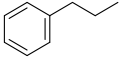
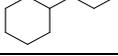
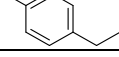
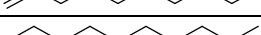
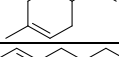
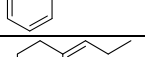
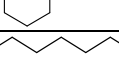
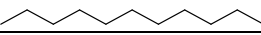
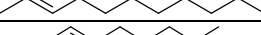
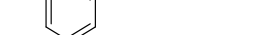
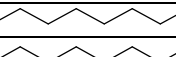
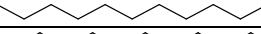
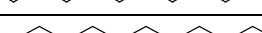
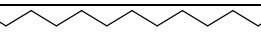
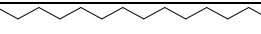
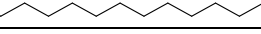
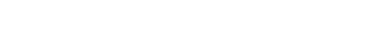
Poor reproducibility was seen in the combined samples (JJ), as only 18 of the 60 products were present in at least four of the six sets of repeats. These products were mainly *n*-alkanes, *n*-alkenes, *n*-cycloalkanes, aromatics, *n*-alkyl-benzenes, a furan and a methyl-alkane nitrile. Set 6 produced the highest number of pyrolysis products (55), while the remaining sets generated relatively few products, with set 2 generating the least (9). Similar to the other combined samples, limonene detected here is attributed to having generated from the used textile utilised in this work.

All of the pyrolysis products generated by porcine bone (Table 2.3) were present in the combined samples (JJ) with the exception of octane and hexadecanitrile. Only six products from the pyrolysis of 100% denim (J) (Table 4.19) were present in the combined samples (JJ). These products were furans (2-methyl-furan, 2,5-dimethyl-furan) and aromatics and *n*-alkyl-benzenes (benzene, toluene, ethyl-benzene, *p*-xylene); the latter group of products were also present in porcine bone. The only two key indicators of denim in the combined samples were 2-methyl-furan and 2,5-dimethyl-furan. No acid, acid esters, ketones or furancarboxyaldehydes, which were detected in 100% denim (J) (Table 4.19), were present in the combined samples (JJ). With only two key indicators of denim present, porcine bone dominated the pyrolytic profile of the combined samples (JJ).

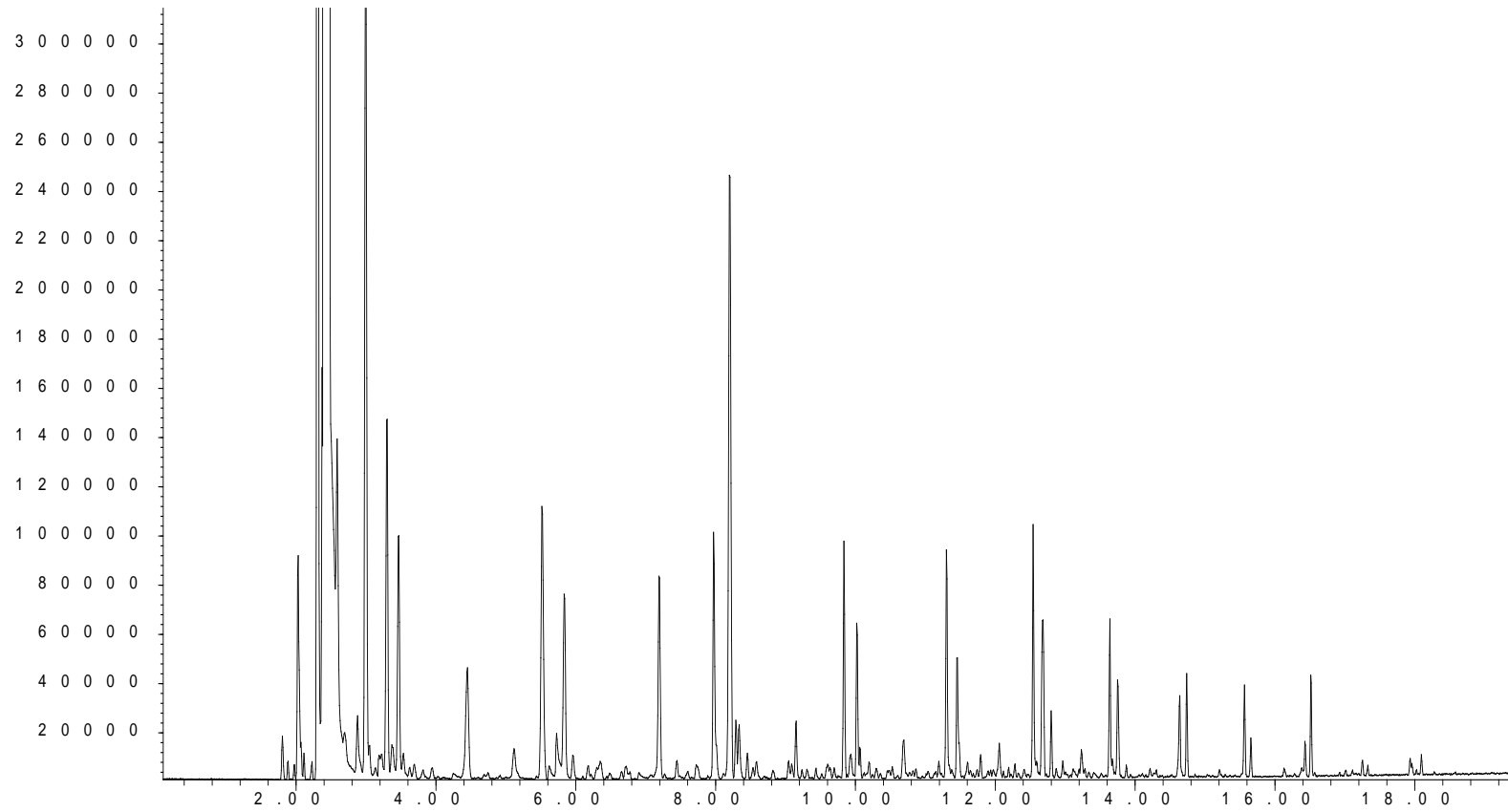
Table 5.8: Pyrolysis products generated from 100% denim in the presence of porcine bone (JJ) across six repeats

No	Retention Time (min)	Compound	Molecular Structure	Set					
				1	2	3	4	5	6
1	3.10	butanal		√		√		√	
2	3.37	2-methyl-furan				√			√
3	3.95	methyl-cyclopentane							√
4	4.12	3-methyl-butanal				√			√
5	4.27	benzene		√	√	√	√	√	√
6	4.74	2-methyl-1,3-pentadiene							√
7	5.11	cyclohexene							√
8	5.14	pentanal		√		√		√	
9	5.61	2-methyl-butanenitrile		√					√
10	5.71	3-methyl-butanenitrile		√			√		√
11	5.75	2,5-dimethyl-furan				√			√
12	6.49	dimethyl disulfide							√
13	7.20	toluene		√		√	√	√	√
14	7.44	1-methyl-cyclohexene							√
15	7.60	1,7-octadiene							√
16	7.70	hexanal		√		√		√	
17	7.97	1-octene		√		√	√	√	√
18	8.29	2-octene				√			√
19	8.33	4-methyl-pentanenitrile		√		√	√		√
20	8.45	octene isomer							√
21	8.53	bicyclooctane							√
22	8.83	1-ethyl-cyclohexane							√
23	9.15	ethyl-benzene		√		√	√	√	√
24	9.31	p-xylene							√
25	9.62	styrene							√
26	9.67	heptanal						√	
27	9.70	o-xylene							√
28	9.80	1-nonene				√	√	√	√
29	10.01	nonane				√	√		√
30	10.06	2-nonene				√			√
31	10.21	nonene isomer							√

Table 5.8 continued

32	10.51	butyl-cyclopentane								√
33	10.69	propyl-benzene								√
34	10.85	propyl-cyclohexane								√
35	11.03	1-ethyl-4-methylbenzene				√	√			√
36	11.19	2-pentyl-furan		√	√	√	√	√	√	√
37	11.30	1-decene				√	√	√	√	√
38	11.46	decane				√	√			√
39	11.74	limonene				√				√
40	12.06	butyl-benzene								√
41	12.28	propylidencyclohexane		√	√	√				√
42	12.58	1-undecene			√	√	√	√	√	√
43	12.68	undecane				√	√			√
44	12.80	2-undecene				√	√			√
45	13.11	pentyl-benzene				√				√
46	13.52	1-dodecene			√	√	√	√	√	√
47	13.63	dodecane				√	√	√	√	√
48	14.60	1-tridecene		√	√	√	√	√	√	√
49	14.73	tridecane				√	√	√	√	√
50	15.56	1-tetradecene			√	√	√	√	√	√
51	15.65	tetradecane				√	√	√	√	√
52	16.40	1-pentadecene		√		√	√	√	√	√
53	16.56	pentadecane		√	√	√	√	√	√	√
54	17.01	nonyl-cyclohexane		√	√					√
55	17.10	1-octadecyne								√
56	17.24	1-hexadecene								√
57	17.32	hexadecane								√
58	17.96	1-heptadecene								√
59	17.98	2-heptadecene								√
60	18.01	heptadecane								√

A b u n d a n c e



T i m e -->

Figure 5.17: A representative TIC of porcine bone + 100% denim (JJ) (set 6)

The combined samples also generated additional *n*-aldehydes, dienes, cyclic compounds, *n*-alkyl-benzenes, methyl-alkane nitrile, alkyne and sulfide that were not present in either of the individual samples. However, these compounds were noted to be present in the cotton and cotton blends in other combined samples (AA), (BB) and (DD). The majority of these compounds, with the exception of *n*-aldehydes and an alkyne, were also noted to have generated, although inconsistently, from porcine bone samples (Appendix 1.0). *n*-Aldehydes of butanal, pentanal and hexanal were present across sets 1, 3 and 5, 3-methyl-butanal was only present in sets 3 and 6, and heptanal was only present in set 5.

The temperature profiles of the six sets of repeats are illustrated in Figure 5.18. Sets 1, 3 and 4 experienced two sharp rises in temperature upon auto-ignition whereas in sets 2 and 5, auto-ignition at the initial stages of heat application generated flames that were self-sustaining. With only nine products detected, the rapid onset of auto-ignition and the short burning duration in set 2 could have prevented the generation of more pyrolysis products. Set 6, with the highest number of products detected experienced three distinctive flaming episodes, whereby the first two extinguished; the final burst of flames that occurred at 759 seconds was self-sustaining, peaking at 615 °C.

The occurrence of flames and the presence of additional pyrolysis products detected in the combined samples (JJ) could have been generated by the pyrolysis of: (1) porcine bone, which could have raised the temperatures in the tin, thus facilitating (2) the auto-ignition of denim, as 100% denim was part of the group of textiles in which four of the six samples did not auto-ignite (Table 4.11 and Figure 4.24), and / or (3) through the pyrolytic interactions between the two samples. Maximum temperatures attained across the six sets of repeats were 519-663 °C.

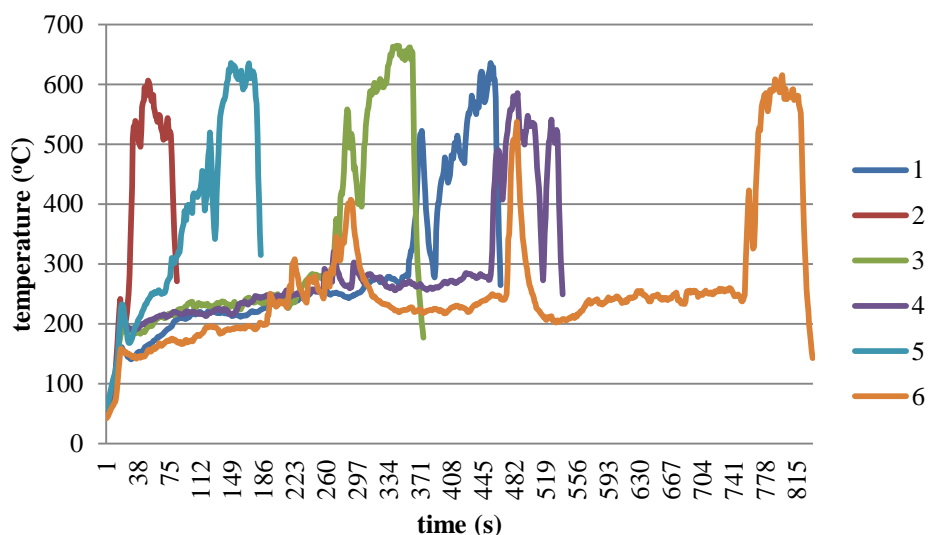


Figure 5.18: Time-temperature profiles of six 100% denim + porcine bone samples (JJ)

5.5.2.8 Porcine Bone + 96% Wool + 4% LYCRA® (LL)

The pyrolysis of 96% wool + 4% lycra® in the presence of porcine bone generated *n*-alkanes, *n*-alkenes, *n*-cycloalkanes and *n*-cycloalkenes, *n*-aldehydes, aromatics, *n*-alkyl-benzenes, dienes, methyl / iso / methyl-alkane nitriles, furans, limonene, pyrrole and sulfide as detailed in Table 5.9. A representative total ion chromatogram of combined sample (LL) is illustrated in Figure 5.19.

Reproducibility was also poor in combined samples (LL) as less than a quarter (17) of the 70 compounds generated were present in at least four of the six repeats. They were mainly *n*-alkanes, *n*-alkenes, aromatics, *n*-cycloalkanes, one *n*-cycloalkene and a furan. Sets 2 and 4 produced the highest number of pyrolysis products (68 and 70, respectively), whereas few products were detected in sets 1 and 6 (3 and 4, respectively). The presence of limonene is attributed to having generated from the used textile utilised in this work.

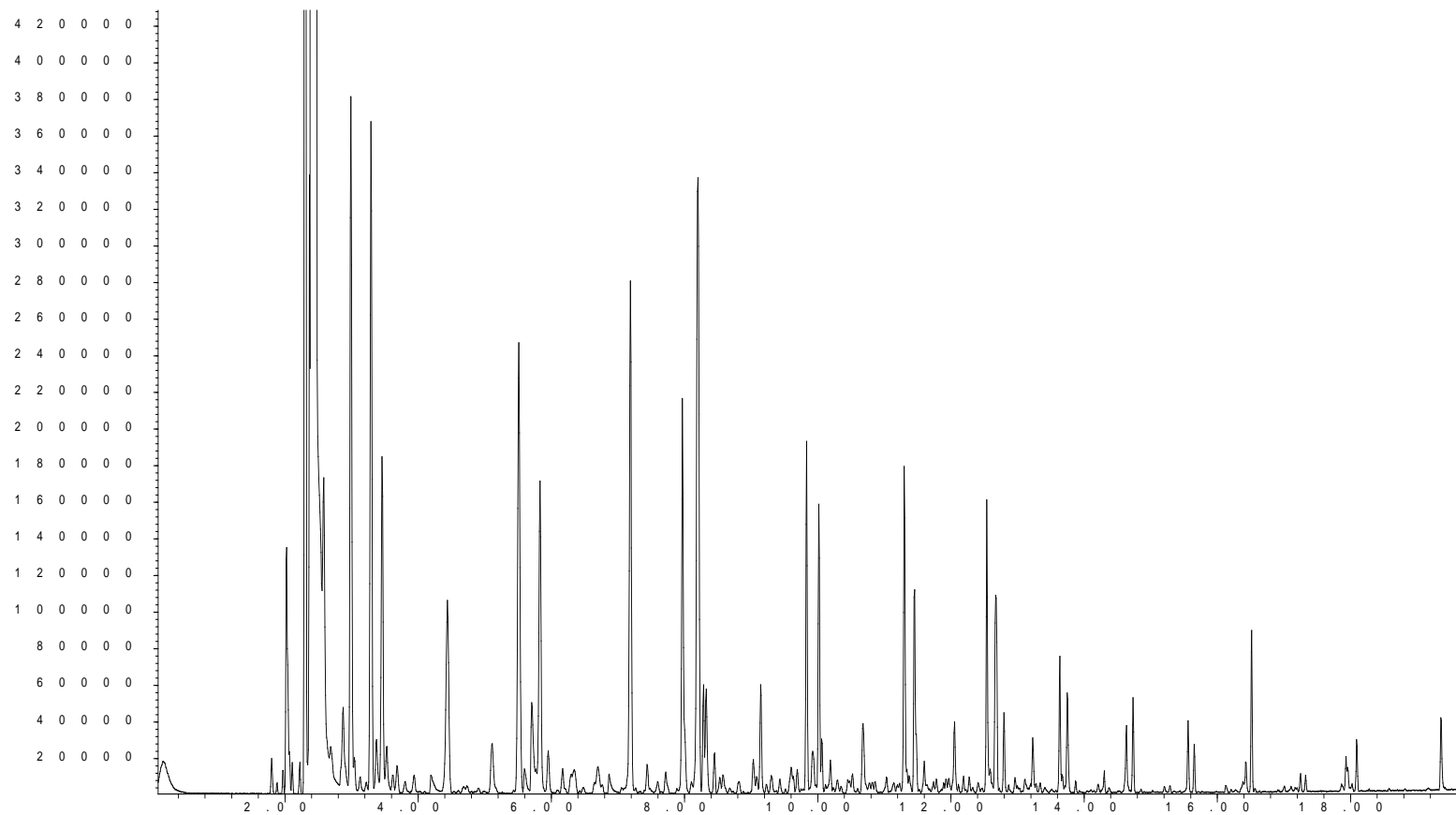
Table 5.9: Pyrolysis products generated from 96% wool + 4% LYCRA® in the presence of porcine bone (LL) across six repeats

No	Retention Time (min)	Compound	Molecular Structure	Set					
				1	2	3	4	5	6
1	3.37	2-methyl-furan			√		√	√	
2	3.38	isobutyronitrile			√		√		
3	3.67	3-methyl-cyclopentene			√		√	√	
4	3.95	methyl-cyclopentane			√	√	√	√	
5	4.2	butanenitrile			√		√		
6	4.27	benzene			√	√	√	√	√
7	5.11	cyclohexene			√	√	√	√	√
8	5.14	pentanal		√					
9	5.61	2-methyl-butanenitrile			√		√	√	
10	5.71	3-methyl-butanenitrile			√		√	√	
11	6.49	dimethyl disulfide			√		√		
12	6.70	vinyl-cyclopentane			√		√		
13	7.20	toluene			√		√	√	√
14	7.44	1-methyl-cyclohexene			√		√	√	
15	7.60	1,7-octadiene			√		√		
16	7.70	hexanal		√					
17	7.97	1-octene			√		√	√	√
18	8.00	1-ethyl-1H-pyrrole			√		√	√	
19	8.29	2-octene			√		√	√	
20	8.33	4-methyl-pentanenitrile			√		√	√	
21	8.45	octene isomer			√		√	√	
22	8.53	bicyclooctane			√		√		
23	8.58	cyclooctene			√		√		
24	8.83	1-ethyl-cyclohexane			√		√		
25	9.04	1,6-undecadiene			√		√		
26	9.15	ethyl-benzene			√		√	√	√
27	9.31	<i>p</i> -xylene			√		√	√	
28	9.44	3-ethyl-cyclohexene			√		√		
29	9.62	styrene			√		√		
30	9.64	1,8-nonadiene			√		√		
31	9.70	<i>o</i> -xylene			√		√		
32	9.80	1-nonene			√		√	√	√

Table 5.9 continued

33	9.93	cyclooctane			√		√		
34	10.01	nonane			√		√	√	√
35	10.06	2-nonene			√		√	√	
36	10.21	nonene isomer			√		√	√	
37	10.30	1-propenyl-cyclohexane			√		√		
38	10.48	propyl-cyclohexane			√		√		
39	10.51	butyl-cyclopentane			√		√		
40	10.69	propyl-benzene			√		√	√	
41	11.03	1-ethyl-4-methyl-benzene			√		√		
42	11.19	2-pentyl-furan		√	√		√	√	
42	11.30	1-decene			√		√	√	
43	11.46	decane			√		√	√	√
44	11.60	5-decene			√		√	√	
45	11.74	limonene			√		√		
46	12.06	butyl-benzene			√		√	√	
47	12.28	propylidencyclohexane		√	√	√	√	√	√
48	12.58	1-undecene			√		√	√	√
49	12.68	undecane			√		√	√	√
50	12.80	2-undecene			√		√	√	
51	12.96	3-hexyl-cyclopentene			√		√		
52	13.11	pentyl-benzene			√		√		
53	13.38	(1,2-dimethylpropyl)-benzene					√		
54	13.52	1-dodecene			√		√	√	
55	13.63	dodecane			√		√	√	
56	13.87	3-dodecene			√		√		
57	14.30	hexyl-benzene			√		√		
58	14.60	1-tridecene			√		√	√	√
59	14.73	tridecane			√		√	√	√
60	15.29	heptyl-benzene			√		√		
61	15.56	1-tetradecene			√		√	√	
62	15.65	tetradecane			√		√	√	√
63	16.40	1-pentadecene			√		√	√	
64	16.56	pentadecane			√		√	√	√
65	17.01	nonyl-cyclohexane			√		√		
66	17.24	1-hexadecene			√		√		
67	17.32	hexadecane			√		√		
68	17.96	1-heptadecene			√		√		
69	18.01	heptadecane			√		√		√
70	19.36	hexadecanitrile					√		

A b u n d a n c e



T i m e -->

Figure 5.19: A representative TIC of porcine bone + 96% wool + 4% LYCRA[®] (LL) (set 6)

With the exception of octane, all of the compounds detected in the pyrolysis of porcine bone (Table 2.3) were detected in the combined samples (LL). Although none of the key indicators of the wool-lycra[®] blend (L) detailed in Table 4.20 (i.e. phenol, 4-methyl-phenol and α -amino acids) were present in the combined samples (LL), nitriles (isobutyronitrile, butanenitrile, 2-methyl-butanenitrile, 3-methyl-butanenitrile, 4-methyl-pentanenitrile), *n*-alkyl-benzenes and aromatics (benzene, toluene, ethyl-benzene, *p*-xylene, styrene, propyl-benzene, 1-methylethyl-benzene,) that were present in the (L) samples were also detected in the combined samples (LL). The aromatic compounds (benzene, toluene, ethyl-benzene, *p*-xylene, propyl-benzene) detected here were also present in the pyrolysis of porcine bone. Once again, porcine bone dominated the pyrolytic profile of the combined samples (LL), as no key indicators of the wool-lycra[®] blend was seen to be present. Similar to the other combined samples, (LL) also generated additional *n*-aldehydes, furans, dienes, cyclic compounds, *n*-alkyl-benzenes, pyrroles and sulfide that were not present consistently in either of the wool-lycra[®] or porcine bone samples.

As evidenced by the temperature profiles across the six sets of repeats (Figure 5.20), all of the sets experienced temperature fluctuations with a series of flaming emissions. Sets 3, 4 and 6 each experienced two distinctive auto-ignitions while sets 1 and 5 each experienced three flaming emissions. In set 2, four distinctive auto-ignitions of the materials were observed, at 448 °C (40 seconds), 367 °C (130 seconds), 521 °C (370 seconds) and 600 °C (571 seconds).

The occurrence of flames and the additional pyrolysis products detected in the combined samples (LL) could have been generated by the pyrolysis of: (1) porcine bone, which could have raised the temperatures in the tin, facilitating (2) the auto-ignition of the wool-lycra[®] blend as it was part of the group of textiles that did not auto-ignite (Table 4.11 and Figure 4.26), and / or (3) through the pyrolytic interactions between the two samples. Maximum temperatures attained across the repeats were 528-664 °C.

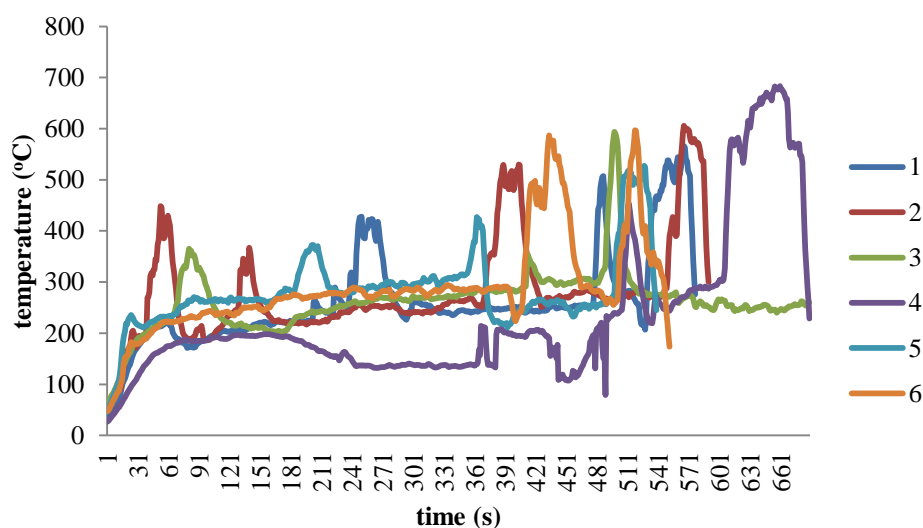


Figure 5.20: Time-temperature profiles of six 96% wool + 4% LYCRA[®] + porcine bone samples (LL)

5.5.2.9 Porcine Bone + 64% Polyester + 33% Rayon + 3% Elastin (NN)

The pyrolysis of 64% polyester + 33% rayon + 3% elastin in the presence of porcine bone generated a range of products: *n*-alkanes, *n*-alkenes, *n*-cycloalkanes and *n*-cycloalkenes, *n*-aldehyde, aromatics, *n*-alkyl-benzenes, dienes, benzo / *n*-alkane / methyl-alkane nitriles, furans, pyrroles, limonene, ketone, an alkyne and a sulfide as detailed in Table 5.10. A representative post heat application of combined sample (NN) is illustrated in Figure 5.21.

Combined samples (NN) displayed good reproducibility as 46 of the 81 products detected, were present in at least four of the six repeats. These products were mainly *n*-alkanes, *n*-alkenes, methyl-alkane and alkane nitriles, aromatics, *n*-alkyl-benzenes, *n*-cycloalkanes, furans, pyrroles, limonene and an alkyne. Sets 1 and 2 generated the highest number of pyrolysis products (78 and 80, respectively), whereas set 3 produced the lowest number of products (13). The presence of limonene is attributed to having generated from the used textile utilised in this work.

Table 5.10: Pyrolysis products generated from 64% polyester + 33% rayon + 3% elastin in the presence of porcine bone (NN) across six repeats

No	Retention Time (min)	Compound	Molecular Structure	Set					
				1	2	3	4	5	6
1	3.13	1,5-hexadiene		√	√				
2	3.37	2-methyl-furan		√	√		√	√	√
3	3.67	3-methyl-cyclopentene		√	√				
4	3.81	tetrahydro-furan		√	√				
5	3.95	methyl-cyclopentane		√	√				
6	4.20	butanenitrile		√	√				
7	4.27	benzene		√	√		√	√	√
8	4.57	3-methyl-3-buten-2-one			√				
9	5.11	cyclohexene		√	√				
10	5.61	2-methyl-butanenitrile		√	√		√	√	√
11	5.71	3-methyl-butanenitrile		√	√		√	√	√
12	5.72	2,5-dimethyl-furan		√	√		√	√	√
13	6.32	1-methyl-1H-pyrrole		√	√				
14	6.49	dimethyl disulfide		√	√		√		
15	6.64	ethyl-cyclopentane		√	√				
16	6.70	vinyl-cyclopentane		√	√				
17	6.86	pentanenitrile		√	√				
18	7.20	toluene		√	√		√	√	√
19	7.44	1-methyl-cyclohexene		√	√				
20	7.60	1,7-octadiene		√	√				
21	7.70	hexanal						√	
22	7.97	1-octene		√	√		√	√	√
23	8.00	1-ethyl-1H-pyrrole		√	√		√	√	√
24	8.29	2-octene		√	√			√	√
25	8.33	4-methyl-pentanenitrile		√	√		√	√	√
26	8.45	octene isomer		√	√			√	√
27	8.53	bicyclooctane		√	√				
28	8.58	cyclooctene		√	√				
29	8.83	1-ethyl-cyclohexane		√	√				
30	9.04	1,6-undecadiene		√	√				

Table 5.10 continued

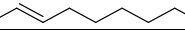
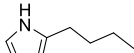
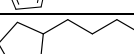
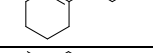
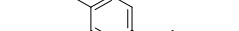
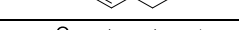
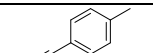
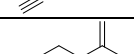
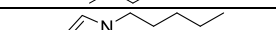
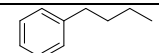
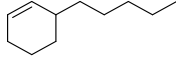
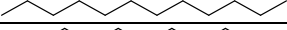
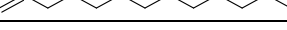
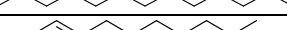
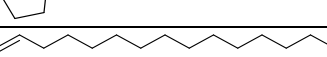
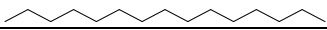
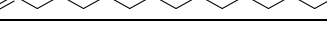
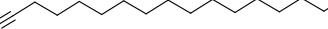
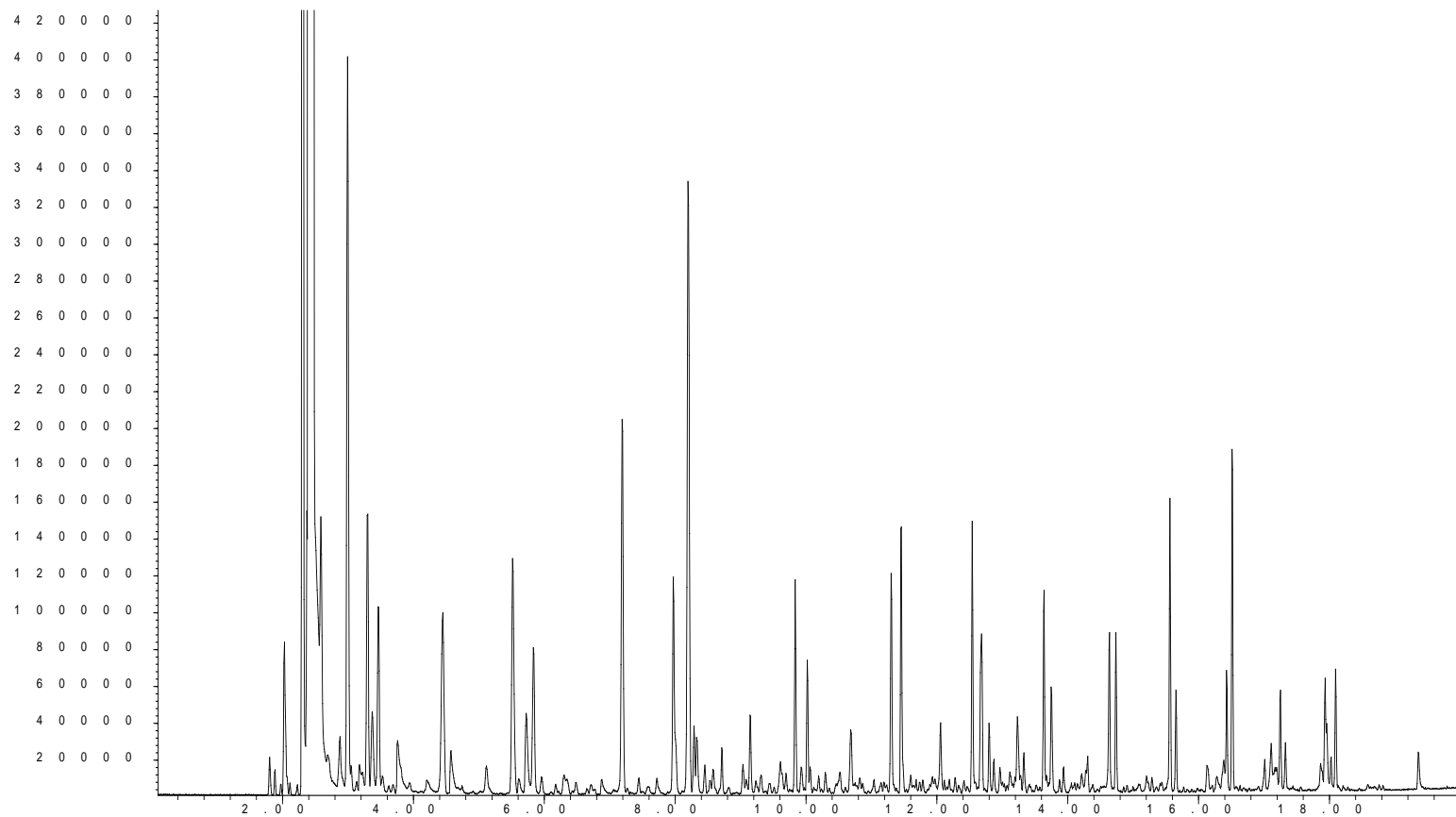
31	9.15	ethyl-benzene		√	√		√	√	√
32	9.31	<i>p</i> -xylene		√	√				
33	9.44	3-ethyl-cyclohexene		√	√				
34	9.62	styrene		√	√				
35	9.70	<i>o</i> -xylene		√	√				
36	9.80	1-nonene		√	√		√	√	√
37	9.93	cyclooctane		√	√				
38	10.01	nonane		√	√		√	√	√
39	10.06	2-nonene		√	√				
40	10.21	nonene isomer		√	√				
41	10.44	1-butyl-1H-pyrrole		√	√		√		
42	10.51	butyl-cyclopentane		√	√				
43	10.69	propyl-benzene		√	√		√	√	√
44	10.74	benzonitrile		√	√				
45	10.78	1-methylethyl-benzene		√	√				
46	10.82	1,3,5-trimethyl-benzene		√	√				
47	10.87	1-propyl-cyclohexene		√	√				
48	11.03	1-ethyl-4-methyl-benzene		√	√				
49	11.19	2-pentyl-furan		√	√	√	√	√	√
50	11.30	1-decene		√	√		√	√	√
51	11.46	decane		√	√		√	√	√
52	11.60	5-decene		√	√				
53	11.66	1-ethynyl-4-methyl-benzene		√	√		√	√	√
54	11.74	limonene		√	√			√	√
55	11.97	1-pentyl-1H-pyrrole		√	√		√	√	√
56	12.06	butyl-benzene		√	√		√	√	√
57	12.58	1-undecene		√	√		√	√	√
58	12.68	undecane		√	√		√	√	√
59	12.80	2-undecene		√	√		√	√	√
60	13.11	pentyl-benzene		√	√		√	√	√

Table 5.10 continued

61	13.27	3-pentyl-cyclohexene			√			√	√
62	13.52	1-dodecene		√	√		√	√	√
63	13.63	dodecane		√	√		√	√	√
64	14.30	hexyl-benzene		√	√		√	√	√
65	14.60	1-tridecene		√	√	√	√	√	√
66	14.73	tridecane		√	√	√	√	√	√
67	15.29	heptyl-benzene		√	√				
68	15.56	1-tetradecene		√	√	√	√	√	√
69	15.65	tetradecane		√	√	√	√	√	√
70	16.14	nonyl-cyclopentane		√	√		√	√	√
71	16.40	1-pentadecene		√	√	√	√	√	√
72	16.56	pentadecane		√	√	√	√	√	√
73	17.01	nonyl-cyclohexane		√	√		√	√	√
74	17.11	1-octadecyne		√	√		√	√	√
75	17.19	cyclohexadecane		√	√		√	√	√
76	17.24	1-hexadecene		√	√	√	√	√	√
77	17.32	hexadecane		√	√	√	√	√	√
78	17.96	1-heptadecene		√	√	√	√	√	√
79	17.98	2-heptadecene		√	√		√	√	√
80	18.01	heptadecane		√	√	√	√	√	√
81	19.36	hexadecanitrile		√	√		√	√	√

A b u n d a n c e



T i m e -->

Figure 5.21: A representative TIC of porcine bone + 64% polyester + 33% rayon + 3% elastin (NN) (set 2)

Similar to the combined samples (AA), (BB), (DD), (HH) and (LL), octane was the only compound from the list of pyrolysis products generated by porcine bone (Table 2.3) that was not detected in combined samples (NN). As with the combined samples (LL), none of the key indicators of the polyester-rayon-elastin blend, detailed in Table 4.21 (i.e. α -methyl-styrene, phenyl and biphenyl compounds, naphthalene and benzoic acid derivatives) were present in the combined samples (NN).

Although no key indicators of the polyester blend were present, a number of products that were present in the 64% polyester + 33% rayon + 3% elastin (N) samples were detected in the combined samples (NN); these products were furans (2-methyl-furan, tetrahydro-furan, 2,5-dimethyl-furan), *n*-alkyl-benzenes and aromatics (benzene, toluene, ethyl-benzene, *p*-xylene, styrene, 1-methylethyl-benzene, propyl-benzene, 1-ethyl-2-methyl-benzene, 1-ethynyl-4-methyl-benzene), nitrile (benzonitrile), ketone (3-methyl-3-buten-2-one), *n*-alkanes and *n*-alkenes (octene, nonene, decene, tridecene, tridecane, tetradecene, pentadecene). The presence of aromatics (benzene, toluene, ethyl-benzene, *p*-xylene, propyl-benzene), *n*-alkanes and *n*-alkenes that were detected in the combined samples (NN) and individual textile (N) were also present in the pyrolysis of porcine bone alone. The furans and 3-methyl-3-buten-2-one detected in the combined samples (NN) are attributed to have generated from the rayon counterpart, as rayon is essentially regenerated cellulose, and known to break down to generate these products [94, 95, 100, 101] plus these products were also detected in the other textile samples containing various forms of cellulose, such as cotton, modal, denim and rayon in textiles (A), (B), (D), (F), (J) and (N); see Tables 4.14-4.16, 4.18 and 4.20. No other key indicators of cellulose (rayon) were detected.

As no key indicators of the polyester-rayon-elastin blend were present, porcine bone dominated the pyrolytic profile of the combined samples (NN) with the majority of its key indicators detected. As with the other combined samples, (NN) also generated additional furans, dienes, cyclic compounds, *n*-alkyl-benzenes, methyl-alkane / alkane nitriles, pyrroles, *n*-aldehyde, alkyne and sulfide that were not present consistently in either of the separate samples. In comparison to other combined

samples, samples (NN) generated the lowest number of *n*-aldehydes with only one, hexanal, detected in set 4.

The time-temperature profiles of the six sets of repeats are displayed in Figure 5.22. Sets 1, 2, 4 and 6 each experienced one auto-ignition with fewer fluctuations in temperature, peaking at 556 °C, 613 °C, 628 °C and 554 °C, respectively. Sets 3 and 5 each underwent three distinctive auto-ignitions. In set 3, initial flaming occurred at 80 seconds with a spike in temperature of 330 °C. The temperature steadily rose, experiencing a second spike at 153 seconds of 540 °C; however, the flames were not self-sustaining and died down. The third temperature increase occurred at 330 seconds and peaked at 600 °C. In set 5, temperatures increased to 419 °C at 100 seconds and dwindled thereafter. The second spike in temperature was noted at 191 seconds to reach 384 °C but, similar to set 3, the flames did not self-sustain and died down. The final temperature increase occurred at 267 seconds to peak at 604 °C.

The flaming events and the presence of additional products could have been a result of: (1) the porcine bone which could have raised the temperatures in the tin, facilitating (3) the auto-ignition of the textile blend, as 64% polyester + 33% rayon + 3% elastin was part of the group of textiles that exhibited an equal mix of auto-ignition as half of the samples auto-ignited but the other half did not (Table 4.11 and Figure 4.28), and / or (4) through the pyrolytic interactions between the two samples. Maximum temperatures attained across the repeats were 554-628 °C.

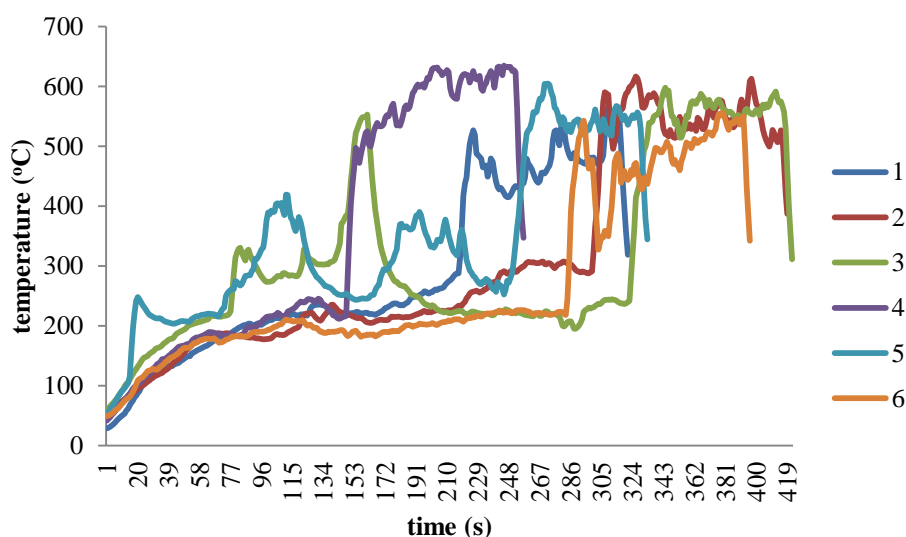


Figure 5.22: Time-temperature profiles of six 64% polyester + 33% rayon + 3% elastin + porcine bone samples (NN)

5.5.2.10 Porcine Bone + 50% Polyester + 50% Viscose (OO)

The pyrolysis of 50% polyester + 50% viscose in the presence of porcine bone generated a similar range of products to those from the combined samples (NN), but with excellent reproducibility and with the additional presence of α -methyl-styrene, dienes, *n*-alkyl cycloalkanes and *n*-alkyl cycloalkenes, as detailed in Table 5.11. In contrast to the combined samples (NN), no ketone, *n*-aldehyde or limonene were detected in combined samples (OO). A representative total ion chromatogram of combined sample (OO) is illustrated in Figure 5.23.

All of the products generated in combined samples (OO) were present in at least four of the six repeats. Sets 3, 4, 5 and 6 produced the most products (70-79), while sets 1 and 2 generated the least with only 25 each.

Similar to previous sample sets, octane was the only compound from the list of pyrolysis products detected in porcine bone (Table 2.3) that was not detected in the combined samples (OO). In contrast to the combined samples (NN), one key indicator (α -methyl-styrene) of the polyester-viscose blend, detailed Table 4.22, was present in the combined samples (OO). However, the naphthalene, acid esters, benzoic acid derivatives, phenyl and biphenyl, *n*-aldehydes, levoglucosenone,

dioxolane and ketones that were detected inconsistently in 50% polyester + 50% viscose (O) samples were not detected in the combined samples (OO).

Only 11 compounds that were present in the 50% polyester + 50% viscose (O) samples were also present in the combined samples (OO). These products include a furan (2-methyl-furan), *n*-alkyl-benzenes and aromatics (benzene, toluene, ethyl-benzene, *p*-xylene, *o*-xylene, styrene, 1-methylethyl-benzene, propyl-benzene, 1-ethyl-2-methyl-benzene), nitrile (benzotrile) and α -methyl-styrene. No *n*-alkanes or *n*-alkenes were present in the (O) samples. Benzene; toluene; ethyl-benzene; *p*-xylene and propyl-benzene that were detected in the combined samples (OO) and in individual textile (O) were also present in the pyrolysis of porcine bone. The furan (2-methyl-furan) in the combined samples (OO) is most likely to have been generated from the viscose (a form of cellulose) within the sample. No ketones, additional furans or other key indicators of cellulose (viscose) were detected.

Similar to combined samples (NN), the pyrolysis profile of porcine bone dominated the pyrolytic profile of the combined samples (OO), with the majority of its key indicators detected. As with combined samples (NN), (OO) generated additional dienes, cyclic compounds, *n*-alkyl-benzenes, methyl-alkane / alkane nitriles, pyrroles, alkyne and sulfide that were not present in either of the separate samples. With the exception of the dienes and an alkyne, all of the additional products detected were noted to have been generated, although inconsistently, from porcine bone samples (Appendix 1.0). In comparison to the previous combined samples, the combined samples (OO) were the only ones to have not generated any *n*-aldehydes.

Table 5.11: Pyrolysis products generated from 50% polyester + 50% viscose in the presence of porcine bone (OO) across six repeats

No	Retention Time (min)	Compound	Molecular Structure	Set					
				1	2	3	4	5	6
1	3.13	1,5-hexadiene				√	√	√	√
2	3.37	2-methyl-furan		√	√	√	√	√	√
3	3.67	3-methyl-cyclopentene				√	√	√	√
4	3.80	3-methyl-1,2-pentadiene				√	√	√	√
5	3.95	methyl-cyclopentane				√	√	√	√
6	4.20	butanenitrile				√	√	√	√
7	4.27	benzene		√	√	√	√	√	√
8	4.74	2-methyl-1,3-pentadiene				√	√	√	√
9	5.11	cyclohexene		√	√	√	√	√	√
10	5.61	2-methyl-butanenitrile		√	√	√	√	√	√
11	5.71	3-methyl-butanenitrile		√	√	√	√	√	√
12	6.49	dimethyl disulfide				√	√	√	√
13	6.64	ethyl-cyclopentane				√	√	√	√
14	6.70	vinyl-cyclopentane		√	√	√	√	√	√
15	6.86	pentanenitrile				√	√	√	√
16	7.20	toluene		√	√	√	√	√	√
17	7.44	1-methyl-cyclohexene				√	√	√	√
18	7.60	1,7-octadiene				√	√	√	√
19	7.62	3,4-nonadiene				√	√	√	√
20	7.97	1-octene		√	√	√	√	√	√
21	8.00	1-ethyl-1H-pyrrole		√	√	√	√	√	√
22	8.29	2-octene				√	√	√	√
23	8.33	4-methyl-pentanenitrile		√	√	√	√	√	√
24	8.45	octene isomer				√	√	√	√
25	8.53	bicyclooctane				√	√	√	√
26	8.58	cyclooctene				√	√	√	√
27	8.83	1-ethyl-cyclohexane				√	√	√	√
28	9.04	1,6-undecadiene				√	√	√	√
29	9.15	ethyl-benzene		√	√	√	√	√	√
30	9.23	2,4-octadiene				√	√	√	√

Table 5.11 continued

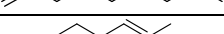
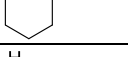
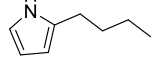
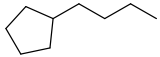
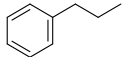
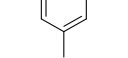
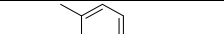
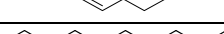
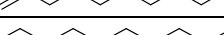
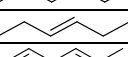
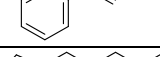
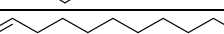
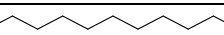
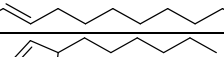
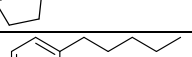
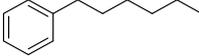
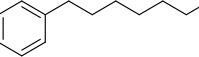
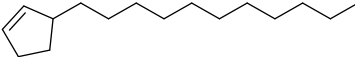
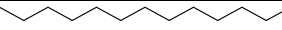
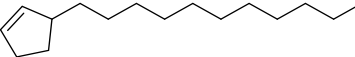
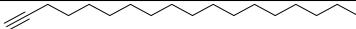
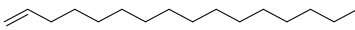
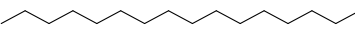
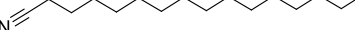
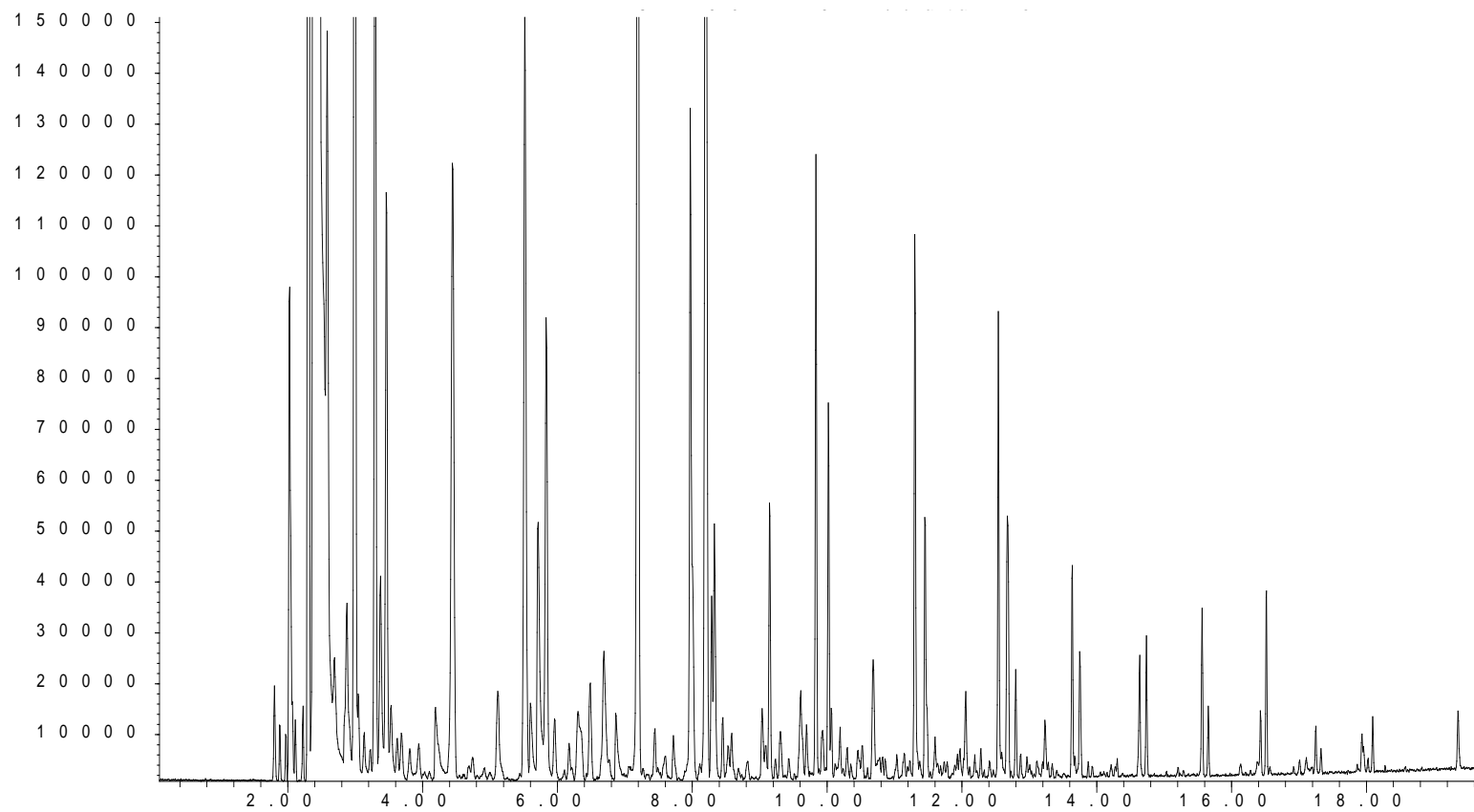
31	9.31	<i>p</i> -xylene				√	√	√	√
32	9.44	3-ethyl-cyclohexene				√	√	√	√
33	9.62	styrene				√	√	√	√
34	9.70	<i>o</i> -xylene				√	√	√	√
35	9.80	1-nonene		√	√	√	√	√	√
36	9.93	cyclooctane				√	√	√	√
37	10.01	nonane		√	√	√	√	√	√
38	10.06	2-nonene				√	√	√	√
39	10.21	nonene isomer				√	√	√	√
40	10.30	1-propenyl-cyclohexane				√	√	√	√
41	10.44	1-butyl-1H-pyrrole				√	√	√	√
42	10.51	butyl-cyclopentane				√	√	√	√
43	10.69	propyl-benzene				√	√	√	√
44	10.74	benzonitrile				√	√	√	√
45	10.78	1-methylethyl-benzene				√	√	√	√
46	10.82	1,3,5-trimethyl-benzene				√	√	√	√
47	10.87	1-propyl-cyclohexene				√	√	√	√
48	11.03	1-ethyl-4-methyl-benzene				√	√	√	√
49	11.30	1-decene		√	√	√	√	√	√
50	11.46	decane		√	√	√	√	√	√
51	11.60	5-decene				√	√	√	√
52	11.80	α -methyl-styrene				√	√	√	√
53	11.97	1-pentyl-1H-pyrrole				√	√	√	√
54	12.06	butyl-benzene				√	√	√	√
55	12.20	1-butyl-cyclohexene				√	√	√	√
56	12.58	1-undecene		√	√	√	√	√	√
57	12.68	undecane		√	√	√	√	√	√
58	12.80	2-undecene				√	√	√	√
59	12.96	3-hexyl-cyclopentene				√	√	√	√
60	13.11	pentyl-benzene				√	√	√	√

Table 5.11 continued

61	13.52	1-dodecene		√	√	√	√	√	√
62	13.63	dodecane		√	√	√	√	√	√
63	14.30	hexyl-benzene				√	√	√	√
64	14.60	1-tridecene		√	√	√	√	√	√
65	14.73	tridecane		√	√	√	√	√	√
66	15.29	heptyl-benzene				√	√	√	√
67	15.56	1-tetradecene		√	√	√	√	√	√
68	15.65	tetradecane		√	√	√	√	√	√
69	16.14	nonyl-cyclopentane				√	√	√	√
70	16.40	1-pentadecene		√	√	√	√	√	√
71	16.56	pentadecane		√	√	√	√	√	√
72	17.01	nonyl-cyclohexane				√	√	√	√
73	17.11	1-octadecyne				√	√	√	√
74	17.24	1-hexadecene				√	√	√	√
75	17.32	hexadecane				√	√	√	√
76	17.96	1-heptadecene				√	√	√	√
77	17.98	2-heptadecene				√	√	√	√
78	18.01	heptadecane				√	√	√	√
79	19.36	hexadecanitrile				√	√	√	√

A b u n d a n c e



T i m e -->

Figure 5.23: A representative TIC of porcine bone + 50% polyester + 50% viscose (OO) (set 3)

The time-temperature profiles of the six sets of repeats, displayed in Figure 5.24 demonstrate that the combined samples (OO) experienced slight fluctuations in temperatures. Sets 4, 5 and 6 experienced a single auto-ignition with minimal temperature fluctuations. Similarly, set 3 also experienced a single auto-ignition but with temperature fluctuations throughout. Sets 1 and 2 each experienced two distinctive auto-ignition events, where the second flames eventually peaked at 624 °C and 603 °C, respectively.

The auto-ignition events were most likely due to (1) ignition of porcine bone, which could have raised the temperature in the tin, facilitating (2) the auto-ignition of the textile blend as 50% polyester + 50% viscose was part of the group of textiles that did not auto-ignite on the whole as four of six samples did not auto-ignite (Table 4.11 and Figure 4.29), and / or (3) through the pyrolytic interactions between the two samples. Maximum temperatures attained across the repeats were in the range of 544-624 °C.

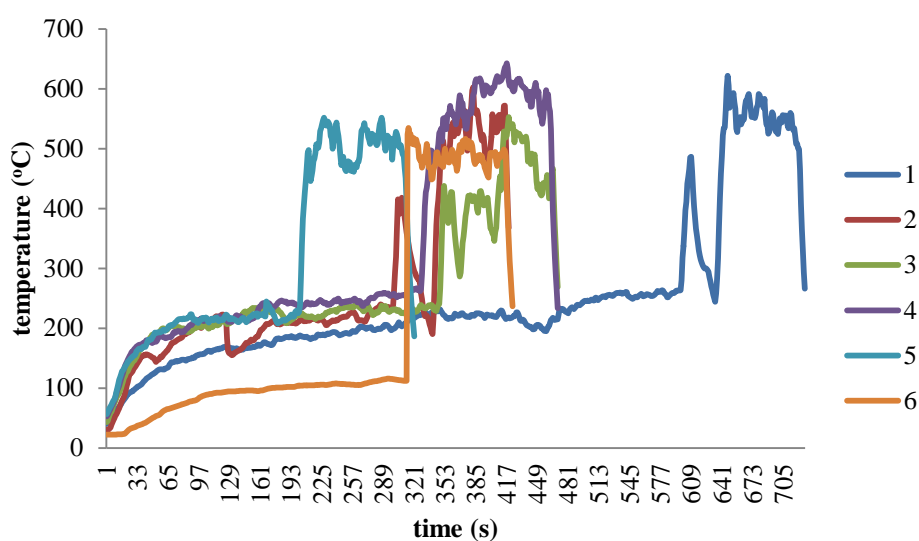


Figure 5.24: Time-temperature profiles of six 50% polyester + 50% viscose + porcine bone samples (OO)

The additional pyrolysis products detected in the polyester blends in (NN) and (OO) could have been generated by the pyrolysis of: (1) the polyester blend, (2) porcine bone, which could have raised the temperatures in the tin, facilitating (3) the auto-ignition of the textile blend, and / or (4) through the pyrolytic interactions between the two samples.

5.5.2.11 Porcine Bone + 100% Leather (QQ)

The pyrolysis of 100% leather in the presence of porcine bone generated 105 pyrolysis products that can be classified into *n*-alkanes, *n*-alkenes, alkyl / *n*-cycloalkanes and *n*-cycloalkenes, pyrroles, chloro-alkanes, dienes, benzo / methyl-alkane / *n*-alkane nitriles, furans, aromatics, *n*-alkyl-benzenes, alkyl-alkane, alkyl-alkene, dichloro-alkene, cyano-alkene, *n*-aldehyde, ketone, an alkyne, limonene and sulfide as detailed in Table 5.12. A representative total ion chromatogram of combined sample (QQ) is illustrated in Figure 5.25.

The combined samples (QQ) exhibited good reproducibility with 80 pyrolysis products detected consistently in at least four of the six sets of repeats. These products were mainly *n*-alkanes, *n*-alkenes, *n*-cycloalkanes, aromatics, methyl nitriles, disulfide, dienes, pyrroles, *n*-alkyl-benzenes, alkyl-alkene, alkyl-alkane, cyano-alkene, furan, limonene and an alkyne. Most of the sets generated considerable numbers of pyrolysis products (82-103), while sets 2 and 6 generated the fewest compounds with 33 and 47, respectively. The presence of limonene is attributed to having generated from the used leather utilised in this work.

Similar to combined samples (AA), (BB), (DD), (HH), (LL), (NN) and (OO), octane was the only compound from the list of pyrolysis products detected in porcine bone (Table 2.3) that was not detected in combined samples (QQ). The major indicators of leather, detailed in Table 4.23, that were detected in the combined samples (QQ) were 1,2-dichloro-propane, dimethyl disulfide, 1-(2-chloroethoxy)-butane and high molecular weight *n*-alkenes. Although dimethyl disulfide was also detected across all types of combined samples utilised in this work, its detection together with other key markers of leather is what that makes it indicative of leather. The only key indicator of leather that was absent in the combined samples (QQ) was dimethyl trisulfide.

Table 5.12: Pyrolysis products generated from 100% leather in the presence of porcine bone (QQ) across six repeats

No	Retention Time (min)	Compound	Molecular Structure	Set					
				1	2	3	4	5	6
1	2.14	ethyl chloride						√	√
2	2.22	3-methyl-1-butene		√	√		√	√	
3	3.13	1,5-hexadiene		√			√	√	
4	3.16	2-butanone				√		√	√
5	3.29	1-hexene		√	√	√	√	√	√
6	3.37	2-methyl-furan		√			√	√	
7	3.67	3-methyl-cyclopentene		√			√		
8	3.80	3-methyl-1,2-pentadiene		√			√	√	
9	3.95	methyl-cyclopentane		√	√		√	√	
10	4.20	butanenitrile		√			√	√	
11	4.27	benzene		√	√	√	√	√	
12	4.75	2-methyl-1,3-pentadiene		√			√	√	
13	4.91	2-methyl-hexane		√	√	√	√		
14	5.11	cyclohexene		√	√	√	√	√	
15	5.21	1,2-dichloro-propane				√	√		
16	5.61	2-methyl-butanenitrile		√		√	√	√	√
17	5.71	3-methyl-butanenitrile		√		√	√	√	√
18	6.09	4,4-dimethyl-cyclopentene		√			√		
19	6.35	3-methyl-cyclohexene		√	√	√	√	√	
20	6.49	dimethyl disulfide		√		√	√	√	
21	6.64	ethyl-cyclopentane		√	√		√	√	
22	6.70	vinylcyclopentane		√			√	√	
23	6.76	methylene-cyclohexane		√			√	√	
24	6.86	pentanenitrile		√			√	√	
25	7.20	toluene		√	√	√	√	√	√
26	7.44	1-methyl-cyclohexene		√		√	√	√	
27	7.60	1,7-octadiene		√		√	√	√	
28	7.70	hexanal				√			√
29	7.92	2-methylene-heptane					√		
30	7.97	1-octene		√	√	√	√	√	
31	8.00	1-ethyl-1H-pyrrole		√		√	√	√	
32	8.29	2-octene		√	√	√	√	√	

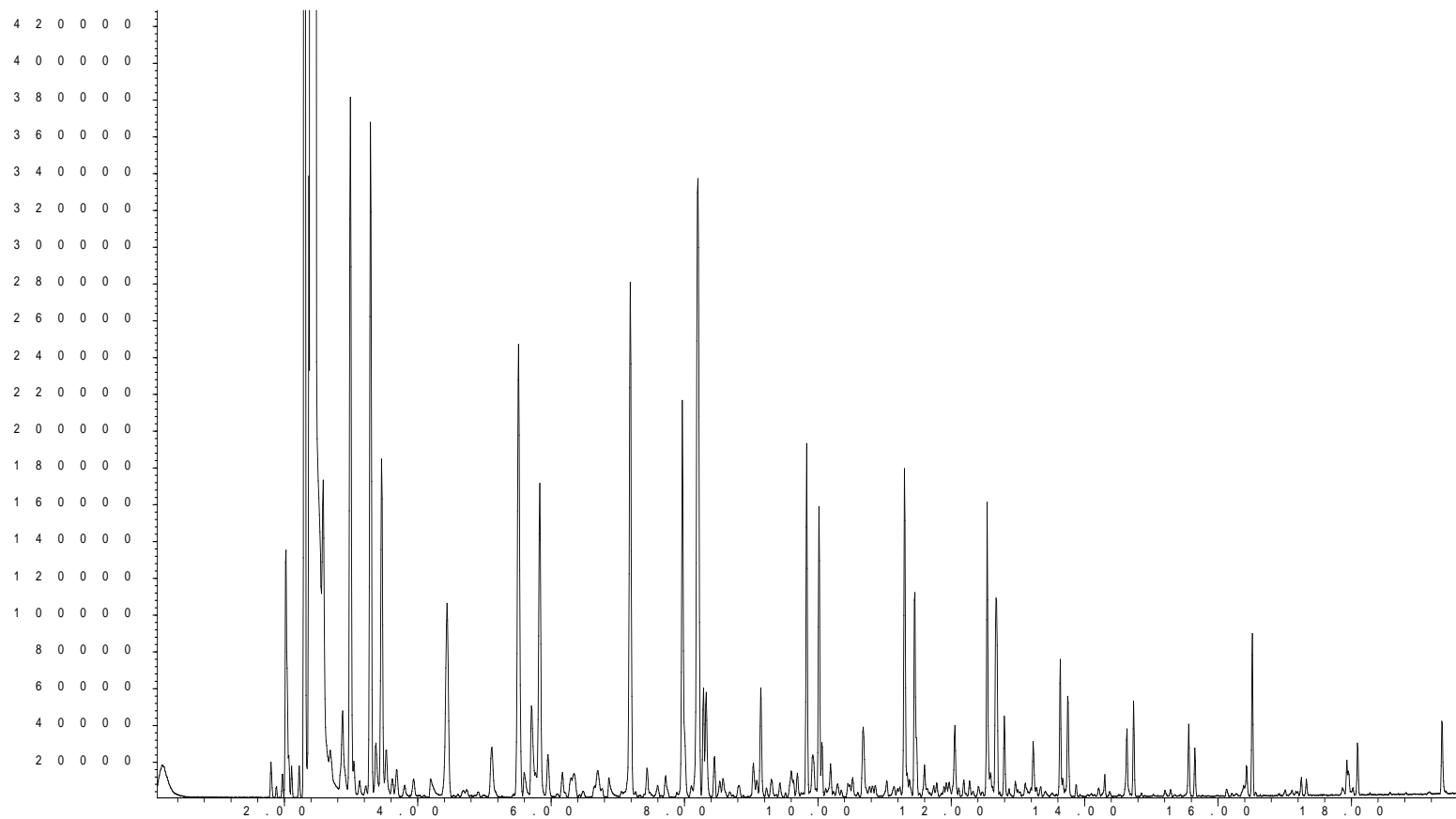
Table 5.12 continued

33	8.33	4-methyl-pentanenitrile		√		√	√	√	√
34	8.45	octene isomer		√	√	√	√	√	
35	8.53	bicyclooctane		√		√	√	√	
36	8.58	cyclooctene		√		√	√	√	
37	8.67	3-methyl-1,5-heptadiene		√			√		
38	8.83	1-ethyl-cyclohexane		√	√		√		
39	9.04	1,6-undecadiene		√		√	√	√	
40	9.09	2-ethyl-cyclohexane		√		√	√	√	
41	9.15	ethyl-benzene		√	√	√	√	√	√
42	9.23	2,4-octadiene		√		√	√	√	
43	9.44	3-ethyl-cyclohexene		√			√	√	
44	9.62	styrene		√		√	√	√	
45	9.70	o-xylene		√		√	√	√	
46	9.80	1-nonene		√	√	√	√	√	√
47	9.93	cyclooctane		√		√	√	√	
48	10.01	nonane		√	√	√	√	√	√
49	10.06	2-nonene		√	√	√	√	√	
50	10.21	cis-2-nonene		√	√	√	√	√	√
51	10.24	1-(2-chloroethoxy)-butane				√	√	√	
52	10.30	1-propenyl-cyclohexane		√		√	√		
53	10.49	propyl-cyclohexane		√	√	√	√		√
54	10.51	6-cyano-1-hexene		√		√	√	√	
55	10.69	propyl-benzene		√	√	√	√	√	
56	10.74	benzonitrile		√			√		
57	10.78	1-methylethyl-benzene		√			√	√	
58	10.81	1-ethyl-2-methyl-benzene		√		√	√	√	
59	10.87	1-propyl-cyclohexene		√		√	√	√	
60	11.03	1-ethyl-4-methyl-benzene		√			√	√	
61	11.18	2-pentyl-furan				√	√	√	√
62	11.30	1-decene		√	√	√	√	√	√
63	11.46	decane		√	√	√	√	√	√
64	11.60	cyclodecene		√		√	√	√	
65	11.68	5-decene		√		√	√	√	
66	11.78	limonene		√		√	√	√	
67	11.97	1-pentyl-1H-pyrrole		√	√	√	√	√	
68	12.06	butyl-benzene		√		√	√	√	√
69	12.20	1-methyl-2-propyl-benzene		√		√	√	√	

Table 5.12 continued

70	12.28	propylidencyclohexane		√		√	√	√	
71	12.58	1-undecene		√	√	√	√	√	√
72	12.68	undecane		√	√	√	√	√	√
73	12.80	2-undecene		√		√	√	√	√
74	12.87	1-cycloundecene		√		√	√	√	√
75	12.96	3-hexyl-cyclopentene		√		√	√	√	
76	13.04	cycloundecene (Z)		√		√	√	√	
77	13.11	pentyl-benzene		√		√	√	√	√
78	13.52	1-dodecene		√	√	√	√	√	√
79	13.63	dodecane		√	√	√	√	√	√
80	13.87	3-dodecene		√		√	√	√	√
81	13.93	cyclododecene		√		√	√	√	√
82	14.30	hexyl-benzene		√		√	√	√	√
83	14.60	1-tridecene		√	√	√	√	√	√
84	14.73	tridecane		√	√	√	√	√	√
85	14.80	4-tridecene		√			√	√	
86	15.20	heptyl-cyclohexane		√		√	√	√	√
87	15.29	heptyl-benzene		√		√	√	√	√
88	15.44	1-cyclohexylheptane		√		√	√	√	√
89	15.56	1-tetradecene		√	√	√	√	√	√
90	15.65	tetradecane		√	√	√	√	√	√
91	15.87	4-tetradecene		√			√	√	
92	16.12	cyclotetradecene		√		√	√	√	√
93	16.14	nonyl-cyclopentane		√		√	√	√	√
94	16.40	1-pentadecene		√	√	√	√	√	√
95	16.56	pentadecane		√	√	√	√	√	√
96	17.01	nonyl-cyclohexane		√		√	√	√	√
97	17.11	1-octadecyne		√		√	√	√	√
98	17.17	cyclohexadecene		√		√	√	√	√
99	17.24	1-hexadecene		√		√	√	√	√
100	17.32	hexadecane		√		√	√	√	√
101	17.88	1,9-hexadecadiene		√		√	√	√	√
102	17.96	1-heptadecene		√		√	√	√	√
103	17.98	2-heptadecene		√		√	√	√	√
104	18.01	heptadecane		√		√	√	√	√
105	19.36	hexadecanitrile		√			√	√	

A b u n d a n c e



T i m e -->

Figure 5.25: A representative TIC of porcine bone + 100% leather (QQ) (set 4)

In contrast to the rest of the combined samples, 100% leather (Q) was the only textile that possessed similar pyrolytic characteristics to porcine bone. This was mainly due to the consistent presence of *n*-alkenes, which were also present in porcine bone pyrolysis. However, through the consistent presence of *n*-alkanes and hexadecanitrile in porcine bone samples but not in leather, it is possible to distinguish between the two samples; in addition to the key indicators from leather pyrolysis.

With 39 compounds and the majority of key indicators which had been found to be present in both the 100% leather (Q) and the combined samples (QQ), the pyrolysis profile of (QQ) was determined to have equal dominance by both leather and porcine bone. The combined samples also generated additional *n*-aldehyde, *n*-alkene, alkyl-alkene, cyano-alkene, ketone, alkyne, dienes, cyclic compounds, methyl-alkane and benzo nitriles, *n*-alkyl-benzenes and pyrroles that were not present consistently in either of the separate samples and as with previous samples, the majority of these compounds could have been generated from the pyrolysis of the porcine bone samples (Appendix 1.0). 1-Hexene, although detected consistently across the combined samples (QQ) was less reproducible in the leather samples (Q). The presence of ethyl chloride in the combined samples (QQ) is also highlighted. Also, hexanal was the only *n*-aldehyde detected in the combined samples (QQ) across sets 3 and 6.

The time-temperature profiles of the six sets of repeats are displayed in Figure 5.26. Sets 3, 5 and 6 experienced the least fluctuations with one auto-ignition event observed. Set 1, 2 and 4 experienced two rapid rises in temperatures but with different flaming duration between them. In set 2, both flaming emissions occurred within 44 seconds of each other whereas sets 1 and 4, the emissions were further apart. The flaming emissions and the presence of additional pyrolysis products detected in the combined samples (QQ) could have been generated by the pyrolysis of: (1) porcine bone, (2) the textile, as 100% leather was part of the group of textiles that auto-ignited (Table 4.11 and Figure 4.31), and / or (3) through the pyrolytic interactions between the two samples. Maximum temperatures attained across the six sets of repeats were in the range of 504-622 °C.

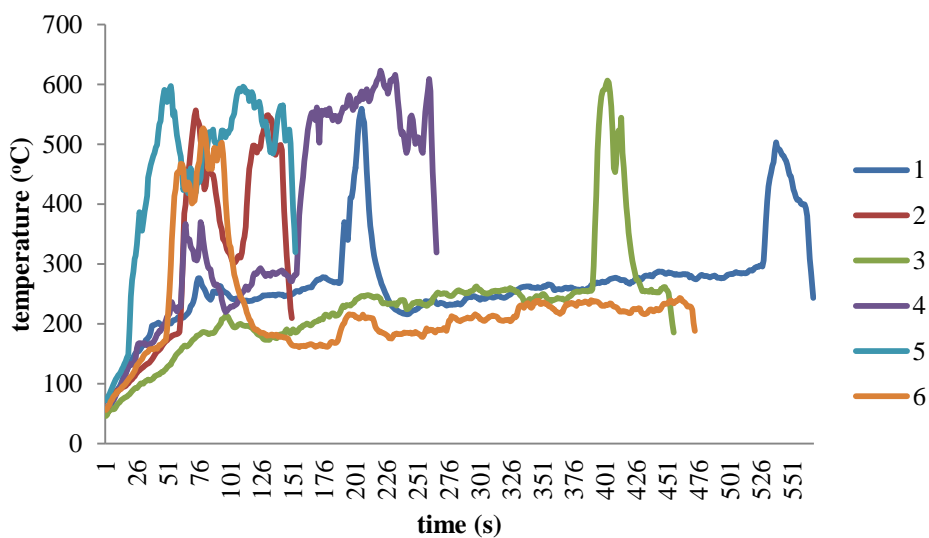


Figure 5.26: Time-temperature profiles of six 100% leather + porcine bone samples (QQ)

The absence of octane across all of the combined samples is highlighted in this study together with the absence of decane, propyl-benzene and hexadecanitrile across some combined samples. The absence of octane could be due to its co-elution with another more dominant compound that could have obscured its presence in the TIC; or octane together with the other three compounds could have undergone molecular interactions and decomposition during the pyrolysis and combustion process. A summary of the results obtained from the pyrolysis of each of the combined sample type is illustrated in Table 5.13.

Table 5:13: Summary of the results obtained from each type of combined sample according to the dominant profile, key indicators absent from the dominant profile, reproducibility and the notable compounds present

Sample + Porcine Bone	Dominant Profile	Key Indicators Absent from Dominant Profile	Reproducibility (%)	Notable Compounds Present
100% cotton (AA)	Porcine Bone	Octane	60	Ethanol, Ethyl Acetate
95% cotton + 5% elastin (BB)	Porcine Bone	Octane	58	-
50% cotton + 50% modal (DD)	Porcine Bone	Octane	76	Propanedioic acid, propyl; Pentanoic acid, 3-methyl, methyl ester;
100% acrylic (EE)	Porcine Bone	Octane, Decane	44	Ethyl Acetate
	Acrylic	Pyridine, Piperidine, Cyanic and Isocyanic Compounds		
50% acrylic + 50% cotton (FF)	Porcine Bone	Octane, Propyl-benzene, Hexadecanitrile	26	-
	Acrylic-Cotton Blend	Pyridine, Piperidine, Cyanic and Isocyanic Compounds		
80% nylon + 20% elastin (HH)	Porcine Bone	Octane	55	6-Cyano-1-hexene, Hexenoic Acid, Oxalic acid, butyl- neopentyl-ester;
100% denim (JJ)	Porcine Bone	Octane, Hexadecanitrile	30	-
96% wool + 4% LYCRA® (LL)	Porcine Bone	Octane	24	-
64% polyester + 33% rayon + 3% elastin (NN)	Porcine Bone	Octane	57	-
50% polyester + 50% viscose (OO)	Porcine Bone	Octane	100	-
100% leather (QQ)	Porcine Bone	Octane	76	1-Hexene, Ethyl Chloride
	Leather	Dimethyl Trisulfide		

5.5.3 Application of Extracted Ion Chromatogram (EIC) and Extracted Ion Profile (EIP) for the Identification of Key Indicators of Porcine Bone

5.5.3.1 EIC and EIP of Porcine Bone (Post-Ignition)

Compounds that consistently appeared across six repeats of porcine bone post-ignition (identified in section 2.5.2.2) were a series of C₈ to C₁₇ *n*-alkanes and *n*-alkenes and hexadecanitrile. *n*-Alkanes and *n*-alkenes were identified based on the *m/z* values detailed in Table 5.0, which also corresponded with the values identified in the standard Grob mixture utilised in this study (detailed in section 2.5.1) that contained *n*-alkanes. Hexadecanitrile was identified based on the *m/z* values obtained from the NIST/EPA/NIH Mass Spectral Library (NIST 08). Their *m/z* values are as follows:

- i. *n*-alkanes, *m/z* = 43, 57, 71, 85, 99
- ii. *n*-alkenes, *m/z* = 41, 55, 69, 83, 97
- iii. hexadecanitrile, *m/z* = 138, 152, 166, 180, 194

It is clearly illustrated in Figure 5.27 that *n*-alkanes were easily extracted from the TIC of porcine bone post-ignition. While the ions 43, 57, 71, 85 and 99 were also present in *n*-alkenes, their abundances in the profiles of *n*-alkanes were much higher and the peaks more prominent (*n*-alkanes marked with arrows in Figure 5.27 (c)). Ion 99 possessed the lowest abundance in comparison to the other ions in the chromatogram.

Comparable outcomes were also observed in the EIC and EIP of *n*-alkenes, as illustrated in Figure 5.28. While the ions 41, 55, 69, 83 and 97 were also detected in *n*-alkanes, their abundances were much higher and more prominent in *n*-alkenes (*n*-alkenes marked with arrows in Figure 5.28 (c)). Contrary to *n*-alkanes, all of the characteristic ions for *n*-alkenes were present at high abundance in the chromatogram.

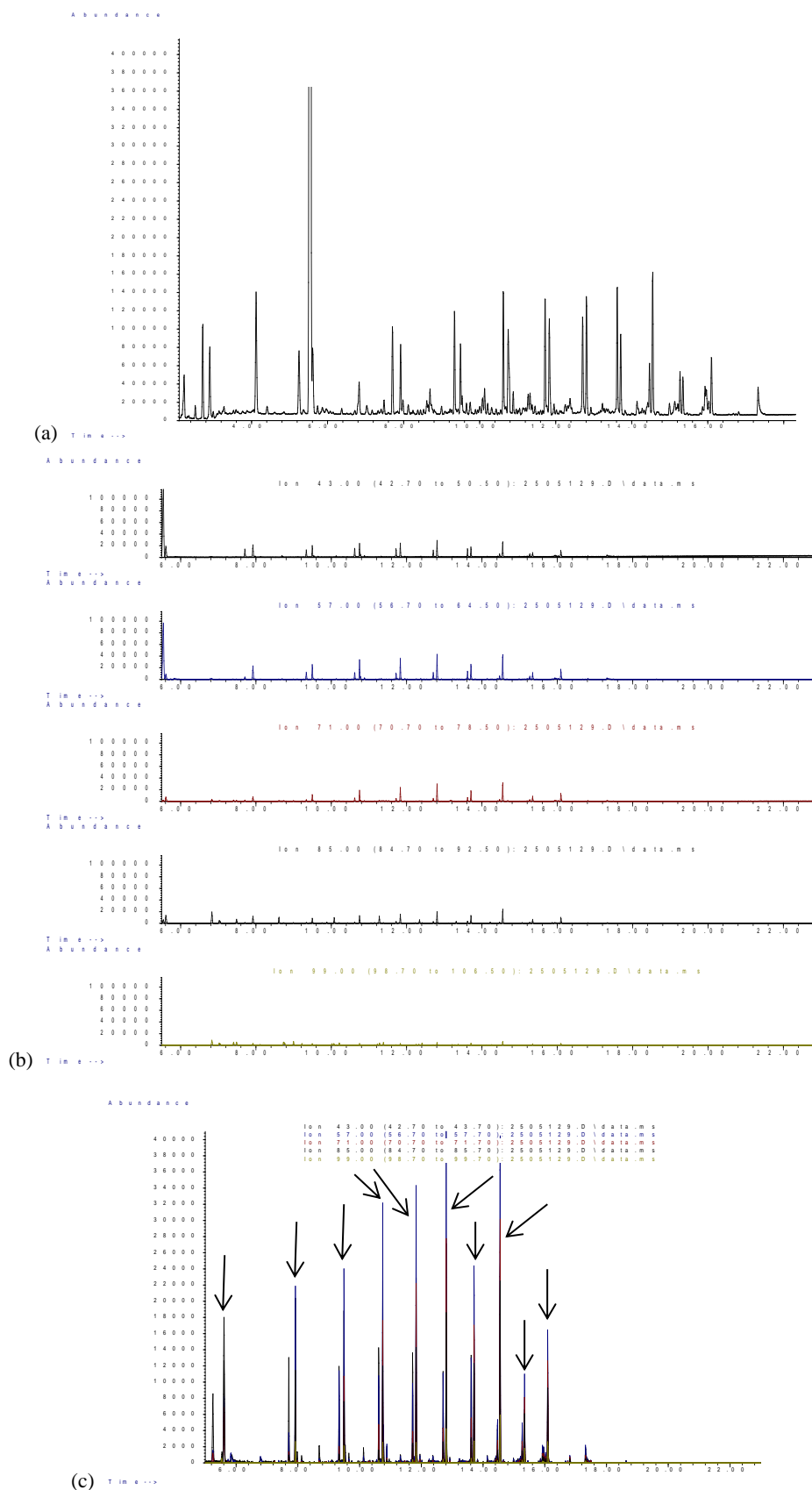


Figure 5.27: (a) TIC of porcine bone (b) EIC of ions 43, 57, 71, 85, 99 and (c) EIP of ions 43, 57, 71, 85, 99 characteristic of *n*-alkanes (marked with arrows)

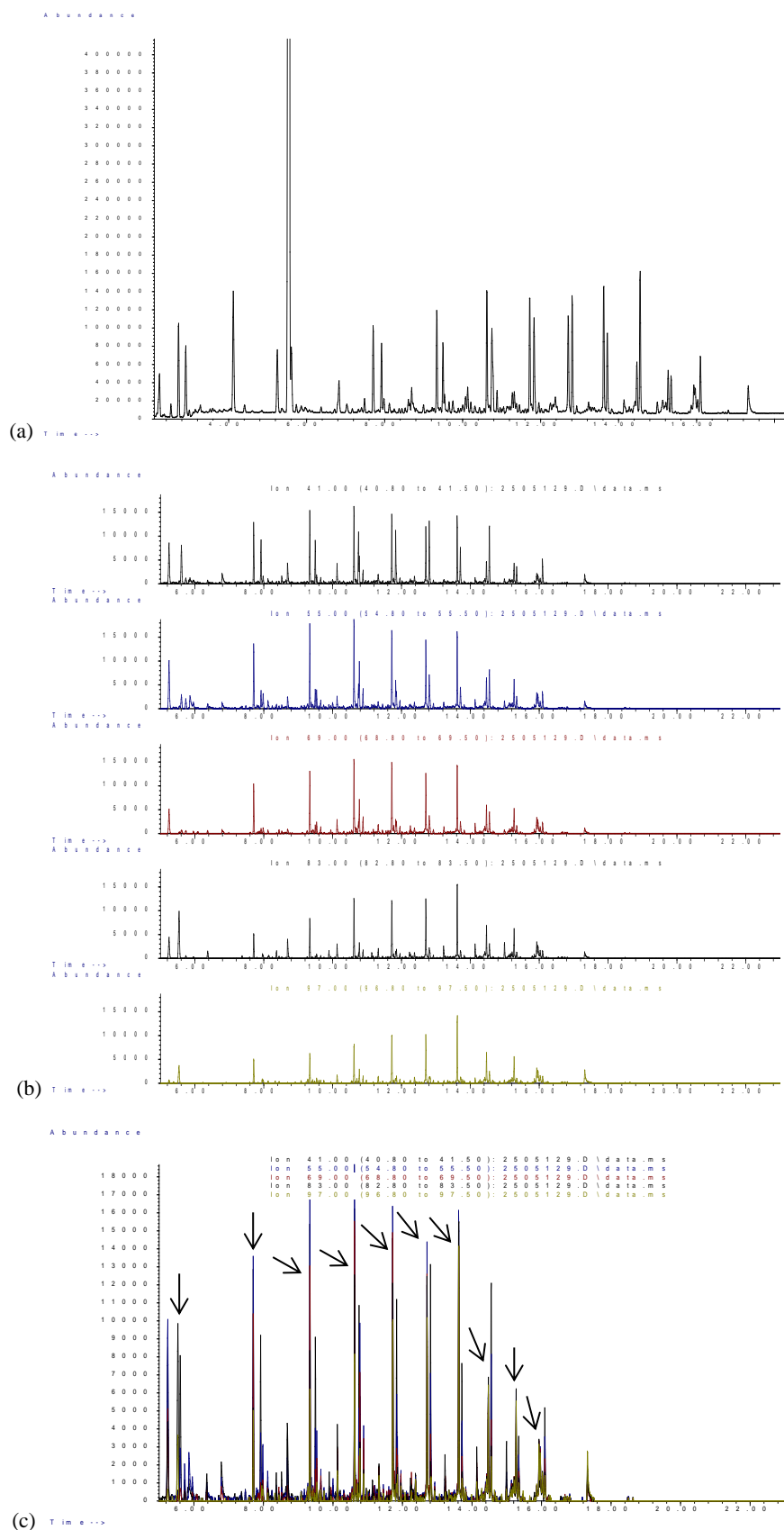


Figure 5.28: (a) TIC of porcine bone (b) EIC of ions 41, 55, 69, 83, 97 and (c) EIP of ions 41, 55, 69, 83, 97 characteristic of *n*-alkenes (marked with arrows)

A number of peaks with ions 138, 152, 166, 180 and 194 were highlighted in both the EIC and EIP of porcine bone (Figure 5.29); however, all of these peaks, with the exception of hexadecanitrile at 17.32 minutes), were present at individual m/z values rather than collectively and at low abundances. At minute 17.32 (marked with an arrow in Figure 5.29 (c)), all of these m/z values were present and at high abundances, thus identifying hexadecanitrile.

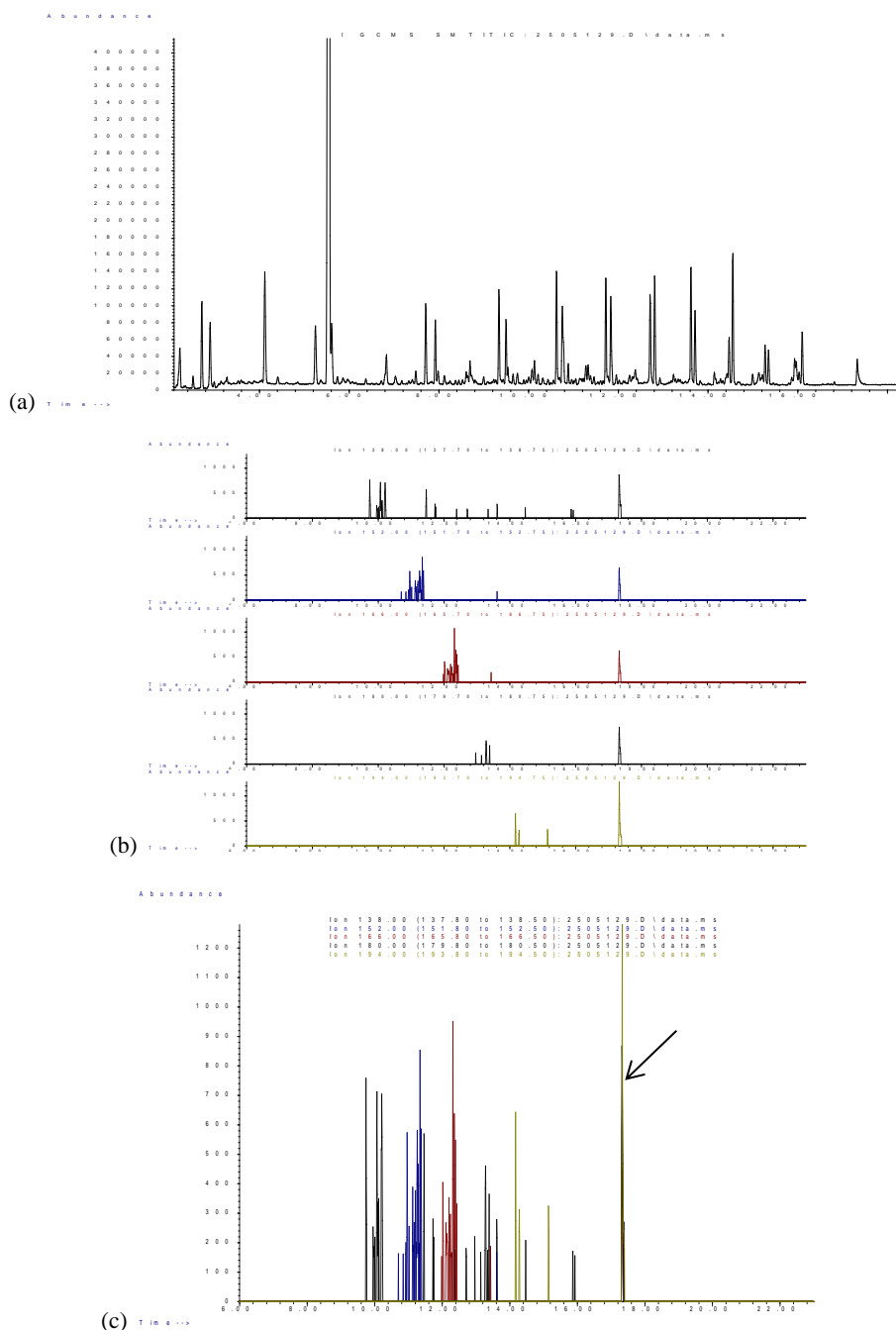


Figure 5.29: (a) TIC of porcine bone (b) EIC of ions 138, 152, 166, 180, 194 and (c) EIP of ions 138, 152, 166, 180, 194 characteristic of hexadecanitrile (marked with arrow)

5.4.3.2 EIC and EIP of Porcine Bone in the Presence of Textiles

EIC and EIP for the combined samples (AA), (BB), (DD), (JJ), (LL), (NN) and (OO) were extracted from 3.00 minutes to 20.00 minutes as the solvent front was present until 3.00 minutes. No peaks were detected after 20.00 minutes. However, for combined samples (EE), (FF) and (HH), EIC and EIP were applied from 2.60 minutes to 20.00 minutes, and for combined samples (QQ), extraction was conducted between 2.00 minutes to 20.00 minutes. The differences in start time applied across these samples were due to the presence of pyrolysis products at an earlier stage of analysis.

The EICs and EIPs of *n*-alkanes and *n*-alkenes for all combined samples, and hexadecanitrile for all but combined samples (FF) and (JJ), (hexadecanitrile was not present across these combined samples) demonstrated separation and characterisation of porcine bone samples with ease, with the exception of leather (QQ), where the *m/z* values of *n*-alkenes in porcine bone coincided with those generated by leather, however the *m/z* values of *n*-alkanes and hexadecanitrile were more useful at this instance. Individual EICs and EIPs for each combined sample are detailed in Appendix 8.0.

5.5.4 Self-Organising Feature Maps (SOFM) Model Validation

The SOFM model was validated using the sample set from each individual textile and porcine bone data that generated the greatest number of pyrolysis products. Results from the test output are revealed in Figure 5.30. The grouping and classification of the textile types and porcine bone demonstrate that the SOFM network was able to fully resolve and classify the textiles (i.e. cotton and cotton blends, acrylic and acrylic blends, nylon-elastin, denim, wool-lycra[®], polyester and polyester blends, leather) and porcine bone (labelled 'pig') correctly with a 100% performance value. Even when there was an overlap in textile composition, for instance, the presence of various cellulose-based materials (i.e. cotton, modal, viscose, rayon, denim) across textiles (A), (B), (D), (F), (J), (N) and (O), the model was not only able to distinguish these compositions but also to display their association / relationship with one another. For example, both (N) and (O) were

classified at the top left side of the map. This is expected as both these textiles contain polyester; however, the network was also able to capture the presence of cellulose (rayon / viscose) in these textiles, segmenting them above the cotton and cotton-blends (A, B, D, J). Similar associations are also observed for acrylic and its blends (E and F). This demonstrates that the SOFM model is capable of providing an objective and accurate interpretation of complex patterns contained in the pyrolysis products of these samples.

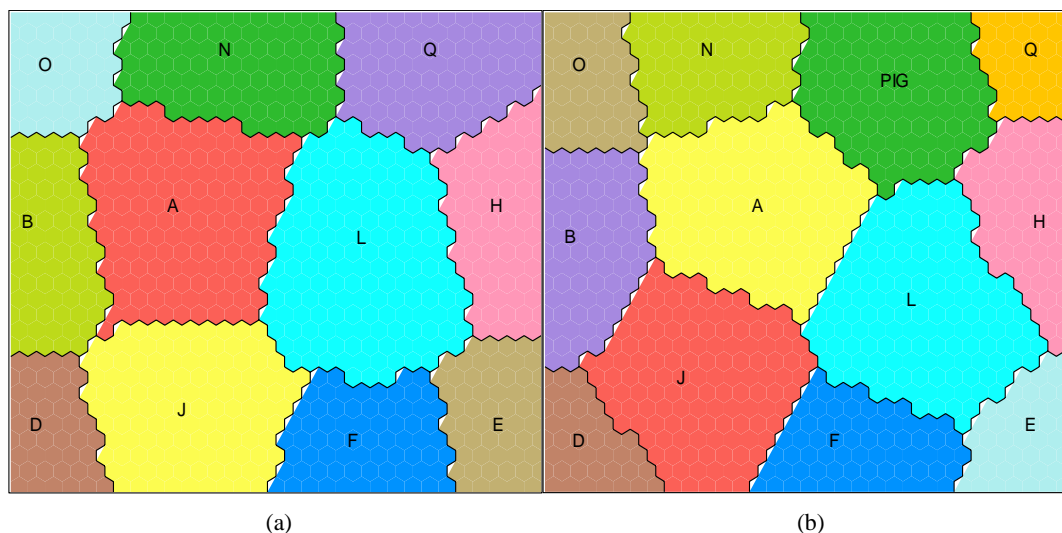


Figure 5.30: Output map of the test set showing classification and association of the textiles based on the presence / absence of the pyrolysis products generated according to the (a) type of textiles and (b) in the presence of porcine bone ('pig'), where the samples are 100% cotton (A), 95% cotton + 5% elastin (B), 50% cotton + 50% modal (D), 100% acrylic (E), 50% acrylic + 50% cotton (F), 80% nylon + 20% elastin (H), 100% denim (J), 96% wool + 4% LYCRA[®] (L), 64% polyester & 33% rayon & 3% elastin (N), 50% polyester + 50% viscose (O) and 100% leather (Q)

5.5.4.1 SOFM Classification of Individual Textile Samples

The output map utilising the presence and absence of pyrolysis products across six sets of repeats for each textile type is presented in Figure 5.31. The output map revealing clusters of all six repeat samples occurred only in the case of 100% acrylic (E) and all other repetitive samples were convoluted to more or lesser degrees, indicating a substantial crossover in some cases of the generated pyrolysis products. This is clearly as a result of the degree of pyrolysis that could be reproducibly achieved and the variation in the chromatographic data obtained as a result.

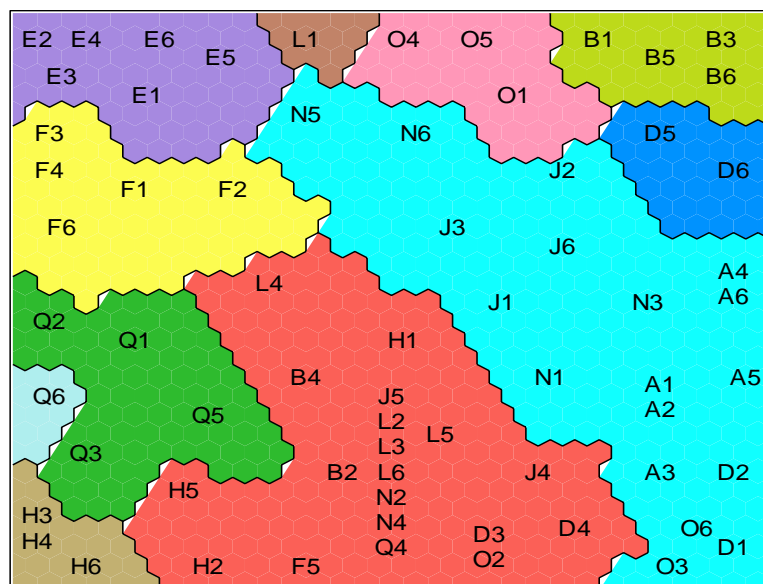


Figure 5.31: Output map for six sets of repeats ($n=6$) for each textile type

In the next stage of the pattern recognition process, the six sets of repeats for each textile were compared according to the number of pyrolysis products present and reported in the form of percentages (100% and decreasing by 10%) of the total pyrolysis products present. Samples which contained between 70% of the maximum number of pyrolysis products were found to represent all of the textiles while providing the best clustering into the originating textiles and this is shown in Figure 5.32.

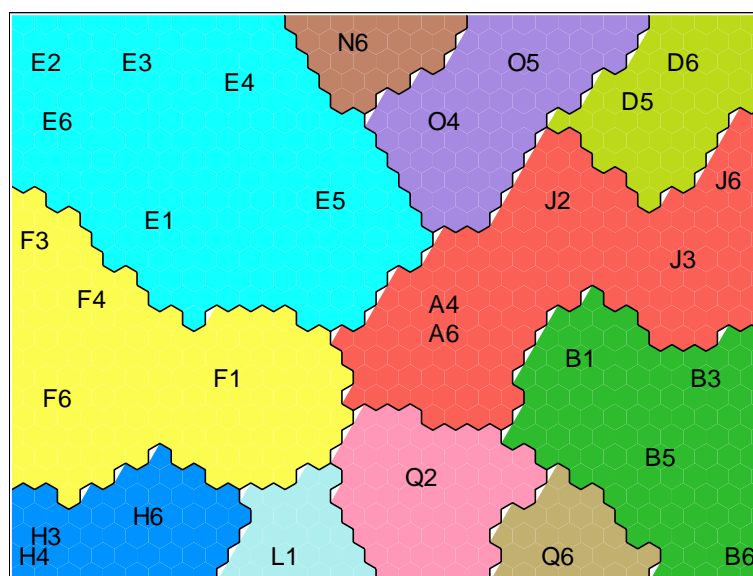


Figure 5.32: Output map for each of the 11 textile sample types for cases which generated 70% of the maximum number of pyrolysis products observed from the textiles

It can still be seen that there was some comingling occurring between the 100% cotton (A) and 100% denim (J) samples, however, when the data at 70% was separated into 11 segments (Figure 5.33) and visualised in the form of U-matrix clusters, as displayed in Figure 5.33 (b), all of the samples are distinguished individually with the presence of additional boundary lines.

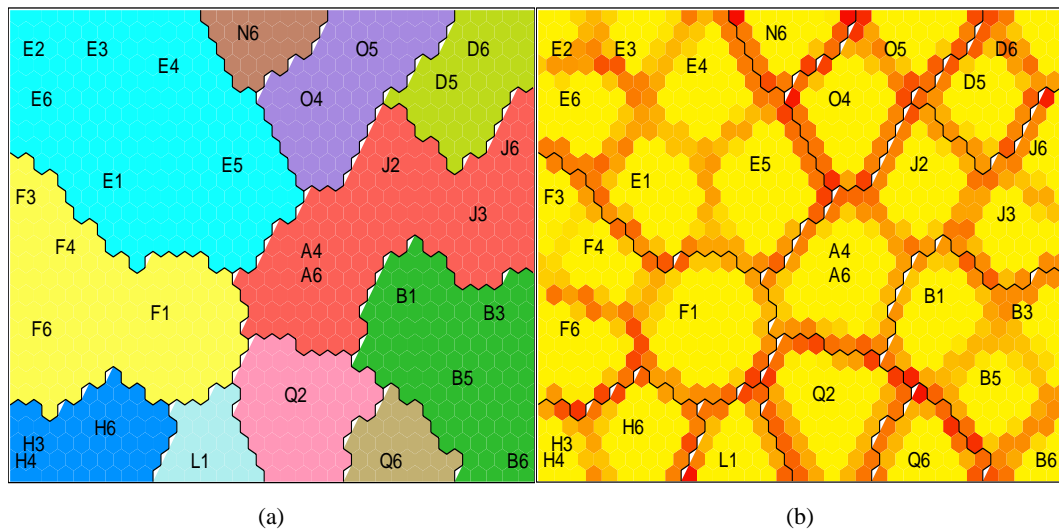


Figure 5.33: 70% map output separated into 11 segments and visualised through (a) flat clusters and (b) U-matrix clusters

When clustering was undertaken across six segments, corresponding to the six group of textiles utilised in this work – cellulose-based (A, B, D, J), acrylic based (E, F), nylon (H), wool (L), polyester-based (N, O), and leather (Q), distinctive classification of 95% cotton + 5% elastin (B), 100% acrylic (E), 50% acrylic + 50% modal (F), 80% nylon + 20% elastin (H) and 100% leather (Q) was demonstrated, as detailed in Figure 5.34. Although the remaining textiles (A, J, D, O, N, F, L) were categorised into two major groups (five in light blue and two in yellow), they were distinguished based on their distinctive position in the flat-cluster output in Figure 5.34 (a) and more so in the U-matrix output in Figure 5.34 (b), as the boundary lines aid in visualising the separation of these six different textile groups into their clusters.

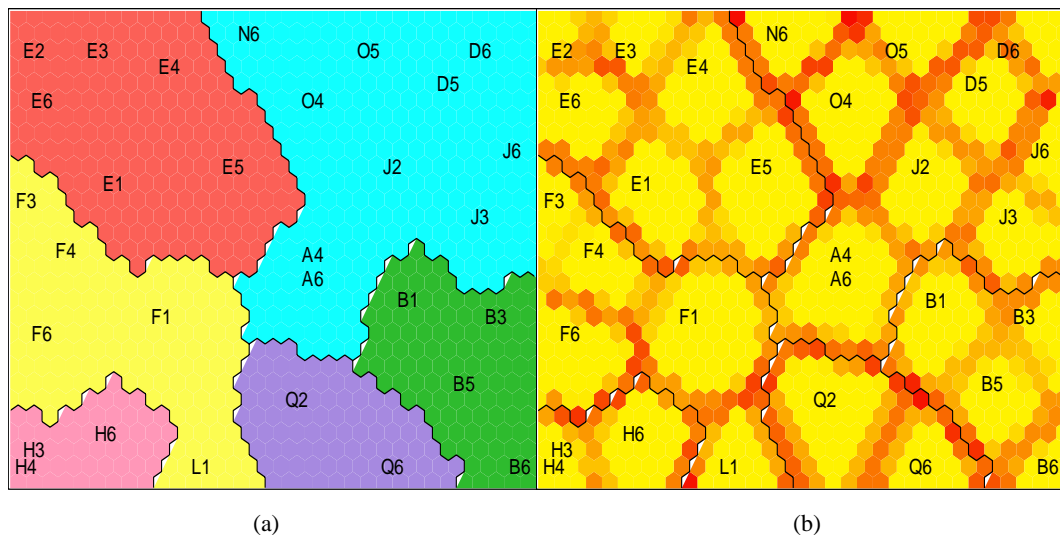


Figure 5.34: 70% map output separated into six segments and visualised through (a) flat clusters and (b) U-matrix clusters

Both output matrix (Figures 5.33 and 5.34) also highlighted the association between textile types that share a similar composition, as they are closely positioned to each other in their respective clusters. This is particularly the case for:

- i. acrylic, positioned at the top left (E) and middle left (F) of the map
- ii. polyester, positioned at the top middle (N and O) of the map
- iii. cellulose, positioned at the middle (A), bottom right (B), top right (D) and middle right (J) of the map

5.5.4.1 SOFM Classification of Combined Samples

The data associated with the textiles burnt in the presence of the porcine samples was also examined using SOFM. Out of the 11 combined samples ($n=6$), only two (i.e. 50% cotton + 50% modal (DD) and 100% acrylic (EE)), were correctly classified into their clusters for all six sets of repeat sample as detailed in Figure 5.35. This is not unexpected given the level of overlap reported in the samples.

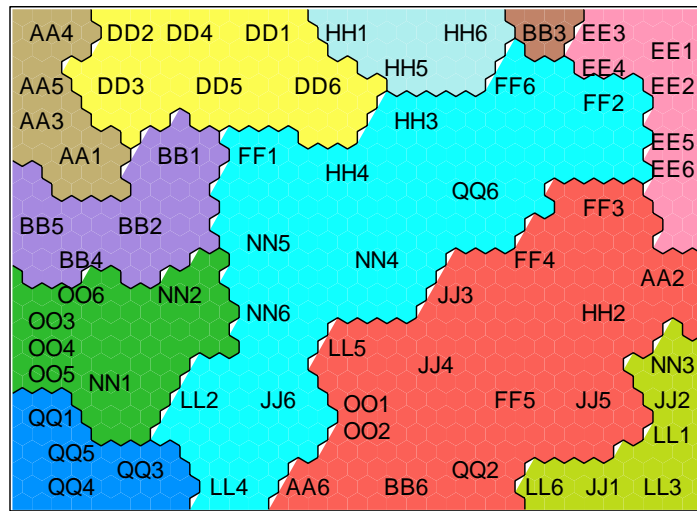


Figure 5.35: Output map for six sets of repeats ($n=6$) for each of the 11 combined samples

Similar observations were noted when porcine bone data (labelled ‘pig’) was added into the dataset of the combined samples (Figure 5.36). Porcine bone clustered into the lower right region of the output map (red), together with a number of sets of combined samples. Its presence did not alter the topography of the total output map as little to no change was noted in the association and position of the sets in the map, however the clustering of 100% acrylic (EE) was reduced.

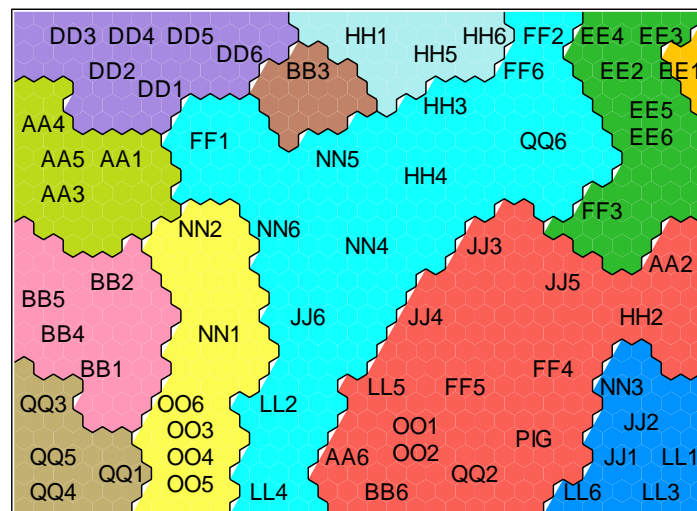


Figure 5.36: Output map for 11 combined textile types ($n=6$ for each), and individual porcine bone (‘pig’) ($n=1$)

When data from the optimised individual textile types were added into the dataset containing the combined samples and porcine bone data, the positions of a number of clusters of combined samples (AA, EE, FF and HH) and some individual sets

changed drastically (Figure 5.37). Although better clustering was noted for 50% acrylic + 50% cotton (FF), a wider spread in classification was noted for 100% cotton (AA) and 50% cotton + 50% modal (DD). The majority of the individual textiles were clustered at the bottom right of the map, with the exception of (E), which clustered at the top right of the map bordering porcine bone ('pig').

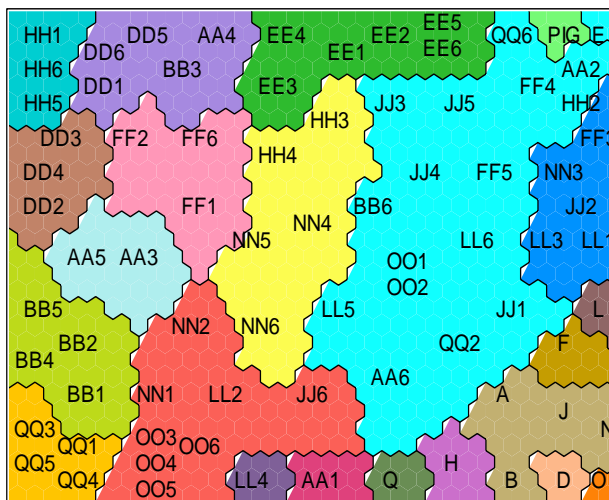


Figure 5.37: Output map for 11 combined samples ($n=6$ for each), individual porcine bone ('pig') ($n=1$) and 11 individual textile types ($n=1$ for each)

Threshold levels for the inclusion of data sets within the combined textile sample sets were explored. In line with the results obtained previously, samples which contained 70% of the maximum pyrolysis products produced, provided the best classification system as illustrated in Figure 5.38, although this was considerable less successful than for the individual textile samples.

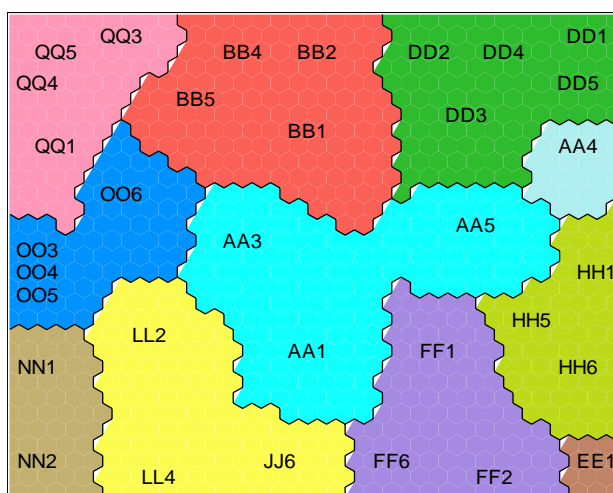


Figure 5.38: Output map for each of the 11 combined sample types for cases which generated 70% of the maximum number of pyrolysis products observed from the textiles

Similarly with the individual textiles, data at 70% was then subjected to separation across 11 segments and results demonstrated full discrimination of the ten but one (AA) combined samples as illustrated in Figures 5.39. The additional boundary lines in the U-matrix output (Figure 5.39 (b)) do distinguish each set and each group of the combined samples individually. Although combined sample (AA4) was separated from the rest of the (AA) samples its position beside the (AA) cluster indicates close association with the combined samples (AA).

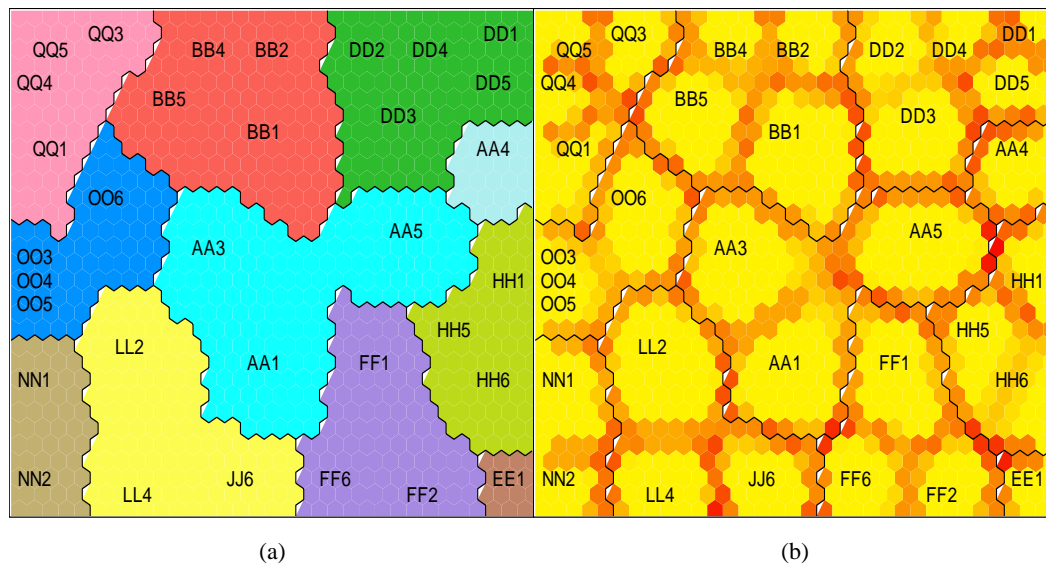


Figure 5.39: 70% map output of the combined samples separated into 11 segments and visualised through (a) flat clusters and (b) U-matrix clusters

With classification into six segments, four distinct clusters of (AA), (BB), (DD) and (QQ) were achieved as illustrated in Figure 5.40. Although the remaining textiles (N, L, J, O, E, F, H) were grouped into two major groups (four in light blue and three in yellow), they were distinguished based on their distinctive position in the flat-cluster output in Figure 5.40 (a) and more so in the U-matrix output in Figure 5.40 (b) as the boundary lines aid in visualising the separation of these seven different combined samples into their clusters.

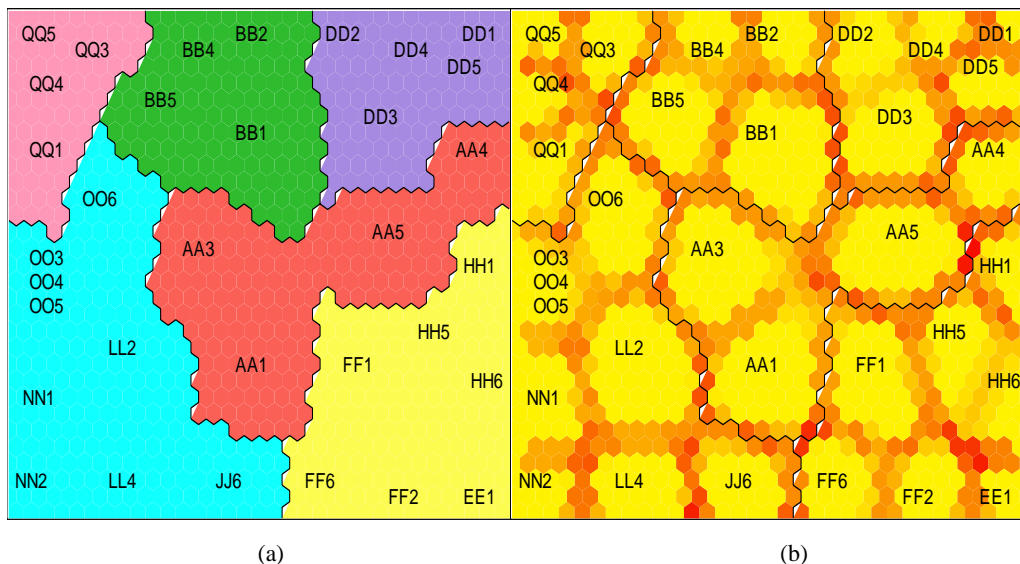


Figure 5.40: 70% map output of combined samples separated into six segments and visualised through (a) flat clusters and (b) U-matrix clusters

Both output matrix (Figures 5.39 and 5.40) also highlighted the association between combined sample types that share similar composition, as they are closely positioned to each other in their clusters, particularly for:

- i. acrylic, positioned at the bottom right of the map (EE and FF)
- ii. polyester, positioned at the bottom left (NN) and middle left (OO) of the map
- iii. cellulose, positioned at the middle and middle right (AA), middle top (BB), top right (DD) and middle bottom (JJ) of the map

When the porcine bone sample (labelled ‘pig’) was added into the 70% dataset for the 11 combined samples and further combined with the 11 individual textile samples, reasonable separation into the 23 groups was revealed, as demonstrated in Figure 5.41. The combined samples (JJ), (LL), (NN) and (OO), were all clustered within the same segment (light blue) or bordered this segment. The combined sample (AA) and (DD) were split across their replicate sample sets however they were all associated together in the sample space. The segments corresponding to the porcine bone sample on its own (‘pig’) and the other textile samples also formed individual clusters with the exception of (A), (N) and (J) which clustered together. When the six textile types were examined; cellulose-based (A, B, D, J), acrylic-based (E, F), nylon

(H), wool (L), polyester-based (N, O), and leather (Q) samples of each textile type were closely associated, in that the clusters were located beside each other.

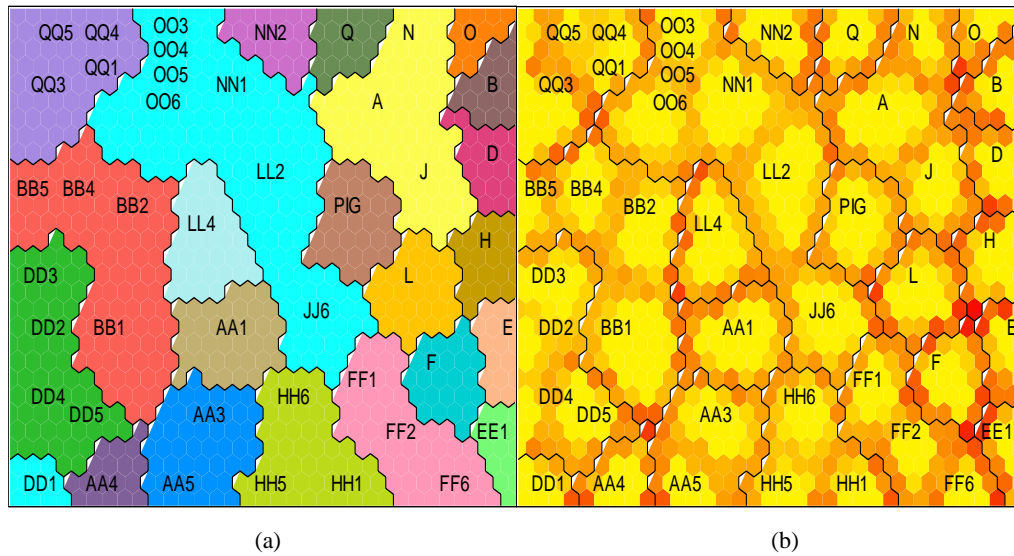


Figure 5.41: 70% map output of 11 combined textile-bone samples, the optimised porcine bone sample ('pig'), and 11 individual textiles classified into 23 segments and visualised through (a) flat clusters and (b) U-matrix clusters

All of the individual textiles and the porcine bone sample were seen to have clustered at the right side of the map. Combined samples (EE) and (FF) were positioned directly next to individual samples (E) and (F), while combined samples (NN), (OO) and (QQ) were positioned at the top left and middle of the map, corresponding to their individual textile samples (N, O and Q) positioned at the top right of the map. The remaining combined samples did not show close association with their respective individual textile samples.

Cellulose-based combined samples (AA, BB, DD and JJ) clustered towards the middle and bottom left of the output maps while polyester-based samples (NN and OO) grouped at the middle top and top left of the maps. While the association between cellulosic (A and B) and polyester-cellulosic blends (N and O) was clearly illustrated for the optimised individual textiles as they were located beside each other (Figure 5.30), their associations were less defined in the combined samples as only (OO) bordered (BB) and no association was noted between (AA) and (NN) or (OO) or between (BB) and (NN).

The porcine bone sample ('pig') was positioned most closely with individual textiles (A), (J) and (L) and combined samples (LL2) and (JJ6) only. Although 100% leather (Q) was expected to be in close association with the porcine bone sample, as they had the most similarities in terms of the type of pyrolysis products detected, this was not directly reflected in the neural network.

5.6 Conclusions

A series of systematic repeat experiments conducted to ascertain the type and consistency of the pyrolysis products detected from the 11 combined samples revealed that, even with similar experimental factors and under controlled laboratory conditions, pyrolytic profiles generated from the same combined samples exposed to an open flame can vary in an unpredictable way. This has been demonstrated clearly in the varying types and reproducibility of pyrolysis products detected within the same textile in the presence of bone, over the six sets of repeats.

The chromatographic profiles of the combined samples varied from those generated from the individual textile samples and, to a lesser extent, porcine bone samples. The influence of porcine bone to the pyrolysis of each textile, and vice versa, is highlighted in this work. Porcine bone influenced the fibre's chemical, thermal and pyrolytic properties; this is distinctively demonstrated across three features: (a) the ability of some textiles to auto-ignite, although they did not when burnt individually (E, F, J, L and O); (b) the dominance of the pyrolytic profile / key indicators of porcine bone over the majority of the textiles, with the exception of combined samples (EE), (FF) and (QQ); and (c) the changes in the temperature profiles across all of the combined samples. Similarly, the textiles also altered the pyrolytic profile of porcine bone, albeit minimally. This is particularly noted with the absence of octane across all of the combined samples, and the absence of decane, propylbenzene and hexadecanitrile in some of the combined samples.

Both the presence of additional pyrolysis products that were not detected in the individual porcine or textile samples and the absence of key indicators of the

majority of the individual textiles support the fact that intermolecular reactions do occur between the molecules from different substrates during pyrolysis, and they can significantly alter the type and presence of characteristic by-products relied on for the identification of a particular target material.

This study also highlighted the use of EIC and EIP as a beneficial tool in identifying key indicators of porcine bone and human toes upon pyrolysis. Although five ions were utilised respectively, the m/z values of 43, 57, 71 and 85 for *n*-alkanes and 41, 55, 69 and 83 for *n*-alkenes were deemed to be most helpful in the extraction process for the identification of porcine / human samples. If present, m/z values of 138, 152, 180 and 194 are most useful for the extraction of hexadecanitrile.

The validation of the SOFM model using optimised individual textile and porcine bone data revealed the ability of the neural network to process complicated data with 100% accuracy in terms of its classification and association so long as a sufficient number of pyrolysis products are present in the samples. For both the individual textile samples and the combined textile-bone samples, the neural network was able to accurately categorise the samples into their respective segments in most cases when 70% of the maximum number of pyrolysis products were present. The SOFM model also showed promise across a range of textile samples that contained overlapping compositions although the number and type of pyrolysis products present is obviously a critical feature. As such, an artificial neural network based statistical approach could be a useful tool in the discrimination of fire debris samples containing textiles and animal / human remains, if the relevant factors are understood and taken into consideration.

5.7 References

1. Stauffer, E., *Identification and Characterization of Interfering Products in Fire Debris Analysis*, in College of Arts and Science. 2001, Florida State University: Miami, USA.
2. Lentini, J.J., Dolan, J.A., and Cherry, C., *The Petroleum-Laced Background*. Journal of Forensic Sciences, 2000. **45**(5): p. 968-989.
3. Lentini, J.J., *Incidental Accelerants*. National Fire and Arson Report, 1983. **2**(3): p. 3.
4. Stauffer, E., *Concept of Pyrolysis for Fire Debris Analysis*. Science and Justice, 2003. **43**(1): p. 29-40.
5. Jhaumeer-Laulloo, S., Maclean, J., Ramtoola, L.L., Duyman, K., and Toofany, A., *Characterisation of Background and Pyrolysis Products That May Interfere with Forensic Analysis of Fire Debris in Mauritius*. Pure and Applied Chemical Sciences, 2013. **1**(2): p. 51-61.
6. Cavanagh, K., Pasquier, E.D., and Lennard, C., *Background Interference from Car Carpets-The Evidential Value of Petrol Residues in Cases of Suspected Vehicle Arson*. Forensic Science International, 2002. **125**(1): p. 22-36.
7. Dehaan, J.D. and Bonarius, K., *Pyrolysis Products of Structure Fires*. Journal of the Forensic Science Society, 1988. **28**(5): p. 299-309.
8. Keto, R.O., *GC/MS Data Interpretation for Petroleum Distillate Identification in Contaminated Arson Debris*. Journal of Forensic Sciences, 1995. **40**: p. 412-412.
9. Nic Daeid, N., *An Introduction to Fires and Fire Investigation*, in Fire Investigation, ed. N. Nic Daeid. 2004, Boca Raton, Florida: CRC Press.
10. Stauffer, E., *Sources of Interference in Fire Debris Analysis*, in Fire Investigation, ed. N. Nic Daeid. 2004, Boca Raton, Florida: CRC Press. p. 191.
11. Drysdale, D., *An Introduction to Fire Dynamics*. 2002, Scotland, UK: John Wiley and Sons.

12. Nowicki, J., *An Accelerant Classification Scheme Based on Analysis by Gas Chromatography/Mass Spectrometry (GC-MS)*. 1990: National Emergency Training Center.
13. Stone, I. and Lomonte, J., *False Positions in Analysis of Fire Debris*. The Fire and Arson Investigator, 1984. **34**(3): p. 36-40.
14. Howard, J. and Mckague, A.B., *A Fire Investigation Involving Combustion of Carpet Material*. Journal of Forensic Sciences, 1984. **29**(3): p. 919-922.
15. Clodfelter, R.W. and Hueske, E.E., *A Comparison of Decomposition Products from Selected Burned Materials with Common Arson Accelerants*. Journal of Forensic Sciences, 1977. **22**: p. 116.
16. Fernandes, M.S., Lau, C.M., and Wong, W.C., *The Effect of Volatile Residues in Burnt Household Items on the Detection of Fire Accelerants*. Science and Justice, 2002. **42**(1): p. 7-15.
17. Curran, A.M., Rabin, S.T.I., Prada, P.A., and Furton, K.G., *Comparison of the Volatile Organic Compounds Present in Human Odor Using SPME-GC/MS*. Journal of Chemical Ecology, 2005. **31**(7): p. 1607-1619.
18. Wells, S.B., *The Identification of Isopar H in Vinyl Flooring*. Journal of Forensic Sciences, 2005. **50**(4): p. 865-872.
19. Bertsch, W., *Volatiles from Carpet: A Source of Frequent Misinterpretation in Arson Analysis*. Journal of Chromatography A, 1994. **674**(1): p. 329-333.
20. ASTM International E1412-07, *Standard Practice for Separation of Ignitable Liquid Residues from Fire Debris Samples by Passive Headspace Concentration with Activated Charcoal*. 2012. American Society for Testing and Materials (ASTM) International: West Conshohocken, PA.
21. ASTM International E1387-01, *Standard Test Method for Ignitable Liquid Residues in Extracts from Fire Debris Samples by Gas Chromatography*. 2002. American Society for Testing and Materials (ASTM) International: West Conshohocken, PA.
22. ASTM International E1618-11, *Standard Test Method for Ignitable Liquid Residues in Extracts from Fire Debris Samples by Gas Chromatography-Mass Spectrometry*. 2012. American Society for Testing and Materials (ASTM) International: West Conshohocken, PA.

23. ASTM International E2154-01, *Separation and Concentration of Ignitable Liquid Residues from Fire Debris Samples by Passive Headspace Concentration with Solid Phase Microextraction (SPME)*. 2012. American Society for Testing and Materials (ASTM) International: West Conshohocken, PA.
24. ASTM International E1388-12, *Standard Practice for Sampling of Headspace Vapors from Fire Debris Samples*. 2012. American Society for Testing and Materials (ASTM) International: West Conshohocken, PA.
25. Clodfelter, R.W. and Hueske, E.E., *A Comparison of Decomposition Products from Selected Burned Materials with Common Arson Accelerants*. *Journal of Forensic Sciences*, 1977. **22**: p. 116.
26. Lennard, C.J., Tristan Rochaix, V., Margot, P., and Huber, K., *A GC-MS Database of Target Compound Chromatograms for the Identification of Arson Accelerants*. *Science and Justice*, 1995. **35**(1): p. 19-30.
27. Almirall, J.R. and Furton, K.G., *Characterization of Background and Pyrolysis Products That May Interfere with the Forensic Analysis of Fire Debris*. *Journal of Analytical and Applied Pyrolysis*, 2004. **71**(1): p. 51-67.
28. Borusiewicz, R., Zięba-Palus, J., and Zadora, G., *The Influence of the Type of Accelerant, Type of Burned Material, Time of Burning and Availability of Air on the Possibility of Detection of Accelerants Traces*. *Forensic Science International*, 2006. **160**(2): p. 115-126.
29. Vella, A.J., *Arson Investigation Using the Ion Trap Detector*. *Journal of the Forensic Science Society*, 1992. **32**(2): p. 131-142.
30. Dehaan, J.D. and Nurbakhsh, S., *Sustained Combustion of an Animal Carcass and Its Implications for the Consumption of Human Bodies in Fires*. *Journal of Forensic Sciences*, 2001. **46**(5): p. 1076.
31. Dehaan, J.D., *Sustained Combustion of Bodies: Some Observations**. *Journal of Forensic Sciences*, 2012.
32. Christensen, A.M., *Experiments in the Combustibility of the Human Body*. *Journal of Forensic Sciences*, 2002. **47**(3): p. 466-470.

33. Dehaan, J.D., Brien, D.J., and Large, R., *Volatile Organic Compounds from the Combustion of Human and Animal Tissue*. Science and Justice, 2004. **44**(4): p. 223-236.
34. Agu, K., *Investigation of the Thermal Degradation Products of Bone*, in Centre for Forensic Science, Department of Pure and Applied Chemistry. 2011, University of Strathclyde: Glasgow, Scotland.
35. Mclellan, S.A., *An Investigation of the Volatiles Produced from Pyrolysis of the Body*, in Centre for Forensic Science, Department of Pure and Applied Chemistry. 1999, University of Strathclyde: Glasgow, Scotland.
36. Almirall, J.R. and Furton, K.G., *Analysis and Interpretation of Fire Scene Evidence*. Forensic Science Techniques Series. 2004, Boca Raton, Florida: CRC Press.
37. Lentini, J.J., *Analysis of Ignitable Liquid Residues*, in Scientific Protocols for Fire Investigation, ed. J.J. Lentini. 2006, Boca Raton, Florida: Taylor and Francis Gp: CRC Press.
38. Brereton, R., *Chemometrics for Pattern Recognition*. 2009, West Sussex, UK: John Wiley and Sons.
39. Mchugh, K.M., *Determining the Presence of an Ignitable Liquid Residue in Fire Debris Samples Utilizing Target Factor Analysis*, in Department of Forensic Science, College of Sciences. 2010, University of Central Florida: Orlando, Florida.
40. Lavine, B.K. and Mirjankar, N., *Clustering and Classification of Analytical Data*. Encyclopedia of Analytical Chemistry. 2000: John Wiley and Sons.
41. Mat Desa, W.N.S., *The Discrimination of Ignitable Liquids and Ignitable Liquid Residues Using Chemometric Analysis*, in Centre for Forensic Science, Department of Pure and Applied Chemistry. 2012, University of Strathclyde: Glasgow, Scotland.
42. Wineman, P.L. and Keto, R.O., *Target-Compound Method for the Analysis of Accelerant Residues in Fire Debris*. Analytica Chimica Acta, 1994. **288**(1-2): p. 97-110.

43. Keto, R.O. and Wineman, P.L., *Detection of Petroleum-Based Accelerants in Fire Debris by Target Compound Gas Chromatography/Mass Spectrometry*. Analytical Chemistry, 1991. **63**(18): p. 1964-1971.
44. Chatfield, C. and Collins, A., *Introduction to Multivariate Analysis*. Vol. **1**. 1981, Boca Raton, Florida: CRC Press.
45. Doble, P., Sandercock, M., Du Pasquier, E., Petocz, P., Roux, C., and Dawson, M., *Classification of Premium and Regular Gasoline by Gas Chromatography/Mass Spectrometry, Principal Component Analysis and Artificial Neural Networks*. Forensic Science International, 2003. **132**(1): p. 26-39.
46. Borusiewicz, R., Zadora, G., and Zieba-Palus, J., *Application of Head-Space Analysis with Passive Adsorption for Forensic Purposes in the Automated Thermal Desorption-Gas Chromatography-Mass Spectrometry System*. Chromatographia, 2004. **60**: p. 133-142.
47. Williams, M.R., *Advances in Fire Debris Analysis*, in Department of Chemistry, College of Sciences. 2007, University of Central Florida: Orlando, Florida.
48. Sigman, M. and Williams, M., *Application of Chemometrics and Fast GC-MS Analysis for the Identification of Ignitable Liquids in Fire Debris Samples*. 2012, U.S. Department of Justice: USA.
49. Stauffer, E., Dolan, J.A., and Newman, R., *Fire Debris Analysis*. 2008, San Diego, USA: Academic Press.
50. Andrews, J.M. and Lieberman, S.H., *Neural Network Approach to Qualitative Identification of Fuels and Oils from Laser Induced Fluorescence Spectra*. Analytica Chimica Acta, 1994. **285**(1): p. 237-246.
51. Tan, B., Hardy, J.K., and Snavelly, R.E., *Accelerant Classification by Gas Chromatography/Mass Spectrometry and Multivariate Pattern Recognition*. Analytica Chimica Acta, 2000. **422**(1): p. 37-46.
52. Sigman, M.E., Williams, M.R., and Ivy, R.G., *Individualization of Gasoline Samples by Covariance Mapping and Gas Chromatography/Mass Spectrometry*. Analytical Chemistry, 2007. **79**(9): p. 3462-3468.

53. Hupp, A.M., Marshall, L.J., Campbell, D.I., Smith, R.W., and McGuffin, V.L., *Chemometric Analysis of Diesel Fuel for Forensic and Environmental Applications*. *Analytica Chimica Acta*, 2008. **606**(2): p. 159-171.
54. Marshall, L.J., *Association and Discrimination of Diesel Fuels Using Chemometric Procedures*, in School of Criminal Justice. 2009, Michigan State University: Michigan, USA. p. 2049-2059.
55. Tobias, R.D., *Chemometrics: A Practical Guide*. *Technometrics*, 1999. **41**(4): p. 375-376.
56. Sandercock, P.M.L. and Du Pasquier, E., *Chemical Fingerprinting of Unevaporated Automotive Gasoline Samples*. *Forensic Science International*, 2003. **134**(1): p. 1-10.
57. Newman, R., *Interpretation of Laboratory Data*, in *Fire Investigation*, ed. N. Nic Daeid. 2004, Boca Raton, Florida: CRC Press. p. 155.
58. Bogusz, M.J., Phipps, R.J., Smith, J.J., Darwin, W.D., Cone, E.J., Cody, J.T., Elsohly, M.A., Gul, W., Salem, M., and Kraemer, T., *Handbook of Analytical Separations*. 2nd Edition. *Forensic Science*, ed. M.J. Bogusz. Vol. **6**. 2000, Amsterdam: Elsevier. p. 1-742.
59. Dolan, J., *Recent Advances in the Applications of Forensic Science to Fire Debris Analysis*. *Analytical and Bioanalytical Chemistry*, 2003. **376**(8): p. 1168-1171.
60. Dehaan, J.D., *Kirk's Fire Investigation*. 5th Edition. 2002, Upper Saddle River, NJ: Prentice Hall.
61. Newman, R., *Modern Laboratory Techniques Involved in the Analysis of Fire Debris Samples*, in *Fire Investigation*, ed. N. Nic Daeid. 2004, Boca Raton, Florida: CRC Press.
62. Radischa, C., Sippula, O., Stengel, B., Sklorz, M., Streibel, T., Rabe, R., and Zimmermann, R., *On-Line and Real Time Analysis of Organic Combustion Products in Ship Diesel Exhaust with Mass Spectrometry Using Various Ionisation Techniques*. 2014, Joint Mass Spectrometry Centre: Helmholtz Zentrum, Munich.

63. Gilbert, M.W., *The Use of Individual Extracted Ion Profiles Versus Summed Extracted Ion Profiles in Fire Debris Analysis*. *Journal of Forensic Sciences*, 1998. **43**: p. 871-876.
64. Sutherland, D., Peer, J., and Almirall, J.R., *Identification of Ignitable Liquid Residue in Fire Debris Analysis by GC/MS/MS*, in *Advances in Forensic Applications of Mass Spectrometry*, ed. J. Yinon. 2003, CRC Press: Boca Raton, Florida.
65. Stauffer, E. and Lentini, J.J., *ASTM Standards for Fire Debris Analysis: A Review*. *Forensic Science International*, 2003. **132**(1): p. 63-67.
66. Nowicki, J., *Analysis of Fire Debris Samples by Gas Chromatography/Mass Spectrometry (GC-MS): Case Studies*. 1991: National Emergency Training Center.
67. Terfloth, L. and Gasteiger, J., *Neural Networks and Genetic Algorithms in Drug Design*. *Drug Discovery Today*, 2001. **6**: p. 102-108.
68. Anzali, S., Gasteiger, J., Holzgrabe, U., Polanski, J., Sadowski, J., Teckentrup, A., and Wagener, M., *The Use of Self-Organizing Neural Networks in Drug Design*. *Perspectives in Drug Discovery and Design*, 1998. **9**: p. 273-299.
69. Marini, F., *Artificial Neural Networks in Foodstuff Analyses: Trends and Perspectives: A Review*. *Analytica Chimica Acta*, 2009. **635**(2): p. 121-131.
70. Cosio, M.S., Ballabio, D., Benedetti, S., and Gigliotti, C., *Geographical Origin and Authentication of Extra Virgin Olive Oils by an Electronic Nose in Combination with Artificial Neural Networks*. *Analytica Chimica Acta*, 2006. **567**(2): p. 202-210.
71. Afkhami, A., Abbasi-Tarighat, M., and Khanmohammadi, H., *Simultaneous Determination of Co^{2+} , Ni^{2+} , Cu^{2+} and Zn^{2+} Ions in Foodstuffs and Vegetables with a New Schiff Base Using Artificial Neural Networks*. *Talanta*, 2009. **77**(3): p. 995-1001.
72. Yang, B-S., Han, T., and An, J.L., *Art-Kohonen Neural Network for Fault Diagnosis of Rotating Machinery*. *Mechanical Systems and Signal Processing*, 2004. **18**(3): p. 645-657.

73. Cheu, R.L. and Ritchie, S.G., *Automated Detection of Lane-Blocking Freeway Incidents Using Artificial Neural Networks*. Transportation Research Part C: Emerging Technologies, 1995. **3**(6): p. 371-388.
74. El Kadi, H., *Modeling the Mechanical Behavior of Fiber-Reinforced Polymeric Composite Materials Using Artificial Neural Networks—A Review*. Composite Structures, 2006. **73**(1): p. 1-23.
75. Thorpe, J.W. and Ismail, D. *Pattern Recognition Procedures for the Classification and Prediction of Stains Originating from Wax-Based Products*, in 108th Semi-annual Seminar (Fall 2006) California Association of Criminalist, October 9th-13th, 2006. Temecula, California: California Association of Criminalist.
76. Fei, B.K.L., Eloff, J.H.P., Venter, H.S., and Olivier, M.S., *Chapter 10: Exploring Forensic Data with Self-Organizing Maps*, in Advances in Digital Forensics, ed. M. Pollitt and S. Shenoj., 2005, Springer: USA. p. 113-123.
77. Mat Desa, W.N.S., Nic Daeid, N., Ismail, D., and Savage, K., *Application of Unsupervised Chemometric Analysis and Self-Organizing Feature Map (SOFM) for the Classification of Lighter Fuels*. Analytical Chemistry, 2010. **82**(15): p. 6395-6400.
78. Fei, B.K.L., Eloff, J.H.P., Olivier, M.S., and Venter, H.S., *The Use of Self-Organising Maps for Anomalous Behaviour Detection in a Digital Investigation*. Forensic Science International, 2006. **162**(1): p. 33-37.
79. Nic Daeid, N. and Ismail, D., *Comparison of Smears of Wax Based Products Using Thin Layer Chromatography (TLC) and Microspectrophotometric (MSP) Detection*. Journal of Forensic Identification, 2011.
80. Kou, C., Tung, C-T., and Fu, H.C. *FISOFM: Firearms Identification Based on SOFM Model of Neural Network*. in Security Technology, in 28th Annual International Carnahan Conference. 1994. Institute of Electrical and Electronics Engineers (IEEE).
81. Ismail, D., *The Application of Pattern Recognition Techniques to Data Derived from the Chemical Analysis of Common Wax Based Products and Ignitable Liquids*, in Centre for Forensic Science, Department of Pure and Applied Chemistry. 2012, University of Strathclyde: Glasgow, Scotland.

82. Reed, G., *Multivariate Profiling of Gel Inks: A Novel Tool for the Discrimination of Within and Between Brand Variation*, in Centre for Forensic Science, Department of Pure and Applied Chemistry. 2013, University of Strathclyde: Glasgow, Scotland.
83. Kohonen, T., *Self-Organized Formation of Topologically Correct Feature Maps*. *Biological Cybernetics*, 1982. **43**(1): p. 59-69.
84. He, Q., *Neural Network and Its Application in IR*, in Graduate School of Library and Information Science,. 1999, University of Illinois: Urbana-Champaign Spring.
85. Kohonen, T. *The Self-Organizing Map*. in *Proceedings of the Institute of Electrical and Electronic Engineering*. 1990: Institute of Electrical and Electronic Engineers (IEEE).
86. Lippmann, R.P., *An Introduction to Computing with Neural Nets*. *ASSP Magazine: Institute of Electrical and Electronic Engineers (IEEE)*, 1987. **4**(2): p. 4-22.
87. Eghbalpour, H., *Artificial Neural Network Lecture_Section 3 (Self Organizing Feature Mapping)*. 2003, BP&A Planning Semiconductors.
88. Vesanto, J., *Som-Based Data Visualization Methods*. *Intelligent Data Analysis*, 1999. **3**(2): p. 111-126.
89. Soria-Frisch, A., *Unsupervised Construction of Fuzzy Measures through Self-Organizing Feature Maps and Its Application in Color Image Segmentation*. *International Journal of Approximate Reasoning*, 2006. **41**(1): p. 23-42.
90. Fincke, T., Lobo, V., and Bação, F., *Visualizing Self-Organizing Maps with GIS*. *GI Days*, 2008.
91. PyMVPA, *Self-Organizing Maps*. [Online] [2006-2013, January 2015] Available from: <http://www.pymvpa.org/examples/som.html>.
92. The National Institute of Standards and Technology (NIST)[®], *NIST/EPA/NIH Mass Spectral Library (NIST 08) V. 2.0f*. 1987-2008. The National Institute of Standards and Technology (NIST)[®].
93. Wakelyn, P.J., Bertoniere, N.R., French, A.D., Thibodeaux, D.P., Triplett, B.A., Rousselle, M-A., Goynes Jr., W.R., Edwards, J.V., Hunter, L., and

- Mcalister, D.D., *Chemical Properties of Cotton*, in Cotton Fiber Chemistry and Technology. 2010, New York, USA: CRC Press.
94. Nakanishi, S., Masuko, F., Hori, K., and Hashimoto, T., *Pyrolytic Gas Generation of Cotton Cellulose with and without Flame Retardants at Different Stages of Thermal Degradation: Effects of Nitrogen, Phosphorus, and Halogens*. Textile Research Journal, 2000. **70**(7): p. 574-583.
 95. Zhu, P., Sui, S., Wang, B., Sun, K., and Sun, G., *A Study of Pyrolysis and Pyrolysis Products of Flame-Retardant Cotton Fabrics by DSC, TGA, and PY-GC-MS*. Journal of Analytical and Applied Pyrolysis, 2004. **71**(2): p. 645-655.
 96. Keheyani, Y., *PY/GC/MS Analyses of Historical Papers*. BioResources, 2008. **3**(3): p. 829-837.
 97. Lin, Y.-C., Cho, J., Tompsett, G.A., Westmoreland, P.R., and Huber, G.W., *Kinetics and Mechanism of Cellulose Pyrolysis*. The Journal of Physical Chemistry C, 2009. **113**(46): p. 20097-20107.
 98. Farooq, A.A., Price, D., Milnes, G.J., and Horrocks, A.R., *Use of Gas Chromatographic Analysis of Volatile Products to Investigate the Mechanisms Underlying the Influence of Flame Retardants on the Pyrolysis of Cellulose in Air*. Polymer Degradation and Stability, 1991. **33**(2): p. 155-170.
 99. Price, D., Horrocks, A.R., Akalin, M., and Farooq, A.A., *Influence of Flame Retardants on the Mechanism of Pyrolysis of Cotton (Cellulose) Fabrics in Air*. Journal of Analytical and Applied Pyrolysis, 1997. **40**: p. 511-524.
 100. Kawamoto, H., Murayama, M., and Saka, S., *Pyrolysis Behavior of Levoglucosan as an Intermediate in Cellulose Pyrolysis: Polymerization into Polysaccharide as a Key Reaction to Carbonized Product Formation*. Journal of Wood Science, 2003. **49**(5): p. 469-473.
 101. Shen, D.K. and Gu, S., *The Mechanism for Thermal Decomposition of Cellulose and Its Main Products*. Bioresource Technology, 2009. **100**(24): p. 6496-6504.

CHAPTER 6: GENERAL CONCLUSIONS AND FUTURE WORK

6.1 Summary of Conclusions

The application of highly discriminative analytical instruments, such as the GC-MS, coupled together with the American Society for Testing and Materials (ASTM) established standards has facilitated the process of analysing and interpreting fire debris samples. When the scene of a fire is suspected of having biological residues (i.e. human or animal), the interpretation process becomes complicated as no reliable key indicators of these remains in a fire have been systematically studied and established. This process is complicated further with fire scenes containing a range of fuel loads, such as upholstery, carpets, textiles, etc. In the little work that has been conducted by a number of researchers, a series of *n*-aldehydes generated from the pyrolysis of human and animal fat has been suggested to be potentially useful as key indicators of human and animal remains in a fire.

This work was undertaken in order to develop a robust and systematic laboratory-based methodology that emulates real fire scenarios in the generation, extraction and analysis of pyrolysis products from biological and non-biological sources. The work was based on the application of passive headspace extraction with activated carbon strips (ACS) coupled with GC-MS. Through repetitive work, experimental factors (ACS sizes, post-deprivation sampling time and sample weight) were optimised and validated to create a reliable and robust system in which the analyses of pyrolysis products across a range of samples were conducted. The experimental procedure for the generation of pyrolysis products was validated using porcine bone samples and the method was proven to generate repeatable and optimal pyrolysis products of C₈ to C₁₇ *n*-alkanes and *n*-alkenes, *n*-alkyl-benzenes, aromatics and a nitrile from a sample weight of 25 g sampled at 4 minutes post-deprivation using a ACS of 10 mm × 20 mm analysed using the GC-MS.

Upon validation, porcine bone and human toe samples were pyrolysed to compare the types of products generated across these samples, and to identify key indicators

of human and animal remains. The hypothesis was that the pyrolysis products from porcine tissues do not differ from those generated from human tissues under similar experimental conditions and, as a consequence, porcine tissues could be a valid representative of human tissues in a fire. Both samples were found to display similar chromatographic profiles, demonstrating the ability of porcine samples to act as a template for human samples in the analysis of pyrolysis products. A database of pyrolysis products across these two species was established, with the identification of key indicators of porcine and human tissues. These are *n*-alkanes and *n*-alkenes, *n*-alkyl-benzenes, aromatics and nitrile(s). For porcine bone samples, additional *n*-alkenes, methyl-alkane nitriles, alkane nitriles, *n*-cycloalkanes and *n*-cycloalkanes, dienes, alkyl-pyrroles, *n*-alkyl-benzenes and substituted alkyl-benzenes, aromatics, substituted benzenes, cyano-alkene, disulfide, an alkyne and a ketone were also detected; for human toe samples, additional *n*-alkyl-benzenes, *n*-alkane, *n*-alkene, a nitrile, disulfide, *n*-alkyl-cycloalkane and an alkyl-furan were also present, however, these products were not consistent across the six sets of repeats and were, therefore, determined to be unreliable indicators of porcine bone and human toe pyrolysis, respectively.

Throughout the analysis of a number of porcine and human tissues post-pyrolysis, the purported series of *n*-aldehydes was not encountered and temperature, rather than exposure duration, was identified as a factor governing the presence or absence of *n*-aldehydes, and its effects were demonstrated across pre-ignition (< 250 °C) and post-ignition (> 250 °C) samples. While pre-ignition porcine bone, muscle and rib samples generated a homologous series of *n*-aldehydes, none were detected in post-ignition samples. The absence of *n*-aldehydes at elevated temperatures in this study demonstrates clearly that their presence or absence is temperature-dependent. This renders unreliable the use of *n*-aldehydes as key indicators of human remains in a fire and has convincingly resolved the previous research literature. Across these three tissues, the main difference noted was the inability of porcine muscle and rib to attain auto-ignition, whereas porcine bone readily auto-ignited; this illustrated that differences in tissue sampling from a fire scene can certainly influence the type of pyrolysis products detected.

In terms of non-biological samples, the pyrolysis and thermal behaviour of 20 common textile types, both pure and blended, were investigated as these materials are commonly used in clothing and could cause potential interferences with the analysis of key indicators human / animal remains. The variation in the burning properties and type of pyrolysis products generated over a range of textiles (i.e. natural, semi-synthetic and synthetic) was highlighted. These variations were not only demonstrated with textiles from different sources (i.e. animal, plant and manufactured) but also within the same group and within the same type of textile. The type and consistency of pyrolysis products detected over repetitive experiments were identified, and this facilitated the process of narrowing down the range of textiles to a manageable number (11) for further experimentation. In this process, key indicators of each textile type were determined. It should be noted, however, that the presence or absence of these characteristic products is largely dependent on temperature and burning duration. The influence of one or more blended fibres in a textile was also emphasised: the presence of the blended fibre did not influence only the major fibre's physical characteristics, but also its chemical, thermal and pyrolytic properties.

Once this stage was completed, porcine bone samples were then combusted in the presence of the optimised textiles (termed 'combined samples'). A series of systematic repeat experiments conducted on the 11 combined samples revealed that, even with similar experimental factors and under controlled laboratory conditions, pyrolysis profiles generated within the same combined sample types exposed to an open flame can vary in an unpredictable way. This has been clearly demonstrated in the varying types and consistencies of pyrolysis products detected within the six sets of repeat experiments for each combined sample.

The chromatographic profiles of the combined samples varied from those generated from the individual textile samples and, to a lesser extent, the porcine bone samples. The influence of the presence of porcine bone in the pyrolysis of each textile, and vice versa, is highlighted in this work. The presence of porcine bone did not influence only the fibre's physical characteristics, but also its chemical, thermal and

pyrolytic properties. Similarly, the textiles were also shown to exert influence, although minimal, on the pyrolytic profile of porcine bone. This is particularly noted in the absence of octane across all combined samples, and the absence of decane, propyl-benzene and hexadecanitrile in some of the combined samples. The presence of additional pyrolysis products that were not detected in the individual porcine and textile samples and the absence of key indicators of the majority of the individual textiles supports the fact that intermolecular reactions do occur between the textile and bone during pyrolysis and they can significantly alter the type and presence of characteristic key by-products which are relied on for identification of a particular target material.

The final stage of this study investigated the usefulness of pattern recognition techniques in separating and identifying key indicators of porcine and textile samples which had been combusted together. This was conducted through a two-fold process. Firstly, the m/z values of the key indicators of porcine samples were identified, and extracted ion chromatogram (EIC) and extracted ion profile (EIP) were conducted on the combined samples to evaluate the ability of these techniques to extract the profiles of human and porcine tissue in the presence of textiles. Both EIC and EIP proved to be useful in identifying key indicators of porcine bone upon pyrolysis. Although five ions were utilised for *n*-alkanes and *n*-alkenes respectively, the m/z values of 43, 57, 71 and 85 for *n*-alkanes and 41, 55, 69 and 83 for *n*-alkenes were deemed to be most helpful in the extraction process for the identification of porcine / human samples. If present, m/z values of 138, 152, 180 and 194 are most useful for the extraction of hexadecanitrile.

In the pattern recognition technique, multidimensional datasets within the self-organising feature map (SOFM) were tested and explored. Through the use of SOFM, the multidimensional data was translated into a two-dimensional, meaningful output (topographic map) to ascertain the ability of the artificial neural network to reveal separation, categorise and identify relationships between the individual textiles and porcine bone, and in the combined samples. The validation of the SOFM model using the optimised individual textiles and porcine bone data revealed the

ability of the neural network to process complicated data with 100% accuracy (100% correctly classified) in terms of classification and association. Even with inconsistent and fairly unreproducible data, the software was able to categorise the samples according to the type and presence / absence of pyrolysis products to a certain degree of certainty for correct classification. This value was determined through the calculation of the percentage of pyrolysis products present to the total pyrolysis products detected in each textile type. For both the individual textile samples and the combined samples (which were textiles in the presence of porcine bone), this degree of certainty was at 70%. This means that the neural network was able to accurately categorise the samples into their respective segments according to the type of pyrolysis products detected at 70%. Clear visualisation of sample linkages, particularly for textiles that contained overlapping compositions, were noted and, as such, SOFM has been proven to demonstrate within the topographic map meaningful connections and associations between samples that are similar to each other. This artificial neural network based statistical approach could potentially be a useful tool in the discrimination of fire debris samples containing textiles and animal / human remains, if the relevant factors are understood and taken into consideration.

6.2 Recommendations for Future Work

Because this work was undertaken with a limited source of human tissue (human toe), pyrolytic experiments using other parts of the human body would be advantageous. This would reveal further information about the type and consistency of pyrolysis products generated by different types of human tissues in a fire.

It would also be particularly interesting to explore tissues of human and porcine origin that have been subjected to decomposition and burnt thereafter. Data generated from this process would be helpful in identifying the effects of decomposition, if any, on the type of pyrolysis products detected across these tissues.

Besides textiles, various types of other materials (e.g. ILR, upholstery, carpets, wood, plastics) that are commonly involved in a fire can be introduced as interfering

compounds in the proper analysis and identification of porcine and human tissues in a fire. Once obtained, this information could then be inserted into a database containing key indicators of the various materials tested, which would be beneficial for the forensic science community in recognising interferences during fire debris analysis.

In addition to the presence / absence classification process utilised in the SOFM model in this work, the use of peak area or height ratio values might also be valuable during analysis, particularly if consistent ratios are produced across the sets of repeats. The potential use of benzene, toluene and ethyl-benzene as an internal standard could also be explored as they have been detected consistently across the individual porcine bone, human toe and combined samples. Normalising the peak areas of the compounds identified in the chromatogram to the peak area of the aromatics and *n*-alkyl-benzenes generated from the pyrolysis process could potentially be useful in determining ratios and reducing the % RSD values of the analysis.

The SOFM network has demonstrated substantial associative abilities in tracing patterns across the pyrolytic data of porcine, human and textile samples, even when dealing with inconsistent data across most of the data sets. With careful consideration, further work could be undertaken in the use of this neural network for classifying complex chromatographic data from fire scenes. Besides SOFM, it would also be interesting to explore the applicability of other statistical tools and chromatographic pattern recognition techniques in the analysis of pyrolytic data.

APPENDICES

Appendix 1.0:

Pyrolysis Products Generated across Six Sets of Repeats from Porcine Bone

In addition to the consistent presence of C₈ to C₁₇ *n*-alkanes and *n*-alkenes together with some aromatics, *n*-alkyl-benzenes and a nitrile, porcine bone samples also generated a range of additional pyrolysis products that were inconsistent across the six sets of repeats. The products were isomers of *n*-alkenes, methyl-alkane nitriles and alkane nitriles, *n*-cycloalkanes and *n*-cycloalkanes, dienes, pyrrole and alkyl-pyrroles, *n*-alkyl-benzenes and substituted alkyl-benzenes, aromatics, substituted benzenes, cyano-alkene, disulfide, an alkyne and a ketone.

Retention Time (min)	Compound	Set					
		1	2	3	4	5	6
2.13	butanenitrile	√				√	√
2.19	3-methyl-cyclopentane	√		√		√	√
2.21	benzene	√	√	√	√	√	√
2.35	2-methyl-1,3-pentadiene	√					
2.85	2-methyl-butanenitrile			√		√	√
3.52	cyclohexene	√		√			√
3.30	1-methyl-1H-pyrrole	√		√		√	√
3.41	dimethyl disulfide					√	√
3.67	pyrrole	√				√	√
3.84	3-methyl-butanenitrile	√					√
3.88	pentanenitrile	√					√
4.12	toluene	√	√	√	√	√	√
4.40	3-methyl-cyclohexane	√					√
5.20	1-ethyl-1H-pyrrole	√	√	√		√	√
5.35	1-octene	√	√	√	√	√	√
5.60	octane	√	√	√	√	√	√
5.72	2-octene	√		√		√	√
5.82	4-methyl-pentanenitrile	√		√		√	√
5.95	3-octene	√		√		√	√
6.14	cyclooctane	√					
6.30	ethyl-cyclohexane	√		√			√
6.77	hexanenitrile	√					
6.82	ethyl-benzene	√	√	√	√	√	√
6.99	2,4-octadiene	√					
7.02	<i>p</i> -xylene	√	√	√	√	√	√
7.40	styrene	√					
7.43	5-methyl-2(1H)-pyridinone					√	√
7.70	1-nonene	√	√	√	√	√	√
7.84	2-nonene	√				√	
7.91	nonane	√	√	√	√	√	√
7.98	nonene isomer	√		√			√
8.12	<i>cis</i> -2-nonene	√		√			√

8.19	3-butyl-cyclopentene	√					
8.24	1-butyl-1H-pyrrole		√	√		√	√
8.34	1,3-nonadiene	√					
8.50	6-cyano-1-hexene	√					
8.60	propyl benzene	√	√	√	√	√	√
8.65	1-butyl-cyclopentene	√				√	√
8.68	octanenitrile	√				√	√
8.73	1-ethyl-2-methyl-benzene	√		√			√
8.99	1-ethyl-3-methyl-benzene	√		√			√
9.26	4-decene	√		√			
9.34	1-decene	√	√	√	√	√	√
9.43	decene isomer	√		√			√
9.50	decane	√	√	√	√	√	√
9.53	<i>cis</i> -3-decene	√		√		√	√
9.66	decene isomer	√		√		√	√
9.74	cyclodecene	√		√			
9.99	1-pentyl-1H-pyrrole	√	√	√		√	√
10.07	butyl-benzene	√		√		√	√
10.12	nonanenitrile	√		√		√	√
10.60	1-undecene	√	√	√	√	√	√
10.67	5-undecene	√		√			
10.70	undecane	√	√	√	√	√	√
10.87	undecene isomer	√	√	√			√
10.95	cycloundecene	√		√			
11.02	1-hexyl-cyclopentene	√		√			
11.27	pentyl-benzene	√	√	√		√	√
11.32	decanenitrile	√		√			√
11.38	1-methylbutyl-benzene	√		√			√
11.71	1-dodecene	√	√	√	√	√	√
11.76	3-dodecene	√		√			
11.84	dodecane	√	√	√	√	√	√
11.95	dodecene isomer	√		√			
12.01	cyclododecene	√					
12.34	hexyl-benzene	√				√	√
12.38	undecanenitrile	√					√
12.41	1,3-dimethylbutyl-benzene	√					√
12.70	1-tridecene	√	√	√	√	√	√
12.80	tridecane	√	√	√	√	√	√
13.33	heptyl-benzene	√					
13.58	7-tetradecene	√		√			
13.65	1-tetradecene	√	√	√	√	√	√
13.71	tetradecane	√	√	√	√	√	√
14.14	nonyl-cyclopentane	√	√	√		√	√
14.42	1-pentadecene	√	√	√	√	√	√
14.47	2-pentadecene	√	√	√		√	
14.56	pentadecane	√	√	√	√	√	√
14.99	nonyl-cyclohexane	√	√	√			√
15.12	1-hexadecyne		√	√			
15.18	1-hexadecene	√	√	√	√	√	√
15.22	3-hexadecene	√	√	√			√

15.27	hexadecene isomer	√	√	√			
15.34	hexadecane	√	√	√	√	√	√
15.85	cyclohexadecane	√		√			√
15.93	8-heptadecene	√		√		√	√
15.96	1-heptadecene	√	√	√	√	√	√
16.09	heptadecane	√	√	√	√	√	√
17.13	hexadecanitrile	√	√	√	√	√	√

Appendix 2.0:

Pyrolysis Products from 50% Cotton + 33% Viscose + 17% Polyester (C)

The pyrolysis of 50% cotton + 33% viscose + 17% polyester (C) generated a range of products, generally representing its cellulose (cotton and viscose) counterpart with most of its key indicators present. However, the consistency of these products across the six repeats was very poor. These products were furans, *n*-aldehydes, aromatics, *n*-alkyl-benzenes, furan alcohol, ketones, acid and acid ester, sugar and levoglucosenone. All of these products were also detected across the textile blends containing cellulose in (A), (B), (D) and a number of these products were also present across textiles (F), (N) and (O) that contained cotton, rayon and viscose, respectively. The isomers of the sugar compound (1,4:3,6-dianhydro- α -D-glucopyranose) detected here was also present across textiles (D) and (F) and is attributed to have generated from the decomposition of cellulose [1] and has been previously mentioned in the literature to be an isomeric form of levoglucosan [2].

Retention Time (min)	Compound	Set					
		1	2	3	4	5	6
2.72	methacrylaldehyde			√			
2.99	pyruvaldehyde			√			
3.20	2-methyl-furan		√	√	√	√	
3.93	2,3-dihydro-furan		√	√			
4.27	benzene	√	√	√	√	√	√
4.38	3-methyl-3-buten-2-one		√	√			
4.97	1-(ethenyloxy)-3-methyl-butane	√	√		√	√	
5.12	propanoic acid			√			
5.56	2,5-dimethyl-furan		√	√	√		
7.06	toluene	√	√	√	√	√	√
9.03	ethyl-benzene	√	√	√	√	√	√
9.20	<i>p</i> -xylene	√	√	√	√	√	
9.60	<i>o</i> -xylene		√				
9.90	2-furanmethanol, tetrahydro-		√				
10.27	propanoic acid, ethenyl ester			√			
10.30	1-(acetyloxy)-2-butanone			√			
10.37	5-methyl-2-furancarboxaldehyde			√			
10.70	1,3,5-trimethyl-benzene			√			
12.15	levoglucosenone					√	
13.30	1,4:3,6-dianhydro- α -D-glucopyranose			√			

Appendix 3.0:

Pyrolysis Products from 100% Nylon (G)

The pyrolysis of 100% nylon (G) generated a range of products that were only present consistently across sets 5 and 6 (the two sets that auto-ignited while the rest did not). These products were dioxolanes, *n*-alkyl- and chloro- benzenes, aromatics and substituted aromatics, *n*-alkyl-benzenes, nitriles, *n*-alkanes and *n*-alkenes, phenyls, alkyl acids and acid esters. Twenty eight of the pyrolysis products detected in 100% nylon (G) were also present in 64% polyester + 33% rayon + 3% elastin (N). This is thought to be due to the chemical nature of these textiles: they are both synthetic petroleum based textiles and, thus, are expected to generate similar pyrolysis products when they decompose under heat [3]. A number of nitriles detected here were also present in the 80% nylon + 20% elastin samples (H). The absence of caprolactam in sample (G) is also highlighted.

Retention Time (min)	Compound	Set					
		1	2	3	4	5	6
3.92	2-methyl-1,3-dioxolane	√				√	√
4.27	benzene	√				√	√
4.78	2-methylene-butanenitrile					√	√
7.06	toluene	√			√	√	√
7.85	1-octene					√	√
8.67	chloro-benzene					√	√
9.04	ethyl-benzene	√				√	√
9.20	<i>p</i> -xylene	√				√	√
9.50	styrene					√	√
9.73	1-nonene	√				√	√
9.85	methoxy-benzene					√	√
10.37	benzaldehyde					√	√
10.56	propyl-benzene					√	√
10.64	benzonitrile					√	√
10.71	1-ethyl-2-methyl-benzene					√	√
10.94	pentanedinitrile	√		√	√	√	√
11.07	benzofuran					√	√
11.18	1-decene					√	
11.30	2-methyl-pentanedinitrile	√				√	√
11.44	heptanedinitrile	√			√	√	√
11.50	α -methyl-styrene	√			√	√	√
11.83	acetophenone					√	√
10.12	1-methylethyl-benzene					√	√
11.74	3-butenyl-benzene					√	

12.24	benzoic acid, methyl ester					√	√
12.42	1-dodecene					√	√
12.73	benzoic acid, ethenyl ester	√				√	√
12.88	benzoic acid					√	√
13.40	naphthalene					√	√
13.52	1-tridecene					√	√
14.02	<i>o</i> -toluic acid, 4-nitrophenyl ester					√	√
14.51	1-tetradecene					√	√
14.34	<i>p</i> -toluic acid, ethyl ester					√	√
15.27	biphenyl					√	√
15.00	4-ethylbenzoic acid, 2,3-dichlorophenyl ester					√	√
15.32	benzoic acid, 2-chloroethyl ester					√	√
15.75	diphenylmethane					√	√
16.20	4-methyl-1,1'-biphenyl					√	√

Appendix 4.0:

Pyrolysis Products from 100% Silk (I)

The pyrolysis of 100% silk (I) generated a range of products that displayed poor reproducibility. These products included various types of nitriles, aromatics and substituted aromatics, isocyanic and phenolic compounds, *n*-alkenes and *n*-alkane, *n*-alkyl-benzenes, imidazole and caprolactam. Fifteen compounds that were detected here were also present in 96% wool + 4% lycra[®] (L). This is believed to be due to the chemical composition of wool and silk as both contain animal proteins and amino acids. The presence of caprolactam in silk is also highlighted. Being a natural polyamide, silk possesses similar chemical structure to synthetic polyamide (nylon-lysine is used to synthesise caprolactam) [3, 4] and, thus, during thermal decomposition it undergoes pyrolytic breakdown to generate caprolactam.

Retention Time (min)	Compound	Set					
		1	2	3	4	5	6
2.64	propanenitrile			√	√	√	
3.19	isobutyronitrile	√		√	√	√	
3.64	3-butenenitrile			√			
3.98	butanenitrile			√	√	√	
4.27	benzene	√		√	√	√	√
5.40	2-methyl-butanenitrile			√	√	√	
5.54	3-methyl-butanenitrile	√		√	√	√	
6.72	pentanenitrile			√			
7.06	toluene	√	√	√	√	√	√
7.80	1-octene			√		√	
7.81	1-isocyano-butane	√					
8.17	<i>bis</i> (1,1-dimethylethyl)-diazene	√		√			
8.20	4-methyl-pentanenitrile	√		√	√	√	
9.04	ethyl-benzene	√		√	√	√	
9.20	<i>p</i> -xylene	√		√	√	√	
9.50	styrene			√		√	
9.73	1-nonene			√		√	
9.90	nonane			√		√	
10.55	propyl-benzene			√		√	
10.63	benzonitrile			√			
10.70	1-ethyl-4-methyl-benzene			√			
10.72	phenol			√		√	
11.92	4-methyl-phenol			√			
12.02	1-methyl-4-nitro-1H-imidazole			√			
12.24	1-isocyano-3-methyl-benzene			√			
12.59	1-methylene-2-benzyloxy-cyclopropene			√			
13.73	caprolactam	√	√	√	√		√

Appendix 5.0:

Pyrolysis Products from 100% Viscose (K)

The pyrolysis of 100% viscose (K) generated a number of products with poor reproducibility across the six repeats with the exception of sets 4 and 6. These products were mainly furans, aromatics, *n*-alkyl-benzene, acid, acid esters and acid salt and ketones. All of these products were present in the 50% polyester + 50% viscose (O) samples and the majority of them were also detected across the textile blends containing cellulose in (A), (B), (C) and (D).

Retention Time (min)	Compound	Set					
		1	2	3	4	5	6
3.20	2-methy-furan	√					√
3.90	2-methyl-1,3-dioxolane						√
4.27	benzene	√	√	√	√		√
4.38	3-methyl-3-buten-2-one				√		√
5.14	propanoic acid				√		√
5.56	2,5-dimethyl-furan	√			√		√
6.80	propanoic acid, 2-methyl				√		
7.06	toluene	√			√		√
8.67	1-(acetyloxy)-2-propanone				√		√
9.04	ethyl-benzene	√			√		√
9.48	2,4-dimethyl-furan				√		
9.53	formic acid, furfuryl ester				√		√
9.60	2-ethyl-5-methyl-furan				√		√
10.25	propanoic acid, ethenyl ester				√		√
10.30	1-(acetyloxy)-2-butanone				√		√
10.37	5-methyl-2-furancarboxyaldehyde				√		√
10.84	2-furanmethanol, acetate				√		√
13.10	benzoic acid, ethyl ester				√		

Appendix 6.0:

Pyrolysis Products from 100% Polyester (M)

The pyrolysis of 100% polyester (M) only generated three products, detected only in set 4. These were *n*-alkyl-benzenes (toluene and ethyl-benzene) and a ketone (cathinone).

Retention Time (min)	Compound	Set					
		1	2	3	4	5	6
7.06	toluene				√		
9.03	ethyl-benzene				√		
12.74	cathinone				√		

Appendix 7.0:

Pyrolysis Products from 64% Polyester + 32% Viscose + 4% Elastin (P)

The pyrolysis of 64% polyester + 32% viscose + 4% elastin (P) generated large number of products, namely *n*-aldehydes, furans, dioxolanes, ketones, acid, acid salt and acid esters, oxy-alkenes and -alkanes, aromatics and derivatives, vinyl benzenes, ether and a benzonitrile. The majority of these products were also detected in the pyrolysis of 64% polyester + 33% rayon + 3% elastin (N), having generated from its polyester counterpart. The additional presence of terephthalic acid, 2-chlorophenyl ethyl ester in samples (P) is also highlighted in this work. This terephthalic acid is expected in polyester-based materials as it is a building block in the synthesis of polyester [5]. While the majority of products were of polyester pyrolysis, the presence of a group of compounds indicates its cellulose contribution: these characteristic by-products are furans (2-methyl-furan, 2,5-dimethyl-furan, tetrahydro-furan, 2-ethyl-5-methyl-furan), ketones (3-methyl-3-buten-2-one, 1-(acetyloxy)-2-butanone, 1-(acetyloxy)-2-propanone) and acid esters (propanoic acid, ethenyl ester;, 2-propenoic acid, methyl ester;).

Retention Time (min)	Compound	Set					
		1	2	3	4	5	6
3.21	2-methyl-furan	√	√	√		√	√
3.56	tetrahydro-furan	√	√			√	
3.89	2-methyl-1,3-dioxolane	√				√	
4.27	benzene	√	√	√		√	√
4.38	3-methyl-3-buten-2-one	√	√			√	
5.56	2,5-dimethyl-furan	√				√	
7.06	toluene	√				√	
7.43	3-butenyl-propyl-ether					√	
7.67	1-propoxy-butane					√	
8.67	1-(acetyloxy)-2-propanone					√	
8.76	1,3-dioxolane					√	
9.04	ethyl-benzene	√				√	
9.16	2-propenoic acid, methyl ester	√				√	
9.20	<i>p</i> -xylene	√				√	
9.34	1-butoxy-butene	√				√	
9.50	styrene	√					
9.60	2-ethyl-5-methyl-furan					√	
10.25	propanoic acid, ethenyl ester					√	
10.30	1-(acetyloxy)-2-butanone					√	
10.37	benzaldehyde					√	

10.56	propyl-benzene					√	
11.07	benzofuran					√	
11.50	1-propenyl-benzene					√	
11.83	acetophenone	√				√	
12.03	3-methyl-benzaldehyde					√	
12.73	benzoic acid, ethenyl ester					√	
12.88	benzoic acid	√				√	
12.24	benzoic acid, methyl ester					√	
13.40	naphthalene					√	
13.21	1-(4-methylphenyl)-ethanone					√	
14.02	<i>o</i> -toluic acid, 4-nitrophenyl ester					√	
14.26	1-(4-ethylphenyl)-ethanone					√	
15.00	<i>p</i> -toluic acid, ethyl ester					√	
15.00	4-ethylbenzoic acid, 2,3-dichlorophenyl ester					√	
15.27	biphenyl	√				√	
15.72	diphenylmethane					√	
16.20	4-methyl-1,1'-biphenyl					√	
17.10	terephthalic acid, 2-chlorophenyl ethyl ester					√	

Appendix 8.0:

EIC and EIP of Porcine Bone in the Presence of Textiles (Combined Samples)

EIC and EIP of Porcine Bone in the Presence of Cotton and Cotton Blends

Figures 8.1, 8.2 and 8.3 illustrate the EICs and EIPs of combined samples (AA) (set 5), (BB) (set 4) and (DD) (set 4), respectively. These were the sets that produced the highest number of pyrolysis products and were subjected to further scrutiny. Although hexadecanitrile was detected in all three combined samples, it was not present in set 4 of combined samples (DD).

For *n*-alkanes and *n*-alkenes, all of the characteristic ions were present across all three combined samples at varying abundances. Across all three combined samples, ion 99 had the lowest abundance for *n*-alkanes; whereas for *n*-alkenes, ions 83 and 97 were the lowest for combined samples (BB) and (DD). In combined samples (AA), all of the characteristic ions for *n*-alkenes were at high abundances.

Similar observations were noted for *m/z* values of hexadecanitrile in combined samples (AA), but this was not the case for combined samples (BB) as two of the five ions (152 and 166) were not present. However, the presence of the other three ions in the peak at 19.36 minutes was sufficient enough to distinguish the alkane-nitrile from the other individual highlighted peaks.

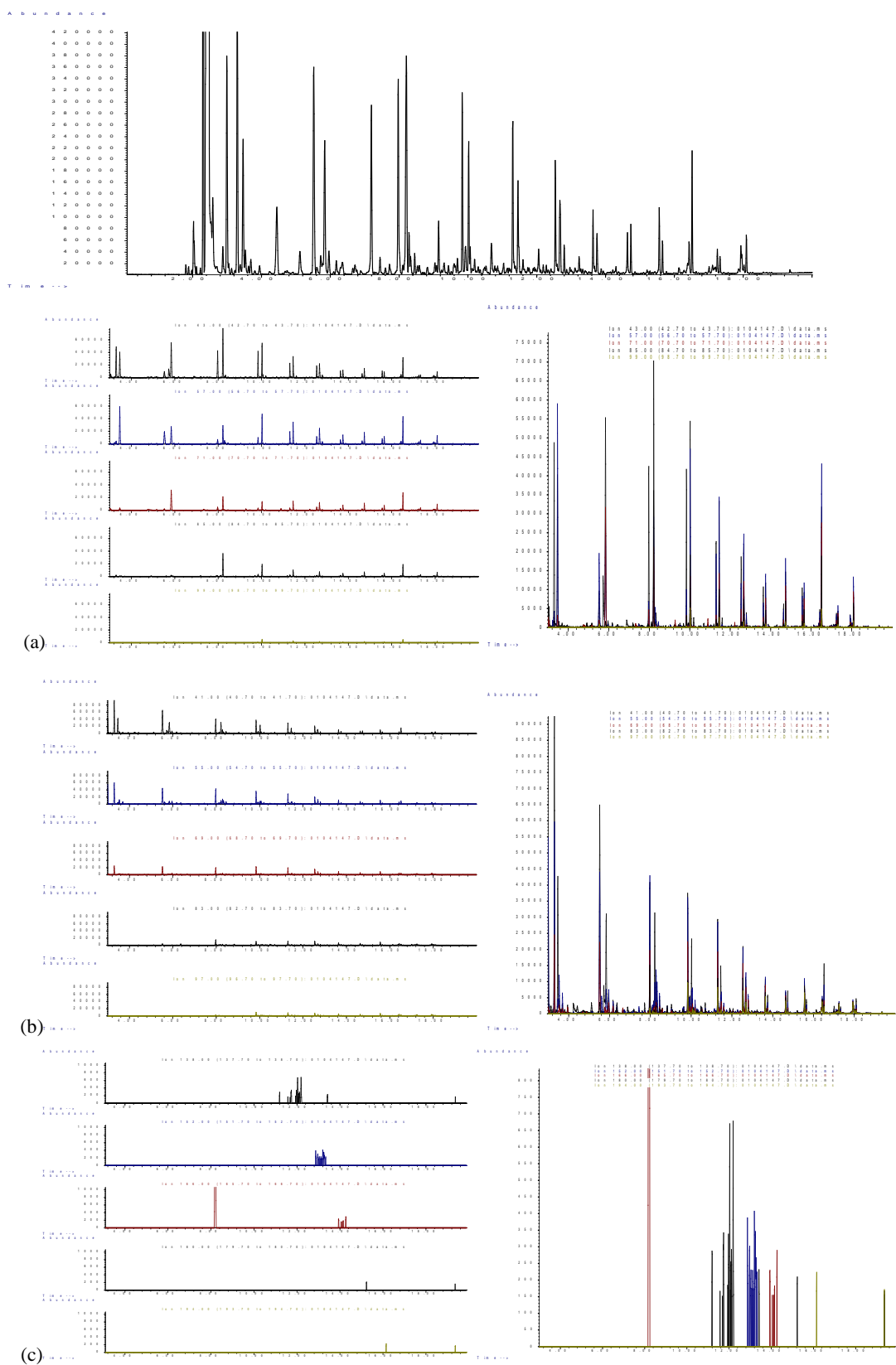


Figure 8.2: EIC and EIP of (a) *n*-alkanes, (b) *n*-alkenes and (c) hexadecanitrile in combined samples (BB)

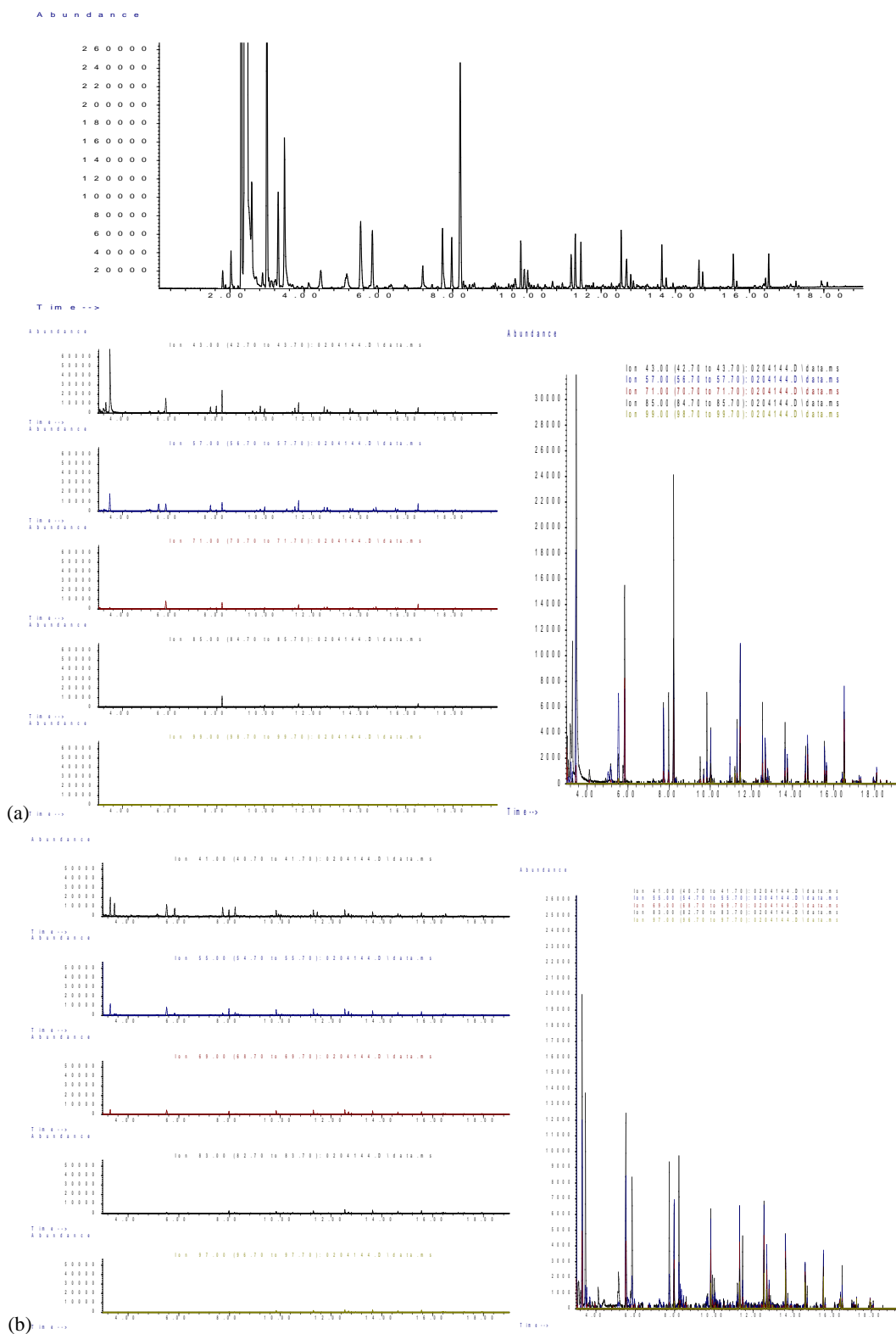


Figure 8.3: EIC and EIP of (a) *n*-alkanes and (b) *n*-alkenes in combined samples (DD)

EIC and EIP of Porcine Bone in the Presence of Acrylic and Acrylic Blends

For combined samples (EE) and (FF), sets 1 and 2, respectively, were the sets that produced the highest number of pyrolysis products and were subjected to further scrutiny. EIC and EIP for each combined samples (EE) and (FF) are displayed in Figures 8.4 and 8.5, respectively. Hexadecanitrile was detected in combined samples (EE), but not in combined samples (FF).

Similar to cotton blends, all of the characteristic ions for *n*-alkanes and *n*-alkenes were present across both combined samples at varying abundances. Across both combined samples, ion 99 had the lowest abundance for *n*-alkanes, whereas for *n*-alkenes ions 69, 83 and 97 were present at low abundances in combined samples (FF) but were at high abundances in combined samples (EE).

Also in combined samples (EE), all five ions characteristic of hexadecanitrile were present. The EIC and EIP of *n*-alkanes and *n*-alkenes contained additional highlighted peaks that are attributed to the presence *n*-alkane- and *n*-alkene-substituted nitrile groups detected across both combined samples.

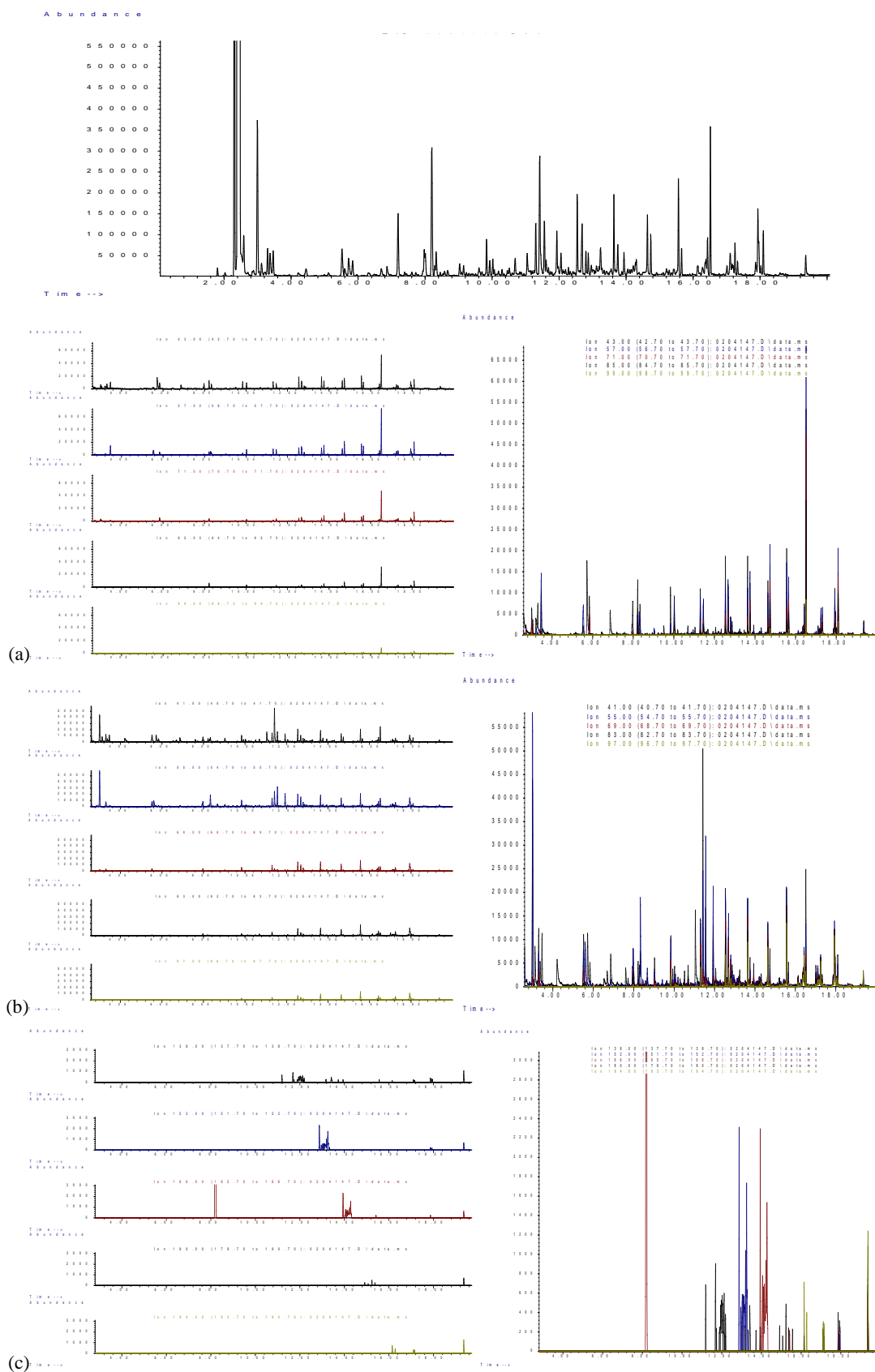


Figure 8.4: EIC and EIP of (a) *n*-alkanes, (b) *n*-alkenes and (c) hexadecanitrile in combined samples (EE)

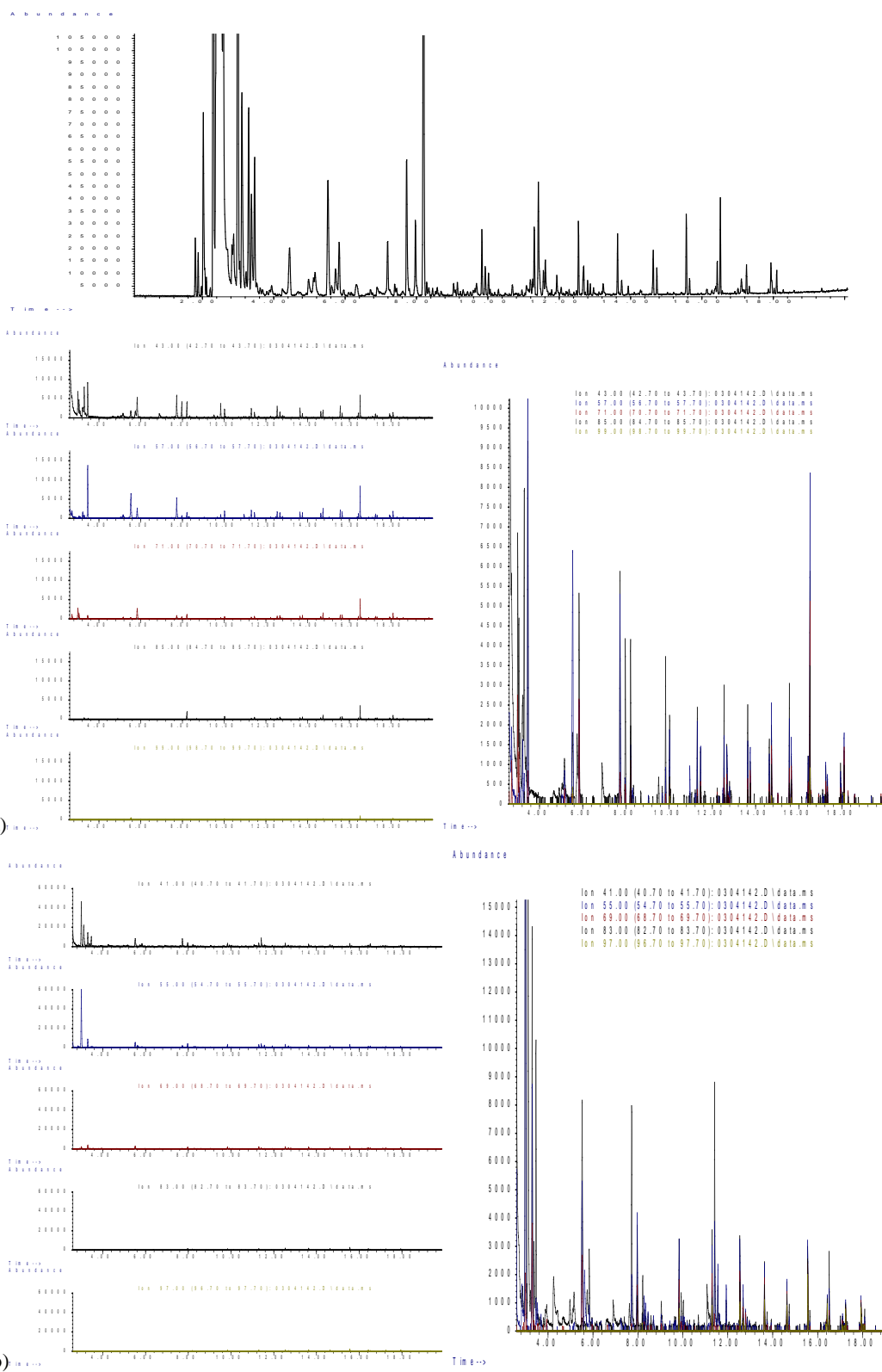


Figure 8.5: EIC and EIP of (a) *n*-alkanes and (b) *n*-alkenes in combined samples (FF)

EIC and EIP of Porcine Bone in the Presence of Nylon-Elastin Blend

Figure 8.6 displays the EIC and EIP of combined samples (HH) utilising the TIC of set 6, the set that generated the highest number of pyrolysis products. With similar results to the cotton and acrylic blends, all of the characteristic ions of *n*-alkanes and *n*-alkenes were present but at varying abundances, with ion 99 for *n*-alkanes and ion 97 for *n*-alkenes present at the lowest abundance in comparison to the other *m/z* values.

Two of the five ions (166 and 180) characterising hexadecanitrile were absent in combined samples (HH). The presence of the other three ions in the peak at minute 19.36 was sufficient for distinguishing the alkane nitrile from the other individual highlighted peaks, as documented in the cotton-elastin blend. Bearing similarities to the acrylic and acrylic blends, the EIC and EIP of *n*-alkanes and *n*-alkenes also contained additional highlighted peaks that are attributed to the presence of *n*-alkane- and *n*-alkene-substituted nitrile groups detected in combined samples (HH).

EIC and EIP of Porcine Bone in the Presence of Denim

As set 6 of the combined sample (JJ) generated the highest number of pyrolysis products, its TIC was subjected to EIC and EIP, as illustrated in Figure 8.7. With similar results to the cotton, acrylic and nylon blends, all of the characteristic ions of *n*-alkanes, *n*-alkenes and hexadecanitrile were present but at varying abundances, with ion 99 for *n*-alkanes present at the lowest abundance. All characteristic ions for *n*-alkenes and hexadecanitrile were present at high abundances.

EIC and EIP of Porcine Bone in the Presence of Wool-LYCRA® Blend

For combined samples (LL), set 4 produced the highest number of pyrolysis products and was subjected to EIC and EIP as detailed in Figure 8.8. As documented in all of the previously detailed combined samples, all of the characteristic ions of *n*-alkanes and *n*-alkenes were present but at varying abundances. Ion 99 had the lowest abundance for *n*-alkanes, whereas for *n*-alkenes ion 97 had the lowest abundance. Also in combined samples (LL), all five ions characteristic of hexadecanitrile were present.

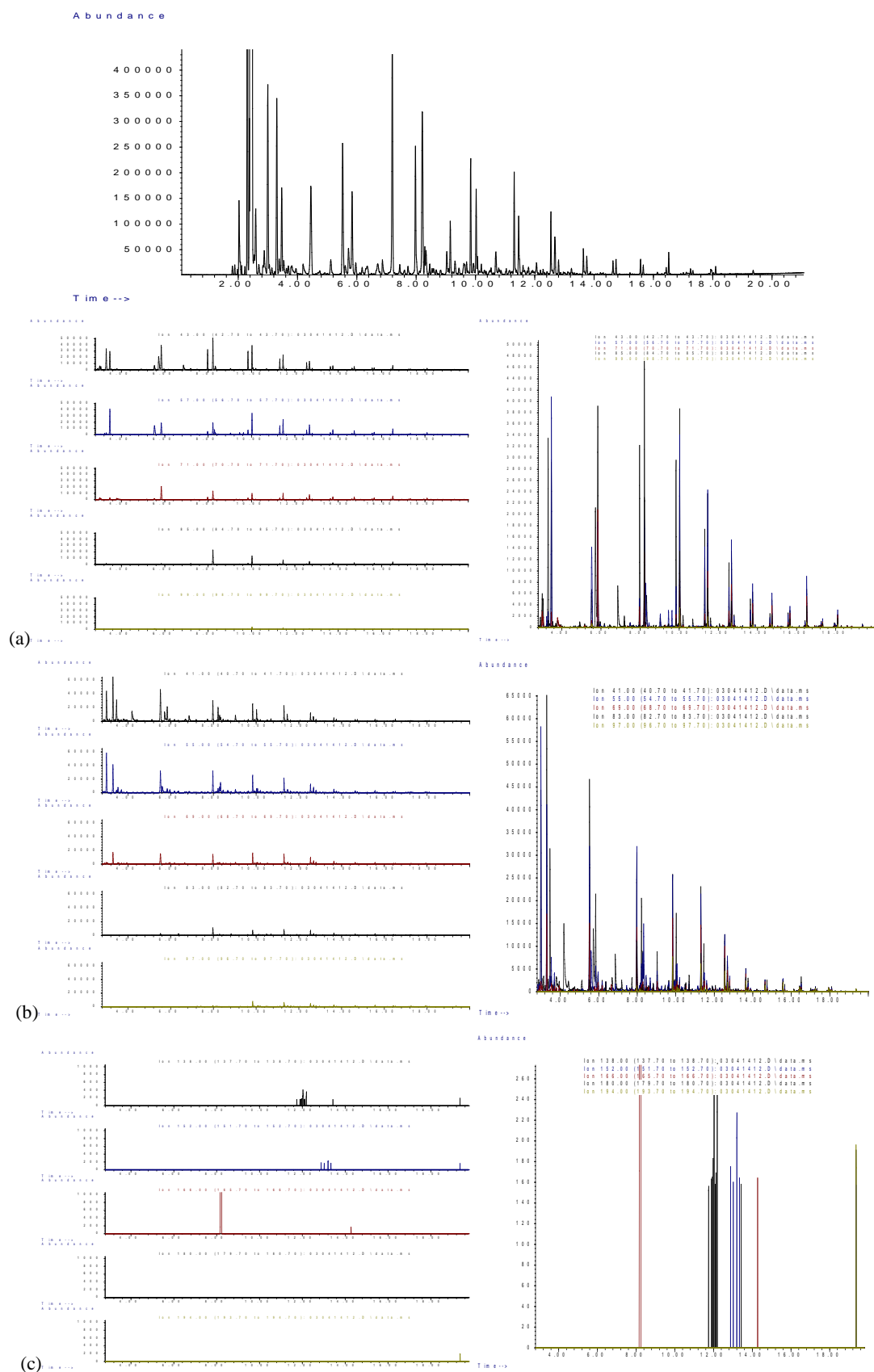


Figure 8.6: EIC and EIP of (a) *n*-alkanes, (b) *n*-alkenes and (c) hexadecanitrile in combined samples (HH)

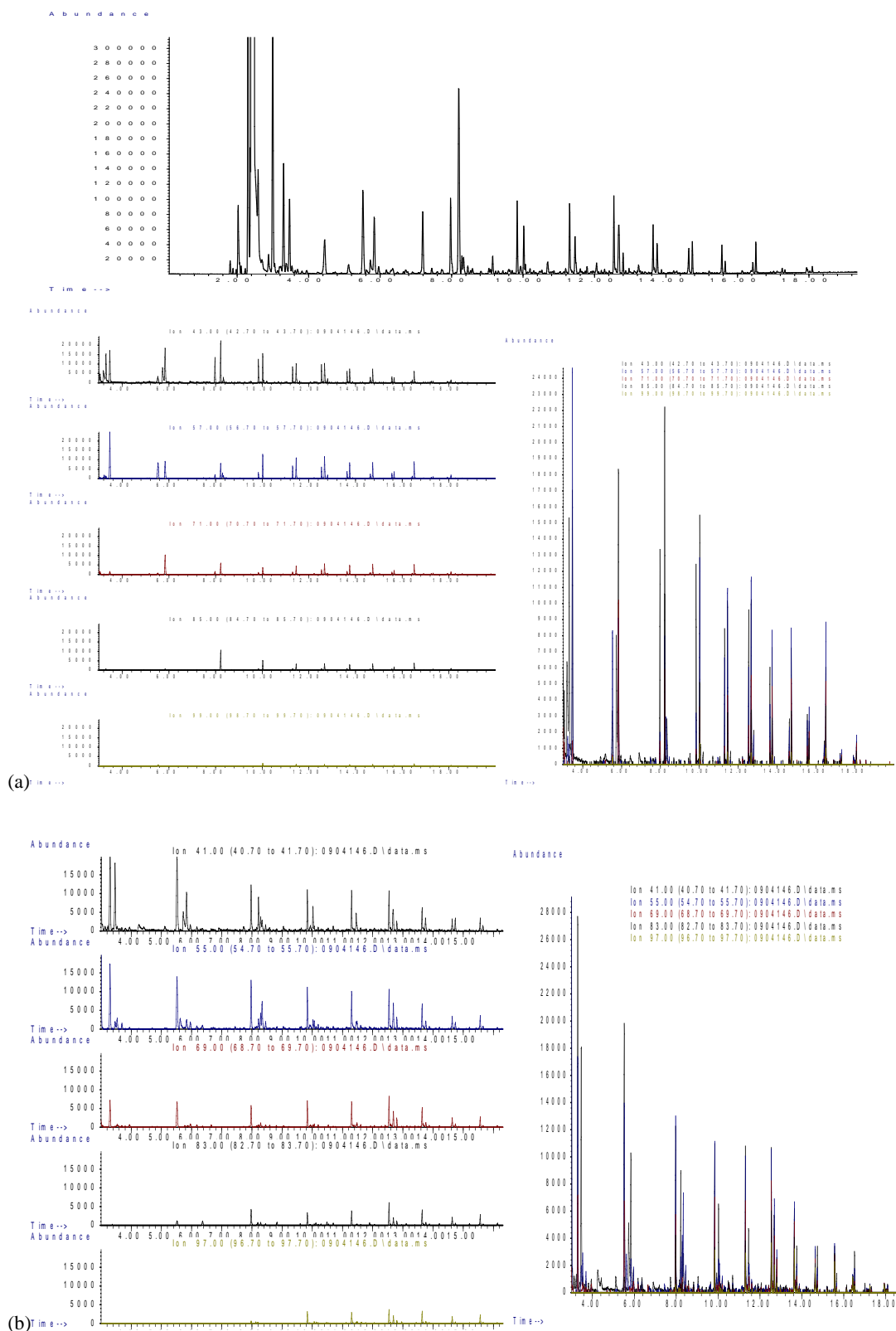


Figure 8.7: EIC and EIP of (a) *n*-alkanes and (b) *n*-alkenes in combined samples (JJ)

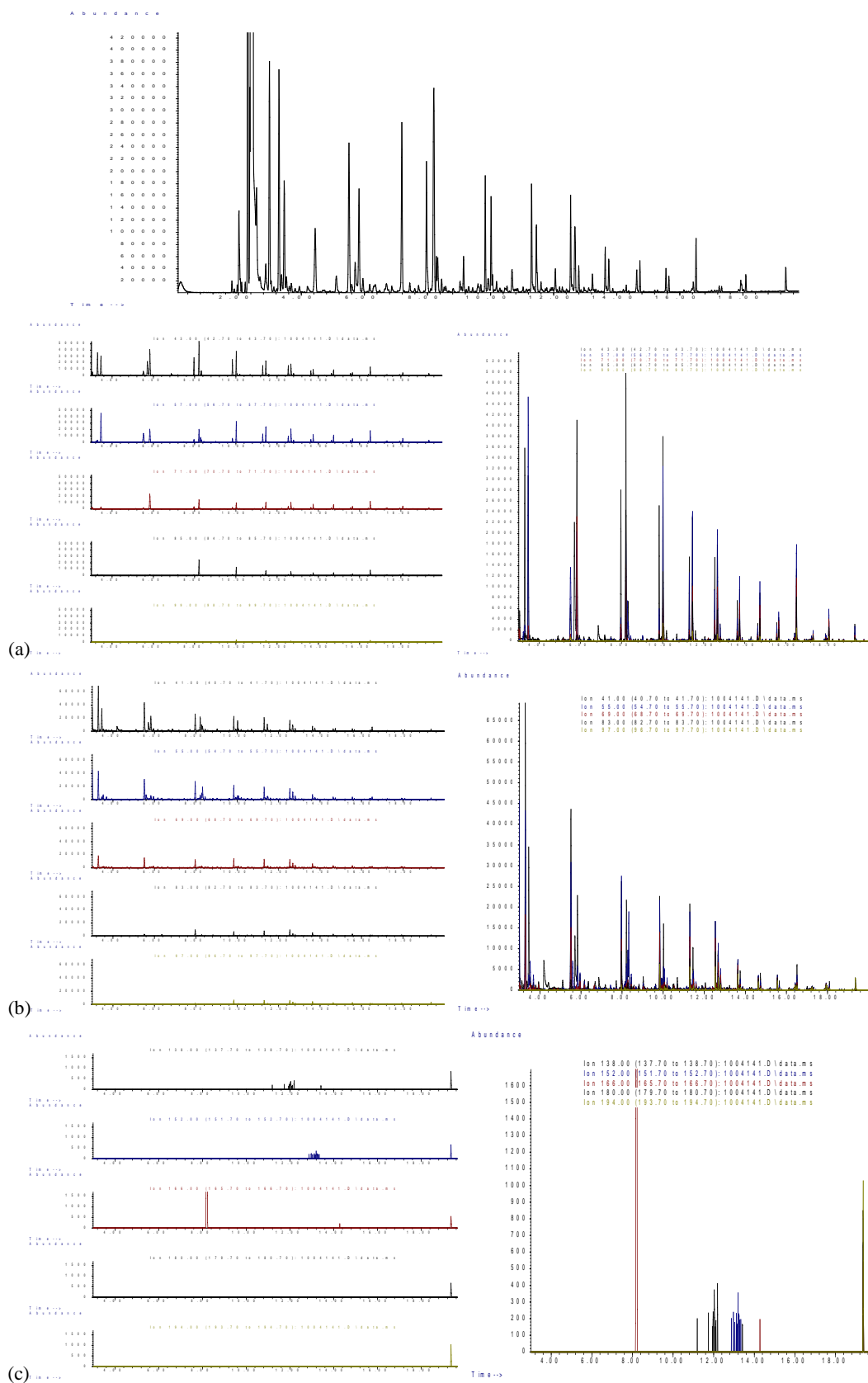


Figure 8.8: EIC and EIP of (a) *n*-alkanes, (b) *n*-alkenes and (c) hexadecanitrile in combined samples (LL)

EIC and EIP of Porcine Bone in the Presence of Polyester and Polyester Blends

Figures 8.9 and 8.10 illustrates the EIC and EIP of combined samples (NN) (set 2) and (OO) (set 3), respectively. For *n*-alkanes, *n*-alkenes and hexadecanitrile, all of the characteristic ions applied were present across both combined samples but at varying abundances.

While ion 99 had the lowest abundance for *n*-alkanes across both combined samples, it was ions 83 and 97 for *n*-alkenes in combined samples (OO). All of the *m/z* values for *n*-alkenes were present at high abundances in combined sample (NN), and hexadecanitrile ions were present across both samples at high abundances.

EIC and EIP of Porcine Bone in the Presence of Leather

For combined samples (QQ), set 4 produced the highest number of pyrolysis products; thus, EIC and EIP exactions were conducted on its TIC and are displayed in Figure 8.11.

For *n*-alkanes, *n*-alkenes and hexadecanitrile, all of the characteristic ions were present across both combined samples but at varying abundances. Ion 99 had the lowest abundance for *n*-alkanes while all of the *m/z* values for *n*-alkenes and hexadecanitrile were present at high abundances.

In contrast to the rest of the combined samples, the TIC of combined samples (QQ) was more complicated and made it difficult to extract the characteristic ion profiles as both contributors (porcine bone and leather) generated similar pyrolytic compounds, particularly heavy molecular weight *n*-alkenes and some less consistent *n*-alkanes. The *m/z* values of a homologous series of *n*-alkanes and hexadecanitrile were more useful in this instance.

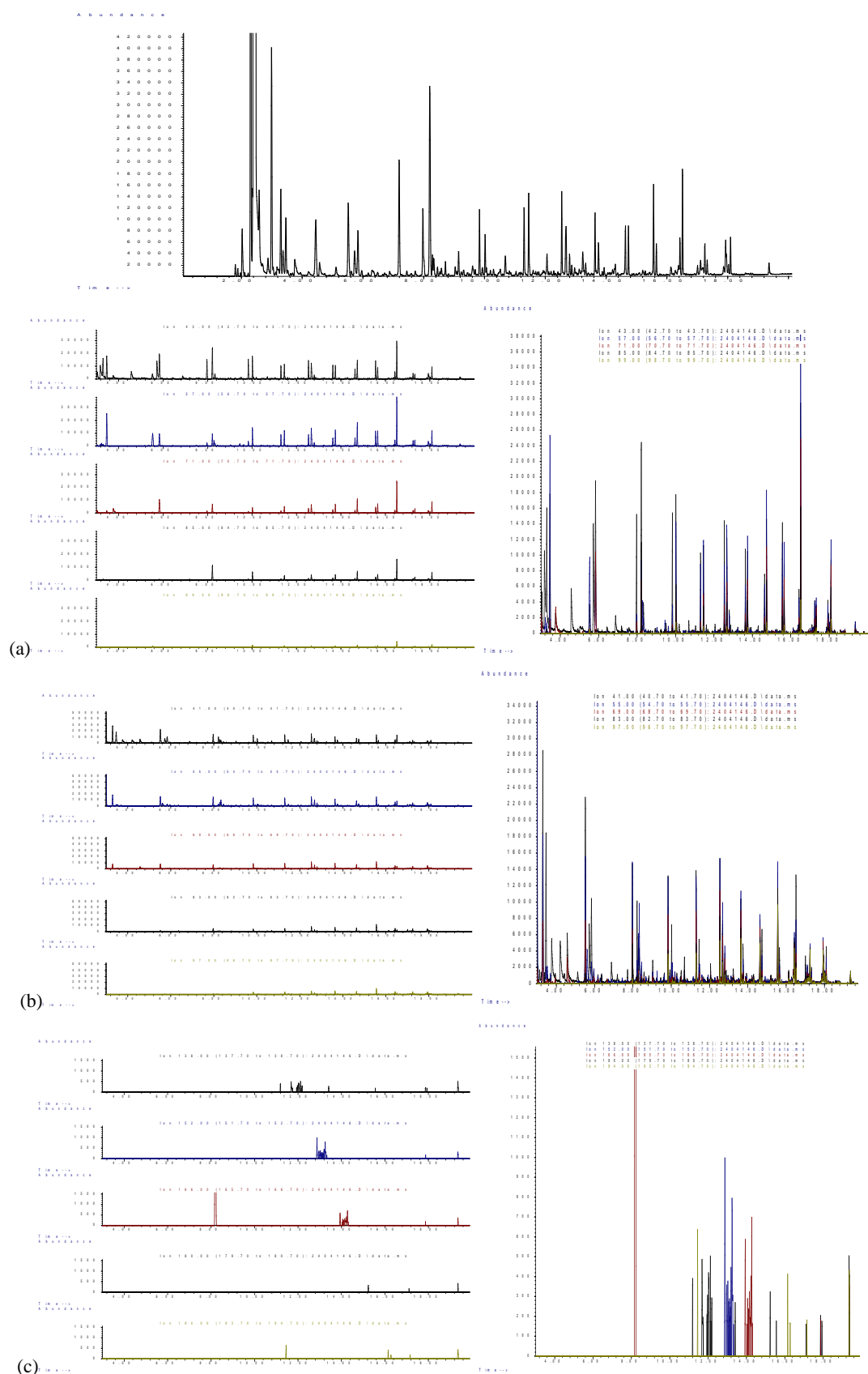


Figure 8.9: EIC and EIP of (a) *n*-alkanes, (b) *n*-alkenes and (c) hexadecanitrile in combined samples (NN)

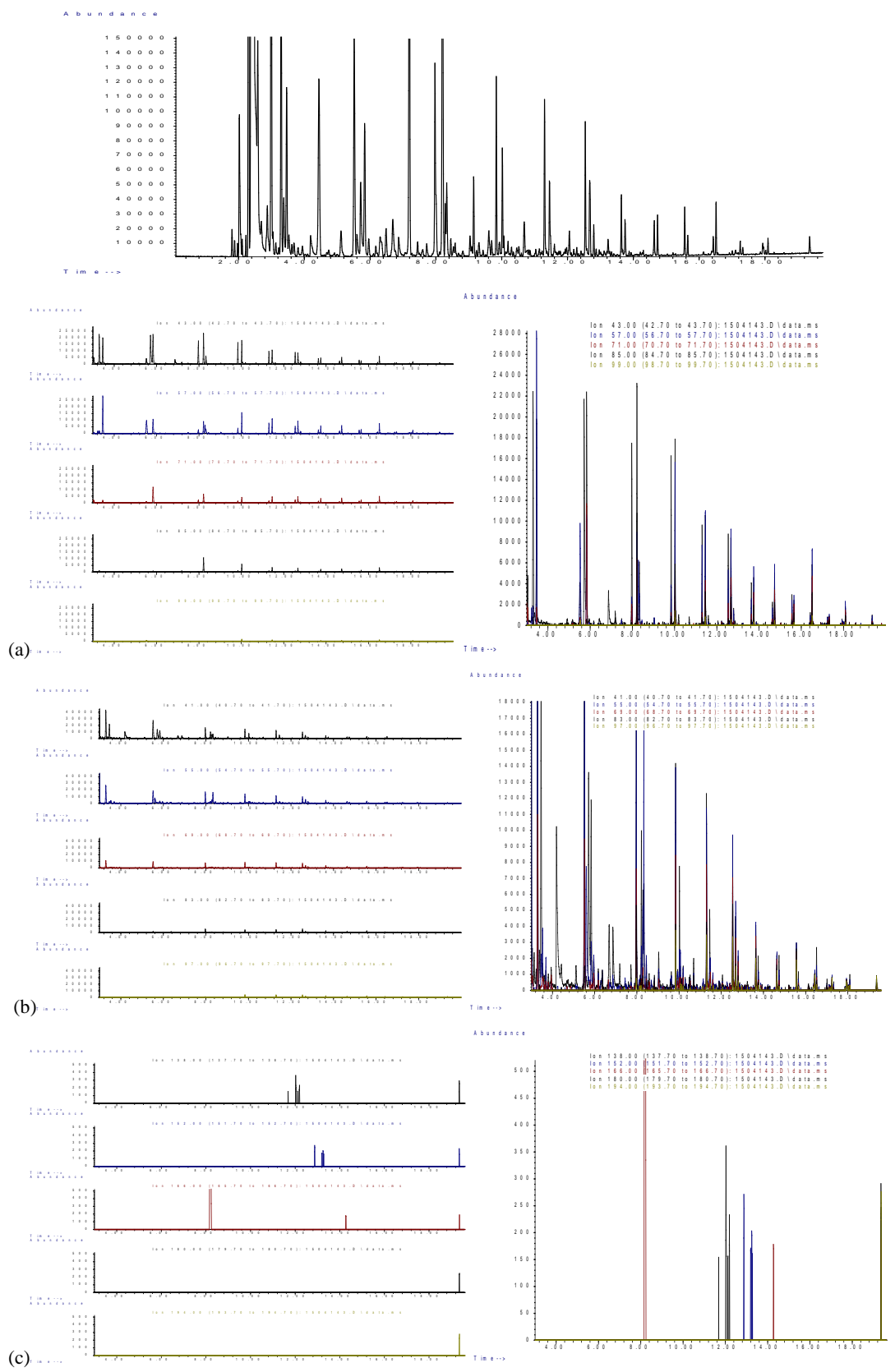


Figure 8.10: EIC and EIP of (a) *n*-alkanes, (b) *n*-alkenes and (c) hexadecanitrile in combined samples (OO)

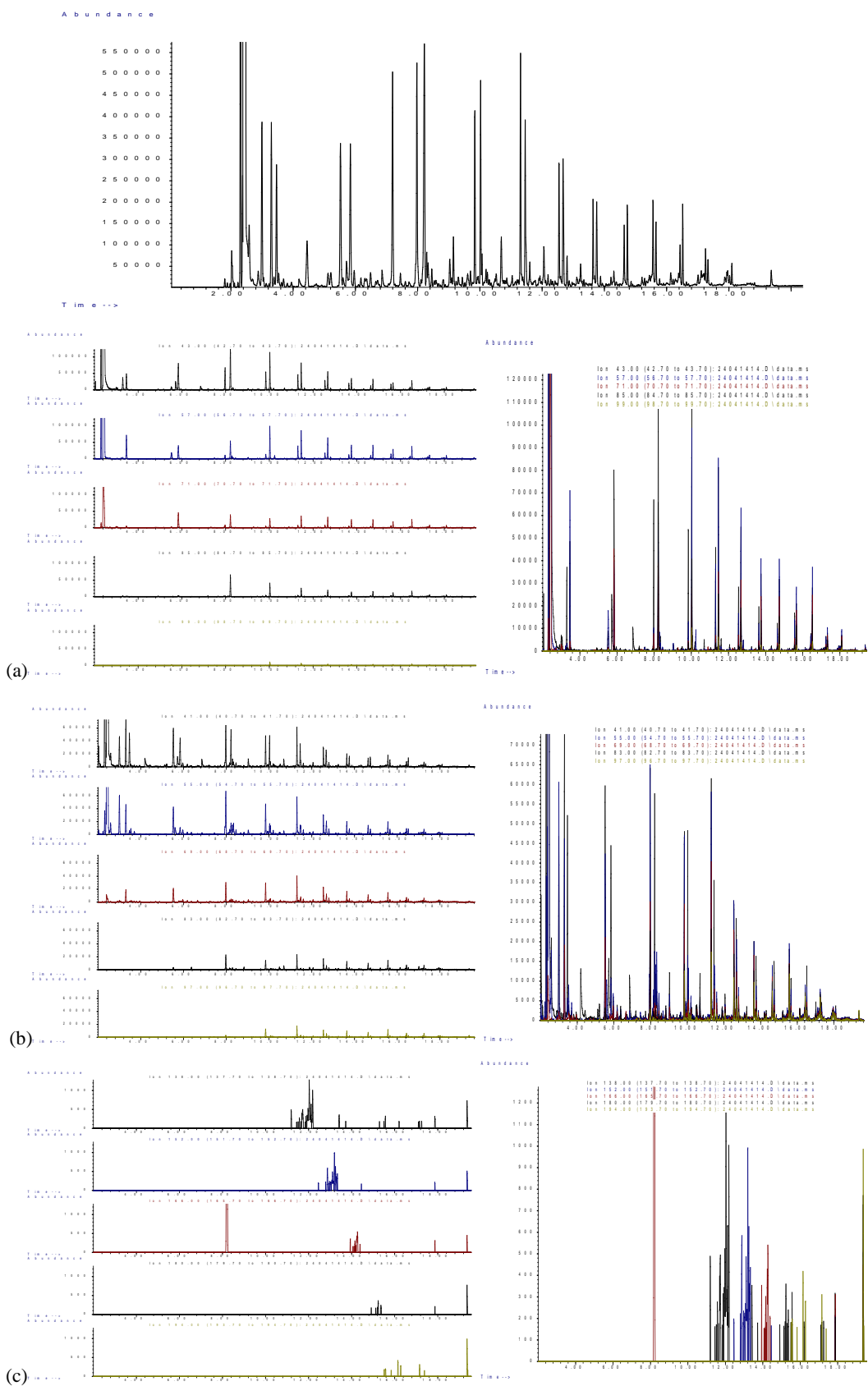


Figure 8.11: EIC and EIP of (a) *n*-alkanes, (b) *n*-alkenes and (c) hexadecanitrile in combined samples (QQ)

References

1. National Center for Biotechnology Information, U.S. National Library of Medicine, *β -D-Allopyranose*. [Online] [April 2013, November 2014]. Available from: <http://pubchem.ncbi.nlm.nih.gov/compound/448388>.
2. Shen, D.K. and Gu, S., *The Mechanism for Thermal Decomposition of Cellulose and Its Main Products*. Bioresource Technology, 2009. **100**(24): p. 6496-6504.
3. Beyler, C.L. and Hirschler, M.M., *Section 1, Chapter 7: Thermal Decomposition of Polymers*, in SFPE Handbook of Fire Protection Engineering ed. P.J. Dinunno. 2002, National Fire Protection Association (NFPA), Quincy, MA.
4. Lawrence, S.A., *Heterocyclic Amines*, in Amines: Synthesis, Properties and Applications, ed. S.A. Lawrence. 2004, Cambridge, UK: Cambridge University Press.
5. Plunkett, J.W., *Plunkett's Chemicals, Coatings & Plastics Industry Almanac*, ed. Plunkett Research Ltd, 2009.